FROM SLAB TO SINTER: THE MAGMATIC-HYDROTHERMAL SYSTEM OF SAVO VOLCANO, SOLOMON ISLANDS

Thesis submitted for the degree of
Doctor of Philosophy
at the University of Leicester

Daniel James Smith MGeol (Leeds)

Department of Geology
University of Leicester

September 2008

FROM SLAB TO SINTER: THE MAGMATIC-HYDROTHERMAL SYSTEM OF SAVO VOLCANO, SOLOMON ISLANDS

Daniel James Smith

The SW Pacific hosts world-class alkaline-related epithermal gold deposits. Savo Island, a recently active volcano in the Solomon Islands, is dominated by alkaline, sodic (≤7.5 wt % Na_2O) lavas and pyroclastic deposits and has an active hydrothermal system, with hot springs and fumaroles. It thus represents a natural laboratory for studying the magmatic and hydrothermal processes that can form epithermal mineralisation.

The magmatic suite is divided into mugearites (plagioclase–clinopyroxene–magnetite ± amphibole ± olivine) and trachytes (plagioclase–amphibole–magnetite ± biotite). Mineralogy, geochemistry, and cumulate xenoliths within the lavas indicate that amphibole fractionation drove magmatic differentiation. Hydrous, alkali-rich magmas were likely derived from partial melting of metasomatised mantle, but radiogenic isotope data cannot discriminate the origin of metasomatic agents.

Hot springs at Savo include high pH, sulphate-rich discharges (with high Na, Si, Ca, K, low Cl^-); atypical for magmatic-hydrothermal systems. These fluids form by the condensation of magmatic volatiles into meteoric-derived groundwater (high Ca, Mg, HCO_3^-) generating acidity by SO_2 disproportionation into H_2SO_4 and H_2S. Water chemistry, $\delta^{18}O$, and δD data indicate that rock reaction, dilution and boiling increase the fluid pH to 7–8. H_2S oxidises at the surface, producing H_2SO_4 and native sulphur in steam-heated springs and fumaroles. The lack of isotopic equilibrium between the various sulphur species indicates that acidity is rapidly neutralised, and that the system is dominated by high pH fluids.

Precipitates around hot springs include sinter, travertine and mixed silica-carbonate. These are often enriched in Au and Te, indicating potential for mineralisation at Savo. Varying contributions from meteoric and hydrothermal fluids leads to alternating carbonate and silica precipitation, underlining the importance of high rainfall to the hydrothermal system. Sinter and travertine may be useful tools for the exploration of alkaline-related epithermal deposits, as they provide preservable records of hydrothermal activity and fluid chemistry.

Acknowledgements

This PhD was made possible by funding from the Natural Environment Research Council and the British Geological Survey. Additional funds came from the Society of Economic Geologists, Robert's Skills Fund, Whitaker Fund, the Mineralogical Society and the Geochemical Society.

From before the project even started, Dr. Gawen Jenkin has provided support, advice, and encouragement. For the duration of the PhD, in the field, laboratory, office, he has pushed me, improved me, and made me a better scientist. I'm proud to call him my boss!

Professor Mike Petterson's passion for geology, keen eye for scientific opportunity and love of the Solomon Islands kick-started this project; his unrivalled optimism and enthusiasm have kept it moving on days when, without him, I might have given up.

Dr. Jon Naden has helped me with advice, encouragement, and information. The PhD has benefited immensely from his experience and insights into hydrothermal systems, and it would be a lesser piece of work without him.

Dr. Adrian Boyce went above and beyond the call of duty with the time he devoted to this project, with his supervision on the stable isotope analyses, manuscripts, and where to find good haggis. Alison McDonald's efforts in the laboratory at East Kilbride made all the data possible. Julie Dougans, Terry Donnelly, Chris Taylor and Andrew Tait all mucked in too; I certainly kept SUERC busy!

Professor Andy Saunders has helped me throughout my time at Leicester. In particular, his help on the igneous petrogenesis and regional tectonics of Savo and the Solomon Islands was invaluable.

Special thanks go to Tom Toba of the Solomon Islands Geological Survey; he was captain of our leaky vessel, our main pathfinder on Savo, logistical mastermind in Honiara, and a fantastic geologist too. I could not have done a thing in the Solomons without him. Alison Papabatu ran around for weeks trying to get my visa and work permit. Gilly Albert is awaiting confirmation of his Michelin Stars for the wonders he worked with megapode eggs and gasoline-contaminated rice. In between kung-fu practice and rearing puppies, Watson "Sato" Satokano was a wonder in the field, and when he was with us, work was a breeze. Alan Ramo had a steady supply of betel nut and an easy-going manner; he kept everyone happy, including me.

The people of Savo Island deserve a special thank you, for allowing us to use their land, their houses, food and water. Chief Melchiot of Lemboni village was a gracious host. Timmy Tambuni had a good eye for xenoliths, and was uncannily good at stopping me from wading through poisonous bushes. Ano was another one of our local guides – without these men the work would have taken forever. Francis and Michael often came along too – their curiosity and growing appreciation for science was a fantastic reward for me.

The British High Commission in the Solomon Islands helped us with transport and storage of chemicals, equipment and computers, provided advice and assistance with the accursed work permits. Richard Lyne and family, and Ray Davidson MBE kept us well fed and watered with barbecues and G & T; their hospitality knew no bounds.

Helen Taylor, Kay Green, Jenny Cook and Richard Shaw (BGS Keyworth) helped with various analyses. At least two chapters of this thesis would be blank if not for their assistance. George Darling (BGS Wallingford) was the mastermind behind the gas and water sampling methodologies; his experience and expertise with geothermal systems has improved the discussion many times over. Ian Millar (NIGL) was my supervisor for the radiogenic isotope analyses. I'm sorry to have provided him with such monotonous samples (better reproducibility than international standards!), but glad to have shared a lab and occasionally a pub with him.

The technical officers and analytical staff in the Department of Geology all provided their time and expertise to help me with this project. My thanks go to Nick Marsh, Rob Kelly, Lin Marvin, Colin Cunningham, Dave York, Andrew Myers and Kevin Sharkey. In particular I would like to thank Sarah Lee and Rob Wilson, who had to put up with an unprecedented amount of nagging. A number of the faculty at Leicester have provided helpful discussion too – thanks to Richard England, Mike Norry, Mark Williams, the late Tim Brewer, Kip Jeffrey, Sarah Gabbott (not least for putting a roof over my head) and Mike Branney. Louise Anderson and Marc Reichow helped me out immensely with my critters and crystals.

Shane Cronin, Mark Reed, David Cooke, Noel White, Peter Schiffman, Bob Fournier, Bruce Gemmell, Jocelyn McPhie, Brian Jones, Bruce Yardley and Daniel Selles all provided helpful and instructive discussion.

A number of my friends and fellow PhD students warrant a big thank you: Simon "The Jow" Jowitt (for all the beers, mineralisation and Bonchurching); James "Jamesor" Blight (for music, bourbon, Halo and The Claw); Steve "Rippers" Rippington (for big hair and aviators); Pablo Dávila Harris (for tea breaks, tequila, and putting up with my music for over two years!); Ben Ellis (for the Bad Attitude); Andy Shore, Pete Fitch, Jo Tudge, Becky Williams, Xiaoya Ma, Dave Baines, Alex and John Lemon, Dave Cornwell, Rowan Whittle, Alex Page and Graham Andrews.

My family have supported me throughout this: Philip, Julie, Becky and Bethany Lowe have kept me supplied with chocolate and liquor, my sister Rachel has fought my corner in darkest Yorkshire, Barney never ate my homework and always wagged at the right times (I'll miss you, little fella), and my Grandma and Granddad (Gladys and Harry Lowe) have always been there for me. I can't thank them enough.

Finally, I'd like to thank my parents. Without David and Sandra Smith, there would be no Daniel Smith. Without their continued love and support, there would be no PhD. It's been four years of hard work for me, but 26 years for them. Anything clever I've done is from the genes, and everything wonderful that's happened for me has been made possible by them.

Daniel Smith

University of Leicester, August 2008.

Contents

List of figures

List of tables

Introduction 1

1.1 Background and rationale

The southwest Pacific is a major gold-rich metallogenic province characterised in particular by unusual alkaline rock-related epithermal deposits. For example, Ladolam, Papua New Guinea, is one of the largest epithermal deposits known, with over 1300 tonnes Au (Simmons and Brown, 2006). Previous studies have linked regional tectonic events, such as subduction polarity reversal, as well as the distinctive alkaline magmas, to the region's spectacular metal endowments. Alkaline-related deposits differ from other epithermal deposits in a number of respects, including ore mineralogy (e.g. abundant tellurides), gangue (abundant carbonates) and alteration (a paucity of acid-related assemblages), that may make recognition during exploration difficult (Jensen and Barton, 2000; Sillitoe, 2002).

Less than 3% of the igneous rocks found in the circum-Pacific arcs are alkaline, yet ~20% of the region's largest gold deposits are associated with them (Sillitoe, 1997; Müller, 2002). Given the low occurrence of alkaline magmatic suites, there are few examples of active hydrothermal systems hosted in such rocks. Ladolam, Papua New Guinea, is one such system – the gold deposit there hosts an active hydrothermal system (Carman, 2003) that is arguably still producing mineralisation at depth (Simmons and Brown, 2006). However, the Luise volcano that hosts the deposit has been modified by sector collapse (Sillitoe, 1994), removing any potential indicators of mineralisation in the lithocap. The study of active analogues is an important method for understanding the formation of epithermal ore deposits, even if the modern system is not mineralised (Henley and Ellis, 1983; Brown, 1986; Hedenquist and Aoki, 1991; Hedenquist et al., 1993).

The early stages of activity in alkaline-related magmatic-hydrothermal systems are undoubtedly important. Richards (1995) noted that sub-economic porphyry-style mineralisation is commonly present at alkaline-related epithermal deposits, and is a key step in the transfer of Au from magmatic to epithermal conditions. At Porgera, Papua New Guinea, the metals in the epithermal deposit may have been derived mostly from leaching of earlier disseminated ore (Richards et al., 1991). As such, magmatic processes, and the early stages of magmatic hydrothermal activity are key research areas.

Savo Island, in the central Solomon Islands, is a historically active volcano with a hydrothermal system manifested at the surface by numerous hot springs, fumaroles and areas of steaming ground. Recent eruptions were dominated by unusually sodic, alkaline magmas (Stanton, 1994; Petterson et al., 2003). Furthermore, the volcano is in a region with established potential for mineral deposit formation – the Gold Ridge epithermal deposit and Koloula copper porphyry prospect are found on nearby Guadalcanal (Petterson et al., 2004). Savo is a natural laboratory to investigate the processes that occur during the earliest stages of magmatic-hydrothermal activity in alkaline-dominated systems, and offers a rare opportunity to examine both products and processes that operate in the uppermost parts of these systems.

1.2 Aims

The aims of this thesis are to:

- Investigate the nature of the hydrothermal and magmatic systems at Savo, discuss its mineralisation potential, and identify the processes and products of the early stages of alkaline-related magmatic-hydrothermal activity.
- Determine the tectonic and petrogenetic processes that lead to the formation of sodic, alkaline magmas at Savo, and the role that these processes could have in the transport of metals and volatiles from subducted slab, mantle and magma to shallow hydrothermal systems.
- Describe the chemical and stable isotope composition of the hydrothermal discharges, determine the key processes that affect them at depth and at surface, and establish a model for the active hydrothermal system.
- Characterise surficial deposits of sinter and travertine from Savo in terms of chemistry, mineralogy and texture, and assess their potential as exploration indicators for other alkaline-related systems, in particular those with intact lithocaps.

1.3 Outline

This thesis describes and discusses the magmatic-hydrothermal system at Savo from slab to sinter.

The nature of subduction and the behaviour of slabs in the sub-arc mantle are principal controls on melt generation and the location of volcanic activity. *Chapter 2* summarises the tectonics, past and present, of the Solomon arc and the geological history of the major islands, including Savo. Various studies in the Solomon Islands and in the wider SW Pacific region have described the complex tectonics of the Melanesian arcs, and identified a number of processes that are favourable to the generation of alkaline magmatic suites and mineral deposits.

Subduction and metasomatism are key processes for the enrichment of the sub-arc mantle in volatiles and alkalis, and for mobilising metals such as gold and copper. However, it is magma that transports them from the mantle to the upper crust. As the melts ascend, they evolve chemically and mineralogically by a range of processes, including crystallisation, fractionation, volatile loss, and assimilation. Each of these can have a profound effect on the behaviour of metals in the system, and ultimately on their availability to hydrothermal fluids. *Chapter 3* provides a detailed description of the mineralogy and geochemistry of unaltered magmatic rocks at Savo, and focuses on the petrogenetic processes that create and modify the alkaline magmas between the mantle and eruption at the surface.

The chemistry of the active hydrothermal system is investigated in *Chapter 4* by the analysis of hot spring discharges. The composition of the hydrothermal fluids can provide evidence for a number of processes at depth, including boiling, water-rock reaction, fluid mixing and mineral precipitation. The composition of the hydrothermal fluids, including their temperature and pH, dictate the alteration of wall rocks and the nature of precipitated minerals (economic and gangue).

Stable isotope ratios of O, H, and S are key tools in understanding aqueous systems; they can provide constraints on fluid sources, boiling, mixing and water-rock reaction that may not be apparent in the fluid chemistry. *Chapter 5* investigates the stable isotope systematics of the hot spring and fumarole discharges at Savo, and is used in parallel with the chemistry data to construct a model for the active hydrothermal system.

The hot spring discharges precipitate a range of deposits (sinter, travertine and mixed silica -carbonate) at the surface. Whereas hot spring discharges are an instantaneous sample of the system, the deposits record longer timescales. As such, they can provide insights into the stability of the hydrothermal system, and the nature of any long-term changes. Many hydrothermal mineral deposits have preserved hot spring sinters associated with them – as such the spring and stream precipitates at Savo may represent a geologically preservable lithocap feature. *Chapter 6* describes the surface deposits at Savo in terms of distribution, mineralogy, chemistry and stable isotope composition. Along with the chemical and stable isotope compositions of major streams on Savo, these data will be used to determine the processes that led to mineral precipitation at the surface, and whether these deposits provide any further information on the hydrothermal system beneath.

Chapters 3–6 are written as independent sections: *Chapter 7* synthesises the observations and conclusions from these chapters into a discussion of the magmatic-hydrothermal system as whole. In particular, the role that the different processes play in gold mineralisation will be discussed; to determine mineralisation potential at Savo, to indicate how processes observed there might inform the debate on the genesis of alkaline-related epithermal deposits, and to identify features that might prove useful as exploration indicators.

The geology and tectonics of the Solomon Islands and Savo Volcano

2

Abstract

The Solomon Islands are one of a series of volcanic arcs that mark the convergence of the Indo-Australian and Pacific Plates. Southward subduction of the Pacific Plate began at the North Solomon Trench System in the Palaeocene, resulting in the earliest arc-related arc activity (62–46 Ma). The Ontong Java Plateau (an Alaska-sized large igneous province) reached the subduction zone 25–20 Ma; its thickened crust "choked" the trench, resulting in a hiatus of magmatism, deformation of the northern islands, and eventually a polarity reversal in subduction. Northward subduction of the Indo-Australian Plate at the South Solomon Trench System began sometime before 6.4 ±1.9 Ma, and resulted in a second stage of arc magmatism that continues today. The Woodlark Basin and its recently active spreading ridge, part of the Indo-Australian Plate, are currently being subducted at the southern trench. A number of studies have concluded that spreading ridge subduction may lead to slab window formation beneath the arc, and is responsible for a number of unusual magma types (picrite, high magnesian andesite) and volcanic positions (volcanism on the fore-arc and downgoing slab).

Savo is a recently active volcano in the central Solomon Islands, dominated by sodic trachyte and mugearite rocks. Eruptive activity (last eruption 19th century) has been dominated by dome formation and subsequent collapse to pyroclastic debris currents (Merapi-type). At present, an active hydrothermal system manifests at the surface in a series of hot springs and fumaroles. Most studies consider Savo to be related to the southern subduction zone (second stage of arc magmatism) and potentially located above a slab window. However, contributions from the northern trench and subducted slab cannot be ruled out.

2.1 Introduction

A series of active and remnant island arcs stretching from Papua New Guinea to Tonga mark the convergence of the Pacific and Indo-Australian plates. This Greater Melanesian Arc System includes the Solomon Islands, situated between Papua New Guinea and Vanuatu (Fig. 2.1). The key tectonic elements of the Solomon Islands arc include the Ontong Java Plateau (OJP) large igneous province to the north and the Woodlark Basin

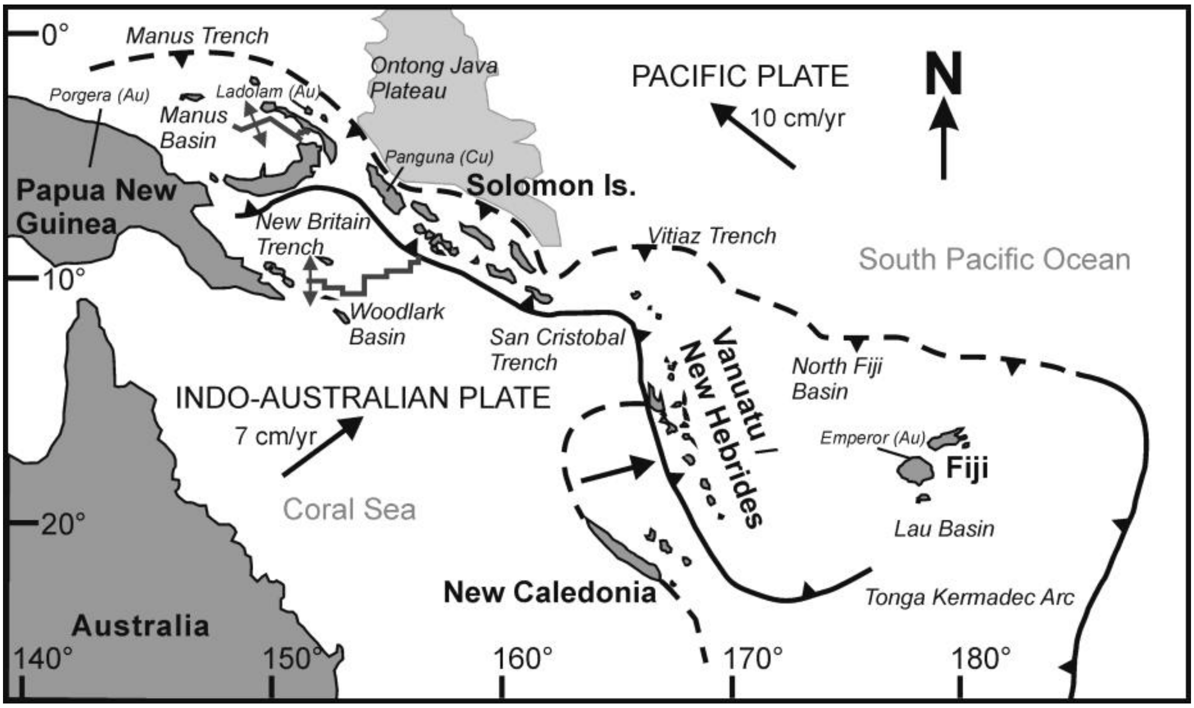

Fig. 2.1: Map of the southwest Pacific and Melanesian Arc systems (after Meffre and Crawford, 2001). Active arcs shown in solid lines (with arrow marks on overriding plate), inactive or intermittently active arcs show as dashed lines. Spreading ridge systems (Manus and Woodlark Basins shown as heavy grey lines. Arrows show relative plate motions (Petterson et al. 1999). Locations of major copper and gold deposits in the region are also shown.

and spreading centre to the south. Subduction zones have been active both north and south of the arc, and the interplay between the thickened crust of the OJP and the young, hot crust of the Woodlark has been a complex yet important control on many of the region's features.

The Solomon Islands (Fig. 2.2) have a complex geological history, with multiple stages of tectonic activity and associated magmatic and deformational events. The various elements that play a role in the Solomon Islands' tectonic history have also led to the development of some unusual features, including opposing subduction zones, obducted oceanic plateau (Malaita), arc picrites (New Georgia Province), anomalously short arc-trench gaps (Kavachi Volcano is only 30 km from the trench), and volcanism on an actively subducting plate (Simbo volcano).

Savo volcano, in the central Solomon Islands, is relatively poorly understood in terms of its relationship to other features in the arc. The edifice is constructed upon unknown basement; it is unclear whether magmatism is related to the northern or southern subduction zones; and the influence of the young, hot slab to the south on melt generation and composition is unconstrained.

Regional scale tectonic processes have led to the development of magmatic and volcanic-related mineral deposits across the southwest Pacific (Fig. 2.1). To the west, Papua New

Guinea boasts world class epithermal gold deposits at Porgera (11 Moz Au reserves; Richards and Kerrich, 1993) and Ladolam (37.1 Moz contained Au; Carman, 2003), and copper–gold porphyry mineralisation at Panguna. East of the Solomon Islands, Fiji has world class gold-telluride mineralisation at Emperor (11 Moz Au; Ahmad et al., 1987; Pals and Spry, 2003). The relationships between geodynamic setting, melt generation and composition, are major factors in the development of mineralisation in these locations (Richards et al., 1990; Eaton and Setterfield, 1993; White et al., 1995; McInnes et al., 2001; Sillitoe and Hedenquist, 2003), and the similarities of tectonic setting suggest that the Solomon Islands may also have the potential for significant volcanic-related mineral deposits. Gold and copper mineralisation has been discovered at Gold Ridge (Tolia and Petterson, 2005) and Koloula (Chivas, 1978) on Guadalcanal (Fig. 2.2); further mineral deposits may yet be found elsewhere in the Solomons.

This chapter provides a review of the geology and tectonic setting of the southwest Pacific, the Solomon Islands and Savo volcano, with particular reference to the role that tectonic processes play in magma genesis, geochemistry and mineralisation.

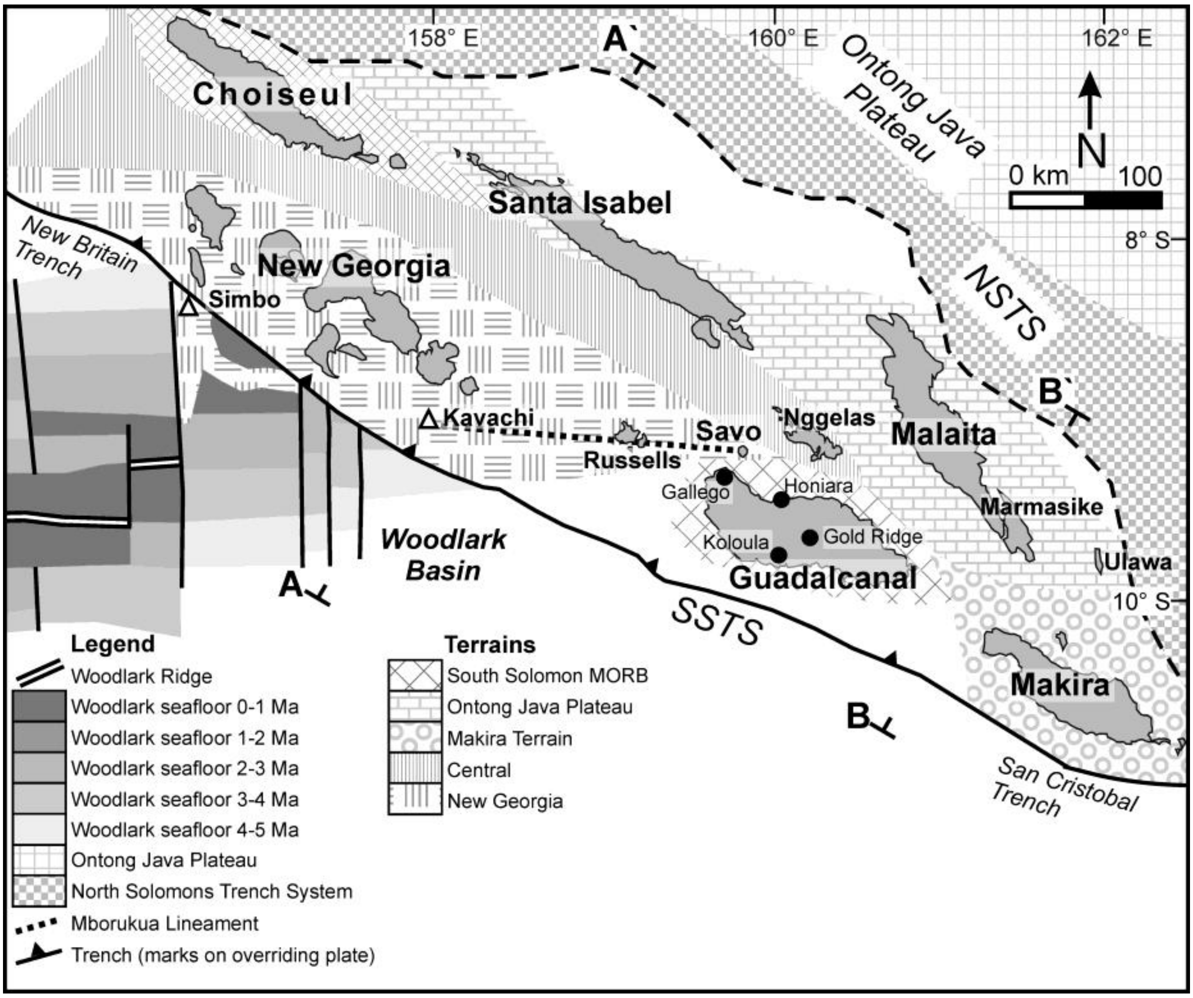

Fig. 2.2: Map of the Solomon Islands showing major tectonic features and geological terrains of Petterson et al. (1999). Age of Woodlark Basin seafloor based on magnetic lineations from Taylor (1987). SSTS = South Solomon trench System. Lines A–A` and B–B` mark seismic lines of Fig. 2.4.

2.2 Regional geology and geological terrains

The Solomon Islands (Fig. 2.2) are the exposed portion of an upstanding block, 1200 by 250 km, oriented northwest–southeast between 5° and 12° S, and 157° and 163° E. The Solomon block is bordered to the northeast by the Vitiaz or North Solomon Trench System (NSTS) and to the southwest by the New Britain–San Cristobal Trench (or South Solomon Trench System, SSTS). The subaerial highs of the Solomon block form a linear double chain of islands.

Coleman (1966) divided the islands into a series of “provinces”, each with distinct geological characteristics. Petterson et al. (1999) revised Coleman’s framework in light of geochemical, geophysical and geological data collected over the intervening decades by numerous workers. Petterson et al. (1999) used a series of geological “terrains” (*sensu lato*) to describe the Solomon Islands. These terrains are distinct from terranes (*sensu stricto*) in that whilst they are geologically distinct, they may not necessarily have unique histories or be separated by terrane-bounding faults. Distinction between terrains is largely based on the basement sequences and subsequent arc development (or lack thereof).

The geological history and major tectonic events are best discussed with reference to the geological terrains, which are discussed below, and summarised briefly on Table 2.1:

i) Ontong Java Plateau Terrain: The basement of the OJPT consists of Cretaceous basaltic lavas and sills, with a smaller volume of coarser-grained plutonic rocks (Petterson et al., 1999). The basement here is geochemically similar to the Ontong Java Plateau to the north (transitional between N-MORB and E-MORB trace element profiles), and shows $^{40}Ar/^{39}Ar$ ages around 122 Ma, with a smaller subset of dates at 90 Ma in the eastern part of the Plateau (Petterson et al., 1997; Tejada et al., 2002).

Post-basement sediments on Malaita, northeast Santa Isabel and Ulawa are of deep pelagic origin, interrupted by alkali basalts and intruded by alnöites during the Oligocene-Eocene (Petterson et al., 1999; Ishikawa et al., 2004). There is no evidence of later volcanic activity on these islands.

ii) The South Solomon MORB Terrain comprises the islands of Choiseul and Guadalcanal. The SSMT contains Cretaceous basalts that are chemically distinct from those of the OJP, with more typical N-MORB trace element profiles, and displays a more varied lithology (including lavas, limestone, chert, basaltic sills and dykes, gabbroic and ultrabasic bodies). The basement Mbirao Volcanics of Guadalcanal have yielded a poorly constrained K–Ar whole-rock age of 92 ± 20 Ma (Hackman, 1980). The basement of the SSMT has been affected by at least two subsequent periods of arc activity, and is overlain by arc-related sequences.

iii) Makira Terrain: The island of Makira is distinct from the other islands in terms of its basement, which is a composite of OJP-like basalt and an N-MORB that shows some signs of plume enrichment. These magma types are found in inter-leaved basaltic lavas. Unlike the OJPT, significant thicknesses of deep pelagic sediments are found between the lavas. $^{40}Ar/^{39}Ar$ plateau age determinations have yielded an age of 35.1 ± 1.1 Ma for one Makira MORB sample, and ages of 63.0 ± 0.5 Ma and 33.9 ± 0.7 Ma for two Makira plateau basalt samples; older ages have been determined but are unpublished (Petterson et al., 1999).

Post-basement arc sequences are seen on Makira, though no volcanic structures are preserved; Petterson et al. (1999) attributed this to increased erosion on Makira as a result of uplift on the fore-arc of the South Solomon Trench.

iv) Central Solomon Terrain: The basement of the CST is dominated by arc-derived material. Basement is basic to ultrabasic with a variety of magma series, including N-MORB, island arc basalt, back-arc basalt and alkali basalt. More evolved calc-alkaline andesites and dacites are present on all islands. The major arc-related activity in this terrain occurred between the Eocene and Early Miocene (Chivas, 1981; Pound, 1986; Petterson et al., 1999).

v) New Georgia Terrain: The NGT is dominated by sialic basement created in the most recent (ongoing) stage of arc activity. Included in this terrain are the New Georgia Group and submarine volcanoes south of New Georgia, Ghizo Ridge, Russell Islands, Kavachi and Savo.

The composition of the volcanic material in this terrain is highly varied. The Woodlark Basin contains silicic to intermediate, calc-alkaline features such as the Ghizo Ridge and Coleman Seamounts, tholeiitic basalt, and unusual Na–Ti rich basalt (Crook and Taylor, 1994). The New Georgia Group contains high-Mg picrite, calc-alkaline basalt, trachybasalt, andesite, dacite and rhyolite (Johnson et al., 1987).

	South Solomon MORB Terrain	**Ontong Java Plateau Terrain**	**Makira Terrain**	**Central Solomon Terrain**	**New Georgia Terrain**
Islands	*Guadalcanal and Choiseul*	*Malaita, North Isabel and Ulawa*	*Makira*	*Ngellas, South Isabel*	*New Georgia, Russell Islands, Savo*
Cretaceous	N-MORB basalt, ultramafic magmatism	Formation of Ontong Java Plateau. Deep sea pelagic sedimentation.	Contemporaneous plume and MORB basaltic magmatism with pelagic sedimentation.		
Paleocene / Eocene to Early Miocene	Stage 1 arc volcanism and related sedimentation	Pelagic and turbiditic sedimentation. Alkaline basalt and alnöitic magmatism.	Plume and MORB magmatism with pelagic sedimentation.	Basement formed by Stage 1 arc magmatism.	
Late Miocene to Recent	Stage 2 arc volcanism, plutonism and related sedimentation	Pelagic and shallow water sedimentation. Accretion to Solomon arc.	Development of Stage 2 arc on plume and MORB basement.	Variable development of Stage 2 arc	Formation of New Georgia Terrain by Stage 2 arc magmatism

Table 2.1: Summary of geological history and terrain development in the Solomon Islands (Petterson et al., 1999). Stage 1 arc activity is that related to the subduction of the Pacific Plate at the North Solomon Trench System; Stage 2 arc activity is that related to the subduction of the Indo-Australian Plate at the South Solomon Trench System.

2.3 Geological and tectonic history

2.3.1 Subduction of the Pacific Plate (Palaeocene to Miocene)

Subduction of the Pacific Plate at the North Solomon Trench began in the Palaeocene, resulting in the earliest stage of arc activity observed in the Solomons (Fig. 2.3). Earthquake hypocentres record the southwest dipping Pacific Plate beneath the Solomon Islands (Fig. 2.4; Cooper and Taylor, 1987). The oldest known arc-related rocks in the Solomons are those of the 62–46 Ma Jajao Igneous Suite on San Jorge, and consist of basaltic to andesitic pillows and lavas, and gabbros from an arc or back-arc setting (Tejada et al., 1996; Berly et al., 2006). Alkaline basalts and more evolved calc-alkaline suites formed the Central Solomon Terrain basement and were intruded into volcanic features on the “typical” seafloor crust of the South Solomon MORB Terrain (Petterson et al., 1999). The Guadalcanal Suta Volcanics and the Poha Diorite (24.4 Ma; Chivas, 1981) that intruded them are attributed to this stage of arc activity.

Subduction at the NSTS brought the Ontong Java Plateau into contact with the Solomon arc. The Ontong Java Plateau is a Cretaceous oceanic large igneous province covering an area approximately the size of Alaska, and with an average crustal thickness of 33 km. Inter-basaltic sheets of sediments are rare, indicating effusion was rapid and continuous (Tejada et al., 2002).

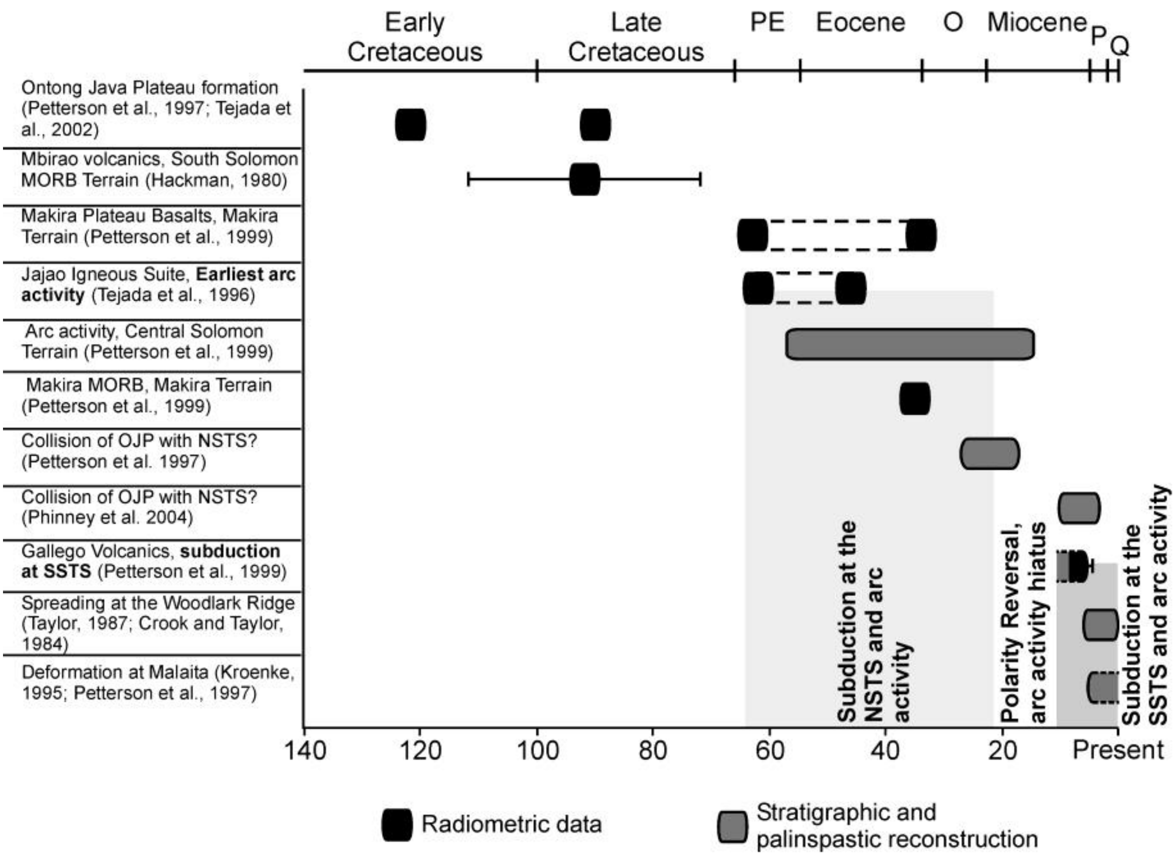

Fig. 2.3: Time–event diagram summarising the major tectonic events of the Solomon Islands, including major periods of terrain formation. PE = Palaeocene; O = Oligocene; P = Pliocene; Q = Quaternary.

The first contact of the OJP with the North Solomon Trench was speculated to be between 25 and 20 Ma, based on a hiatus of arc activity (Petterson et al., 1997). Early and mid-Miocene sequences from Malaita do not record major compressional deformation during their deposition – Petterson et al. (1997; 1999) therefore consider the initial contact of the OJP with Solomon arc to be a “soft docking” collision. Phinney et al. (2004) suggest a much more recent age for first collision (6 to 8 Ma) based on palinspastic modelling.

Much of Malaita (an OJPT-dominated island) has been deformed in a compressive regime with an element of transpression (Auzende et al., 1996; Petterson et al., 1997). Folding and faulting is commonplace, and Petterson et al. (1997) calculated local crustal shortening to be 23–46%. Much of the deformation (i.e. “hard docking”) seen on Malaita has occurred since 4 Ma (Kroenke, 1995; Petterson et al., 1997; Petterson et al., 1999).

The OJPT is thought to represent an obducted accretionary prism containing material derived from the Ontong Java Plateau (Auzende et al., 1996; Petterson et al., 1997; Birkhold et al., 1998; Tejada et al., 2002; Phinney et al., 2004), attached to the Solomon Block as the Pacific Plate was subducted south-westwards under the Australian Plate at the North Solomon Trench System.

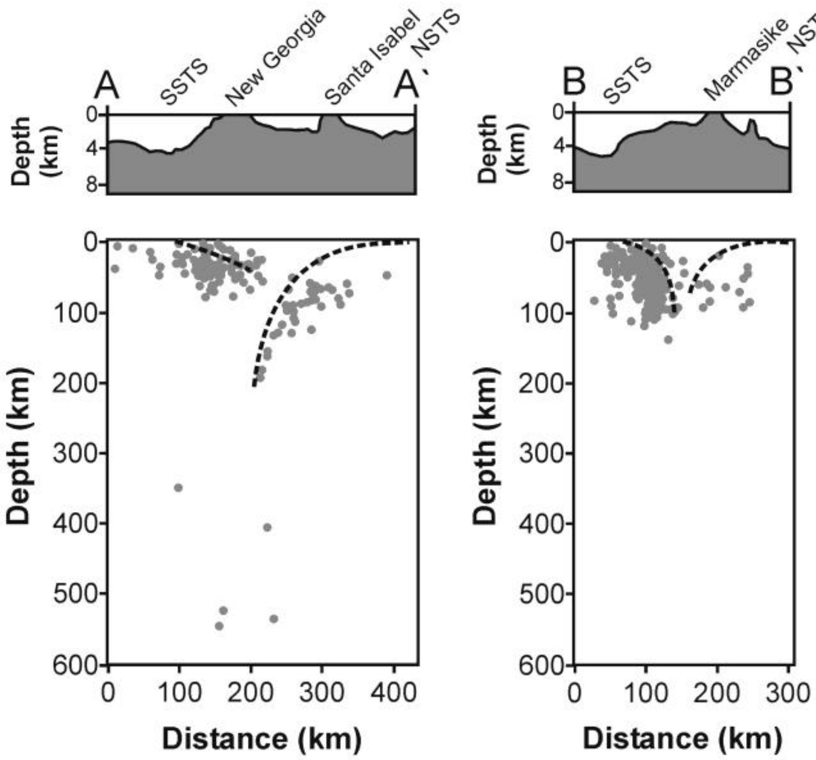

Fig. 2.4: Seismic profiles along lines A–A` and B–B` (Fig. 2.2) showing earthquake hypocentres (with body wave magnitude > 4.7, detected by 15 or more World Seismograph Station Network in the period 01/01/1964 to 06/30/1984) projected onto vertical planes. Dashed line shows inferred location of the top of the Wadati–Benioff Zones for the subducted slabs. Image reproduced from Cooper and Taylor (1987).

Eventually the thicker crust of the OJP "choked" the NSTS resulting in a polarity reversal of subduction and the initiation of the subduction of the Indo-Australian Plate at the SSTS (Cooper and Taylor, 1987; Petterson et al., 1999; Phinney et al., 2004). The timing of this event is unclear, but on the basis of major changes in arc activity, assumed to have occurred sometime before 6.4 ± 1.9 Ma (Petterson et al., 1999). Seismicity, submarine mapping and structural dating have shown that intermittent subduction along the North Solomon Trench still occurs (Cooper and Taylor, 1987; Kroenke, 1995; Auzende et al., 1996).

2.3.2 Subduction of the Indo-Australian Plate (Miocene to Present)

The Indo-Australian Plate began subducting beneath the Solomon block at the SSTS, and was accompanied by a second major stage of arc activity that initiated sometime before 6.4 ± 1.9 Ma (based on K–Ar dating of samples from the Gallego Volcanic Field, Guadalcanal; Petterson and Biliki, 1994; Petterson et al., 1999). The New Georgia Terrain is dominated by Miocene to Recent volcanic activity, and contains the only two historically active volcanoes in the Solomon arc (the other being Kavachi). Most of the islands in the arc show evidence for activity during the second major period of subduction (Petterson et al., 1999).

The reversal in subduction polarity resulted in what were previously back-arc environments being subjected to fore-arc uplift and activity (e.g. Makira, Guadalcanal). Uplift in the central Solomon Islands has been locally accelerated by the subduction (or impingement onto the trench) of significant seafloor features in the Woodlark Basin, e.g. the Coleman Seamount (Mann et al., 1998).

The second stage of arc activity has continued to the present day. Earthquake hypocentres (Fig. 2.4) show the Australian Plate beneath the Solomon Islands dips vertically to 200 km in the western region of the arc (New Britain Trench) and vertically to 100 km in the eastern end of the arc (San Cristobal Trench). However, in the central Solomon Islands seismicity is low magnitude, shallow and diffuse (Cooper and Taylor, 1987). The poor definition of the slab in seismic studies is thought to be a result of the relative warmth of the young lithosphere of the Woodlark Basin compared to the older, colder lithosphere to the east and west (Cooper and Taylor, 1987; Mann et al., 1998).

2.3.2.1 Subduction of the Woodlark Basin

The subduction of the Woodlark Basin is considered to be a major influence on structure and magmatism in the Solomon Islands (Cooper and Taylor, 1987; Johnson et al., 1987; Taylor and Exon, 1987). Spreading at the Woodlark Ridge began before 5 Ma (based on magnetic lineations; Taylor, 1987) and ceased approximately 0.5 Ma (Crook and Taylor, 1994). One of the Woodlark Ridge transform faults intersects the SSTS to produce a trench -trench-transform triple junction east of Simbo Island (Crook and Taylor, 1994). The combined divergence and subduction of the Woodlark Ridge is believed to have led to the formation of “windows” in the Indo-Australian slab beneath the arc (Johnson et al., 1987; Perfit et al., 1987; Taylor, 1987; Taylor and Exon, 1987). Divergence at the surface leads to the development of new oceanic crust at the ridge; when the slab is subducted, the temperature of the mantle may be close to the solidus and thus gaps or windows can develop (Thorkelson, 1996).

The development of slab windows is believed to be responsible for fore-arc magmatism at Kavachi (Johnson et al., 1987); tholeiitic basalts and basaltic andesite with typical island arc trace element affinities are erupted less than 30 km from the convergence of the Indo-Australian Plate and Solomon Block. Fore-arc volcanism has been related to ridge subduction and slab window formation in Japan, California and Chile, for example

(Thorkelson, 1996; and references therein). Melts are generated by decompression of asthenospheric material as it upwells through the slab window (Marshak and Karig, 1977), a process referred to as the “blow-torch effect” by DeLong et al. (1979).

Picrites in New Georgia may also be related to ridge subduction and slab window development (Johnson et al., 1987; Perfit et al., 1987). Recent studies suggest that the New Georgia picrites are the result of an initially picritic–basaltic melt (14 wt% MgO) mixing with mantle wedge peridotite to generate the high MgO contents observed (up to 30 wt%; Schuth et al., 2004; Rohrbach et al., 2005). Additional heat provided by the spreading centre and/or slab windows leads to unusually high degrees of melting and possibly a collapse of the peridotite matrix (Rohrbach et al., 2003; Schuth et al., 2004).

Partial melting of the downgoing slab in areas of ridge subduction has been suggested to be significant for the generation of melts, particularly those with adakitic affinities, and adakitic rocks have been identified in the Solomon Islands (Schuth et al., 2006). In areas where the spreading ridge is < 5 Ma, the slab may be sufficiently hot to melt (Defant and Drummond, 1990; Peacock et al., 1994); slab melting may also occur at the edges of slab windows by thermal erosion, as hot asthenospheric mantle upwells through the window (Rogers et al., 1985; Johnston and Thorkelson, 1997; Yogodzinski et al., 2001; Breitsprecher et al., 2003; Thorkelson and Breitsprecher, 2005). This partial melting produces magmatic rocks characterised by ≥ 56% SiO_2, Al_2O_3 ≥ 15%, MgO < 3%, La/Yb > 8, low Y and HREE relative to island arc ADRs (andesites, dacites and rhyolites), high Sr relative to island arc ADRs and $^{87}Sr/^{86}Sr$ < 0.7040 (Defant and Drummond, 1990; Castillo, 2006 and references therein), with high Sr reflecting plagioclase melting, and HREE depletions a result of residual garnet at source. However, the significance of these geochemical characteristics has been challenged, as they are non-unique, and can be generated by other petrogenetic processes (Garrison and Davidson, 2003; Castillo, 2006; Richards and Kerrich, 2007), including partial melting of lower crust garnet amphibolite (Yumul et al., 2000; Conrey et al., 2001; Chung et al., 2003; Saleeby et al., 2003; Hou et al., 2004; Wang et al., 2005), the interaction of asthenospheric melts with crustal (in particular lower crustal) material (Feeley and Hacker, 1995; Streck et al., 2007), and by extensive differentiation of a parental basaltic melt (Castillo et al., 1999; Dreher et al., 2005; Macpherson et al., 2006; Rodriguez et al., 2007). In light of these alternative processes, the importance of slab melting to adakite genesis, and to arc magmatism as a whole, is questionable (Richards and Kerrich, 2007), and the role of slab melting in the Solomons should be considered critically.

Various authors have recognised a relationship between copper–gold mineralisation and the occurrence of adakites (Thieblemont et al., 1997; Sajona and Maury, 1998; Oyarzun et al., 2001). Mungall (2002) suggested that slab melts are capable of oxidising mantle sulphides (due to higher Fe^{3+} contents compared to aqueous fluids), and releasing copper and gold into the ascending magmas. However, this body of work has been subject to criticism, not least because of the non-unique geochemical characteristics of adakites, and the potential for their formation by non-slab melting processes (Rabbia et al., 2002; Richards, 2002; Macpherson et al., 2006; Richards and Kerrich, 2007). The role of slab melting in island arc magmatism is an important consideration for any discussion of both magmatism and mineralisation.

Dredges in the vicinity of Simbo Ridge, in the Woodlark Basin, have recovered Na–Ti rich basalt. Unlike the majority of the basaltic material recovered from the basin, these samples do not show unequivocal arc signatures. In contrast with the "typical" Woodlark basalt, the NaTi basalts do not have high LFS and low HFS element contents; some LFS elements are relatively enriched (Sr) and others depleted (Ba, K) and Zr is high. Perfit et al. (1987) suggested that the NaTi basalts were generated from a MORB source highly depleted in highly incompatible elements (Ba, K), then later melted to a very small extent, resulting in basalts strongly enriched in moderately incompatible elements (Na, Sr). The significance of the tectonic setting of the Solomon Islands to the generation of NaTi basalts is unclear; and the potential role that the basalts or their mantle source might play in generating arc magmas is unknown.

2.3.2.2. The influence of the Pacific slab

Seismic profiles suggest that the Pacific slab still underlies the arc (Fig. 2.4), and may be responsible for the near vertical dip of the Indo-Australian slab (Cooper and Taylor, 1987). Coleman and Kroenke (1981) suggested that to the east of Savo, the cold, refractory and thick crust of the OJP abuts directly onto the Indo-Australian slab, limiting magma generation and resulting in no recent volcanism in that part of the arc. However, west of Savo, the relict Pacific slab is believed to play an important role in melt generation. König et al. (2007) identified Pacific slab melt contributions to magmas at Simbo volcano (on the Indo-Australian Plate) on the basis of lead isotopes. König et al. (2007) speculated that slab melting of the relict slab could occur at fractured edges of the slab exposed by thermal erosion, or due to the higher mantle geotherms in the vicinity of the triple junction.

Metasomatism of mantle peridotite by fluids derived from the Pacific slab was responsible for the generation of pyroxenites from San Jorge and Santa Isabel (Berly et al., 2006). McInnes et al. (2001) suggested that metasomatic additions to the mantle wedge are responsible for the oxidised, sulphur- and alkali-rich volcanics of Lihir (New Ireland, Papua New Guinea), host to the Ladolam alkaline-related epithermal Au deposit (Müller et al., 2001). The Pacific slab may play an important role in metallogenesis in the Solomon Islands, without directly generating magmas; metasomatism of the mantle may prime it for later extraction of Cu, and Au fertile melts.

Rocks recovered in dredges the from Woodlark Basin also show the effects of fluids from the Pacific slab. Rather than displaying N-MORB trace element characteristics, these rocks are typically enriched in the low field strength elements (Sr, Ba, etc.) a feature more typical of arc rocks (Perfit et al., 1987). The Woodlark Ridge is for the most part orthogonal to the North Solomon Trench System, and it seems improbable that the Woodlark Basin is a former back-arc spreading centre related to the subduction of the Pacific Plate. There is no evidence for the slab underlying the Woodlark Basin in any location (Cooper and Taylor, 1987; Johnson et al., 1987; Perfit et al., 1987), other than perhaps Simbo, which suggests that fluids from the Pacific slab carrying LFS elements enrich the mantle over a large "footprint", rather than immediately above the slab.

Lead isotope studies by Schuth et al. (2006; 2007) have identified minor Pacific slab contributions in a number of locations along the arc. The Pacific Pb isotope signature is interpreted to be a result of fluid (and/or sediment) flux from the slab, rather than melt contributions (c.f. Simbo), as Hf and Nd isotope systematics suggest an Indo-Australian origin in most cases. The mantle domain beneath the Solomon arc is Indo-Australian (König et al., 2007; Schuth et al., 2007), despite the SSTS marking the current Indo-Australian~Pacific boundary, as prior to the initiation of the SSTS, the NSTS was the boundary zone, and presumably the boundary of the mantle domains.

2.4 The geology of Savo

Savo volcano is 35 km northwest of Honiara, the Solomon Islands capital, and is considered to be at the easternmost limit of the New Georgia Terrain (Petterson et al., 1999). The volcano has a basal diameter of 9 km and a height of approximately 1400 m. The upper portion of the volcano is above sea level – Savo Island is approximately 7 km long (N–S) by 6 km wide (E–W), with a high point of 485 m (Fig. 2.5).

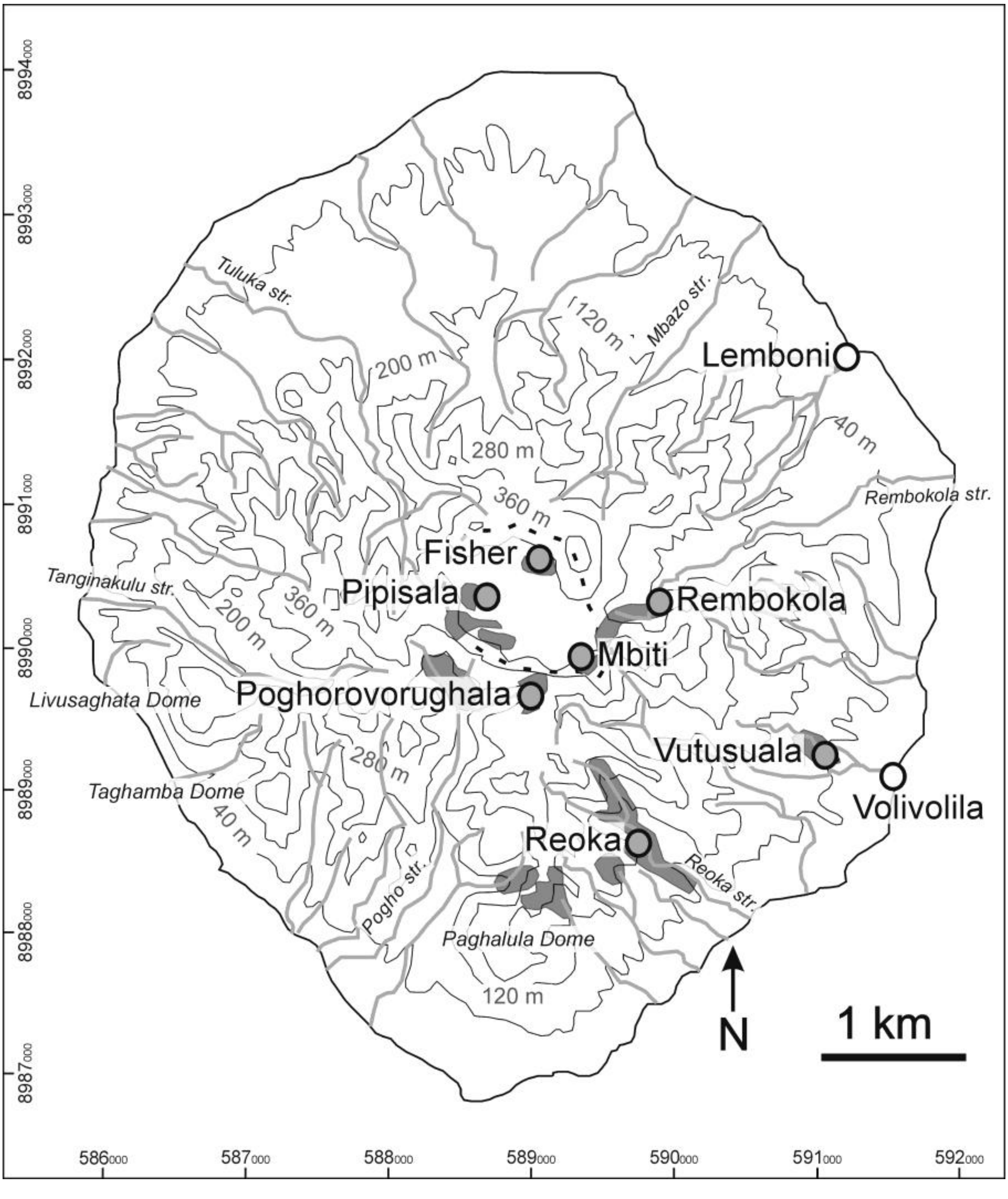

Fig. 2.5: Map of Savo Island showing location of major thermal areas (shaded), hot spring sampling sites (filled circles) and well sampling sites (open circles). Also shows names of major streams and domes. Grid references for UTM zone 57L.

The centre of the island is marked by a 1.5 km wide, approximately 80 m deep crater. At least two heavily vegetated, small crypto- or lava domes are visible in the central crater, along with a number of steeper domes in the south and southwest of the island (Paghalula, Taghamba, and Livusughata). The coastal areas and the north of the island are relatively flat and low lying in comparison with the central and southwest of the island.

Fig. 2.6: Photograph of the Paghalula Dome from the northeast.

Streams drain from the outer crater wall in a radial pattern, dissecting the island into a series of steep-sided gorges and valleys. A number of stream channels are seasonal or only flow during high rainfall. Major streams in the south and east of the island (Poghorovorughala, Reoka, Vutusuala, Rembokola, Mbazo, and Tanginakulu) are fed by hot springs located inland.

With the exception of the steep domes in the southwest of the island, pyroclastic and reworked pyroclastic deposits are ubiquitous on the island, and include block and ash flow (BAF), debris flow, tephra fall, lahar, and surge deposits. Coherent lavas (and/or intrusive bodies) are limited to the domes in the crater and southwest (Fig. 2.6) and discontinuous, heavily weathered exposures in valleys.

Primary, unaltered magmatic rocks at Savo are dominantly sodic trachytes, with lesser amounts of sodic trachyandesite (benmoreite), basaltic trachyandesite (mugearite), trachybasalt (hawaiite) and basalt. The most mafic compositions commonly occur as enclaves within more felsic rocks. Typical mineralogies are feldspar + amphibole +

Fig. 2.7: Selection of typical trachyte and trachyandesite (benmoreite) samples from Savo, containing ultramafic enclaves/ autoliths (amphibolites and clinopyroxenites).

magnetite ± biotite for trachytes; and feldspar + clinopyroxene + magnetite ± olivine for basaltic compositions.

As well as the mafic enclaves, autoliths and xenoliths are abundant in erupted blocks and domes. Autoliths and xenoliths include amphibolites, clinopyroxenites, amphibole + plagioclase, clinopyroxene + plagioclase, glimmerite. (Fig. 2.7; discussed in detail in Chapter 3).

2.4.1 Eruptive History, Stratigraphy and Eruptive Style

Savo is one of only three volcanoes in the Solomon Islands with known historical eruptions (the others being submarine volcano Kavachi, and Tinakula in the east, considered to be part of the Vanuatu arc in geological terms). The earliest recorded eruptive activity was in 1568, when the Spanish explorer Mendaña recorded "smoke" from the crater and "white roads" running from the central crater to the northern coast (Amherst et al., 1901; Petterson et al., 2003). Oral histories of eruptions in the 1830s to mid-1840s were recorded by the visiting Bishop Aubin in 1906 (Grover, 1958). Descriptions of historical eruptions are consistent with Merapi-type events, in which pyroclastic density currents are derived from the gravitational collapse and mass wasting events from a largely degassed dome (Grover, 1958; Rose et al., 1976; Wright et al., 1980; Petterson et al., 2003).

The volcaniclastic deposits at Savo can be subdivided and described as a number of separate lithofacies. Lithofacies are distinguished on the basis of field observation, and are described below briefly, with respect to their interpreted origin.

Block and ash flow deposits are typically massive, very poorly sorted and poorly consolidated deposits with blocks and lithics of variable size (from centimetres to metres diameter) supported in a lapilli–ash matrix (typically fine sand to gravel equivalent; Fig. 2.8). The largest clasts are typically found at the top of the unit, but otherwise no internal grading is observed. Aligned natural remnant magnetism of blocks can be identified in some locations with a portable fluxgate magnetometer, indicating juvenile origin (records in-situ cooling of clasts from >350°C; Petterson et al. 2003), but for the most part, entrained lithics and juvenile blocks are indistinguishable due to the limited sediment sources on Savo (i.e. all available material is derived from volcanic eruptions). Most blocks are angular, subrounded, dense and poorly- to non-vesiculated, crystal rich sodic trachyte, with lesser amounts of basaltic and ultramafic (xenolith/autolith) material. BAF deposits are laterally discontinuous and cannot generally be correlated between adjacent valleys, suggesting that the flows were topographically confined.

Fig. 2.8: Photograph of contact between two poorly sorted block and ash flow deposits, from the coastal section north of Lemboni. Note hammer for scale.

Tephra /ashfall deposits and surges are common in the crater wall and on interfluvial high ground towards the coast. Fall deposits are very well sorted ash (silt to sand equivalent), with occasional accretionary lapilli (up to 0.5 cm diameter) and charcoal fragments. Soil horizons overprint ash fall deposit layers at the interfluve exposures. Surge deposits are most common in the crater wall exposures, associated with and within fall deposits, and occur as laterally discontinuous lenses, often only a few centimetres thick, of poorly sorted ash and lapilli (silt to coarse sand equivalent) with weak cross bedding.

Lahar deposits are very poorly sorted, matrix supported deposits. They are polymict, with larger subangular to subrounded clasts consisting predominantly of trachyte, along with basalt, ultramafic (xenolith/autolith) and hydrothermally altered material. The matrix is typically poorly sorted silt to gravel. Lahar deposits may be massive or irregularly bedded, and may or may not display sorting, horizontal fabrics, cross bedding and clast trains. Lahar deposits occur from the outside of the crater wall to the coast, but are more common in the major drainage areas towards the coast. They represent primary deposits reworked in largely grain-supported flows minutes to decades after eruptions. Major lahar events were reported as recently as 1953 (Petterson et al., 2003).

Hyperconcentrated debris flow deposits are very poorly to poorly sorted, matrix supported deposits. They are polymict, with similar clast populations to lahar deposits. The matrix varies from silt to gravel grade. Diffuse bedding is common. Cross bedding occurs, and channel structures and lensoid beds are frequently observed. These deposits are more common towards the coast in the major drainage systems. They represent the reworking of unconsolidated and poorly consolidated sediments in water-supported flows.

The predominance of dense, poorly vesiculated, crystal-rich material in the juvenile material of the BAF deposits and reworked equivalents, as well as topographic confinement of those deposits, is consistent with Merapi-type eruptions (Wright et al., 1980; Miyabuchi, 1999; Petterson et al., 2003). Crater morphology and in particular, low points in the crater wall, affect how ground-hugging density currents are distributed around the island.

Phreatomagmatic events may have accompanied dome collapse at Savo; oral histories report explosions during eruptive events, and major changes to the distribution and nature of hydrothermal features prior to eruption (Grover, 1958; Petterson et al., 2003). The dome in the centre of the crater at present day is much lower than the crater wall (by 50–90 m), is interpreted to have a pristine morphology and not represent the remnants of a larger, collapsed structure, leading Petterson et al. (2003) to suggest that the most recent recorded activity (1830s–1840s) was dominantly explosive in nature; explosions were generated either by phreatomagmatic activity or perhaps by Pelean-style eruptive activity (i.e. explosions driven by gas overpressures within the dome; Fisher and Heiken, 1982; Sparks, 1997; Ui et al., 1999). However, the vesiculated pyroclasts that would be expected from such an explosive event are rarely found on Savo.

2.4.2 Geodynamic Setting

The geodynamic setting of Savo is poorly constrained. Although the consensus is that Savo is related to subduction of the Indo-Australian Plate at the South Solomon Trench System (Stanton, 1994; Petterson et al., 1999; Petterson et al., 2003), the influence of the Pacific Plate on the location of the volcano and magma genesis cannot be ruled out (Cooper and Taylor, 1987).

Petterson et al. (1999) considered Savo to be part of the New Georgia Terrain – the volcano is recently active, constructed above an unknown basement, similar to the volcanoes of the New Georgia Group – and thus related to the subduction of the Indo-Australian Plate at the South Solomon Trench System (Petterson et al., 2003). The age of the volcanic edifice at Savo is unknown. The lava domes in the southwest of the island are considered to be the oldest exposed features on the island, but are too young for K–Ar dating (i.e. < 100,000 years old; Petterson et al. 2003).

The subduction of the Woodlark Ridge system may also be an important influence on the magma genesis and location of Savo as in the western Solomon Islands (Johnson et al., 1987; Perfit et al., 1987). The subduction of fracture zones in other arc systems such as the New Hebrides (Vanuatu) and Aleutian arcs is suggested to be responsible for the generation of sodic alkaline magmas that are relatively unusual in arc environments (DeLong et al., 1975; Pearce, 1982). The presence of highly sodic rocks in the Woodlark Basin – the NaTi basalts discussed in section 2.3.2 – is interesting, and may point to a melt source region with unusually high Na/K beneath the Woodlark Basin, and following subduction, beneath the western and central Solomon Islands.

Savo is the easternmost member of the “Mborukua Lineament” a line of Quaternary volcanoes that includes Kavachi, Mborukua and the Russell Islands, and is approximately parallel to the trends of the Woodlark Ridge south of the SSTS (Fig. 2.2). Recent bathymetric studies have identified at least one (inactive) submarine volcano on this lineament (Cowley et al., 2004). The relevance of this feature has been questioned (Johnson et al., 1987) as there are no other identified bathymetric features on the line, and the Quaternary Gallego Volcanic Field on northwest Guadalcanal is not considered part of the trend.

Petterson et al. (2003) considered Savo to be a modern extension of the older Gallego Volcanic Field (GVF) of northwest Guadalcanal (Fig. 2.2), on the basis of similar geochemical and petrological features (Stanton, 1994) and that Savo is situated along a north-northeast trending lineament system that appears to have been a major structural control on the location of volcanic centres in the Gallego Volcanic Field (Hackman, 1980; Petterson and Biliki, 1994).

2.5 Conclusions

The Solomon Islands record the complex history of the interplay between the Pacific and Indo-Australian Plates. The oldest exposed rocks in the Solomons arc represent pre-subduction Cretaceous ocean floor, with arc activity and island uplift commencing in the Palaeocene as the Pacific Plate began to subduct at the North Solomon Trench System. In the Miocene the thickened crust of the Ontong Java Plateau blocked this trench, and subduction commenced at the South Solomon Trench System, resulting in a second distinct stage of arc magmatism (Fig. 2.3).

In the present day, the two subduction zones and the motions of the two plates still play a crucial role in the structure, magmatism, seismicity and morphology of the arc. In particular, the young, hot crust of the Woodlark Basin at the southern trench is considered to be an important control on magma genesis in the Western and Central Solomon Islands. Most authors consider Savo to be the easternmost extension of the Indo-Australian controlled volcanism within the Solomon arc. The nature of the subducted slab beneath Savo is unknown; it may have formed “windows” as beneath New Georgia, with the melting of the mantle wedge driven by hot mantle material upwelling through those windows. Although Savo is presumed to be related to the active subduction at the SSTS, fluid flux from the intermittently subducting Pacific slab may be responsible for adding mobile elements and lowering solidus temperatures in the overlying mantle wedge, in the region beneath Savo.

Magmatism at Savo has resulted in a number of historical eruptions, typically of Merapi-type (mass wasting from a largely degassed dome). Erupted compositions are dominantly sodic trachytes, with the unusual chemistry perhaps a result of its ambiguous and complex geodynamic setting.

The igneous petrogenesis of Savo Volcano 3

Abstract

Savo, Solomon Islands, is a historically active volcano dominated by sodic, alkaline lavas and pyroclastic rocks with up to 7.5 wt % Na_2O. The suite at Savo is divided into mugearites (plagioclase–clinopyroxene–magnetite ± amphibole ± olivine) and trachytes (sodic plagioclase–amphibole–magnetite ± biotite). Whole rock and mineral chemistry, and studies of abundant xenoliths within the lavas, indicate that amphibole played an important role during fractionation suggesting high magmatic water contents (>3.5 wt %). It is proposed that the hydrous, alkali-rich magmas were derived from partial melting of metasomatised mantle. Radiogenic isotope data indicate an Indo-Australian mantle domain beneath Savo, but cannot discriminate the origin of metasomatic agents.

3.1 Introduction

The Solomon Islands have been subject to a complex subduction history, involving the collision of an oceanic large igneous province (the Ontong Java Plateau; Petterson et al., 1997; Hughes, 2004), initiation of a second subduction zone (Petterson et al., 1999), and the subduction of a young oceanic spreading ridge and resulting slab window formation (Johnson et al., 1987; Taylor and Exon, 1987). The tectonic processes at the Solomons arc generated magmas atypical of island arcs, including picrites (Staudigel et al., 1987; Schuth et al., 2004), high magnesisan andesites and adakites (König et al., 2007), and alkaline magmas (DeLong et al., 1975).

Savo, in the central Solomon Islands, is one of only three historically active volcanoes in the country (along with Kavachi in the west, and Tinakula in the east). The role that the various tectonic elements and events have played in magma genesis at Savo remains unclear. Previous studies at Savo have provided brief summaries of chemistry and petrology (Petterson et al., 2003), or larger datasets in the context of arc-wide studies, with little specific attention focussed on Savo (Stanton, 1994). The unaltered magmatic rocks at Savo display a number of unusual characteristics, including high sodium contents (up to 7.5 wt % Na_2O), increasing Sr with fractionation, and abundant ultramafic nodules.

Savo occupies a relatively ambiguous tectonic position, approximately equidistant from the two opposing subduction zones that define the arc (Figs. 2.2 and 2.4). Previous authors have related the magmatism at Savo to the subduction zone to the south (Petterson et al., 2003) but a relationship to the northern subduction zone has not been ruled out (Cooper and Taylor, 1987). In light of recent studies at Simbo volcano (König et al., 2007), there is scope for interaction between *both* subduction zones in magmatic processes in the Solomon Islands; a critical assessment of petrogenesis Savo is therefore an important contribution to the understanding of tectonic and large-scale chemical processes in the Solomon Islands in particular, and in the southwest Pacific in general.

3.2 Sampling and analytical methods

Due to intense tropical weathering, in-situ outcrops were rarely suitable for any analytical work. Fresh samples were collected from volcaniclastic deposits, stream-cut exposures, beaches and wherever possible from exposed coherent lavas (Fig. 3.1). A number of samples were nodules (enclaves, autoliths, xenoliths or cumulates) within a larger body of host rock, and some of the samples collected as individual blocks (particularly the most mafic) may represent nodules separated from the host rock during transport.

3.2.1 X-ray fluorescence

Weathered surfaces were removed from samples by splitter or rock saw prior to crushing. Samples for XRF analysis were crushed to coarse chips using a hardened steel press and powdered using an agate planetary mill at the University of Leicester. Loss on ignition was determined from powders dried overnight at 105°C, then ignited at 950°C for 1 hour.

Samples SV1–65 were analysed with a Philips PW1400 X-ray fluorescence spectrometer at the University of Leicester. All major element determinations were carried out on fused glass discs prepared from ignited sample powders with an 80% lithium metaborate–20% tetraborate flux. Analytical conditions were optimised to avoid significant line overlaps. Samples were ratioed against monitor samples to minimise the effect of any drift. Count data were processed using a de Jongh (1973) based model. Trace elements were determined on pressed powder pellets (prepared with Moviol 88 binding agent) using analytical conditions optimised to balance sensitivity and stability. Elements with characteristic X-rays at wavelengths higher than Fe-K absorption edge were corrected following the method of Reynolds (1967), and elements with characteristic X-rays between Fe-K and Ca-K absorption edges were corrected with the method of Nesbitt et al. (1976).

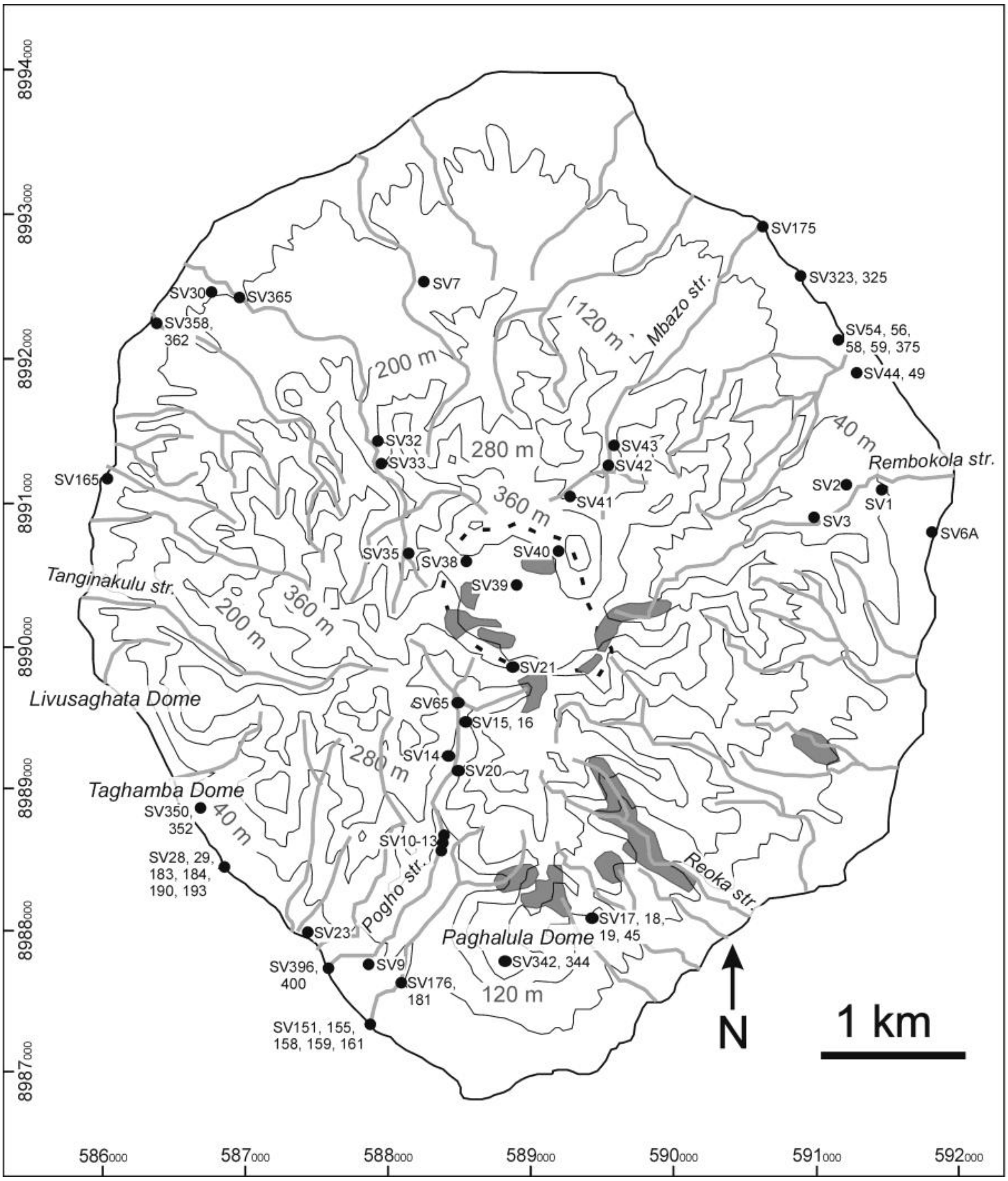

Fig. 3.1: Map of Savo Island showing sample locations. Shaded areas mark major hydrothermal zones (hot springs, fumaroles and steaming ground). Volcanic domes in the south of the island are named. Grid references are for UTM zone 57L.

Samples SV151–400 were analysed with a PANalytical PW4400 Axios Advanced XRF spectrometer, operating under PANalytical SuperQ software, at the University of Leicester. Elements with X-ray energies between Fe-K and Ca-K absorption edges were corrected with mass absorption coefficients calculated from the major element compositions (Thinh and Leroux, 1979).

A range of reference materials (RMs) were used to calibrate both instruments. The precision (1σ) of the major element data, across a range of compositions, was estimated to be <3% for SiO_2, Al_2O_3, Fe_2O_3, MgO, CaO and Na_2O; <7% for TiO_2 and MnO; <10% for K_2O and P_2O_5. For trace element concentrations above 10 ppm the precision was <15% for Ba; <10% for Ce, Co, Cr, Cu, Ni, Sc; and <5% for Ga, Rb, Sr, V, Zn, Zr. For trace element concentrations below 10 ppm, the precision was <1 ppm for Ga, Nb, Rb; <2 ppm for Co, Cu, La, Nd, Ni, Y; <4 ppm for Ba, Cr, Th, Zr. Measured values for RMs were within 1σ of accepted values (Govindaraju 1994; Jochum et al. 2005). There was no significant difference between results from the two spectrometers.

3.2.2 Rare earth element chemistry

Samples were crushed and milled as in section 3.2.1. A 0.2 g sub-sample was fused with sodium peroxide at 480°C for 1 hour. The fused material was leached with 20 ml deionised water, followed by 12.5 ml 50% HCl. All washings were retained in a 250 ml plastic volumetric flask to which 12.5 ml 50% HCl and 1 ml concentrated HF had been added. On making up to volume with deionised water, the final solution was in 5% HCl with a trace of HF, at a dilution of 1250.

All sample solutions were analysed at the British Geological Survey (Keyworth) with a VG PQ ExCell ICP-MS. Accuracy was estimated from analysis of certified RMs and was typically within 10% of the accepted values. Precision (1σ) was estimated to be <0.05 for Eu, Ho, Lu, Pr, Tb, Tm; <0.1 for Eu, Pr; <0.2 for Dy, Er, Sm, Yb; <1 Ce, Gd, La, Nd.

3.2.3 Electron probe micro-analysis

All data were collected using a JEOL 8600 Superprobe at the University of Leicester, using a wavelength dispersive system. A 30 nA current and 15 kV accelerating voltage were used for all analyses; a 10 μm beam was used for most analyses, with a 5 μm beam used for a small subset of amphibole analyses. A subset of feldspar analyses were analysed for SrO and BaO in addition to the major elements. Precision for electron probe analysis was determined from counting statistics, and is summarised in Table 3.1. Complete data tables of probe analyses can be found in Appendix I.

3.2.4 Strontium and neodymium isotopes

Samples were crushed and milled as in section 3.2.1. All further sample preparation and analysis was carried out at the NERC Isotope Geosciences Laboratory (NIGL). In order to determine whether any minor alteration had modified isotope values, a portion of each powder was leached in 6 M HCl for one hour; the resulting residues were run as "leached" samples and the supernatant liquid as "leachate". Samples were dissolved in Savillex

Mineral	Plagioclase			Plagioclase			Na Plagioclase			Na Plagioclase		
Analysis	04-002			04-013			04-022			04-102		
	Wt %	Error ± 2σ	Error %	Wt %	Error ± 2σ	Error %	Wt %	Error ± 2σ	Error %	Wt %	Error ± 2σ	Error %
SiO_2	61.04	0.27	0.436	58.34	0.26	0.443	64.97	0.28	0.426	66.63	0.29	0.421
Al_2O_3	24.28	0.12	0.483	25.91	0.13	0.477	21.71	0.11	0.493	19.98	0.11	0.501
FeO	0.11	0.05	42.6	0.07	0.05	67.4	0.18	0.05	27.43	0.22	0.06	23.9
CaO	5.94	0.11	1.716	7.73	0.12	1.506	2.96	0.08	2.456	1.34	0.06	3.842
Na_2O	7.96	0.14	1.707	6.80	0.13	1.832	9.42	0.15	1.59	10.02	0.16	1.551
K_2O	0.36	0.03	8.252	0.27	0.03	9.889	0.74	0.04	5.055	1.06	0.05	4.111
BaO	0.03	0.03	76.72	0.03	0.03	78.29	0.09	0.03	29.94	0.18	0.03	14.92
SrO	0.35	0.04	12.59	0.71	0.05	7.608	0.10	0.04	37.51	0.06	0.03	58.31

Table 3.1: Analytical error for electron probe microanalysis for different minerals A) feldspar only analyses (above); B) general analyses (right).

Mineral	Ca Plagioclase			Magnetite			Clinopyroxene		
Analysis	10-035			09-080			12-113		
	Wt %	Error ± 2σ	Error %	Wt %	Error ± 2σ	Error %	Wt %	Error ± 2σ	Error %
SiO_2	45.97	0.23	1	0.03	0.05	162	52.37	0.25	1
TiO_2	0.01	0.08	1400	4.77	0.12	2	0.36	0.08	20
Al_2O_3	33.97	0.22	1	1.02	0.06	5	2.66	0.06	2
Cr_2O_3	0.00	0.13	6488	0.10	0.06	53	0.15	0.07	41
FeO	0.18	0.06	30	84.98	0.75	1	5.10	0.17	3
MnO	0.01	0.05	391	1.36	0.11	7	0.07	0.06	78
MgO	0.00	0.01	9315	0.73	0.07	8	15.29	0.14	1
CaO	17.70	0.18	1	0.00	0.01	9512	23.38	0.21	1
Na_2O	1.24	0.06	5	0.00	0.01	9330	0.25	0.05	17
K_2O	0.00	0.03	1212	0.00	0.01	9132	0.00	0.01	9330
NiO	0.00	0.01	7976	0.06	0.07	105	0.00	0.01	8277

Mineral	Olivine			Amphibole			Biotite		
Analysis	12-125			08-122			11-027		
	Wt %	Error ± 2σ	Error %	Wt %	Error ± 2σ	Error %	Wt %	Error ± 2σ	Error %
SiO_2	39.88	0.22	1	42.39	0.23	1	37.28	0.21	1
TiO_2	0.00	0.08	1869	1.73	0.09	5	2.47	0.10	4
Al_2O_3	0.00	0.01	9733	12.67	0.13	1	14.20	0.13	
Cr_2O_3	0.00	0.01	6565	0.04	0.06	116	0.00	0.01	6935
FeO	18.15	0.32	2	11.66	0.25	2	14.16	0.28	2
MnO	0.29	0.07	21	0.19	0.06	30	0.39	0.07	16
MgO	41.86	0.25	1	14.11	0.14	1	15.83	0.15	1
CaO	0.06	0.04	61	11.48	0.14	1	0.04	0.04	93
Na_2O	0.04	0.04	97	2.92	0.10	3	0.86	0.06	7
K_2O	0.01	0.03	246	1.11	0.05	4	9.12	0.13	1
NiO	0.08	0.06	68	0.02	0.05	248	0.01	0.06	418

bombs using 2 ml 6 M Teflon Distilled (TD) HNO_3 and 10 ml Romil Supra-Pure HF at 105°C overnight. Samples were dried down on a hot plate. 2 ml TD HNO_3 was added and the dry-down was repeated. Dried samples were dissolved with 10 ml 6 M HCl and transferred to Savillex beakers. After another dry-down step 2 ml 2.5 M HCl was used to dissolve the samples and transfer to a centrifuge. Strontium fractions were prepared from centrifuged solutions with standard techniques using Dowex AG50W-X8 ion exchange resin (Royse et al., 1998). Samples were loaded onto single Re filaments using a TaO activator, and analysed using a Thermo-Finnigan Triton mass spectrometer in static multicollection mode. The blank at the time of analysis was 111 pg total Sr. Replicate analyses of the SRM987 standard solution gave an average value of 0.710263 ± 4 (1σ, *n*=50). Data are reported normalised to SRM987 = 0.710250.

Following collection of the Sr fraction the Nd fraction was separated and collected following procedures described in Royse et al. (1998). Separated samples were loaded onto single Ta filaments and analyses performed using a Thermo-Finnigan Triton mass spectrometer in static multicollection mode. The blank at the time of analysis was 132 pg total Nd. Replicate analyses of the J&M standard solution gave an average value of 0.511104 ± 0.000012 (2σ, *n*=50). Data are reported normalised to J&M standard solution = 0.511123.

3.2.5 Lead isotopes

Samples for Pb isotope analysis were coarsely crushed as in section 3.2.1. Samples were powdered in a tungsten carbide mill at the University of Leicester to avoid potential Pb contamination from galena veinlets within agate (Jochum et al., 1990). Samples were processed as described by Kempton and McGill (2002). Pb isotope ratios were determined at NIGL using a VG Axiom, MC-ICP-MS. Prior to analysis, each sample was centrifuged at 13000 rpm for 10 minutes and then spiked with a Tl solution. Samples were then introduced into the instrument via an ESI 50 µl/min PFA micro-concentric nebuliser attached to a Cetac Aridus desolvating unit. For each sample, five ratios were simultaneously measured ($^{206}Pb/^{204}Pb$, $^{207}Pb/^{204}Pb$, $^{208}Pb/^{204}Pb$, $^{207}Pb/^{206}Pb$, $^{208}Pb/^{206}Pb$).

The precision and accuracy of the method was assessed through repeat analysis of a NBS 981 standard solution spiked with Tl. Mass fractionation was corrected for using the isotopes of Tl as an internal monitor. All Pb isotope ratios have been corrected relative to the NBS 981 composition of Thirlwall (2002). Blanks at the time of analysis were 2 ng total Pb.

3.3 Results

Samples from Savo are divided into two groups: the *main suite* consists of crystal rich trachytes, mugearites and occasional benmoreites, defined on the basis of total alkalis vs. silica (Fig. 3.2); *nodules* commonly occur as inclusions within main suite samples.

Nodules include a wide variety of mineralogies, and occur in range of sizes, from 30 cm in diameter, to xenocrysts and micro-nodules identifiable only at thin section scale.

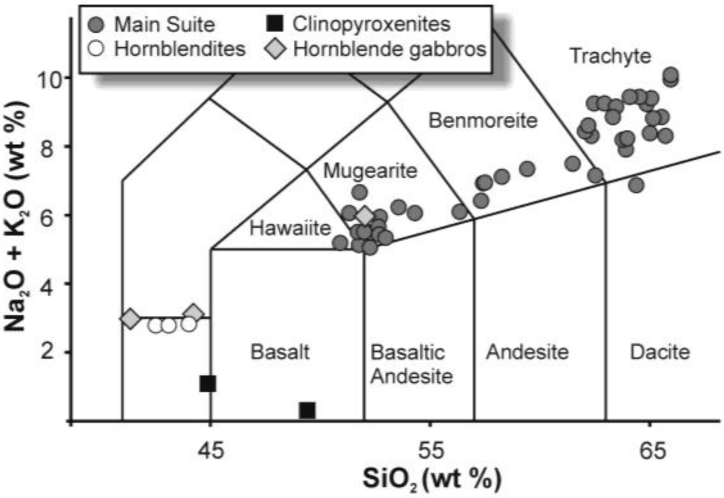

Fig. 3.2: Total alkalis vs. silica for samples from Savo (after Le Maitre et al., 1989). Samples recalculated to 100% on a volatile-free basis. Samples are sodic ($Na_2O-2>K_2O$) and contain less than 20% normative quartz, and are thus classified as a hawaiite – trachyte series.

3.3.1 Petrography and mineral chemistry – main suite

Samples in the main suite are typically crystal-rich (55–70% crystals by volume) and porphyritic with hyalopilitic groundmass (Fig. 3.3A), although a small number of the mafic (hawaiite and mugearite) samples collected from small exposures of lava flow deposits are entirely crystalline, with phenocrysts of clinopyroxene and olivine (0.5–3 mm) in a groundmass of plagioclase crystals (0.3–3 mm; Fig. 3.3C).

Plagioclase and magnetite occur in all samples. There is a progressive change in the mafic mineral assemblage with increasing whole rock SiO_2, from clinopyroxene mugearites to clinopyroxene–amphibole mugearites, amphibole benmoreites and finally amphibole–biotite trachytes (Fig. 3.4). Partially iddingsitised olivine is present in a small number of mugearite and hawaiite samples. Anhydrite was observed in one trachyte sample (SV40; Fig. 3.3E).

Plagioclase is ubiquitous throughout the suite, and constitutes 25–35% of the sample volume of mugearites, and 40–45% of benmoreites and trachytes (Fig. 3.4). Crystals are typically euhedral laths in thin section at <0.2 mm to over 10 mm in rare cases, but more typically 2–3 mm. A significant quantity of fragmented crystals may also be present. Normal zoning is common, with calcic cores and sodic rims (Fig. 3.3B; Fig. 3.5; Table 3.2). Mugearites analysed range from An_{85}–An_{50}, often within a single crystal; benmoreite plagioclase ranged from An_{80}–$An_{30.}$ Plagioclase within trachytes is commonly An_{40}–$An_{10,}$ although some crystals were An_{75}–An_{20}. The potassium contents of feldspars were low in

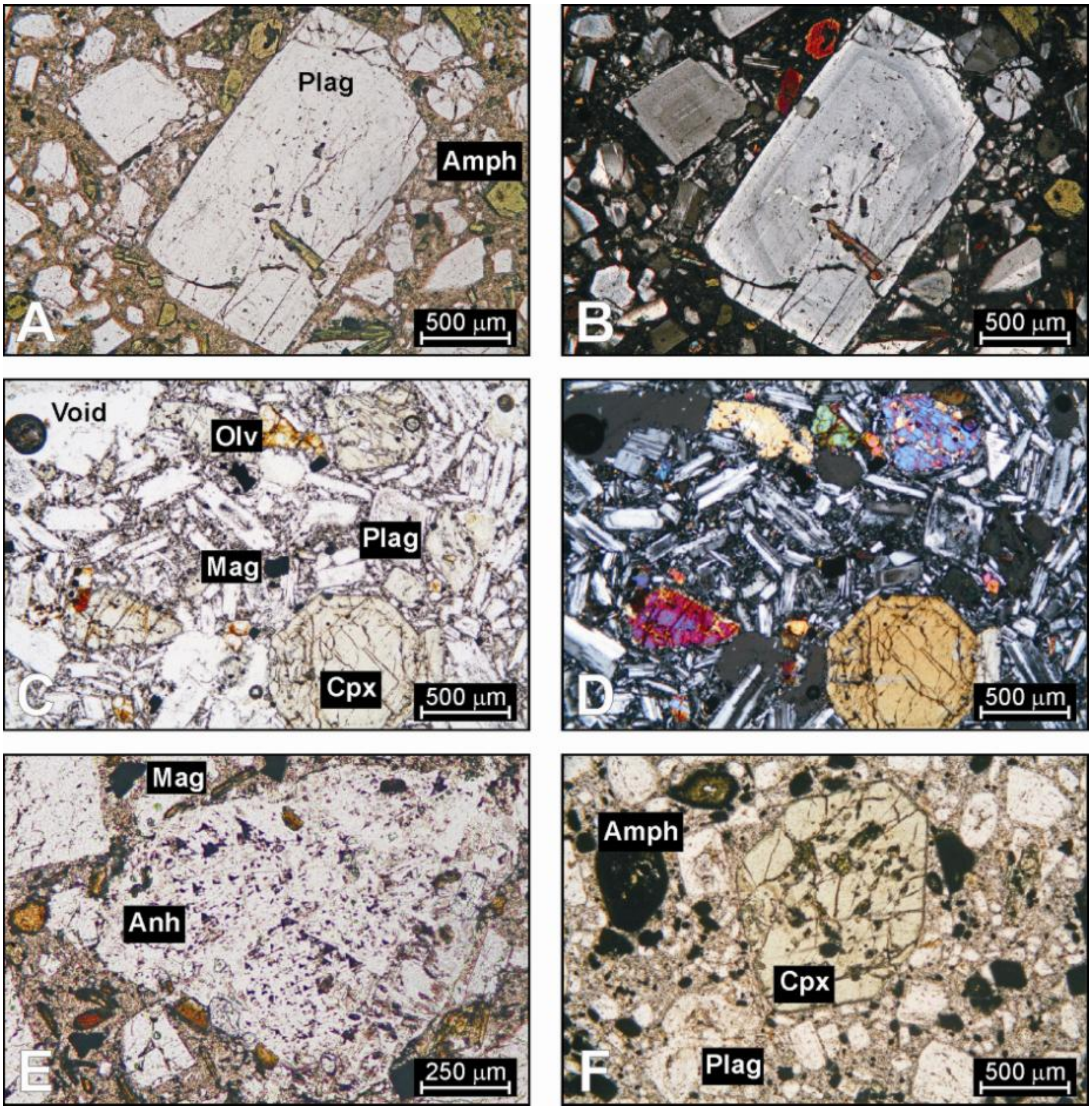

Fig. 3.3: Thin section photomicrographs of main suite samples: A) typical crystal-rich trachyte (SV10); B) as before in cross polarised light; C) crystalline olivine–clinopyroxene mugearite (SV1); D) as before in cross polarised light; E) anhydrite (with triangular cleavage pits) in trachyte (SV40); F) benmoreite with fresh clinopyroxene, and amphibole replaced by a mixture of clinopyroxene + magnetite + plagioclase (SV12).

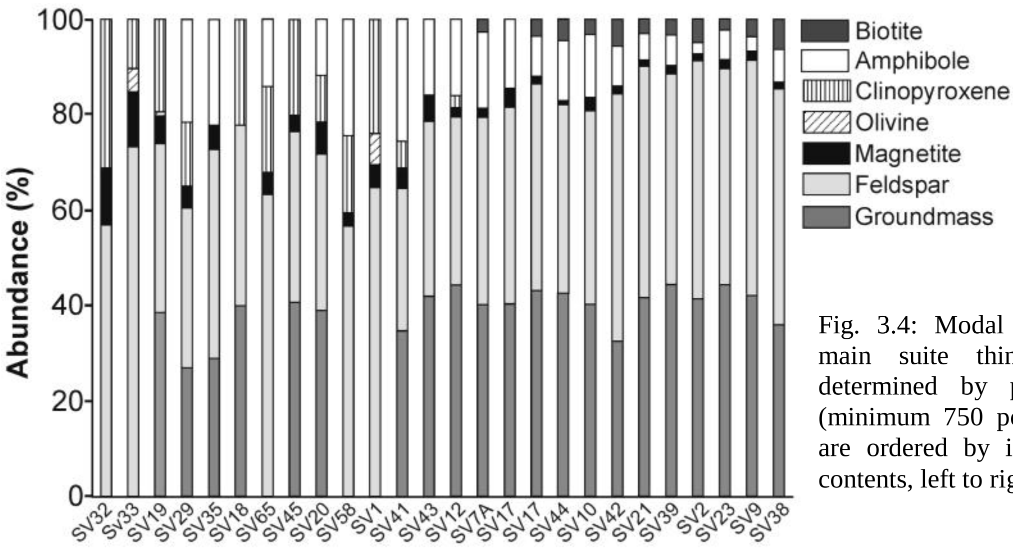

Fig. 3.4: Modal mineralogy of main suite thin sections as determined by point counting (minimum 750 points). Samples are ordered by increasing SiO_2 contents, left to right.

Analysis	06-044	06-051	12-050	12-051	11-008	11-010	03-058	10-035
Sample	SV19	SV19	SV12	SV12	SV40	SV40	SV38	SV181
Rock type	MUG	MUG	BEN	BEN	TRAC	TRAC	HBLITE	HBLITE
Crystal Position	Core	Rim	Core	Rim	Core	Rim		
SiO_2	47.75	52.75	51.08	57.89	58.85	65.47	45.90	45.97
TiO_2			0.00	0.03	0.00	0.00	0.00	0.01
Al_2O_3	32.22	28.91	30.77	25.36	25.16	21.26	34.60	33.97
Cr_2O_3			0.01	0.00	0.00	0.03	0.00	0.00
FeO_T	0.67	0.67	0.32	0.53	0.22	0.22	0.22	0.18
MnO			0.00	0.02	0.01	0.00	0.00	0.01
MgO			0.01	0.18	0.01	0.01	0.00	0.00
CaO	16.36	12.51	14.33	8.12	7.24	2.68	18.21	17.70
Na_2O	2.25	4.44	3.40	6.46	7.27	9.38	1.16	1.24
K_2O	0.09	0.26	0.18	0.45	0.30	1.15	0.01	0.00
NiO			0.00	0.04	0.01	0.02	0.00	0.00
BaO	0.02	0.02						
SrO	0.16	0.16						
Total	99.51	99.71	100.11	99.06	99.07	100.22	100.10	99.08
An %	80	60	69	40	35	13	90	89
Ab %	20	39	30	57	63	81	10	11
Or %	1	1	1	3	2	7	0	0

Table 3.2: Representative electron microprobe analyses of plagioclase crystals. MUG= mugearite; BEN = benmoreite; TRAC = trachyte; HBLITE = hornblendite. Blank cells not analysed.

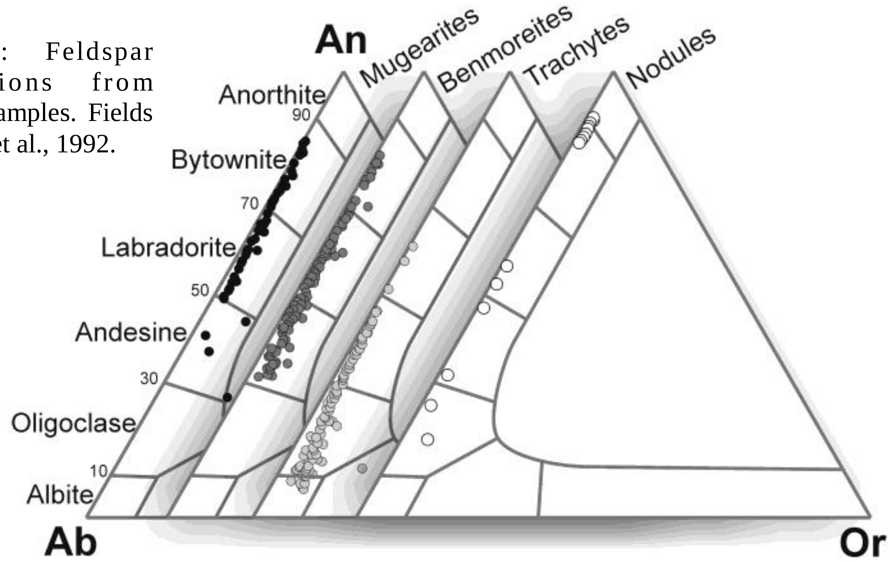

Fig. 3.5: Feldspar compositions from unaltered samples. Fields from Deer et al., 1992.

nearly all crystals analysed; rare outliers with Or >5% may be a result of minor alteration. Feldspar crystals occasionally contain inclusions of amphibole and magnetite.

Magnetite occurs throughout the suite as a minor phenocryst phase (1–12% by volume; Fig. 3.4), with crystals typically <0.3 mm. Magnetite has been observed as inclusions within all major phenocryst phases. Many magnetite crystals show well developed exsolution lamellae under reflected light. Electron microprobe analysis of magnetite (Table 3.3) frequently returned analyses with totals <90 wt %, with iron analysed as FeO . This may be a result of an excess of the Fe_2O_3 component, i.e. the magnetites are approaching

Analysis	11-114	11-066	12-073	09-080	09-026	11-028	12-112	10-047
Sample	SV45	SV45	SV12	SV10	SV17	SV40	SV158	SV181
Rock type	MUG	MUG	BEN	TRAC	TRAC	TRAC	CPXITE	HBLITE
SiO_2	0.00	0.11	0.00	0.03	0.00	0.01	0.00	0.05
TiO_2	6.82	4.96	1.84	4.77	4.99	0.76	4.09	4.07
Al_2O_3	4.27	3.49	1.10	1.02	0.88	0.61	3.48	2.53
Cr_2O_3	0.15	0.38	0.51	0.10	0.05	0.07	4.99	0.04
FeO_T	76.78	73.10	82.27	84.98	80.98	83.90	70.93	81.98
MnO	0.49	0.65	1.13	1.36	1.68	1.82	0.28	0.51
MgO	4.02	4.00	2.32	0.73	1.42	1.23	2.17	1.44
CaO	0.02	0.09	0.00	0.00	0.04	0.00	0.00	0.00
Na_2O	0.01	0.00	0.00	0.00	0.00	0.13	0.01	0.04
K_2O	0.00	0.04	0.00	0.00	0.00	0.01	0.01	0.03
NiO	0.02	0.03	0.01	0.06	0.02	0.03	0.05	0.01
Total	92.57	86.85	89.17	93.04	90.05	88.57	86.01	90.69

Table 3.3: Representative electron microprobe analyses of iron oxides. CPXITE = clinopyroxenite.

the maghemite endmember. Magnetite–maghemite solid solution is probably a result of subsolidus oxidation (Haggerty, 1976).

Clinopyroxene occurs in the hawaiites, mugearites and one benmoreite (SV12) sample, typically as well developed phenocrysts between 0.5 and 2 mm diameter that represent up to 30% of the sample's volume (Fig. 3.4). Zoning, exsolution lamellae and reaction rims were rarely observed. Clinopyroxene crystals occasionally contain inclusions of magnetite (up to 0.3 mm, typically well developed crystals), and rarely feldspar (<0.2 mm, poorly developed crystals). Clinopyroxenes analysed by EPMA (Table 3.4) were classified using PX-NOM (Sturm, 2002). Pyroxenes from the main suite fall in a narrow compositional range that spans the augite–diopside boundary on Figure 3.6; the pyroxenes are typically aluminian and aluminian-ferrian diopsides/augites, with a smaller proportion (<10% of

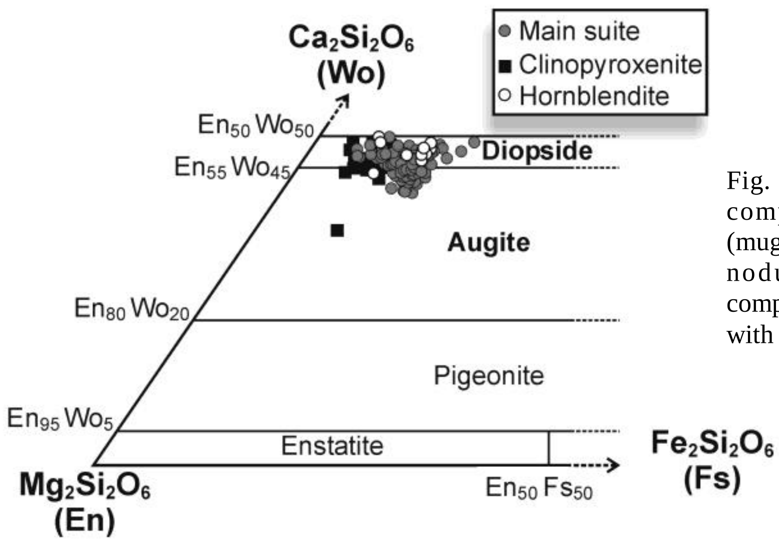

Fig. 3.6: Plot of clinopyroxene compositions from main suite (mugearites and benmoreites) and nodules from Savo. Mineral compositions calculated and plotted with PX-NOM (Sturm, 2002).

Analysis	05-001	05-041	05-087	12-069	12-113	07-037	03-004	07-087
Sample	SV1	SV19	SV20	SV12	SV158	SV165	SV6A	SV183
Rock type	MUG	MUG	MUG	BEN	CPXITE	CPXITE	HBLITE	HBLITE
Mineral Name	Aluminian Augite	Aluminian Ferrian Diopside	Aluminian Ferrian Diopside	Aluminian Diopside	Aluminian Diopside	Aluminian Chromian Ferrian Augite	Aluminian Ferrian Diopside	Diopside
SiO_2	52.54	49.51	49.00	50.73	52.37	52.16	50.99	53.37
TiO_2	0.49	0.70	0.30	0.58	0.36	0.17	0.13	0.04
Al_2O_3	2.97	4.91	2.27	3.71	2.66	2.93	3.60	1.16
Cr_2O_3	0.01	0.07	0.00	0.00	0.15	0.58	0.04	0.05
FeO_T	7.37	7.84	7.00	8.05	5.10	5.87	7.45	6.45
MnO	0.23	0.17	0.39	0.48	0.07	0.17	0.31	0.44
MgO	15.17	14.41	14.44	12.98	15.29	16.84	14.38	15.27
CaO	20.42	22.14	21.98	22.42	23.38	21.25	23.00	23.15
Na_2O	0.03	0.00	0.00	0.01	0.00	0.02	0.00	0.02
K_2O	0.48	0.39	0.40	0.53	0.25	0.76	0.43	0.46
NiO	0.03	0.00	0.05	0.00	0.00	0.08	0.02	0.03
Total	99.75	100.15	95.81	99.48	99.62	100.83	100.35	100.43
En %	44	41	42	38	44	47	41	43
Fs %	13	13	12	14	8	10	12	11
Wo %	43	46	46	48	48	43	47	47

Table 3.4: Representative electron microprobe analyses of clinopyroxene crystals. Mineral names obtained with PX-NOM (Sturm, 2002).

analyses) of chromian diopsides and augites. There is little observable, systematic variation of pyroxene chemistry with whole rock chemistry.

Analysis	05-020	05-027	07-056	12-125
Sample	SV1	SV1	SV165	SV158
Rock Type	MUG	MUG	CPXITE	CPXITE
SiO_2	38.07	38.13	39.21	39.88
TiO_2	0.00	0.00	0.04	0.00
Al_2O_3	0.05	0.01	0.02	0.00
Cr_2O_3	0.00	0.00	0.04	0.00
FeO_T	22.97	25.08	17.77	18.15
MnO	0.49	0.72	0.36	0.29
MgO	38.74	37.80	43.38	41.86
CaO	0.19	0.17	0.08	0.06
Na_2O	0.05	0.01	0.02	0.04
K_2O	0.02	0.00	0.00	0.01
NiO	0.03	0.01	0.15	0.08
Total	100.61	101.92	101.08	100.37
Fo %	75	72	81	80
Fa %	25	27	19	20

Table 3.5: Representative electron microprobe analyses of olivine crystals.

Olivine occurs as phenocrysts (up to 2 mm diameter) in a small number of mugearitic samples, where it constitutes up to 7% of the sample's volume (Fig. 3.4). Crystals are typically rounded with the margins altered to iddingsite. Microprobe analyses are available only for sample SV1 in the main suite; analysed crystals are $Fo_{70–80}$, with Ca contents of 0.15–0.20 wt % (Table 3.5).

Amphibole occurs over a wide range of whole rock SiO_2 values (from <52 to >65), and is the most abundant phenocryst mineral after plagioclase. Amphibole is commonly present as well developed crystals and laths, typically between 0.5 and 1 mm but occasionally over 3 mm in length. Amphibole is strongly pleochroic in either deep green to pale green, or red-brown to straw/ colourless. Zoning was observed in a number of well-formed crystals.

Analysis	05-085	08-021	12-057	08-117	08-122	03-066	10-081	12-124
Sample	SV20	SV41	SV12	SV40	SV40	SV38	SV181	SV158
Rock type	MUG	MUG	BEN	TRAC	TRAC	HBLITE	HBLITE	CPXITE
Mineral Name	Ferrian Titanian M.hastingsite	Pargasite	Ferrian M.hastingsite	Pargasite	M.hastingsite	Pargasite	Pargasite	M.hastingsite
SiO_2	41.90	41.08	43.47	39.35	42.39	43.89	40.49	43.92
TiO_2	2.64	1.60	1.59	1.72	1.73	0.69	1.60	1.08
Al_2O_3	11.40	13.09	11.75	16.06	12.67	12.29	15.04	11.87
Cr_2O_3	0.03	0.01	0.02	0.01	0.04	0.11	0.00	0.01
FeO_T	0.21	0.10	0.15	0.33	0.19	0.22	0.26	0.08
MnO	11.56	10.17	10.46	15.34	11.66	10.98	14.25	9.02
MgO	14.65	14.27	15.55	9.96	14.11	14.47	11.19	16.14
CaO	10.76	12.25	11.33	11.54	11.48	12.11	11.64	11.77
Na_2O	2.59	2.56	2.47	2.71	2.92	2.86	2.51	2.26
K_2O	0.61	0.80	0.71	1.16	1.11	0.42	0.77	0.68
NiO	0.00	0.02	0.03	0.01	0.02	0.05	0.01	0.03
Total	96.34	96.19	97.52	98.39	98.36	98.08	97.75	96.85

Table 3.6: Representative electron microprobe analyses of amphibole crystals. Mineral names obtained with AMPH-CLASS (Esawi, 2004). M.hastingsite= magnesiohastingsite.

Amphibole stoichiometric and structural formulae were determined with AMPH-CLASS (Esawi, 2004) and named according to the IMA 97 scheme (Leake et al., 1997). All fresh amphiboles analysed by electron microprobe (Table 3.6) were hornblende group (*sensu lato*), with the majority being pargasites and magnesiohastingsites, with a smaller number of edenites and magnesiohornblendes (Fig. 3.7). Significant variations in composition (e.g. Si, Na_A+K_A, Mg#) can occur within single samples, and even within single crystals. For

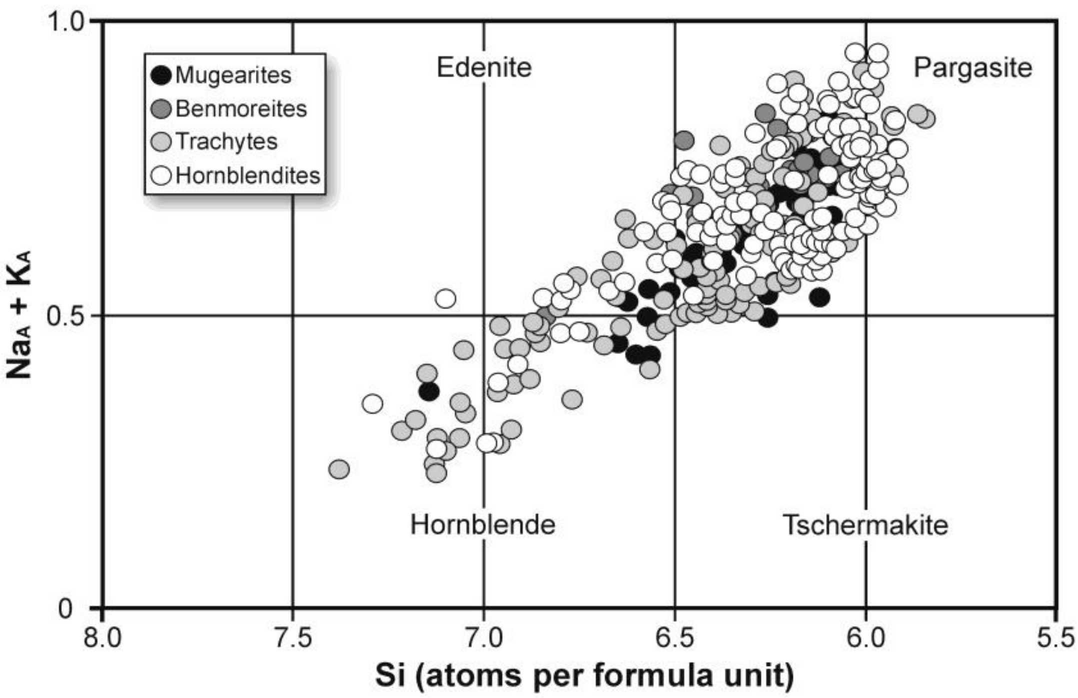

Fig. 3.7: Amphibole chemistry for main suite and nodule samples. Stoichiometry calculated using AMPH-CLASS (Esawi, 2004); mineral names according to Leake et al. (1997).

example, a single crystal in SV40 was found to be normally (with oscillations) zoned from Mg# (Mg/Mg+Fe) 0.79 to 0.55, as Na_A+K_A varied from 0.55 to 0.9. No systematic variation in zoning was observed for the suite (i.e. normal, reverse and oscillatory zoning all occur, as do homogeneous crystals).

In a number of sections, hornblende displays opaque rims, and in a small number of samples (including SV12, 20, 29) is completely replaced and pseudomorphed by finely crystalline opaque minerals (Fig. 3.3F); extensive microprobe and X-ray diffraction study of pseudomorphed and rimmed amphiboles from Guadalcanal and Savo was carried out by Stanton (1994) who found the replacing assemblage to be a mixture of clinopyroxene, magnetite and plagioclase with trace quartz and hematite.

Biotite occurs in benmoreite and trachyte samples, typically as small (<0.5 mm) crystals; rare examples with long axes of up to 2 mm were observed. Biotite crystals are often deformed, and in rare examples may be seen as inclusions within large amphibole crystals. Biotite typically constitutes between 3 and 7% by volume of samples with whole rock SiO_2 >60 wt %. Biotites analysed in this study (Table 3.7) are relatively magnesium rich (Mg# typically 0.6–0.7). The majority of analysed samples are part of the annite–phlogopite series (*sensu* Tischendorf et al. 2007), with a significant proportion sufficiently Mg-rich to fall within the phlogopite field (Fig. 3.8) of the *mgli*–*feal* plot (Tischendorf et al., 2004; Li contents estimated using equations therein).

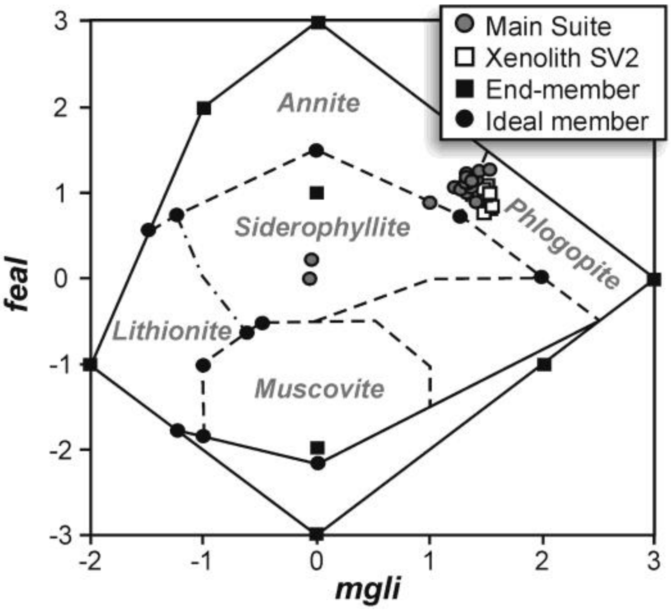

Fig. 3.8: Biotite compositions from Savo main suite and xenolith within SV2, plotted by the methods outlined in Tischendorf et al. (2004). *feal* = (Fe_T + Mg + Ti − ^{VI}Al) and *mgli* = (Mg − Li), all in a.p.f.u.; Li estimated using equations of Tischendorf et al. (2004).

Analysis	03-107	11-027	09-087	01 -048
Sample	SV38	SV40	SV44	SV2
Rock type	TRAC	TRAC	TRAC	NOD
Mineral	Phlog.	Phlog.	Annite	Phlog.
SiO_2	36.66	37.28	37.36	37.12
TiO_2	2.67	2.47	4.08	2.40
Al_2O_3	14.77	14.20	13.12	14.10
Cr_2O_3	0.00	0.00	0.04	0.00
FeO_T	14.98	14.16	14.27	13.99
MnO	0.39	0.39	0.33	0.33
MgO	15.69	15.83	15.63	16.51
CaO	0.01	0.04	0.02	0.00
Na_2O	0.85	0.86	1.03	0.82
K_2O	8.44	9.12	8.86	8.90
NiO	0.01	0.01	0.07	0.02
Total	94.45	94.36	94.81	94.20
Li_2O	*0.043*	*0.042*	*0.043*	*0.037*
Mg #	0.65	0.67	0.66	0.68

Table 3.7: Representative electron microprobe analyses of biotite crystals. Named according to the scheme of Tischendorf et al. (2004). Li2O = [2.1/(0.356 + MgO)]−0.088. Phlog. = Phlogopite; NOD = nodule.

3.3.2 Petrography and mineral chemistry – nodules

Nodules are abundant and diverse in rocks at Savo, ranging from mm-scale clusters of xenocrysts, to inclusions of material over 20 cm in diameter. Nodules are subdivided on the basis of dominant mineralogy:

Hornblendites (*sensu lato*) are composed of amphibole (>90%) with minor clinopyroxene and magnetite ± plagioclase ± apatite. Amphibole crystals are typically >2 mm, and can measure up to 3 cm. Texture varies according to mineralogy: plagioclase ± apatite-bearing samples typically have euhedral amphibole crystals, with anhedral (interstitial) feldspar and apatite; feldspar-free and feldspar-poor samples are much more common on Savo, and are dominated by anhedral amphiboles. The samples are consistent with cumulate textures, with feldspar-free orthocumulates (Fig. 3.9A) and feldspar-bearing adcumulates (Fig. 3.9B). Amphibole compositions in nodules overlap with those analysed from the main suite (Fig. 3.7). Plagioclase analysed from hornblendites may be more calcic than feldspar in the main suite (SV38, SV181 nodules are An_{80-90}) but not in all cases (Fig. 3.5).

Clinopyroxenites are dominated by clinopyroxene, with olivine, minor amphibole, and magnetite, and display orthocumulate textures (Fig. 3.9C). Amphibole can be seen to be replacing clinopyroxene in a number of samples, especially at the contact between the host rock and the nodule (Fig. 3.9D), and also occurs as an intercumulus phase, typically leading to poikilitic textures. Clinopyroxene chemistries overlapped with those of the main suite, tending to be slightly more Mg-rich (Fig. 3.6). From the small number of olivine analyses there is no appreciable difference in Fo% between the nodules and main suite, but the nodule olivines look to be less calcic than those of the main suite (>0.1 vs. ~0.2 wt % CaO, respectively).

Amphibole gabbros are coarsely crystalline (1–5 mm) with plagioclase, amphibole, clinopyroxene and magnetite (Fig. 3.9E). Amphiboles are often blackened or partially replaced by clinopyroxene and magnetite. Amphibole gabbros are transitional between hornblendites and main suite hawaiites and mugearites in terms of mineralogy and texture. No microprobe data are available for amphibole gabbros.

3.3.3 Major element chemistry

Samples from Savo are mildly alkaline and sodic ($K_2O < Na_2O-2$), and are classed as mugearites, benmoreites and trachytes, with occasional hawaiite and dacite samples (Fig.

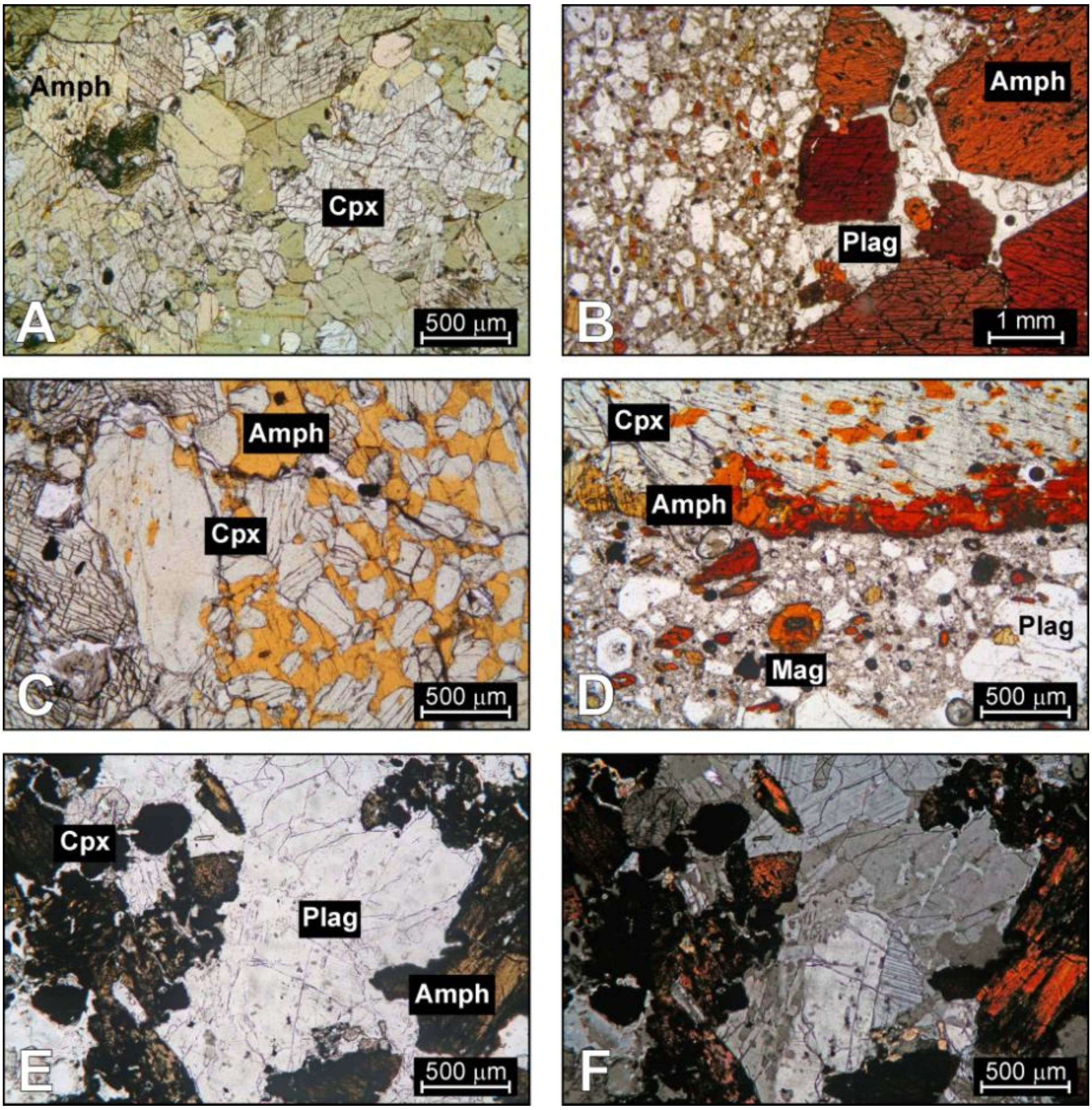

Fig. 3.9: Thin section photomicrographs of nodules from Savo (plane polarised light unless noted otherwise): A) hornblendite with clinopyroxene (SV175); B) hornblendite with intercumulus plagioclase in trachyte host rock (SV181); C) clinopyroxenite with amphibole replacing pyroxene (SV158); D) amphibole reaction rim at contact between clinopyroxenite nodule and trachyte host (SV158); E) amphibole–clinopyroxene gabbro (SV55); F) as before in cross polarised light.

3.2; Table 3.8). The majority of analysed samples are silica saturated and metaluminous, but a small number of mugearites are nepheline-normative.

Major element trends for the main suite and nodules are shown in Harker variation diagrams in Figure 3.10. Samples from the main suite show well defined linear relationships for all elements relative to SiO_2 increase. There is a paucity of benmoreite samples relative to the mugearites and trachytes; to what extent this reflects a sampling bias rather than a real lack of benmoreites in the erupted material at Savo is difficult to ascertain.

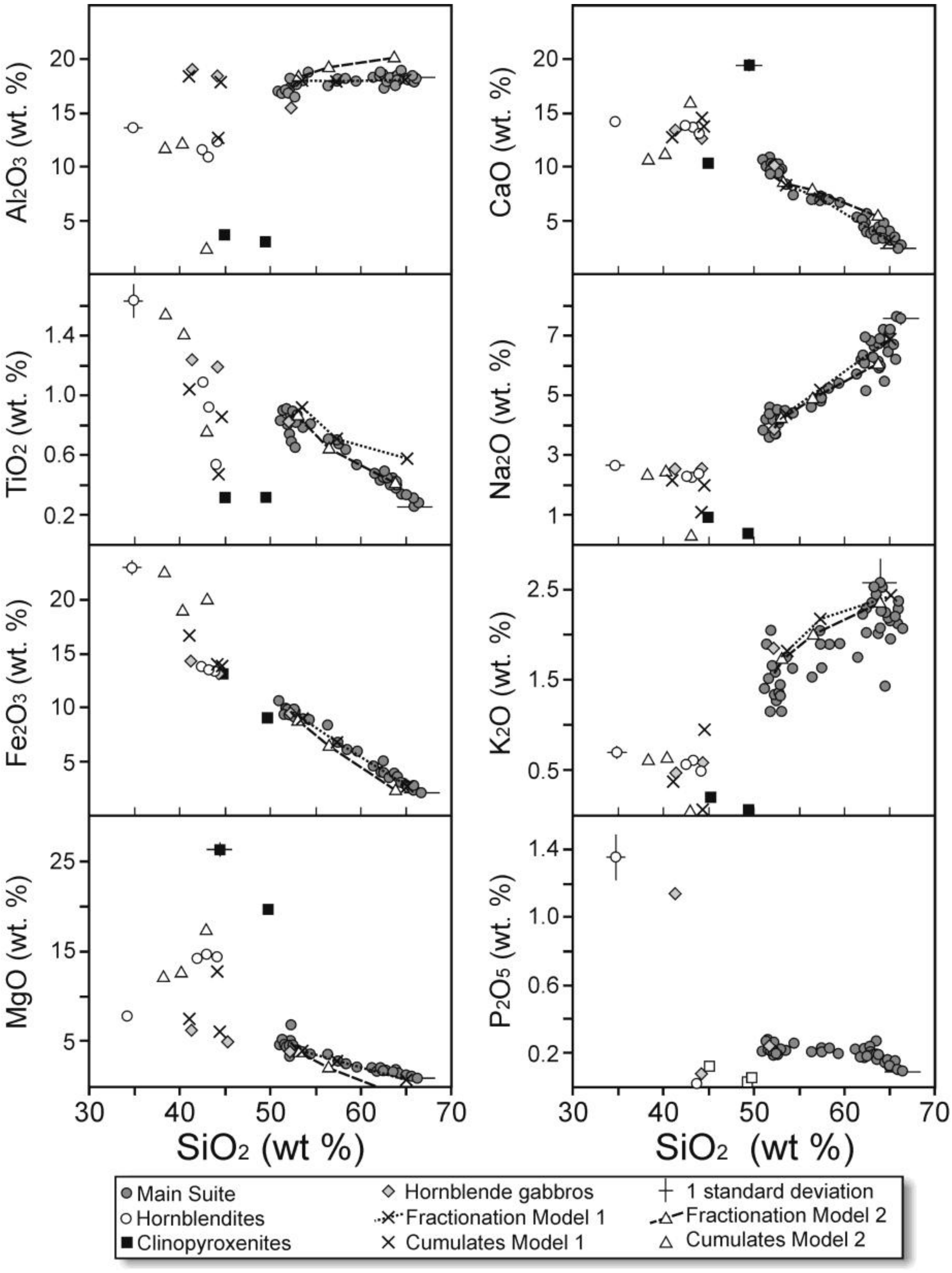

Fig. 3.10: Major element Harker variation diagrams for main suite samples and nodules from Savo Island. All data recalculated to 100% on a volatile-free basis. Also shows results of least-squares fractionation models discussed in text.

TiO_2, Fe_2O_3 (Fe_T), MgO and CaO all show progressive decrease with increasing SiO_2; these elements are compatible with the fractionating mineral assemblage between 50 and 70 wt % SiO_2. Na_2O increases linearly with increasing SiO_2; K_2O data is scattered, but

Sample	SV32	SV151	SV33	SV19	SV362	SV29	SV35	SV18	SV65	SV45	SV20	SV58	SV1	SV56	SV7B	SV41	SV11	SV352
Location	Tuluka	Solo.	Tuluka	Pogho.	Tuluka	Kalaka	Tuluka	Pagha.	Pogho.	Pagha.	Pogho.	Mbonala	Rembo.	Mbonala	Tana.	Mbazo	Pogho.	Kalaka
Rock Type	MUG	HAW	MUG	MUG	MUG	MUG	MUG	HAW	MUG	MUG	MUG	MUG	MUG	MUG	MUG	MUG	BEN	BEN
SiO_2 (wt %)	50.05	50.53	50.75	51.00	51.19	51.41 (0.40)	51.61	51.66	51.67	51.84	51.89	52.10	52.35	52.51	52.83	55.51	56.76	56.93
TiO_2	0.88	0.82	0.86	0.72	0.84	0.90 (0.01)	0.84	0.80	0.80	0.63	0.75	0.87	0.68	0.89	0.78	0.69	0.67	0.69
Al_2O_3	16.35	16.82	16.82	16.55	16.87	16.93 (0.15)	17.25	16.78	17.24	16.11	17.42	17.60	15.33	17.25	18.26	17.32	17.76	18.12
Fe_2O_3	9.05	10.58	9.07	9.31	9.51	9.95 (0.02)	9.01	9.61	8.98	9.83	8.76	8.93	9.31	9.58	8.64	8.29	6.77	6.85
MnO	0.16	0.14	0.16	0.14	0.14	0.16 (0.01)	0.20	0.12	0.21	0.12	0.13	0.16	0.15	0.17	0.13	0.27	0.11	0.13
MgO	5.18	4.47	4.54	4.78	4.95	5.02 (0.01)	3.82	4.67	3.95	4.41	3.68	4.63	6.88	4.61	3.48	3.48	2.80	2.63
CaO	9.70	10.50	9.04	10.02	8.95	9.39 (0.14)	9.33	10.83	9.16	9.95	8.00	8.93	10.18	9.08	7.05	6.78	6.86	6.74
Na_2O	4.05	3.79	4.50	3.74	3.84	4.33 (0.13)	4.06	3.61	4.38	3.98	4.32	4.28	3.71	4.30	4.27	4.50	5.00	4.86
K_2O	1.84	1.39	2.02	1.63	1.56	1.15 (0.05)	1.12	1.51	1.41	1.34	1.72	1.30	1.35	1.27	1.59	1.51	1.88	2.04
P_2O_5	0.26	0.21	0.27	0.22	0.23	0.19 (0.003)	0.22	0.22	0.21	0.19	0.21	0.21	0.19	0.20	0.25	0.20	0.21	0.23
LOI	2.18	0.57	2.13	1.09	1.06	0.72 (0.02)	2.84	0.57	0.35	1.12	1.99	0.48	-0.12	0.23	1.52	1.11	0.21	0.44
Total	99.71	99.82	100.17	99.19	99.46	100.17	100.28	100.37	98.36	99.52	98.87	99.48	100.01	100.08	98.78	99.66	99.03	99.67
Ba (ppm)	473	287	527	525	328	273 (6)	277	466	303	494	331	297	327	307	334	338	348	441
Ce	21	16	31	40	20	18 (4)	17	27	19	28	28	22	19	16	30	18	26	21
Co	24	33	34	27	29	29 (2)	30	31	28	27	24	30	35	29	25	31	17	18
Cr	48	91	77	98	31	51 (10)	119	95	31	92	10	110	214	18	bdl	49	bdl	bdl
Cu	123	69	105	88	130	92 (4)	93	95	37	110	77	124	103	115	83	89	10	50
Ga	22	19	20	20	19	21 (1)	23	18	22	24	21	24	19	23	22	23	22	22
La	10	8	14	11	10	7 (1)	7	13	7	14	6	8	10	8	8	9	8	13
Nb	2	bdl	bdl	bdl	2	bdl	bdl	bdl	3	2	bdl	bdl	bdl	2	2	bdl	bdl	3
Nd	16	11	11	16	12	14 (1.5)	12	15	9	17	12	12	10	12	16	16	12	12
Ni	11	19	19	24	15	8 (0.2)	7	22	bdl	7	9	16	43	bdl	12	17	bdl	bdl
Pb	8	bdl	bdl	bdl	bdl	bdl	bdl	8	bdl	11	bdl	8	bdl	bdl	bdl	bdl	bdl	bdl
Rb	26	13	23	22	18	17 (2)	20	18	22	34	26	22	21	22	24	27	26	30
Sc	34	32	39	32	32	29 (2)	38	29	29	44	30	33	28	26	21	22	21	16
Sr	1172	704	849	849	827	654 (22)	731	855	776	1215	762	736	709	706	658	720	837	733
Th	bdl	bdl	6	7	bdl	bdl	7	bdl	bdl	4	5	bdl	6	bdl	8	7	6	bdl
U	bdl	bdl	bdl	bdl	bdl	bdl	bdl	bdl	bdl	bdl	bdl	bdl	bdl	bdl	bdl	bdl	bdl	bdl
V	317	246	438	460	290	196 (5)	296	423	290	305	273	285	225	187	291	222	258	169
Y	18	18	16	20	19	18 (0.5)	21	22	20	20	17	18	19	19	20	24	19	19
Zn	56	62	85	89	66	66 (3)	67	74	62	55	64	75	61	70	69	111	50	56
Zr	75	54	61	68	67	65 (9)	81	54	75	77	79	79	63	75	88	85	105	103

Table 3.8: Whole rock major and trace element chemistry as determined by XRF analysis. Abbreviations used: MUG = mugearite; HAW = hawaiite; BEN = benmoreite; TRAC = trachyte; DAC = dacite; CPXITE = clinopyroxenite; HBLITE = hornblendite; GAB = amphibole gabbro; bdl = below detection limits; Pagha. = Paghalula Dome; Pogho. = Poghorovorughala catchment; Rembo. = Rembokola catchment; Soulo. = Soulomata catchment; Tana. = Tanavalea catchment; Pogholav. = Pogholavka. A small number of samples were analysed in triplicate; analyses listed are average values, with 1 standard deviation shown in parentheses.

Sample	SV43	SV54	SV12	SV7A	SV13	SV344	SV17	SV342	SV40	SV323	SV16	SV44	SV400	SV10	SV30	SV396	SV15	SV42	SV14
Location	Mbazo	Mbonala	Pogho.	Mega.	Pogho.	Pagha.	Pagha.	Pagha.	Mbazo	Tana.	Pogho.	Lemboni	Pogho.	Pogho.	Tuluka	Pogho.	Pogho.	Mbazo	Pogho.
Rock Type	BEN	BEN	BEN	BEN	BEN	TRAC	TRAC	TRAC	TRAC	TRAC	TRAC	TRAC	TRAC	TRAC	DAC	TRAC	TRAC	TRAC	TRAC
SiO_2 (wt %)	57.53	58.41	58.55 (0.53)	61.32	61.87	60.89	61.50	61.89	62.26	62.53	62.67	62.87	62.96	63.13	63.23	63.25	63.63	63.67	63.94
TiO_2	0.70	0.63	0.52 (0.08)	0.47	0.49	0.42	0.42	0.43	0.45	0.44	0.39	0.44	0.40	0.37	0.37	0.39	0.42	0.33	0.39
Al_2O_3	18.51	18.19	17.65 (0.07)	18.30	17.06	18.03	18.52	18.52	17.71	18.07	18.00	17.86	17.75	18.16	18.51	17.77	17.40	17.97	18.43
Fe_2O_3	6.78	6.18	5.84 (0.06)	4.63	5.02	3.98	4.11	3.93	3.84	3.70	3.67	3.67	3.45	3.37	3.28	3.36	3.99	2.87	3.69
MnO	0.11	0.16	0.13 (0.008)	0.10	0.09	0.10	0.10	0.10	0.09	0.06	0.09	0.09	0.07	0.10	0.12	0.07	0.09	0.08	0.08
MgO	2.85	2.55	1.93 (0.07)	2.10	1.71	1.43	1.48	1.38	2.07	1.40	1.45	1.81	1.46	1.26	1.15	1.40	1.83	1.22	1.49
CaO	7.21	6.80	6.48 (0.43)	5.21	5.47	4.83	4.16	4.68	3.74	3.14	3.85	3.68	3.20	4.31	4.63	3.14	4.19	3.15	3.52
Na_2O	4.82	5.23	5.33 (0.29)	5.72	5.08	6.09	6.23	6.05	6.94	6.59	6.20	6.84	6.63	6.10	5.35	6.79	5.87	7.08	5.98
K_2O	1.63	1.90	1.88 (0.19)	1.75	2.00	2.21	2.27	2.23	2.29	2.41	2.52	2.36	2.55	1.99	1.40	2.53	2.05	2.23	2.27
P_2O_5	0.21	0.23	0.19 (0.004)	0.22	0.18	0.18	0.17	0.18	0.23	0.27	0.19	0.24	0.21	0.16	0.16	0.19	0.19	0.16	0.17
LOI	0.51	0.18	0.57 (0.05)	0.83	0.33	0.16	0.58	0.34	0.26	0.79	0.19	0.30	0.88	0.16	0.91	0.65	0.27	0.67	0.30
Total	100.84	100.44	99.07	100.65	99.32	98.32	99.53	99.73	99.89	99.46	99.21	100.16	99.61	99.11	99.10	99.57	99.94	99.43	100.24
Ba (ppm)	374	448	425 (5)	708	439	689	737	723	881	822	789	854	839	733	650	838	707	882	770
Ce	19	17	20 (4)	16	23	18	19	18	20	31	21	24	17	21	9	20	17	10	22
Co	18	16	15 (1)	11	12	9	9	11	11	8	9	15	8	7	10	9	9	11	8
Cr	12	28	29 (18)	22	9	23	bdl	12	30	bdl	5	7	11	15	bdl	bdl	7	bdl	29
Cu	106	46	8 (3)	10	35	4	9	12	25	17	9	21	5	21	14	bdl	16	10	8
Ga	24	22	22 (2)	24	21	23	25	24	24	24	25	25	22	26	24	23	23	24	24
La	6	13	10 (1)	11	8	11	11	9	15	19	12	15	12	9	10	12	9	9	11
Nb	bdl	3	2 (0.3)	5	3	3	4	4	3	3	5	2	3	4	5	3	2	3	5
Nd	14	16	10 (2)	12	10	12	13	12	14	16	14	13	11	11	9	11	9	9	11
Ni	bdl	bdl	bdl	13	bdl	bdl	bdl	bdl	bdl	bdl	bdl	bdl	bdl	bdl	bdl	bdl	bdl	bdl	bdl
Pb	bdl	8	bdl	11	17	bdl	bdl	7	16	10	12	17	12	13	13	12	13	12	12
Rb	29	36	31 (3)	38	34	34	40	34	43	29	45	42	36	45	27	36	46	44	46
Sc	22	14	13 (3)	bdl	16	bdl	bdl	bdl	bdl	bdl	bdl	bdl	bdl	bdl	bdl	bdl	bdl	bdl	bdl
Sr	765	794	863 (31)	1152	827	1338	1506	1348	1606	1604	1543	1630	1477	1427	1170	1417	1141	1468	1516
Th	5	5	bdl	bdl	8	bdl	5	bdl	8	bdl	5	10	bdl	6	4	bdl	7	6	6
U	bdl	bdl	bdl	bdl	bdl	bdl	bdl	bdl	bdl	bdl	bdl	bdl	bdl	bdl	bdl	bdl	bdl	bdl	bdl
V	208	135	183 (11)	84	148	77	83	71	91	89	73	83	77	62	57	78	83	52	87
Y	16	19	16 (2)	12	15	10	10	10	11	9	12	11	7	12	12	7	10	9	10
Zn	59	53	46 (1)	48	40	47	47	53	42	41	44	45	42	47	55	43	39	40	42
Zr	95	119	102 (11)	126	117	117	136	122	130	117	141	135	117	136	147	116	125	130	142

Table 3.8 contd.

Sample	SV21	SV375	SV3	SV39	SV2	SV23	SV9	SV38	SV49	SV159	SV161	SV181	SV155	SV175	SV6A	SV59	SV350	SV365
Location	Pogho.	Lemboni	Rembo.	Crater	Rembo.	Koela	Pogho.	Crater	Lemboni	Soulo.	Soulo.	Soulo.	Soulo.	Soulo.	Pogholav.	Mbonala	Kalaka	Tuluka
Rock Type	TRAC	TRAC	TRAC	TRAC	TRAC	TRAC	TRAC	TRAC	TRAC	CPXITE	CPXITE	HBLITE	HBLITE	HBLITE	HBLITE	GAB	GAB	GAB
SiO_2 (wt %)	64.06 (0.4)	64.18	64.61	64.92	65.08	65.11	65.44	65.75	66.57	44.44	49.79	34.13	42.03	42.79	43.39	40.65	43.81	49.74
TiO_2	0.30 (0.01)	0.34	0.32	0.33	0.25	0.28	0.25	0.33	0.27	0.31	0.31	1.61	1.07	0.91	0.52	1.22	1.18	0.79
Al_2O_3	18.02 (0.21)	17.91	17.99	18.21	17.66	17.92	18.10	18.40	18.31	3.47	2.95	13.39	11.27	10.85	12.16	18.64	18.24	17.37
Fe_2O_3	2.77 (0.05)	3.10	3.06	2.85	2.36	2.68	2.27	2.83	2.16	13.18	8.47	22.72	13.66	13.37	12.45	14.13	13.51	8.73
MnO	0.05 (0.02)	0.07	0.06	0.07	0.06	0.06	0.06	0.07	0.06	0.21	0.12	0.23	0.12	0.12	0.22	0.18	0.12	0.17
MgO	1.05 (0.03)	1.02	1.13	1.19	0.87	1.10	0.88	1.16	0.78	26.30	19.74	7.92	14.37	14.81	14.19	6.26	6.59	3.10
CaO	3.04 (0.21)	3.78	3.15	3.07	2.41	3.27	2.28	2.98	2.58	10.11	19.10	13.89	13.57	13.59	12.90	13.15	12.53	9.66
Na_2O	6.05 (0.20)	6.36	6.62	7.08	7.56	6.66	7.61	7.27	7.62	0.90	0.29	2.56	2.25	2.22	2.34	2.50	2.51	3.92
K_2O	2.08 (0.13)	1.94	2.15	2.20	2.35	2.16	2.29	2.20	2.08	0.17	0.03	0.68	0.54	0.58	0.46	0.44	0.56	1.77
P_2O_5	0.10 (0)	0.12	0.14	0.16	0.10	0.12	0.10	0.15	0.09	0.01	bdl	1.34	0.01	0.00	0.01	1.13	0.08	0.25
LOI	2.12 (0.02)	0.35	0.33	0.32	0.26	0.15	0.41	0.35	0.61	1.43	-0.09	0.47	0.22	0.28	0.30	0.74	0.35	3.80
Total	99.63	99.17	99.55	100.40	98.97	99.51	99.68	101.50	101.12	100.55	100.71	98.95	99.12	99.55	98.95	99.05	99.49	99.61
Ba (ppm)	740 (14)	654	777	893	931	750	927	889	966	26	9	107	61	67	33	97	139	383
Ce	17 (5)	17	17	17	4	9	6	17	4	4	2	17	5	5	11	22	12	21
Co	7 (5)	7	bdl	12	bdl	bdl	bdl	9	7	103	55	39	60	63	52	38	43	25
Cr	17 (7)	bdl	40	7	bdl	8	bdl	bdl	bdl	1236	1871	40	249	345	731	28	bdl	11
Cu	5 (3)	30	4	11	bdl	6	bdl	10	bdl	bdl	bdl	109	bdl	81	8	225	102	87
Ga	23 (1)	22	23	24	22	23	24	24	23	6	5	21	15	12	17	23	23	22
La	10 (1.6)	9	4	8	7	9	6	10	5	4	2	6	3	bdl	2	6	5	10
Nb	4 (0.8)	4	5	4	4	2	4	4	4	bdl	bdl	bdl	bdl	bdl	2	2	bdl	2
Nd	8 (1.5)	10	9	13	6	8	4	13	9	2	3	13	7	5	9	14	7	14
Ni	bdl	bdl	bdl	bdl	bdl	bdl	bdl	bdl	bdl	414	163	7	89	86	183	bdl	bdl	7
Pb	9 (3)	bdl	8	15	12	12	12	14	12	bdl	bdl	bdl	bdl	bdl	bdl	bdl	bdl	bdl
Rb	49 (1)	38	45	47	49	45	49	44	47	4	3	4	4	4	4	5	4	23
Sc	bdl	bdl	bdl	bdl	bdl	bdl	bdl	bdl	bdl	45	85	36	75	71	63	32	45	29
Sr	1298 (11)	1124	1174	1497	1206	1238	1238	1420	1220	112	52	463	261	193	179	674	667	921
Th	5 (1)	bdl	bdl	7	6	6	bdl	8	6	bdl	bdl	bdl	bdl	bdl	5	5	bdl	bdl
U	bdl	bdl	bdl	bdl	bdl	bdl	bdl	bdl	bdl	bdl	bdl	bdl	bdl	bdl	bdl	bdl	bdl	bdl
V	81 (5)	58	66	55	46	57	52	53	40	130	185	459	572	503	214	430	444	266
Y	9 (1)	8	5	8	7	10	7	8	6	6	6	26	13	11	17	24	15	19
Zn	31 (1)	43	29	38	31	34	32	38	30	76	33	97	52	41	98	74	70	67
Zr	125 (4)	119	134	124	127	124	133	124	128	10	6	31	16	10	19	34	30	73

Table 3.8 contd.

shows an increase from ~1 to ~2.5 wt % with increasing SiO_2. Al_2O_3 shows a weakly defined linear increase as SiO_2 increases from 50–55 wt % SiO_2¸ and plateaus at approximately 18 wt % at higher SiO_2 values. P_2O_5 is relatively constant at 0.18–0.26 for samples with low SiO_2; at SiO_2 >62 wt % phosphorous contents decrease steadily as silica increases.

Major element trends for nodules are more scattered, a feature accounted for by the varied mineralogy and small sample populations. Clinopyroxenite samples (SV159 and SV161) show features – low Al, Ti, Na, K and P; high Fe, Mg and Ca – that reflect the mineralogy being dominated by clinopyroxene, with increased olivine contents in SV159 leading to higher Mg and lower Ca contents.

Hornblendites SV6A, 155 and 175 cluster closely on plots of all major element oxides with the exception of Ti; most likely a reflection of TiO_2 being controlled by magnetite, which is a variable minor phase in these specimens. Notably, the hornblendites are co-linear with main suite samples for the major elements except Al and P. Sample SV181 plots separately from the other hornblendites, with lower SiO_2 and Mg, and significantly higher Ti, Fe and P (as a result of intercumulus apatite). Al, Na, K contents are similar for SV181 and the other hornblendites analysed. The differences between SV181 and the main hornblendite cluster are likely to be due to decreased clinopyroxene (lower Mg and Si) and higher magnetite and apatite (increased Fe and P) in SV181.

Amphibole gabbro nodules are approximately co-linear with the main suite for the elements Al, Ca, Na, K and Fe (vs. SiO_2; Al co-linear for main suite samples with SiO_2 >55 wt %; Fig. 3.10). Magnesium contents are more varied, but as displayed by the hornblendites and clinopyroxenites, Mg is susceptible to large changes as olivine and clinopyroxene abundances vary.

3.3.4 Trace element chemistry

Trace element data are shown in Table 3.8, and Harker variation diagrams are shown in Figure 3.11. In the main suite Ba, Rb, Sr and Zr all increase as SiO_2 increases, whereas Co, Cr, Cu, V, Y and Zn all decrease. Ga increases from 50–55 wt % SiO_2, and remains constant at around 22 ppm at higher SiO_2 contents. Ba and Sr show a weakly bimodal distribution, with a cluster of mugearite and benmoreite samples at lower concentrations, and a trachyte cluster at higher contents. To a certain extent these effects are exaggerated by the small number of benmoreite samples, but the more mafic clusters of data on both

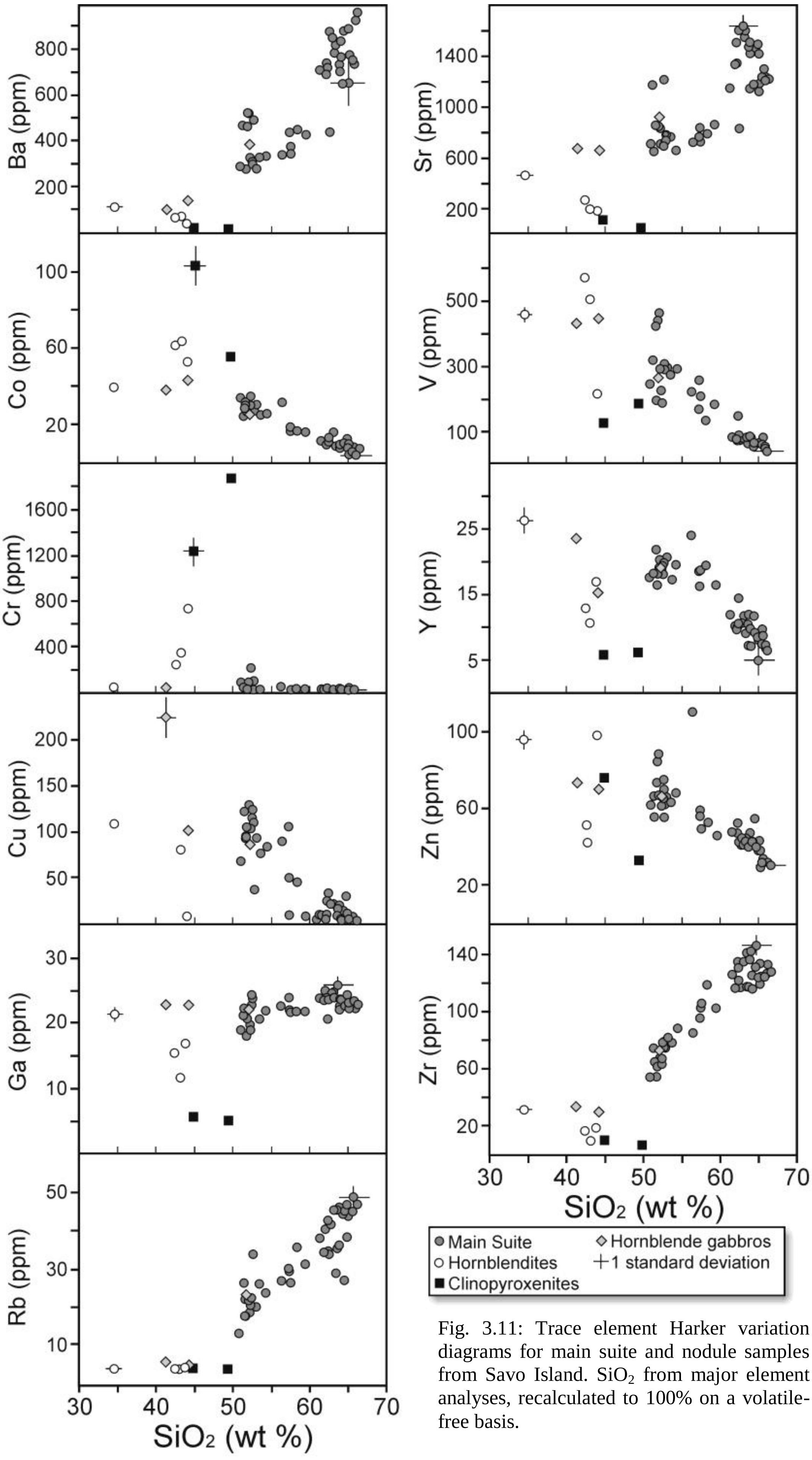

Fig. 3.11: Trace element Harker variation diagrams for main suite and nodule samples from Savo Island. SiO_2 from major element analyses, recalculated to 100% on a volatile-free basis.

the Sr and Ba plots show a plateau rather than a linear increase to the high contents seen in the trachyte samples.

For nodules, Ba, Rb, Sr and Zr are approximately co-linear with the main suite. The compatible elements show significant scatter for the nodules relative to the main suite; Cr in particular shows significant enrichment (relative to the overall trend) in the clinopyroxenites and clinopyroxene-bearing hornblendites (i.e. excluding SV181).

3.3.5 *Rare earth element chemistry*

	SV33	SV19	SV45	SV20	SV1	SV12	SV17	SV40	SV44	SV10	SV39	SV2	SV38	SV181	SV6A
	MUG	MUG	MUG	MUG	MUG	BEN	TRAC	TRAC	TRAC	TRAC	TRAC	TRAC	TRAC	HBLITE	HBLITE
La	10.81	11.02	11.47	7.58	7.85 (0.05)	9.32 (0.50)	10.92	14.12	14.49	9.94	8.87	5.94	9.81	5.56	1.01
Ce	22.9	22.8	22.1	17.0	15.51 (0.16)	19.15 (1.23)	21.1	27.1	28.2	19.4	17.1	11.4	19.4	13.8	4.3
Pr	3.05	2.90	2.80	2.41	2.28 (0.08)	2.50 (0.15)	2.63	3.30	3.34	2.38	2.07	1.26	2.42	2.67	0.97
Nd	14.8	13.1	12.3	11.1	10.59 (0.37)	10.86 (0.85)	10.9	13.1	13.5	10.1	8.7	5.7	10.0	16.3	5.7
Sm	3.37	3.13	2.81	2.73	2.44 (0.11)	2.27 (0.09)	1.96	2.27	2.49	2.05	1.33	1.04	1.69	4.71	1.91
Eu	1.00	1.00	0.88	0.96	0.79 (0.03)	0.74 (0.04)	0.72	0.69	0.69	0.67	0.52	0.37	0.49	1.60	0.64
Gd	3.30	2.77	2.76	2.93	2.37 (0.07)	2.36 (0.14)	1.70	1.84	1.92	1.70	1.24	0.86	1.16	5.65	2.33
Tb	0.45	0.45	0.41	0.46	0.39 (0.01)	0.36 (0.05)	0.25	0.28	0.25	0.28	0.17	0.13	0.19	0.75	0.39
Dy	2.85	2.71	2.56	2.85	2.38 (0.04)	2.25 (0.06)	1.56	1.50	1.53	1.52	0.98	0.84	1.19	4.68	2.34
Ho	0.56	0.58	0.55	0.62	0.51 (0.02)	0.48 (0.06)	0.33	0.33	0.27	0.30	0.19	0.19	0.25	0.96	0.51
Er	1.61	1.87	1.65	1.74	1.43 (0.05)	1.32 (0.10)	0.90	0.83	0.87	0.89	0.71	0.50	0.75	2.80	1.36
Tm	0.22	0.26	0.20	0.26	0.21 (0.01)	0.20 (0.03)	0.14	0.13	0.12	0.15	0.09	0.08	0.11	0.37	0.20
Yb	1.90	1.65	1.52	1.74	1.42 (0.11)	1.45 (0.13)	0.96	1.05	0.95	1.14	0.65	0.63	0.84	2.36	1.23
Lu	0.24	0.24	0.20	0.27	0.20 (0)	0.22 (0.01)	0.16	0.15	0.13	0.17	0.11	0.10	0.12	0.32	0.24

Table 3.9: Rare earth element chemistry for samples from Savo. All values in mg/kg. Samples SV1 and SV12 run in triplicate; values are averages, with one standard deviation in parentheses. Abbreviations and samples locations as in Table 3.8.

Rare earth element chemistry for a subset of the main suite samples is summarised in Table 3.9. All samples are enriched relative to average C1 chondrite (Fig. 3.12). As SiO_2 increases, the REE profiles become steeper due to progressive depletion of the MREE and HREE. The change in slope of the REE profile can be expressed as the increase in La_N/Yb_N and La_N/Dy_N from 3–4 to 6–10 as SiO_2 increases from 50–66 wt %; over the same silica range, Dy_N/Yb_N increases from 2 to 4 (Fig. 3.13). Europium anomalies are absent in most samples, with only trachytes SV2, 17 and 39 showing weak positive anomalies (Eu/Eu^*=1.2, based on the deviation from the geometric mean of Sm_N and Gd_N).

The rare earth profiles for the two hornblendites analysed (SV181 and SV6A) is also shown on Figure 3.12. The two differ in terms of LREE, with SV181 considerably more enriched in La–Nd compared to SV6A. This is

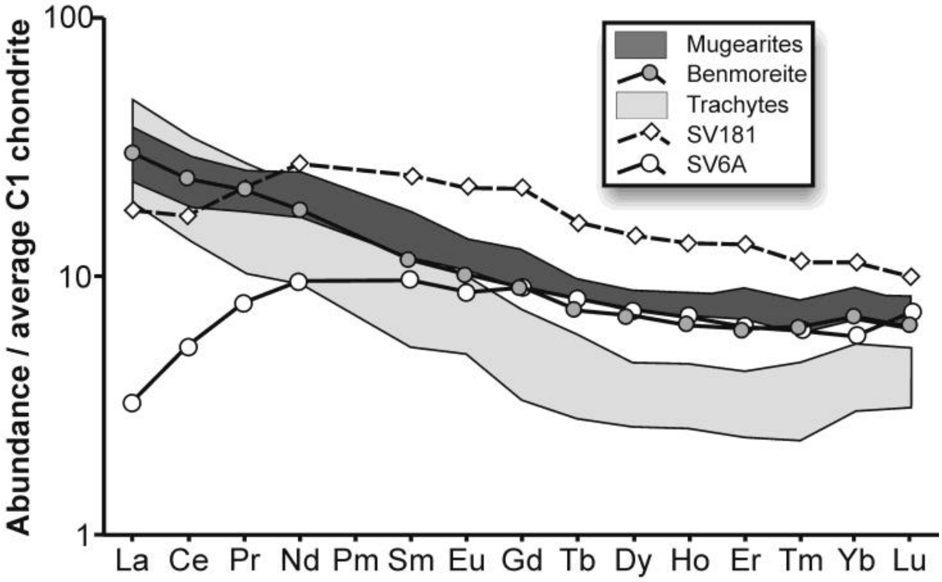

Fig. 3.12: Chondrite-normalised REE plots, for a subset of samples from Savo. Normalising values from Boynton (1984). Hornblendite sample SV181 has a significant quantity of apatite (P_2O_5 >1 wt %) causing LREE enrichment.

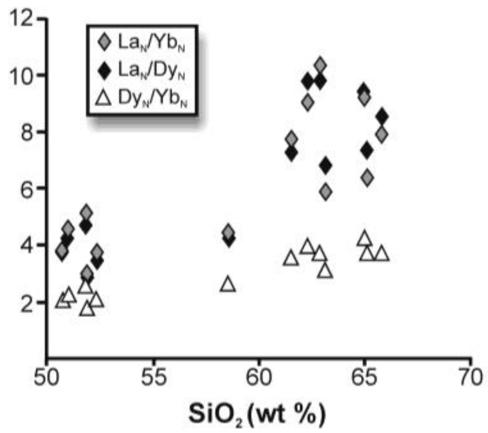

Fig. 3.13: Variation of normalised REE ratios with SiO_2. Shows increase in LREE (La) relative to MREE (Dy) and HREE (Yb) with increasing SiO_2; ratio of MREE to HREE increases less over same interval, indicating predominance of amphibole in the fractionating assemblage. Variation in La due to variable apatite fractionation. Normalising values from Boynton (1984), SiO_2 from major element XRF analysis, recalculated to 100% on a volatile-free basis.

assumed to be a result of high apatite content in SV181, also reflected in the high phosphorous content.

3.3.6 Radiogenic isotopes

Neodymium isotope data are summarised in Table 3.10. There is no observable variation of $^{143}Nd/^{144}Nd$ with increasing SiO_2. Average $^{143}Nd/^{144}Nd$ is 0.512965 with $2\sigma = 0.000022$, which is close to the reproducibility the standard solution ($2\sigma = 0.000012$).

Strontium isotope analysis was performed on leached and unleached samples and the corresponding leachate (Table 3.11). Leachates produced slightly different $^{87}Sr/^{86}Sr$ values to the leached and unleached samples, but in all cases, leached and unleached samples produced results within analytical uncertainty indicating that any alteration was minimal (Fig. 3.14). In the main suite, $^{87}Sr/^{86}Sr$ increases slightly with increasing SiO_2 and total Sr from 0.7040 for mugearites to approximately 0.7042 for trachytes. Sample SV2 yielded significantly higher $^{87}Sr/^{86}Sr$ at 0.7044. The original block from which SV2 was prepared contained an unusual finely crystalline feldspar + amphibole + biotite xenolith; it is highly likely that this nodule represents exotic material rather than a cognate xenolith, and that the higher $^{87}Sr/^{86}Sr$ value of this sample may be a result of metasomatism of the volume of rock surrounding the xenolith.

Lead isotopes show no resolvable variation with increasing whole-rock SiO_2 (Table 3.12). $^{206}Pb/^{204}Pb$ ratios average 18.454 ($1\sigma = 0.012$), $^{207}Pb/^{204}Pb = 15.521$ ($1\sigma = 0.001$), and $^{208}Pb/^{204}Pb = 38.273$

Label	Sample	Nd ppm	$^{143}Nd/^{144}Nd$	± 2SE	εNd
N565:1	SV1	6.820	0.512970	0.000005	6.477644
N565:2	SV2	9.639	0.512977	0.000015	6.614198
N565:3	SV6A	7.752	0.512961	0.000003	6.302075
N565:4	SV12	16.080	0.512972	0.000005	6.51666
N565:5	SV17	10.558	0.512967	0.000013	6.419121
N565:6	SV19	13.383	0.512943	0.000045	5.950937
N565:7	SV20	10.380	0.512978	0.000009	6.633706
N565:8	SV33	14.455	0.512972	0.000003	6.51666
N565:9	SV38	9.180	0.512968	0.000012	6.438629
N565:10	SV10	9.449	0.512961	0.000005	6.302075
N565:11	SV45	12.161	0.512957	0.000010	6.224045
N565:12	SV39	9.054	0.512949	0.000006	6.067983

Table 3.10: Neodymium isotope data for samples from Savo. SE = Standard error.

Batch	Label	Sample	Type	$^{87}Sr/^{86}Sr$	$^{87}Sr/^{86}Sr$ error
N565	1	SV1	U	0.703992	0.000004
N566	1.1	SV1	LA	0.704045	0.000006
N566	1.2	SV1	L	0.703994	0.000004
N565	2	SV2	U	0.704425	0.000006
N566	2.1	SV2	LA	0.704402	0.000006
N566	2.2	SV2	L	0.704431	0.000006
N583	2.3	SV40	L	0.704164	0.000006
N565	3	SV6A	U	0.7042	0.000004
N566	3.1	SV6A	LA	0.704742	0.000008
N566	3.2	SV6A	L	0.704183	0.000004
N565	4	SV12	U	0.704108	0.000004
N566	4.1	SV12	LA	0.704086	0.000008
N566	4.2	SV12	L	0.704116	0.000018
N565	5	SV17	U	0.704188	0.000004
N566	5.1	SV17	LA	0.704313	0.000008
N566	5.2	SV17	L	0.704195	0.000016
N565	6	SV19	U	0.704035	0.000006
N566	6.1	SV19	LA	0.70406	0.000008
N565	7	SV20	U	0.704019	0.00001
N566	7.1	SV20	LA	0.704081	0.00001
N565	8	SV33	U	0.704103	0.000004
N566	8.1	SV33	LA	0.704188	0.000008
N566	9.1	SV38	LA	0.70413	0.000008
N566	9.2	SV38	L	0.704167	0.000012
N565	10	SV10	U	0.704167	0.000012
N566	10.1	SV10	LA	0.704176	0.000008
N566	10.2	SV10	L	0.704195	0.000006
N565	11	SV45	U	0.704028	0.000012
N566	11.1	SV45	LA	0.704082	0.000014
N566	11.2	SV45	L	0.704006	0.000008
N565	12	SV39	U	0.704147	0.000008
N566	12.1	SV39	LA	0.704097	0.000008
N566	12.2	SV39	L	0.704158	0.00001
N565	13	SV44	U	0.704131	0.000006
N566	13.1	SV44	LA	0.704095	0.000008
N566	13.2	SV44	L	0.704125	0.000012

Table 3.11: Strontium isotope data for samples from Savo. U = unleached; LA = leachate; L = leached.

Label	Sample	$^{206}Pb/^{204}Pb$	% 1σ	±1σ abs	$^{207}Pb/^{204}Pb$	% 1σ	±1σ abs	$^{208}Pb/^{204}Pb$	% 1σ	±1σ abs
P412:1	SV1	18.4508	0.0062	0.0011	15.5180	0.0081	0.0013	38.2734	0.0095	0.0036
P412:2	SV10	18.4445	0.0055	0.0010	15.5202	0.0071	0.0011	38.2655	0.0080	0.0030
P412:3	SV12	18.4545	0.0057	0.0011	15.5208	0.0070	0.0011	38.2681	0.0077	0.0029
P412:4	SV17	18.4429	0.0039	0.0007	15.5196	0.0055	0.0009	38.2629	0.0076	0.0029
P412:5	SV19	18.4851	0.0049	0.0009	15.5236	0.0064	0.0010	38.3171	0.0083	0.0032
P412:6	SV20	18.4490	0.0051	0.0009	15.5201	0.0069	0.0011	38.2650	0.0096	0.0037
P412:6 Repeat	SV20	18.4508	0.0040	0.0007	15.5218	0.0054	0.0008	38.2678	0.0073	0.0028
P412:8	SV33	18.4494	0.0042	0.0008	15.5210	0.0059	0.0009	38.2694	0.0080	0.0031
P412:9	SV38	18.4612	0.0045	0.0008	15.5218	0.0062	0.0010	38.2767	0.0081	0.0031
P412:10	SV39	18.4612	0.0041	0.0008	15.5207	0.0057	0.0009	38.2688	0.0076	0.0029
P412:11	SV44	18.4489	0.0053	0.0010	15.5195	0.0072	0.0011	38.2679	0.0097	0.0037
P412:18	JB1	18.3805	0.0054	0.0010	15.5628	0.0072	0.0011	38.6968	0.0094	0.0036

Table 3.12: Whole rock lead isotope data for samples from Savo.

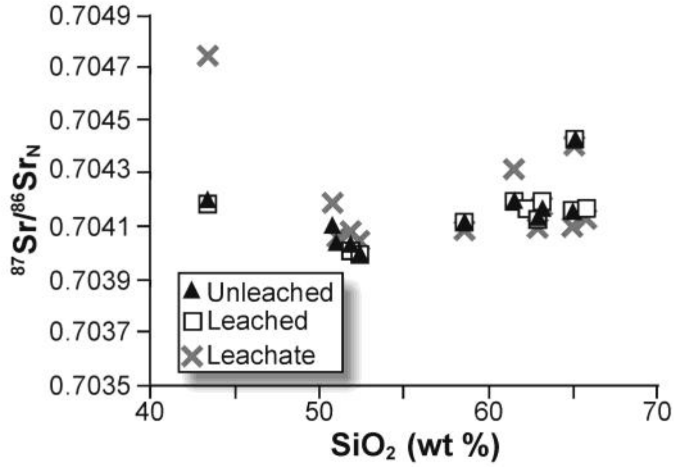

Fig. 3.14: $^{87}Sr/^{86}Sr$ for samples from Savo. Leached and unleached samples are generally within error, indicating minimal alteration. Outlier SV2 contains xenolith of exotic origin, possibly metasedimentary. Error (2σ) within point size.

(1σ = 0.015). Lead isotope ratios are similar to those determined by König et al. (2007) for volcanic samples from the western Solomon Islands.

3.4 Discussion

3.4.1 Crystal fractionation models for Savo

Crystal fractionation is one of the most important mechanisms for deriving felsic magmatic rocks from parental basalts in arc terrains (Gill, 1981). The presence of cumulates such as the hornblendites and clinopyroxenites is consistent with a crystal fractionation process at Savo. Least-squares modelling was used to investigate this process at Savo (Table 3.13). Modelling was performed over three steps, to account for changes in mineralogy observed in the main suite samples. All main suite samples from Savo are phenocryst rich, and as such are unlikely to represent liquid compositions. Whole rock and mineral chemistries were recalculated to 100 wt % on an anhydrous basis with Fe_T as Fe_2O_3. P_2O_5 (and apatite) was not used in the modelling. Mineral data were based on average values from all samples for clinopyroxene, olivine, biotite and magnetite; feldspar compositions used a nodule average (An_{78}) over the interval 52–57 wt % SiO_2 and a mugearite average (An_{68}) for the interval 57–65 wt %; amphibole composition was averaged from nodule data.

Model 1 uses all available minerals observed in the main suite samples for the relevant SiO_2 interval; relative abundances of minerals and total amount of melt extracted are calculated to minimise residuals. Model 1 closely reproduces the observed major element trends in the main suite, with the exception of TiO_2 (Fig. 3.10). However, TiO_2 is controlled mostly by magnetite fractionation, and therefore the model is sensitive to its abundance in that mineral; as discussed in section 3.3.1 the magnetite crystals may have been subject to subsolidus oxidation thus limiting the reliability of data obtained from them.

	Plag (xen. avg.)	CPX avg.	Olivine avg.	Oxide avg.	Total extracted (%)	Parent SV362	Daughter SV20	Daughter Model 1	Residue Model 1	Daughter Model 2	Residue Model 2
SiO_2	48.64	51.36	37.47	0.07		52.20	53.55	53.54	44.18	53.48	42.99
TiO_2	0.01	0.37	0.00	4.01		0.86	0.78	0.89	0.47	0.82	0.75
Al_2O_3	32.45	2.92	0.01	1.86		17.20	17.98	17.97	12.58	18.17	2.33
Fe_2O_3	0.33	7.35	23.01	91.20		9.70	9.04	9.02	13.98	9.04	19.91
MnO	0.01	0.24	0.44	1.09		0.14	0.13	0.12	0.26	0.12	0.37
MgO	0.00	15.32	38.86	1.71		5.04	3.80	3.79	12.80	3.72	17.47
CaO	16.05	22.01	0.14	0.03		9.13	8.25	8.23	14.68	8.45	15.86
Na_2O	2.40	0.41	0.05	0.03		3.91	4.46	4.34	1.01	4.18	0.31
K_2O	0.10	0.02	0.01	0.01		1.59	1.77	1.82	0.04	1.75	0.02
Proportion (%):											
Model 1	34.6	41.4	16.3	7.8	14.0			Σr^2 =0.04			
Model 2		72.0	16.0	12.0	7.99					Σr^2 =0.80	

	Plag (xen. avg.)	CPX avg.	Amph. (xen. avg.)	Oxide avg.	Total extracted (%)	Parent SV20	Daughter SV11	Daughter Model 1	Residue Model 1	Daughter Model 2	Residue Model 2
SiO_2	48.64	51.36	43.07	0.07		53.55	57.44	57.29	40.97	56.44	38.30
TiO_2	0.01	0.37	1.22	4.01		0.78	0.68	0.70	1.04	0.64	1.53
Al_2O_3	32.45	2.92	12.83	1.86		17.98	17.98	17.87	18.35	19.19	11.62
Fe_2O_3	0.33	7.35	13.95	91.20		9.04	6.85	6.74	16.79	6.50	22.51
MnO	0.01	0.24	0.25	1.09		0.13	0.11	0.10	0.25	0.10	0.34
MgO	0.00	15.32	13.49	1.71		3.80	2.84	2.72	7.44	2.22	12.19
CaO	16.05	22.01	11.91	0.03		8.25	6.94	6.95	12.64	7.81	10.59
Na_2O	2.40	0.41	2.59	0.03		4.46	5.06	5.15	2.15	4.87	2.31
K_2O	0.10	0.02	0.68	0.01		1.77	1.90	2.19	0.37	1.99	0.60
Proportion (%):											
Model 1	36.4	4.7	48.4	10.5	22.9			Σr^2 =0.15			
Model 2			88.9	11.1	15.9					Σr^2 =3.79	

	Plag (mug. avg.)	CPX avg.	Amph. (xen. avg.)	Bio. avg.	Oxide avg.	Total extracted (%)	Parent SV11	Daughter SV38	Daughter Model 1	Residue Model 1	Daughter Model 2	Residue Model 2
SiO_2	50.84	51.36	43.07	39.71	0.07		57.44	65.01	65.01	44.50	63.73	40.27
TiO_2	0.03	0.37	1.22	3.20	4.01		0.68	0.33	0.57	0.85	0.41	1.14
Al_2O_3	30.37	2.92	12.83	14.56	1.86		17.98	18.19	18.08	17.79	20.12	12.12
Fe_2O_3	0.75	7.35	13.95	16.21	91.20		6.85	2.80	2.76	13.84	2.41	18.97
MnO	0.02	0.24	0.25	0.37	1.09		0.11	0.07	0.04	0.23	0.04	0.30
MgO	0.09	15.32	13.49	15.77	1.71		2.84	1.14	0.88	6.19	-0.78	12.73
CaO	14.19	22.01	11.91	0.46	0.03		6.94	2.95	3.00	13.67	5.40	11.14
Na_2O	3.48	0.41	2.59	1.03	0.03		5.06	7.19	6.86	1.98	6.02	2.42
K_2O	0.23	0.02	0.68	8.69	0.01		1.90	2.18	2.46	0.94	2.36	0.64
Proportion (%):												
Model 1	50.6	29.3		9.4	10.7	36.9			Σr^2 =0.34			
Model 2			93.5		6.5	26.8					Σr^2 =16.7	

Table 3.13: Summary of major element least squares fractionation models.

The solids extracted in Model 1 can be compared to analysed nodules (Fig. 3.10). For the earliest SiO_2 interval (52.2–53.6 wt %), the residual solids are olivine-clinopyroxene gabbros, similar in bulk chemical composition to the nodule sample SV6A (but dissimilar in terms of observed mineralogy; SV6A is a hornblendite); the residual solids from the higher SiO_2 intervals are hornblende gabbros, similar in composition and predicted mineralogy to the hornblende gabbro cumulates SV59 and SV350.

Sr	**SV362–SV20**	**SV20–SV11**	**SV11–SV38**
Fspr	1.83	1.80	2.84
Ol	0.01	0.01	0.00
Bio	0	0	0.45
FeOx	0.00	0.01	0.00
Cpx	0.06	0.08	0.52
Hbl	0.46	0.46	0.02
Model 1			
Bulk K_D	0.66	0.88	1.63
Initial Sr	827	871	898
Daughter Sr	871	898	671
Model 2			
Bulk K_D	0.05	0.41	0.02
Initial Sr	827	896	992
Daughter Sr	896	992	1347

Zr	**SV362–SV20**	**SV20–SV11**	**SV11–SV38**
Fspr	0.0	0.013	0.135
Ol	0.012	0.01	0
Bio	0	0	1.197
FeOx	0.1	0.2	0.8
Cpx	0.1	0.162	0.6
Hbl	0.5	0.5	0.31
Model 1			
Bulk K_D	0.07	0.28	0.39
Initial Zr	67	77	93
Daughter Zr	77	93	123
Model 2			
Bulk KD	0.09	0.47	0.34
Initial Zr	67	72	79
Daughter Zr	72	79	97

Table 3.14: Trace element modelling results for Sr and Zr variation with least squares fractionation Model 1 and Model 2. Uses Rayleigh fractionation equations and K_D values from Rollinson (1993). Initial Sr and Zr values from model starting composition SV362.

The behaviour of Sr and Zr in Model 1 was determined using Rayleigh fractionation equations and trace element distribution coefficients collected in Rollinson (1993), summarised in Table 3.14. Stanton (1994) calculated K_D values for Sr for various minerals in Solomon Islands lava sequences, including “hornblende andesites” of Savo (trachytes), that are similar to those used in this study. Stanton (1994) does not provide data for samples analogous to mugearites analysed in this study.

Model 1 closely reproduces the Zr enrichment observed in the main suite samples, but fails to reproduce the high Sr contents of the trachytes (Fig. 3.15). The first two stages of Model 1 (52.2–57.44 wt % SiO_2) show relatively flat enrichment trends in Sr, similar to the observed mugearite and benmoreite data. Model 1 predicts decreasing Sr contents in the more felsic samples, rather than the observed enrichment. This is a function of plagioclase fractionation, as Sr behaves compatibly with feldspar minerals (K_D >1).

In the absence of any obvious indicators of assimilation (Fig. 3.16), the progressive enrichment of Sr with increasing fractionation (i.e. SiO_2, Zr) dictates that the element is behaving incompatibly with respect to the bulk mineralogy of extracted solids. Therefore, the involvement of plagioclase must be limited, and Model 1 clearly removes too much

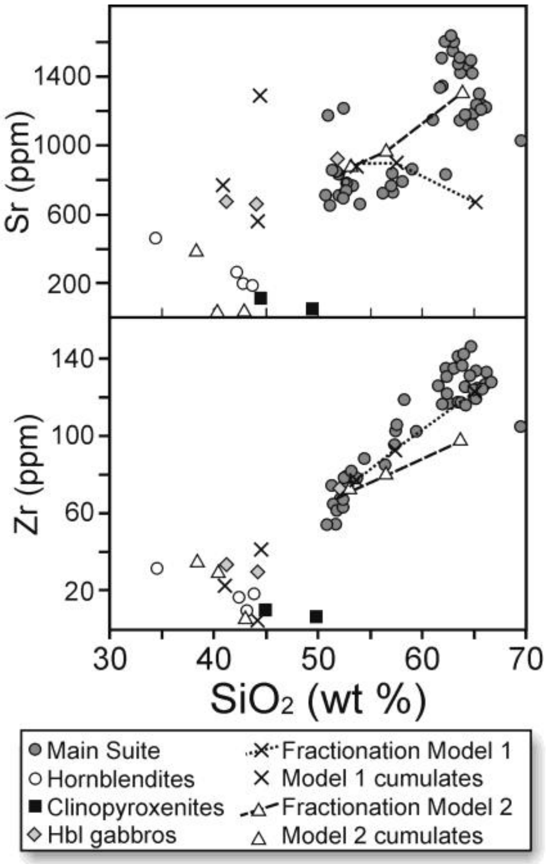

Fig. 3.15: Trace element variations determined by Rayleigh fractionation equations (Rollinson, 1993), based on least-squares fractionation modelling, compared to observed variations. K_D values from Rollinson (1993) and summarised in Table 3.14.

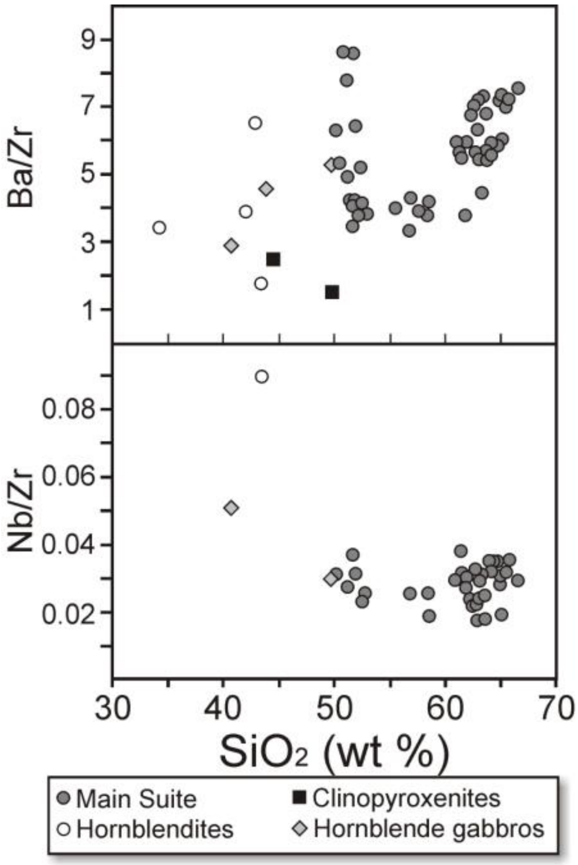

Fig. 3.16: Plot of trace element ratios Ba/Zr and Nb/Zr vs. SiO2. The suite shows no systematic variation, limiting possible contributions by the assimilation of compositionally distinct crustal material.

plagioclase to account for the Sr enrichment observed in the trachytes (Fig. 3.15). In addition, the paucity of highly calcic (>An_{50}) plagioclase in the trachytes (Fig. 3.5) and only slight increase in the modal abundance of feldspar with increasing SiO_2 (Fig. 3.4) suggests that accumulation of feldspar crystals is not responsible for the increasing Sr contents.

Model 2 uses the same rock and mineral compositions as Model 1, but this time plagioclase was excluded from the modelled minerals. The residuals are significantly larger than those of Model 1, and are driven primarily by Al_2O_3 being higher in the modelled values relative to the analysed samples (Fig. 3.10). Residual solids correspond to the clinopyroxenites for the first SiO_2 interval (with differences in MgO and CaO controlled by variation in olivine content, as discussed in section 3.3.3), and to the range of values displayed by the hornblendite samples for the high SiO_2 intervals. Modelling cannot adequately account for variation in amphibole chemistry (Fe, Mg, Al), which contributes to higher residuals.

Trace element characteristics of Model 2 are more effective at reproducing the Sr enrichments seen in the trachyte samples (Fig. 3.15); Zr estimates are low in Model 2, reflecting smaller proportions of melt being extracted than compared to Model 1.

For extensive amphibole fractionation without apatite, as in Model 2, the ratios La_N/Yb_N and La_N/Dy_N should increase with SiO_2, whereas Dy_N/Yb_N should remain constant. At Savo, La_N/Yb_N and La_N/Dy_N do increase (due to amphibole fractionation); Dy_N/Yb_N increases much less over the corresponding SiO_2 range (Fig. 3.13).

Model 2 does not take into account plagioclase in the fractionation (the fractionating amount is set to 0 for all intervals). The presence of small amounts of feldspar in the cumulate samples dictates that this is not a valid assumption, as does the failure of Model 2 to account for the Al_2O_3 plateau (Fig. 3.10) and Zr enrichment (Fig. 3.15). In reality, the system probably fractionates small amounts of plagioclase and felsic melt (trapped as intercumulate liquid), although the amount removed must be less than that determined by Model 1 to account for the Sr enrichment observed in the trachytes. A further refinement of Model 2 may be to adjust the Al contents of amphibole, which contains increasing Al at higher temperature and pressure (Hammarstrom and Zen, 1986).

The overlap between observed nodules and those predicted by the mass balance of both fractionation models suggests that both fractionation schemes may operate, under slightly different conditions. Model 2 fractionation is appropriate for the lowest SiO_2 interval, given the presence of plagioclase-free clinopyroxene (+ olivine) nodules and low residual error of that particular mass balance. At higher SiO_2 intervals, different fractionation models are appropriate: mugearites and benmoreites develop by the fractionation of plagioclase + amphibole + clinopyroxene + magnetite (Model 1); and trachytes have developed by amphibole + magnetite removal, with relatively minor amounts of plagioclase extracted (Model 2). All compositions can be derived from a more mafic parent, such as a hawaiite; the overlap of mineral chemistry between trachytes and mugearites suggests a common origin, and differing fractionation histories.

Phosphorous was not included in the fractionation models, but the high P_2O_5 contents of some of the cumulate samples indicate that apatite fractionation has occurred, and apatite may play an important role in LREE variation. Comparison of REE profiles for SV181 (P_2O_5 >1 wt %) and SV6A (P_2O_5 <0.05 wt %) shows that the presence of apatite offsets the REE effects of amphibole removal, in that apatite extracts large amounts of LREE whereas amphibole removes MREE and HREE. Apatite removal and/or accumulation may account for the variation seen in La_N/Yb_N and La_N/Dy_N (Fig. 3.13).

3.4.2 The role of water in petrogenesis at Savo

Water plays a key role in island arc magmatism, including the initiation of partial melting (e.g. Gill, 1981; Plank and Langmuir, 1988; Pearce and Peate, 1995), influencing magma chemistry (Pearce, 1982); melt viscosity (Lange, 1994); crystallisation (Sisson and Layne, 1993); mineralogy (Sisson and Grove, 1993); volcanic eruptions (Roggensack et al., 1997); and ore genesis (Henley and McNabb, 1978). A number of petrological and geochemical features point to high pre-eruptive water contents in the magmas at Savo – high concentrations of fluid-mobile elements (Sr, Ba, Rb) in mafic samples are consistent with melt generation from hydrated mantle (Fig. 3.17; Pearce, 1982), and the presence of the hydrous minerals amphibole and biotite requires high water contents (>3 wt %) in the crystallising magmas (Gill, 1981; Sisson and Grove, 1993; Moore and Carmichael, 1998; Barclay and Carmichael, 2004).

Pre-eruptive conditions (temperature, pressure, pH_2O) are difficult to determine with any specificity due to the mineralogy (e.g. one pyroxene, no ilmenite) and degree of crystallinity (leading to a lack of homogeneous glass representative of liquid/melt). However, numerous experiments have been undertaken on arc basalts and the generalities of those experiments should apply to Savo.

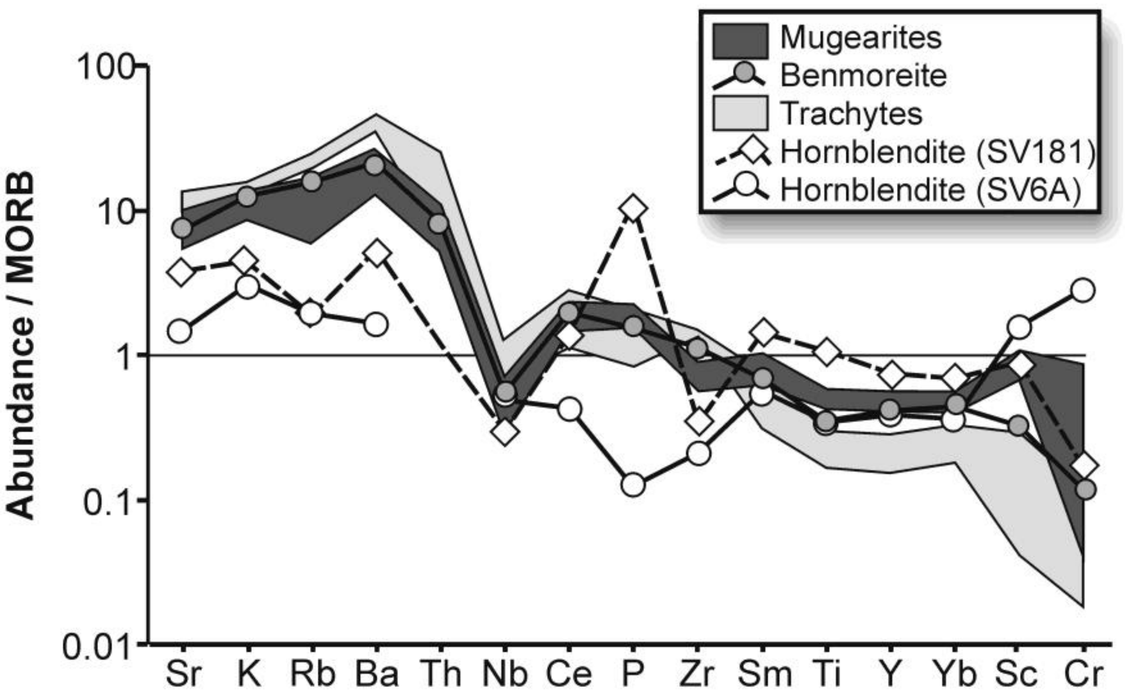

Fig. 3.17: MORB-normalised multi-element variation diagrams for samples from Savo, showing typical island arc trends. Normalising values from Pearce (1982).

High water contents in basaltic melts have the effect of destabilising silicate minerals, plagioclase in particular, relative to oxides (Gill, 1981; Gaetani et al., 1993; Sisson and Grove, 1993). Plagioclase is suppressed at high water contents, and occurs as a liquidus phase at lower temperatures and pressures in hydrous basalts than it does in anhydrous equivalents (Gaetani et al., 1993). Oxides are affected much less than silicates by high water contents. Thus, arc basalts typically fractionate assemblages (in order of appearance, rather than abundance) of magnetite > olivine > clinopyroxene > plagioclase (Sisson and Grove, 1993). High fO_2 (the presence of anhydrite in SV40 indicates $fO_2 \geq$ NNO+1; Carroll and Rutherford, 1987) would also stabilise oxide phases relative to silicates.

Amphibole is a stable mineral phase at temperatures below 1000°C and water contents >3 wt %; higher water contents are needed to stabilise it as a liquidus phase (Gill, 1981). Experiments by Sisson and Grove (1993) showed that amphibole stability is also controlled by the sodium content of magma. Melt experiments on basaltic andesite with 6 wt % H_2O did not produce amphibole as a liquidus phase; however, addition of NaOH sufficient to make the basaltic andesite Ne-normative produced abundant pargasitic hornblende as a stable liquidus phase at temperatures below 1000°C.

Differentiation at Savo is consistent with fractionation of hydrous, sodic basalt (hawaiite); at high temperatures, magnetite, clinopyroxene and olivine are liquidus phases, and fractionate extensively; at lower temperatures amphibole (pargasite) becomes stable, and drives the differentiation. Differences between the more mafic end of the suite (mugearites and benmoreites) and the felsic (trachytes) develop during lower temperature and/or pressure differentiation, following the common stage of clinopyroxene + olivine + magnetite fractionation.

As outlined in section 3.4.1, trachytes develop by Model 2-type fractionation. Plagioclase is limited to a subliquidus phase by high water contents, and plays little role in driving the major chemical trends (i.e. Al_2O_3 static, Sr increases), until the magma is at low enough pressures to reach water saturation. When the magma becomes water saturated, aqueous fluids are discharged, and the melt undergoes a period of rapid crystallisation (with little differentiation). Limited fractionation of plagioclase results in high whole rock Sr; crystallising feldspars have high initial Sr, decreasing rapidly with continued crystallisation (Fig. 3.18). The degree of crystallinity dictates the eruptability of the magma (Barclay and Carmichael, 2004); it may be that significant volumes of melt are “frozen” in the crust as hypabyssal intrusions as a result of rapid water loss and concomitant rapid crystallisation.

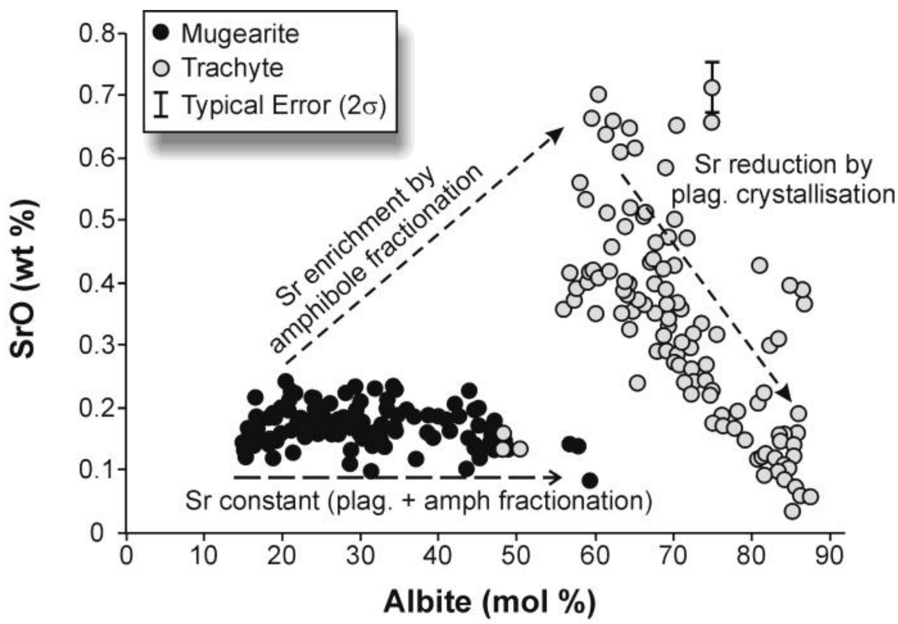

Fig. 3.18: Behaviour of SrO with increasing Na (mole % albite) in feldspar for a subset of electron probe microanalyses. Mugearite plagioclase has constant SrO with an increasing albite component, reflecting behaviour of Sr in the liquid (c.f. Fig. 3.15); trachyte has high initial SrO due to lack of plagioclase fractionation, decreasing rapidly with crystallisation and increasing albite. Whole rock Sr does not decrease with trachyte crystallisation, as plagioclase fractionation is minor.

Model 1 fractionation is consistent with a lower H_2O than Model 2, with plagioclase a more abundant fractionating phase. Lower H_2O could be a result of either lower total pressure or lower water contents of the magma, but without independent estimates of those parameters it is not possible to determine which (if either) is the major control on differing fractionation schemes. The presence of amphibole in both mugearites and trachytes dictates that both magmas have minimum 3 wt % H_2O (Sisson and Grove, 1993). Thus assuming 3 wt % as a common minimum water content, the lower solubility of water in the mugearitic magmas (Fig. 3.19) dictates that H_2O will be equal to or lower than for trachytic magma at a given depth (total pressure). As a consequence, plagioclase is capable of crystallising earlier from mugearitic magma, and will play a more important role in driving chemical trends.

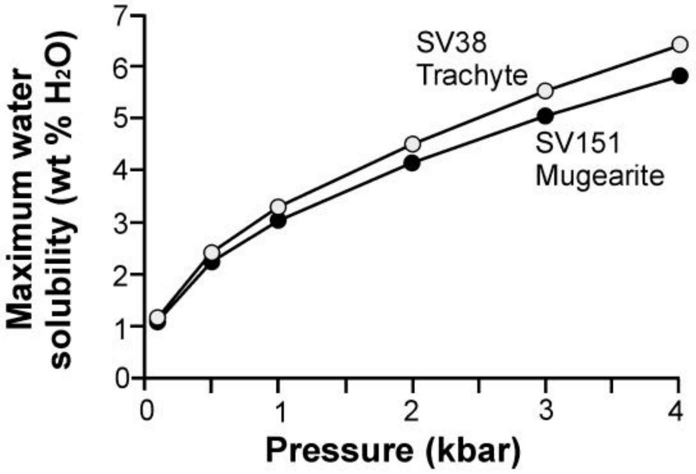

Fig. 3.19: Maximum idealised water solubility with pressure for different melt compositions. SV151 is a mugearite (SiO_2 = 50 wt %); and SV38 a trachyte (66 wt %). Water solubility calculated by the Burnham Model (Burnham, 1994), using temperatures of 1000°C for both compositions. Mafic compositions have lower maximum water contents than the more felsic samples; this results in increased plagioclase stability in the mugearites.

In the "hot zone" model of Annen et al. (2006), parental magmas undergo significant amounts of differentiation in lower crustal intrusions, with periodic release of fractionated daughter magmas into shallow chambers. To apply this model to compositions at Savo, trachytes have fractionated clinopyroxene, olivine and amphibole extensively in deeper intrusions, then evolved magmas ascend to shallow chambers where plagioclase is "frozen in" by rapid crystallisation as the pressure and water solubility drops; mugearites have undergone significantly less deep fractionation, and their chemistry is influenced to a greater extent in the shallow crust, chiefly by plagioclase and amphibole crystallisation and fractionation.

3.4.3 Adakitic compositions at Savo

The felsic samples at Savo show a number of geochemical characteristics in common with adakites – andesitic (and more evolved) magmas derived by partial melting of subducted oceanic crust (Defant and Drummond, 1990), rather than the partial melting of hydrated asthenospheric mantle more commonly invoked for subduction zone magmatism (Gill, 1981; Plank and Langmuir, 1988; Pearce and Peate, 1995; Poli and Schmidt, 2002). Defant and Drummond (1990) defined adakites on the basis of major and trace element characteristics, and $^{87}Sr/^{86}Sr$ ratios; this definition has since been modified by a number of researchers (see Castillo, 2006; Richards and Kerrich, 2007 and references therein). The trachytes and benmoreites of Savo fulfil many of these criteria (Table 3.15).

Parameter	Defant and Drummond (1990)	Richards and Kerrich (2007)	Savo Main Suite benmoreites and trachytes Only	Savo Main Suite
SiO_2 (wt %)	≥ 56	≥ 56	≥ 56	**≥ 50**
Al_2O_3 (wt %)	≥ 15	≥ 15	≥ 15	≥ 15
MgO (wt %)	Usually < 3, rarely > 6	Usually < 3	≤ 2.85	**≤ 6.88**
Mg #		~0.5	0.19–0.32	0.19–0.39
Na_2O (wt %)		≥ 3.5	≥ 4.82	≥ 3.61
K_2O (wt %)		≤ 3	≤ 2.55	≤ 2.55
K_2O/Na_2O		~0.42	0.26–0.42	0.26–0.46
Rb (ppm)		≤ 65	≤ 49	≤ 49
Sr (ppm)	≥ 400	≥ 400	≥ 732	≥ 654
Y (ppm)	≤ 18	≤ 18	**≤ 19**	**≤ 24**
Yb (ppm)	≤ 1.9	≤ 1.9	≤ 1.5	≤ 1.9
Ni (ppm)		≥ 20	**≤ 13**	**≤ 13**
Cr (ppm)		≥ 30	**5.3–40.4**	**5.3–214**
Sr/Y		≥ 20	≥ 39.5	≥ 29.9
La/Yb		≥ 20	**6.6–16.2**	**6.6–16.2**
$^{87}Sr/^{86}Sr$	≤ 0.7040	≤ 0.7045	0.7040–0.7044	0.7040–0.7044
Age of subducted oceanic crust	≤ 25 m.y.	≤ 25 m.y.	≤ 5 m.y.	≤ 5 m.y.

Table 3.15: Summary of adakite characterisitcs of Defant and Drummond (1990) and Richards and Kerrich (2007), with characteristics of trachytes and benmoreites, and all Main Suite samples from Savo shown for comparison. Data in bold fail to meet the criteria for adakites.

Adakite genesis occurs under a number of specific conditions: the subduction of young (<25 m.y.) oceanic crust, sufficiently hot to melt during subduction (Defant and Drummond, 1990; Peacock et al., 1994); the subduction of a spreading ridge, leading to the development of slab windows, "mantle blowtorch" melting and thermal erosion of the subducted slab (Marshak and Karig, 1977; DeLong et al., 1979; Thorkelson and Breitsprecher, 2005); the flattening of the subducting slab (Gutscher et al., 2000); and the heating of a stalled slab (Mungall, 2002). The subduction of both young oceanic crust and a spreading centre occurs at the South Solomon Trench System (Cooper and Taylor, 1987; Taylor and Exon, 1987); moreover, previous studies in the Solomon Islands have concluded that slab window formation occurs in the western part of the arc (see Section 2.3.2.1), and plays a crucial role in petrogenesis there – including the generation of adakitic and related melts (e.g. high-Mg andesite; König et al., 2007). In addition to the South Solomon Trench System conditions, the North Solomon Trench System is a stalled subduction zone, and the recovery of mantle geotherms may have generated adakitic melts beneath Papua New Guinea, to the northwest (Fig. 2.1; Kamenov et al., 2008).

Given the favourable conditions for adakite genesis at the Solomon arc, coupled with prior reports of adakitic magmas in the region, it is therefore important to examine in detail the adakitic characteristics of the samples from Savo, as well as the evolution of those characteristics across the suite. Table 3.15 compares data from the main suite at Savo, compared to the geochemical characteristics of adakites. The benmoreites and trachytes at Savo satisfy nearly all criteria, with notable exceptions being La/Yb, and Ni and Cr contents.

A number of studies have shown that the geochemical signatures of adakite magmas are non-unique, and may develop by a range of processes without requiring melt to originate from subducted oceanic crust. Such processes include partial melting of lower crustal garnet amphibolite (Yumul et al., 2000; Hou et al., 2004), interaction between asthenospheric melts and lower crust (Feeley and Hacker, 1995; Streck et al., 2007), partial melting of amphibole-bearing lithospheric mantle (Saunders et al., 1987), and fractional crystallisation, from a basaltic melt, of minerals such as hornblende that preferentially remove Y and Yb over La and Sr (Castillo et al., 1999; Dreher et al., 2005; Macpherson et al., 2006; Rodriguez et al., 2007).

Already the importance of amphibole fractionation has been demonstrated at Savo, particularly for trachyte compositions, and the late crystallisation of plagioclase further emphasises the high Sr/Y value of the magma as Sr behaves as an incompatible element on plots of whole rock geochemistry. The most likely explanation for the "adakitic signatures" at Savo is that initially Sr-rich, hydrous arc basalt/ hawaiite magmas fractionate an amphibole dominated assemblage, resulting in increasing La/Yb, and Sr/Y (Fig. 3.20).

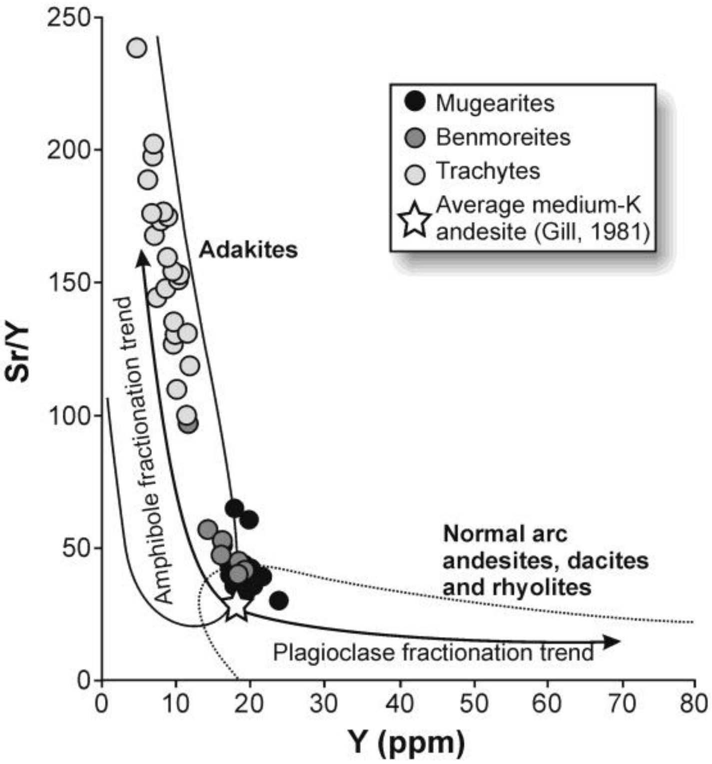

Fig. 3.20: Plot shows increasing Sr/Y and decreasing Y with continued fractionation (mugearite – benmoreite – trachyte). Amphibole-dominant fractionation, particularly for the trachytes, leads to adakite like Sr/Y values. Adakite fields from Richards and Kerrich (2007), typical arc andesite from Gill (1981).

3.4.4 Sodic magmas at Savo

Sodic magmas are unusual occurrences in arcs, although they may be generated by a number of mechanisms, including partial melting of subducted slabs (generating adakites, as discussed above); partial melting of underplated basaltic crust (Atherton and Petford, 1993); assimilation of basaltic lower crustal material (Feeley and Hacker, 1995); partial melting of mantle metasomatised by aqueous fluids (McInnes and Cameron, 1994; Kamenov et al., 2008) and/or melts from subducted slabs (Kepezhinskas et al., 1995); and small degrees of partial melting of the mantle in truncated melt columns (Plank and Langmuir, 1988; Hole and Saunders, 1996).

Models involving extensive interaction with crustal material are unlikely at Savo. Radiogenic isotope data preclude the involvement of compositionally (or temporally) distinct material (Fig. 3.14), and crustal thickness beneath Savo (approximately 14 km; Petterson et al., 2003) is much thinner than in those examples that conclude extensive crustal interaction (Atherton and Petford, 1993; Feeley and Hacker, 1995).

DeLong et al. (1975) compiled data for sodic magmas in intra-oceanic arcs and observed that they occurred in a number of specific tectonic settings: 1) near lateral edges of subduction zones where hinge faulting is occurring (Bering, Fiji, Grenada) and 2) where fracture zones and ridges are being subuducted at a high angle (Kanaga, Aoba and Ambrym, New Georgia, Iwo-jima). DeLong et al. (1975) suggested that the subduction of these linear features provides pathways for magmas from regions beneath or within the subducted lithosphere, an idea further developed into a model of slab window development (DeLong et al., 1979; Thorkelson and Breitsprecher, 2005). Thorkelson and Breitsprecher (2005) predicted that melts above such a slab window would likely be adakitic, due to thermal erosion of the slab window margins during mantle upwelling. The slab window model is viable for the Solomon Arc, and explains a number of features in the western portion of the arc, including forearc volcanism (Johnson et al., 1987), island arc picrites (Schuth et al., 2004), and volcanism on the down-going slab (König et al., 2007).

Melts and aqueous fluids from subducted slabs can enrich the mantle by metasomatism (Kepezhinskas et al., 1995; Pearce and Peate, 1995; Rapp et al., 1999; Gregoire et al., 2001; McInnes et al., 2001). At low melt: rock ratios, slab melts enrich the mantle wedge with adakitic components (Na, Al, Si, Sr, La) rather than ascending to the surface as pristine adakites or mantle-hybridised high magnesian andesites (HMAs; Kepezhinskas et al., 1995; Rapp et al., 1999). Given the presence of HMAs in the western Solomon Islands, as well as the favourable tectonic setting for partial melting of the subducted slab, this is an appealing agent for enriching mantle-derived melts with Na at Savo.

Enrichment of the mantle has occurred further west in the Tabar–Lihir–Tanga–Feni (TLTF) island arc of Papua New Guinea, where alkaline eruptive suites commonly contain mantle xenoliths that indicate widespread metasomatism beneath the arc (McInnes and Cameron, 1994; Gregoire et al., 2001; Kamenov et al., 2008). Various interpretations have been made of the origin of the metasomatism in this region, including partial melting of subducted crust as the geotherms recover at the stalled slab, resulting in adakite genesis (Kamenov et al., 2008). However, other studies have concluded that the metasomatic agent was a hydrous fluid (Gregoire et al., 2001). Under high pressure and temperature conditions (1250°C, 15–25 kb), aqueous fluids derived from a dehydrating slab are capable of carrying significant volumes of fluid mobile elements. Under such conditions, aqueous fluids and silicate melts may be entirely miscible, and would have similar solvent properties (Ayers and Eggler, 1995; Bureau and Keppler, 1999). It therefore makes it difficult to discriminate between slab melt and hydrous metasomatism on the basis of trace and major elements alone.

Radiogenic isotopes from Savo provide little conclusive evidence for slab melts vs. hydrous metasomatism. Due to the subduction reversal, the Indo-Australian slab is subducting into Indo-Australian mantle domain, i.e. the SSTS defines the current limit of the Indo-Australian Plate, but not the limit of its mantle isotope signature. As a result, $^{87}Sr/^{86}Sr$ and $^{143}Nd/^{144}Nd$ data from Savo show Indo-Australian affinity, and they would be expected to regardless of whether they were partial melts of the Indo-Australian slab or hydrated mantle melts. The Indo-Australian signature of Sr–Nd (Fig. 3.21) and $^{208}Pb/^{204}Pb$ (Fig. 3.22) would appear to rule out major contributions of Pacific slab melt as a metasomatic agent, but hydrous metasomatism cannot be ruled out; in fact the presence of arc-like Ba and Sr enrichments in basalts erupted in the Woodlark Basin suggests that the Pacific slab has a "hydrous footprint" that extends a considerable distance south of the arc (Perfit et al., 1987; Woodhead et al., 1998).

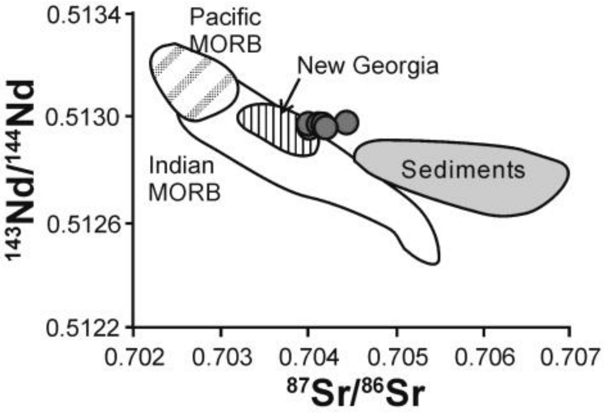

Fig. 3.21: Sr–Nd diagram for samples from Savo. Fields for Pacific and Indo-Australian MORB from Hofmann (1997), New Georgia field from Schuth et al. (2004), and sediments field from König et al. (2007). Error within point size.

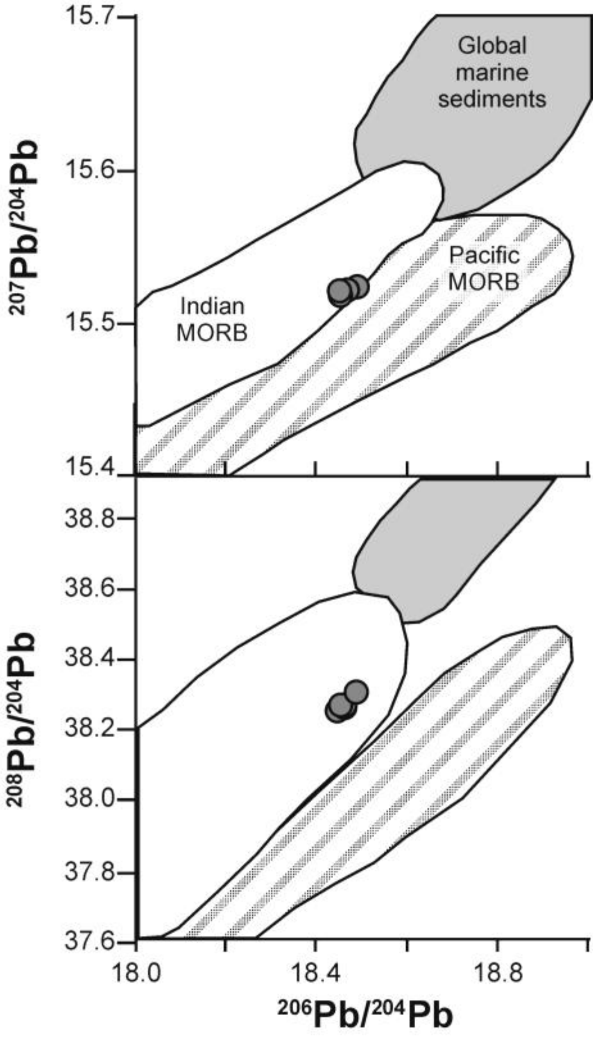

Fig. 3.22: Whole rock common lead isotopes for Savo. Fields from Peate et al. (1997). Error within point size.

The geographical location of Savo places it in an ambiguous position above both the Pacific and Indo-Australian slabs. Both slabs have the potential to dehydrate, or partially melt, given the unusual tectonic scenario (stalled subduction, young crust, and slab window development) but the depth-to-slab (50–100 km) dictates that any slab melt will interact with large volumes of Indo-Australian type mantle; this has the effect of rendering such a slab melt, particularly one derived from the Indo-

Australian slab, as "cryptic". Hydrous metasomatism cannot be ruled out as an alternative to melt metasomatism; in fact, both processes could occur in tandem (Fig. 3.23), given the two subducted slabs present beneath the arc.

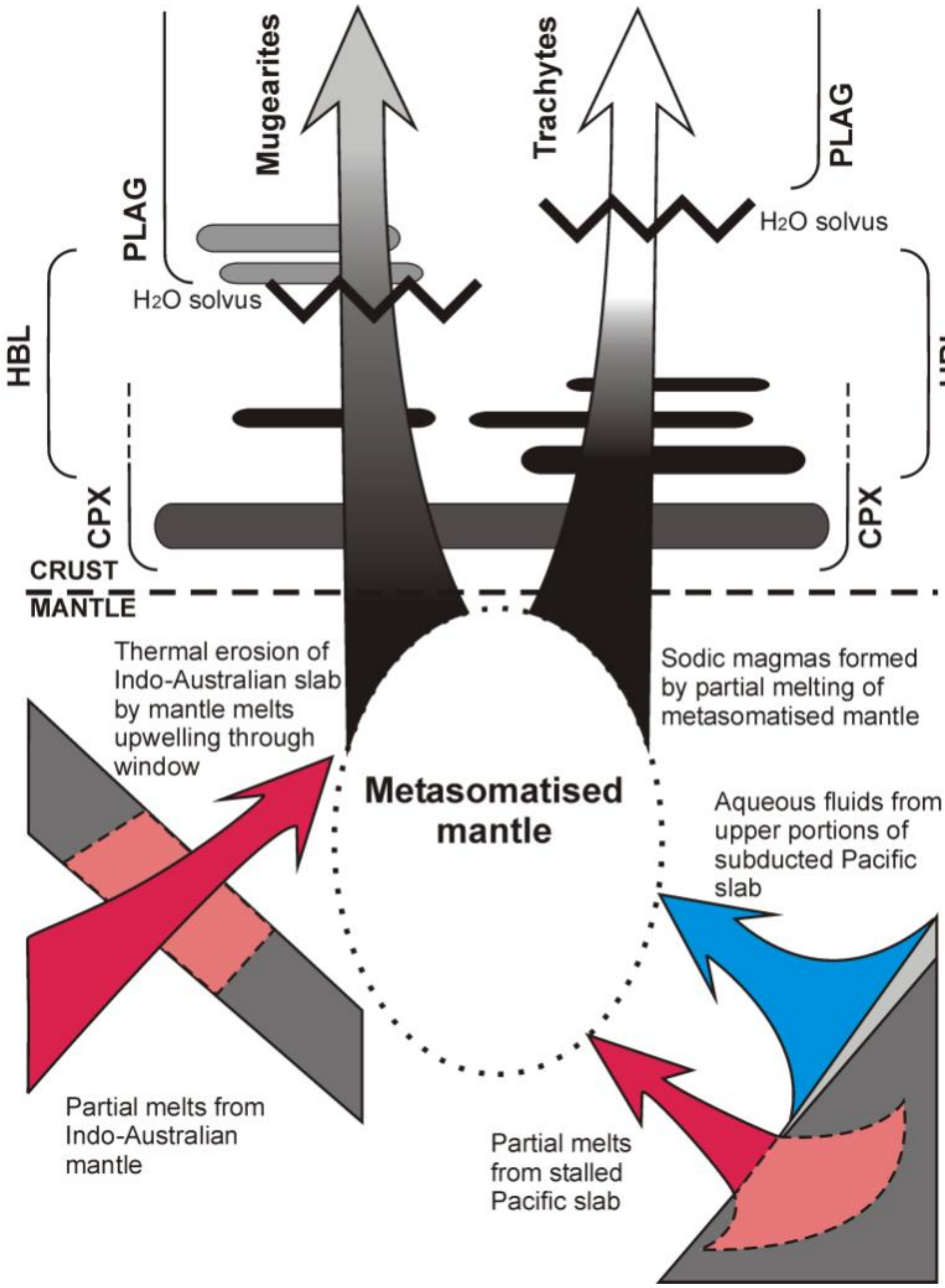

Fig. 3.23: Summary diagram for petrogenetic processes at Savo (not to scale). Slab contributions (either silicate melts or aqueous fluids) metasomatise the mantle, ultimately resulting in the genesis of sodic magmas. Mugearites develop by fractionation of a clinopyroxene-rich assemblage, then a plagioclase-amphibole assemblage (due to either lower initial water contents, or reaching water saturation at greater depths, as suggested by Fig. 3.19), whereas trachytes develop by extensive clinopyroxene and amphibole fractionation, with limited involvement of plagioclase.

3.5 Conclusions

The erupted material at Savo spans a broad range of compositions, from mafic to felsic, with abundant nodules of cognate ultramafic material. The trace element, isotopic and mineral chemistry of the samples analysed in this study indicate that the various compositions at Savo have a common origin, but have undergone different differentiation histories, a feature reflected in the variety of nodules.

A simple fractionation model cannot account for the observed trace element characteristics, in particular the apparently incompatible behaviour of Sr in the more felsic samples. Instead, it appears that two distinct fractionation systems occur. Early clinopyroxene + olivine + magnetite fractionation is common to all magmas. Trachytes are generated by amphibole-dominated fractionation; crystallisation of plagioclase is limited, resulting in high Sr in the crystal rich trachytes. Mugearites are less differentiated, and their fractionating assemblage is clinopyroxene + amphibole + plagioclase, resulting in only moderate Sr increase with continued fractionation.

The presence of amphibole over a large range of whole-rock SiO_2 (52–68 wt %) reflects high water contents of the magmas; coupled with unusually high sodium contents, this favours amphibole stability, and suppresses plagioclase. Amphibole fractionation is the dominant control on trace element chemistry in the trachytes. The lesser role of amphibole and increased importance of plagioclase in the more mafic mugearites is a result of either lower pressure or lower H_2O contents. In fact, the different solubility of water in the two compositions suggests that mugearites will have lower H_2O than a trachyte at similar crustal depths, and therefore plagioclase is more likely to play a role in fractionation for mugearites, particularly at shallow depths.

The fractionation models at Savo are consistent with “hot zone” models of arc magmatism, where primitive mantle melts are emplaced at deep crustal levels, and undergo high temperature and pressure differentiation, and major chemical variations are established; more evolved magmas ascend to shallower chambers, where crystallisation and minor fractionation influence physical characteristics and minor chemical changes (Annen et al., 2006). At Savo, mafic and felsic magmas may evolve from primitive mantle melts in deep zones, and undergo limited fractionation in shallow magma chambers to generate the mugearites, benmoreites and trachytes that are ultimately erupted (Fig. 3.23). The shallow fractionation results in differences of trace element chemistry, mostly due to the behaviour of plagioclase with changing pressure and H_2O contents.

Extensive amphibole fractionation with limited plagioclase removal leads to high Sr/Y and La/Yb in the trachytes. Although these features are characteristic of adakites, they can be shown to develop by fractionation from compositions that are too mafic to represent partial melt of subducted slab. However, such slab melting processes can and likely do occur in the Solomons Islands (Defant and Drummond, 1990; König et al., 2007), and the sodic nature of magmas at Savo may reflect mantle metasomatism by slab melts, a process documented in a number of areas in the region.

In the Solomon Islands, slab melts may be derived by subduction of young, hot oceanic crust, by the thermal erosion of slab window margins (with subduction of the Woodlark Ridge generating slab windows) or by recovery of mantle geotherms leading to partial melting of the stalled Pacific slab. Savo could feasibly be affected by any three of those processes, but radiogenic isotope data rule out major contributions from Pacific slab melts. Equally possible is that hydrous fluid metasomatism, with or without partial slab melts, can account for the chemistry, but the chemistry of hydrous fluids and silicate melts are analogous at high temperatures and pressures, and it is not possible to distinguish one particular source at Savo.

Alkaline fluids produced in the magmatic-hydrothermal environment at Savo Volcano 4

Abstract

Savo, Solomon Islands is a volcano with an active hydrothermal system, manifested at surface by hot springs, steaming ground and fumaroles. A number of hot springs (90–100°C) discharge unusual high pH (7–8), dilute, chloride-poor, sulphate-rich fluids (and with high Na, Ca, K, Si) classified as alkaline sulphate type. Other springs discharge acid sulphate waters, and Ca–Mg–HCO_3^- enriched waters occur in warm springs (40–60°C). The alkaline sulphate waters are produced by mixing a sulphate-rich hydrothermal endmember fluid with Ca–Mg–HCO_3^- fluids. High pH is generated by water–rock interaction, reaction between acid species and HCO_3^-, and continued dilution by meteoric-derived groundwater. Mixing of sulphate and calcium rich fluids leads to anhydrite precipitation in the subsurface; this then provides a buffer to sulphate concentrations in the fluids, as further mixing of sulphate-poor fluids dissolves the anhydrite.

Ca–Mg–HCO_3^- fluids form by CO_2 dissolving into meteoric-derived groundwater in peripheral, low temperature areas of the hydrothermal system. Ca and Mg are introduced by low temperature (<100°C) interaction with the host rocks. Acid sulphate springs develop by the oxidation of H_2S at the surface. Water in the springs is derived from nearby surface water runoff, and as a result the acid springs often have chemical compositions similar to nearby streams. The distribution, occurrence and chemistry of the acid sulphate springs are consistent with a steam heated origin.

The dilute chemistry of all discharges at Savo, and the high pH of the alkaline sulphate fluids, are a result of the high rainfall of the region, thus climate may be an important control on the chemistry and mineralogy of shallow hydrothermal systems.

4.1 Introduction

Studies of active magmatic-hydrothermal systems (e.g. Delmelle et al., 2000; Giggenbach et al., 2003) typically identify acidic fluids discharging from springs in close proximity to the crater and/or centre of hydrothermal activity. However, near-crater hot springs on Savo, Solomon Islands discharge high pH (7–8) sulphate-rich fluids which precipitate silica sinter and mixed silica–carbonate deposits at the surface.

The pH of fluids is an important parameter of any hydrothermal system as it controls: the porosity, permeability and strength of the volcanic host rock through rock dissolution and/ or secondary mineral precipitation; the relative importance of various complexing metal ligands in element transport; the secondary mineral assemblages that develop; and elemental fluxes between fluid and rock.

The origin of the high pH fluids at Savo may have implications for the study of mineral deposits in the region. Typically, epithermal gold deposits directly associated with magmatic-hydrothermal activity have distinctive alteration assemblages that indicate activity of highly acidic fluids (Heald et al., 1987; Stoffregen, 1987; Simmons et al., 2005). However, in the southwest Pacific, there are epithermal deposits such as Porgera and Ladolam (Papua New Guinea), hosted in alkaline rocks, that show relatively little evidence for acidic fluids (Jensen and Barton, 2000; Sillitoe, 2002). It is unclear why these systems show a paucity of evidence for acidic fluids, although it has been suggested that the role of buffering by the alkali (Na, K) rich rocks may be important (Sillitoe, 2002). The magmatic rocks at Savo are alkali-enriched too, with up to 7.5 wt% Na_2O in evolved trachytes (Chapter 3).

This chapter uses the chemistry of hot springs at Savo to investigate the processes which contribute to high fluid pH there, and what products might be expected at depth in the hydrothermal system.

4.2 Hydrothermal areas

Areas of hot springs (60–100°C) and steaming ground are found on the upper flanks of the volcano (Fig. 4.1). The crater has no hot springs, but areas of fumaroles (<120°C) and steaming ground can be found. Areas of steaming ground usually had a strong smell of H_2S, and native sulphur was precipitated at higher temperature steam and gas outlets. Grey pyrite-bearing mud was often observed just beneath the surface at the larger thermal areas (Poghorovorughala, Vutusuala and Reoka). The important characteristics of the major thermal areas are summarised in Table 4.1.

Inland cold springs (with temperature below ambient air temperature) are rare on Savo; most springs are in excess of 40°C. Groundwater-recharged wells in the coastal villages are usually slightly above ambient temperature, between 30–40°C.

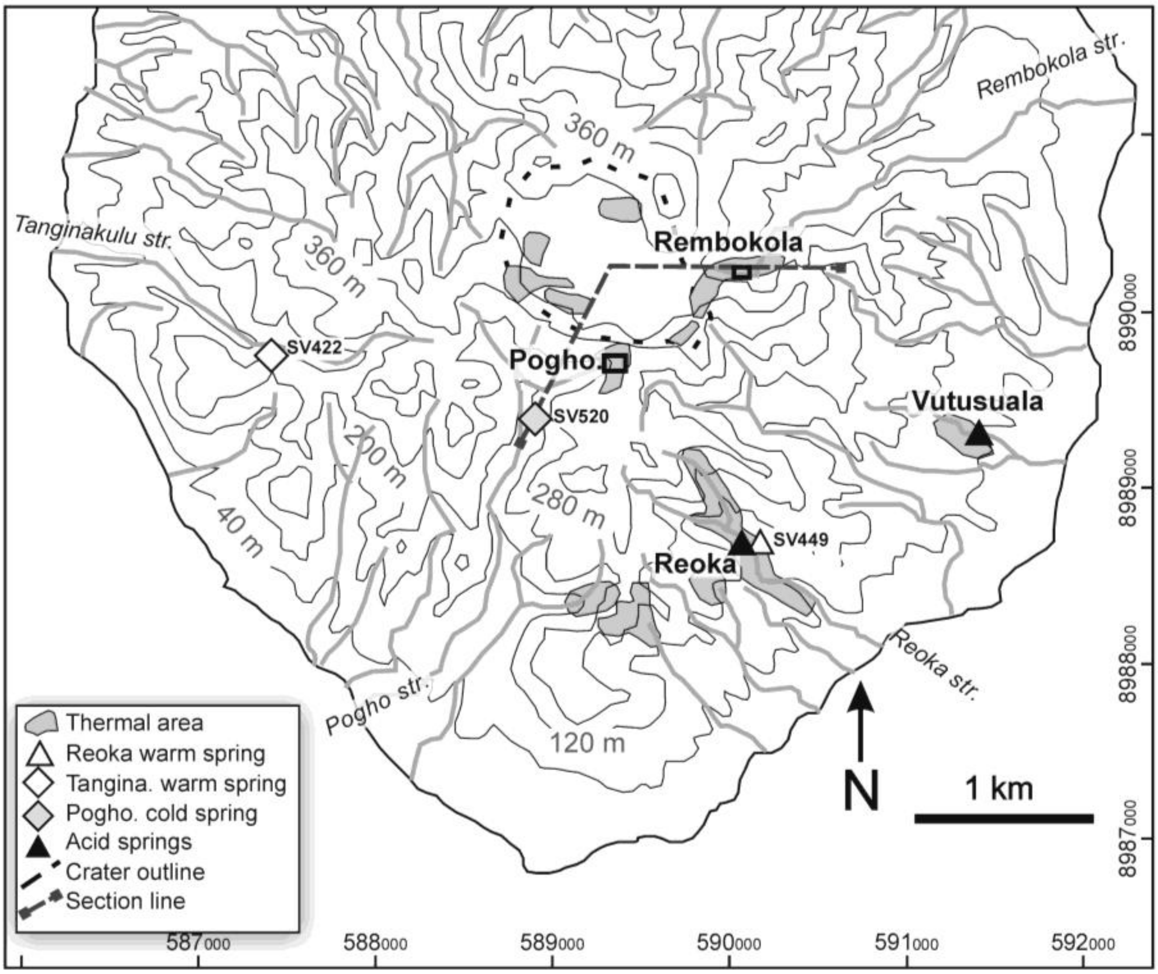

Fig. 4.1: Map of the south of Savo Island showing location of major thermal areas, streams and a selection of spring samples. Springs from the Rembokola and Poghorovorughala area shown in detail on Figures 4.2 and 4.5 respectively (locations marked with boxes). Specific sample locations for Reoka and Vutusuala are too close together to display clearly at this scale. Section line marks approximate location of Figure 4.15. Grid references are for UTM zone 57L.

Location	Spring T°C	Spring pH	Deposits	Area of >60°C activity*	Typical spring discharge rates (total for area)
Rembokola	~100	7–8	Sinter	10 m^2	1 kg/s (10–50 kg/s)
Reoka	56–100	3–7†	None‡	50 m^2	<0.01 kg/s
Vutusuala	90–100	5–8†	None	5 m^2	<0.01 kg/s
Poghorovorughala	~100	3–4 7–8	None Mixed travertine-sinter	2000 m^2	<0.01 kg/s 0.1–1 kg/s (10–50 kg/s)
Tanginakulu	<50	7	Travertine	N/A	<0.01 kg/s

Table 4.1: Summary of the major thermal areas of Savo discussed in this study. † High pH observed in springs mixing freely with adjacent high pH stream. ‡ No deposits around springs, but abundant travertine developed in the stream. * Lower temperature thermal activity may be considerably more extensive; see Figure 4.1.

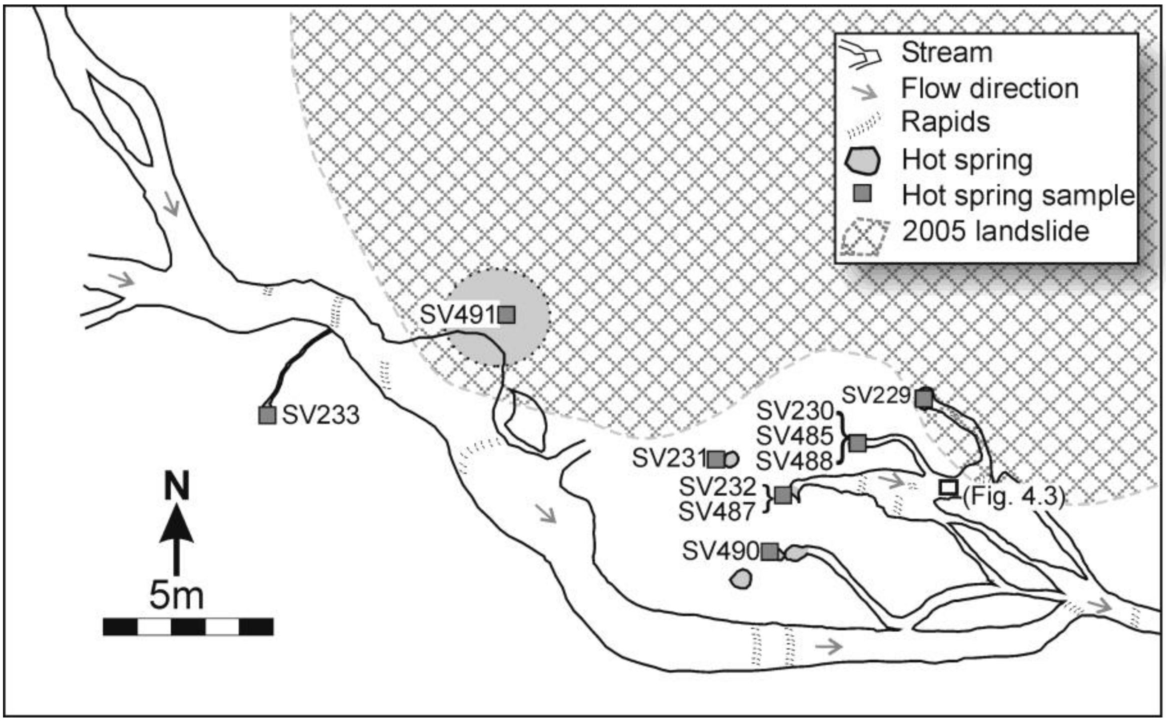

Fig. 4.2: Map of sampling sites in the Rembokola (Toakomata) thermal area. Heavy rainfall prior to 5/6/2005 triggered landslides that buried a number of springs in this area, subsequent to sampling. The spring at SV491 developed within the landslide deposits in 2006. Also shows location of Figure 4.3.

4.2.1 Rembokola

The major hot spring area of the Rembokola catchment (also known as Toakomata) is an approximately 10 m^2 area of alkaline (pH 7–8) hot springs towards the upper reaches of the valley (Fig. 4.2). The hot springs at Rembokola are 80–100°C and many boil upon discharge. Flow rates could be seen to vary over relatively short (minutes) timescales. In general, springs are estimated to discharge at rates no greater than 1 kg/s. The Rembokola stream is dominated by thermal water contributions in the upstream part of the catchment resulting in water temperatures up to 80°C. Discharge of the entire stream just below the main area of springs shown in Figure 4.2 was estimated to be 10–50 kg/s.

The springs are hosted in unlithified to poorly lithified volcaniclastics (Section 2.4.1); reworking by mass wasting processes has destroyed any original depositional fabrics making it impossible to distinguish to which lithofacies the sediments belong. White siliceous sinter forms a crust over much of the stream bed and the sediments adjacent to the hot springs (Fig. 4.3).

During the 2006 field work, a “new” spring formed (SV491). It grew from a small fissure in the ground into a 2 m^2 collapse crater with boiling water in the bottom. It developed in sediments deposited by landslides in 2005, and may represent the re-emergence of springs buried by those slides. Away from the landslide, spring locations were stable between 2005 and 2006.

Upstream of the main area of hot springs is an area of highly altered steaming ground, known informally as Toakomata Two. It extends approximately 250 m NNE from the crater wall to the source of the Rembokola stream (i.e. the major hot spring area, Toakomata). The area is elongate, being confined to a gorge. Following heavy rainfall, the water table is sufficiently high that small ephemeral hot springs develop at the northern end of the area.

The steaming ground and weak fumaroles are hosted in unconsolidated clastic deposits similar to those at Toakomata. The surface mineralogy is largely kaolinite + residual silica + native sulphur + minor alunite (as determined by Portable Infra-red Mineral Analyser and X-ray diffraction) at the surface. However, 15–30 cm beneath the surface is grey–black pyrite-bearing mud.

Fig. 4.3: Silica sinter developed on leaf litter in the Rembokola stream. Downstream from SV230 (Fig. 4.2).

4.2.2. Reoka

The Reoka hydrothermal field is an area (approximately 50 m^2) of hot springs and fumarolic ground in the lower reaches of the Reoka stream. It is the closest active hydrothermal area to sea level. Ground and hot spring water temperatures were typically 100°C. Alteration mineralogy was similar to that seen in the upper reaches of the Rembokola valley (Toakomata Two), with grey mud (containing minor pyrite) beneath up to 30 cm of kaolinite dominated-alteration. Minor sulphate minerals (mostly anhydrite) occur in a number of small patches on the steaming ground. In 2005, acid hot springs (pH 2–5) occurred in depressions within the thermal area. The springs were isolated from the stream, and had very low discharge rates (<0.01 kg/s). Landslides in 2006 changed both the flow path of the stream and the location of hot springs, and as such the same springs could not be sampled on the two field campaigns. In 2006, most springs were connected to the stream, and had pH 5–7.

Upstream of the main thermal area, the stream is fed by a number of small warm (c. 50°C) springs. Warm and cold springs are often pH >7, and have travertine associated with them. A number of small springs are >60°C, pH <7, and typically precipitate an orange iron oxide rich sludge where they emerge from the host rock. Many of the upstream springs are hosted in massive, jointed dacite, as opposed to the clastic material downstream. One warm spring was observed immediately downstream of the thermal area (SV449).

4.2.3 Vutusuala

Vutusuala is a small (5 m^2) hydrothermal area in the SE of the island (Fig. 4.4). The Vutusuala stream runs through the area, dividing it into a steep bank of fumarolic ground to the north, and a small flat strip of hot ground to the south. Digging into the altered sediment on either side of the stream exposes hot black pyrite-bearing mud. On the north side, the surface of the bank shows kaolinite-dominated alteration. Native sulphur can be found, but is not abundant. Small acidic springs occur, typically perched in the steaming ground. Temperatures are around 100°C.

The Vutusuala area is extensively reworked by human activity. This is the closest hydrothermal area to any village, and easily accessible. As a result, it is used heavily for cooking. Villagers typically dig holes into the fumarolic ground, allowing them to fill with water from below or from the stream, and steam their food. The digging turns over the sediments, and introduces large amount of organic material.

Fig. 4.4: Photograph of the Vutusuala thermal area. The Vutusuala stream flows through an area of steaming ground and small, transient acid sulphate hot springs.

4.2.4 Poghorovorughala

Poghorovorughala is the largest of the hydrothermal areas outside of the crater, as well as the most vigorous. It can be found in the upper reaches of the Poghorovorughala stream, in the south of the island. The area extends approximately 200 m along the stream valley from the crater wall (Fig. 4.5). It appears to be confined to the valley, with less than 30 m lateral extent from the stream.

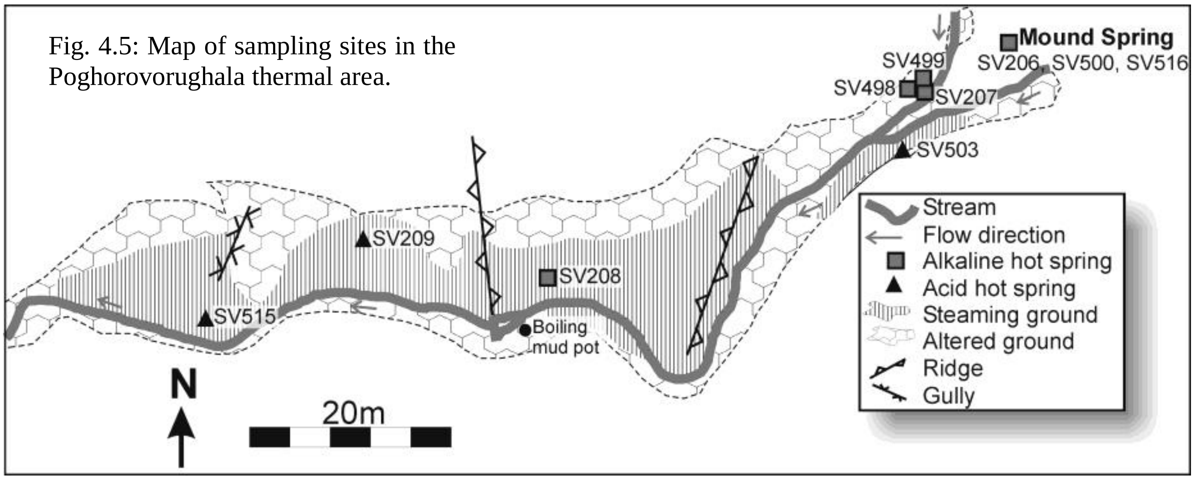

Fig. 4.5: Map of sampling sites in the Poghorovorughala thermal area.

There is extensive fumarolic ground at the Poghorovorughala area, particularly on the northern side of the stream. This is marked by kaolinite and abundant native sulphur at the surface and black pyrite-bearing mud beneath. Boiling alkaline hot springs are common, and a number occur in the stream bed, marked only by bubbling and boiling water as they vent into the stream. There are a small number of mud pots, and some small spouters. Many of the springs produce unusual carbonate + opal-A + anhydrite deposits, as both layered structures and as rounded (lobate) structures surrounding springs and spouters (Fig. 4.6). The Mound Spring (Fig. 4.7) is surrounded by a significant thickness of these deposits; perhaps as much as three metres thickness, based on its height above the

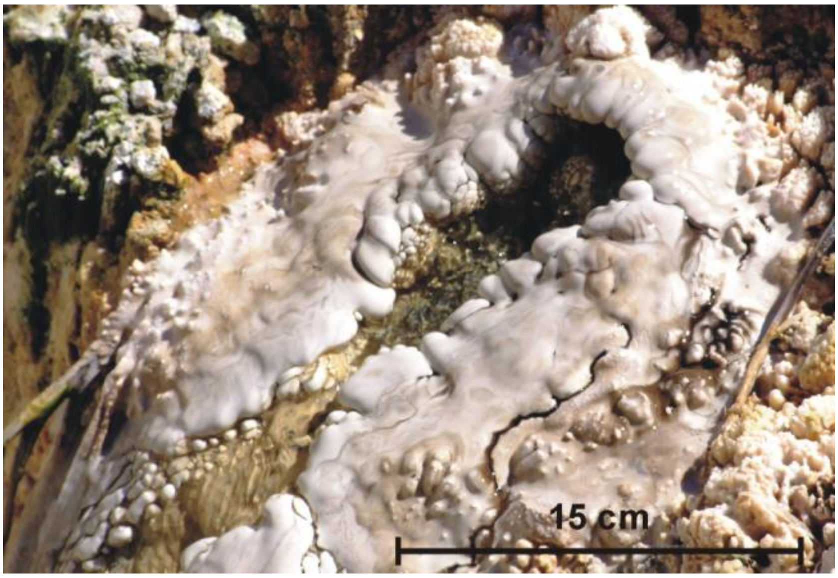

Fig. 4.6: Carbonate–sulphate–silica travertine around a boiling alkaline sulphate hot spring (SV501; Fig. 4.5), at Poghorovorughala.

Fig. 4.7: View of the Poghorovorughala thermal area, taken from location of boiling mud pot (Fig. 4.5) towards the Mound Spring. Note people for scale.

surrounding ground. Many of the springs identified in 2005 were still active in 2006, although some had deposited sufficient travertine to block the conduits, thus greatly reducing discharge. For unblocked springs, discharge rates were similar to those of the Rembokola area, estimated to be 0.1–1 kg/s. The combined discharge of the springs is similar to that of the Rembokola area; stream discharge at SV515 (Fig. 4.5) is estimated to be 10–50 kg/s.

Acid hot springs also occur in the Poghorovorughala area. Rather than depositing travertine and constructing mounds, the acid hot springs are destructive, and are hosted within cavities. These springs typically have very low discharges (on the order of 0.001–0.010 kg/s) and some are entirely isolated. These springs were not persistent features over the two sampling periods.

4.2.5 Tanginakulu

Tanginakulu is a stream (28–35°C) fed by small, low discharge springs (~0.001 kg/s) with a "warm" temperature (45–50°C). Travertine deposits occur for much of the stream's length, and range from thin veneers cementing clasts together on the stream bed, to >10 cm thick beds of layered travertine. There are no major thermal areas within the Tanginakulu catchment.

4.3 Sampling and analytical methods

To investigate the nature of the hydrothermal system and the development of high pH fluids at Savo, two field campaigns (April – May 2005; September – October 2006) were carried out. It has been noted where sampling protocol or analytical technique was modified for the second campaign.

Water samples were collected directly from springs and streams. The water was pumped through a <0.45 μm in-line PTFE syringe filter using silicone tubing and a hand vacuum pump and collected in a vacuum flask. To ensure all equipment was free from contamination by previous samples, approximately 150 ml of sample was pumped and discarded three times before sample collection.

pH was determined in the field from filtered and cooled (c. 50°C) samples using digital pH meters with automatic temperature calibration (Hanna Instruments HI98128 and 991001). For hot springs, pH was corrected to spring temperature (pH_C) using SOLVEQ (Reed, 1982; Reed and Spycher, 1984), and using estimated HCO_3^- contents where necessary. Correction factors are small, generally resulting in changes of around 0.2 pH units.

Dissolved inorganic carbon (DIC) content was determined in the field from filtered samples using a titration method: pH was adjusted to 8.3 by addition of NaOH, then titrated to pH 3.8 using a Hach® Digital Titrator with sulphuric acid. Titrations were repeated until three results within 5% were obtained. Purging of CO_2 and back titration was not possible. Results were corrected for interference from water, SiO_2 and boron, as per Arnórsson (2000). Bisulphide (HS^-) analysis was not possible, and this species may provide interference for the titration (resulting in over-estimation of total carbonate) for alkaline fluids. Results are expressed as mg/l HCO_3^- equivalent, although for acidic (pH <3.8) values likely represent dissolved CO_2.

For each sample, an unacidified fraction for anion determination was decanted into a 28 ml HDPE bottle. A fraction for major and trace elements and species was collected in a 28 ml HDPE bottle and acidified by addition of 0.3 ml Tracepur® 69 % HNO_3 (samples SV197 – SV215 acidified with 1 ml Tracepur® 69 % HNO_3).

All laboratory-based analyses were carried out at the British Geological Survey at Keyworth, UK, a UKAS Accredited laboratory that participates in the Aquacheck proficiency testing scheme. Analyses conform to ISO 17025.

Major and trace elements and species, including total sulphur (as sulphate) were determined from acidified fractions using a Fisons/ARL3580 ICP-AES with Gilson 222 Autosampler, using the procedures described in Ault et al. (1999). Samples for ICP-AES were diluted by five times (2005) or two times (2006) using 1% Aristar® grade HNO_3 to avoid precipitation of solids in the nebuliser. A subset of trace elements were analysed by VG Elemental PQ ExCell quadrupole ICP-MS for 2006 samples using procedures outlined in Cook et al. (2002). Accuracy and precision were determined from repeat analysis of quality control solutions over a period of 12 months, and are summarised for ICP-AES in Table 4.2 and for ICP-MS in Table 4.3. Detection limits vary between instruments and samples due to different dilutions; detection limits are summarised in Table 4.4.

Anions were determined from unacidified fractions using a Dionex DX-600 Ion Chromatograph system with ED50A Electrochemical Detector and AD20 Absorbance Detector modules, using the procedures outlined in Charlton et al. (2003). Precision on IC data (based on long term quality control solution data, with >500 analyses) is F^{-} = 3%;

		QCS10 Target	2005 Mean	2σ	Prec. %	Acc. %	2006 Mean	2σ	Prec. %	Acc. %	QCS11 Target	2005 Mean	2σ	Prec. %	Acc. %	2006 Mean	2σ	Prec. %	Acc. %
Al	ug/l	**200**	195	18	9	-3	195	20	10	-2	**100**	102	13	13	2	101	20	20	1
As	ug/l	**500**	483	15	3	-3	494	22	4	-1									
B	µg/l	**0.5**	0.51	0.02	4	2	0.51	0.02	4	2	**0**	0.26	0.01	5	4	0.26	0.01	5	4
Ba	mg/l	**0.2**	0.216	0.006	3	8	0.198	0.004	2	-1	**0**	0.110	0.003	3	10	0.110	0.003	3	10
Be	ug/l	**100**	103.0	2.8	3	3	101.4	1.2	1	1	**50**	51.7	1.1	2	3	51.4	1.3	2	3
Ca	mg/l	**20**	21.58	0.69	3	8	20.88	0.29	1	4	**50**	54.41	1.44	3	9	54.99	0.57	1	10
Cd	ug/l	**100**	98	3	3	-2	98	3	4	-2	**200**	198	6	3	-1	199	7	3	-1
Co	ug/l	**200**	195	9	4	-2	196	9	5	-2	**100**	98	6	6	-2	98	6	6	-2
Cr	ug/l	**100**	97	6	7	-3	97	7	7	-3	**200**	194	8	4	-3	184	18	10	-8
Cu	ug/l	**100**	96	4	4	-4	96	4	4	-4	**200**	195	7	3	-3	195	7	3	-2
Fe	mg/l	**0.5**	0.49	0.01	3	-2	0.49	0.01	3	-2	**0**	0.25	0.01	4	1	0.25	0.01	4	1
K	mg/l	**10**	10.0	0.4	4	0	10.2	0.4	4	2	**5**	5.0	0.2	4	0	5.1	0.1	2	3
La	ug/l	**100**	98	5	5	-2	98	6	6	-2	**200**	200	7	3	0	200	7	3	0
Li	ug/l	**100**	103	4	4	3	103	4	4	3	**200**	210	10	5	5	210	9	4	5
Mg	mg/l	**10**	9.92	0.23	2	-1	10.21	0.28	3	2	**5**	5.16	0.11	2	3	5.24	0.18	3	5
Mn	mg/l	**0.1**	0.091	0.002	3	-9	0.092	0.003	3	-9	**0**	0.046	0.002	3	-9	0.046	0.002	3	-8
Mo	ug/l	**100**	98	6	6	-2	97	6	6	-3	**200**	197	6	3	-1	196	8	4	-2
Na	mg/l	**50**	51.93	1.14	2	4	50.08	1.02	2	0	**25**	26.79	0.51	2	7	25.96	0.22	1	4
Ni	ug/l	**200**	196	9	4	-2	196	9	5	-2	**100**	96	7	7	-4	96	7	7	-4
P	mg/l	**1**	1.08	0.05	5	8	1.08	0.05	5	8	**1**	0.53	0.03	5	7	0.53	0.03	5	7
Pb	ug/l	**500**	482	19	4	-4	483	20	4	-3	**250**	243	15	6	-3	243	15	6	-3
Si	mg/l	**1**	1.10	0.04	3	10	1.09	0.07	6	9	**2**	2.17	0.04	2	8	2.16	0.04	2	8
SO_4^{2-}	mg/l	**102**	103.96	2.15	2	2	105.40	1.49	1	3	**51**	52.31	0.64	1	3	52.36	0.62	1	3
Sr	mg/l	**0.1**	0.098	0.002	2	-2	0.098	0.002	2	-2	**0**	0.200	0.005	2	0	0.201	0.005	2	0
V	ug/l	**100**	100	7	7	0	100	7	7	0	**200**	203	5	3	1	202	6	3	1
Y	ug/l	**100**	98	2	2	-2	98	2	2	-2	**50**	49	1	3	-1	49	1	3	-1
Zn	ug/l	**100**	100	5	5	0	100	5	5	0	**200**	199	7	3	-1	199	7	3	0
Zr	ug/l	**100**	97	5	5	-3	97	5	5	-3	**50**	50	3	7	-1	49	3	7	-1

Table 4.2: Summary statistics for ICP-AES quality control solutions QCS10 and QCS11 for the 12 month periods in which Savo samples were analysed. Precision is 2σ as a percentage of the target value, accuracy is the percentage difference between mean and target values.

Element	Target	Mean	2σ	% Prec.	% Acc.
Ag	2.5	2.5	0.2	7	0
Al	10.0	9.7	1.4	14	-3
As	10.0	10.0	0.8	8	0
Ba	10.0	9.8	0.6	6	-2
Be	10.0	9.8	0.7	8	-2
Bi	10.0	9.9	0.7	7	-1
Cd	10.0	9.9	0.6	6	-1
Co	10.0	10.0	0.7	7	0
Cr	10.0	9.8	0.8	8	-2
Cs	10.0	10.0	0.7	7	0
Cu	9.5	9.5	0.7	8	0
Ho	8.5	9.5	0.6	7	12
La	9.5	9.4	0.6	7	-1
Mo	10.0	10.0	0.7	7	-1
Nd	8.5	9.6	0.7	7	13
Ni	9.7	9.7	0.7	7	0
Pb	10.0	9.9	0.6	6	-1
Rb	10.0	10.0	0.8	8	0
Sb	9.0	9.9	0.6	6	10
Se	10.0	9.9	1.0	11	-1
Sn	9.7	9.7	0.6	6	0
Th	9.5	9.6	0.6	7	1
Tl	9.7	9.6	0.6	6	-1
U	10.0	9.9	0.6	6	-1
V	10.0	10.0	0.7	7	0
Y	9.0	9.1	0.6	7	1
Zn	10.0	10.0	1.1	11	0
Zr	10.0	10.0	0.8	8	0

Table 4.3: Summary statistics for ICP-MS quality control solution. Statistics calculated as in Table 4.2. All values in µg/l.

Cl^- = 5%; NO_2^- = 3%; NO_3^- = 4%; Br^- = 2%; and HPO_4^- = 3%. Accuracy (percent difference between mean and target value) is <1% for F^-, NO_2^-, Br^- and HPO_4^-; 2% for NO_3^-; and 6% for Cl^-.

Comparison of SO_4^{2-} as determined by ICP-AES (as total sulphur; SO_4^{2-} should be the dominant species in acidified samples) and IC shows significant discrepancy between the two techniques, particularly for 2006 hot springs, with SO_4^{2-} concentrations lower when determined by IC. Sulphate content was also calculated by a gravimetric method, with barium sulphate precipitated from acidified samples by addition of an excess of 5% $BaCl_2$ (barium sulphate used for isotopic analysis; Chapter 5). Sulphate contents determined by gravimetric calculation were similar to ICP-AES data (within 10%, excluding two outliers with insufficient $BaCl_2$), not IC data, suggesting that the sulphate in the latter (unacidifed) samples have been subject to modification, either by bacterial action or mineral precipitation. Logistical constraints meant that time between sampling and analysis was at least one month; in ideal circumstances, this time would be much less, and would be expected to produce better IC SO_4^{2-} data. Consequently, ICP-AES data for SO_4^{2-} are used in preference to results obtained by IC. For further discussion, see Appendix II.

Charge balance error (CBE) was calculated for major species (H^+, Al^{3+}, Fe^{2+}, Ca^{2+}, K^+, Mg^{2+}, Mn^{2+}, Na^+, SO_4^{2-}, Cl^-, HCO_3^-) using the equation:

$$CBE\,(\%) = 100 \times \frac{\sum m_c z_c - \sum m_a z_a}{\sum m_c z_c + \sum m_a z_a} \qquad \mathbf{1}$$

Where m = moles per litre; z = charge on ion; c = cations; a = anions. Total carbonate is presented as HCO_3^-, and is calculated as a monovalent anionic species for the purposes of charge balance. Charge balance error is higher for 2005 samples as no carbonate analyses were made. For samples where all major species have been included, CBE should ideally

		ICP-AES 2005	ICP-AES 2006	ICP-MS 2006
Ag	µg/l			0.1
Al	µg/l	350		2
As	µg/l	350		2
B	mg/l	0.4	0.08	
Ba	µg/l	30		5
Be	µg/l	5		0.1
Bi	µg/l			0.02
Ca	mg/l	0.25	0.05	
Cd	µg/l	80		0.04
Ce	µg/l			0.02
Co	µg/l	250		0.1
Cr	µg/l	300		1
Cs	µg/l			0.05
Cu	µg/l	70		2
Fe	mg/l	0.1		0.02
Ho	µg/l			0.02
K	mg/l	1	0.2	
La	µg/l	100		0.02
Li	µg/l	50	10	
Mg	mg/l	0.6	0.12	
Mn	mg/l	0.03	0.006	
Mo	µg/l	140		0.5
Na	mg/l	0.75	0.15	
Nd	µg/l			0.02
Ni	µg/l	300		2
P	mg/l	1	0.2	
Pb	µg/l	500		0.2
Rb	µg/l			0.5
Sb	µg/l			0.1
Se	µg/l			2
Si	mg/l	0.8	0.16	
Sn	µg/l			0.5
SO_4^{2-}	mg/l	1.2	0.24	
Sr	mg/l	0.01	0.002	
Te	µg/l			0.05
Th	µg/l			0.02
Ti	µg/l	60	12	
Tl	µg/l			0.02
U	µg/l			0.02
V	µg/l	120		1
Y	µg/l	20		0.02
Zn	µg/l	350		4
Zr	µg/l	60		0.02
		IC 2005	**IC 2006**	
Cl^-	mg/l	0.25	0.05	
NO_3^-	mg/l	0.1	0.02	
Br	mg/l	0.1	0.02	
NO_2^-	mg/l	0.05	0.01	
HPO_4^{2-}	mg/l	0.5	0.1	
F^-	mg/l	0.02	0.01	

Table 4.4: Detection limits for different techniques and dilutions used in the analysis of water samples from Savo.

be within ±5%. High CBE may occur due to inappropriate choice of valency for carbonate species (i.e. carbonate species are dominated by CO_3^{2-}, rather than HCO_3^-).

4.4 Results

4.4.1 Hot spring classification

Hot spring discharges (T >80°C) are usually classified according to dominant anion composition and pH, leading to four main categories: alkaline (or near neutral) chloride, acid sulphate, acid sulphate–chloride, and bicarbonate (Ellis and Mahon, 1977). Hot springs from Savo are sulphate dominated, with occasional sulphate–bicarbonate springs (Fig. 4.8). However, alkaline sulphate springs do not readily fit into any of the classical categories, and as such are classified separately. Incorporating them with the traditional acid sulphate category is unsatisfactory, as acid sulphate springs also occur on Savo; thus there are two groups of sulphate-rich hot springs at Savo, which can be defined separately on the basis of chemistry, stable isotope ratios and physical nature of the spring.

Hot springs defined as alkaline sulphate type are pH_C 7–8 and have $\delta^{34}S_{SO4}$ values >4‰ and $\delta^{18}O_{H2O}$ values slightly greater than local non-thermal groundwater (Chapter 5). Flow rates are visibly higher than in acid sulphate springs, with the alkaline sulphate springs being the major contributors to water in the streams in the south of the island. Sinter and mixed silica–carbonate deposits are found surrounding and downstream from alkaline sulphate springs.

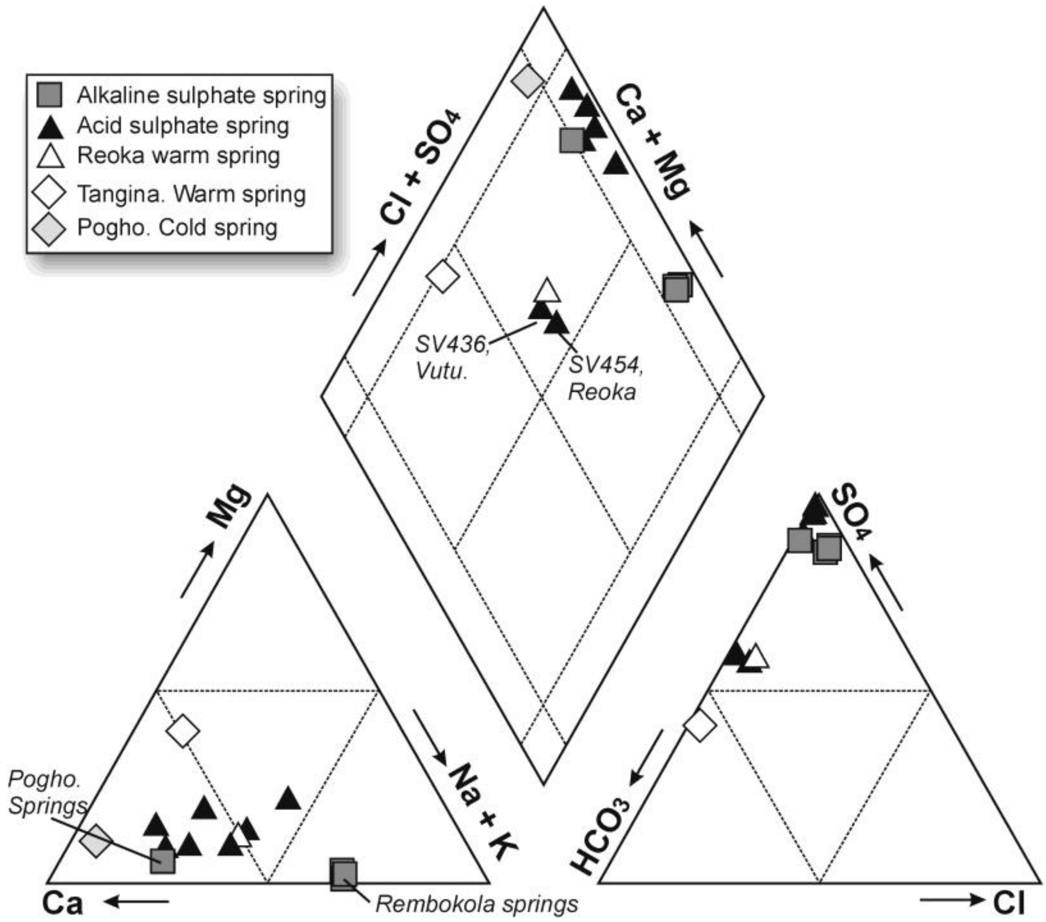

Fig. 4.8: Piper diagram for spring samples from Savo. The majority of hot springs are classified as sulphate springs, with a smaller number bicarbonate–sulphate springs. SV454 and SV436 are included with the acid sulphate group on the basis of physical appearance. Rembokola springs are more sodium-rich than springs elsewhere; Poghorovorughala springs are more calcium-rich. Pogho. = Poghorovorughala.

Springs classified as acid sulphate type have $\delta^{34}S_{SO4}$ values <2‰, high $\delta^{18}O_{H2O}$ and δD_{H2O} relative to non-thermal groundwater (Chapter 5), and pH_C typically <7 and often <4. Acid sulphate springs are found in areas of steaming ground and advanced argillic alteration (silica + kaolinite ± native sulphur). Acid sulphate springs are slow to recharge if emptied, and may be better described as stagnant pools rather than springs. There are no sinters or travertine deposits found surrounding acid sulphate springs.

A number of springs from Reoka and Vutusuala have a physical appearance more consistent with acid sulphate springs than that of the alkaline sulphate springs, and are classified as such despite near-neutral pH_C. The two bicarbonate-rich samples from 2006 (SV454 and SV436) fall within this group. For springs in these groups where sulphate yield was sufficiently high for stable isotope analysis, $\delta^{34}S_{SO4}$ values were <2‰ (Chapter 5), consistent with the acid sulphate springs.

4.4.2 Alkaline sulphate hot springs

Alkaline sulphate springs are found in two of the major thermal areas, Rembokola and Poghorovorughala, although the similarity between the chemistry of these springs (Table 4.5 and Table 4.6) and those of other major streams on Savo indicates that similar springs must occur outside of these major thermal areas to feed those streams. All alkaline sulphate springs have near neutral to slightly alkaline pH (pH_C 7–8), with sulphate as the dominant anion (600–700 mg/l), and are generally boiling at discharge. The two areas have differences in major and trace element chemistry.

Sample	SV498	SV206[1]	SV500[1]	SV516[1]	SV207	SV499	SV208
Area	Pogho.	Pogho.	Pogho.	Pogho.	Pogho.	Pogho.	Pogho.
Date	18/10/06	25/05/05	18/10/06	21/10/06	25/05/05	18/10/06	25/05/05
T (°C)	100	100	100	100	100	96	99
pH (T)	8.0 (58)	6.7 (42)	7.8 (45)	7.7 (58)	7.2 (49)	8.0 (49)	7.4 (37)
pH_C	7.7	6.8	7.5	7.5	7.1	7.7	7.2
HCO_3^- eqv.	94		86	88		90	
Ag (µg/l)	bdl		0.1	0.1		bdl	
Al (µg/l)	35	bdl	11	13	bdl	13	bdl
As (µg/l)	bdl	bdl	bdl	bdl	bdl	bdl	bdl
B	2.22	1.95	2.15	2.11	2.06	2.21	19.79
Ba (µg/l)	61.2	49.6	40.9	58.9	49.6	59.8	59.6
Be (µg/l)	0.5	bdl	0.4	bdl	bdl	0.1	bdl
Ca	247	207	239	240	224	247	160
Co (µg/l)	0.8	bdl	0.5	0.3	bdl	0.4	bdl
Cs (µg/l)	3.8		2.6	3.7		3.7	
Fe	0.04	bdl	0.04	0.04	bdl	0.05	bdl
K	17.0	16.6	16.8	16.7	17.0	17.0	17.3
Li (µg/l)	301	298	290	288	318	301	233
Mg	12.9	10.5	12.0	12.0	11.3	12.9	11.1
Mn	0.84	1.08	0.71	0.75	1.39	0.85	0.56
Mo (µg/l)	bdl	bdl	bdl	bdl	bdl	bdl	bdl
Na	82	97	81	80	98	82	111
Ni (µg/l)	7	bdl	4	3	bdl	4	bdl
P	0.22	bdl	bdl	bdl	bdl	bdl	bdl
Pb (µg/l)	0.3	bdl	bdl	bdl	bdl	bdl	bdl
Rb (µg/l)	65.8		44.0	60.4		65.5	
Sb (µg/l)	bdl		bdl	bdl		bdl	
Si	120	117	120	118	118	120	129
SO_4^{2-}	681	602	669	661	623	679	619
Sr	3.34	2.76	3.25	3.23	3.02	3.34	2.13
Ti (µg/l)	19	bdl	16	21	bdl	20	bdl
Tl (µg/l)	bdl		bdl	bdl		bdl	
V (µg/l)	bdl	bdl	bdl	bdl	bdl	bdl	bdl
Y (µg/l)	0.11	bdl	0.06	0.03	bdl	0.05	bdl
Zn (µg/l)	9	bdl	bdl	bdl	bdl	bdl	bdl
Zr (µg/l)	0.05	bdl	0.04	0.02	bdl	0.06	bdl
Cl^-	4.3	5.2	4.4	4.4	5.2	4.5	4.4
NO_3^-	0.024	bdl	0.020	0.067	0.035	0.804	0.035
Br	bdl	bdl	bdl	bdl	bdl	bdl	bdl
NO_2^-	bdl	bdl	bdl	bdl	bdl	bdl	bdl
F^-	0.226	0.348	0.220	0.234	0.325	0.229	0.385
CBE (%)	5	11	5	5	13	5	4

Table 4.5: Data for Poghorovorughala alkaline sulphate springs. All values in mg/l unless noted otherwise. bdl = below detection limits; Pogho. = Poghorovorughala; [1] = all samples from Mound Spring. Blank cells denote no analysis. Number in brackets next to pH denotes measurement temperature (°C). The following elements (and species) were below detection limits for all analyses, and are omitted from the table: Bi, Cd, Ce, Cr, Cu, Ho, La, Nd, P, Se, Sn, Te, Th, U, HPO_4^-.

Sample	SV491	SV230[1]	SV485[1]	SV488[1]	SV229	SV232[2]	SV487[2]	SV231	SV490	SV233
Area	Remb.	Remb.	Remb.	Remb.	Remb.	Remb.	Remb.	Remb.	Remb.	Remb.
Date	16/10/06	29/05/05	15/10/06	16/10/06	29/05/05	29/05/05	16/10/06	29/05/05	16/10/06	29/05/05
T (°C)	99	100	100	82	100	100	100	100	99	97
pH (T)	8.0 (46)	8.2 (39)	7.8 (50)	7.9 (45)	8.0 (40)	8.2 (41)	8.1 (51)	8.0 (42)	7.9 (50)	8.3 (31)
pH_C	7.6	7.8	7.5	7.6	7.6	7.8	7.8	7.6	7.6	7.8
HCO_3^- eqv.	23		38	33			38		43	
Ag (µg/l)	bdl		bdl	bdl			bdl		bdl	
Al (µg/l)	7	bdl	7	7	bdl	bdl	9	bdl	6	bdl
As (µg/l)	49	bdl	50	49	bdl	bdl	53	bdl	51	bdl
B	8.19	8.26	8.78	8.97	8.12	8.09	8.66	7.83	8.69	14.37
Ba (µg/l)	56.6	49.7	55.8	53.7	59.6	49.7	61.0	49.7	60.0	49.7
Be (µg/l)	bdl	bdl	bdl	bdl	bdl	bdl	bdl	bdl	bdl	bdl
Ca	96	120	96	97	121	133	95	144	97	129
Co (µg/l)	0.1	bdl	0.2	0.2	bdl	bdl	0.2	bdl	0.2	bdl
Cs (µg/l)	54.9		49.4	45.0			47.9		47.8	
Fe	0.03	bdl	bdl	bdl	bdl	bdl	bdl	bdl	0.02	bdl
K	28.4	26.8	28.5	29.3	27.2	26.6	28.2	25.4	28.6	29.7
Li (µg/l)	1591	1621	1684	1696	1655	1582	1644	1472	1635	1657
Mg	2.0	10.0	4.4	4.4	10.7	10.9	6.5	10.6	6.5	5.5
Mn	0.04	0.42	0.14	0.12	0.42	0.56	0.27	0.41	0.27	0.20
Mo (µg/l)	7.9	bdl	7.1	7.8	bdl	bdl	8.1	bdl	7.9	bdl
Na	208	206	216	218	209	201	210	189	210	220
Ni (µg/l)	bdl	bdl	2	2	bdl	bdl	3	bdl	2	bdl
P	bdl	bdl	bdl	bdl	bdl	bdl	bdl	bdl	bdl	bdl
Pb (µg/l)	0.3	bdl	0.5	bdl	bdl	bdl	bdl	bdl	0.4	bdl
Rb (µg/l)	110.6		121.7	119.0			124.5		121.1	
Sb (µg/l)	0.6		0.6	0.7			0.6		0.6	
Si	174	176	175	168	179	175	183	162	184	164
SO_4^{2-}	624	633	627	643	639	635	614	642	620	652.76
Sr	2.68	3.40	2.74	2.75	3.45	3.70	2.72	4.01	2.74	3.73
Ti (µg/l)	bdl	bdl	bdl	bdl	bdl	bdl	bdl	bdl	bdl	bdl
Tl (µg/l)	0.09		0.11	0.12			0.14		0.13	
V (µg/l)	2	bdl	bdl	1	bdl	bdl	bdl	bdl	bdl	bdl
Y (µg/l)	0.02	bdl	0.04	0.04	bdl	bdl	0.04	bdl	0.04	bdl
Zn (µg/l)	bdl	bdl	bdl	bdl	bdl	bdl	7	bdl	bdl	bdl
Zr (µg/l)	0.03	bdl	0.05	bdl	bdl	bdl	0.04	bdl	0.02	bdl
Cl^-	45.2	41.5	46.7	47.7	41.8	30.3	45.7	38.1	45.3	49.6
NO_3^-	bdl	bdl	0.332	bdl	bdl	bdl	0.445	bdl	0.028	bdl
Br	0.070	bdl	0.073	0.086	bdl	bdl	0.081	bdl	0.063	bdl
NO_2^-	bdl	bdl	0.014	bdl	bdl	bdl	bdl	bdl	bdl	bdl
F^-	0.245	0.368	0.302	0.294	0.347	0.293	0.263	0.400	0.258	0.499
CBE (%)	0	7	1	1	7	9	1	8	1	7

Table 4.6: Data for Rembokola alkaline sulphate springs. All values in mg/l unless noted otherwise. bdl = below detection limits; Remb. = Rembokola; [1] = samples from F1 spring; [2] = samples from F3 spring. Blank cells denote no analysis. Number in brackets next to pH denotes measurement temperature (°C). The following elements (and species) were below detection limits for all analyses, and are omitted from the table: Bi, Cd, Ce, Cr, Cu, Ho, La, Nd, P, Se, Sn, Te, Th, U, HPO_4^-.

Poghorovorughala springs are calcium and sulphate-rich (Fig. 4.8), with very low chloride contents (~5 mg/l) and moderate DIC (~90 mg/l HCO_3^- equivalent) and Si (~120 mg/l). Ca can reach as high as ~250 mg/l, Na ~90 mg/l, K ~17 mg/l, and Mg ~12 mg/l. Fe, Al are present in only trace amounts (<0.05 μg/l). Important trace elements include Li (300 μg/l), Rb (60 μg/l), and Sr (3 mg/l). In general, the analysed springs are dilute.

Rembokola springs have similar sulphate contents to the Poghorovorughala springs, but higher chloride (~40 mg/l; still remarkably low), lower DIC (~40 mg/l HCO_3^- eqv.) and higher Si (~175 mg/l). Na and K concentrations are higher (concentrations are ~200 and 28 mg/l respectively), and Ca and Mg (~100 and 5–10 mg/l) lower than the Poghorovorughala springs (Figs. 4.8 and 4.9). As with the Poghorovorughala samples trace element concentrations are low overall, but with increased alkali metals (Rb ~120 μg/l, Cs ~50 μg/l) relative to Poghorovorughala. Arsenic contents are slightly higher at Rembokola, with samples analysed by ICP-MS containing ~50 μg/l.

4.4.3 Acid sulphate hot springs

Acid sulphate springs occur in a number of areas, including Poghorovorughala where they occur within 5 m of alkaline sulphate springs. Acid sulphate springs have a varied chemistry, in part a result of including bicarbonate–sulphate springs (e.g. SV454, Table 4.7) within the classification.

The Poghorovorughala acid springs are low pH (<4) with high but variable sulphate (480–820 mg/l), Si ~130 mg/l, and low chloride (<6 mg/l). Alkali metals are very similar between acid sulphate and alkaline sulphate springs in Poghorovorughala, whereas the alkali earths tend to have slightly lower concentrations in the acid springs (Sr <2 mg/l, Ca <200 mg/l). Iron and aluminium concentrations are 3 orders of magnitude higher in the acid springs (Fig. 4.9). Acid springs elsewhere show similar chemical trends. Concentration of alkali metals and alkali earths varies between locations; carbonate, Al and Fe are strongly influenced by pH (Fig. 4.9).

The Reoka thermal area hosts acid sulphate springs of both subdivisions (i.e. acid sulphate *sensu stricto* and bicarbonate–sulphate springs too). The bicarbonate–sulphate springs in particular have chemistry similar to that of the adjacent stream most likely as a result of mixing between the two waters; e.g. SV453 has highly similar Ca, Na, Mg, Si, and K to SV460 (Table 4.8). However, the Reoka springs all have Al and Fe concentrations at least one order of magnitude higher than the adjacent stream (Table 4.8), a feature particularly pronounced in the most acidic of the springs (SV213). The composition of the springs is closest to that of the stream at high pH (>6), with increasing differences as pH decreases.

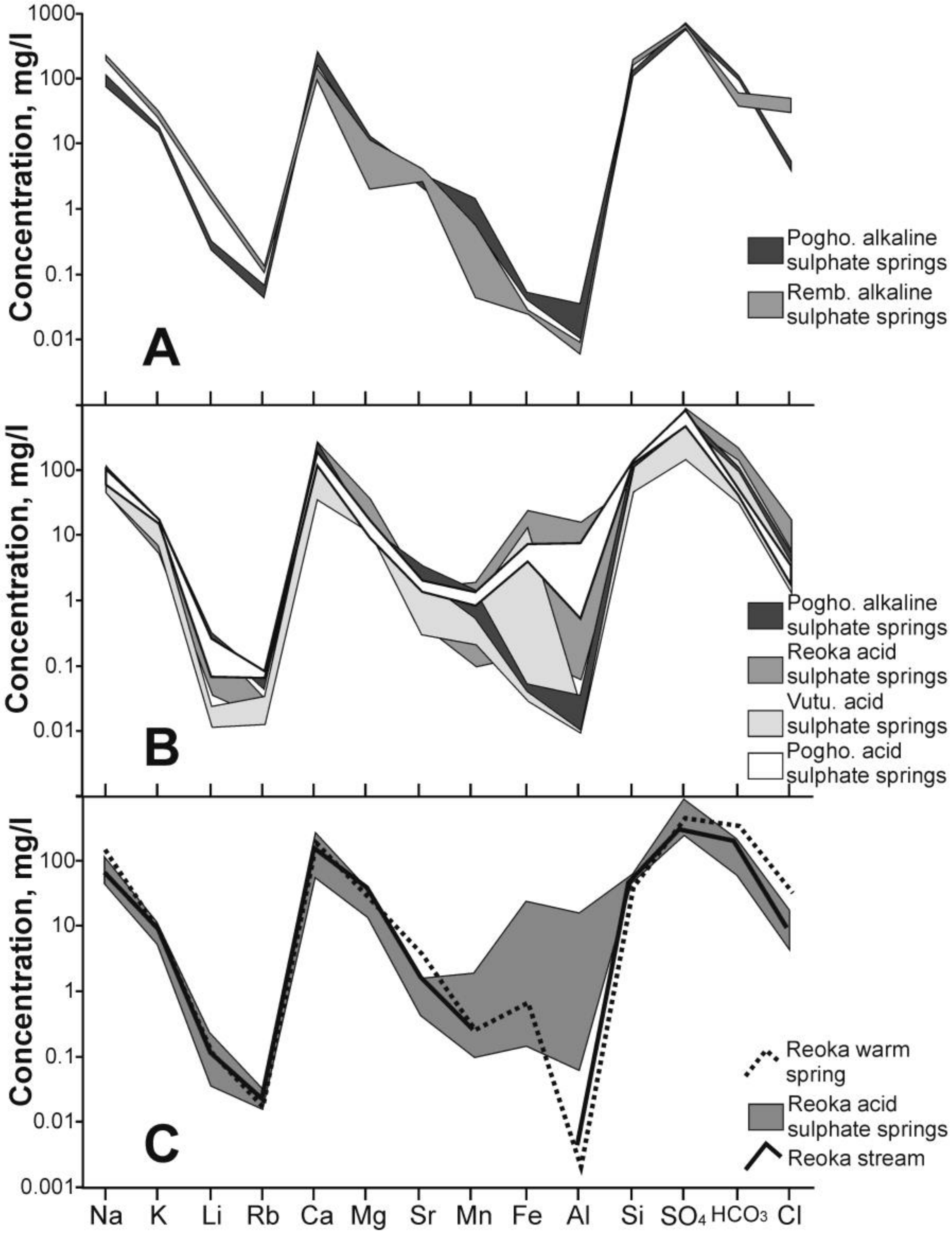

Fig. 4.9: Major and trace element (and species) variation for A) alkaline sulphate springs; B) acid sulphate springs (Poghorovorughala alkaline sulphate springs shown for comparison); C) Reoka warm spring, stream and acid springs.

As with the Reoka samples, the Vutusuala springs show a variable chemistry. Springs in this area are in close proximity to the Vutusuala stream, and as with the Reoka area, water may be exchanged between the two.

Sample	SV209	SV503	SV515	SV212	SV213	SV453	SV454	SV458	SV201	SV435	SV436
Area	Pogho.	Pogho.	Pogho.	Reoka	Reoka	Reoka	Reoka	Reoka	Vutu.	Vutu.	Vutu.
Date	25/05/05	18/10/06	21/10/06	26/05/05	26/05/05	10/10/06	10/10/06	11/10/06	24/05/05	08/10/06	08/10/06
T (°C)	100	98	103	100	100	89	83	91	100	98	95
pH	3.8 (40)	2.9 (55)	2.7 (50)	6.8 (36)	2.5 (33)	6.9 (45)	7.4 (42)	6.7 (40)	5.4 (44)	7.1 (49)	7.8 (49)
pH_C	4.1	3.2	3.0	6.1	2.7	6.9	7.3	6.7	5.5	7.0	7.6
HCO_3^- eqv.		36	29			67	208	50		19	130
Ag (µg/l)		bdl	0.2			bdl	bdl	bdl		bdl	bdl
Al (µg/l)	540	6449	7629	827	15787	308	62	108	bdl	10	21
As (µg/l)	bdl	bdl	3	bdl	bdl	bdl	55	bdl	bdl	bdl	bdl
B	5.07	1.76	3.05	bdl	bdl	0.71	2.79	0.40	bdl	0.15	0.10
Ba (µg/l)	69.5	30.9	25.5	129.1	59.6	97.0	32.4	128.0	39.7	102.9	97.1
Be (µg/l)	bdl	0.4	0.6	bdl	bdl	bdl	bdl	bdl	bdl	bdl	bdl
Ca	120	186	140	66	58	149	82	265	34	143	70
Cd (µg/l)	bdl	bdl	0.11	bdl	bdl	bdl	bdl	bdl	bdl	bdl	bdl
Ce (µg/l)		2.72	2.19			0.05	0.06	0.57		bdl	bdl
Co (µg/l)	bdl	1.3	1.8	bdl	bdl	0.4	0.2	0.6	bdl	0.9	0.2
Cr (µg/l)	bdl	2	bdl	bdl	bdl	bdl	bdl	bdl	bdl	bdl	bdl
Cs (µg/l)		3.2	3.4			0.7	2.0	0.6		0.8	0.3
Fe	4.92	7.08	4.03	6.76	24.09	0.48	0.14	0.52	12.99	0.03	bdl
Ho (µg/l)		0.16	0.26			bdl	bdl	bdl	bdl	bdl	bdl
K	16.4	15.1	16.7	6.3	5.5	7.5	11.2	8.2	15.6	13.7	7.3
La (µg/l)	bdl	0.83	0.83	bdl	bdl	0.04	0.04	0.31	bdl	bdl	bdl
Li (µg/l)	72	255	117	bdl	bdl	61	236	35	bdl	24	12
Mg	9.5	16.3	14.0	14.0	15.5	31.3	31.1	34.8	13.5	11.2	11.7
Mn	0.88	1.11	1.33	0.45	0.60	0.51	0.10	1.88	0.76	0.99	0.22
Mo (µg/l)	bdl	bdl	bdl	bdl	bdl	bdl	5.6	bdl	bdl	bdl	0.8
Na	61.33	83.9	102.0	52.27	45.35	78.8	111.9	74.6	63.40	46.1	60.9
Nd (µg/l)		3.01	2.24			0.02	0.06	0.36		bdl	bdl
Ni (µg/l)	bdl	6	6	bdl	bdl	4	2	6	bdl	7	2
P	bdl	bdl	bdl	bdl	bdl	bdl	bdl	bdl	bdl	0.39	bdl
Pb (µg/l)	bdl	5.0	2.7	bdl	bdl	0.5	bdl	1.3	bdl	2.2	0.4
Rb (µg/l)		67.8	78.3			16.2	31.7	15.7		33.7	13.4
Si	130	136	140	52	63	45	58	57	109	69	48
SO_4^{2-}	481	817	774	342	516	561	247	865	332	508	151
Sr	1.38	2.00	1.41	0.70	0.43	1.59	0.75	1.49	0.30	1.34	0.68
Th (µg/l)		bdl	0.05			bdl	bdl	bdl		bdl	bdl
Ti (µg/l)	bdl	17	15	bdl	bdl	15	bdl	17	bdl	bdl	bdl
Tl (µg/l)		bdl	0.07			bdl	bdl	bdl		bdl	bdl
U (µg/l)		0.11	0.09			bdl	bdl	bdl		bdl	bdl
V (µg/l)	bdl	11	3	bdl	bdl	6	4	5	bdl	2	1
Y (µg/l)	bdl	4.33	7.40	bdl	bdl	0.09	0.15	0.58	bdl	0.04	bdl
Zn (µg/l)	bdl	75	86	bdl	bdl	23	bdl	22	350	16	bdl
Zr (µg/l)	bdl	0.06	0.11	bdl	bdl	0.05	bdl	0.10	bdl	0.05	0.05
Cl^-	2.6	3.3	1.7	5.6	4.4	7.7	17.3	5.9	5.8	1.3	4.1
NO_3^-	bdl	0.027	0.132	bdl	0.161	0.300	0.150	0.487	0.321	0.280	0.362
Br	bdl	bdl	bdl	bdl	bdl	bdl	0.021	0.059	bdl	bdl	bdl
NO_2^-	bdl	bdl	bdl	bdl	bdl	0.032	bdl	0.013	bdl	0.021	0.228
HPO_4^{2-}	bdl	bdl	bdl	bdl	bdl	bdl	bdl	bdl	bdl	0.269	bdl
F^-	0.473	0.344	0.319	0.308	0.405	0.294	0.337	0.505	1.72	0.223	0.178
CBE (%)	1	-2	-2	0	4	3	16	2	-4	-2	18

Table 4.7: Data for acid sulphate springs. All values in mg/l unless noted otherwise. bdl = below detection limits; Pogho. = Poghorovorughala; Vutu. = Vutusuala. Blank cells denote no analysis. The following elements were below detection limits for all analyses, and are omitted from the table: Bi, Cu, Sb, Se, Sn, Te.

Sample	SV449[1]	SV460	SV422[2]
Location	Reoka	Reoka stream	Tangina.
Date	09/10/06	11/10/06	07/10/06
T (°C)	56	33	47
pH	7.0	8.1	6.7
HCO_3^- eqv.	315	199	513
Al (µg/l)	2	4	2
As (µg/l)	bdl	5	19
B	1.92	0.94	0.20
Ba (µg/l)	43.8	34.0	44.3
Ca	186	151	204
Ce (µg/l)	0.07	bdl	bdl
Co (µg/l)	0.5	0.6	2.5
Cs (µg/l)	2.4	1.4	3.9
Fe	0.66	bdl	3.03
K	8.5	8.1	5.9
La (µg/l)	0.06	bdl	bdl
Li (µg/l)	120	106	55
Mg	25.6	39.2	98.5
Mn	0.26	0.23	0.56
Mo (µg/l)	1.8	2.7	2.0
Na	150	66	48.3
Nd (µg/l)	0.06	bdl	bdl
Ni (µg/l)	5	5	7
P	bdl	bdl	0.20
Pb (µg/l)	bdl	0.6	1.5
Rb (µg/l)	17.0	19.1	24.5
Sb (µg/l)	bdl	bdl	bdl
Si	40	45	73
SO_4^{2-}	419	311	294
Sr	3.72	1.56	1.49
Tl (µg/l)	bdl	bdl	0.03
V (µg/l)	1	2	bdl
Y (µg/l)	0.38	0.08	0.22
Zn (µg/l)	14	bdl	11
Zr (µg/l)	0.05	bdl	0.03
Cl^-	32.4	9.0	7.6
NO_3^-	0.148	0.369	1.49
Br	0.047	bdl	bdl
NO_2^-	0.022	0.027	0.031
F^-	0.403	0.312	bdl
CBE (%)	10	16	17

Table 4.8: Data for Reoka and Tanginakulu warms springs, ([1] and [2] respectively) and a typical Reoka stream sample. All values in mg/l unless noted otherwise. [1] = warm spring feeding into stream; bdl = below detection limits. The following elements (and species) were below detection limits for all analyses, and are omitted from the table: Ag, Be, Bi, Cd, Cr, Cu, Ho, Se, Sn, Te, Th, Ti, U, HPO_4^-. High CBE may be a result of carbonate speciation (i.e. CO_3^{2-}> HCO_3^-).

Sample	SV235	SV211	SV520
Area	Remb.	Pogho.	Pogho.
Date	29/05/05	25/05/05	21/10/06
T (°C)	26	26	26
pH	7.5	8.1	8.0
HCO_3^- eqv.			52
Ag (µg/l)			0.1
Al (µg/l)	bdl	bdl	3
As (µg/l)	bdl	bdl	2
Ba (µg/l)	bdl	bdl	23.3
Ca	42	104	153
Co (µg/l)	bdl	bdl	0.3
Cs (µg/l)			0.1
Fe	bdl	bdl	bdl
K	1.9	2.5	3.1
Mg	12.9	8.0	12.1
Mo (µg/l)	bdl	bdl	4.6
Na	11.6	7.9	9.3
Ni (µg/l)			2
Rb (µg/l)			6.7
Si	18	16	18
SO_4^{2-}	107	213	329
Sr	0.31	0.68	0.99
V (µg/l)	bdl	bdl	1
Zn (µg/l)	bdl	bdl	5
Cl^-	3.1	4.0	4.6
F^-	0.367	0.241	0.226
CBE (%)	24	16	7

Table 4.9: Data for cold spring samples. All values in mg/l unless noted otherwise. bdl = below detection limits. The following elements (and species) were below detection limits for all analyses, and are omitted from the table: B, Be, Bi, Cd, Ce, Cr, Cu, Ho, La, Li, Mn, Nd, P, Pb, Sb, Se, Sn, Te, Th, Ti, Tl, U, Y, Zr, HPO_4^-, NO_3^-, Br, NO_2^-.

4.4.4 *Warm and cold springs*

Warm (~50°C) springs were sampled in Reoka and Tanginakulu (Table 4.8). Both springs were bicarbonate-sulphate type, with near neutral pH. The springs are notably rich in Mg (25–100 mg/l) and Ca (180–200 mg/l).

Cold springs (<30°C) were sampled from the Rembokola and Poghorovorughala catchments, in both cases a short distance downstream of the major thermal areas. Cold springs are high pH (7.5–8.0), and have low concentrations of most dissolved species, with the exception of Ca, which dominates the cation composition (40–150 mg/l), and sulphate, the major anionic species (100–300 mg/l; Table 4.9; Fig. 4.8). All species occur in lower concentrations in cold springs relative to hot springs from the same catchments, with the exception of Mg (8–13 mg/l).

4.5 Discussion

4.5.1 Anion composition – a genetic classification

The classification of hot springs according to the relative proportions of anions (as discussed in section 4.4.1) is a useful tool, as they relate to the origin and evolution of fluids in a hydrothermal system. The classification of springs is a first step towards a genetic model for the hydrothermal fluids. In magmatic–hydrothermal systems there is a generally observed evolution of fluids in terms of changing anion composition (Giggenbach, 1997). Condensation of magmatic volatiles (including SO_2) into groundwater, or contraction of a magmatic vapour phase, leads to highly acidic, sulphate-dominated fluids, with variable chloride contents (Giggenbach, 1997; Symonds et al., 2001); "immature" volcanic fluids therefore plot towards the sulphate apex of the anion ternary (Fig. 4.10). As the fluid reacts with host rocks and approaches equilibrium, sulphate content decreases by precipitation of minerals such as anhydrite and alunite, and chloride content increases, both relative to the decrease in sulphate, and as a result of leaching from the host rocks (Giggenbach, 1997; Reed, 1997). pH increases as H^+ ions are consumed in base exchange reactions (Reed, 1997):

$$\underset{\text{(albite)}}{2H^+ + 2NaAlSi_3O_8} = 2Na^+ + 2SiO_2 + \underset{\text{(pyrophyllite)}}{Al_2Si_4O_{10}(OH)_2} \qquad \mathbf{2}$$

The "mature" near-neutral (or alkaline) fluids produced by water-rock reaction plot in the chloride-dominant sector of the anion ternary (Fig. 4.10). At lower temperature (<100°C) zones in the hydrothermal system, significant amounts of magmatic CO_2 can dissolve into the water, leading to increased bicarbonate concentrations. Where fluids boil at depth, steam and relatively non-condensable gases (H_2S, CO_2) ascend and condense into cool, shallow aquifers, generating chloride-free, bicarbonate-rich waters. If the steam and gases condense into surface waters, H_2S is oxidised to sulphate, leading to fluids that plot towards the sulphate apex. Thus, sulphate-rich fluids are generally produced by two distinct processes: condensation of primary magmatic volatiles (including SO_2) into

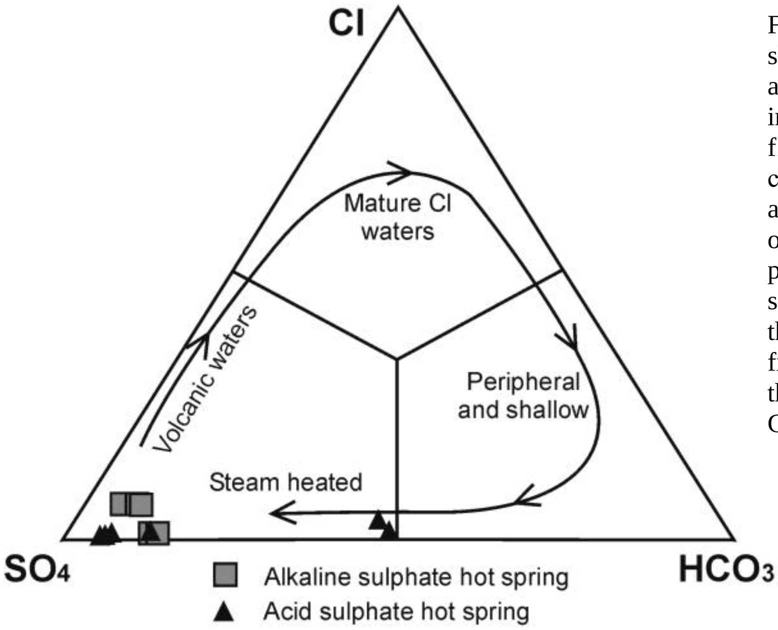

Fig. 4.10: Anion ternary with arrow showing general evolution of fluids in a magmatic-hydrothermal system from initial magmatic sulphate dominated fluids to rock-buffered, neutral chloride "mature" fluids. Bicarbonate and steam heated acid sulphate waters occur in the near surface and peripheral parts of hydrothermal system. Acid sulphate springs plot in the bicarbonate-sulphate and sulphate fields; alkaline sulphate fields plot at the sulphate apex. Diagram after Giggenbach (1997).

groundwater; and oxidation of H_2S from a secondary steam phase in surface waters, as described by the following reactions:

$$4SO_2 + 4H_2O = 3H_2SO_4 + H_2S \quad \mathbf{3}$$

$$H_2S + 2O_2 = H_2SO_4 \quad \mathbf{4}$$

The first reaction involves the disproportionation of magmatic SO_2 upon reaction with water at temperatures below about 350°C (Holland, 1965). This reaction produces H_2S, which may be eventually oxidised at the surface as in equation 4.

Both alkaline sulphate and acid sulphate hot springs from Savo plot at the sulphate apex of Figure 4.10, with only a small number of acid sulphate springs having increased bicarbonate. With respect to stable isotope compositions (discussed extensively in Chapter 5), alkaline sulphate springs have uniformly high $\delta^{34}S_{SO4}$ (4 to 7‰), and acid sulphate springs lower and more variable $\delta^{34}S_{SO4}$ (2 to −4‰). The sulphur isotope data show that acid sulphate and alkaline sulphate springs have distinct sulphate sources, consistent with the two processes shown in equations 3 and 4. However, regardless of sulphur source, both processes generate initially acidic fluids as H_2SO_4 dissociates to SO_4^{2-} and H^+, and so the processes which generate high pH in the alkaline sulphate springs must be discussed on detail.

4.5.2 Alkaline sulphate springs

It is important to critically assess the degree to which a hydrothermal fluid has "matured", or reached equilibrium with its host rock, as mineral–fluid equilibria form the basis of thermometric calculations, and can provide insight into mineral assemblages and alteration regimes in the deeper parts of hydrothermal systems. Water–rock equilibrium may be assessed by the application of various major element ratios (Giggenbach, 1988).

In hydrothermal systems the ratio K/Na is controlled by exchange of alkalis between aqueous fluids and coexisting feldspars, and is the basis of a widely used chemical thermometer (Fournier, 1979; Truesdell, 1984). Equilibrium K/Na values can be derived by the equation:

$$L_{kn} = \log\left(c_K / c_{Na}\right) = 1.75 - 1390 / T \qquad \mathbf{5}$$

where c is concentration in mg/kg, and T is temperature in °C (Giggenbach, 1988). A similar equation can be written for K and Mg:

$$L_{km} = \log\left(c_K^2 / c_{Mg}\right) = 14.0 - 4410 / T \qquad \mathbf{6}$$

The K/Mg ratio is controlled by equilibration with chlorite and other Mg-containing clays, and with biotite at high temperatures (Ellis and Mahon, 1977). The K/Na ratio of a hydrothermal fluid is slower to re-equilibrate down-temperature than K/Mg, and as a result is less subject to progressive resetting upon ascent and discharge.

K/Mg and K/Na ratios can be compared graphically using the method of Giggenbach (1988). Fluid compositions are plotted in terms of Na/1000, K/100 and √Mg (all in mg/kg)

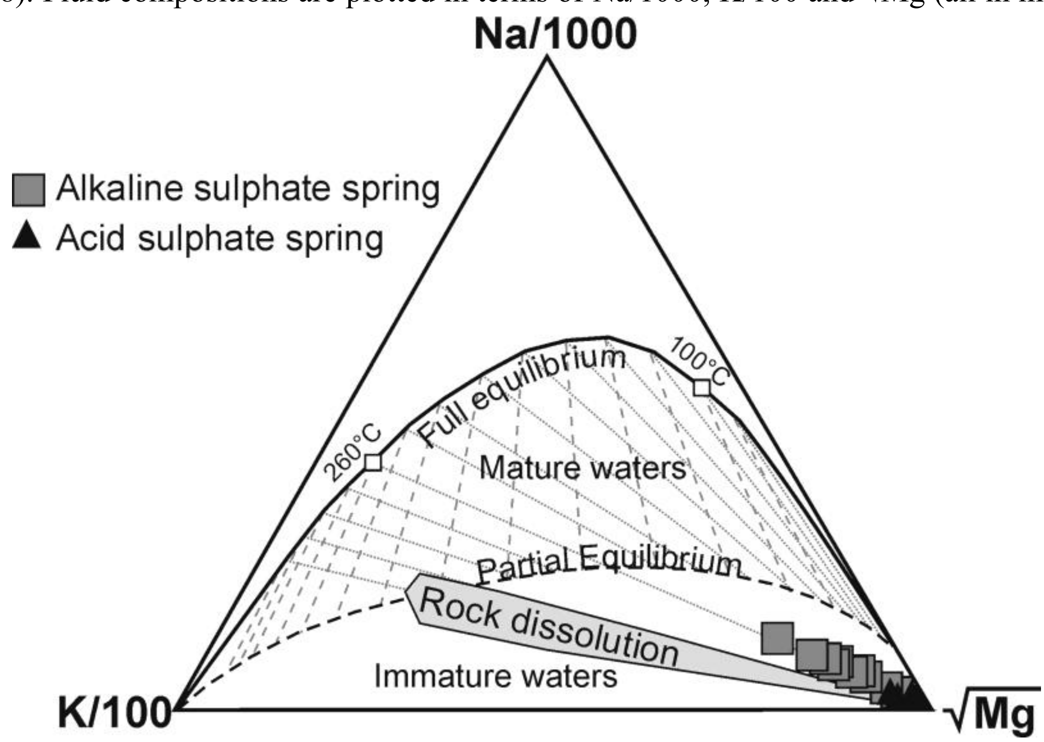

Fig. 4.11: Na–Mg–K ternary diagram, after Giggenbach (1988). Full equilibrium line plotted by intersection of K/Na and K/Mg isotherms (equations 5 and 6; plotted as fine dotted and dashed lines respectively, 100° and 260°C intersections marked); partial equilibrium line defined by equation 7. Rock dissolution field shows fluid compositions expected by isochemical dissolution of up to 1000g rock per kg water, using local rock compositions (Chapter 3). Hot spring waters from Savo fall well below the partial equilibrium line, and close to the rock dissolution field.

on a ternary diagram (Fig. 4.11). Where isotherms defined by equations 5 and 6 meet, a fluid can be assumed to be in equilibrium with a typical hydrothermal alteration assemblage at that temperature; the full equilibrium line is a curve which joins equilibrium compositions at varying temperatures. The partial equilibrium line is defined as having a Maturity Index (MI) of 2 (Giggenbach, 1988):

$$MI = 0.315L_{km} - L_{kn} \qquad \textbf{7}$$

Waters lying within the field defined by the partial and full equilibrium lines are referred to as "mature waters", those below the partial equilibrium line (with MI <2) are "immature". Isochemical dissolution of rocks generates immature fluids.

Giggenbach (1988) noted that both "volcanic waters" and steam-heated waters (Fig. 4.10) tend to plot as immature waters on plots such as that of Figure 4.11, and usually fall close to the field defined by isochemical rock dissolution. The alkaline sulphate springs from Savo form an array of points with slightly higher Na/K ratios than the rocks. The position and distribution of the alkaline sulphate spring data can be explained in two ways:

1. Hydrothermal fluids are initially acidic and attack the host rocks, resulting in isochemical dissolution. As reaction continues and pH increases, potassium bearing minerals such as alunite precipitate, increasing the Na/K ratio. The sulphate-rich nature of the fluids also favours the formation of alunite.

2. Hydrothermal fluids are initially at unknown pH, but equilibrated with a feldspar-bearing assemblage between 300 and 260°C (by projecting back to the equilibrium line on Fig. 4.11). During ascent, dilution (mixing with Mg-rich, cold spring-type water) shifts the compositions to higher √Mg at constant Na/K ratios.

The two processes are not mutually exclusive. The alkaline sulphate springs at Poghorovorughala have higher Mg and lower K and Na concentrations than the Rembokola springs. Considering the two processes above, such differences could result from:

1. Isochemical dissolution of rock with higher Mg and lower Na and K, such as a mugearite rather than a trachyte, at Poghorovorughala.

2. Increased dilution / fluid mixing at Poghorovorughala.

Comparison of the conservative elements Cl, B and Li between the two areas (Fig. 4.12) shows that mixing of Rembokola spring fluid with a fluid similar to those discharged at cold springs or Tanginakulu would produce the conservative element characteristics of the

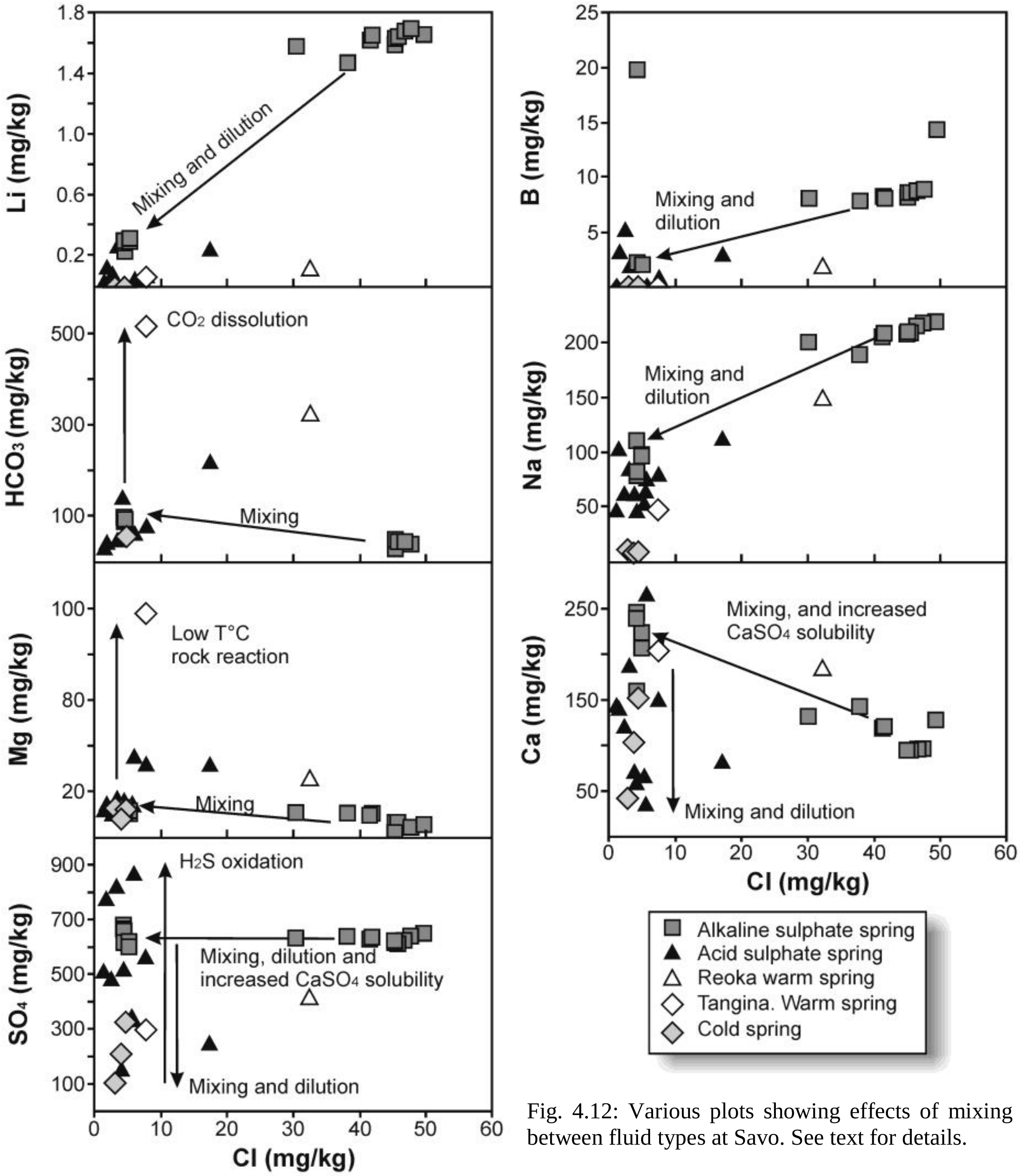

Fig. 4.12: Various plots showing effects of mixing between fluid types at Savo. See text for details.

Poghorovorughala springs. It seems likely that mixing with cool, Mg-enriched groundwater (Table 4.9) is responsible for producing the variation between Rembokola and Poghorovorughala, and also for the overall position of all alkaline sulphate fluids on the Na–Mg–K ternary (Fig. 4.11). The position of the Rembokola springs on the Na–Mg–K plot indicates that they too have been diluted by cooler waters; thus, the most Cl-rich endmember is unknown. K/Na temperature calculations are relatively robust with respect to dilution (Giggenbach, 1988), and the back projected temperatures along the K/Na isotherms are likely to be valid in spite of the significant changes to K/Mg and conservative elements. K/Na temperatures are much higher than values expected for steam-heated environments (~100°C) where reaction 4 dominates sulphate generation; high temperatures require a deeper environment where reaction 3 might be expected to dominate sulphate production.

Dilution and fluid mixing limits the applicability of chemical thermometers to the waters. Clearly, the K/Mg thermometer is inappropriate, but other calculations in common usage for geothermal waters are also dilution-limited. Other chemical thermometers include those based on equilibrium with quartz, and stable isotope thermometers based on $\Delta^{18}O_{SO4\text{-}H2O}$ (discussed further in Section 5.3.4). The quartz no steam loss thermometer (Truesdell, 1984) is described by the equation:

$$T°C = \frac{1309}{5.19 - \log \mathrm{SiO}_2} - 273.15 \qquad \mathbf{8}$$

The quartz maximum steam loss thermometer by:

$$T°C = \frac{1522}{5.75 - \log \mathrm{SiO}_2} - 273.15 \qquad \mathbf{9}$$

The sulphate oxygen stable isotope thermometer (McKenzie and Truesdell, 1977) by:

$$T°C = \sqrt{\frac{10^6}{\Delta_{\mathrm{SO4-H2O}} + 4.1 / 2.88}} - 273.15 \qquad \mathbf{10}$$

As the silica thermometers are based on concentration, mixing of a silica-rich thermal fluid with cooler, silica undersaturated groundwater leads to underestimates of reservoir temperature. The sulphate oxygen thermometer will also underestimate reservoir temperature, as cold waters samples at Savo plot at lower $\delta^{18}O_{H2O}$ values than thermal waters.

Comparison of the various thermometers (Fig. 4.13) shows that K/Na calculations result in higher temperatures for Poghorovorughala springs, but the K/Mg, silica and stable isotope temperatures are lower, reflecting increased dilution at Poghorovorughala.

The Rembokola alkaline sulphate springs have been subject to less mixing with cold spring -type waters, but comparison of the various thermometers shows that they are not pristine (Fig. 4.13). On the various plots of Figure 4.12, the Rembokola and Poghorovorughala alkaline sulphate springs define a mixing line, with the latter approaching cold spring water chemistry (or intermediate between cold springs and warm bicarbonate springs as sampled at Tanginakulu), and the former towards an unknown (deep reservoir) water. By comparison of Poghorovorughala and Rembokola springs, and assuming that changes in Cl^-, B and Li are controlled by mixing with the more dilute cold water, there is a decrease

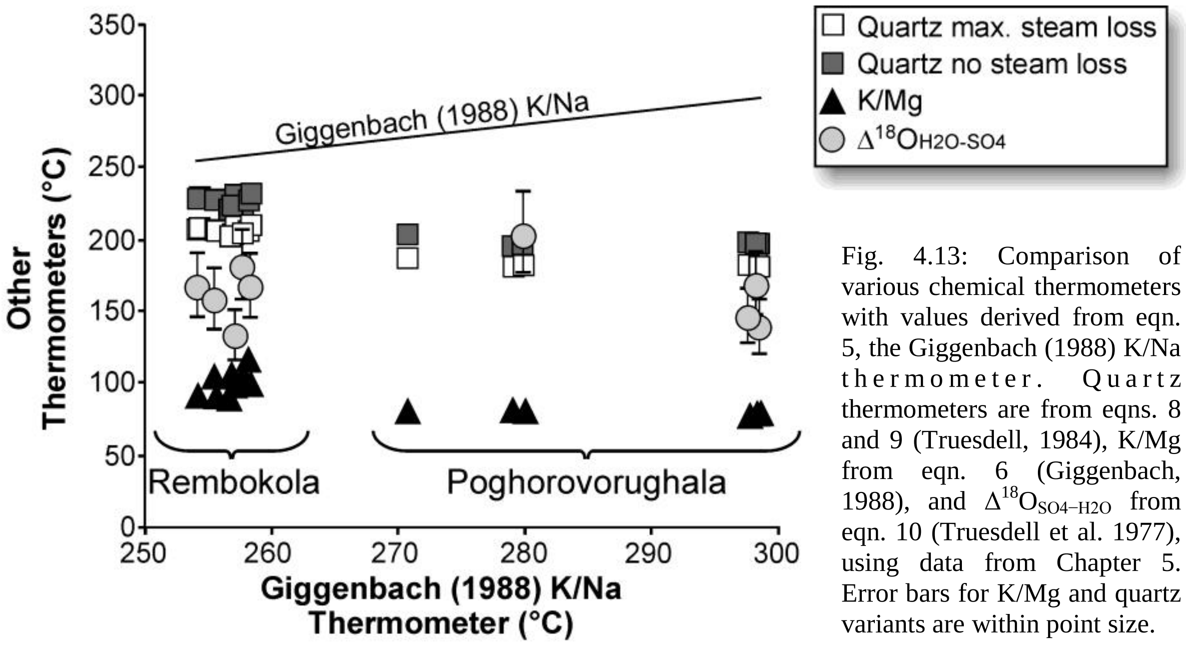

Fig. 4.13: Comparison of various chemical thermometers with values derived from eqn. 5, the Giggenbach (1988) K/Na thermometer. Quartz thermometers are from eqns. 8 and 9 (Truesdell, 1984), K/Mg from eqn. 6 (Giggenbach, 1988), and $\Delta^{18}O_{SO4-H2O}$ from eqn. 10 (Truesdell et al. 1977), using data from Chapter 5. Error bars for K/Mg and quartz variants are within point size.

in concentration (dilution) of Na, K, Cs, Rb, Si and As; an increase in concentration of HCO_3^-, Ca, and Mg; and SO_4^{2-} and Sr remain relatively constant. The increase in bicarbonate reflects the increased solubility of CO_2 in cooler water. The Poghorovorughala fluids have mixed with a relatively dilute (low conservative element concentrations) HCO_3^-–Ca–Mg fluid. Such fluids are produced by CO_2 dissolving into cool groundwater to produce bicarbonate, and low temperature water rock reaction to increase Ca and Mg contents (essentially weathering processes).

The HCO_3^-–Ca–Mg fluid may have a more important role than just diluting deep reservoir fluids. In equation 3, magmatic SO_2 condenses into water to generate H_2SO_4 – that water may initially be HCO_3^-–Ca–Mg rich. Symonds et al. (2001) modelled the condensation of a HCl and SO_2-rich magmatic gas to both air saturated water (ASW) and bicarbonate water (ASW with added $NaHCO_3$). Both systems produce increasingly acidic fluids as more magmatic gas is added, chiefly through the dissociation of HCl and H_2SO_4. However, in the water with additional $NaHCO_3$, bicarbonate can increase pH by the reaction:

$$HCO_3^-{}_{(aq)} + H^+{}_{(aq)} = H_2O_{(aq)} + CO_{2\,(g)} \qquad \textbf{11}$$

Magmatic gases condensing into HCO_3^-–Ca–Mg fluids will tend to be less acidic than fluids condensing into ASW, and these bicarbonate-rich fluids may represent an early step in producing high pH fluids at Savo.

Acid fluids will react with the host rocks, and H^+ will be consumed by reactions such as that described by equation 2. These reactions alter the host rocks, and the alteration mineral assemblage depends on temperature and pH of the fluids. Under acidic conditions, assemblages such as silica + kaolinite + alunite (advanced argillic alteration) may develop, but dilution and interaction with bicarbonate may limit the generation of acidic fluids; hydrothermal alteration may not feature the assemblages that indicate the highly acidic fluids.

The sodic nature of the host rocks at Savo means that there is abundant albite for reactions such as equation 2, and so acidic fluids can be neutralised by reaction with a smaller volume of rock compared to a less sodic system. However, this neutralising capacity does not dictate the final, water-rock equilibrium pH. The full equilibrium, or "propylitic" pH, is controlled by buffers such as (Reed, 1997):

$$\underset{}{2H^+} + \underset{\text{(albite)}}{2NaAlSi_3O_8} + \underset{\text{(microcline)}}{KAlSi_3O_8} = \underset{\text{(muscovite)}}{KAl_3Si_3O_{10}(OH)_2} + 2Na^+ + 6SiO_2 \qquad \textbf{12}$$

From this, it can be seen that pH is controlled by the concentration of the base cations in solution, which in turn are limited by the balancing anions (Reed, 1997). In the hydrothermal fluids at Savo, sulphate is the dominant anion. Thus any process that reduces the concentration of sulphate (and to a lesser extent chloride) will cause Na^+ to decrease and by reaction 12, lead to an increase in pH. The concentration of the balancing anions can be lowered by dilution (as already demonstrated in Fig. 4.12), or by removal in minerals. Sulphate can be precipitated as anhydrite, a mineral which will be particularly important if Ca-rich groundwater is mixed with sulphate-rich hydrothermal water.

The solubility of anhydrite is therefore a crucial control on the fluid composition, and in particular the pH. Anhydrite is more soluble in cooler waters. In a situation where cool, sulphate-poor water is mixed with hot sulphate-rich hydrothermal water, there are competing processes whereby increasing Ca concentration favours anhydrite formation, but a lower temperature favours its dissolution. Anhydrite solubility will be further modified by the sodium content of the fluids, as $NaSO_4^-$ is a relatively stable aqueous species (Rimstidt, 1997).

CHILLER (Reed, 1982) was used to calculate the speciation of the fluid chemistry at equilibrium, and it was found that Poghorovorughala springs are saturated with anhydrite at the discharge temperature of 100°C (and in fact precipitate anhydrite within mixed carbonate–silica deposits; Chapter 6) whereas Rembokola springs are slightly undersaturated (saturation temperature 110–120°C). All springs are supersaturated at K/Na temperatures. This reflects the addition of Ca to the springs at temperatures lower than $T_{K/Na}$ (Fig. 4.12 shows that the fluid added to the hydrothermal endmember is more Ca-rich).

Primary igneous anhydrite was identified in only one unaltered trachyte from Savo (from more than 50 samples studied in detail; Chapter 3). Anhydrite content was calculated to be ~0.17 wt %, by assuming that total sulphur (400 ppm, as analysed by Leco Carbon–Sulphur analyser) occurred as anhydrite. In more sulphate-rich systems, primary anhydrite can be a significant source of solutes for hydrothermal and non-thermal groundwaters, e.g.. El Chichón, Mexico (Taran et al., 1998), and Pinatubo, Philippines (Stimac et al., 2004). However, given its paucity, primary igneous anhydrite is unlikely to be a major sulphate source at Savo. If sulphate is derived from primary igneous anhydrite dissolution (Fig. 4.14A), then high temperature waters (i.e. those at K/Na temperatures) would contain lower sulphate contents than those observed, due to saturation considerations (anhydrite exhibits retrograde solubility). The cold water analyses (e.g. Table 4.9, SV422, and SV449) are all sulphate undersaturated, and so mixing with K/Na temperature fluids would actually lead to progressive *undersaturation*, not saturation. Additional anhydrite may be sourced on cooling by continued water-rock reaction, but other highly soluble, conservative elements are lower in Poghorovorughala springs than Rembokola (Cl^- 5 vs. 50 mg/l; Li 300 vs. 1600 μg/l, Cs 4 vs. 50 μg/l). This suggests dilution and not additional water–rock reaction is the dominant process differentiating Poghorovorughala and Rembokola springs, despite the fact that the former is closer to anhydrite saturation. To generate the observed characteristics, saturation with anhydrite must be achieved by mixing Ca-rich and hot, sulphate-rich waters to generate an anhydrite supersaturated fluid (Fig. 4.14B). Conservative, highly soluble elements would be retained in solution, and a “clean” (Cl, B, Li, Cs–poor) anhydrite would be rapidly precipitated. Continued addition of cool water (causing anhydrite undersaturation) leads to the dissolution of the hydrothermal anhydrite and dilution of Cl, Li, etc. Sulphate concentrations are maintained at (temperature-dependent) anhydrite saturation levels until the anhydrite has been entirely dissolved away.

The retrograde solubility of carbonate minerals may also lead to their precipitation in the subsurface, in particular as Ca–HCO_3^- rich water is heated by mixing with hydrothermal fluids. The alkaline sulphate waters have sufficiently high pH to allow travertine to deposit in the immediate vicinity of the springs (Chapter 6), but deeper in the system, pH is unknown and may be lower, depending on the proportion of magmatic volatiles and degree of rock reaction. Carbonates are likely to be important hydrothermal minerals where alkaline sulphate-type water boils below the surface (Simmons and Christenson, 1994).

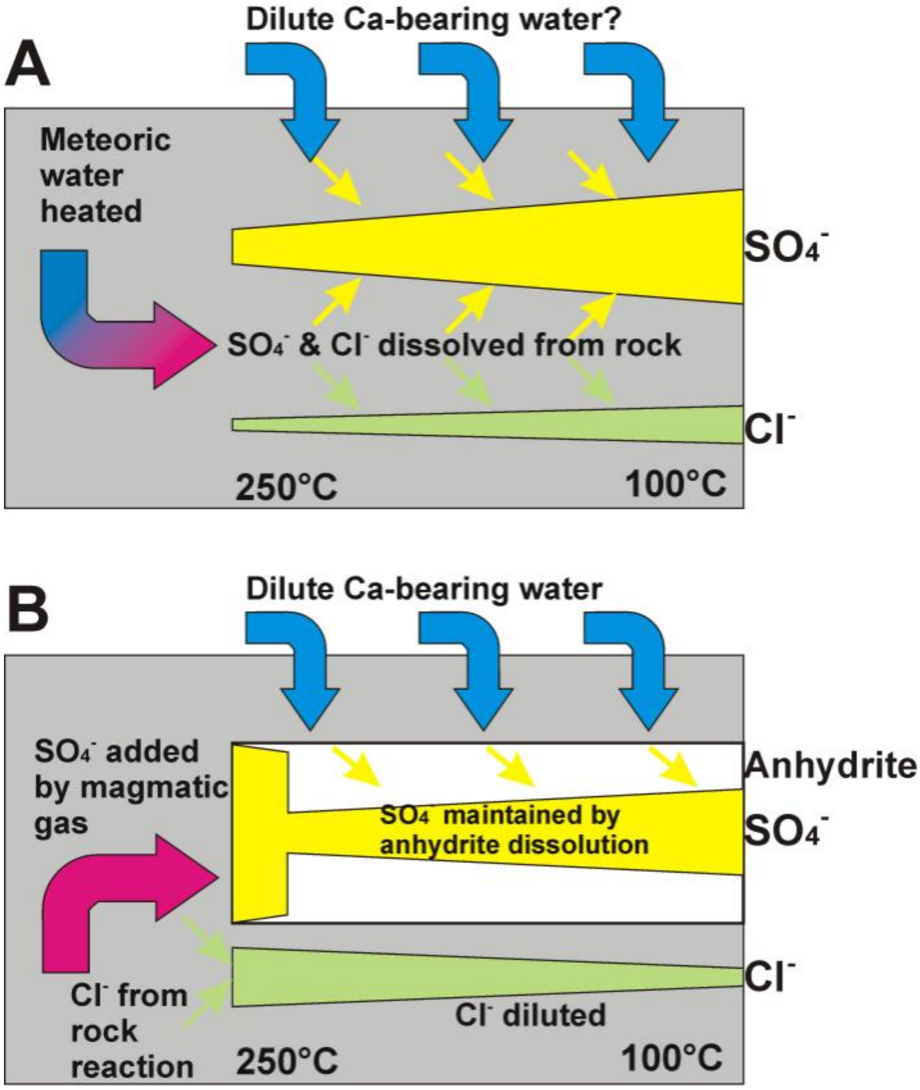

Fig. 4.14: Schematic diagram showing potential sources of sulphate for the hydrothermal fluids. The thickness of the bars for SO_4^{2-} and Cl^- is representative of concentration in solution. In A, sulphate is sourced from the host rocks; as such, SO_4^{2-} contents should correlate with Cl^- (also present in the host rocks). Anhydrite precipitation is limited, as addition of cold waters and cooling of hydrothermal water leads to progressive anhydrite undersaturation. In B, sulphate is derived from the disproportionation of SO_2 from a magmatic volatile phase. Cl^- is either magmatic or rock derived. Addition of cooler Ca-rich fluids leads to dilution of Cl^-; SO_4^- concentration is maintained at anhydrite saturation by precipitation and dissolution of anhydrite. Measured springs are consistent with model B: sulphate concentration does not co-vary with Cl^- (Fig. 4.12).

Loss of dissolved CO_2, for example during boiling, can lead to increase in pH and carbonate precipitation (Chafetz et al., 1991; Fouke et al., 2000)

Mixing of a hot, silica (as quartz) saturated fluid with a cooler silica undersaturated fluid may result in the precipitation of quartz, as silica solubility is temperature dependent (Fournier, 1985). However, dilution may lower the concentration of silica in solution such that quartz is undersaturated. Changes in pH have little to no effect below pH 8 (Rimstidt, 1997). Silica is precipitated at the Rembokola alkaline sulphate springs as sinter (Fig. 4.3; Chapter 6), and along with anhydrite and calcite at the Poghorovorughala springs (Fig. 4.6); similar mineral assemblages may be precipitated in the subsurface.

4.5.3 Acid sulphate springs

The acid sulphate springs discharge immature, non equilibrium fluids, based on Figures 4.10 and 4.11. The stable isotope systematics (Chapter 5) indicate a steam-heated origin for these springs – water is mostly meteoric or stream-derived surface water, with steam and gas providing additional heat, and sulphate is derived from the oxidation of H_2S, as in equation 4. Some of the springs are relatively isolated – typically those with the lowest pH (<4), high Al and Fe, and greatest $\delta^{18}O_{H2O}$ and δD_{H2O} enrichments (up to 15‰ and 40‰ greater than meteoric, respectively; Chapter 5) – whereas others are relatively open to periodic recharge from streams (e.g. SV454 in the Reoka area). The springs are all low discharge (only a few grams per second), and do not appear to have significant inputs from groundwater – in that respect they are perhaps better described as pools rather than springs.

Comparison of acid waters with other fluids in the nearby area, including alkaline sulphate springs (Fig. 4.9B) and streams (Fig. 4.9C), shows that acid springs have much higher Mn, Al, and Fe concentrations than any other nearby water types, reflecting the high solubility of these elements at low pH. The alkalis and alkali earths are generally closer in concentration to nearby stream waters, but acid springs show a much more variable concentrations of those elements, probably due to acid attack of surrounding host rocks and sediments. This results in alteration of surrounding rocks to a base-depleted assemblage of kaolinite + silica ± anhydrite ± alunite. Two of the acid sulphate springs analysed in 2006 (SV454 and SV436) had high DIC. This is likely a result of recharge from the HCO_3^--rich stream waters (e.g. Table 4.8).

4.5.4 Warm bicarbonate springs

Small bicarbonate-rich warm springs occur at Tanginakulu and Reoka (SV449 and SV422). Discharge rates are lower than the alkaline sulphate springs, but higher than the acid sulphate springs (on the order of 0.1 kg/s). In contrast with the acid sulphate springs, the warm springs are recharged by groundwater rather than surface water. Bicarbonate and bicarbonate-sulphate fluids are relatively common in geothermal areas, occurring in parts of the system where CO_2 condenses into cold groundwater (Ellis and Mahon, 1977), either at depth, or at the periphery of steam heated areas.

Sulphate and bicarbonate are the dominant anion species. Sulphate is derived from oxidation of H_2S, or by small amounts of mixing with other sulphate-rich fluids. The elevated Ca and in particular Mg concentrations indicate that the water discharged at these springs has undergone moderate to low temperature (<100°C) reaction with the host rocks

(Fig. 4.12). The Reoka warm spring shows a position somewhat intermediate between the Tanginakulu spring and the Rembokola alkaline sulphate springs, and as such may represent a mixture of the two fluid types. As discussed in section 4.5.2, cool bicarbonate-rich groundwater similar to that discharged at Tanginakulu may be responsible for the mixing characteristics seen in the alkaline sulphate springs.

4.5.5 A model for the hydrothermal system of Savo

The hydrothermal system and the distribution of the various fluid types is summarised schematically on Figure 4.15. The system is divided into zones where a particular water type is expected to dominate; in reality, the distribution of a particular fluid will be controlled by fractures and permeable horizons in the volcanic edifice.

Heat and magmatic volatiles, chiefly water vapour, CO_2, SO_2 and H_2S, condense into meteoric-derived groundwater to produce initially acidic, ~300°C hydrothermal fluids. Acidity will be progressively neutralised by reaction with surrounding host rocks. Alteration assemblages will depend on the pH. If initial pH is <2, base leaching will be near-total at the core of the condensation zone resulting in an advanced argillic mineral assemblage dominated by residual silica, kaolinite and its polymorphs, and alunite (Stoffregen, 1987). As pH increases (or at higher initial pH), fluid composition is controlled by minerals such as clinochlore, paragonite and secondary albite (Reed, 1997).

The composition of the fluids discharged at the surface is controlled by a combination of water–rock reaction and fluid mixing. Cool waters at Savo generally have high Ca, Mg and HCO_3^-, and it can be seen by comparison of Poghorovorughala and Rembokola springs that the former have a greater component of cool water. The role of these cool waters could be an important control on the hydrothermal system's chemistry at depth, as the initial pH of magmatic volatiles condensing into such waters will be controlled by both dilution and reaction with HCO_3^- (equation 11). Anhydrite may precipitate by the mixing of sulphate-rich and Ca-rich fluids. Continued flushing with cool waters would lead to dissolution of anhydrite though – final discharged fluids have a sulphate content dictated by competition between dissolution and dilution.

The alkaline sulphate fluids generated by the combination of magmatic condensation, rock reaction and mixing boil beneath the surface to generate widespread areas of steaming ground on the flanks and in the central crater. Hydrogen sulphide is oxidised at the surface and generates zones of acid alteration. Where steam condenses into surface waters, acid springs develop. Initial chemistry is controlled by water origin (in most cases, nearby

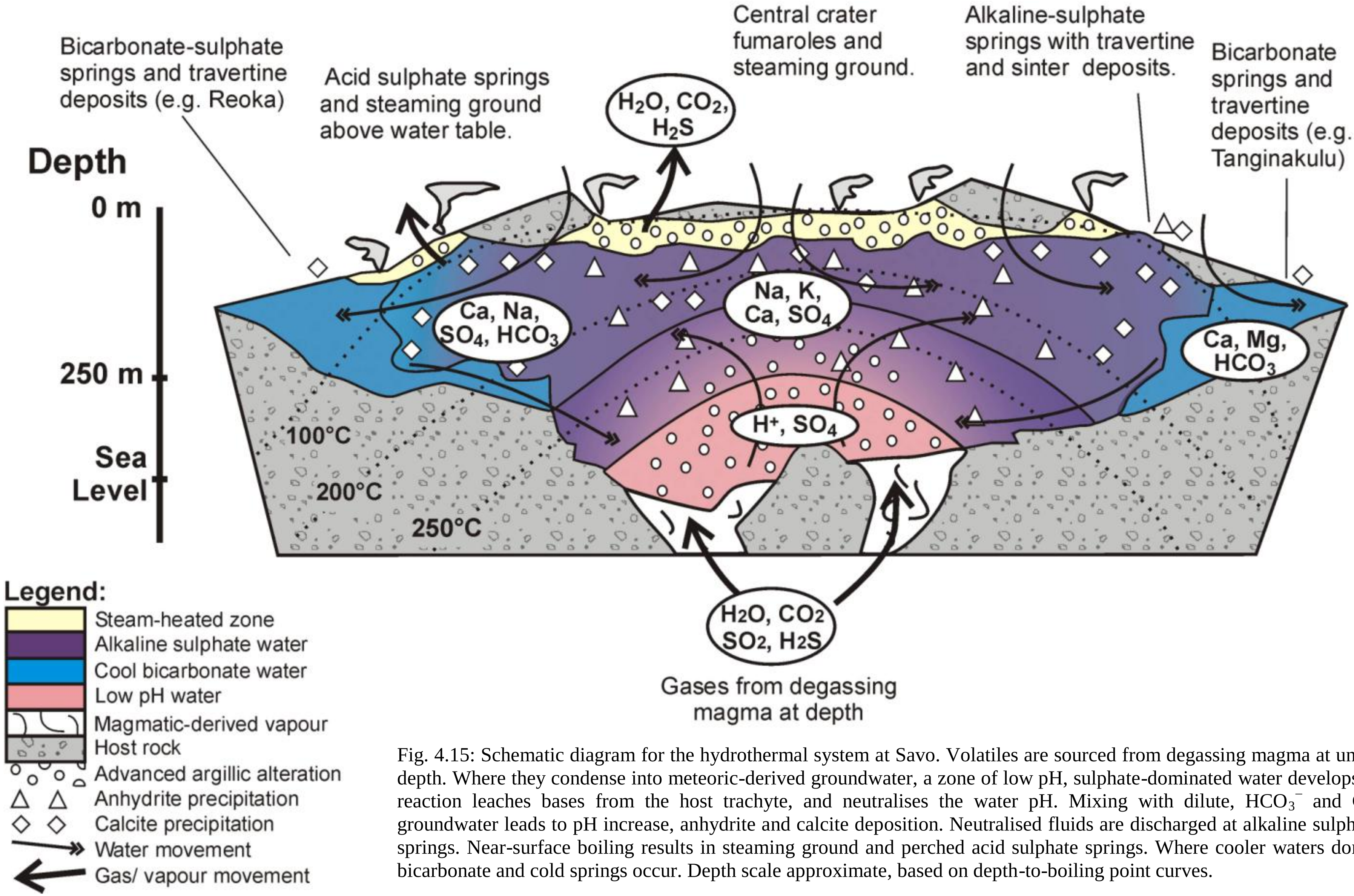

Fig. 4.15: Schematic diagram for the hydrothermal system at Savo. Volatiles are sourced from degassing magma at unknown depth. Where they condense into meteoric-derived groundwater, a zone of low pH, sulphate-dominated water develops. Rock reaction leaches bases from the host trachyte, and neutralises the water pH. Mixing with dilute, HCO_3^- and Ca-rich groundwater leads to pH increase, anhydrite and calcite deposition. Neutralised fluids are discharged at alkaline sulphate hot springs. Near-surface boiling results in steaming ground and perched acid sulphate springs. Where cooler waters dominate, bicarbonate and cold springs occur. Depth scale approximate, based on depth-to-boiling point curves.

stream water), but as pH decreases by addition of steam, surrounding rocks are leached, and the springs becomes enriched in both base cations (Na, K, Ca, Mg) but also silica and aluminium.

Where cooler waters dominate, CO_2 will dissolve to produce bicarbonate waters. Low temperature water–rock reactions lead to fluids with high Mg and Ca relative to the high temperature fluids. These fluids ultimately discharge as springs such as the Tanginakulu warm spring. This dilute, bicarbonate rich fluid is a good candidate for the low temperature contributor to the Poghorovorughala springs. Reoka stream waters are intermediate between Tanginakulu and Rembokola springs; such waters are produced by combined dilution of the high temperature hydrothermal fluid and CO_2 absorption as temperature decreases.

Thermal waters dominate Savo, as nearly all springs and wells have temperatures above mean annual air temperature. Rembokola springs represent the most "hydrothermal-dominated" waters, and the cold springs the most dilute, but neither is a true endmember. The hydrothermal system at Savo may be considered an open system, with relatively free mixing of fluids at depth. The abundance of cooler waters to dilute the hydrothermal system reflects the tropical climate of the Solomon Islands and high annual rainfall (annual rainfall 3–5 m; Solomon Islands Meteorological Service). Climate may be a crucial influence on the hydrothermal system, particularly to generate high pH.

4.6 Conclusions

The high pH fluids discharged at Savo are the result of a combination of processes, including the formation of initially sulphate-rich, acidic fluids at depth, their subsequent dilution and modification by rock reaction and mixing with cooler waters, and by precipitation and dissolution of minerals such as anhydrite.

Although the trachyte host rocks play an important role in neutralising any acidity, dilution is the key process whereby the alkaline sulphate fluids derive their high pH and general chemical characteristics. Continued mixing with meteoric-dominated, Ca–Mg–HCO_3^- fluids results in spring discharges that only partially record reservoir conditions; at discharge the chemistry has been greatly modified from that which was presumably in equilibrium with a hydrothermal mineral assemblage at depth.

Chloride in particular provides evidence for heavily diluted hydrothermal fluids; sulphate is the major anion but responds differently to fluid mixing and dilution than chloride because of its precipitation as anhydrite, and subsequent dissolution as a mineral with retrograde solubility. Anhydrite is initially precipitated by fluid mixing between a sulphate rich hydrothermal fluid and a cool, calcium rich groundwater; sulphate concentrations are buffered to anhydrite saturation by continued dilution – at least until all the anhydrite is dissolved. Significant deposits of hydrothermal anhydrite are likely to exist at depth on Savo.

Stable isotope evidence for magmatic contributions to the alkaline hydrothermal system at Savo

5

Abstract

The presence of HCl and SO_2 in magmatic volatiles commonly results in the development of low pH fluids in magmatic-hydrothermal environments. However, epithermal Au deposits related to alkaline magmatism rarely show evidence for acidic fluids, despite significant magmatic contributions. Savo volcano, Solomon Islands, is a trachyte-dominated stratovolcano with a hydrothermal system that discharges alkaline (pH 7–8) waters at a number of hot springs from the upper flanks of the edifice, as well as a smaller number of low discharge acid springs (pH 2–7). A stable isotope study of the hot springs was carried out to determine whether or not magmatic volatiles are an important contributor to these fluids. Aqueous sulphate for alkaline springs had significantly higher $\delta^{34}S$ (3.8 to 6.8‰) values than fumarolic sulphur and sulphate in acid springs (−6 to 2‰). The isotopic distinction between these two species of sulphate is interpreted to be due to the disproportionation of magmatic SO_2 into H_2SO_4 and H_2S upon reaction with water. Oxygen and hydrogen isotope ratios of water indicate that the hydrothermal fluids are dominantly meteoric. $\delta^{18}O$ and δD enrichments in the hydrothermal fluids (relative to local meteoric water) are generated by additions from magmatic fluids, water–rock reaction and boiling. Any acidity from magmatic volatiles is neutralised by rock reaction and dilution; the resulting hydrothermal water is discharged as high pH hot springs. Where this water boils at depth, steam and H_2S separate to form a shallow steam-heated zone and acid springs. The hydrothermal system at Savo is a potential analogue for alkaline rock-related epithermal deposits.

5.1 Introduction

Shallow hydrothermal systems in subduction-related volcanic settings are the most important environment where epithermal gold deposits form (Henley and Ellis, 1983; Hedenquist and Henley, 1985; Hedenquist et al., 1993; Hedenquist and Lowenstern, 1994; Simmons and Brown, 2006). Volcanoes and volcanic areas such as White Island and the Taupo Volcanic Zone are widely recognised to be the active analogues for the two main styles of epithermal gold mineralisation (Table 5.1), high and low sulphidation. However, in the southwest Pacific, there are notable epithermal Au deposits such as Ladolam

(37.1 Moz contained Au; Carman, 2003) and Porgera (11 Moz Au reserves; Richards and Kerrich, 1993), Papua New Guinea and Emperor, Fiji (11 Moz Au; Ahmad et al., 1987; Pals and Spry, 2003), hosted in alkaline volcanic rocks, that do not fit these models. Studies of these deposits suggest that, as in high sulphidation epithermal mineralisation, magmatic fluid contributions are an important component for metallogenesis (Richards, 1995; Jensen and Barton, 2000; Simmons and Brown, 2006), but hydrothermal alteration suggests neutral fluids (Sillitoe, 2002), more typical of volcanic environments dominated by surficial waters.

Here, we present elemental and isotope geochemical data for Savo, an active magmatic-hydrothermal system in the central Solomon Islands. Savo is a recently active volcano that hosts a hydrothermal system manifested at the surface by abundant hot springs and fumaroles. Unaltered magmatic rocks, like those that host mineralisation at Ladolam, Porgera and Emperor, are alkalic, and the majority of hot springs discharging from the upper flanks of the volcano are high pH (typically 7–8), with a smaller number with acid pH (2–7). The study was carried out to assess the magmatic contributions to the hydrothermal system, to examine the early stages of magmatic-hydrothermal activity in alkaline rock-related systems, and to determine whether the system at Savo is an active analogue for alkaline rock-related magmatic-hydrothermal gold deposits in the southwest Pacific.

5.1.1 Classification of epithermal hydrothermal systems and related mineral deposits

Magmatic-hydrothermal systems and their mineral deposit equivalents are classified according to a number of characteristics. An exhaustive review of the spectrum of epithermal hydrothermal systems and mineral deposits is beyond the scope of this paper, and thorough reviews on the topic are provided in Cooke and Simmons (2000), Heald et al. (1987), Hedenquist et al. (2000), Sillitoe and Hedenquist (2003) and Simmons et al. (2005). A brief summary of the three main classes of epithermal hydrothermal systems – magmatic-hydrothermal, hydrothermal/geothermal, and alkalinerock -associated magmatic -hydrothermal – is provided in Table 5.1, together with the characterisation of their associated epithermal mineral deposit and alteration styles.

From Table 5.1 it is clear that fluid pH and host rock composition alone is insufficient to classify the system at Savo as alkaline rock-related; magmatic contributions to the hydrothermal system are an important characteristic of this class of system. For Savo to be

System (Pseudonyms)	Typical Host Rocks	Fluid Sources	General Fluid Characteristics	Alteration	Epithermal Mineral Deposit Type (Pseudonyms)	Metals	Examples	Mineral Deposit Examples	Selected References
Magmatic Hydrothermal (Volcanic Hydrothermal)	Calc-alkaline andesite to rhyodacite	Magmatic + meteoric ± marine	Acidic (H_2SO_4 + HCl) Oxidised <2–15 wt.% NaCl, occasionally much higher	Vuggy silica, alunite, kaolinite, dickite, pyrophyllite	High Sulphidation (acid sulphate)	Au, Ag, Cu, As, Sb	White Island, New Zealand; Vulcano, Italy	El Indio, Chile; Lepanto, Philippines	Boyce et al. 2007; Fulignati et al. 1998; Giggenbach et al. 2003; Hedenquist et al. 1993; Stoffregen, 1987
Hydrothermal (Geothermal)	Andesite to rhyodacite Bimodal basalt-rhyolite	Meteoric ± Magmatic ± marine	Neutral pH Reduced <10wt% NaCl	Quartz, chalcedony, calcite, adularia, illite	Low Sulphidation (adularia-sericite; hot spring type)	Au, Ag	Broadlands-Ohaaki, New Zealand	Waihi, New Zealand; Midas, Nevada	Christenson et al. 2002; Giggenbach 1988; Heald et al. 1987; Henley & Ellis, 1983; Hedenquist & Henley 1985; Simmons & Browne, 2000
Alkaline Associated Magmatic Hydrothermal	Alkaline	Magmatic + meteoric ± marine	Neutral to alkaline pH Oxidised? <10 wt.% NaCl	Calcite, chalcedony, quartz, roscoelite, adularia	Alkaline-associated epithermal (Au-telluride; alkalic low sulphidation)	Au, Te	Ladolam, Papua New Guinea; *Savo?*	Emperor, Fiji; Porgera, PNG; Ladolam, PNG	Carman 2003; Eaton & Setterfield 1993; Jensen & Barton 2000; Muller, 2002; Richards 1995; Sillitoe 2002; Simmons & Brown 2006

Table 5.1: Classification and key features of the three major classes of epithermal hydrothermal systems and associated mineral deposits. Follows summaries by Cooke and Simmons (2000), Heald et al. (1987), Hedenquist et al. (2000), Sillitoe and Hedenquist (2003) and Simmons et al. (2005).

discussed as analogous to alkaline rock-related deposits, the contributions of magmatic fluids (if any) to the system must be determined.

5.2 Sampling and analytical methods

To investigate the hydrothermal system at Savo, two field campaigns (April–May 2005; September–October 2006) were carried out. Where sampling protocol or analytical technique were modified for the second campaign has been noted. Sampling areas are marked on Figures 5.1, 4.2 and 4.5.

5.2.1 Water and steam sampling

Water samples were collected directly from springs, or from large containers of well water. The water was pumped through a <0.45 μm in-line PTFE syringe filter using silicone

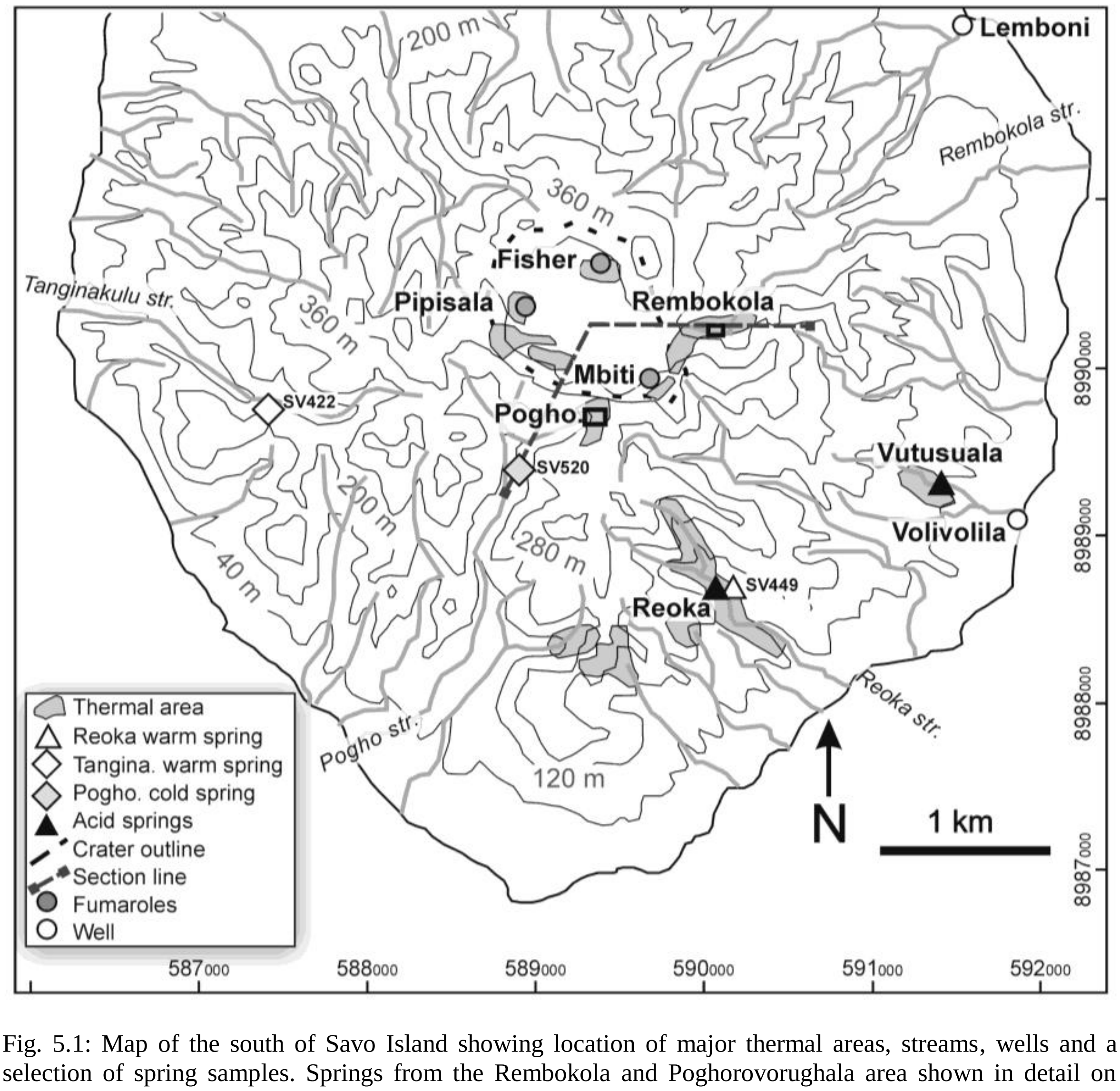

Fig. 5.1: Map of the south of Savo Island showing location of major thermal areas, streams, wells and a selection of spring samples. Springs from the Rembokola and Poghorovorughala area shown in detail on Figures 4.2 and 4.5 respectively (locations marked with boxes). Specific sample locations for Reoka and Vutusuala are too close together to display clearly at this scale. Grid references are for UTM zone 57L.

tubing and a hand vacuum pump. To ensure all equipment was free from contamination by previous samples, approximately 150 ml of sample was pumped and discarded three times before collecting the sample.

Steam and gas were collected from fumaroles and steaming ground by burying a polypropylene funnel at the hottest part. Steam and gas were pumped through silicone tubing and a stainless steel cooling coil into two borosilicate glass flasks with stopcocks at each end. Condensed steam was collected in the first flask and non-condensable gases in the second (Darling and Talbot, 1991).

5.2.2 Water chemistry

In the field, pH measurements were determined from filtered samples as soon as possible after collection using Hanna Instruments digital pH meters HI98128 and HI991001with automatic temperature calibration. Samples were cooled to <60°C before pH measurement. Hot spring pH measurements were corrected to discharge temperature (pH_C) using major cations and anion composition (Chapter 4) with SOLVEQ (Reed, 1982) by the method outlined in Reed and Spycher (1984).

Total sulphur content was determined from 30 ml samples acidified in the field with 0.3 ml Tracepur® 69% HNO_3. Analysis was by ICP-AES using a Fisons/ARL3580 spectrometer with Gilson 222 Autosampler at BGS Keyworth, using the procedures described in Ault et al. (1999). Samples for ICP-AES were diluted by five times (2005) or two times (2006) using 1% Aristar® grade HNO_3 to avoid precipitation of solids in the spectrometer's nebuliser apparatus. Total sulphur represents sulphate content of acidified samples, and data are reported accordingly. BGS Keyworth is a UKAS Accredited laboratory and participates in the Aquacheck proficiency testing scheme. Analyses conform to ISO 17025, and reported values have an uncertainty within 2%.

5.2.3 Sulphur isotopes

For aqueous sulphate analysis, 75 ml (100 ml for 2006 samples) was decanted in the field into a HDPE bottle and acidified with 1 ml Tracepur® 69% HNO_3, and an excess of 5% $BaCl_2$ solution was added slowly to the sample to precipitate $BaSO_4$. In the laboratory, precipitated $BaSO_4$ was separated from the water by centrifuge. Resulting solids were rinsed with deionised water and dried at 80°C overnight. Recovered solids were weighed and the gravimetric yield was used to calculate SO_4^{2-} contents of the water samples. These data were compared with the ICP-AES results as an approximate measure of recovery; recoveries were 100% ± 10% with the exception of SV212 (80%).

Native sulphur crystals were hand picked from altered rocks collected at fumarolic areas, washed in deionised water in an ultrasonic bath for five minutes and dried in a desiccator overnight.

Sulphur and sulphate samples were converted to SO_2 for mass spectrometry at the Scottish Universities Environmental Research Centre (SUERC) by conventional combustion procedures (Robinson and Kusakabe, 1975; Coleman and Moore, 1978). Determination of the sulphur isotope composition of the purified SO_2 gas was carried out using a VG SIRA II gas mass spectrometer and standard corrections applied to raw $\delta^{66}SO_2$ values to produce true $\delta^{34}S$. Calibration, reproducibility and accuracy were monitored through replicate measurements of international standards NBS 123 (17.7 ± 0.3‰, n = 16), IAEA S3 (−31.6 ± 0.3‰, n = 16), NBS 127 (21.2 ± 0.8‰, n = 17) and SUERC internal laboratory standard CP-1 (−4.6 ± 0.7‰, n = 24); mean values for standards are within error of the accepted values (Coplen et al., 2002; Lipfert et al., 2007). All sulphur isotope compositions were calculated relative to Vienna Cañon Diablo Troilite (V-CDT), and are reported in standard permil notation. Sulphur isotope data are further discussed in Appendix II.

Primary igneous anhydrite was observed in an unaltered trachydacite sample (SV40). Approximately 50 g of sample was leached in 1 M HCl at 40°C, filtered, and 5% BaCl2 added to the resulting liquid to precipitate BaSO4, which was subsequently separated, washed and analysed as above.

5.2.4 Oxygen and hydrogen isotopes

In the field, an unacidified fraction for isotopic analysis was decanted into a 14 ml glass McCartney bottle with a rubber lined cap. Oxygen was analysed at SUERC using an automated CO_2 equilibration technique (after Epstein and Mayeda, 1953) using 1 ml of sample and analysing the resulting equilibrated CO_2 on an Analytical Precision AP2003 continuous-flow isotope ratio mass spectrometer. Water was reduced to H_2 using a chromium furnace (Donnelly et al., 2001) and analysed using a VG SIRA 9 mass spectrometer (2005 samples) and a VG Optima (2006 samples). Reproducibility was within ± 1.0‰ for $\delta^{18}O$ and ± 5‰ for δD.

Steam condensates were measured at the British Geological Survey in Wallingford for $\delta^{18}O$ by equilibration with CO_2 at 25°C; and for δD by reduction to H_2 with zinc at 450°C for one hour. Analysis of both was carried out with a VG Optima mass spectrometer. Reproducibility was within ±0.2 ‰ for $\delta^{18}O$ and ±2 ‰ for δD. All oxygen and hydrogen isotope data are reported in standard notation with respect to V-SMOW.

The $\delta^{18}O$ of precipitated sulphate was measured at SUERC using the technique of Hall et al. (1991). Barium sulphate was mixed with pure carbon in a platinum crucible and heated in a vacuum line to produce CO_2. Any CO produced was converted to C and CO_2 in a Pt-electrode vessel. The resulting CO_2 was analysed on a VG Isogas SIRA 10 mass spectrometer. Reproducibility was monitored by repeat analysis of international standard NBS 127 (8.6 ± 0.4‰, n = 10, accepted value 8.7‰; Kornexl et al. 1999).

5.2.5 Strontium isotopes

Sr analysis was performed on unacidified water fractions at the NERC Isotope Geosciences Laboratories (NIGL). Sr was separated by standard techniques using Dowex AG50W-X8 ion exchange resin (Royse et al., 1998). Samples were loaded onto single Re filaments using a TaO activator, and analysed using a Thermo-Finnigan Triton mass spectrometer in static multicollection mode. The Sr blank at the time of analysis was 111 pg. Replicate analyses of the SRM987 standard solution gave an average value of 0.710263 ± 0.000004 (1σ, n=50). Data are reported normalised to SRM987 = 0.710250.

5.3 Results

5.3.1 Spring classification

Hot springs defined as alkaline sulphate type are >80°C, and pH 7–8; anions are dominated by sulphate (600–680 mg/l); chloride contents are very low in all springs analysed (Tables 4.5 and 4.6). Na and Ca are the dominant cations, although their relative abundance varies with location (Na is more abundant in Rembokola springs, as discussed in Chapter 4). Flow rates are visibly higher than the acid sulphate springs, with the alkaline sulphate springs being the major contributors to water in the streams in the south of the island. Mixed silica–carbonate–sulphate sinters are found surrounding and downstream of alkaline sulphate springs.

Springs classified as acid sulphate type have temperature >80°C, pH typically <7 and often <3. Acid sulphate springs are found in areas of steaming ground and advanced argillic alteration (silica + kaolinite ± native sulphur). Acid sulphate springs are slow to recharge if emptied, and may be better described as stagnant pools rather than springs. There are no sinters or travertine deposits found surrounding acid sulphate springs. Although some of the springs are pH >6, their chemical composition (significant Al and Fe contents, low $\delta^{34}S_{SO4}$ values) and physical appearance means it is more appropriate to classify them with the low pH springs.

Cold springs (<30°C) show similar pH values to alkaline sulphate hot springs, but have more dilute chemistry (Table 4.9). Recharge and discharge of the cold springs was visibly slower than the alkaline sulphate hot springs.

5.3.2 Sulphur isotopes

Aqueous sulphate from alkaline sulphate hot springs were found to have a narrow range of $\delta^{34}S$ values, from +3.8 to +6.8‰ (Table 5.2) . There is no significant variation with time or location, and no correlation with total sulphate content (Fig. 5.2).

Cold springs, where sulphate contents were sufficiently high for analysis, showed $\delta^{34}S$ values similar to the alkaline hot springs at +5‰. The warm spring at Tanginakulu had similar sulphate concentrations and $\delta^{34}S$ values to the cold springs.

Acid sulphate springs have $\delta^{34}S$ values ranging from −3.6 to +2.0‰ (Table 5.2), showing a weak correlation between increasing $\delta^{34}S$ value and total sulphate content (Fig. 5.2).

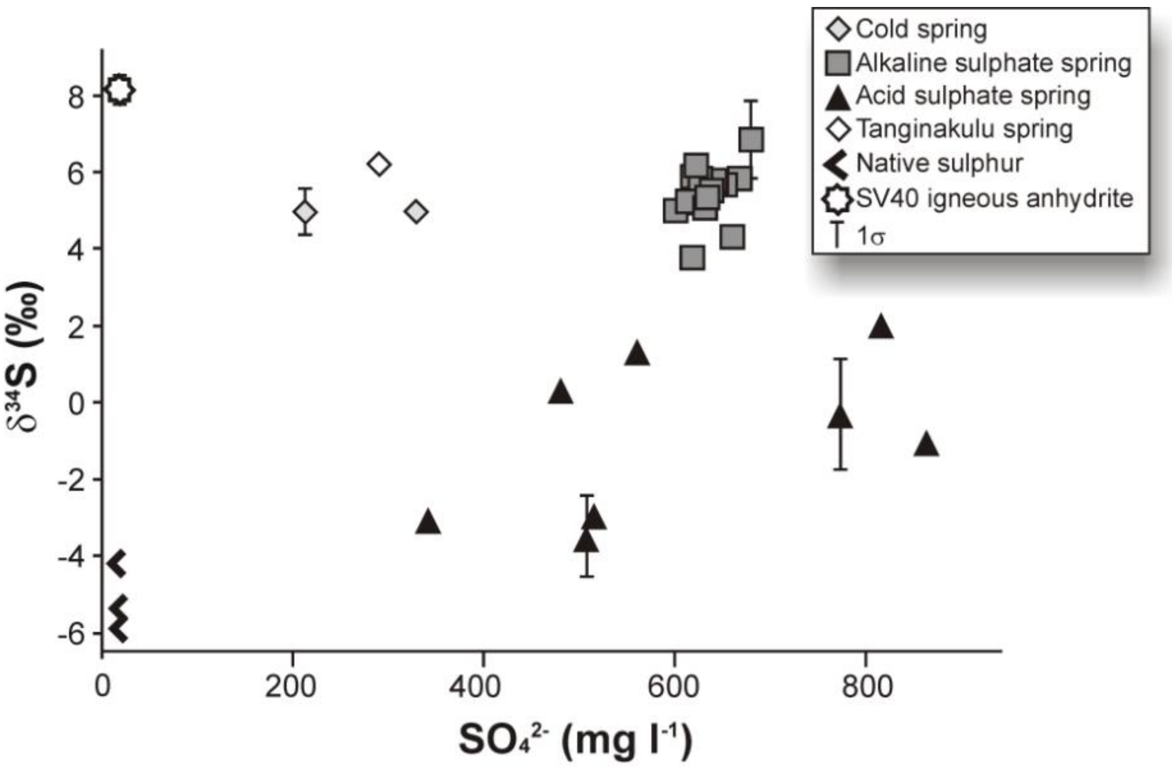

Fig. 5.2: $\delta^{34}S_{SO4}$ vs. total sulphate content of alkaline and acid hot springs, cold and warm springs from Savo. $\delta^{34}S$ values for igneous anyhdrite and native sulphur shown for comparison. For replicated analyses, error bars represent one standard deviation; most are within symbol size.

Label	Area	Site	Type	Date	T °C	pH	SO_4 mg l^{-1}	$\delta^{34}S_{SO4}$	$\delta^{18}O_{SO4}$	$\delta^{18}O_{H2O}$	δD_{H2O}	$^{87}Sr/^{86}Sr$
SV208	Pogho.		Alk.	25/05/05	99	7.2	619	3.8	4.0	3.0 ± 0.2	–13 ± 1.6	0.704199
SV498	Pogho.		Alk.	18/10/06	100	7.7	681	6.8 ± 1.0	7.7	–3.7 ± 0.6	–35 ± 2.3	
SV206	Pogho.	Mound	Alk.	25/05/05	100	6.8	602	5.0		–3.2	–35 ± 1.7	
SV500	Pogho.	Mound	Alk.	18/10/06	100	7.5	669	5.8 ± 0.4	6.1	–3.7 ± 0.7	–36 ± 3	
SV516	Pogho.	Mound	Alk.	21/10/06	100	7.5	661	4.3	7.2	–4.7 ± 0.1	–39 ± 0.5	
SV207	Pogho.		Alk.	25/05/05	100	7.1	623	6.2	5.8	–2.0	–29 ± 2.8	0.704178
SV499	Pogho.		Alk.	18/10/06	96	7.7	679			–3.6 ± 0.7	–37 ± 1.0	
SV491	Remb.		Alk.	16/10/06	99	7.6	624	5.2	6.7	–4.5 ± 0.2	–36 ± 0.3	
SV230	Remb.	F1	Alk.	29/05/05	100	7.8	633	5.0 ± 0.1	6.0	–4.4	–36 ± 4.7	
SV485	Remb.	F1	Alk.	15/10/06	100	7.5	627	5.8	6.7	–3.9 ± 0.5	–25 ± 4.5	
SV488	Remb.	F1	Alk.	16/10/06	82	7.6	643	5.8	6.2	–4.1 ± 0.1	–33 ± 0.1	
SV229	Remb.		Alk.	29/05/05	100	7.6	639	5.5 ± 0.7		–4.6	–36 ± 2.3	0.704109
SV232	Remb.	F3	Alk.	29/05/05	100	7.8	635	5.4 ± 0.4		–3.7	–36 ± 4.7	0.704111
SV487	Remb.	F3	Alk.	16/10/06	100	7.8	614	5.2	7.9	–4.6	–35 ± 0.1	
SV231	Remb.		Alk.	29/05/05	100	7.6	642	5.7 ± 0.01		–4.5	–38 ± 4.7	0.704115
SV490	Remb.		Alk.	16/10/06	99	7.6	620	5.9 ± 0.5	5.6	–4.2 ± 0.1	–34 ± 0.8	
SV233	Remb.		Alk.	29/05/05	97	7.8	653	5.7 ± 0.4	5.6	–3.5	–38 ± 4.9	
SV503	Pogho.		Acid	18/10/06	98	3.2	817	2.0 ± 0.1		0.7 ± 0.5	–27 ± 3.3	
SV515	Pogho.		Acid	21/10/06	100	3.0	774	–0.4 ± 1.5		7.7 ± 0.2	–8 ± 0.5	
SV209	Pogho.		Acid	25/05/05	100	4.1	481	0.3	5.2	6.8 ± 0.3	–3 ± 1.7	0.704241
SV213	Reoka		Acid	26/05/05	100	2.7	516	–3.0	2.2	3.8 ± 0.5	–3 ± 1.9	
SV212	Reoka		Acid	26/05/05	100	6.1	342	–3.1	1.3	–0.9 ± 0.5	–24 ± 2.3	0.704161
SV453	Reoka		Acid	10/10/06	89	6.9	561	1.3		0.0 ± 0.1	–21 ± 1.5	
SV458	Reoka		Acid	11/10/06	91	6.7	865	–1.1 ± 0.4		4.6 ± 0.8	–3 ± 0.3	
SV454	Reoka		Acid	10/10/06	83	7.3	247			–5.9 ± 0.1	–39 ± 3.1	
SV201	Vutu.		Acid	24/05/05	100	5.5	332			2.8	–7 ± 3.9	0.704290
SV435	Vutu.		Acid	08/10/06	98	7.0	508	–3.6 ± 1.0		4.7 ± 0.2	–7 ± 2.2	
SV436	Vutu.		Acid	08/10/06	95	7.6	151			–3.6 ± 0.4	–34 ± 2.2	
SV211	Pogho.		Cold	25/05/05	26	8.1	213	5.0 ± 0.6		–8.1 ± 0.2	–47 ± 2.7	0.704167
SV520	Pogho.		Cold	21/10/06	26	8.0	329	5.0 ± 0.04		–8.0 ± 0.1	–43 ± 1.3	
SV235	Remb.		Cold	29/05/05	26	7.5	107			–8.1	–45 ± 4.8	0.704129
SV422	Tangina.		Warm	07/10/06	47	6.7	294	6.1		–7.4 ± 0.4	–42 ± 1.0	
SV199	Lemboni	1	Well	24/05/05	34	6.9	113	4.9		–7.3 ± 0.4	–41 ± 1.7	0.704419
SV379	Lemboni	1	Well	28/09/06	36	7.3	162			–7.2	–41 ± 7.2	
SV197	Lemboni	2	Well	24/05/05	33	7.2	58			–7.6 ± 0.2	–46 ± 1.2	
SV410	Lemboni	2	Well	03/10/06	34	7.2	94			–7.6	–46 ± 3.5	
SV200	Lemboni	3	Well	24/05/05	39	6.3	103	5.6		–7.8	–44 ± 3.6	
SV204	Volivolila		Well	24/05/05	29	7.0	24			–7.7	–41	0.704674
SV244	Crater	Fisher	St.	30/05/05	100					–5.0	–51	
SV246	Crater	Fisher	St.	30/05/05	100					–7.1	–69	
SV305	Crater	Fisher	St.	11/09/06	100					–6.6	–56	
SV306	Crater	Fisher	St.	11/09/06	100					–6.6	–50	
SV307	Crater	Fisher	St.	11/09/06	100					–7.2	–47	
SV247	Crater	Mbiti	St.	30/05/05	100					–7.7	–57	
SV248	Crater	Mbiti	St.	30/05/05	100					–13.0	–84	
SV301	Crater	Mbiti	St.	10/09/06	100					–8.6	–56	
SV302	Crater	Mbiti	St.	10/09/06	100					–6.9	–59	
SV303	Crater	Mbiti	St.	10/09/06	98					–14.3	–80	
SV240	Crater	Pipisala	St.	30/05/05	101					–14.7	–106	
SV133	Reoka		S	16/05/05				–5.4				
SV216	Pogho.		S	25/05/05				–4.2				
SV217	Pogho.		S	25/05/05				–5.6 ± 0.3				
SV237	Crater	Pipisala	S	30/05/05				–5.9				
SV40	Crater		Ig					8.1 ± 0.4				

Table 5.2: Isotopic compositions of samples from Savo volcano. Samples are from unique sites unless specifically named and noted in the "site" column. All isotope values in standard notation. Results of multiple analyses are shown as averages ± 1σ. Abbreviations as follows: Pogho. = Poghorovorughala; Remb. = Rembokola; Vutu. = Vutusuala; Alk. = Alkaline sulphate spring; St. = steam sample; S = native sulphur sample, Ig= igneous anhydrite

Native sulphur collected from areas of steaming ground and fumarolic / solfataric activity shows negative $\delta^{34}S$ values, ranging from −4.2 to −5.9‰ (Table 5.2).

Sulphate leached from trachyte SV40 has a value of +8.1‰ SV40 has a total sulphur content of approximately 400 ppm (analysed by Leco CS230 Carbon/Sulphur Determinator at the University of Leicester).

5.3.3 Oxygen and hydrogen isotopes of water

Figure 5.3 shows oxygen and hydrogen isotope compositions of water and steam from Savo. Alkaline sulphate hot springs are clustered at $\delta^{18}O = -4 \pm 0.8$‰ and $\delta D = -36 \pm 3$‰, with three outliers, all showing enrichment of the heavier isotopes. SV208 shows considerable enrichment of both ^{18}O and D, and also has the lowest $\delta^{34}S_{SO4}$ value (+3.8‰) of the alkaline sulphate springs.

Acid sulphate springs range from $\delta^{18}O = -5.9$‰ and $\delta D = -39$‰ to $\delta^{18}O = +6.8$‰ and $\delta D = -3$‰. The data form a linear array with slope 2.9 (1σ scatter around line is ±5.4‰ δD). Two of the alkaline sulphate outliers (SV207 and the most extreme outlier, SV208) also lie on this trend.

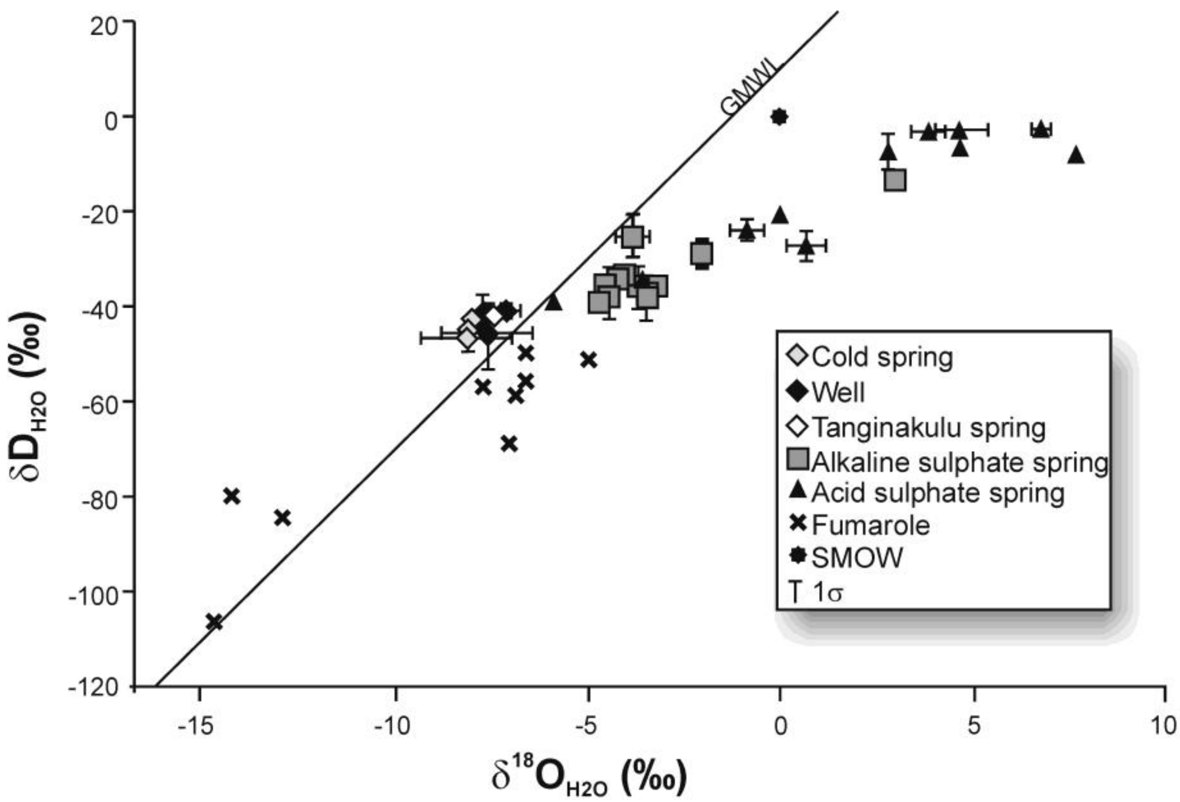

Fig. 5.3: δD_{H2O} vs. $\delta^{18}O_{H2O}$ for alkaline and acid sulphate hot springs, warm and cold springs, wells, and condensed fumarole steam. Error bars represent one standard deviation from mean value for samples analysed in triplicate; most are within symbol size. GMWL = Global meteoric water line.

Cold spring samples cluster around $\delta^{18}O = -8‰$ and $\delta D = -45‰$, depleted in the heavy isotopes of oxygen and hydrogen relative to the alkaline hot springs. The cold springs lie just above the global meteoric water line, and overlap with compositions of waters collected from cold wells and the Tanginakulu warm spring.

Condensed steam collected from fumaroles and steaming ground in the crater plots on an array with a slope of 4.8 (1σ scatter around line is ±8.9‰ δD). Isotopically heavy steam samples (from Fisher Voghala and the crater floor fumarole of the Mbiti Voghala area; Fig. 5.1) have δD values similar to those of cold springs, but are shifted to higher $\delta^{18}O$ values. The isotopically light steam samples (from the Mbiti Voghala crater wall area and Pipisala) sit above the global meteoric water line, around $\delta^{18}O = -15‰$ and $\delta D = -100‰$.

5.3.4 Sulphate oxygen $\delta^{18}O$

Sulphate oxygen $\delta^{18}O$ values for alkaline hot springs vary between 4.0 and 7.9‰, and acid springs from 1.3 to 5.2‰ (Table 5.2). Application of the sulphate oxygen isotope thermometer (McKenzie and Truesdell, 1977) to alkaline sulphate springs gives temperatures ranging from 143–218°C, with one outlier at 476°C (Fig. 5.4). Acid hot springs yield unrealistically high temperatures for SO_4^{2-}–H_2O equilibration, from 400° to 800°C.

The rate of oxygen isotope exchange between water and dissolved sulphate is slow in neutral to alkaline fluids below 200°C, but much faster at lower pH (McKenzie and Truesdell, 1977). In the case of initially acidic fluids that increase their pH by wall-rock reaction, the sulphate oxygen should record pre-reaction composition, and is relatively resistant to progressive resetting by water-rock interaction. However, it is likely that the oxygen isotope compositions of the water will have changed *en route* to the surface (by boiling, water-rock interaction or dilution), and so any temperature data derived from the use of sulphate oxygen thermometry will be approximations at best.

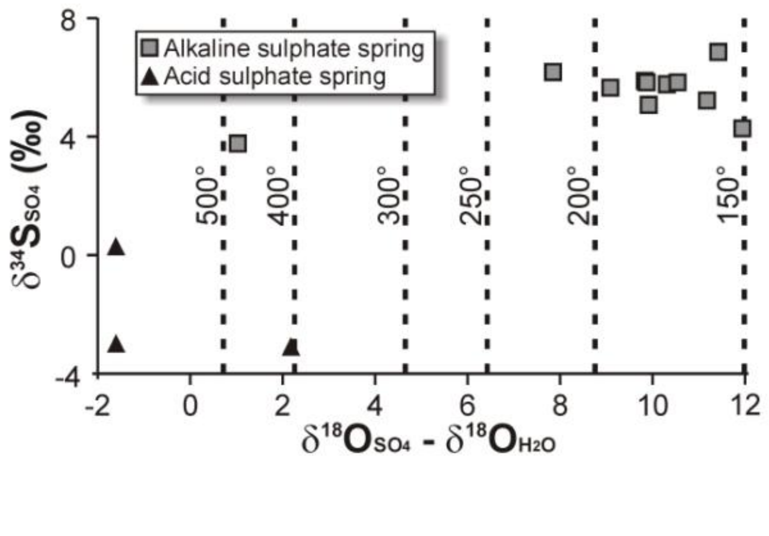

Fig. 5.4: Oxygen fractionation between water and sulphate against sulphur isotope values for acid and alkaline springs. Temperature values derived from McKenzie and Truesdell (1977).

5.3.5 Strontium isotopes

$^{87}Sr/^{86}Sr$ values for all hot springs and cold springs (average = 0.70420 ± 9) overlap with the values for local rocks (average = 0.70414 ± 11, based on 14 samples ranging from basalt to trachyte). A seawater sample collected by the same method from offshore Savo has a $^{87}Sr/^{86}Sr$ value of 0.709164 ± 12 (accepted value for modern seawater is 0.709211 ± 37; Elderfield 1986). Coastal wells analysed in this study have $^{87}Sr/^{86}Sr$ values slightly higher (0.70442–0.70467) than those of the inland springs.

5.4 Discussion

5.4.1 Sources of dissolved sulphate

Sulphate dissolved in hydrothermal fluids may be derived from a number of sources, including entrained seawater (Delmelle et al., 1998), dissolution of sulphate minerals (Shevenell and Goff, 1993; Stimac et al., 2004), oxidation of reduced sulphur species (sulphides, native sulphur and H_2S; Rye et al., 1992), and disproportionation of SO_2 (Holland, 1965). Each of these mechanisms are discussed below.

5.4.1.1 Sulphate from entrained seawater

Hydrothermal systems in emergent and coastal volcanoes may entrain significant amounts of seawater. A marine contribution has been recognised at Milos (Naden et al., 2005) and Nysiros, Greece (Brombach et al., 2003); White Island, New Zealand (Giggenbach et al., 2003); Vulcano, Italy (Chiodini et al., 1995; Leeman et al., 2005); and Taal, Philippines (Delmelle et al., 1998).

Very low chloride contents in hot spring waters from Savo (Tables 4.5–4.9), and $^{87}Sr/^{86}Sr$ values overlapping with whole rock values – and distinctly lower than seawater – rule out major contributions of seawater to the hot springs; there is no measurable effect on sulphate content or $\delta^{34}S$ from seawater entrainment (Fig. 5.5). Furthermore, even assuming that all chloride in the springs is seawater derived, the calculated maximum seawater contents of the hot spring waters are <0.5%.

The coastal wells are a maximum of 5 m from the high tide mark, and have slightly elevated $^{87}Sr/^{86}Sr$ values and chloride contents (up to 125 mg l^{-1}; Appendix III), indicating perhaps small amounts (~ 1%) of seawater from groundwater or sea spray contamination. The absence of a seawater contribution is remarkable given the setting of the system, but not without precedent, e.g. Hakone volcano, Japan (Oki and Hirano, 1978).

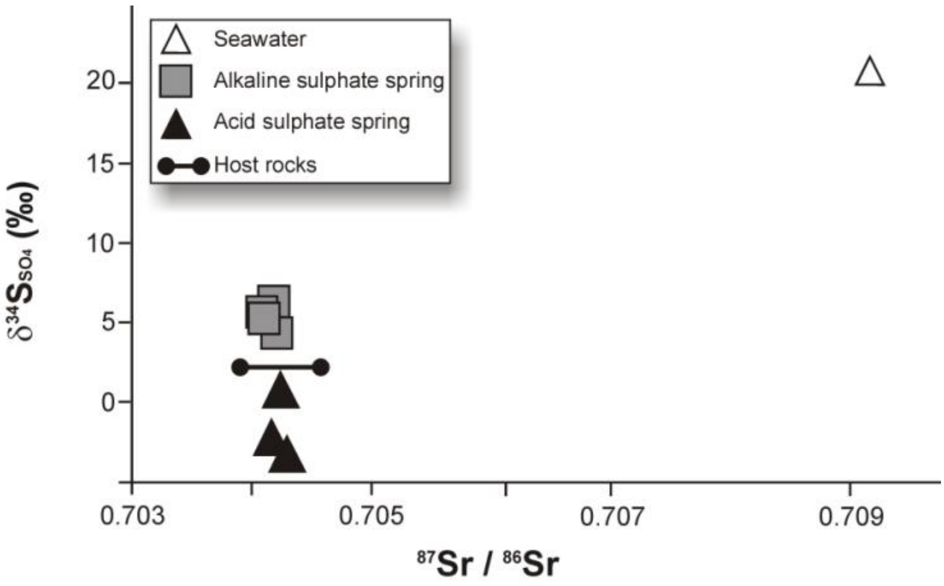

Fig. 5.5: $^{87}Sr/^{86}Sr$ versus $\delta^{34}S$ for hot springs and seawater (this study). Range of whole rock $^{87}Sr/^{86}Sr$ for local unaltered rocks also shown.

5.4.1.2 Sulphate from dissolution of existing minerals

Dissolution of existing sulphate minerals is possible at Savo, but the majority of sulphate minerals observed are secondary (i.e. precipitated *from* hydrothermal fluids). The only primary sulphate mineral observed was rare anhydrite in one unaltered trachyte (Fig. 3.3), occurring as microphenocrysts associated with apatite, suggesting an igneous (non-hydrothermal) origin (Luhr et al., 1984). Dissolution of primary sulphate minerals on a large scale can generate sulphate-rich springs (e.g. the "Red Waters" of El Chichon, Mexico; Taran et al., 1998). Anhydrite dissolves congruently, leading to dissolved sulphate with the same $\delta^{34}S$ values as the primary mineral (Sakai, 1968; Shelton and Rye, 1982). The $\delta^{34}S$ values obtained from the trachydacite (8.1‰) are heavier than the values obtained from the alkaline sulphate springs (3.8–6.8‰), thus simple dissolution of primary magmatic anhydrite cannot explain the lighter hot spring $\delta^{34}S_{SO4}$. In addition, the high solubility of anhydrite in water would lead to its removal from the system over time (Shevenell and Goff, 1995; Stimac et al., 2004) assuming a finite source. Given the rarity of primary anhydrite in samples at Savo (observed in one sample out approximately 50 unaltered specimens examined), the length of time since last eruption (160 years), and the stability of the hydrothermal system (location and temperature of main hydrothermal areas consistent from at least 1956 onwards; Grover, 1958; Toba, 1995), it seems highly unlikely that the majority of the dissolved sulphate in the spring waters is derived from dissolved anhydrite. Furthermore, the role of primary anhydrite dissolution as the major sulphate source can be dismissed on the basis of dilution and saturation trends observed in the major springs (Section 4.5.2).

5.4.1.3 Sulphate from oxidation of reduced sulphur species

Oxidation of reduced sulphur-bearing species, such as pyrite or H_2S, is an important mechanism for generating sulphate and acidity in the upper levels of volcanic-hydrothermal systems, particularly in the "steam-heated zone" – the vadose zone above boiling water, where oxidising conditions generally prevail.

Oxidation of H_2S, native sulphur and sulphides in steam-heated zones results in sulphate with approximately the same $\delta^{34}S$ value; full equilibrium fractionations between H_2S and sulphate (i.e. large $\Delta^{34}S_{SO4-H2S}$ values) rarely develop (Rye et al., 1992). Native sulphur samples collected from fumaroles and areas of steaming ground had consistently negative $\delta^{34}S$ values. Native sulphur forms by the oxidation of H_2S, and may be further oxidised to sulphate in the subaerial environment, with very little change in $\delta^{34}S$ accompanying either oxidation reaction. Aqueous sulphate from acid hot springs, commonly in close proximity to steaming ground, often has $\delta^{34}S$ values similar to native sulphur values. The similar $\delta^{34}S$ values indicate that the sulphate in the acid springs is generated by oxidation of H_2S gas that accompanies steam discharges or by further oxidation of H_2S-generated sulphur and sulphide minerals.

Although the oxidation of the sulphur species at the surface should lead to native sulphur, sulphate and H_2S with similar $\delta^{34}S$, a number of the acid sulphate springs have $\delta^{34}S$ values higher than native sulphur samples. Progress towards sulphide–sulphate equilibrium will result in higher $\delta^{34}S$ values in sulphate. For example, Fifarek and Rye (2005) reported full equilibrium values for steam-heated alunite at the Pierina high sulphidation Au deposit in Peru (Fig. 5.6), as a result of long residence times for sulphate and rapid $H_2S–SO_4^{2-}$ isotopic equilibration due to unusually high temperature and low pH. Higher $\delta^{34}S_{SO4}$ values may also result from mixing with waters containing heavier $\delta^{34}S_{SO4}$ (e.g. those of the alkaline hot springs and the streams fed by alkaline hot springs).

The alkaline sulphate springs have a significantly different $\delta^{34}S$ value to the native sulphur samples and acid sulphate waters (Fig. 5.2). Equilibrium between sulphate and sulphide in the alkaline waters is less likely than in the acid springs, as the isotopic equilibration rate is strongly controlled by pH (Fig. 5.7). It is unlikely that the higher $\delta^{34}S_{SO4}$ values in the alkaline sulphate springs are a result of better-developed $H_2S–SO_4^{2-}$ equilibrium. The most obvious explanation is that it the alkaline springs have a distinct sulphur source to the acid sulphate springs and native sulphur deposits.

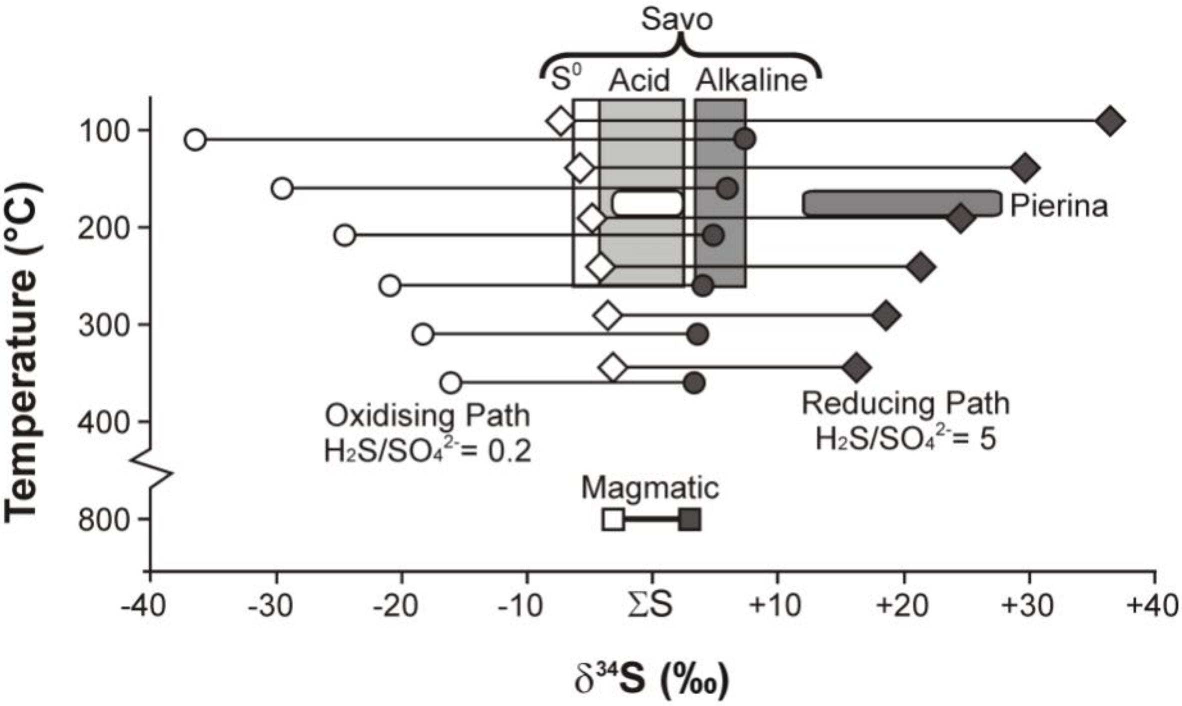

Fig. 5.6: Equilibrium values for co-existing sulphate and reduced sulphur species (H_2S, sulphide, native sulphur) against temperature (Ohmoto and Rye, 1979; Rye, 1993). The two paths show oxidising (sulphate dominant) and reducing (sulphide dominant) paths. Equilibrium paths are shown relative to bulk sulphur (ΣS) = 0. Plot shows data from steam-heated zone at Pierina, Peru, where full equilibrium developed under reducing conditions (Fifarek and Rye, 2005). Data from Savo do not correspond to equilibrium conditions at temperatures <400°C.

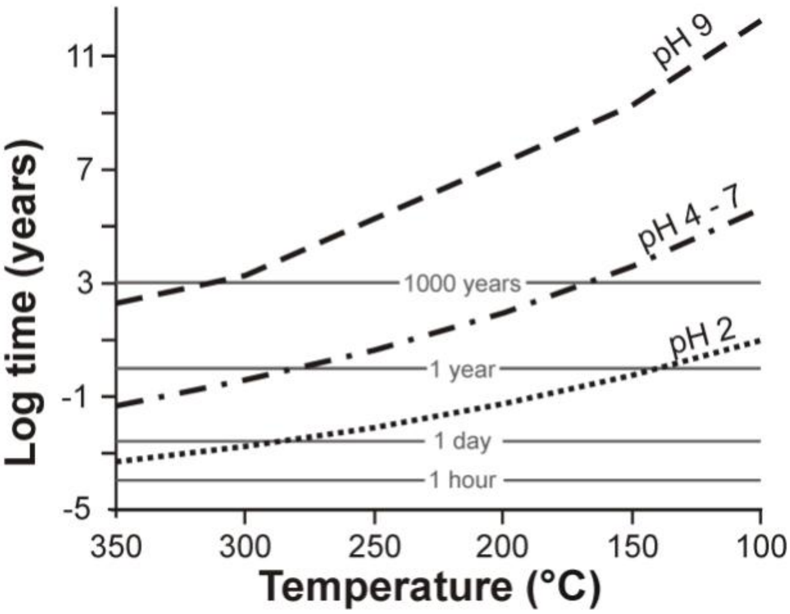

Fig. 5.7: Time taken (log years) for sulphate and sulphide (H_2S) to attain equilibrium at a given temperature and pH. Values from Ohmoto and Lasaga (1982).

5.4.1.4 *Sulphate from SO_2 disproportionation*

Degassing magmas release SO_2 and H_2S which can be "scrubbed out" by overlying hydrothermal systems (Symonds et al., 2001). The proportions of H_2S to SO_2 in fluids released from subduction-related magmas are controlled by the oxidation state of the magma, pressure and temperature (Ohmoto, 1986). The presence of magnetite in unaltered magmatic rocks at Savo, and primary anhydrite in unaltered trachydacite SV40 suggest relatively oxidising magmatic conditions (Chapter 2; Carroll and Rutherford, 1987), and any fluids released would be expected to have a relatively low H_2S/SO_2.

At temperatures below 400°C, SO_2 reacts with water according to the disproportionation reactions:

$$4SO_2 + 4H_2O = 3H_2SO_4 + H_2S \quad \textbf{1}$$

$$3SO_2 + 2H_2O = S + 2H_2SO_4 \quad \textbf{2}$$

(Holland, 1965). These reactions remove virtually all SO_2 and produce acidic condensates (Symonds et al., 2001). Accompanying the disproportionation of SO_2, sulphur isotopes fractionate between the different phases. Kinetic isotope effects result in SO_4^{2-} being enriched in ^{34}S, and the reduced H_2S or S^0 species depleted in ^{34}S (Ohmoto and Rye, 1979). In volcanic hydrothermal systems, H_2S produced by disproportionation may be oxidised in the near-surface environment to produce native sulphur or sulphate depleted in ^{34}S, relative to the bulk sulphur value for the magma (Rye, 1993).

The sulphur isotope systematics of the hot springs at Savo are best explained by the disproportionation of SO_2: the ^{34}S-enriched SO_4^{2-} is found in the alkaline hot springs, the corresponding ^{34}S-depleted H_2S is oxidised to native sulphur and sulphate in the acid springs, as discussed in section 5.4.1.3.

Excluding waters of steam heated origin (where temperatures are too low and residence time too short to develop equilibrium except in rare circumstances, as discussed in section 5.4.1.3), the norm is for sulphate and sulphide in hypogene magmatic-hydrothermal fluids to equilibrate, as a result of the low pH and high temperature conditions that predominate (Rye, 1993). It would be reasonable to expect the alkaline sulphate $\delta^{34}S$ to be approximately in equilibrium with the reduced sulphur species (i.e. native sulphur). However, this is not the case assuming temperatures <400°C (Fig. 5.6); the most obvious explanation is that the high pH waters discharged at the springs are derived from a slightly acid to neutral pH (4–7) reservoir, where H_2S–SO_4^{2-} equilibration times are much longer than the residence time of those components (Fig. 5.7). The disproportionation of SO_2 forms acidic fluids but at Savo they must have been buffered to higher pH before sulphur species could equilibrate; the isotopic difference between alkaline sulphate and S^0 and/or acid sulphate species is either inherited from magmatic fractionations or generated by instantaneous kinetic isotope fractionation upon disproportionation (Kusakabe et al., 2000). Rapid changes in chemistry (and/or temperature) control the sulphur isotope equilibrium or lack thereof at Savo and elsewhere (Shelton and Rye, 1982; Zhang, 1986). Significant amounts of mixing and dilution are indicated by the chemistry of hot spring waters at Savo, and these processes can lead to relatively high pH even where there are considerable magmatic inputs (Section 4.5.2). Cold springs and the Tanginakula are a result of the continued dilution of the hydrothermal fluids, with low sulphate concentrations and the isotopic characteristics of the alkaline sulphate springs (see also Section 4.5.4).

5.4.2 Magmatic anhydrite as a source of SO_2

Anhydrite has been reported in unaltered magmatic rocks from a number of volcanic systems, most notably El Chichón, Mexico (Luhr et al., 1984), Mount Pinatubo, Philippines (Bernard et al., 1991) and Mount Lamington, Papua New Guinea (Arculus et al., 1983). Anhydrite may be more common in magmas than reported, owing to its high solubility in water and the efficacy of its removal during weathering processes (Carroll and Rutherford, 1987).

As a magma ascends, progressive degassing of both H_2S and SO_2 from an initially sulphur-rich, anhydrite-bearing magma leads to crystal-rich, anhydrite-free lava at surface (Luhr and Logan, 2002), perhaps providing a mechanism by which the majority of Savo's crystal rich rocks are sulphur-poor and anhydrite-free, as well as providing a major source of SO_2 to an overlying hydrothermal system.

The $\delta^{34}S$ value of +8‰ obtained for the anhydrite-bearing trachyte SV40 in this study is unlikely to represent the bulk sulphur value for the system, as degassing leads to preferential enrichment of high-^{34}S anhydrite in magmas (Rye et al., 1984). The anhydrite in sample SV40 is likely to be the residue from a degassed, initially sulphate-rich magma.

5.4.3 Oxygen and hydrogen isotopes

Cold springs and wells analysed for $\delta^{18}O$ and δD plot in a narrow field of values just above (0.5 to 1‰ lower with respect to $\delta^{18}O$) of the Global Meteoric Water Line (Craig, 1961). The deviation from the GMWL is likely to be a result of a local meteoric water line with a different slope, commonly observed for tropical islands (Jouzel et al., 1987). Data for the range of meteoric water isotope compositions in the Solomon Islands are unavailable, but comparison with data from Madang, Papua New Guinea (GNIP, 2004) suggests that the values of Savo groundwater are representative of an average meteoric water composition for the southwest Pacific (Madang varies from $\delta^{18}O = -14$ to -2‰ and $\delta D = -92$ to -3‰, average -7, -46‰). Thus, for the purposes of the following discussion, the average isotopic composition of well and cold spring waters is used as the meteoric-derived groundwater on Savo. The presence of sulphate in the cold spring waters – with $\delta^{34}S$ comparable to alkaline sulphate springs – suggests that these fluids are not isolated from the hydrothermal fluids. Likewise, wells on the island often have temperatures above ambient air temperature, indicating that hydrothermal contributions to groundwater are commonplace on Savo. It may be more appropriate to consider cold springs, wells, and warm springs such as that of Tanginakulu, as being dominantly meteoric-derived groundwater, with minor contributions from hydrothermal fluids.

Relative to local meteoric-derived groundwater, both alkaline and acid sulphate hot springs are dominated by higher $\delta^{18}O$ and δD values, particularly the acid springs (Fig. 5.3). ^{18}O enrichment, and to a lesser extent, D enrichment, in hydrothermal waters is commonplace, and may be due to isotopic exchange between heated meteoric-derived groundwater and host rocks (Craig, 1963; Truesdell, 1984; Field and Fifarek, 1985); evaporation from bodies of water (lakes, pools, stagnant springs) at the surface (Craig, 1963; Giggenbach and Stewart, 1982; Varekamp and Kreulen, 2000); phase changes and phase separation processes, including boiling (Truesdell et al., 1977) and subsurface condensation (Darling et al., 1989); or addition of isotopically heavy H_2O from a second fluid such as seawater or magmatic vapour (Hedenquist and Aoki, 1991; Giggenbach, 1992; Taran et al., 1995; Delmelle et al., 2000; Varekamp and Kreulen, 2000; Giggenbach et al., 2003; Wagner et al., 2005). In some systems, combinations of the above processes have been invoked to describe oxygen and hydrogen isotope relationships in hydrothermal fluids (Chiodini et al., 1995; Delmelle et al., 1998). These processes and their relevance to the different springs at Savo are discussed below.

5.4.3.1 Alkaline sulphate springs

Evaporative enrichment of the heavy isotopes from surface pools is unlikely to be the major control on the composition of the alkaline sulphate springs; the springs discharge and recharge rapidly, and the residence time of any mass of water in the spring is short. In this case, the isotopic composition of the fluids is likely to represent the isotopic composition at depth, rather than recording post-discharge evaporation.

Water-rock isotopic exchange in hydrothermal systems is dominated by oxygen exchange in most cases, due to the higher oxygen content of rocks relative to hydrogen. Hydrogen exchange only becomes important at very low water/rock ratios (<0.1; Campbell et al., 1984). As a result, fluids in most systems tend to show sub-horizontal (oxygen) shifts on $\delta^{18}O$ and δD plots.

The following equations can be used to predict the isotopic composition of water following exchange with a felsic rock for a range of temperatures and water/rock ratios (Field and Fifarek, 1985):

$$\delta^{18}O_w^f = \frac{7 - \Delta_{r-w} + 1.8R \times \delta^{18}O_w^i}{1 + 1.8R} \qquad \textbf{3}$$

$$\delta D_w^f = \frac{-40 - \Delta_{r-w} + 100R \times \delta D_w^i}{1 + 100R} \qquad \textbf{4}$$

$\delta^{18}O^f_w$ and δD^f_w and are the final oxygen and hydrogen isotope compositions of the water discharged from the spring, $\delta^{18}O^i_w$ and δD^i_w are the initial isotope compositions of the water (in this case, meteoric-dominated groundwater), R is the water/rock mass ratio, and Δ_{r-w} is the equilibrium isotope fractionation factor between rock and water. The relative abundances of oxygen and hydrogen in water as compared to typical andesites, dacites and rhyolites are accounted for by the numerical coefficients 1.8 for oxygen and 100 for hydrogen (Field and Fifarek, 1985).

For oxygen Δ_{r-w}-, the trachyandesite–H_2O fractionation factor calculated by Zhao and Zheng (2003) is used in this study. For hydrogen Δ_{r-w}, Field and Fifarek (1985) assumed that rock–H_2O fractionation was equivalent to chlorite–H_2O fractionation, based on comparison of various mineral–H_2O fractionations with experimental rock–H_2O fractionations. The chlorite–H_2O fractionation factors of Graham et al. (1987) and references therein are used in this study.

Using local meteoric-derived groundwater compositions for Savo, an estimated δD value for the initial rock (−40‰), and initial $\delta^{18}O$ = +7‰ based on the mean of 14 unaltered samples from Savo (Appendix IV), at temperatures between 100 and 200°C isotopic exchange could result in the observed fluid compositions (Fig. 5.8). However, the water/ rock mass ratios required for the range of observed hydrogen values are small (<0.1), and it is questionable whether such ratios are capable of sustaining a hydrothermal system without the water becoming fixed into hydrous secondary minerals (Reed, 1997). The dilute chemistry and in particular low chlorinity of the springs also rules out low water/ rock ratios (Hattori and Sakai, 1979).

Changing the initial rock δD value or the choice of mineral–H_2O proxy for hydrogen Δ_{r-w} does affect the maximum possible δD^f_w, but the inflection of the curve (i.e. the point at which water–rock interaction begins to influence the δD value of the water) is controlled by R, the water/rock mass ratio; if typical whole rock hydrogen contents are appropriate for Savo, then water–rock interaction alone cannot explain the higher δD values of the alkaline

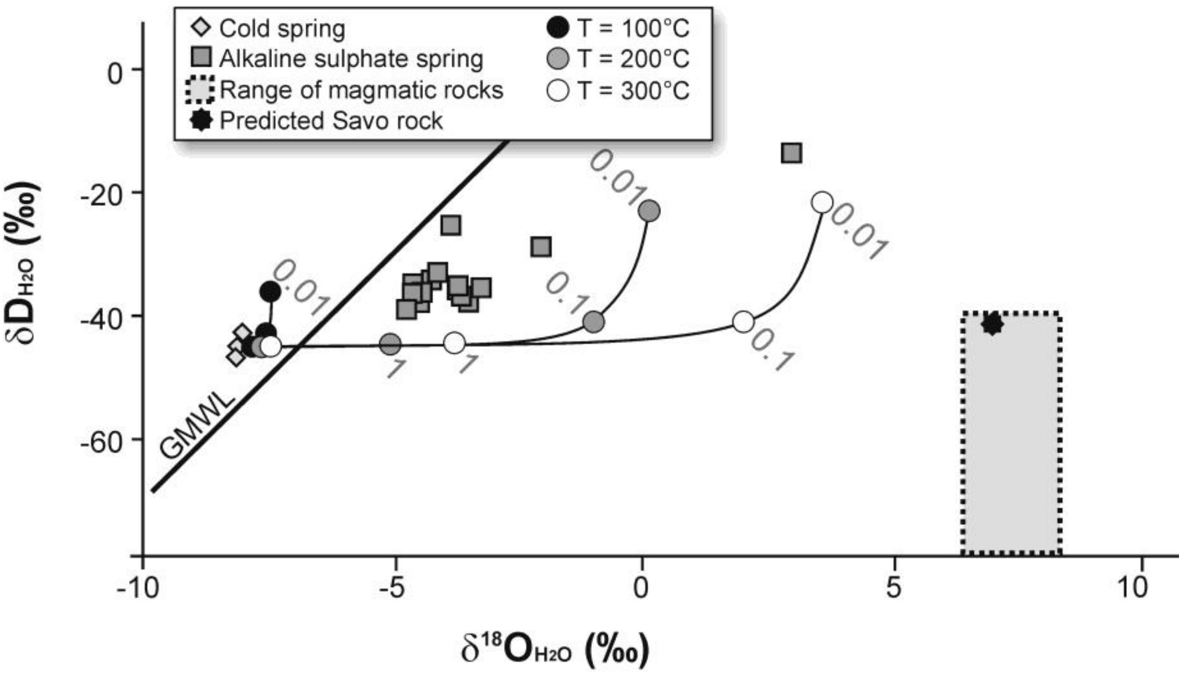

Fig. 5.8: δD_{H2O}–$\delta^{18}O_{H2O}$ plot showing alkaline sulphate springs and modelled water–rock exchange curves at 100, 200 and 300°C. Curves constructed using equations from Field and Fifarek (1985). Oxygen fractionation factors based on trachyandesite–H_2O (Zhao and Zheng, 2003), hydrogen fractionation factors based on chlorite–H_2O (Graham et al., 1987). Numbers in grey are values of water/rock mass ratio R.

sulphate waters. Water–rock interaction may contribute to higher $\delta^{18}O$ seen in the alkaline sulphate springs however, as significant oxygen exchange can occur even at high water/ rock ratios, assuming rapid equilibration.

Boiling of liquid water causes the separation of vapour (steam). Oxygen and hydrogen isotopes fractionate between the liquid and vapour phase. At the temperatures of interest (100–300°C) the vapour phase is depleted in ^{18}O and D, and the liquid phase enriched relative to the initial liquid. Maximum isotopic enrichment in the residual liquid can be obtained by single-step steam separation (steam remains mixed with water and separates at a lower, single temperature, rather than separating continuously over a range of temperatures; Truesdell et al., 1977).

Compositions of steam and residual liquid can be modelled from a hypothetical starting liquid using the single-step steam separation equations of Giggenbach and Stewart (1982):

$$\delta_s = \delta_o - \Delta_{w-s}\ 1 - y_s \qquad \mathbf{5}$$

$$\delta_w = \delta_o + y_s \Delta_{w-s} \qquad \mathbf{6}$$

where δ_s is the isotopic composition of the steam, δ_o is the initial isotopic composition of the source water, δ_w is the isotopic composition of the residual liquid water, Δ_{w-s} is the fractionation factor between water and steam at the separation temperature, and y_s is the fraction of steam separated, calculated by:

$$y_s = \frac{H_o - H_w}{H_s - H_w} \qquad \mathbf{7}$$

where H_o, H_s, and H_w are the enthalpies of the original fluid at the reservoir temperature, the steam enthalpy at separation temperature, and the enthalpy of the residual water at the separation temperature respectively (values from Keenan et al., 1969).

To determine whether boiling contributes to the measured isotope composition of the alkaline sulphate springs, the following parameters were used with the above equations: an assumed reservoir temperature of 200°C (based on sulphate oxygen thermometry of alkaline sulphate waters; section 5.3.4); separation temperatures of 180–120°C (resulting in y_s values of 0.04 to 0.16) ; assumed $\delta_{o\text{-}}$ of groundwater enriched in ^{18}O following water–rock interaction at R = 1 and 200°C ($\delta^{18}O = -5.1‰$, $\delta D = -45‰$; "shifted meteoric" on figure); and Δ_{w-s} values from Truesdell et al. (1977). The results are shown on Figure 5.9. The residual liquids show higher δD values than the initial fluid, but the maximum enrichment still produces δD values consistently lower than the analysed values for alkaline sulphate waters. Nevertheless, predicted values are close to measured values, and therefore water–rock interaction and boiling are capable of generating waters with the $\delta^{18}O$ and δD composition close to that of the alkaline sulphate springs from an initial groundwater, but it is unclear how these processes alone can generate the observed sulphur isotope systematics.

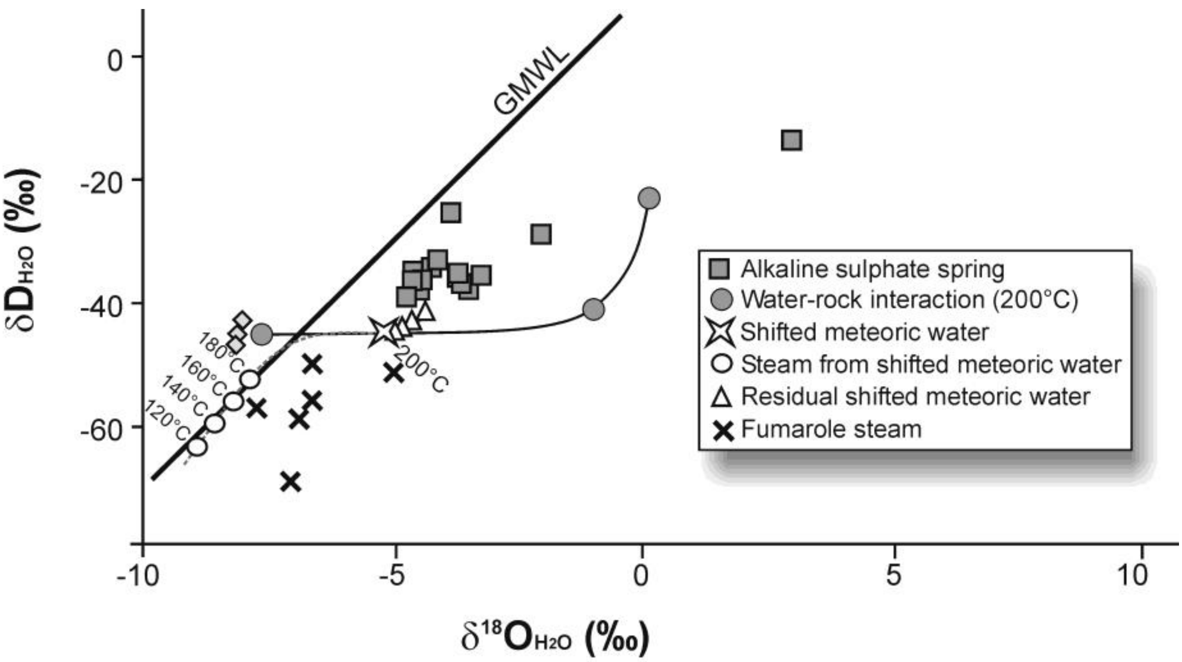

Fig. 5.9: δD_{H2O}–$\delta^{18}O_{H2O}$ plot showing steam and residual liquids after boiling of meteoric-derived groundwater equilibrated with rock (at 200°C and R = 1; Fig. 5.8). Initial liquid temperature 200°C, with single step steam separation at 180–120°C.

Mixing of meteoric derived groundwater with ^{18}O and D enriched fluids is an important process in many hydrothermal systems. On the basis of $^{87}Sr/^{86}Sr$ and chloride content (section 5.4.1.1), seawater involvement is negligible. Magmatic fluids are typically enriched with respect to ^{18}O and D, and a magmatic input is indicated at Savo given the presence of disproportionated SO_2 in the alkaline sulphate springs (section 5.4.1.4) and high CO_2 contents of crater fumaroles.

Based on studies of high temperature (>300°C) fumaroles from a number of Pacific arc volcanoes, Giggenbach (1992) observed that discharged H_2O had a common isotopic end-member, most likely seawater recycled through subduction and magmatism. This "andesitic water" has approximate δD of −20 ± 10‰ and $\delta^{18}O$ close to that of the original magma (Giggenbach et al., 2003).

On $\delta^{18}O$–δD plots, the addition of magmatic vapour to groundwater produces a straight mixing line between the two end-member compositions (Hedenquist and Aoki, 1991). Application of a mixing line to Savo (using "andesitic water" δD from Giggenbach, 1992; and $\delta^{18}O$ = 7.3‰) is shown on Figure 5.10. Alkaline sulphate springs are indicated to have maximum contributions of 30% magmatic fluids.

However, the chemistry of the springs (Chapter 4) is more dilute than other systems with similar magmatic end-member contributions to discharged fluids (c.f. White Island, NZ; Giggenbach et al., 2003), and thus meteoric–magmatic mixing is unlikely to be the sole

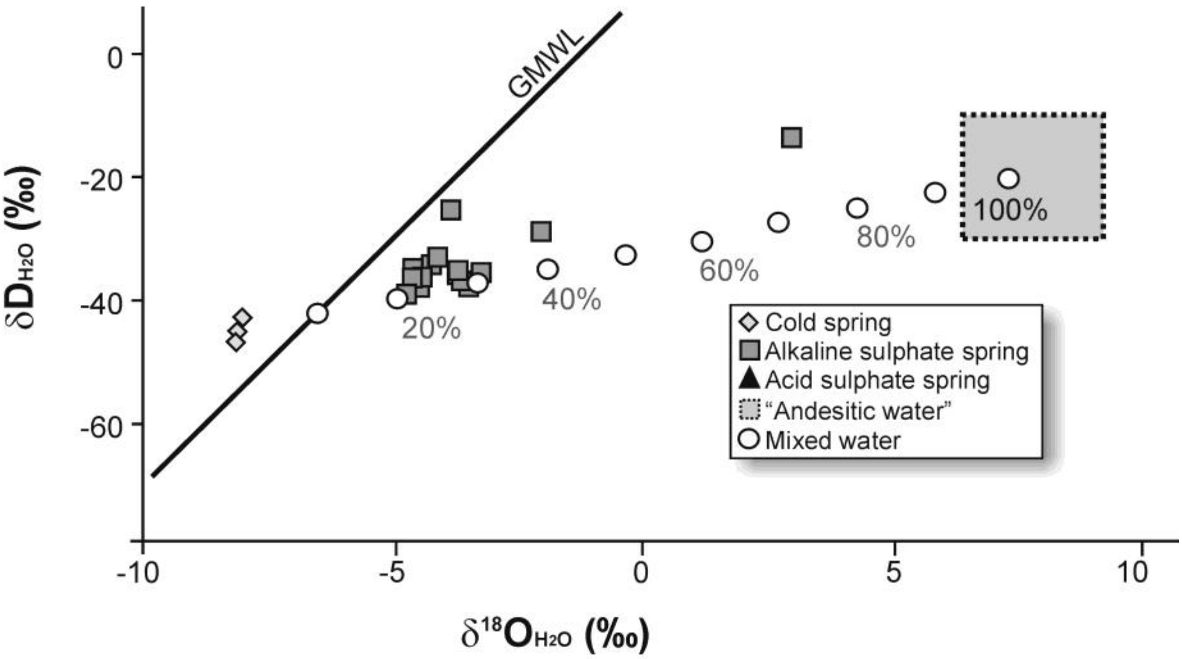

Fig. 5.10: δD_{H2O}–$\delta^{18}O_{H2O}$ plot showing theoretical mixing line between typical subduction-related magmatic water ("andesitic water" Giggenbach, 1992) and local groundwater compositions. Percentage contribution from magmatic fluid is marked on the diagram. Alkaline sulphate springs lie on this trend, suggesting maximum 30% magmatic fluid contribution.

process determining the isotopic composition of the alkaline sulphate springs. Instead, the most likely explanation for the observed $\delta^{18}O$ and δD, taking into account the $\delta^{34}S$ data, is that small (<<30%) additions of magmatic vapour to a meteoric-dominated groundwater led to an increase in temperature, $\delta^{18}O$ and δD and addition of SO_4^{2-}. This fluid subsequently reacts with the host rocks, leading to further ^{18}O enrichment (Fig. 5.8). The fluid boils before and at discharge at alkaline sulphate springs, leading to further $\delta^{18}O$ and δD increase (Fig. 5.9). The range of $\delta^{18}O$ values in the analysed alkaline sulphate springs is a result of varying contributions from the magmatic end-member, meteoric-derived groundwater, and varying degrees of water–rock exchange.

5.4.3.2 Fumarole steam

Steam separation from boiling liquid has been discussed in Section 5.4.3.1. The steam generated by the boiling of a rock-reacted groundwater calculated by eqns. 5–7 is shown on Figure 5.9. The steam generated by this process does not account for the majority of samples; many have much higher $\delta^{18}O$, and three samples have much lower $\delta^{18}O$ and δD values (shown in the lower right hand corner of Fig. 5.3).

The fumarole steam samples with higher $\delta^{18}O$ require separation from water with a higher $\delta^{18}O$ to begin with. Considering the processes discussed in section 5.4.3.1, the $\delta^{18}O$-enriched fluid is either groundwater equilibrated with host rock at higher temperatures, or has a larger contribution from the magmatic vapour. Both are feasible at Savo, and given the data available, it is impossible to distinguish the two. Figure 5.11 shows the steam that would separate from more ^{18}O-enriched water. In this case, one based on 40% "andesitic water" (Fig. 5.10).

The steam is generated from a reservoir that is similar to the parental water for the alkaline sulphate springs: the liquid left as residue following steam separation is discharged at alkaline sulphate springs.

The samples most depleted in ^{18}O and D can be explained by Rayleigh condensation at temperatures between 100 and 150°C. The equation used to plot the condensation trends on Figure 5.11 is:

$$\left(1000+\delta_r\right) = \left(1000+\delta_i\right) \times f^{\alpha-1} \qquad \textbf{8}$$

(Darling et al., 1989) where δ_r is the isotopic value of the resulting steam composition after condensation, δ_i is the initial steam isotopic value, f is the fraction of steam remaining, and

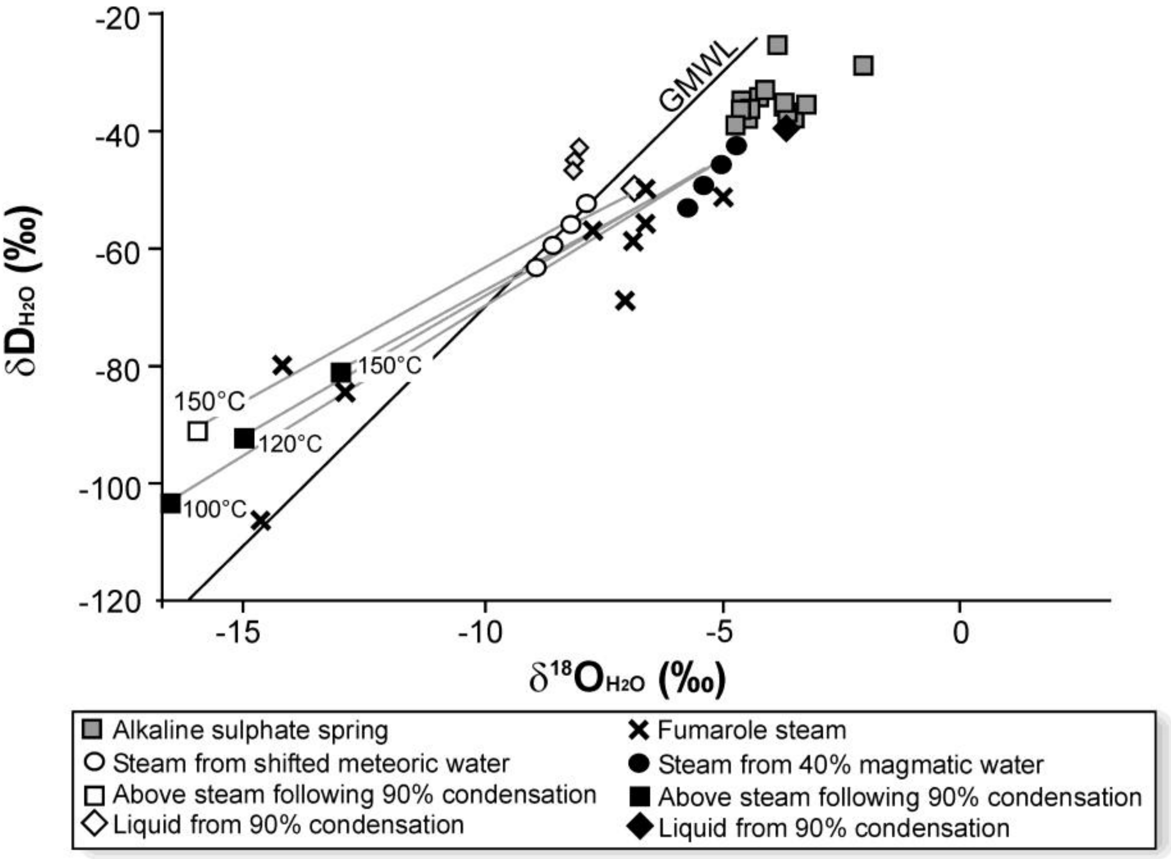

Fig. 5.11: δD_{H2O}–$\delta^{18}O_{H2O}$ plot showing steam separated from shifted groundwater (Fig. 5.9), subsequent condensation of 90% of the steam at 100°C and the resulting liquid condensate. The array of observed steam samples is most likely a result of condensation, but the ^{18}O compositions of the observed steam are higher than predicted by steam separation from "shifted groundwater". In this case, a groundwater with 40% magmatic contributions (Fig. 5.10) is used to represent a heavier source, but the position on the plot is non-unique, and may be generated by water-rock interaction (Fig. 5.8).

a is related to the permil equilibrium isotopic fractionation factor between liquid water and steam (Δ_{w-s}) by the equation:

$$\Delta_{w-s} \approx 1000 \ln \alpha \qquad \textbf{9}$$

From these equations, it can be shown that a steam condensing only a small portion of its original mass is shifted to slightly lighter $\delta^{18}O$ and δD values. As condensation continues and a greater portion of the steam condenses the isotopic composition of the steam progresses to lower $\delta^{18}O$ and δD values. The steam samples with the lowest $\delta^{18}O$ and δD values are a result of the condensation of approximately 90% of the original mass of steam, at temperatures 100–150°C. As condensation continues, the liquid produced approaches the isotopic composition of the initial steam ; the resulting condensate may show similar isotopic composition to the alkaline sulphate springs (Fig. 5.11; liquid from condensing steam of 40% magmatic water).

5.4.3.3 Acid sulphate waters

The high $\delta^{18}O$ and δD values seen in the acid sulphate waters are much greater than can be accounted for by water–rock interaction and boiling of an originally meteoric-derived groundwater. Mixing can be ruled out in terms of temperature and chemistry; if mixing with the "andesitic water" magmatic fluid is to account for the $\delta^{18}O$ and δD composition, then up to 100% of the final fluid is of the magmatic end-member. Fluid (vapour) samples showing close to 100% magmatic contributions are only found at very high temperature fumaroles (e.g. Taran et al., 1995), and the sulphur isotope composition of the acid springs is more typical of secondarily derived hydrothermal fluids rather than pristine magmatic fluids (section 5.4.1.3).

Evaporation from surface waters such as hot springs (Craig, 1963) and crater lakes (Varekamp and Kreulen, 2000) is an important process in shallow hydrothermal environments. The kinetic isotope fractionation effect that accompanies evaporation from thermal (>50°C) waters at the surface results in the residual liquid becoming enriched in the heavy isotopes of O and H.

Craig (1963) compiled data from a number of low pH, sulphate-rich springs from geothermal areas. He interpreted them to be superficial waters, with sulphate and acidity derived from the oxidation of H_2S to H_2SO_4 (in the same manner as acid sulphate springs of Savo discussed in sections 5.4.1.3 and 5.4.1.4), and heat derived by addition of steam. The observed ^{18}O and D enrichments were ascribed to purely evaporative processes, with kinetic isotopic fractionation between liquid and vapour resulting in trends with a slope of approximately 3 on $\delta^{18}O$–δD plots. The acid sulphate springs analysed at Savo (plus two of the outliers from the alkaline sulphate cluster) lie on a trend with a slope close to 3 (Fig. 5.3), suggesting evaporation is an important control on the isotopic composition on these springs (slope of best fit line for acid sulphate springs only is 2.9, ; for acid *and* cold spring samples, slope is 2.9, i.e. acid sulphate springs and cold springs are co-linear).

Giggenbach and Stewart (1982) suggested that the contributions from steam might be more significant than just heat, and they modelled the isotopic effects of steam addition to small, evaporating pools at the surface. Giggenbach and Stewart (1982), derived a number of equations that can be used to predict the isotopic composition of the steam-heated springs following the addition of steam to groundwater:

$$\delta_{wo} = \delta_{wi} + x\ \delta_{si} - \delta_{wi} + \varepsilon' \qquad \textbf{10}$$

where δ_{wo} is the isotopic composition of the liquid discharge of the steam-heated pool, δ_{wi} is the water supplied to the pool (groundwater) before addition of steam with composition δ_{si}, x is the fraction of steam in the total amount of water ($wi + si$) entering the pool, and ε' is the non-equilibrium fractionation factor:

$$\varepsilon' = \Delta_{w-s} + 1000n\ D/D' - 1 \qquad \mathbf{11}$$

where Δ_{w-s} is the equilibrium fractionation factor between water and water vapour at the surface temperature of the analysed pool or spring for oxygen or hydrogen (using values from Truesdell et al. 1977), *D/D´* is the ratio of diffusion coefficients and largely a function of the mass ratios of the diffusing molecules – it is assumed to be 1.024 for HDO and 1.028 for $H_2{}^{18}O$ (Giggenbach and Stewart 1982), and *n* is an empirically derived coefficient relating to the size of the evaporating water body, and can be assumed to be 0.35 (Giggenbach and Stewart, 1982), although it should be noted that the final values of ε' are relatively sensitive to small changes in *n*.

Using SV306 as δ_{si} to heat groundwater ($\delta^{18}O = -8‰$, $\delta D = -44‰$; the sample least affected by condensation), and assuming surface temperature of the water to be between 100 and 60°C, the modelled enrichment trends shown on Figure 5.12 are close to those observed in the acid sulphate springs. The most ^{18}O and D enriched samples (SV515 and SV209) require approximately 90% of fluid added to be steam; recharge with surface water

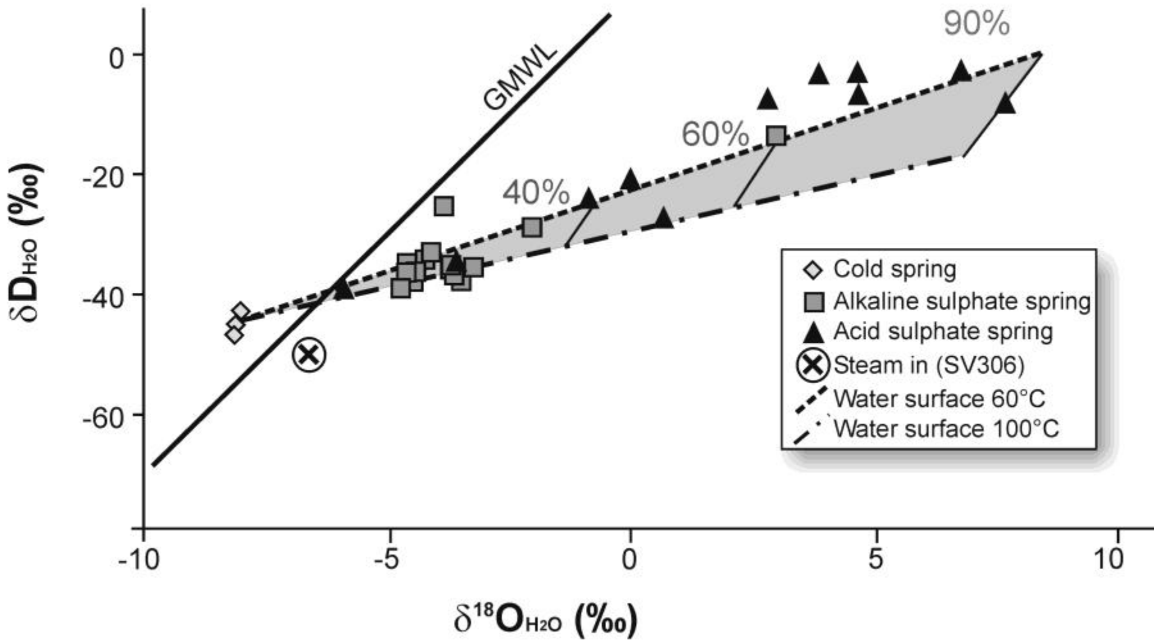

Fig. 5.12: δD_{H2O}–$\delta^{18}O_{H2O}$ plot showing modelled isotopic enrichment trends for evaporation of meteoric-derived water in a pool at 60 and 100°C after addition of steam. Acid sulphate and some alkaline sulphate springs develop observed enrichments by this process. Percentage contributions of steam to total fluid input are marked on evaporation field; the most enriched samples have relatively small amounts of recharge from groundwater and are dominated by steam input and evaporation.

is either limited or intermittent (i.e. the “springs” would be more appropriately described as pools or puddles).

The steam that provides the heat, H_2S (oxidised to SO_4^{2-}), ^{18}O and D isotopic enrichment observed in the acid sulphate water is derived from a boiling reservoir at depth, and the residual liquid is discharged at alkaline sulphate springs.

The unrealistically high temperature estimates calculated from $\Delta^{18}O_{SO4-H2O}$ for acid sulphate springs is therefore explained by the evaporative enrichment of $\delta^{18}O_{H2O}$ at the surface.

5.4.3.4 Transitional springs

For the most part, evaporative enrichment is a minor influence on the isotopic composition of the alkaline sulphate springs (section 5.4.3.1), with the exception of samples SV208 and SV207. These samples show ^{18}O and D enrichments similar to the acid sulphate springs, and are interpreted to be alkaline sulphate springs that have become isolated from the underlying reservoir, rendering them stagnant and susceptible to evaporation. It is important to note that SV208 has a relatively light $\delta^{34}S_{SO4}$ value (3.8‰) compared to the majority of alkaline sulphate springs, also suggesting it is transitional to the acid sulphate type spring. Changes in sub-surface hydrology may lead to the closure of fluid pathways and/or water table changes, and consequent modification of the hydrothermal environment in overlying and laterally equivalent areas (e.g. Bolognesi, 2000).

5.5 A model for the magmatic-hydrothermal system at Savo

Sulphate-dominated fluids in volcanic-hydrothermal environments can have either a magmatic vapour (sulphate from SO_2 disproportionation) or steam-heated (oxidation of H_2S) origin (discounting seawater contamination, shown in section 5.4.1.1 to be unimportant at Savo). Considering the sulphur, oxygen and hydrogen isotope data, it is clear that both types are present at Savo: waters with contributions from magmatic vapour discharge at the surface as alkaline hot springs; acid sulphate springs are steam-heated in origin.

As shown on Figure 5.13, magmatic vapours ascend through the volcanic edifice, potentially exploiting faults and similar structures (Giggenbach et al., 1990; Reyes et al., 2003), condensing into meteoric-derived groundwater at high levels. Disproportionation of SO_2 upon reaction with water leads to the generation of ^{34}S-enriched sulphuric acid. The initial condensate is therefore expected to be acidic, and capable of generating intense alteration (Stoffregen, 1987; Boyce et al., 2007), although mixing with bicarbonate-rich groundwater may limit the level of acidity (Section 4.5.2). Reaction with the sodic host rocks neutralises the acidity (Reed, 1997). The resulting fluids are modified by dilution and boiling, then discharged from the flanks as alkaline sulphate springs. The high pH of these fluids, and the stabilisation of silica, anhydrite and carbonate (precipitated as sinters or

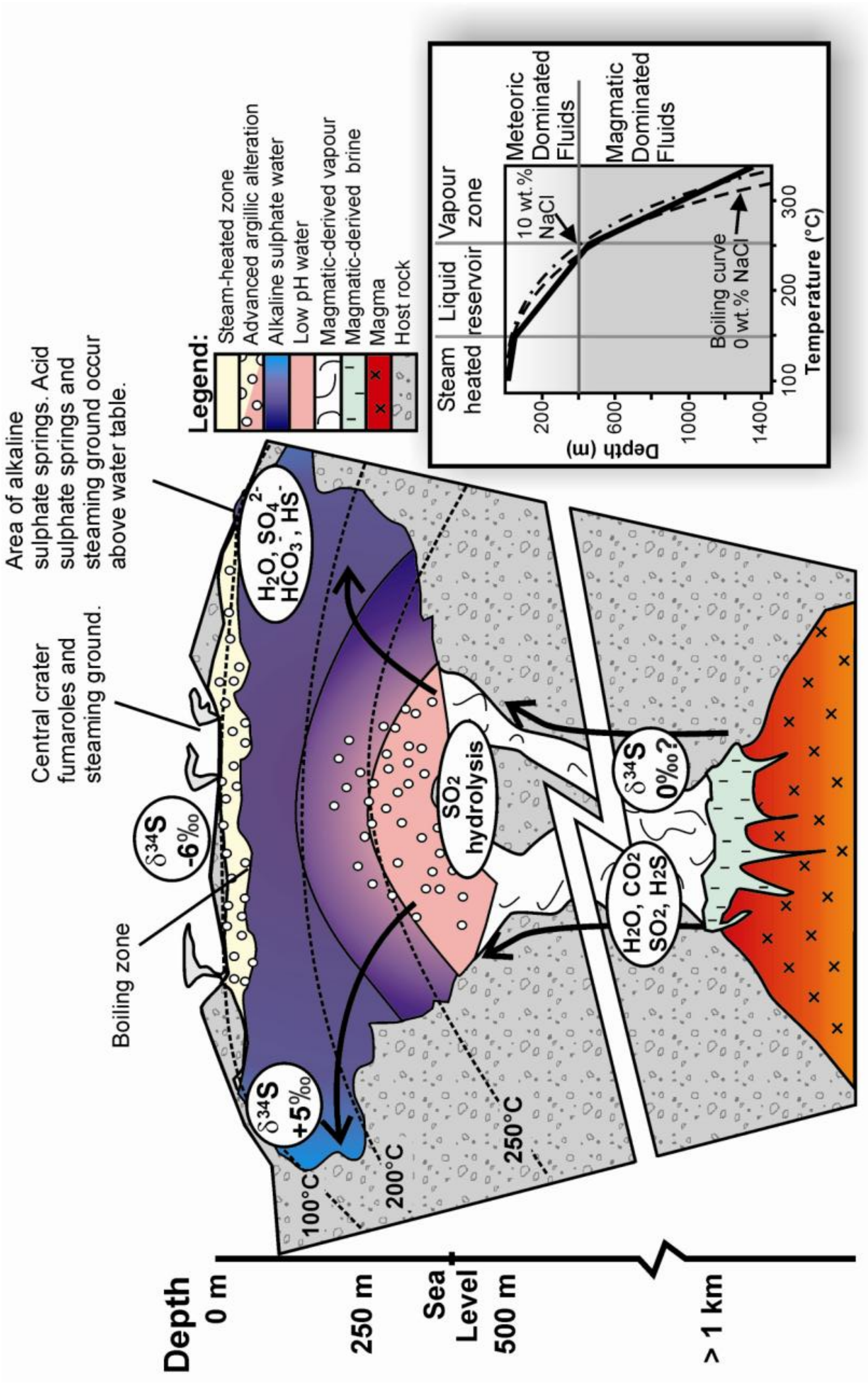

Fig. 5.13: Schematic model for the hydrothermal system of Savo. Section based on dashed line shown on Fig. 5.1. Inset shows tentative depth vs. temperature curve for Savo, superimposed onto boiling curves for water (with up to 10 wt. % NaCl; Henley, 1984). Curve shows magmatic dominated vapour zone at depth; increased meteoric water contributions lead to rapid decrease in temperature at depths less than 400 m below surface and the formation of a liquid reservoir. This reservoir may boil in the near surface, generating a steam heated zone above the water table.

travertines around hot springs, and expected at depth based on thermodynamic calculations) suggest that the neutralisation process is highly efficient at Savo – perhaps because of the alkaline chemistry of the host rocks, and in part because of the dilute chemistry (Chapter 4) – and the amount of acid-related alteration at depth is probably limited in volume and extent. Sillitoe (2002) commented on the relative paucity of such alteration and associated mineralisation in alkaline rock-hosted epithermal deposits, ascribing it to highly efficient acid-buffering.

Where temperatures are high and pressures low enough, the mixed magmatic–meteoric fluid may boil at depth. ^{34}S-depleted H_2S generated during the disproportionation of SO_2 partitions strongly into the steam; where this steam reaches the surface it results in fumaroles and steaming ground, as observed in the crater and on the flanks of Savo. Oxidation of H_2S produces native sulphur and H_2SO_4 which leaches the rock to produce the advanced argillic alteration typical of the steam-heated environment (Rye et al., 1992). Where the steam encounters surface water, or perched aquifers, condensation of steam and H_2S oxidation produces acid sulphate type fluids. Surface water may be derived from alkaline sulphate springs initially, resulting in pools or springs with intermediate sulphur isotope signatures.

The sulphur isotope systematics of the system show that little progress was made towards sulphur isotope equilibrium between SO_4 and H_2S in the system, either as a function of high pH, low temperature, rapid ascent and separation of the phases, or a combination of all three. Given the high pH of the fluids, this is an important factor to consider at Savo, and may well be a relatively common feature of epithermal and porphyry deposits in alkaline host rocks.

The magmatic contributions come from a degassing magma at an unknown depth. Epithermal-related magmatic-hydrothermal systems may extend as far as 6 km below the surface (Dilles and Einaudi, 1992), but are likely to be much shallower. High SO_2/H_2S values are favoured by lower pressures (Carroll and Webster, 1994), and the salinity (NaCl content) of the vapour phase increases with pressure of phase separation (Sourirajan and Kennedy, 1962; Fournier, 1999; Driesner and Heinrich, 2007). The low chlorinity of the alkaline sulphate hot spring waters suggests a relatively shallow depth-to-degassing (<3 km).

High sulphidation epithermal deposits typically show evidence of two stages of formation. Genetic models include an early “ground preparation” stage, where magmatic gases condense and produce highly acidic hydrothermal fluids that leach the host rocks and generate the alteration assemblages that host mineralisation; metals are introduced at a later stage (Hedenquist and Lowenstern, 1994; Arribas, 1995; Cooke and Simmons, 2000; Boyce et al., 2007). The early stages of epithermal alteration may be synchronous with porphyry-type mineralisation at depth (Arribas et al., 1995; Hedenquist et al., 1998; Muntean and Einaudi, 2001). Stable isotope evidence from fluids at Savo suggest that it may be in a “ground preparation” stage with low salinity magmatic-hydrothermal fluids generating alteration, but the alteration assemblages and potentially any mineralisation that may occur are more likely to be low sulphidation in style due to the alkaline nature of the host rocks; this is certainly consistent with the presence of sinter and travertine around hot springs and in stream channels fed by alkaline-sulphate springs. Alkaline rock-related epithermal deposits commonly show major contributions from magmatic sources and low sulphidation mineralisation (Ahmad et al., 1987; Richards et al., 1997; Alderton and Fallick, 2000; Jensen and Barton, 2000). Given the stable isotope evidence for magmatic contributions to the hydrothermal fluids at Savo, the high pH of the hot springs, and the deposition of sinter and travertine around the hot springs, it is clear that Savo has affinities with alkaline rock-related epithermal deposits.

Carman (2003) suggested that at the earliest stage of mineralisation at Ladolam, subvolcanic intrusions were generating a magmatic-hydrothermal system and porphyry mineralisation, with an advanced argillic lithocap hosted in the overlying stratovolcano. The volcano and the alteration (and possibly mineralisation) it hosted was subsequently removed by sector collapse (Sillitoe, 1994; Carman, 2003) to form the present day Luise caldera and the Ladolam deposits. The present day system at Savo is somewhat analogous to the earliest stages at Ladolam, but it is clear from this study that alkaline fluids are at least as important as acidic in the lithocap environment, and that the products of the alkaline sulphate springs (silica, carbonate and sulphate sinters) may be useful exploration targets for alkaline epithermal deposits.

5.6 Conclusions

Hot springs discharging high pH, sulphate-rich water have been identified at Savo. The sulphur, oxygen and hydrogen stable isotope systematics indicate that these formed by the condensation of magmatic vapour into meteoric-derived groundwater. Sulphate is derived from the hydrolysis of SO_2; H_2S generated by this reaction is oxidised in the near-surface steam-heated environment.

The alkaline sulphate waters form a reservoir with temperatures between 200 and 300°C, at depths shallow enough to permit boiling. Stable isotopes of oxygen and hydrogen in water and steam show that the alkaline sulphate fluids are residual liquids after boiling; the steam produced by boiling discharges at the crater, and condenses into acid sulphate springs on the flanks of the volcano.

The condensation of SO_2-rich magmatic vapours typically results in highly acidic fluids; the high pH of the alkaline sulphate fluids is potentially a result of buffering by the sodic host rocks. High pH conditions lead to slow rates of equilibration between aqueous (and gaseous) sulphur species, resulting in isotopic disequilibrium. Sulphur isotope disequilibrium may be common within alkaline rock-related epithermal deposits.

The stable isotope data from Savo indicate that there are significant magmatic contributions to the hydrothermal fluids, and that the system is analogous to the upper levels of alkaline rock-related epithermal deposits.

Unusual mixed silica–carbonate deposits from magmatic-hydrothermal hot springs 6

Abstract

The volcanic island of Savo, Solomon Islands, hosts an active hydrothermal system discharging unusual alkaline (pH 7–8) sulphate-rich, chloride-poor fluids, with variable admixtures of Ca–Mg–HCO_3^- rich fluids. Hot springs and related streams precipitate a variety of deposits, including travertine, silica sinter and unusual mixed silica–carbonate rocks. Water chemistry and stable isotopes of oxygen, hydrogen and carbon indicate that evaporation and CO_2 degassing are the most important processes causing silica and calcite precipitation. Travertine fabrics are dominated by ray-crystal calcite, associated with rapid abiotic precipitation from a supersaturated solution. Sinter is produced by evaporation of thermal waters, and downstream samples contain preserved traces of micro-organisms, which potentially acted as templates for precipitation. Springs are close to or at saturation with both calcite and amorphous silica, though increased contributions from the Ca–Mg–HCO_3^- endmember favours calcite formation. This fluid is of low temperature origin, and as such is favoured by high rainfall. Mixed samples showing cyclical changes between silica and carbonate precipitation are therefore assumed to be a result of seasonal rainfall variations at Savo. Trace element chemistry of sinters and travertines includes anomalously high levels of Au and Te, suggesting that the system could be producing gold mineralisation at depth.

6.1 Introduction

Travertine ($CaCO_3$) and silica sinter are common features around hot springs and the streams they feed. However, mixed silica–carbonate deposits are rare; only a few are recognised worldwide, most notably at Ohaaki, Ngatamariki, and Waikite, New Zealand (Jones et al., 1996; Campbell et al., 2002; Jones and Renaut, 2003a). Such deposits are found at springs and thermal streams at Savo, Solomon Islands, along with separate deposits of sinter and travertine.

Sinter is most commonly associated with discharge of near-neutral, chloride-rich thermal waters (Hedenquist et al., 2000), or more rarely with acid sulphate waters (Rodgers et al., 2004). The acid systems have different microbial populations and sinter morphology to the

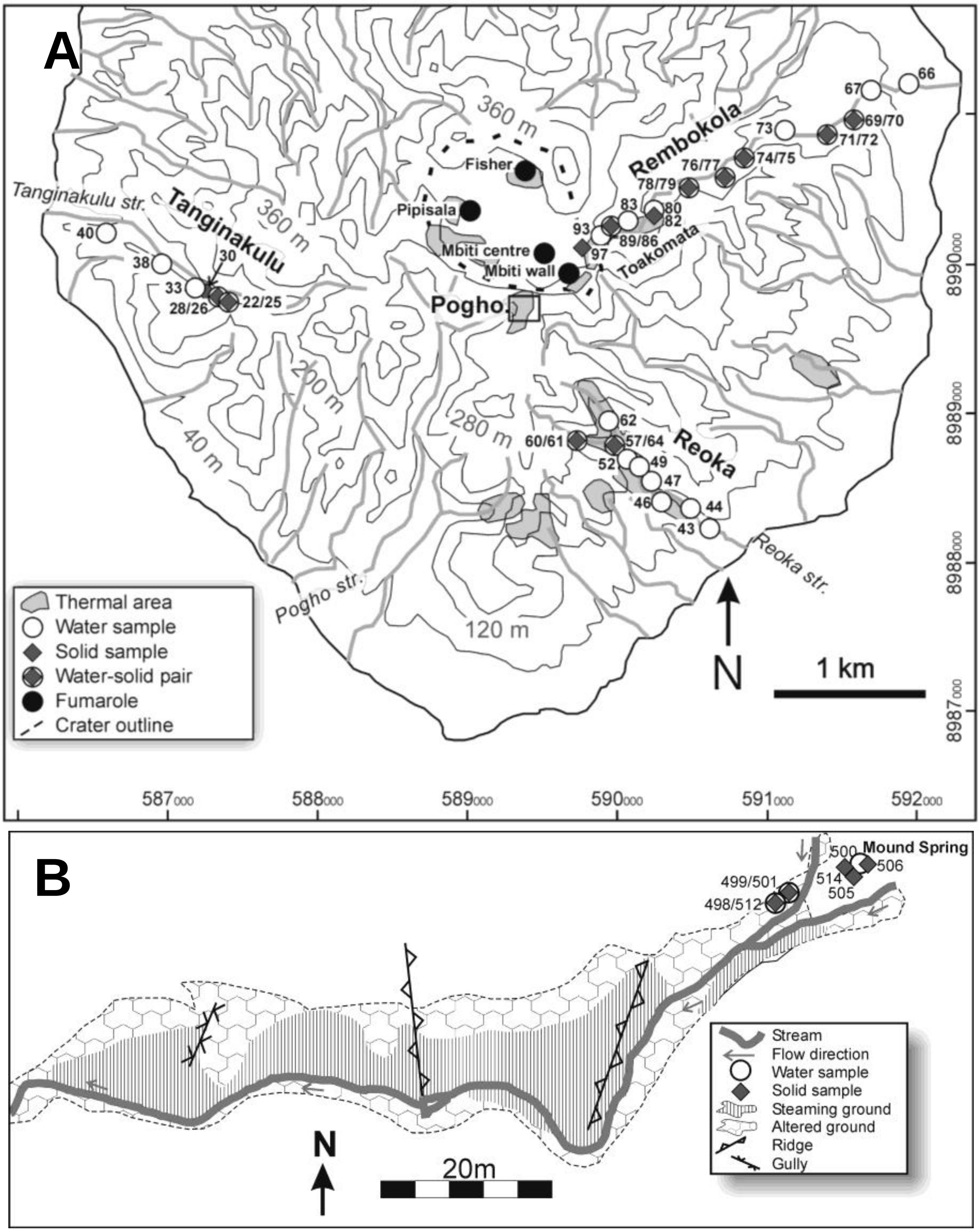

Fig. 6.1A: Map of southern Savo showing location of major streams, thermal areas, and samples discussed in this study. Co-ordinates are for UTM zone 57L. Only the last two digits of the samples numbers are shown, full samples are SV4##. B) Detailed map of Poghorovorughala (Pogho.) sampling areas. See Figure 4.5 for map of Poghorovorughala water samples.

neutral-chloride counterparts (Jones et al., 2000). The fluids discharged at Savo are alkaline sulphate fluids with very low chloride (Chapter 4). Thus the alkaline sulphate springs on Savo represent an environment of sinter formation not previously described, and as such may have distinct microbial ecology and sinter morphology.

As the surface expression of a hydrothermal system, sinter and travertine may provide insights into the chemistry of the fluids at depth, and can be shown to be the surface manifestation of a mineralised system (e.g. Vikre, 2007). Savo occurs in a region prized for epithermal deposits hosted by alkaline rocks, including the world class Ladolam deposit of Lihir, Papua New Guinea (Carman, 2003). Sinters within the Tavua Caldera, Fiji have been related to the giant epithermal Emperor gold-telluride deposit nearby (Eaton and Setterfield, 1993). Sinter and travertine may be useful for identifying otherwise "blind" mineral deposits.

This chapter describes the morphology and mineralogy of the travertine, sinter and mixed silica–carbonate deposits on Savo, including the chemistry and stable isotope compositions of the deposits and the waters from which they precipitate. The aims of the study are: to identify the mechanisms which precipitate travertine, sinter and mixed deposits; to determine the processes behind changes between carbonate-dominant, silica-dominant and mixed deposit precipitation; to determine the significance of gold and pathfinder element concentrations in the precipitates.

6.2 Distribution, morphology and mineralogy

6.2.1 Rembokola deposits

The Rembokola stream, in the east of the island, is fed by hot springs on the upper flanks of the volcano (SV497; Fig. 6.1). These springs discharge small volumes of fluid, and have produced terraced sinter deposits (Fig. 6.2A). Individual benches are no more than a few square centimetres, and in the terminology of Fouke et al. (2000) are considered micro-terracettes. The sinter is highly porous and friable opal-A (X-ray amorphous silica, using a

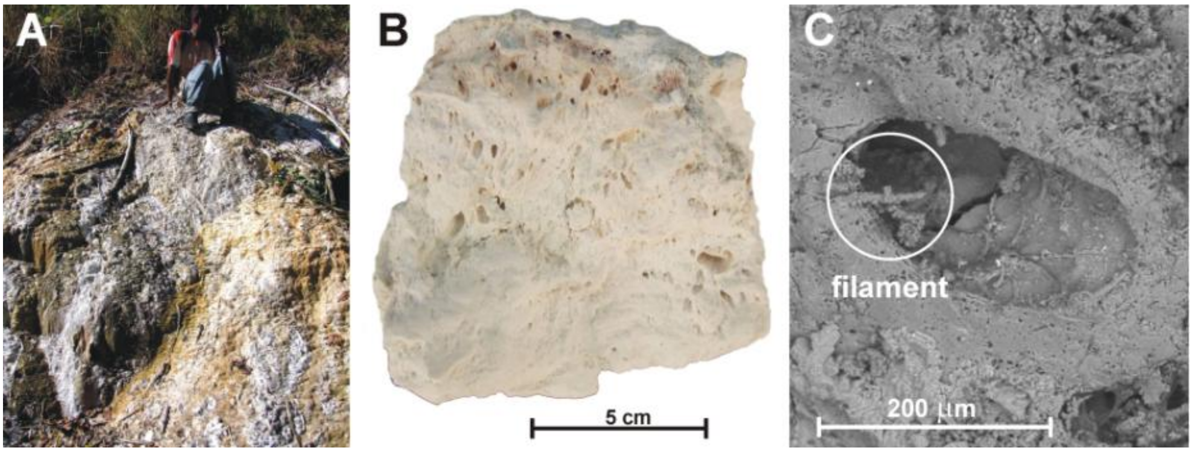

Fig. 6.2: Rembokola terraced sinter (SV497). A) Terraced sinter, on the slopes above the Toakomata hot spring area (Rembokola catchment). Deposit is composed of micro-terracettes of opal-A. B) Photograph of the interior of the sinter, showing highly porous opal-A. C) BSE (back scattered electron) image from broken surface showing small tubes within the void.

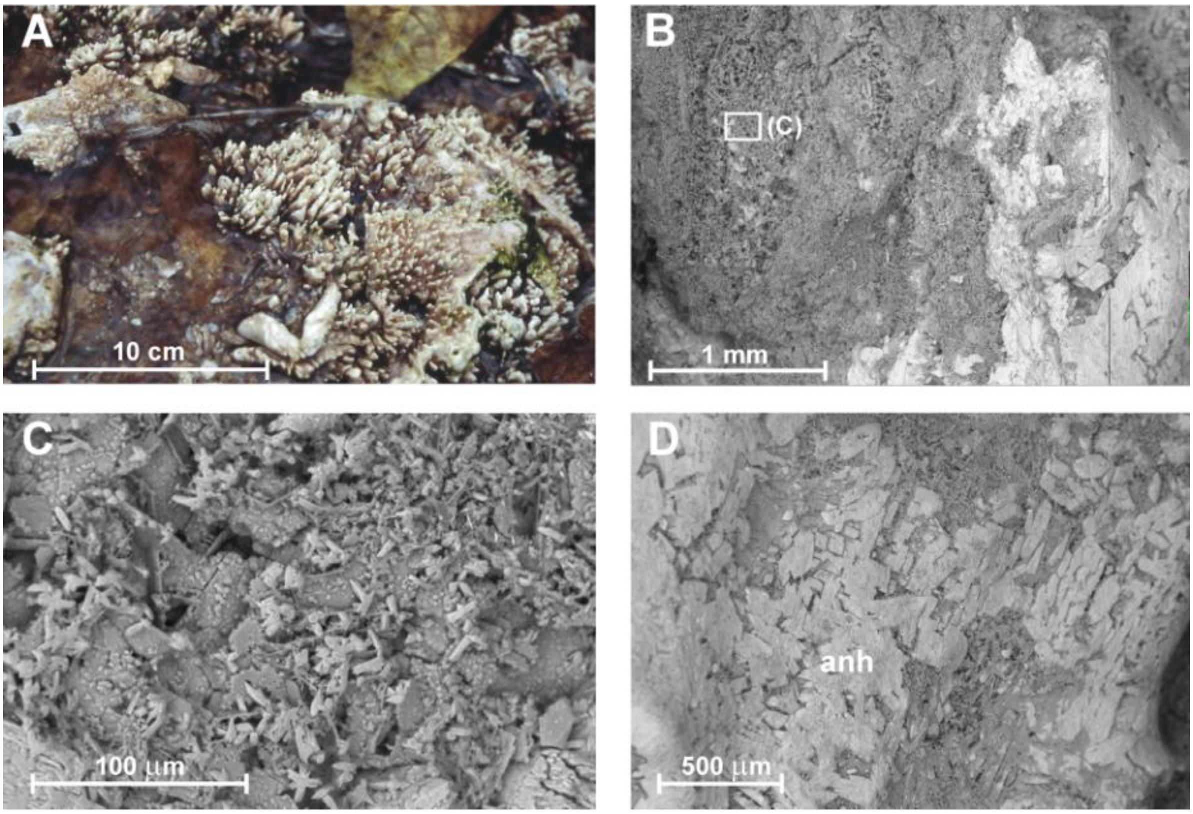

Fig. 6.3: Rembokola spike sinter (SV486). A) Opal-A sinter growing on leaf litter in the Rembokola stream, at the Toakomata hot spring area. B) Back scattered electron (BSE) image of Rembokola spike sinter. Upper surface is to the right of the field of view, and contains more anhydrite (white) than the underside, which is dominated by opal-A. C) BSE image of the interior of a spike; image shows opal-A with small needles of anhydrite. D) BSE image of the upper surface of a spike showing crystalline anhydrite (*anh*) on opal-A.

Philips PW 1716 X-ray diffractometer; Fig. 6.2B–C) with small amounts of anhydrite. Small filaments (<5 µm diameter) are occasionally visible, particularly within pore spaces (Fig. 6.2C).

Downstream, in an area of numerous, vigorous hot springs known as Toakomata (Fig. 6.1), sinter grows above the water surface on stream detritus, usually developing into small (1–2 cm) pointed columns (Fig. 6.3A). SEM and XRD analysis of the spike sinter shows that it is opal-A, often with anhydrite crystals on the top surface (Fig. 6.3 B–D).

Downstream of the hot springs, sinter coats and cements sediment and leaf litter in the stream channel, and forms crusts in the stream channel and banks where accumulations are thicker (Fig. 6.4A). It is often finely laminated (layers <1 mm; Fig. 6.4B). Some of the layers are non-porous opal-A (Fig. 6.4C), others a mixture of non-porous opal-A and hollow filaments up to 5 µm in diameter and 100 µm in length (Fig. 6.4D–E), aligned orthogonally to the layers.

In some locations along the Rembokola stream, mixed silica–carbonate terraces occur above the current water level (upper surface approximately 30 cm above water level at time of observation; Fig. 6.5A). The appearance of the small terraces suggests that they are

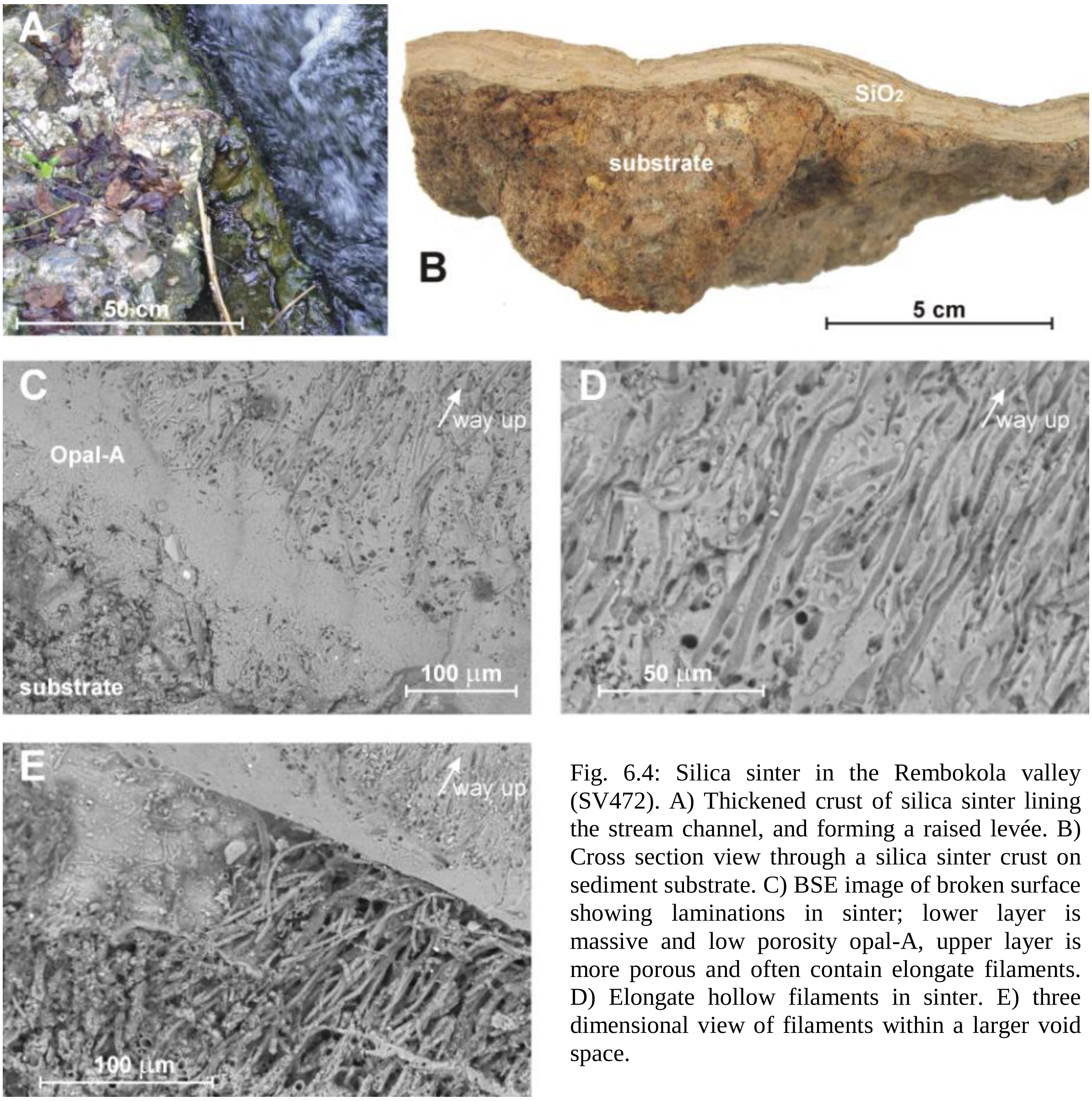

Fig. 6.4: Silica sinter in the Rembokola valley (SV472). A) Thickened crust of silica sinter lining the stream channel, and forming a raised levée. B) Cross section view through a silica sinter crust on sediment substrate. C) BSE image of broken surface showing laminations in sinter; lower layer is massive and low porosity opal-A, upper layer is more porous and often contain elongate filaments. D) Elongate hollow filaments in sinter. E) three dimensional view of filaments within a larger void space.

older than the silica-only sinters: they occur well above the current water level, and exposed surfaces show signs of weathering and erosion. These deposits consist of alternating layers of opal-A and calcite. Individual layers are up to 10 mm thick, and unconformities are often visible (Fig. 6.5B, D). Carbonate layers are formed from ray-crystals of calcite (Folk et al., 1985; Chafetz and Guidry, 1999), organised into near-vertical fans (Fig. 6.5C, E). Silica layers are for the most part non-porous, but in cavities where a three dimensional view is possible, small filaments are visible (Fig. 6.5F, G; cf. Fig. 6.4E).

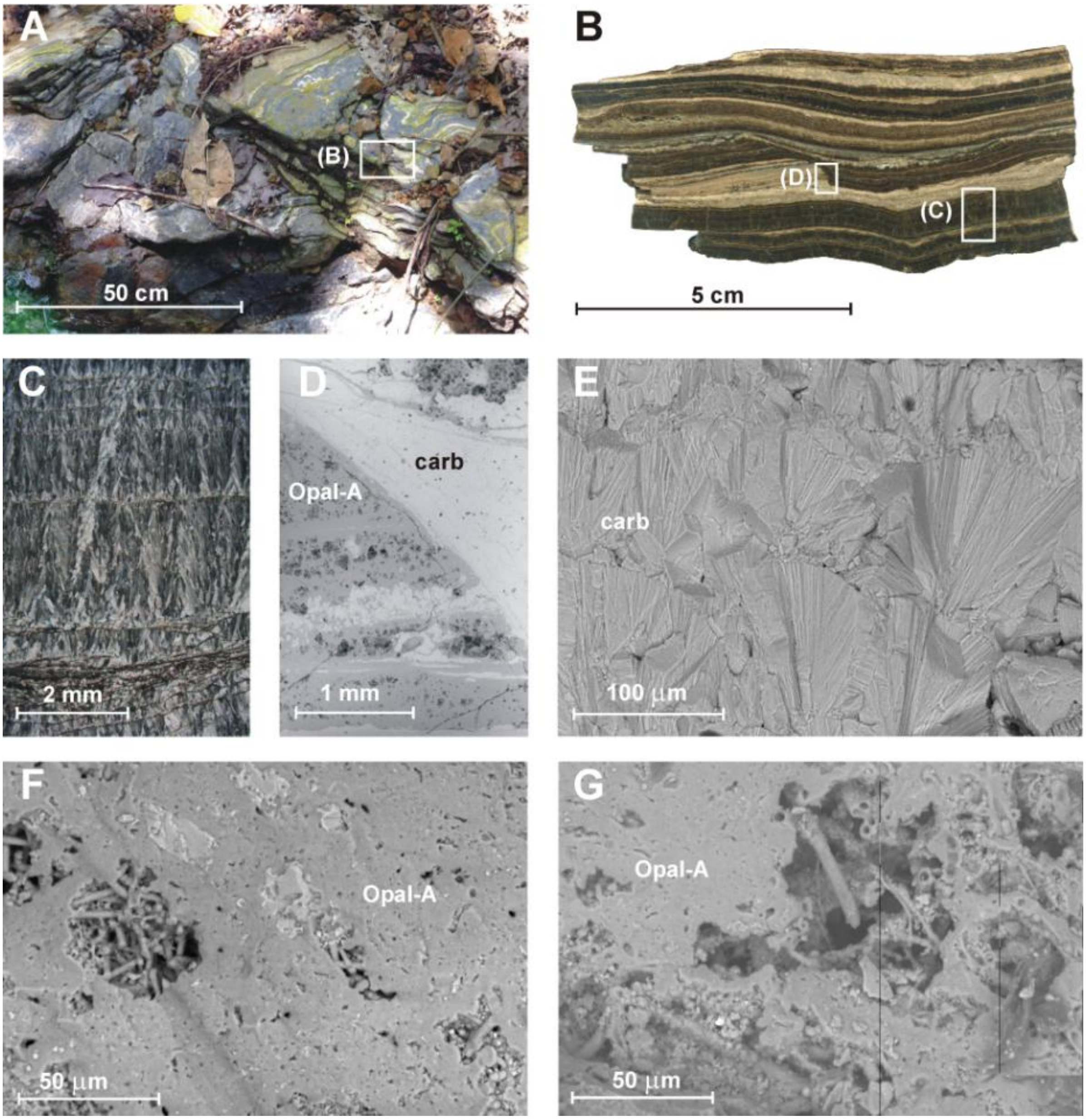

Fig. 6.5: Mixed silica–carbonate sinter, Rembokola valley (SV482). A) Terrace of mixed sinter above current stream water level. B) Cross section through sinter showing layers of calcite (dark) and opal-A (pale). C) Thin section through carbonate layers showing fans of ray crystals (cross polarised light). D) BSE image showing calcite layer onlapping onto older silica and carbonate layers. E) BSE image of calcite fans (determined by bulk XRD analysis, confirmed with EDX SEM analysis). F) BSE image of silica layer, with filaments visible in void space. G) BSE image of filaments in void space.

6.2.2 Poghorovorughala deposits

Silica–carbonate deposits were collected from the Poghorovorughala thermal area (Fig. 6.1). Deposits form around alkaline sulphate hot springs and in the base of the stream. Deposits are carbonate-dominated (aragonite and calcite) with opal-A. Distinct depositional facies can be observed (Fig. 6.6):

- Lobate deposits form adjacent to alkaline sulphate springs, in areas frequently splashed and bathed by thermal waters. They typically have smooth, rounded upper

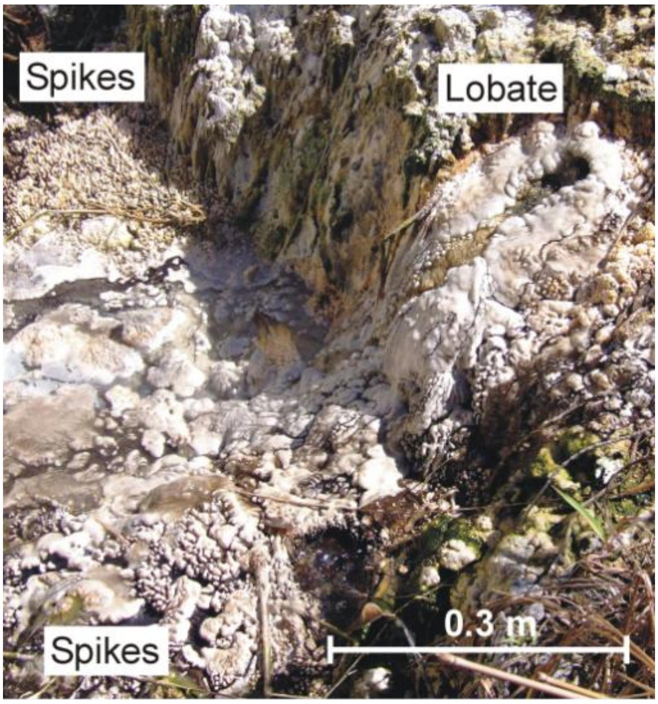

Fig. 6.6: Precipitates surrounding an alkaline sulphate hot spring at Poghorovorughala. Lobate deposits surround the spring and the discharge channel; spikes occur on the periphery.

surfaces of carbonate (microcrystalline aragonite or calcite) with opal-A and minor anhydrite (Fig. 6.7A–D). Individual lobes are finely laminated in cross section (Fig. 6.7B). Trigonal prisms of calcite are visible on SEM images, typically in sheltered areas between lobes (Fig. 6.7E, G–H). Pyrite and some manganese oxide precipitate on the underside of the lobes (i.e. slightly submerged or at the contact with the hot spring water; Fig. 6.7F).

- Spike deposits form slightly further from the springs, typically in areas splashed and bathed infrequently. The physical appearance is identical to the spiked sinter that grows on leaf litter near the Rembokola springs (Fig. 6.3), although contains more carbonate. Spiked growths were observed developing on a lobate travertine substrate (Fig. 6.6).
- Layered silica–carbonate deposits occur in the discharge channels of springs and in the stream. The ~2 m high Mound Spring (Fig. 6.8A) is constructed of layered precipitates (based on surface exposure) with micro-terracetted (Fig. 6.8B) surface texture. The layers are 5–50 mm thick, and generally pale in colour though occasional dark layers do occur (Fig. 6.8C). Dark layers tend to be dominated by opal-A (Fig. 6.8D), whereas the pale layers are composed of ~1 mm long calcite ray-crystals organised into fans that diverge upwards (Fig. 6.8F; mineralogy confirmed with XRD). Minor anhydrite is present, mostly within the carbonate dominated layers (Fig. 6.8G).

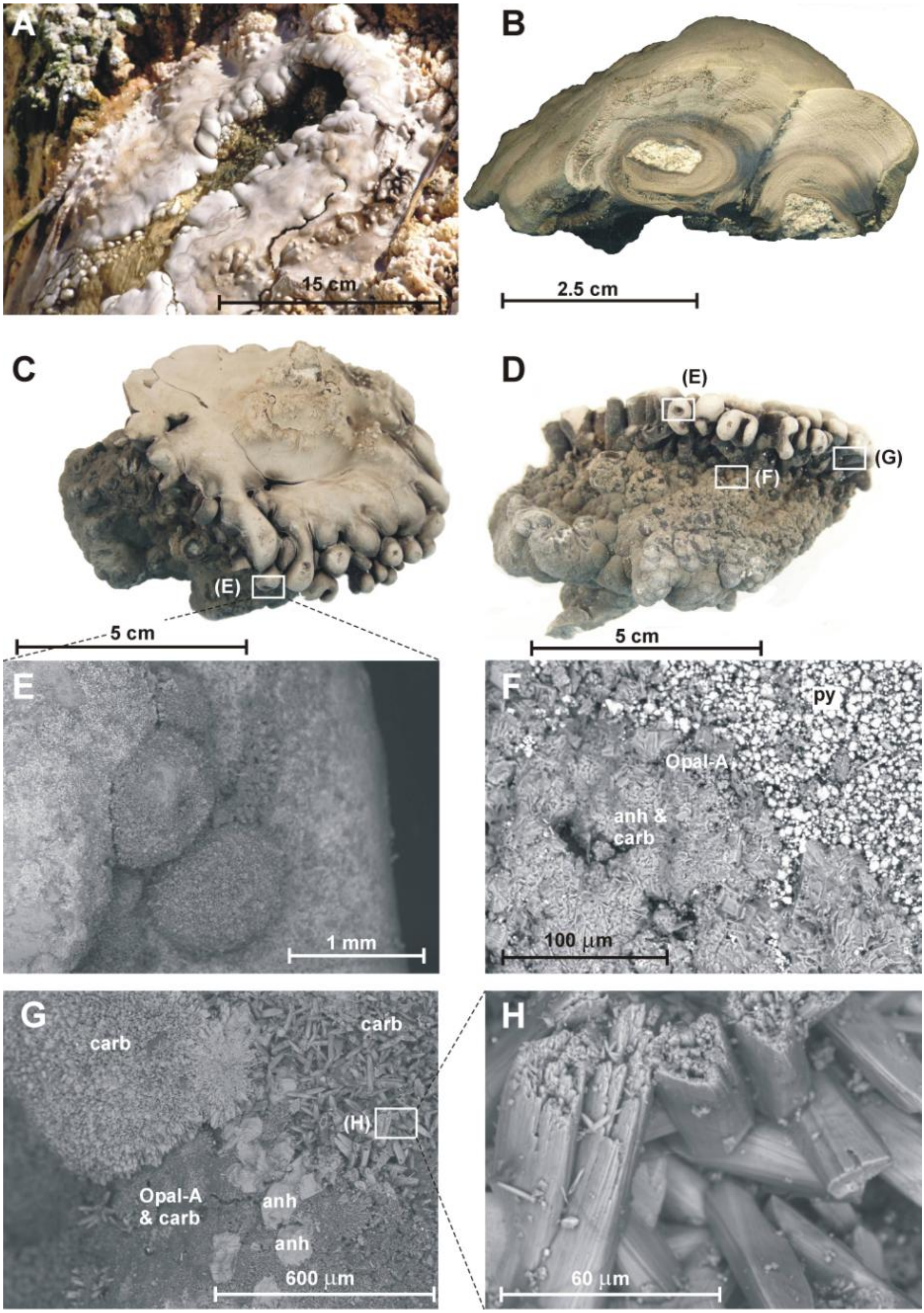

Fig. 6.7: Lobate deposits, Poghorovorughala. A) Lobes surrounding boiling hot spring (SV512). B) Cross section through lobes, showing concentric laminations (SV512). C) Upper surface of SV501. D) Underside of SV501 (submerged portion). E) Rounded lobes of carbonate developing on subaerially exposed / splashed portion (SV501). F) Pyrite on surface of carbonate, opal-A and minor anhydrite in submerged portion (SV501). G) Carbonate and opal-A, with occasional anhydrite crystals, on splashed area of deposit (SV501). H) Detail view of calcite, showing trigonal crystal form (SV501).

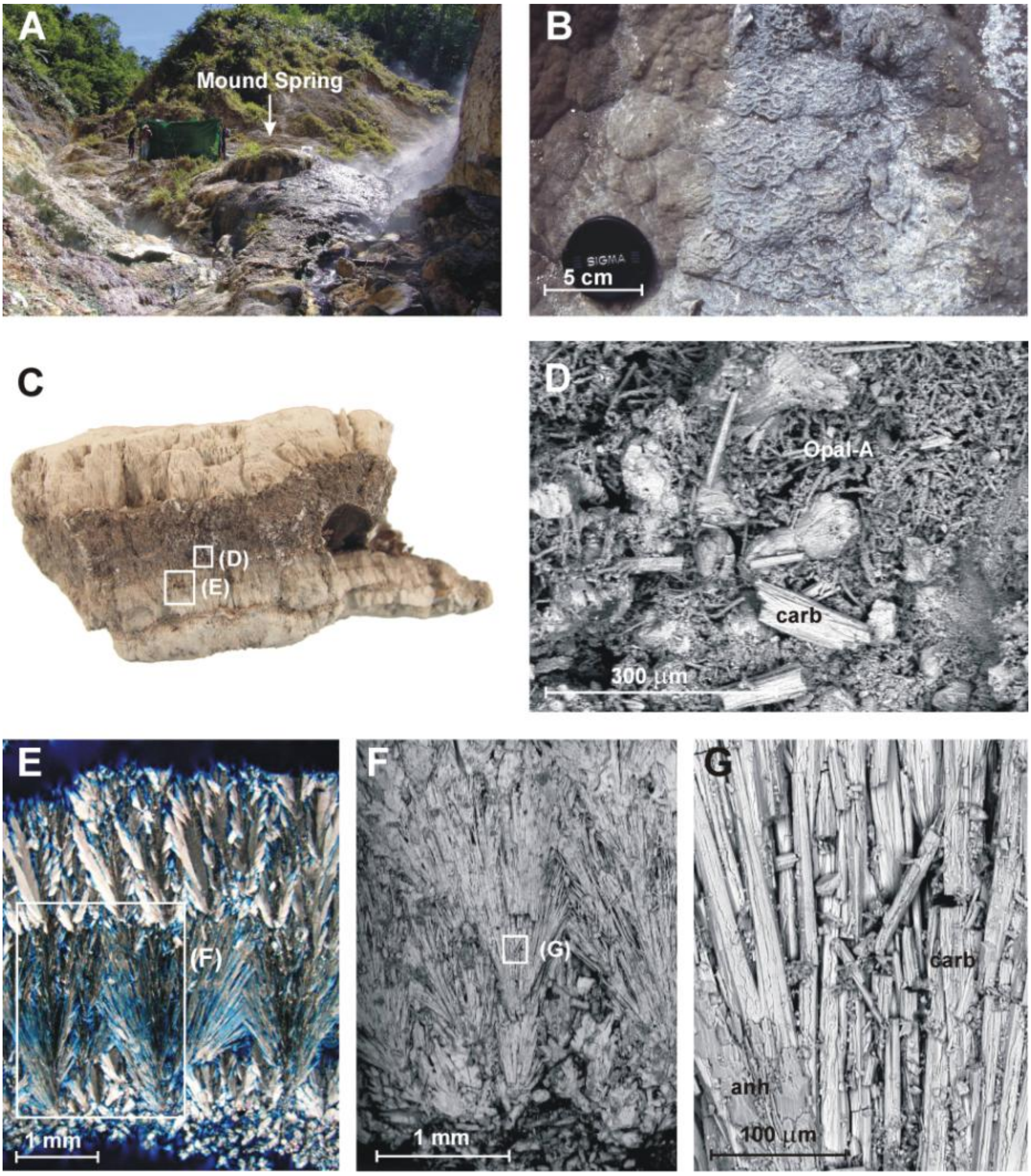

Fig. 6.8: Mixed silica–carbonate deposits, Poghorovorughala (SV505). A). View of Mound Spring, a 3 m high deposit of layered travertine. A hot spring discharges from the summit of the mound. B) Micro-terracette texture on surface of the Mound Spring. C) Cross section through layered travertine of the Mound Spring. D) Dark layer is a mixture of tubes/ filaments of opal-A, and crystals of calcite. E) Thin section view of carbonate fans (cross polarised light; sample mounted in blue resin). F) BSE image of carbonate fans. G) Detail view of calcite ray crystals, showing minor anhydrite.

6.2.3 Reoka and Tanginakulu travertines

Travertine is abundant in the stream channels of both tributaries upstream of the Reoka thermal area (Fig. 6.1). Downstream of the thermal area, no major travertine deposits were observed, other than transported blocks (SV448 and SV450). Travertine forms laminated crusts on material in the tributary channels, developing terracettes in some areas (Fig. 6.9A). Layers are finer than those observed in the Poghorovorughala layered deposit

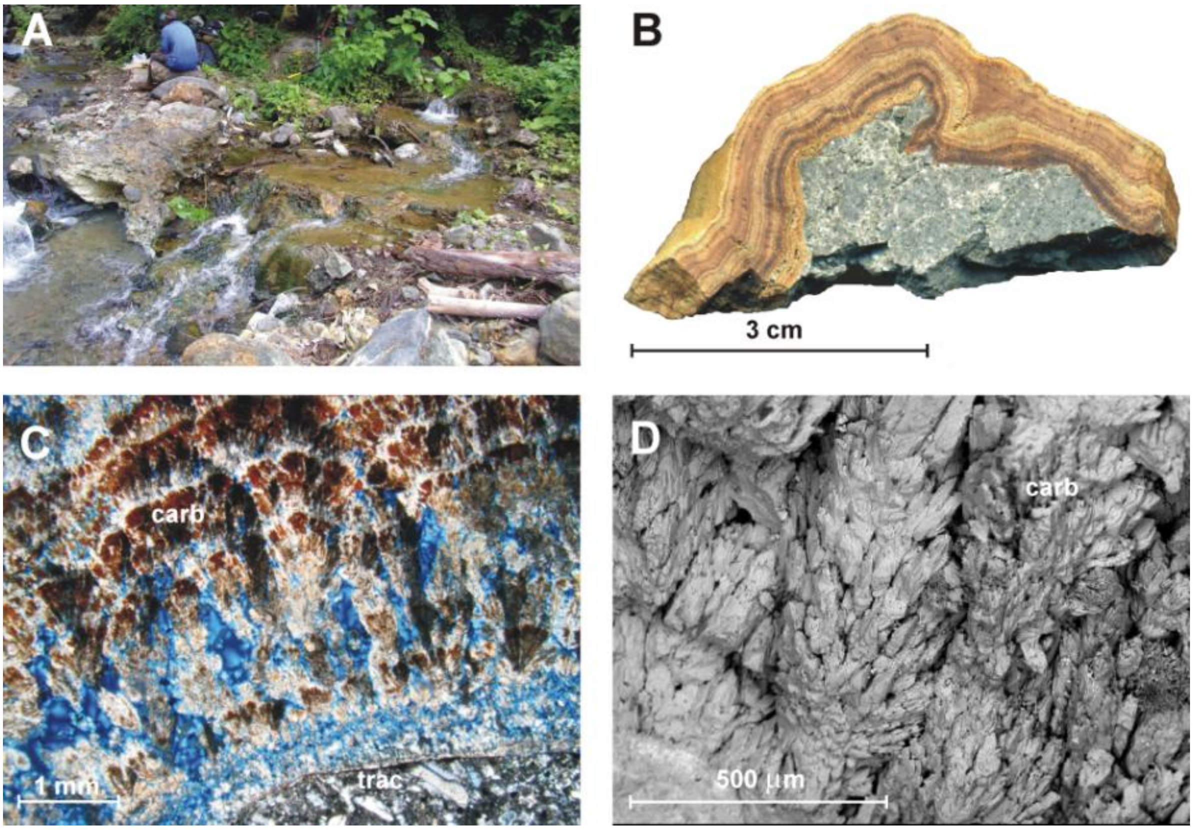

Fig. 6.9: Reoka travertine deposits. A) Terraces in the stream channel are deposits of travertine (SV464). B) Laminated travertine crust on trachyte substrate. C) Thin section of Reoka travertine SV461. Fans of calcite ray-crystals form lobate top surfaces of individual layers (cross polarised light; sample mounted in blue resin). D) BSE image of calcite fan showing three dimensional structure (SV461).

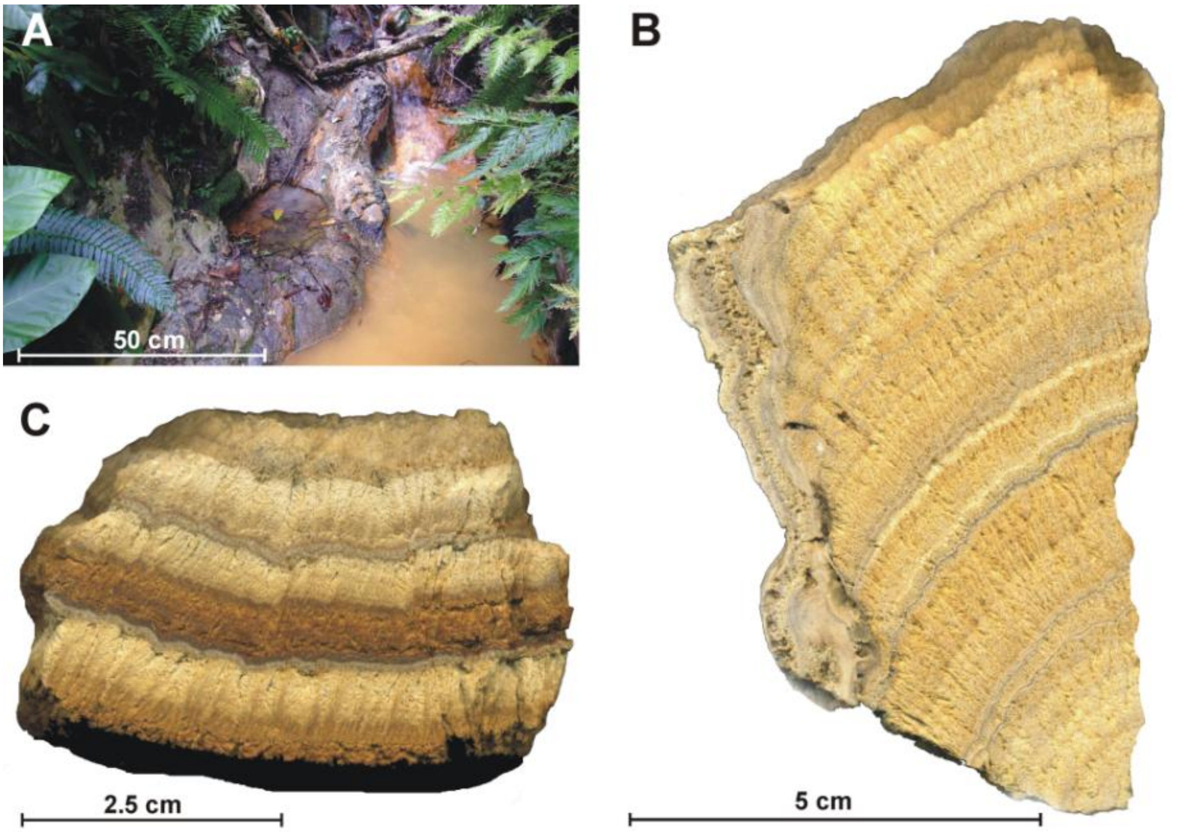

Fig. 6.10: Tanginakulu travertine deposits. A) Travertine deposited at small stream rapids. B & C) Cross sections views through travertine blocks showing laminations of carbonate and fans of elongate calcite ray-crystals (samples SV427 and SV425 respectively).

(generally <5 mm thick; Fig. 6.9B), but the calcite has a similar morphology, with elongate calcite ray crystals in upwards-diverging fans (Fig. 6.9C–D).

Travertine occurs in the stream channel over the whole length of the Tanginakulu stream. In relatively flat areas, travertine coats and cements stream detritus, whereas sizeable thicknesses of layered travertine develop at rapids and waterfalls (Fig. 6.10A). Internal structure of the deposits is similar to that of the Reoka travertine samples, with layers of calcite ray-crystal fans (Fig. 6.10B–C).

6.3 Sampling and analytical methods

6.3.1 Travertines and sinters – chemistry and stable isotopes

Samples were sequentially leached in three steps to attempt to separate the anhydrite, carbonate and silicate fractions. Samples were crushed using a hardened steel press and milled to a fine powder with an agate planetary mill. Samples were dried overnight at 100°C. 100 mg sample was transferred to a centrifuge tube and 50 ml deionised H_2O was added to dissolve the anhydrite portion. The tube was placed in an ultrasonic bath at 30°C for 30 minutes. The sample was centrifuged and the supernatant liquid transferred to a clean glass beaker by pipette. This step was repeated 5 times. The resulting 250 ml solution was evaporated to dryness on a hot plate, re-dissolved in 15 ml 32% HCl, and evaporated to dryness again. The resulting chloride salts were re-dissolved in 15 ml 1.7 N HCl and transferred to sample containers. The residual solids were left in the tube, dried and weighed.

To dissolve the carbonate portion 25 ml 0.1 M acetic acid was added to the solid residue from the first leach, and the centrifuge tube was placed in the ultrasonic bath at 30°C for 30 minutes. The sample was centrifuged, and the supernatant liquid transferred to a clean glass beaker by pipette. 10 ml deionised water was added to the sample, which was briefly shaken, then centrifuged, and the resulting supernatant liquid transferred to the beaker with the acetic solution. This was repeated three times to remove any acetic acid from the residual solids. The resulting solution was dried and redissolved as for water-soluble fraction.

To dissolve the silicate portion, the residual solids from the second leach were transferred into open PTFE beakers. 5 ml 70% HNO_3 was added and the sample heated at 50°C overnight; 1 ml 60% perchloric acid and 5 ml 48% HF were then added, and the mixture left at 90°C for 3 hours, at 140°C for a further 3 hours, and at 190°C overnight to fume off silica (not analysed for the final fraction). 1 ml 32% HCl was added to the resulting residue, and left for 1 hour at 50°C. The solution was quantitatively transferred to sample containers and diluted to 15 ml by adding deionised H_2O. Samples with <10 mg of solid remaining after the water and acetic leaches were not HF leached. For samples that underwent HF leach, no solid residue remained after that step.

All sample solutions were analysed for As, Ba, Ca, Cu, Fe, K, Mg, Mn, Na, Pb, S, Sb, Sr, V and Si (water and acetic portions only) with a JY Ultima 2 ICP-OES at the University of Leicester. The accuracy for solutions at the ICP-OES was <5% for all fractions and analytes with the exception of As (water and acetic, 8%, HF fraction 6%), and Sr (HF fraction 6%). The accuracy was propagated through the dilution and sample mass correction steps, assuming cautious weighing errors of ±2 mg and ±1 ml on volume measurement. For small fractions, the weighing errors are the principal source of uncertainty. The final error values are shown graphically where appropriate.

Eight sinter and travertine samples were sent for chemical analysis and precious metal assay at Acme Analytical Laboratories, Canada. Samples were crushed and powdered as above, and analysed by ICP-MS following aqua regia digestion. Precision and accuracy were estimated by duplicate analysis of standard DS7; precision (2σ) was <5% for all species except Al, Ca, Cr, B, La, Na, Sc (<10%); Zn, Hg, Se, Ag (<15%); Cu (43%) and Au (63%). The low reproducibility of Cu and Au indicates a nugget effect with standard DS7. Similar values were obtained for repeat analysis (n = 4) of a Savo carbonate. The accuracy (mean measured DS7 vs. accepted value) was better than +5% for Ca, Fe, Ga, Hg, La, Mg, Mn, Mo, P, Th, Tl, U, V, Zn; −5% for Ag, Co, Ni, Pb, Se, W; +10% for Al, As, Au, B, Ba, Cd, Sc; −10% for S, Ti; +15% for Bi, Sr, K, Cr, Cu; −12% for Sb, +19% for Te and +26% for Na (NB. accepted Na contents are 0.073 wt %)

Representative bulk travertine samples were analysed for $\delta^{13}C$ and $\delta^{18}O$. Samples were crushed and powdered as above, and prepared using the phosphoric acid method of McCrea (1950) as modified by Rosenbaum and Sheppard (1986). The final purified CO_2 fraction was analysed with a VG SIRA 10 mass spectrometer at SUERC (East Kilbride, Scotland). Repeat analysis of laboratory standard MAB 2b (calibrated against NBS 19) indicates that the precision of the technique is better than 0.2‰ for $\delta^{13}C$ and 0.3‰ for $\delta^{18}O$. The $\delta^{18}O$ data for MAB 2b show a slight bias (0.5‰) to lower than expected values, though the difference is small when taking into account the precision and so no correction was made. $\delta^{13}C$ values show no bias.

For finely layered travertine blocks, samples were obtained from individual layers with a small diamond-tipped drill. Samples were analysed with an Analytical Precision AP2003 mass spectrometer equipped with a separate acid injector system, after reaction with 105% H_3PO_4 under He atmosphere at 70°C. Accuracy and precision were similar to that of the above technique. All stable isotope values are reported relative to V-PDB (carbon) and V-SMOW (oxygen) in standard permil notation, and are calibrated against reference material NBS 19.

6.3.2 Water chemistry and stable isotopes

Water samples were collected and analysed as in Chapters 4 and 5.

For comparison with travertine samples, stream and spring waters were analysed for $\delta^{13}C$ of dissolved inorganic carbon (DIC). The water was collected as in Section 4.3. In the field, 75 ml was decanted into a HDPE bottle and made alkaline with the addition of 2 ml 0.1 N NaOH, and an excess of 5% $BaCl_2$ solution was added slowly to the sample to precipitate $BaCO_3$ (with co-precipitation of $BaSO_4$). In the laboratory, precipitated $BaCO_3$ was separated from the water by centrifuge. Resulting solids were rinsed with deionised water and dried at 80°C overnight. Dried samples were prepared for isotopic analysis using the phosphoric acid method discussed above. The final CO_2 fraction was analysed with a VG SIRA 10 mass spectrometer at SUERC (East Kilbride, Scotland); accuracy and precision for the techniques are the same as for the travertine samples.

Carbon dioxide samples were collected from fumaroles and steaming ground by burying a polypropylene funnel at the hottest part. Steam and gas were pumped through silicone tubing and a stainless steel cooling coil into two borosilicate glass flasks with stopcocks at each end. Condensed steam was collected in the first flask and non-condensable gases in the second (Darling and Talbot, 1991). CO_2 from the gas samples was separated from other gases and moisture by the use of liquid nitrogen and methanol traps. The separated CO_2 was analysed on a VG Optima mass spectrometer at the British Geological Survey, Wallingford, to determine carbon and oxygen stable isotope compositions. $\delta^{13}C$ values were calculated using laboratory standard MCS, calibrated against reference materials NBS 19 and NBS 22. Repeat analysis of samples gives a precision of $< \pm 0.2‰$ (1σ).

6.4 Results

6.4.1 Streams and fumaroles

The Rembokola stream is fed by alkaline sulphate hot springs in the Toakomata area, and has similar chemistry to them, with high Na, Ca, Si, K, and SO_4^{2-}, and low Cl^-. (Table 6.1; Table 4.6). Important trace elements include Sr, Li, Rb and Cs. Arsenic occurs in concentrations of 60–70 μg/l; for comparison, typical seawater concentrations are only 1 μg/l (Cabon and Cabon, 2000). The chemistry shows no abrupt downstream changes, reflecting the fact that there are no tributaries. There are, however, gradual changes to the stream chemistry. Heading downstream, there is a decrease in temperature, DIC, Mn, and Si; whereas B, Li, Cl^- and the pH all increase (Table 6.1, Fig. 6.11). $\delta^{18}O_{H2O}$ may increase by ~1‰ downstream, but the reproducibility of the most downstream samples was poor; δD shows ~4‰ increase, but again is within error (Fig. 6.11). $\delta^{18}O$ and δD are close to those of the alkaline hot springs in the upstream area (Fig. 6.12).

In contrast with the Rembokola, the Reoka thermal area is not the source for the waters of the stream. Rather, the hot springs of the Reoka thermal area are periodically flooded by the stream, resulting in springs with chemistry similar to that of the adjacent stream (Tables 6.2 and 4.7). Water chemistry is dominated by Ca, Na, and Mg, with high

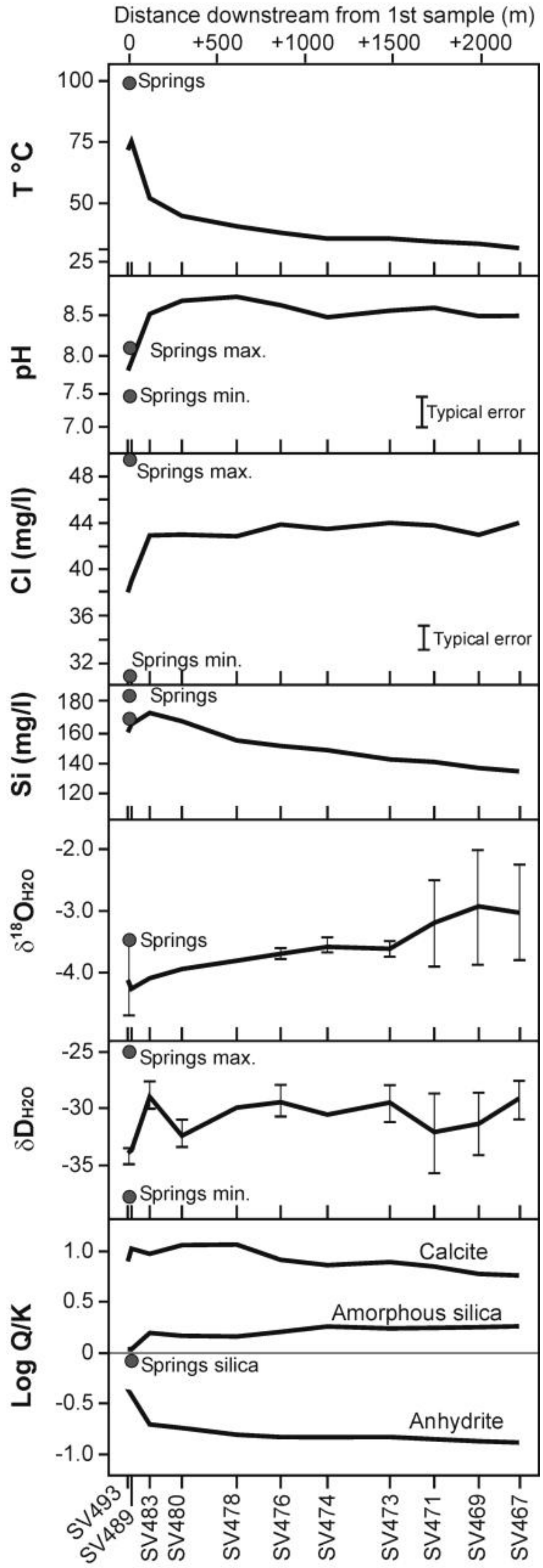

Fig. 6.11: Changes in temperature, pH, Cl^- and Si concentrations, stable isotopes of water and saturation index of important minerals in the Rembokola stream. Representative alkaline sulphate springs (or maximum and minimum values in the case of a range) shown for comparison. Moving downstream from left to right. Error bars are ±1σ; not shown when within point size.

Sample	SV493	SV489	SV483	SV480	SV478	SV476	SV474	SV473	SV471	SV469	SV467
Date	16/10/06	16/10/06	15/10/06	15/10/06	15/10/06	15/10/06	14/10/06	14/10/06	14/10/06	14/10/06	14/10/06
Distance	0.00	0.01	0.11	0.30	0.61	0.86	1.13	1.48	1.73	1.98	2.21
T (°C)	72	75	52	45	40	38	35	35	34	33	31
pH	7.9	8.1	8.5	8.7	8.8	8.6	8.5	8.6	8.6	8.5	8.5
DIC	72	62	49	44	42	47	53	47	44	47	49
Ag (µg/l)	bdl	bdl	bdl	bdl	bdl	bdl	bdl	bdl	bdl	0.7	bdl
Al (µg/l)	7	6	3	bdl	2	3	bdl	2	2	4	9
As (µg/l)	68	65	66	69	70	70	73	69	72	73	69
B	7.37	7.89	8.58	8.75	8.79	8.91	8.81	8.81	8.77	8.66	8.7
Ba (µg/l)	63.5	60.6	66.3	66.1	63.3	64.5	66.8	63.2	64.7	64.1	62
Ca	169	152	152	153	152	153	155	154	154	153	154
Co (µg/l)	0.3	0.3	0.3	0.3	0.3	0.3	0.3	0.3	0.3	0.3	0.3
Cs (µg/l)	44.4	42.6	45.4	46.3	44.2	44.9	46.8	44.3	43.9	44.2	43
Fe	0.04	0.03	0.03	0.03	bdl	bdl	bdl	bdl	bdl	0.03	0.03
K	25.6	26.2	28.1	28.5	28.3	28.5	29	29	28.7	28.5	28.3
Li (µg/l)	1313	1377	1492	1514	1515	1537	1532	1546	1546	1534	1521
Mg	8.8	7.7	8	8	8	8.1	8.3	8.2	8.2	8.2	8.2
Mn	0.39	0.33	0.31	0.22	0.15	0.15	0.14	0.08	0.07	0.07	0.08
Mo (µg/l)	14.9	13.5	13.4	14	13.7	14.1	14.2	13.4	14	13.9	13.4
Na	174.8	184.1	198.1	200.6	200.4	203.3	202.7	203.9	203.6	202.4	200.9
Ni (µg/l)	3	3	3	3	4	3	4	4	4	4	4
Pb (µg/l)	0.5	0.3	bdl	0.2	0.2	0.2	bdl	bdl	0.4	0.4	0.7
Rb (µg/l)	113.4	112.3	118.6	123.3	122.7	124.6	126.5	120.8	122.7	123.7	120.2
Sb (µg/l)	0.9	0.9	0.8	0.8	0.8	0.8	0.9	0.8	0.8	0.8	0.8
Si	160	164	172	165	154	150	148	142	141	136	135
SO_4^{2-}	684	668	696	710	711	719	715	716	717	713	713
Sr	4.34	4.01	4.02	4.06	4.05	4.09	4.1	4.1	4.11	4.09	4.07
Ti (µg/l)	21	bdl	bdl	bdl	bdl	bdl	bdl	bdl	bdl	bdl	bdl
Tl (µg/l)	0.13	0.12	0.13	0.13	0.12	0.11	0.13	0.12	0.11	0.11	0.1
U (µg/l)	0.04	0.03	bdl	bdl	bdl	bdl	bdl	bdl	bdl	bdl	bdl
V (µg/l)	2	2	1	1	1	1	2	1	2	2	2
Y (µg/l)	0.05	0.05	0.05	0.05	0.07	0.06	0.07	0.06	0.07	0.08	0.07
Zr (µg/l)	0.03	0.02	0.03	0.02	0.1	bdl	bdl	bdl	0.02	0.07	0.04
Cl^-	38	38.9	43	42.9	42.8	44	43.4	44	43.8	43	43.9
NO_3^-	0.11	0.065	0.307	0.254	0.314	0.036	0.274	0.101	0.089	0.103	0.112
Br^-	0.069	0.071	0.066	0.077	0.082	0.068	0.067	0.074	0.076	0.078	0.079
NO_2^-	0.056	0.017	0.041	0.018	0.016	bdl	bdl	bdl	0.013	0.015	bdl
F^-	0.297	0.315	0.305	0.305	0.323	0.441	0.323	0.278	0.332	0.325	0.321
CBE (%)	5	5	4	3	4	4	3	4	4	4	5
$\delta^{18}O_{H2O}$	−4.1	−4.2	−4.1	−3.9	−3.8	−3.7	−3.6	−3.6	−3.2	−2.9	−3.0
1σ	0.7	0.1	0	0	0	0.1	0.1	0.1	0.7	0.9	0.8
δD_{H2O}	−34	−34	−29	−33	−30	−29	−31	−30	−32	−32	−29
1σ	1	0	1	1	1	2	1	2	4	3	2

Table 6.1: Water chemistry data for Rembokola stream samples. All values in mg/l unless noted otherwise. Distance is measured in kilometres downstream from first sample. bdl = below detection limits; DIC = dissolved inorganic carbon as mg/l HCO_3^- eqv.; CBE = charge balance error. The following elements and species were below detection limits for all analyses, and are omitted from the table: Be, Bi, Cd, Ce, Cr, Cu, Ho, La, Nd, P, Se, Sn, Te, Th, Zn, HPO_4^-.

SO_4^{2-} and low Cl^-; trace elements of note include Sr and As, although neither are present in concentrations as high as the Rembokola waters.

The Reoka stream has multiple tributaries. Comparison of samples from the two feeder streams (SV460 and SV462) shows a number of small but significant differences in As, B, Ca, K, Na, Rb, Si, DIC and Cl; samples downstream of the confluence of these tributaries have intermediate chemistries (SV457–443; Table 6.2 and Fig. 6.13). The water

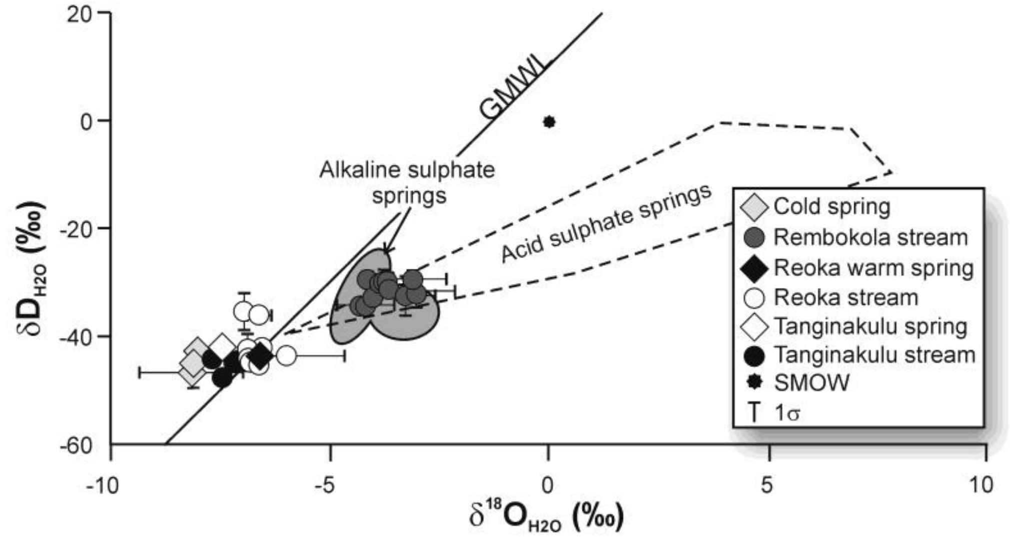

Fig. 6.12: Oxygen and hydrogen stable isotope of stream and spring waters from Savo Island. Alkaline sulphate and acid sulphate spring waters are shown for reference. Rembokola stream waters have isotopic values similar to the alkaline sulphate springs found in the upstream area of that catchment; Reoka and Tanginakulu waters are similar to cold springs and warm springs. GMWL = global meteoric water line.

Sample	SV460	SV462	SV457	SV452	SV447	SV446	SV444	SV443
Date	11/10/06	11/10/06	11/10/06	10/10/06	09/10/06	09/10/06	09/10/06	09/10/06
Distance	0.00	(0.04)	0.13	0.17	0.35	0.55	0.78	1.00
T (°C)	33	38	34	38	37	38	37	35
pH	8.1	8.3	8.1	7.7	8	8.2	8.3	8.2
DIC	199	237	205	220	218	220	216	216
Al (µg/l)	4	4	3	7	6	4	3	3
As (µg/l)	5	69	22	40	34	28	25	21
B	0.94	3.1	1.5	2.12	2.02	1.89	1.83	1.79
Ba (µg/l)	34	35.8	33.6	34.3	39.8	43.8	41.8	43.5
Ca	151	96	140	116	132	135	136	137
Co (µg/l)	0.6	0.3	0.4	0.4	0.4	0.5	0.4	0.4
Cs (µg/l)	1.4	3.1	1.7	2.2	1.9	1.8	1.6	1.3
Fe	bdl	0.05	bdl	0.03	0.04	0.03	0.02	0.05
K	8.1	12.4	9.2	10.5	10.2	9.8	9.7	9.4
Li (µg/l)	106	275	148	200	185	169	165	158
Mg	39.2	34.4	39.1	35.9	35.9	34.7	34.6	34.3
Mn	0.23	0.09	0.09	0.09	0.1	0.08	0.05	0.05
Mo (µg/l)	2.7	6.4	4	4.7	4.4	4.5	4.1	3.7
Na	66	124	83	100	101	100	99	96
Ni (µg/l)	5	3	4	4	4	4	4	4
Pb (µg/l)	0.6	0.3	1.2	0.5	2.4	0.9	0.9	1
Rb (µg/l)	19.1	35.1	23.9	28.4	26.8	25.9	23.9	22.3
Sb (µg/l)	bdl	0.1	bdl	bdl	bdl	bdl	bdl	bdl
Si	45	68	50	57	55	52	52	49
SO_4^{2-}	311	248	316	284	309	307	308	309
Sr	1.56	0.73	1.44	1.11	1.37	1.45	1.45	1.44
Tl (µg/l)	bdl	0.04	0.02	0.03	0.03	0.03	0.03	0.02
V (µg/l)	2	2	2	2	2	3	3	3
Y (µg/l)	0.08	0.11	0.08	0.1	0.11	0.12	0.1	0.07
Zr (µg/l)	bdl	0.04	0.02	0.08	0.04	0.04	0.02	0.06
Cl^-	9	18.1	13.3	14.8	15.5	14.9	14.6	13.9
NO_3^-	0.369	0.876	1.65	0.056	0.681	0.038	bdl	0.63
Br^-	bdl	0.036	0.022	0.022	0.026	0.028	0.02	0.021
NO_2^-	0.027	0.039	0.034	bdl	0.042	bdl	bdl	0.506
F^-	0.312	0.431	0.267	0.348	0.294	0.234	0.294	0.256
CBE (%)	16	17	15	15	15	15	15	15
$\delta^{13}C_{DIC}$	8.4	5.5	8.1	8.9	9.4	8.3	8.2	9.7
1σ			1.4	1.5				
$\delta^{18}O_{H2O}$	−6.9	−6.5	−6.8	−6.6	−5.9	−6.5	−6.5	−6.8
1σ	0.1	0.3	0	0.1	1.4	0.4	0.4	0
δD_{H2O}	−35	−36	−42	−43	−43	−41	−44	−44
1σ	3	0	3	0	1	2	2	1

Table 6.2: Water chemistry data for Reoka stream samples. All values in mg/l unless noted otherwise. Distance is measured in kilometres downstream from first sample (tributary marked in brackets). bdl = below detection limits; DIC = dissolved inorganic carbon as mg/l HCO_3^- eqv.; CBE = charge balance error. The following elements (and species) were below detection limits for all analyses, and are omitted from the table: Ag, Be, Bi, Cd, Ce, Cr, Cu, Ho, La, Nd, P, Se, Sn, Te, Th, Ti, U, Zn, HPO_4^-. High CBE may be a result of carbonate speciation (i.e. $CO_3^{2-} > HCO_3^-$).

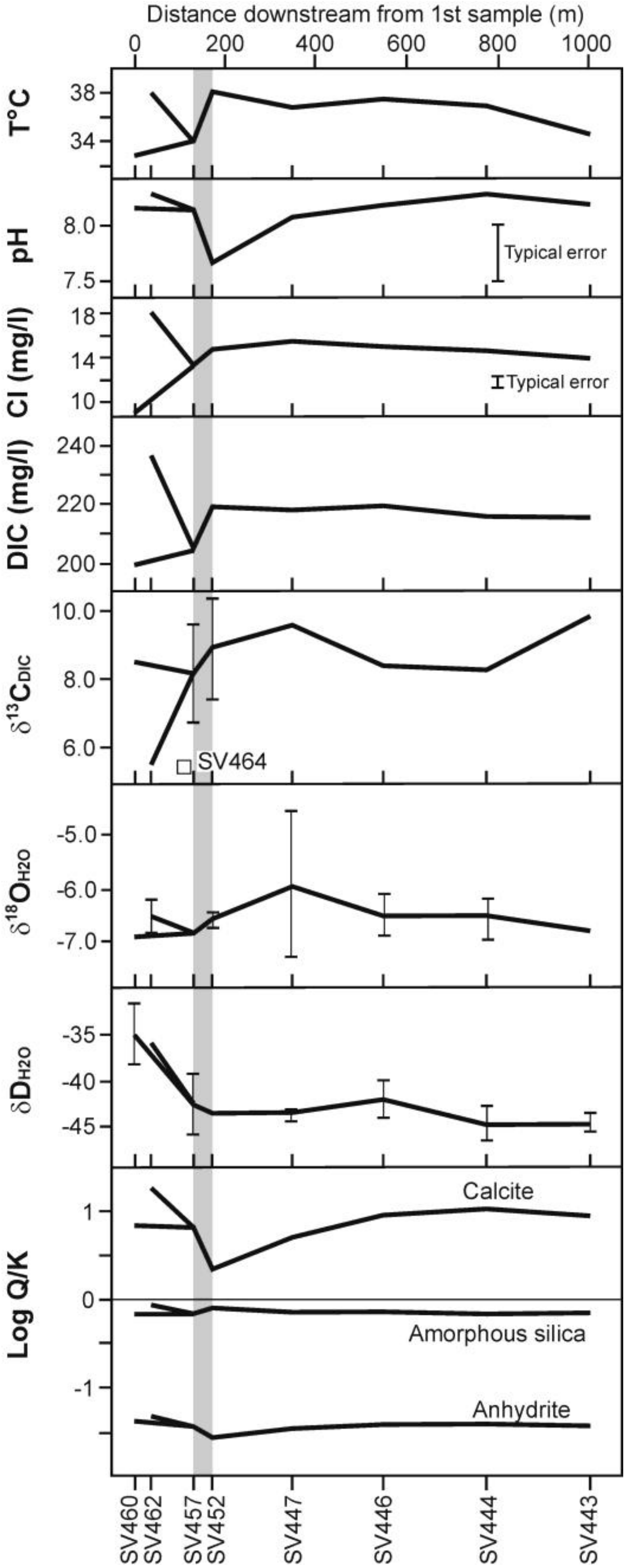

temperature upstream of the thermal area (<30°C) is warmer than would be expected for a typical groundwater-fed stream, indicating that this stream also has contributions from thermal waters. Stream chemistry shows little change downstream of the thermal area other than a slight increase in DIC and 0.5 unit drop in pH (Fig. 6.13); the springs are relatively dilute and low discharge, so contributions to the stream are minimal. Stable isotope composition varies between the two tributaries, but downstream of the confluence (SV457 –443) there is no systematic variation of $\delta^{13}C$, $\delta^{18}O$, or δD. $\delta^{13}C$ values are high (6 to 10‰). Oxygen and hydrogen isotope values are similar to those of cold springs and the warm spring at Reoka (Fig. 6.12).

The Tanginakulu stream is fed by low discharge warm springs of bicarbonate –sulphate type, and high in Mg relative to other areas (Table 6.3). Moving downstream, temperature, DIC, Ca, SO_4^-, Sr, B, Ba, and Cs, all decrease steadily, whereas pH increases (Fig. 6.14). Unlike the Rembokola stream, there are no consistent changes in the

Fig. 6.13: Changes in temperature, pH, Cl^-, DIC (as HCO_3^- eqv.) stable isotope composition, and saturation index of important minerals in the Reoka stream. Moving downstream from left to right. Samples SV462 and SV460 are tributaries, with the confluence at SV457; SV457 is intermediate between the two tributary compositions. Shaded box marks major thermal area (principally stream-fed acid sulphate springs and steaming ground) between SV457 and SV452, and is responsible for changes to pH, temperature, chemistry and mineral saturation states. $\delta^{13}C$ value for travertine SV464 is also shown. Error bars are $\pm 1\sigma$; not shown when within point size.

Sample	SV428	SV433	SV438	SV440
Date	07/10/06	07/10/06	08/10/06	08/10/06
Distance	0.00	0.24	0.56	1.00
T (°C)	35.4	32	29.9	28
pH	8.1	8.1	8.4	8.5
DIC	295	232	199	163
Al (µg/l)	13	bdl	3	bdl
As (µg/l)	7	8	10	11
B	0.18	0.17	0.17	0.14
Ba (µg/l)	30.9	26.2	22.1	18.8
Ca	166	113	88	82
Co (µg/l)	1.2	0.4	0.2	0.2
Cs (µg/l)	2.4	2.4	2.2	1.2
Fe	0.06	0.02	bdl	bdl
K	5.8	5.7	6.0	5.2
Li (µg/l)	49	50	51	35
Mg	76.9	75.2	79.5	54.1
Mn	0.18	0.01	bdl	bdl
Mo (µg/l)	1.6	1.8	1.8	1.7
Na	40.9	40.0	43.0	33.7
Ni (µg/l)	5	3	4	3
P	bdl	bdl	0.39	bdl
Pb (µg/l)	0.7	0.7	1.1	0.5
Rb (µg/l)	18.4	19.3	20.6	15.4
Si	60	60	62	53
SO_4^{2-}	286	268	266	190
Sr	1.22	1.04	0.97	0.76
Tl (µg/l)	0.02	bdl	0.02	bdl
U (µg/l)	0.02	0.02	0.03	0.06
V (µg/l)	1	3	4	13
Y (µg/l)	0.05	0.03	0.02	0.03
Zn (µg/l)	50	bdl	14	7
Zr (µg/l)	0.04	0.03	0.09	0.03
Cl^-	7.5	6.8	7.6	8.0
NO_3^-	3.16	3.64	1.91	0.071
NO_2^-	0.067	0.161	0.134	bdl
F^-	0.120	0.071	0.086	0.139
CBE (%)	24	17	19	19
$\delta^{13}C_{DIC}$	7.4	7.7	5.4	2.0
1σ				0.2
$\delta^{18}O_{H2O}$	−7.0	−7.6	−7.4	−7.1
1σ	1.0	0.3	0.1	0.4
δD_{H2O}	−44	−44	−47	−45
1σ	1	1	1	0

Table 6.3: Water chemistry data for Tanginakulu stream samples. All values in mg/l unless noted otherwise. Distance is measured in kilometres downstream from first sample. bdl = below detection limits; DIC = dissolved inorganic carbon as mg/l HCO_3^- eqv.; CBE = charge balance error. The following elements (and species) were below detection limits for all analyses, and are omitted from the table: Ag, Be, Bi, Cd, Ce, Cr, Cu, Ho, La, Nd, Sb, Se, Sn, Te, Th, Ti, HPO_4^-, Br. High CBE may be a result of carbonate speciation (i.e. $CO_3^{2-} > HCO_3^-$), or unanalysed HS^-.

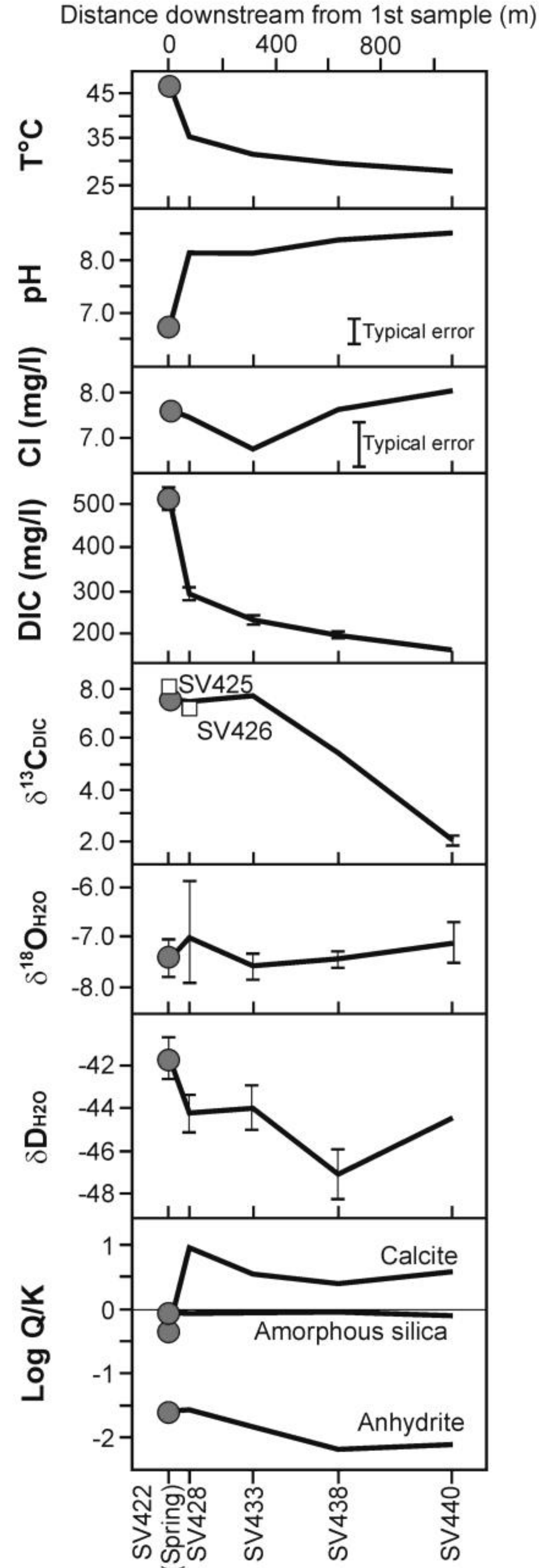

Fig. 6.14: Changes in temperature, pH, Cl^-, DIC (as HCO_3^- eqv.), stable isotope composition, and saturation index of important minerals in the Tanginakulu stream. Moving downstream from left to right, with SV422 a warm spring in the upper reaches of the stream. $\delta^{13}C$ values for travertines SV425 and SV426 are also shown. Error bars are ±1σ; not shown when within point size.

concentrations of conservative elements (Cl^-, Li, Cs). $\delta^{18}O$ and δD do not vary significantly downstream and are similar to those of cold springs and the Reoka stream waters (Fig. 6.12). $\delta^{13}C$ is high (2 to 7.7‰), with the lower values downstream.

The stable isotope composition of fumarolic CO_2 was analysed (Table 6.4). $\delta^{13}C_{PDB}$ values of +1 to +3‰ are unusually high for a volcanic system (mantle-derived CO_2 typically −8 to −5‰; Taylor, 1986).

Sample	$\delta^{13}C_{PDB}$	$\delta^{18}O_{SMOW}$	Location
SV244	2.4	21.1	Fisher Voghala
SV246	2.0	19.9	Fisher Voghala
SV305	2.7	20.9	Fisher Voghala
SV306	2.9	19.3	Fisher Voghala
SV307	2.7	18.8	Fisher Voghala
SV247	2.2	22.8	Mbiti Voghala
SV301	2.4	15.5	Mbiti Voghala - Central Fumarole
SV302	2.7	19.3	Mbiti Voghala - Central Fumarole
SV303	2.6	11.8	Mbiti Voghala - Crater Wall Fumarole
SV304	2.5	20.7	Mbiti Voghala - Northern Fumarole
SV239	2.0	11.7	Pipisala
SV240	2.3	10.4	Pipisala
SV328	1.0	16.7	Rembokola F1 (hot spring)
SV329	1.1	15.8	Rembokola F1 (hot spring)

Table 6.4: Stable isotope composition of fumarolic CO_2.

6.4.2 Sinters and travertines

6.4.2.1 Chemistry

The Rembokola sinters analysed in this study were dominated by opal-A, with maximum water and acetic acid soluble contents leaches of 27%, but more commonly <4% (Table 6.5). The near-spring spike sinter (SV486) has a sizeable water-soluble fraction (18%), as would be expected from the more anhydrite-rich mineralogy (Fig. 6.3), but is otherwise similar to the downstream precipitates. The obvious exception to the common chemistry is the mixed silica–carbonate sample of SV482.

For the stream-deposited sinters, major element chemistry is dominated by silica, with only small amounts of Ca, Fe, Mg, Mn and S (Table 6.5). As, Cu and V concentrations are enriched in the sinters relative to the stream water (Table 6.1) by factors of approximately 500, >10,000 and >10,000 respectively. Fe and V concentrations both approximately double downstream of SV472 (Fig. 6.15).

Sinter samples analysed by ICP-MS following aqua regia digestion (SV475 and SV479; Table 6.6) have results that differ from the ICP-OES results (see comparison plots in Fig. 6.15); always with lower concentrations for the MS analyses. It is possible that the aqua regia digestion resulted in incomplete dissolution of the silica, and as a result, only partial recovery of trace elements. As a result, the two datasets are not easily comparable.

Sample	SV486			SV482			SV479		SV477		SV475	SV475	SV475	SV472	SV470		SV466
Location	Rembokola			Rembokola			Rembokola		Rembokola		Remb.	Remb.	Remb.	Remb.	Rembokola		Remb.
Type	Spike sinter			Mixed carbonate / silica			Sinter		Sinter		Sinter	Sinter	Sinter	Sinter	Sinter		Sinter
Fraction	A	B	C	A	B	C	A	C	B	C	C	C	C	C	B	C	C
Wt %	18	9	74	8	75	17	4	96	3	96	98	98	98	98	3	96	96
Ca wt %	18.7		1.6	26.6	40.4	9.8		1.6		1.2	1.4	1.3	1.3	1.3		1.5	1.5
Fe wt %			0.36		0.1	1.43	0.97	1.84		0.85	0.88	0.9	0.92	2.01	1.19	2.25	2.82
Mg wt %	0.84	5.4	1.36	0.24	0.19	0.53	0.91	0.56		0.37	0.41	0.41	0.41	0.55		0.61	0.59
Mn wt %		0.3	0.18	0.33	0.8	0.73	0.21	0.24	1.82	0.39	0.33	0.33	0.33	0.28	1.52	0.16	0.25
Na wt %	1.82																
S wt %	19.49	1.12		1.5	1.31	0.46		0.05	0.29	0.1	0.1	0.1	0.1	0.16	0.49	0.13	0.2
As ppm	48	280	9	186	287	251		33		10	16	17	17	22		28	25
Ba ppm	148	296	59	112	130		136	280		66	130	127	135	124	614	290	204
Cu ppm								33		18	18	22	22	57	1142	33	23
K ppm	4479						12432										
Pb ppm		23			3			12	69	8	9	10	10	9	109	14	12
Sb ppm		8			3				2						44		
Si ppm	2605	3029	na		1124	na		na	3497	na	na	na	na	na	5952	na	na
Sr ppm	6081	5527	426	3110	4206	1589	1002	830	1286	356	541	522	547	465	1373	862	723
V ppm	13	70	26		3		44	67	22	31	33	34	35	76	36	82	105
Comments							B bdl.		A bdl.		A & B bdl.	A & B bdl.	A & B bdl.	A & B bdl.	A bdl.		A & B bdl.

Table 6.5: Rembokola sinter chemistry as determined by ICP-OES on sequential leaches. Values are concentration in fraction. A = water soluble fraction; B = acetic acid soluble fraction; C = HF soluble fraction; bdl = below detection limits; na = not analysed. Blank cells denote analyte below detection limits.

However, with the assumption that the MS results represent minimum values, there are a number of interesting values: Au is present in low but significant concentrations (1–3 ppb), and Te is present in concentrations of 0.04 ppm; at least 2000 times higher than in the water (which is <0.02 ppb), and ~8 times greater than average crustal abundances (Fig. 6.16; Wedepohl, 1995).

Sample SV482 has a significant acetic-soluble fraction (75%; Table 6.5) as would be expected from the more carbonate-rich mineralogy. The bulk chemistry of the mixed silica–carbonate sample differs from the other Rembokola samples in a number of respects (Fig. 6.15); Ca and Sr are obviously higher, due to the increased calcite contents; As, Mn, S and Te are higher in SV482, and Cu and V lower. The Te contents are >50 times higher than average crustal abundance (Fig. 6.16; Wedepohl, 1995).

The near-spring deposits of the Poghorovorughala area also have mixed mineralogy – individual samples can have significant water-soluble, acetic soluble and HF-soluble fractions (Table 6.7). Silica (HF-soluble) contents are highest in the near-spring facies (lobate = 15–20 wt %; spikes = 28 wt %), and sulphate (water soluble) contents are highest in the spike facies (SV506), similar to the Rembokola spike sinter (SV486; Table

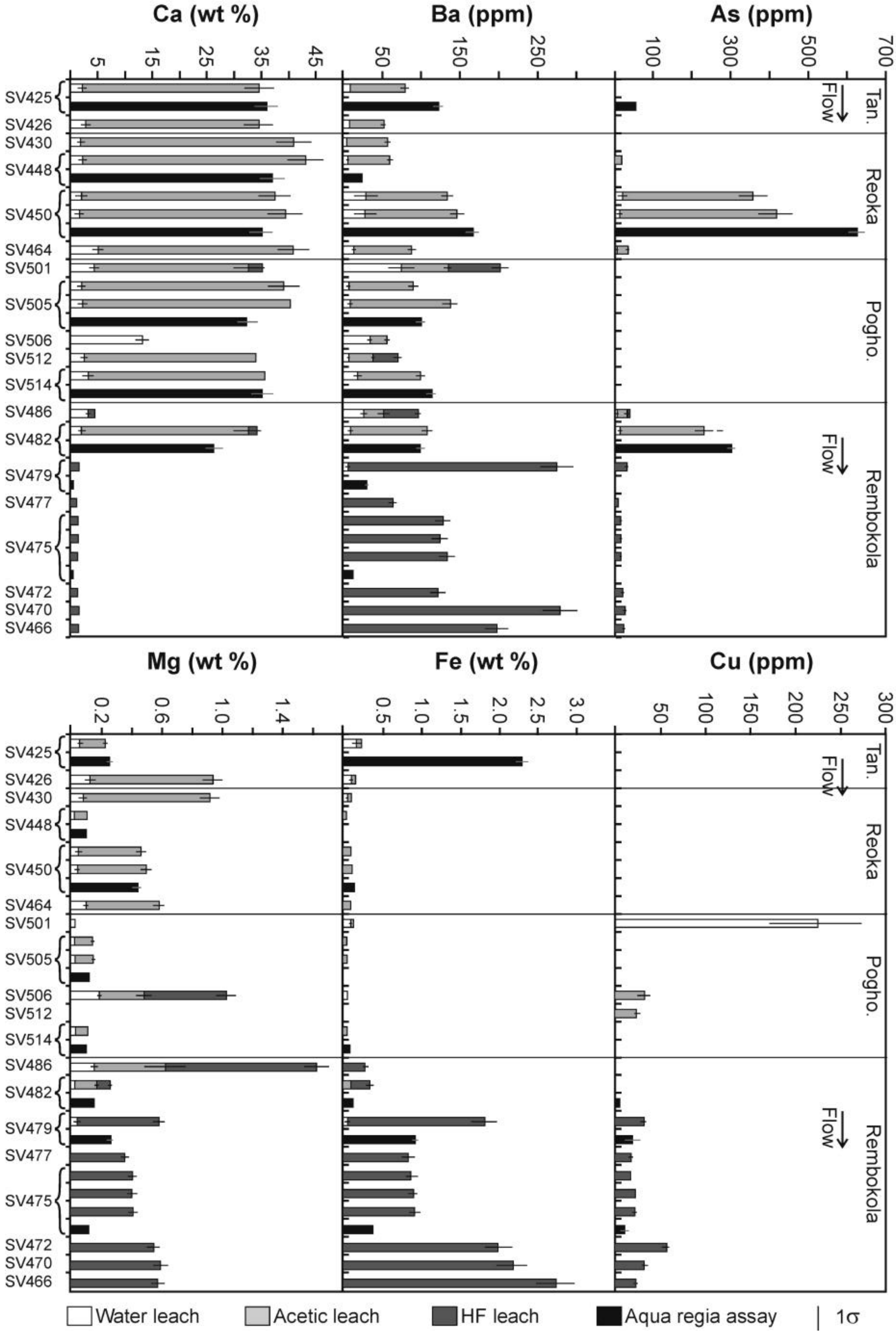

Fig. 6.15: Chemistry of precipitates analysed in this study. Plots show relative contributions from water, acetic acid and HF soluble-fractions and aqua regia digested assay results. Differences between assay and step-leach results may be due to limited solubility of high-silica samples in aqua regia digest (see SV475 and SV479). Error bars are 1σ, estimated by repeat analysis of reference materials, for ICP-MS results. For ICP-OES results, error bars are calculated as 1σ error on calibration line, combined with errors inherent in weighing and diluting during the sequential leach process.

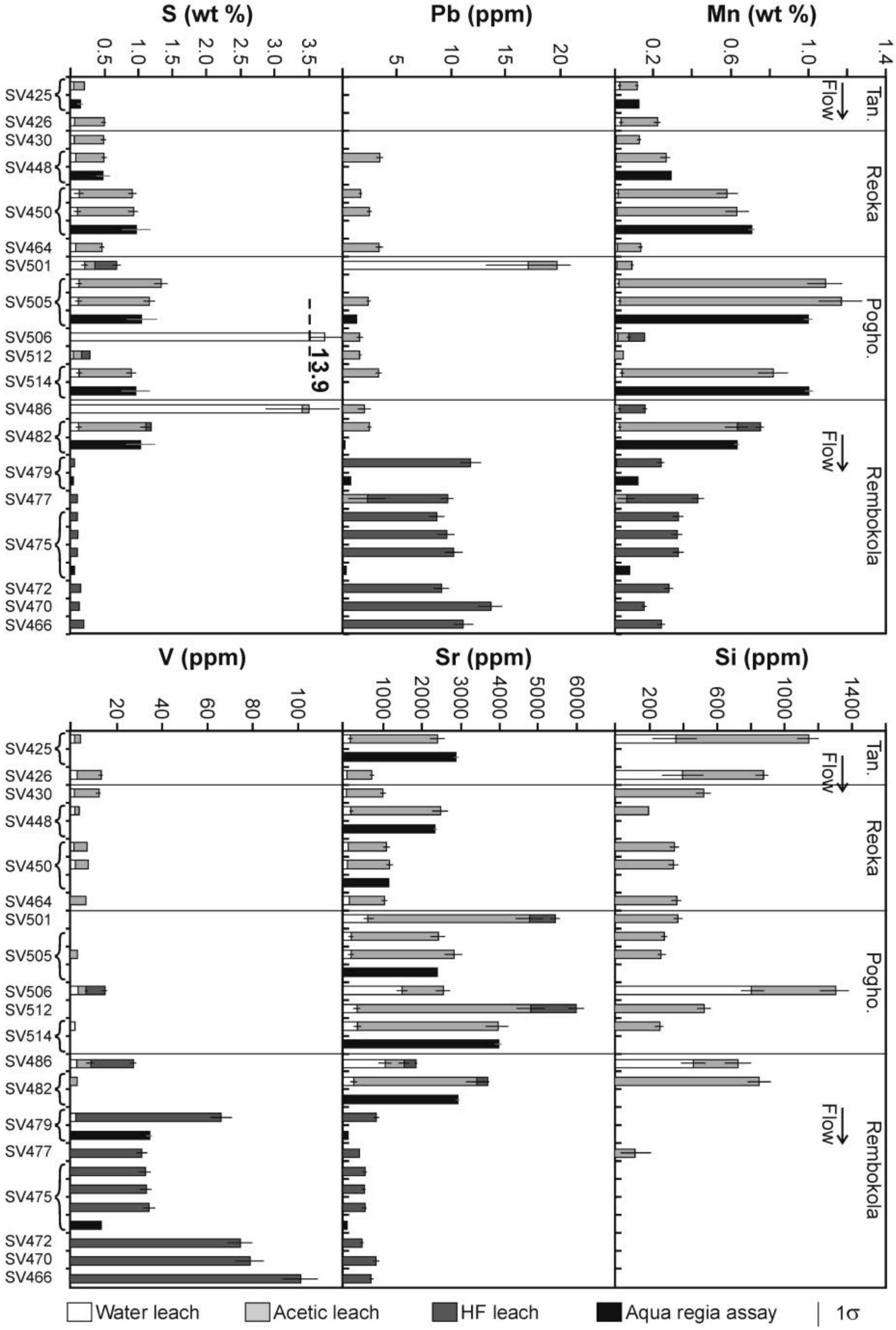

Fig. 6.15: Continued.

Sample	**MDL**	**SV425**	**SV448**	**SV450**	**SV475**	**SV479**	**SV482**	**SV505**	**SV514**
Location		Tang.	Reoka	Reoka	Remb.	Remb.	Remb.	Pogho.	Pogho.
Type		Trav.	Trav.	Trav.	Sinter	Sinter	Mixed	Trav.	Trav.
Al wt %	0.01				0.15	0.38	0.02		
Ca wt %	0.01	35.90	37.04	34.99	0.42	0.51	26.38	32.39	35.21
Fe wt %	0.01	2.29		0.12	0.36	0.90	0.10		0.06
K wt%	0.01	0.01		0.01	0.04	0.08	0.01		
Mg wt%	0.01	0.25	0.09	0.43	0.11	0.25	0.14	0.11	0.09
Na wt %	0.001	0.044	0.014	0.063	0.035	0.081	0.036	0.030	0.030
P wt %	0.001	0.029	0.009	0.041	0.023	0.028	0.037	0.028	0.040
S wt %	0.02	0.15	0.48	0.97	0.06	0.04	1.03	1.05	0.96
Ti wt %	0.001				0.011	0.029	0.001	0.009	
Ag ppb	2			35	6	9	3	3	
As ppm	0.1	54.3		625.6	2.1	3.1	302.5	0.7	0.6
Au ppb	0.2				2.9	1.3	1.9		
B ppm	20			36	77	96	35		
Ba ppm	0.5	122.1	23.3	166.5	12.2	30.0	98.8	99.1	113.3
Bi ppm	0.02					0.02			
Cd ppm	0.01	0.05		0.36	0.04	0.02	0.11		
Co ppm	0.1	2.9	0.1	0.4	0.9	2.5	1.4		
Cr ppm	0.5				2.5	5.8		1.7	
Cu ppm	0.01	0.37	0.20	0.78	10.18	18.23	4.19	0.67	0.15
Ga ppm	0.1			0.2	0.8	1.8	0.2	0.3	0.3
Hg ppb	5			7	17	25	14	9	
La ppm	0.5		2.7		0.7	1.5			
Mn ppm	1	1260	2889	7064	763	1210	6319	>10000	>10000
Mo ppm	0.01	0.04	0.05	0.17	0.28	0.84	0.11	0.09	0.08
Ni ppm	0.1	1.8	3.1	1.5	1.5	2.9	3.0	2.6	4.0
Pb ppm	0.01	0.03	0.03	0.15	0.34	0.72	0.13	1.25	0.08
Sb ppm	0.02	0.09			0.02	0.03	0.03		
Sc ppm	0.1	0.4	0.1	0.2	0.6	1.3	0.2	0.2	0.2
Se ppm	0.1	0.2	0.2	0.1	0.4	0.2	0.2		0.1
Sr ppm	0.5	2885.2	2352.1	1151.6	74.6	107.3	2927.0	2383.5	3974.0
Te ppm	0.02	0.41	0.31	0.20	0.04	0.04	0.30	0.25	0.38
Tl ppm	0.02				0.06		0.02		
U ppm	0.1	0.2					0.1		
V ppm	2				13	34			
Zn ppm	0.1	21.0	0.3	0.8	6.9	18.2	3.6	5.6	0.3

Table 6.6: Whole rock sinter and travertine chemistry as determined by ICP-MS analysis following aqua regia digestion. Blank cells denote analyte below detection limits. Analyses marked “>” are above calibration range. MDL = method detection limit.

6.5). The layered deposits from the Mound Spring are carbonate-dominated, with a small water-soluble contribution (<10%). The insoluble fraction was small (<9%), but layers dominated by opal-A have been observed under SEM (Fig. 6.8D).

In the Poghorovorughala deposits Sr and Mn are abundant (up to 0.6 wt % and 1 wt % respectively); Cu is typically <50 ppm, but up to 200 ppm in the water soluble portion of SV501 (Fig. 6.15); arsenic is generally below detection limits. Assay results reproduce the step-leach results relatively well (Fig. 6.15), indicating that aqua regia digestion was effective for these samples. Au concentrations are below detection limits (Table 6.6) and the low As concentrations are confirmed by ICP-MS (<1 ppm). As with the Rembokola sinters, Te contents of the deposits are high relative to the spring waters (enrichment factor >5000).

The travertine deposits of the Reoka and Tanginakulu contain low concentrations of Si (<0.2 wt %), Mn (<0.2 wt %) and S (<0.5 wt %; Table 6.8; Fig. 6.15), but the mineralogy

Sample	SV501			SV505		SV505		SV506			SV512			SV514	
Location	Poghorovorughala			Pogho.		Pogho.		Poghorovorughala			Poghorovorughala			Pogho.	
Type	Lobate Travertine			Mixed layers		Mixed layers		Spikes			Lobate Travertine			Mixed layers	
Fraction	A	B	C	A	B	A	B	A	B	C	A	B	C	A	B
Wt %	13	68	19	7	94	7	93	55	17	28	9	76	16	9	82
Ca wt %	34.3	41.4	13.7	29.0	39.4	31.7	40.8	24.0			28.9	41.6		36.6	39.4
Fe wt %	0.58	0.05			0.02		0.03	0.05							0.0[illegible]
Mg wt %	0.14			0.24	0.13	0.26	0.13	0.33	1.75	1.93				0.27	0.1[illegible]
Mn wt %	0.09	0.12		0.29	1.14	0.37	1.22	0.03	0.33	0.28		0.06		0.44	0.9[illegible]
Na wt %								0.35							
S wt %	1.65	0.21	1.68	1.79	1.28	1.72	1.11	25.27	0.42	0.10	0.49	0.16	0.79	1.43	0.9[illegible]
As ppm													28		
Ba ppm	587	89	349	88	89	115	138	61	129		75	41	204	202	98
Cu ppm	1761								187			31			
K ppm								1195							
Pb ppm	135	4					3		9			2			4
Sb ppm		1													1
Si ppm		536	na		304		291	1460	2877	na		691	na		311
Sr ppm	4896	6115	3393	2519	2384	2679	2835	2731	6219		3863	5938	7492	3936	4397
V ppm							2	5	21	29				15	1
Comments														C fraction 9%, not analysed	

Table 6.7: Poghorovorughala travertine and mixed deposit chemistry as determined by ICP-OES on sequential leaches. Values are concentration in fraction. A = water soluble fraction; B = acetic acid soluble fraction; na = not analysed. Blank cells denote analyte below detection limits.

Sample	SV425		SV426		SV430		SV448		SV450		SV450		SV464	
Location	Tang.		Tang.		Tang.		Reoka (not *in situ*)		Reoka (not *in situ*)		Reoka (not *in situ*)		Reoka	
Type	Layered Trav.		Layered Trav.		Layered Trav.		Layered Trav.		Layered Trav.		Layered Trav.		Layered Trav.	
Fraction	A	B	A	B	A	B	A	B	A	B	A	B	A	B
Wt %	8	82	9	85	7	90	7	94	5	86	5	88	15	83
Ca wt %	28.4	39.7	30.3	37.4	28.6	43.1	27.7	43.6	43.1	41.3	31.6	42.6	33.3	43.2
Fe wt %	1.91	0.08	0.88	0.06	0.45	0.05		0.02		0.09		0.10	0.14	0.06
Mg wt %	0.67	0.21	1.30	0.96	1.07	0.93	0.20	0.09	0.98	0.48	0.67	0.52	0.60	0.58
Mn wt %	0.34	0.11	0.36	0.22	0.10	0.13	0.11	0.27	0.38	0.66	0.21	0.70	0.10	0.14
Na wt %	3.10		2.35											
S wt %	0.48	0.20	0.64	0.50	0.63	0.48	0.94	0.45	2.70	0.92	1.94	0.93	0.53	0.45
As ppm	80							19	456	394	255	456	49	34
Ba ppm	104	87	79	52	57	58	65	58	619	123	524	133	87	90
Cu ppm														
K ppm														
Pb ppm								4		2		3		4
Sb ppm								7		2		2		
Si ppm	4494	963	4187	560		572		202		406		385		432
Sr ppm	2114	2750	784	767	896	1040	2298	2459	2173	1156	1701	1227	913	1081
V ppm	16	3	27	12	19	12	17	2	20	7	26	7		8
Comments	C fraction 9%, not analysed		C fraction 6%, not analysed		C fraction 3%, not analysed				C fraction 9%, not analysed		C fraction 6%, not analysed		C fraction 3%, not analysed	

Table 6.8: Tanginakulu and Reoka travertine chemistry as determined by ICP-OES on sequential leaches. Values are concentration in fraction. A = water soluble fraction; B = acetic acid soluble fraction. Blank cells denote analyte below detection limits.

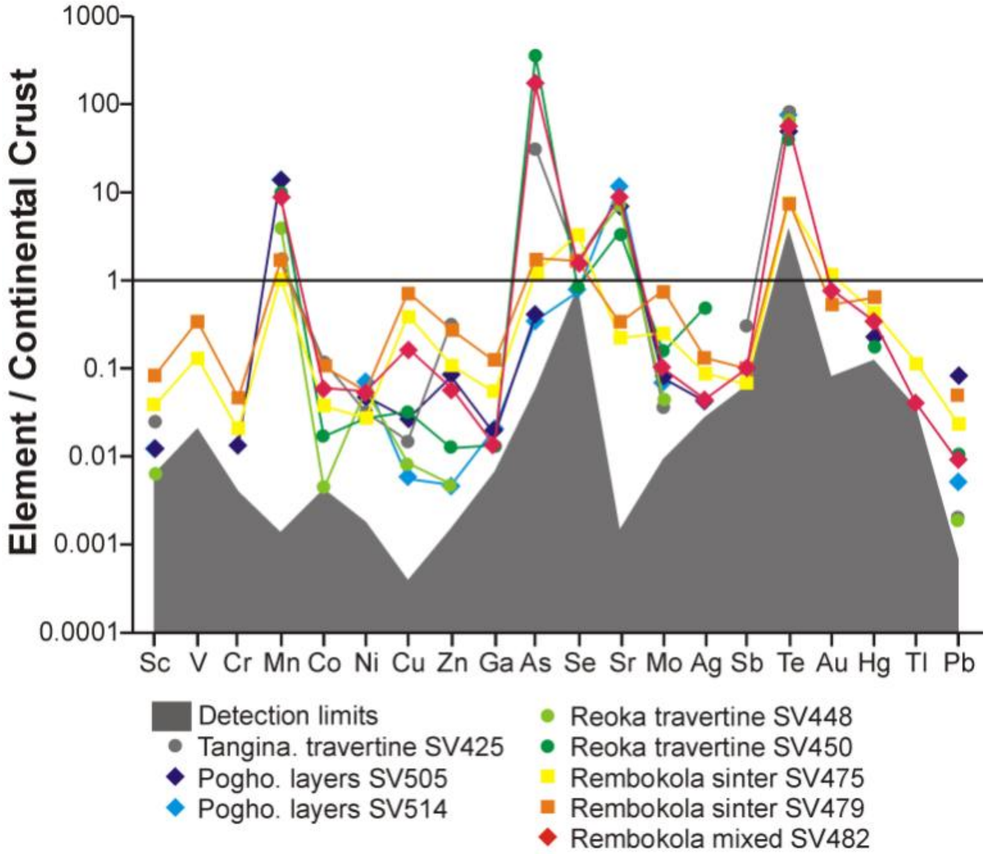

Fig. 6.16: ICP-MS analysis of sinter, travertine and mixed silica–carbonate deposits from Savo normalised against average continental crust (Wedepohl, 1995). Samples show anomalous enrichments of Te and Mn; arsenic is enriched in all samples except from Poghorovorughala. Au shows crustal concentrations to slight enrichment in the Rembokola samples.

and chemistry is dominated by calcite. Arsenic is present in significant concentrations in the Reoka samples (~400 ppm), and as with carbonate samples from the other locations on Savo, Te occurs in concentrations 0.2–0.4 ppm (Table 6.6).

6.4.2.2. Stable isotopes

The carbonate layers of mixed Rembokola sample SV482 were analysed for stable isotope composition (Fig. 6.17). The stable isotope composition does not show any major variation between layers, with total range of $\delta^{13}C$ = 0.6‰ and $\delta^{18}O$ = 1.2‰ in the samples analysed. All layers are enriched in ^{13}C relative to most typical carbon reservoirs (Hoefs, 1997), although they are in a similar range as the DIC analysed from the various water samples in this study (section 6.4.1; Rembokola stream water had insufficient DIC to analyse). $\delta^{18}O$ values are much higher than those of the Rembokola stream waters (Table 6.1).

For the Poghorovorughala deposits $\delta^{13}C$ is high (4 to 12‰), and $\delta^{18}O$ is variable (13 to 23‰; Table 6.9). The spiked growths show the highest $\delta^{13}C$ value of all samples analysed in this study at 11.7‰. $\delta^{13}C$ values obtained from DIC in the hot springs at

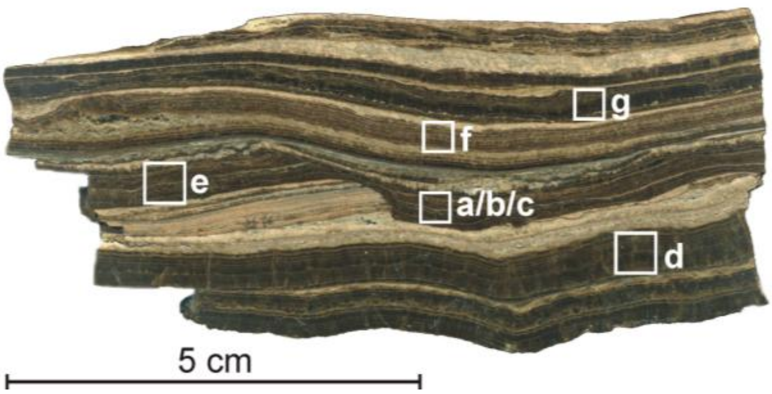

	$\delta^{13}C_{PDB}$	$\delta^{18}O_{SMOW}$
SV482a	7.3	21.0
SV482b	7.4	21.1
SV482c	7.5	21.5
Average	7.4	21.2
1σ	0.1	0.2
SV482d	7.9	20.3
SV482e	7.3	20.8
SV482f	7.7	21.2
SV482g	7.7	20.7

Fig. 6.17: Stable isotope composition of carbonate layers from Rembokola mixed silica–carbonate sample SV482.

Sample	Location	Type	$\delta^{13}C_{PDB}$ (‰)	$\delta^{18}O_{SMOW}$ (‰)	Method
SV425	Tangina.	Layered Trav.	8.1	20.6	AP
SV425	Tangina.	Layered Trav.	8.1	20.3	Line
SV426	Tangina.	Layered Trav.	7.2	19.9	Line
SV430	Tangina.	Layered Trav.	7.0	20.8	Line
SV448	Reoka	Layered Trav.	4.3	13.5	Line
SV450	Reoka	Layered Trav.	5.9	18.1	Line
SV464	Reoka	Layered Trav.	5.5 ±0.1	22.3 ±0.2	AP
SV464	Reoka	Layered Trav.	5.4 ±0.1	20.3 ±0.2	Line
SV501	Pogho.	Lobate Trav.	8.7	15.5	Line
SV505	Pogho.	Mixed layers	6.8	16.8	Line
SV506	Pogho.	Spikes	11.7	20.5	Line
SV512	Pogho.	Lobate Trav.	8.1	14.7	Line
SV514	Pogho.	Mixed layers	7.7 ±0.2	17.6 ±0.3	Line

Table 6.9: Stable isotope composition of various travertines from Savo. Where repeat measurements were made, values are shown as averages ± 1σ. Samples marked "line" were analysed with a VG Sira 10 mass spectrometer, and those marked "AP" by Analytical Precision AP2003 mass spectrometer. See text for details of techniques.

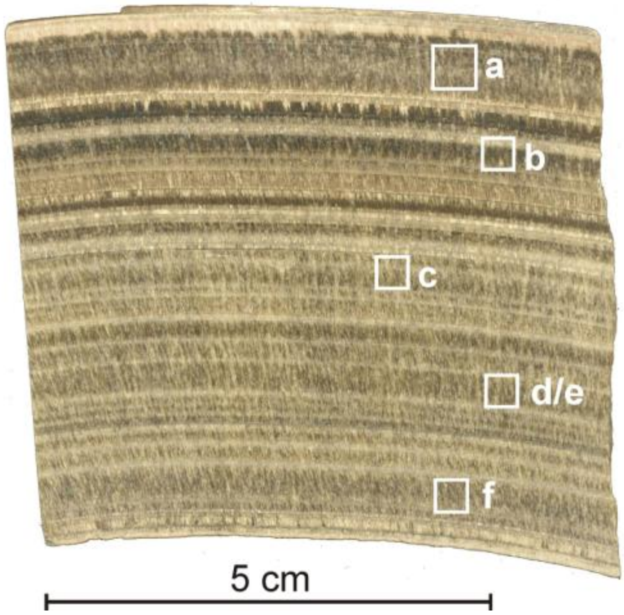

	$\delta^{13}C_{PDB}$	$\delta^{18}O_{SMOW}$
SV450a	5.7	19.5
SV450b	5.7	19.4
SV450c	5.6	19.2
SV450d	5.7	19.2
SV450e	5.7	19.4
Average	5.7	19.3
1σ	0.0	0.1
SV450f	5.7	19.1

Fig. 6.18: Stable isotope composition of layers from Reoka travertine sample SV450.

					DIC		Water	
Sample	Location	Spring Type	T°C	pH	mg/l (HCO_3^- eqv)	$\delta^{13}C_{PDB}$	$\delta^{18}O_{SMOW}$	δD_{SMOW}
SV422	Tangina.	Warm	47	6.7	513	7.5 ±0.1	−7.4 ±0.4	−42 ±1
SV449	Reoka	Warm	56	7.0	315	8.2 ±2.2	−6.5 ±0.2	−42 ±2
SV498	Pogho.	Alk.	100	7.7	94	−0.4	−3.7 ±0.6	−35 ±2
SV499	Pogho.	Alk.	96	7.7	90	4.6	−3.6 ±0.7	−37 ±1
SV500	Pogho.	Alk.	100	7.5	88	0.2 ±0.3	−3.7 ±0.7	−36 ±3
SV516	Pogho.	Alk.	100	7.5	88	−0.6 ±0.8	−4.7 ±0.1	−39 ±1

Table 6.10: Stable isotopes of water and dissolved inorganic carbon for selected springs at Savo. Chemistry is discussed in Chapter 4. Tangina. = Tanginakulu; Pogho. = Poghorovorughala; Alk. = alkaline sulphate hot spring.

Poghorovorughala are lower than the associated travertine samples (−0.6 to 4.6‰; Table 6.10), and the $\delta^{18}O$ values from the water are lower than the solids by approximately 20‰.

Bulk $\delta^{13}C$ values for Reoka and Tanginakulu travertine samples were also high, with Reoka samples at 4 to 6‰ and Tanginakulu specimens higher at 7 to 8‰ (Table 6.9). $\delta^{18}O$ values were in a similar range to previously discussed samples (15–21‰). Individual layers of sample SV450 were analysed (Fig. 6.18) and the variability was negligible. In comparison with water samples collected from the same locations (where possible; Fig. 6.1; Table 6.2), Reoka travertine samples have lower $\delta^{13}C$ and higher $\delta^{18}O$ values, whereas Tanginakulu travertines have similar $\delta^{13}C$ and higher $\delta^{18}O$ values.

6.5 Discussion

6.5.1 The hydrothermal system of Savo

Various different water types can be identified in springs at Savo on the basis of chemistry and stable isotope chemistry. The system is meteoric water-dominated, resulting in near-meteoric stable isotope signatures and generally dilute chemistry in springs and streams (Chapters 4 and 5). Alkaline sulphate springs are generated by magmatic volatiles (chiefly H_2O, SO_2 and some CO_2) condensing into meteoric-derived groundwater. Rock reaction and continued mixing and dilution reduce the acidity generated by SO_2 hydrolysis. Comparison of the water chemistry of Rembokola and Poghorovorughala alkaline hot springs indicates that there is a "high temperature" end-member fluid, characterised by high Si, SO_4^{2-}, Cl^-, and Na, mixed with a "low temperature" end-member fluid, with high Ca, Mg, and DIC. The Rembokola springs have a larger contribution of the former, and the Poghorovorughala springs the latter; exact proportions are difficult to constrain due to non-ideal (i.e. reactive) mixing between the two end-members. Warm springs at Reoka and Tanginakulu and cold springs around the island discharge fluids dominated by the low temperature (Ca–Mg–HCO_3^-) end-member.

6.5.2 Travertines

The Reoka and Tanginakulu streams are both dominated by the Ca–Mg–HCO_3^- type fluid. The stretch of the Reoka stream system sampled in this study consists of two tributaries that converge at a major thermal area; although the two tributaries have slightly differing chemistry, both are typical of the Ca–Mg–HCO_3^- rich waters. The high magnesium contents indicate a low temperature (<100°C) origin for these waters, as at high temperatures Mg is readily removed by the formation of minerals such as chlorite (Giggenbach, 1988).

The Reoka and its tributaries (Fig. 6.13), and the Tanginakulu (Fig. 6.14) are moderately supersaturated with respect to calcite, with log Q/K = 0.5 to 1.5 (where Q is the ion activity product and K is the equilibrium constant of the calcite-forming reaction, as calculated with SOLVEQ; Reed, 1982, 1998).

Travertine precipitation from stream and spring waters initially enriched with calcium and bicarbonate is typically driven by CO_2 removal (Pentecost, 2003):

$$Ca^{2+} + 2HCO_3^{-} = H_2O + CaCO_3 + CO_2 \qquad \mathbf{1}$$

Removal of carbon dioxide can be biotic (photosynthesis), or abiotic (degassing). The latter mechanism is the predominant process in most streams and springs, and is particularly effective where water is turbulent (Pentecost, 2003). There is a strong association with travertine deposition (and thicker travertine deposits) in areas of waterfalls and rapids on Savo; CO_2 loss to the atmosphere is therefore the most likely cause of calcite supersaturation and precipitation.

Examination of travertine blocks from both areas (Figs. 6.9 and 6.10) shows that they are composed of layers of calcite ray crystals. Calcite is the dominant $CaCO_3$ polymorph at temperatures <40°C (Jones et al., 1996), and so its predominance over aragonite in these deposits is unsurprising. Ray crystal layers are common in travertine, and are typically abiotic in origin, formed by rapid precipitation of calcite from supersaturated solutions (Folk et al., 1985; Chafetz and Guidry, 1999).

As well as causing carbonate precipitation, CO_2 loss is an important mechanism for increasing water pH (Chafetz et al., 1991; Fouke et al., 2000):

$$HCO_3^{-} + H^{+} = H_2O + CO_2 \qquad \mathbf{2}$$

Figure 6.14 shows the changes in DIC and pH moving down the Tanginakulu stream. In particular there is a rapid drop in DIC and corresponding increase in pH after discharge from the warm spring (SV422) into the stream proper. Combined CO_2 loss and travertine precipitation is capable of producing the relationships displayed in Figure 6.14. The situation at Reoka is more complicated due to the confluence of the two tributaries, and the flow of the stream through a major thermal area. Stream water DIC actually increases as the Reoka flows through the thermal area (note increase in DIC between SV457 and SV452 on Fig. 6.13) most likely by the addition of fumarolic / steaming ground CO_2.

Tellurium in notably enriched in all travertine samples, and arsenic in a high proportion of those analysed (Fig. 6.16). Although Te is below detection limits in all water samples in this study, As is associated with the higher temperature component: its concentration is higher in the Rembokola springs and stream than in the Ca–Mg–HCO_3^- enriched springs (Section 4.4). Te would also be expected to be associated with a the high temperature fluids, given that it can be transported in a magmatic vapour phase (Cooke et al., 1996). The high concentrations of arsenic and tellurium in the travertine may reflect the fact that carbonate minerals are more suitable hosts for As and Te species than opal-A (which generally has lower concentrations of both elements, despite being associated with the high temperature endmember).

6.5.3 Sinters

Sinter is deposited within the Rembokola valley. The stream is a relatively simple system: there are few major springs feeding the stream other than those of the upstream thermal area, and there are no major tributaries into the stream. Heading downstream, evaporation causes a decrease in temperature, and increases in conservative elements such as Cs, B, Li, Cl^- and $\delta^{18}O$ (Fig. 6.11). Simple calculations indicate that approximately 10% of the original mass of water is lost between SV493 and SV476 to produce the observed Cl^- and Li increases. Mn and Si decrease by mineral precipitation, whereas CO_2 loss leads to pH increase (Eqn. 2) and DIC decrease (Fig. 6.11)

The combined effects of evaporation, cooling and CO_2 loss is that amorphous silica (equivalent to opal-A) becomes increasingly supersaturated (increasing log Q/K) downstream (Fig. 6.11). Calcite is also supersaturated (*decreasing* downstream, due to decreasing temperature and retrograde calcite solubility) but the DIC contents of the waters are low (<50 mg/l HCO_3^- eqv.), and it is likely that any precipitated carbonate is masked by greater volumes of silica.

Silica precipitates near hot springs in two distinct facies – as terraced deposits on the steep slopes in the upper Rembokola valley, and as spikes on subaerially exposed substrate in the relatively flat-lying thermal area. The spiked sinter described in this study is morphologically similar to the silica–carbonate “meringue” deposits of the Pavlova Spring, Ngatamariki, New Zealand (Campbell et al., 2002). These authors concluded that the Pavlova deposits formed by evaporation of hot spring-derived water from subaerially exposed surfaces, typically partially submerged detritus (principally leaf litter). Meniscoid and capillary creep ("wicking"; Hinman and Lindstrom, 1996; Campbell et al., 2002), as well as sporadic bathing and splashing in the case of the Savo deposits, replenish fluids. The spikes reach a maximum height (~2 cm) above which the wicking process can no longer replenish moisture in sufficient quantity to allow further growth (Campbell et al., 2002). Further evidence of evaporation as a precipitation mechanism is the presence of anhydrite on the upper surfaces of the spikes (Fig. 6.3). At spring temperatures and below, anhydrite is undersaturated (Fig. 6.11). The only effective mechanism for precipitating anhydrite is evaporation.

The upstream terraced sinter may also be precipitated through evaporation, but in the case of the deposits on the steep slopes, wicking is less important than direct evaporation from the surface. Water and dissolved silica is supplied constantly by the spring's fluids bathing the discharge apron, whilst never submerging it entirely. Terrace-type constructions are common in both travertine and siliceous sinter deposits, and occur where precipitation is from a sheet flow (Guidry and Chafetz, 2003a). The stair-step morphology of the micro-terracettes is produced by random perturbations in deposition (perhaps produced by debris or microbial mats; Chafetz and Folk, 1984; Guidry and Chafetz, 2003a) that eventually reorganise into linear or curvilinear ridges (Hammer et al., 2007).

Evaporation and cooling of the hot spring fluids as they flow downstream leads to an increase in the saturation index of amorphous silica (Fig. 6.11) and sinter precipitation (Rimstidt and Cole, 1983). Unlike in the immediate surroundings of the hot springs, sinter is deposited in wholly submerged parts of the stream channel. A further feature of significance to the sinters is the near-ubiquitous presence of filaments or tubes preserved by opal-A, often aligned and orthogonal to the growth laminations of the sinter (Fig. 6.4). The orientation may be a result of filaments aligning with flow direction in the stream (Jones et al., 2003). Filaments were not observed in the spike facies, and only rarely in the terraced sinter (Fig. 6.2). Such filamentous structures are commonplace in siliceous sinters, and are the result of the enclosure and partial preservation of microbes (Jones and Renaut, 2003a; Jones and Renaut, 2003b; Jones et al., 2003; Lynne and Campbell, 2003; Konhauser et al., 2004; Fernandez-Turiel et al., 2005; Jones et al., 2005).

Thermal waters may be colonised by a range of micro-organisms, including cyanobacteria, bacteria and fungi; however, low preservation fidelity of the organisms following silicification (replacement and/or encasement with silica, during or shortly after life) often makes taxonomic identification difficult (Jones et al., 2003). The fossils preserved in the Rembokola stream sinters are simple, non-branching filaments, approximately 5 μm in diameter (although silica cementation means that the diameter of the preserved filament may be significantly different to that of the living organism; Jones et al., 2003) and 100 µm in length. Cyanobacteria of the *Phormidium* sp. are common in thermal areas, and have an appropriate morphology (Pentecost, 2003) but the lack of more complex features preserved in the Rembokola sinters preclude definitive classification.

The role of micro-organisms, including cyanobacteria and thermophilic prokaryotes, in precipitating sinter can be important (Guidry and Chafetz, 2003b). For example, the vital activities of organisms may modify water pH and trigger silica saturation (Birnbaum and Wireman, 1984), or may act as templates for the precipitation of silica (Konhauser and Ferris, 1996; Jones et al., 1997). Biotic substrates may be important in the formation of the downstream Rembokola sinters, but the chemistry of the stream water combined with downstream cooling and evaporation leads to silica supersaturation without requiring biological control.

The chemistry of the sinters is relatively constant moving downstream, although Fe, Mn and V increase in the downstream sinters (Fig. 6.15). This change is not recorded in the water chemistry, and so may be a result of detrital material within the sinters, rather than trace elements within the amorphous silica. There is a change in land use between SV472 and SV475; the surrounding land downstream is used for agriculture which will overturn and disturb the soil more frequently, leading to higher particulate inputs to the stream.

Some noteworthy aspects of the sinters are the low but significant As concentrations, and ~20 ppm Cu (Table 6.5). Despite the Cu and Fe contents of the samples, no sulphide minerals (pyrite, chalcopyrite) were observed under SEM; in fact, with the exception of anhydrite in the spike and terraced sinter and occasional clasts of substrate material (trachytic volcaniclastics), no minerals other than opal-A were observed. Accessory elements can be bound into the structure of opal-A without requiring distinct mineral phases (Jones and Renaut, 2003a).

ICP-MS analysis of a subset of the sinter samples (Table 6.6) show that trace amounts of Au (1–2 ppb) are present, and Se is above detection limits as with the Reoka and Tanginakulu carbonates. Te is significantly lower than in the travertine samples analysed though, and may reflect a mineralogical control. The presence of even small amounts of gold may indicate a mineralising system at depth, as sinter deposits can be considered an extension of a deeper vein system (Vikre, 2007).

6.5.4 Mixed deposits

Mixed carbonate-silica deposits are found above present stream levels in the mid- to upper reaches of the Rembokola (SV482; Fig. 6.1). The silica layers include filaments in void spaces, similar to those observed in the stream sinters (Fig. 6.4E; Fig. 6.5F–G). The silica layers tend to be more massive than in the silica-only sinters, with fewer preserved filaments and lower porosity, perhaps as a function of age. Over time, diagenetic transformation in sinter leads to the destruction of primary depositional fabrics (Jones and Renaut, 2003a). The mixed deposits are clearly older than the silica sinters, as they are above the present day stream level, and have indurated and weathered upper surfaces (Fig. 6.5A).

Carbonate layers in SV482 consist of ray-crystal calcite (Fig. 6.5C), similar to the travertines at Reoka and Tanginakulu. Similar precipitation mechanisms for the Rembokola carbonates are envisaged – CO_2 degassing in an area of turbulent flow leads to calcite supersaturation and precipitation. Chemically, SV482 represents a combination between the sinter and travertine samples from this study having Au concentrations similar to the sinters, and As and Te levels typical of the travertines. Te and As are considered pathfinder elements for epithermal Au deposits (White and Hedenquist, 1995), with Te in particular associated with alkaline-related epithermal deposits (Jensen and Barton, 2000). SV482 in particular shows enrichments of these elements (Fig. 6.16).

Mixed, layered silica–carbonate deposits are also found surrounding the Mound Spring at Poghorovorughala (Fig. 6.8). Layers of opal-A contain filaments similar to the sinters elsewhere on the island (Fig. 6.8D; Fig. 6.4D). The lack of alignment in the filaments is most likely a result of the low flow rate on the Mound Spring’s discharge apron relative to the Rembokola stream.

Although calcite and silica can be found in the same deposits, (Jones et al., 1996; Campbell et al., 2002), the situation is rare, as the two minerals are associated with different fluid types (in terms of origin and chemistry) in most geothermal areas (Canet et al., 2005). SV482 and SV505 show that the Rembokola stream and Poghorovorughala Mound Spring have historically alternated between travertine and sinter formation. Carbonate precipitation is from waters with a higher contribution from low-temperature fluid (e.g. Reoka and Tanginakulu warm-spring type), and silica precipitation is from waters dominated by the high temperature end member fluid (Section 4.5). The periodic switching between the two situations reflects changes in the degree of mixing between the two end member fluids at source (Fig. 6.19). If DIC contents are too low, then calcite precipitation is masked by silica precipitation, or simply prohibited by the lack of sufficient supersaturation.

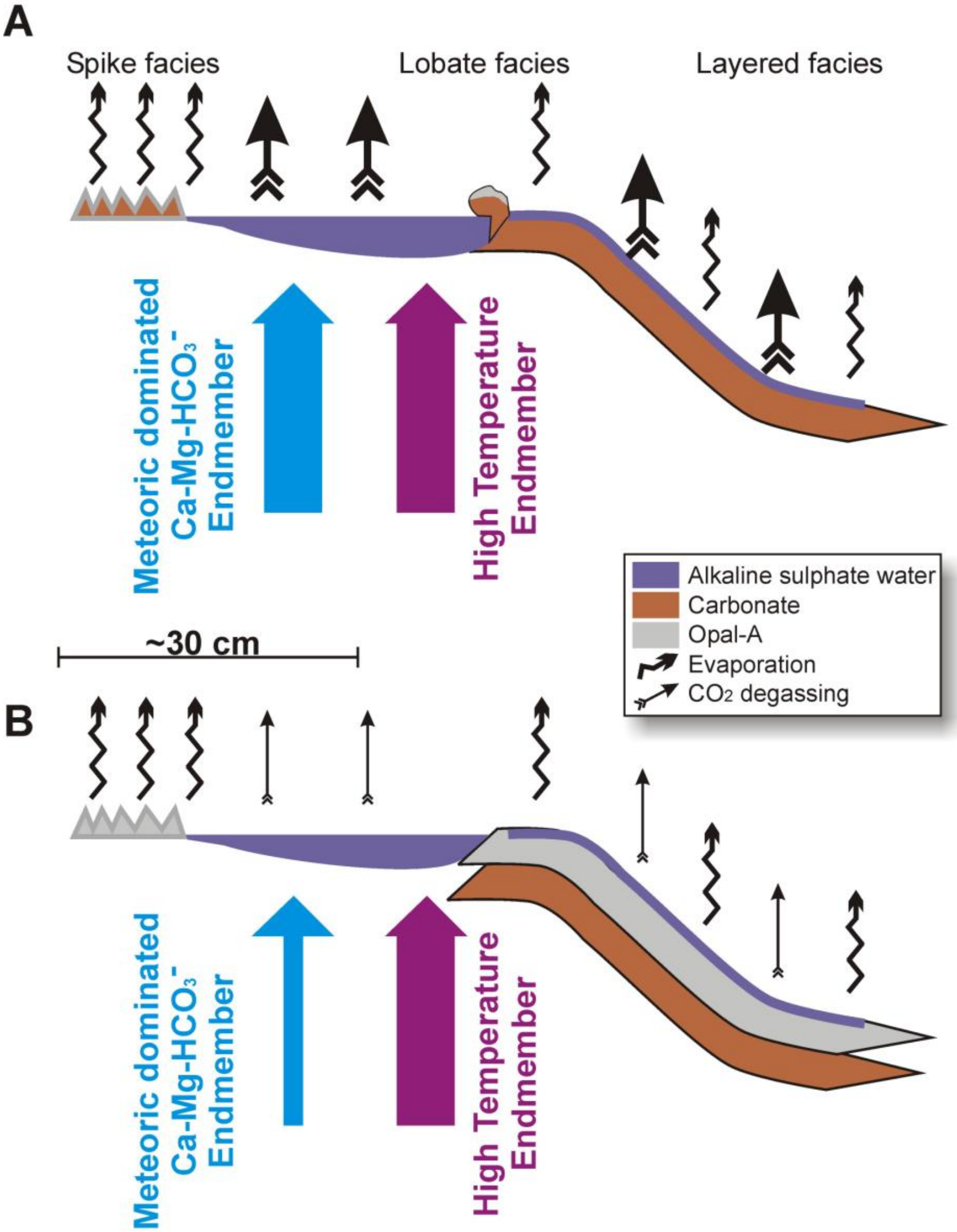

Fig. 6.19: Diagram showing how variation in the relative contributions from meteoric-dominated and high temperature endmember fluids leads to changes in mineral precipitation around alkaline sulphate hot springs, such as the Mound Spring. Thicker arrows denote greater contributions from that process or fluid. A) Carbonate precipitation during periods of large contributions from meteoric-dominated fluid. CO_2 degassing is the main process contributing to deposition. Evaporation leads to the precipitation of opal-A in spikes and lobes. B) Low contributions from meteoric water lead to opal-A being the dominant mineral, and evaporation being the main cause of precipitation.

Comparison between the Rembokola and Poghorovorughala springs shows that differential fluid mixing was occurring during the sampling for this study (Section 4.5); for example, Mg contents were far higher than would be expected for waters at the temperatures recorded (Giggenbach, 1988). The Poghorovorughala springs have a higher contribution from the Ca–Mg–HCO_3^- endmember fluid compared to the Rembokola springs. Poghorovorughala spring water samples are supersaturated with a number of mineral phases at discharge temperature, most notably with calcite (log Q/K ≈ 1.2), and aragonite (log Q/K ≈ 1.1), and saturated with anhydrite (log Q/K ≈ 0.1). The waters are undersaturated with respect to amorphous silica (log Q/K ≈ −0.2) although should saturate upon cooling to approximately 60°C (calculated with SOLVEQ; Reed, 1982; Reed, 1998). At the time of sampling, the Rembokola was precipitating only opal-A (and minor anhydrite) whereas the Poghorovorughala springs were precipitating carbonates, opal-A and anhydrite.

What causes the cyclical changeover between carbonate and silica precipitation in samples such as SV482 and SV505 is unknown. Three principal mechanisms can be defined:

1. That there are changes in the relative contribution of magmatic fluids to the hydrothermal system;
2. There are seasonal changes in the rainfall and thus the contributions of the low temperature component vary:
3. There are changes in the hydrology and plumbing of the system and the contributions / mixing of both components varies.

Seasonal variation in rainfall is the simplest mechanism to change the water chemistry periodically; regular, cyclical changes to the physical structure or magmatic inputs of the hydrothermal system are difficult to envisage compared to the simple wet-dry seasonality typical of the Solomon Islands. The mixed silica–carbonate deposits therefore reinforce the importance of meteoric water inputs and climate to the chemistry of the hydrothermal system at Savo (Sections 4.5.5 and 5.5).

Mixed carbonate-silica-anhydrite spikes grow on the periphery of Poghorovorughala hot springs, upon infrequently splashed and bathed surfaces (Fig. 6.6). The increased proportion of opal-A and anhydrite (Table 6.7) in these samples indicates that they are precipitated from more highly evaporated spring waters, as anhydrite and amorphous silica are marginally saturated and undersaturated (respectively) in the spring waters. The spikes here are morphologically similar to those of the Rembokola area (albeit with more carbonate). Mineralogy is closer to the Pavlova Spring deposits referred to in section 6.5.3 (Campbell et al., 2002), with both carbonate and silica phases, and the spikes at Poghorovorughala are interpreted to form in the same way – by wicking of hydrothermal fluids from infrequently bathed and splashed surfaces, resulting in evaporative precipitation of sinter/travertine (Fig. 6.19).

The lobate silica-carboante deposits surrounding Poghorovorughala hot springs (Fig. 6.7A) contain carbonates, with anhydrite and opal-A. In these deposits, CO_2 loss (by largely by boiling) causes carbonate precipitation, and evaporation precipitates anhydrite and silica, similar to the spike facies. For the most part, deposits are microcrystalline to amorphous, with the exception of well-developed trigonal prisms of calcite in sheltered areas between lobes (Fig. 6.7H). At precipitation temperatures above 40°C, aragonite is the expected polymorph of $CaCO_3$, with some exceptions (Jones et al., 1996). Jones et al. (1996) described calcite deposited from Waikite Hot Springs, New Zealand, where water temperatures are >90°C. The near-spring deposits at Poghorovorughala contain both calcite and aragonite, and water temperatures are >90°C; however, as the deposits are formed in splashed and bathed areas, rather than submerged, it is possible that there is precipitation both above *and* below the 40°C boundary temperature. Without real-time observations of precipitation and without a detailed micro-facies model of the deposits (i.e. on a sub-centimetre scale) it is difficult to determine whether calcite is precipitating at an unusually high temperature.

6.5.5 Stable isotopes

6.5.5.1 Fumarole CO_2

The $\delta^{13}C$ of CO_2 released from fumaroles in the crater is high (+1 to +3‰) – typically volcanic CO_2 is in the range −10 to −2‰ (Taylor, 1986; Sano and Marty, 1995). High $\delta^{13}C$ values in fumarolic CO_2 (−2 to +3‰) are reported from Iwojima, Izu-Ogasawara arc, Japan (Ohsawa and Yusa, 2001; Sumino et al., 2004; Notsu et al., 2005), where ^{13}C enrichment has been attributed to a number of different processes. Ohsawa and Yusa (2001) and Sumino et al. (2004) favoured increased contributions from subducted slab components, including marine carbonates, and related the high $\delta^{13}C$ to the unusual (alkaline) magmatism at Iwojima, suggesting that both indicated an anomalously high sediment (carbonate) input into the subduction zone. Notsu et al. (2005) instead concluded that high $\delta^{13}C$ was a result of CO_2 equilibrating with calcite at temperatures >200°C. Ohsawa and Yusa (2001) also considered subsurface processes, chiefly kinetic isotope fraction of CO_2 dissolving into steam condensates, to be additional possible causes of the unusual CO_2.

Similar arguments can be made for the system at Savo – melt compositions are alkaline and atypical of arc magmatism, and indicate significant inputs of slab-derived fluids (Section 3.4.4); subsurface temperatures >200°C are indicated by thermometric calculations, and subsurface calcite formation is possible given the pH of the fluids in the system (Sections 4.5.2 and 4.5.5); steam condensation is indicated clearly by the $\delta^{18}O$ and δD of crater fumarole steam samples (Section 5.4.3.2). It should be noted that the processes are not exclusive; potentially all three occur at Savo and Iwojima in unison. The origin of the high $\delta^{13}C$ values may be better constrained by noble gas samples – increased sediment inputs during subduction may result in noble gas isotope ratios (He, Ne, Ar) that depart from mantle ranges (Sano and Marty, 1995; Sumino et al., 2004).

6.5.5.2 Travertine and travertine depositing waters

Stable isotope studies of travertine depositing springs and streams have concluded that CO_2 -loss as a precipitation mechanism commonly results in DIC and solid carbonates with high $\delta^{13}C$ values (Friedman, 1970; Usdowski et al., 1979; Amundson and Kelly, 1987; Fouke et al., 2000). The CO_2 loss results in a Rayleigh distillation process, coupled with kinetic effects, with $^{12}CO_2$ preferentially lost to the atmosphere, resulting in an increase in $\delta^{13}C$ for the precipitated minerals and residual DIC (Usdowski et al., 1979; Dandurand et al., 1982; Michaelis et al., 1985). The fumarolic CO_2 analyses indicate that $\delta^{13}C_{DIC}$ is likely to be initially high at Savo, and therefore high values in the travertines cannot be presumed to result from CO_2 degassing alone.

The high $\delta^{13}C$ values of DIC and travertine analysed in this study are consistent with CO_2-loss as the principal precipitation mechanism, and are generally higher than the fumarolic CO_2 values. However, stream relationships do not show the steady increase in $\delta^{13}C$ and decrease in DIC that would be predicted by a Rayleigh distillation model alone (eg. Usdowski et al., 1979). Reoka is complicated by the hydrological situation and addition of CO_2 at the thermal area, but Tanginakulu should be a simple system. Although the latter shows steady DIC decrease, $\delta^{13}C$ values also decrease (Fig. 6.14), contrary to the expected Rayleigh fractionation. It is unclear why the stable isotope data contradict the chemical data (and distribution of travertine deposits, which also suggests CO_2-loss precipitation). It may be that after early degassing (i.e. prior to SV438) pH and CO_3^{2-} activity are high enough that CO_2 degassing is no longer required for precipitation. Unfortunately, the small number of data obtained in this study are insufficient to investigate this as a potential process.

The Poghorovorughala springs have DIC with lower $\delta^{13}C$ than the Reoka and Tanginakulu stream samples, yet the travertines show high $\delta^{13}C$ values (Table 6.9). The $\delta^{13}C_{DIC}$ values are close to zero, and therefore lower than the fumarolic CO_2 samples. The cause of lower $\delta^{13}C$ values of DIC here compared to the crater CO_2 and other streams is unclear.

Comparison of $\delta^{13}C$ of travertine and paired water samples shows a close match for the Tanginakulu specimens (Fig. 6.14); the Reoka sample collected *in-situ* (SV464) has a lower $\delta^{13}C$ than the equivalent water sample. However, the area from which SV464 and SV457 were sampled is the confluence of two tributaries, and slight difference in the relative flow of each stream may affect the stable isotope composition of the travertine deposit produced. In that context, it is worth noting that SV464 is isotopically very similar to the DIC of the feeder stream typified by SV462. It should also be noted that the data for travertine and water are not strictly comparable, as the travertine is always older than the water in which it is immersed.

According to equilibrium fractionation factors, at the sampled water temperatures $\delta^{13}C_{calcite}$ should be approximately 1–2‰ greater than $\delta^{13}C_{HCO3}$ (Deines et al., 1974; Chacko et al., 2001). Paired travertine-water samples from Reoka and Tanginakulu have $\Delta^{13}C_{calcite-HCO3}$ values close to zero (Fig. 6.20A); equilibrium values are not attained, and nor are they in many travertine depositing systems (Dandurand et al., 1982; Michaelis et al., 1985; Fouke et al., 2000). There is relatively little fractionation observed between $\delta^{13}C_{DIC}$ and $\delta^{13}C_{calcite}$ in systems where calcite is supersaturated, as upon nucleation, precipitation occurs more rapidly than isotopic equilibration (Usdowski et al., 1979). However, the Poghorovorughala springs all produce travertine ^{13}C-enriched relative to the spring, suggesting that significant evaporation and CO_2 degassing occurs prior to the precipitation. ^{12}C preferentially degasses from the spring waters during evaporation, and resulting precipitates are ^{13}C-enriched. The travertine deposits at Poghorovorughala are somewhat decoupled from the spring water – instead, the deposits are a result of spring water modification in micro-environments (mostly splashed areas surrounding the springs).

The $\delta^{18}O_{H2O}$ and δD_{H2O} values of the Reoka and Tanginakulu streams do not vary significantly between samples. CO_2 degassing is unlikely to affect the oxygen stable isotope composition of the water as re-equilibration is almost instantaneous between atmospheric CO_2, DIC and H_2O (Fouke et al., 2000). Unless significant evaporation of the

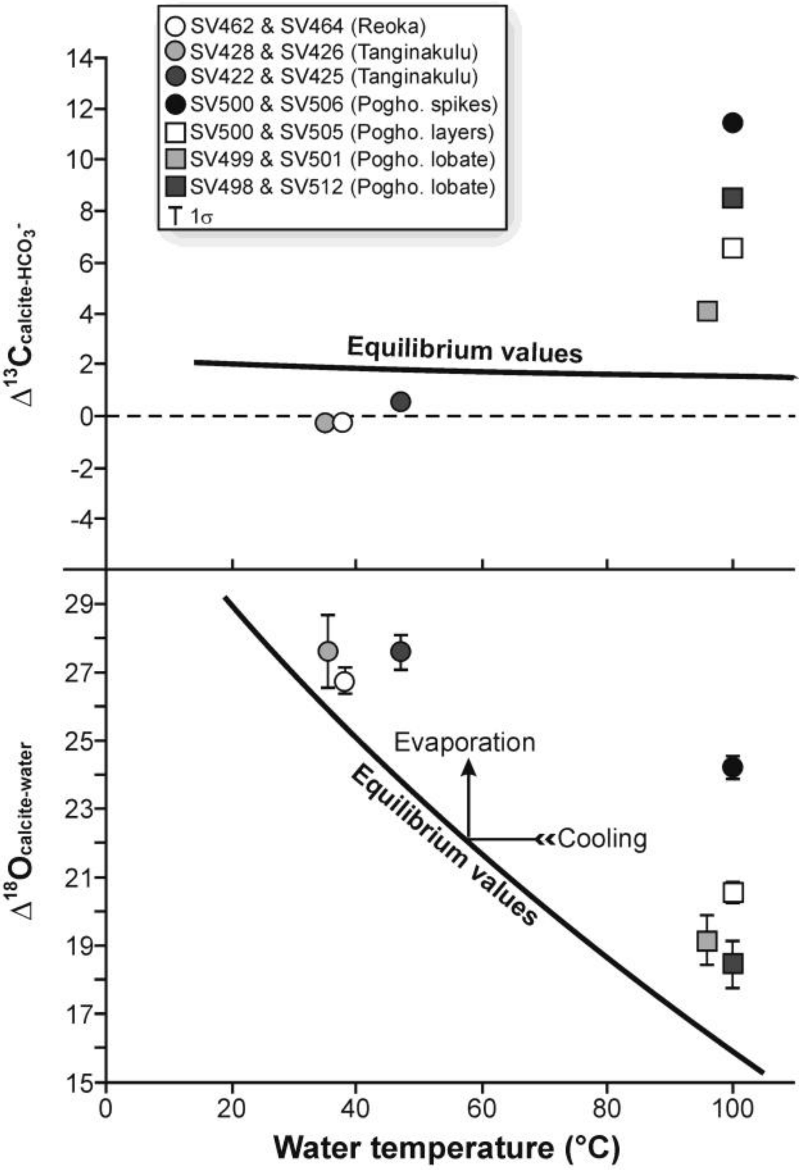

Fig. 6.20: A) $\Delta^{13}C_{calcite\text{-}HCO3}$ values from travertines and paired DIC samples. Curves show equilibrium values (Deines et al., 1974). Travertine precipitated from supersaturated solutions typically has the same $\delta^{13}C$ value as the DIC (dashed line); at Savo, hot spring deposits show enrichment of ^{13}C. B) $\Delta^{18}O_{calcite\text{-}H2O}$ values from travertines and paired water samples. Equilibrium values from Kim and O'Neil (1997). Arrows show effect of evaporation (increase in $\delta^{18}O_{calcite}$ relative to measured water) and cooling (sample plotted at higher temperature than true equilibration temperature). SV506 and SV505 are different facies from the Mound Spring. Error (1σ) within point size.

stream occurs (which would be indicated by progressive Cl^- increase), there are relatively few surface process which substantially modify those values.

The rapid oxygen isotope equilibration between atmospheric CO_2, DIC and H_2O means that the calcite precipitated should be in equilibrium with the water from which it precipitated (Friedman, 1970). Comparison of travertine and paired stream water analyses (Fig. 6.20B) shows that the low temperature (<40°C) deposits are close to the equilibrium values. However, travertine from the area surrounding the Tanginakulu warm spring (SV422) has higher $\Delta^{18}O_{calcite-H2O}$ values than expected from equilibrium. The most likely explanation for this is that calcite precipitation is triggered by combined evaporation and CO_2 degassing from the warm spring. SV422 is undersaturated with respect to calcite at discharge temperature (Fig. 6.14), and thus to produce the observed travertine deposits, its chemistry must be modified by CO_2 loss and evaporation to precipitate calcite. It should be noted that the temperature of calcite precipitation will necessarily be lower than the spring temperature if evaporation occurs; this results in an upwards shift of points on Fig. 6.20B.

$\delta^{18}O$ of the Poghorovorguhala carbonates and springs indicate that evaporation plays a role in precipitation here. As with the warm spring at Tanginakulu, $\Delta^{18}O_{calcite-H2O}$ values are greater than would be expected for equilibrium (Fig. 6.20B), and the most likely explanation for this is that evaporation leads to lower temperatures of calcite precipitation, and actual equilibrium is with higher $\delta^{18}O_{H2O}$ than discharged at the spring.

The spike facies deposits around the Mound Spring show the greatest $\Delta^{13}C_{calcite-HCO3}$ and $\Delta^{18}O_{calcite-H2O}$ values. As discussed in section 6.5.4, the mineralogy of the spike deposits requires significant evaporation of the starting spring water, as the fluids are initially undersaturated with amorphous silica (which comprises approximately 30% by mass of the solid). Extensive evaporation results in greatly increased $\delta^{13}C$ and $\delta^{18}O$ values in the final solids.

The stable isotope variation over a number of carbonate layers in samples SV482 and SV450 is minimal (Fig. 6.17, Fig. 6.18). In SV482, this indicates that whatever changes occurred between carbonate and silica-precipitating conditions, they were at least consistent between carbonate-precipitating conditions. This regularity, combined with the fact that ray crystal layers can develop over very short (seasonal) timescales (Folk et al., 1985), is possibly a reflection of the wet-dry seasonality of the Solomon Islands and a climatic control on the mineralogy of the stream deposits at Rembokola.

6.6 Conclusions

Hydrothermal discharges at Savo produce a range of deposits, including travertine, sinter and unusual mixed carbonate-silica rocks. Previous work has shown that there are multiple fluid types within the hydrothermal system, including a silica-rich end member associated with high temperature water-rock-gas interaction, and a Ca–Mg–HCO_3^- end member derived by low temperature water-rock-gas interaction. The streams and springs discussed in this study can be classified according to which component dominates: the Rembokola is high temperature dominated, the Reoka and Tanginakulu are low temperature rich, and the Poghorovorughala springs are mixed.

The Reoka and Tanginakulu streams have significant deposits of travertine, particularly in areas of rapids and waterfalls. Although the springs that feed these streams are generally saturated with calcite upon discharge, degassing of CO_2 in areas of turbulent water is important for calcite supersaturation and precipitation. Oxygen and carbon stable isotope data on DIC and the travertine further supports CO_2 loss as the most important mechanism. Textural analysis of the travertines does not indicate biological activity was involved in the precipitation; abiotic ray-crystal calcite is the dominant fabric.

The Rembokola stream system is fed by alkaline sulphate springs dominated by the high temperature endmember fluid. Unlike the Reoka and Tanginakulu streams, the majority of the Rembokola deposits are opal-A sinter. Calcite is supersaturated in these waters at discharge, but DIC contents are low as a result of a lower proportion of the Ca–Mg–HCO_3^- endmember. Any carbonate deposition is presumably masked by greater silica deposition. Near the springs, silica is deposited by evaporative processes, or wicking, typically on the exposed surfaces of debris. Near-spring “spike sinters” commonly contain significant quantities of anhydrite, which can only be precipitated from these initially undersaturated waters by evaporation. Where the springs discharge onto steep slopes, evaporation from the surface leads to the construction of terraced sinter.

Downstream from the main thermal area at Rembokola, layered sinter deposits line the stream channel. Stream water chemistry indicates that evaporative concentration, as well as significant cooling, are responsible for the supersaturation and ultimately precipitation of opal-A. The layered sinters commonly contain micro-fossils in the form of filaments. They are likely to be produced by the encasement and replacement of thermophilic cyanobacteria. Thus microbial activity may assist silica precipitation.

Poghorovorughala hot springs precipitate mixed silica–carbonate deposits in a variety of facies, including lobate precipitates in the area immediately surrounding discharge, spikes on surfaces infrequently bathed and splashed, and layered deposits on sloped surfaces. Stable isotopes indicate that evaporation and CO_2 loss are important for precipitation of these deposits, with the facies produced a function of the degree of evaporation and/or frequency of water supply.

Layered mixed silica–carbonate deposits occur in the Rembokola stream system and surrounding the Mound Spring at Poghorovorughala. The carbonate layers are similar to the travertines found in the Reoka and Tanginakulu streams, and the silica layers similar to the sinters currently forming in the Rembokola stream. The samples are interpreted to reflect meteorological changes, possible seasonal, with periods of high rainfall leading to increased contributions from the low temperature, carbonate-forming, fluid endmember.

Sinter and travertine samples are variably enriched in arsenic, selenium and tellurium, all important “pathfinder” elements for gold deposits, particularly for alkaline rock hosted epithermal deposits. The presence of trace amounts of gold in the Rembokola sinters may indicate potentially mineralising fluids at depth.

Synthesis: The magmatic-hydrothermal system and metallogenic processes at Savo 7

7.1 Introduction

The southwest Pacific is highly prospective for a number of ore deposit types, most importantly copper–gold porphyry (e.g. Panguna, Bougainville; Ok Tedi and Frieda River, Papua New Guinea) and epithermal gold (e.g. Emperor, Fiji; Porgera and Ladolam, PNG; Gold Ridge, Solomon Islands). The copper and gold deposits of the SW Pacific are amongst the largest and highest grade examples of those deposit types: Ladolam is the world's largest known epithermal gold deposit, with 1300 t Au (Simmons and Brown, 2006); Grasberg, Irian Jaya, is the most gold-rich porphyry known, with 2600 t Au and 28 Mt Cu (Cooke and Hollings, 2005).

The system at Savo shares many gross characteristics with the aforementioned deposits, including arc setting, alkaline magmatic products, and high rainfall climate, and as such may represent a modern, active analogue for the early stages of those systems. Analysis of the rocks, waters, gases and hydrothermal minerals at Savo can inform the debate on the origin of alkaline-epithermal deposits of the southwest Pacific, identify processes that are crucial to their development, and describe features from the uppermost parts of such a system that may aid the recognition of further deposits.

Also, irrespective of metal contents and metallogenic processes, a thorough description of the features and processes at Savo is necessary for our understanding of the diversity and complexity of volcanic and hydrothermal systems. This thesis has shown it is a highly unusual system with respect to tectonics, magma genesis, hydrothermal activity, and surface hydrothermal deposits.

This chapter will integrate the disparate aspects of the system; for example, the role that magma genesis plays in the evolution of the hydrothermal system. The impact of the processes and products of Savo in metallogenesis and the identification of mineral deposits in the region will also be stressed.

7.2 Regional tectonics and metallogenesis in the southwest Pacific

The SW Pacific mineral deposits represent a spectrum of ages, from the 17 Ma Frieda River porphyries (Solomon, 1990), to the 0.4 Ma Ladolam epithermal deposit – the latter arguably still active (Simmons and Brown, 2006). As such, the formation of specific deposits has been related to a number of tectonic events and processes. Furthermore, the spectacular accumulations of metal and unusual mineralogy of the deposits (both ore, gangue and host rock) have led to a number of studies relating major tectonic events to favourable conditions for metallogenesis on a large (arc-wide) scale.

Sillitoe (1997) identified stalled subduction as process that appears to favour the generation of large gold deposits. Stalled subduction may lead to partial melting of the stalled slab, or extensive mantle metasomatism (by aqueous fluids or silicate melts); this is capable of generating oxidised magmas that destabilise sulphide minerals and allows for the release of chalcophile Au and Cu into ascending melts (McInnes and Cameron, 1994; Sillitoe, 1997; Mungall, 2002). Solomon (1990) noted that stalled subduction was often related to or followed by reversal of subduction polarity, which again was related temporally and spatially to ore formation. Stalled subduction and polarity reversal events occur as a result of arc–arc, continent–arc, or in the case of the Solomons, plateau–arc collisions (Petterson et al., 1999): globally important examples of deposits related to such situations include Panguna, Bougainville; Koloula copper prospect, Guadalcanal, Solomon Islands (Solomon, 1990); Ladolam (McInnes and Cameron, 1994); Grasberg, Irian Jaya (Sillitoe, 1997); Pueblo Viejo, Dominican Republic (Lebron and Perfit, 1993); and Cadia, Australia (Wyborn, 1992). As detailed in Chapter 2, Savo is in a central position in the arc (Fig. 2.2). Magma genesis related to the Pacific slab has occurred further south (e.g. the Poha Diorite and Suta Volcanics of Guadalcanal; Chivas, 1981), and König et al. (2007) concluded that Pacific derived melts contributed to magma genesis at Simbo, *south* of the South Solomon Trench System (i.e. on the down-going Indo-Australian Plate; Fig. 2.2), therefore indicating that Savo is well within the metasomatic "footprint" of the stalled Pacific slab.

An extensional geodynamic setting – such as incipient back-arc rifting – has been suggested to be important in the genesis of a number of the SW Pacific deposits (Sillitoe and Hedenquist, 2003), including Emperor (Eaton and Setterfield, 1993) and Ladolam (Carman, 2003). Extensional stress regimes may also operate on a local level within regional compressive tectonics, by the operation of composite transform-convergent tectonic zones (CTCs; Coleman, 1991; Petterson et al., 2004). Such structures are important at the New Guinea deposits (Hill et al., 2002; Gow and Walshe, 2005). Petterson et al. (2004) suggested that CTCs may be important regional structures in the central Solomons, including at Gold Ridge and Savo (Petterson and Biliki, 1994).

The formation of slab windows can also contribute to an extensional geodynamic setting (Sillitoe and Hedenquist, 2003), or at least the arc inherits characteristics of extensional-type magmas from the underlying window (Thorkelson, 1996). A number of studies in the Solomon Islands have concluded that slab windows are forming beneath the arc as a result of the subduction of the Woodlark spreading ridge at the South Solomon Trench System, and that it has a significant effect on magma genesis and chemistry (Johnson et al., 1987; Johnson and Tuni, 1987; Perfit et al., 1987; Schuth et al., 2004; König et al., 2007). Whether or not these slab windows form as far west as Savo and Guadalcanal is unknown, but a number of studies speculate that the Mborukua Lineament (an E–W trending chain of Quaternary volcanoes including Kavachi and Savo; Fig. 2.2) is a surface expression of a slab window (Johnson et al., 1987; Cowley et al., 2004).

7.3 Petrogenesis and ore deposit formation

In the circum-Pacific region, there is a strong relationship between alkaline rocks and copper–gold deposits – alkalic and shoshonitic rocks constitute less than 3% by volume of igneous rocks in those arc terranes, yet ~20% of the largest gold deposits are associated with such rocks (Sillitoe, 1997; Müller, 2002). For epithermal deposits, there are a number of features that distinguish alkaline-related deposits from the calc-alkaline equivalents – including high telluride contents (Ahmad et al., 1987; Jensen and Barton, 2000); telescoping or transitioning downwards into porphyry-type mineralisation (Eaton and Setterfield, 1993; Richards and Kerrich, 1993; Carman, 2003); and widespread carbonate precipitation (rather than quartz; Sillitoe, 2002).

Highly potassic rocks are more frequently associated with gold mineralisation than sodic suites, partly because K-rich rocks are more common in arc settings (Baker, 1982; Sillitoe, 1997) and in part because the IUGS nomenclature gives potassium greater emphasis in whole rock chemistry, as “sodic” rocks are defined as having $Na_2O-2 > K_2O$. Jensen and Barton (2000) pointed out that although shoshonites are potassic basalts they may have molar contents of Na 3.5 times greater than K.

Why alkaline rocks should be so favourable for gold metallogenesis is unclear. At Ladolam, mantle enrichment appears to have taken place by the addition of fluids and partial melts from the upper parts of the subducted Pacific slab (McInnes and Cameron, 1994; McInnes et al., 2001; Kamenov et al., 2008. Addition of fluid-mobile alkalis, sulphate and carbonate to the mantle leads to the genesis of alkaline, oxidised melts. Gold and copper sulphides in the mantle are destabilised by the oxidising conditions, and taken into the melts (Sillitoe, 1997; Mungall, 2002); later fractionation of Cu–Au sulphides is limited, allowing for Au and Cu to be carried to high crustal levels (Müller et al., 2001).

It can be speculated that similar conditions exist at Savo. Certainly, the enrichment of Na and fluid mobile elements (Sr, K, Rb, Ba; Fig. 3.17) in the parental melts, and the high water content of the magmas, point to a metasomatised mantle origin. The paucity of sulphide minerals and the presence of magmatic anhydrite indicate relatively oxidising conditions.

Magmatic anhydrite was only observed in one trachyte sample, though may have been more prevalent. As an anhydrite-bearing magma ascends, progressive degassing of SO_2 leads to the breakdown of anhydrite (Luhr and Logan, 2002), perhaps providing a mechanism by which the majority of Savo's crystal rich rocks are sulphur-poor and anhydrite-free. The chemistry and sulphur isotope data of the hot spring discharges (Sections 4.5.2 and 5.4.1) indicate that significant contributions of SO_2 are made to the shallow hydrothermal system.

Hydrous magmas are likely to be essential to the formation of magmatic hydrothermal ore deposits. Models of epithermal and porphyry deposits involve the release of magmatic fluids as sources of complexing ligands and the ore metals themselves (Henley and McNabb, 1978; Henley and Ellis, 1983; Simmons et al., 2005). The mineralogy of the magmatic rocks at Savo requires that water contents are high (>3.5 wt % to stabilise amphibole; Burnham, 1979), and water solubility and crystallisation considerations require that water must be exsolved as magmas ascend (Section 3.4.2; Fig. 7.1).

Extensive magmatic fractionation results in aqueous phases being enriched in chloride; although amphibole and biotite may contain chlorine, often the amount is low relative to the water content of the mineral (Webster and De Vivo, 2002; Webster, 2004). Chloride is probably the most important ligand for metal complexes upon exsolution of fluid from a crystallising magma (i.e. porphyry-type conditions, with T >400°C and P >1 kbar), largely due to its abundance (Seward, 1991; Seward and Barnes, 1997). Extensive silicate fractionation (Section 3.4.1) combined with little to no sulphide fractionation at Savo means that exsolved fluids should be chloride and gold enriched relative to the parental melt.

Fig. 7.1: Schematic diagram of the magmatic and hydrothermal system at Savo, highlighting key processes, and in particular how gold and related pathfinders behave.

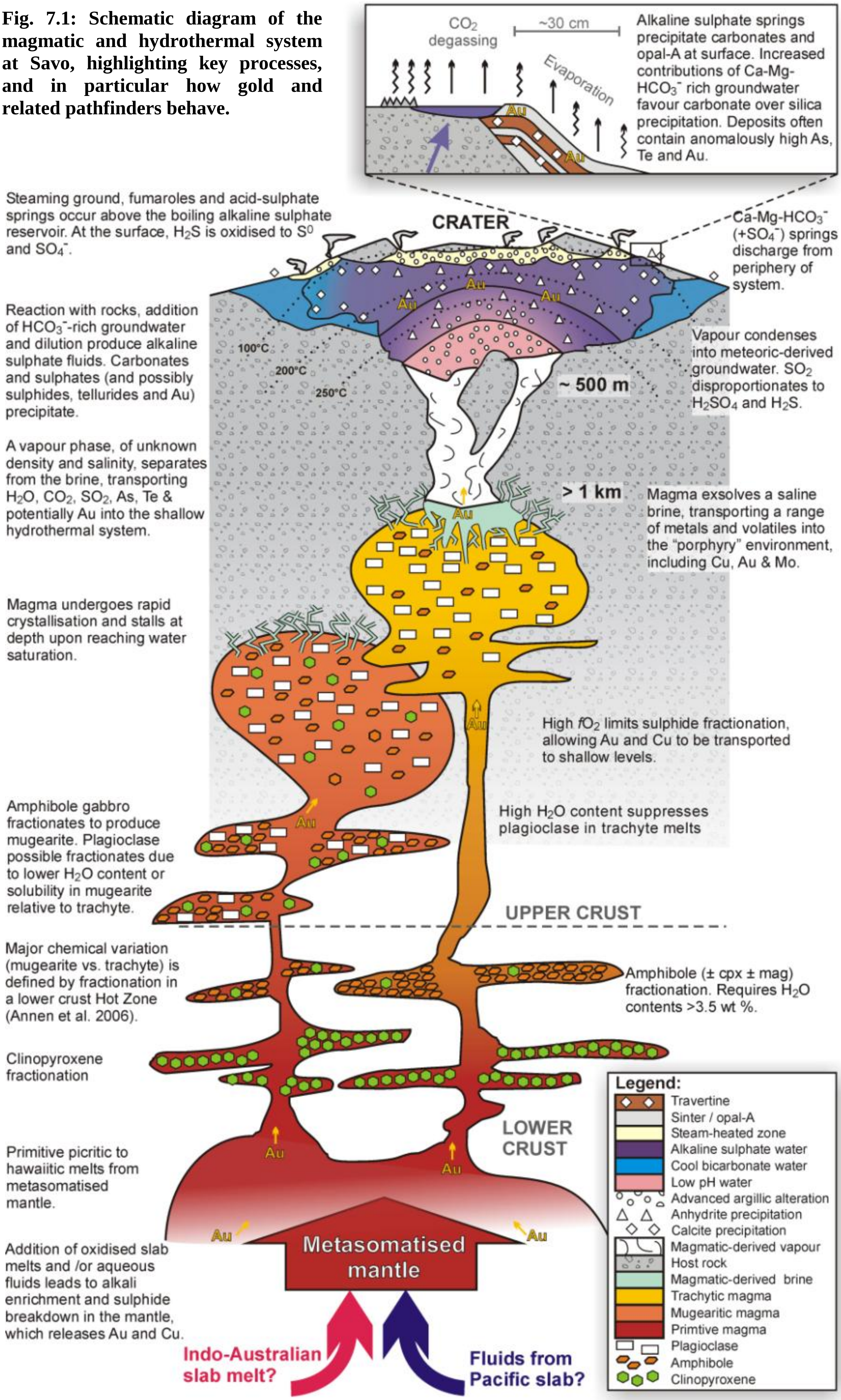

Copper is less abundant in the evolved trachytes of Savo relative to the mugearites (~10 ppm vs. >100 pm); concentrations are high in a number of the amphibole-bearing cumulates analysed in this study (up to 225 ppm; Table 3.8), but more commonly are less than 100 ppm. Stanton (1994) determined the crystal: melt distribution coefficients (K_D) for the Solomon Islands "Hornblende Andesites" lavas (which includes Savo) and found that the only abundant mineral to have K_D >1 was magnetite, and that it fractionated in insufficient amounts to produce the observed Cu depletions. He speculated that copper might be removed in a volatile phase.

Along with abundant nodules of cumulate material at Savo, inclusions of trachyte / mugearite stockworked by quartz veins can be found (Fig. 7.2). These samples represent hydrothermal fluids exsolved during an earlier magmatic event, with the resulting rocks then entrained and erupted by a later magma. Aqua regia digestion and ICP-MS analysis of two such veined xenoliths (Table 7.1; technique described in Section 6.3.1) gives a semi-quantitative measure of the chemistry. The samples contain small amounts of Au (3.8–32.6 ppb; Fig. 7.3); whilst one sample is enriched in Cu (204 ppm) the other is within the range represented by unaltered magmatic rocks (73 ppm). Unlike some of the surface hydrothermal deposits analysed in this study, the veined materials do not show particularly high arsenic contents (≤0.2 and <1 ppm respectively), and Te is close to instrumental detection limits (0.02 ppm; but still considerably enriched relative to typical arcs, at 0.002 –0.006 ppm; Yi et al., 2000). Molybdenum is also enriched (4.8–7 ppm; unaltered igneous rocks are

Sample	**MDL**	**SV227**	**SV322**	**SV368**	**SV368**
Type		Quartz veined xenolith	Quartz veined xenolith	Anhydrite w/ sulphides	Anhydrite w/ sulphides
Al wt %	0.01	0.40	0.51	0.02	0.02
Ca wt %	0.01	0.14	0.15	13.45	13.21
Fe wt %	0.01	0.56	0.54	0.21	0.21
K wt%	0.01	0.40	0.50	0.01	bdl
Mg wt%	0.01	0.55	0.66	bdl	bdl
Na wt %	0.001	0.124	0.183	0.004	0.004
P wt %	0.001	0.051	0.054	0.008	0.009
S wt %	0.02	bdl	0.02	>10.00	>10.00
Ti wt %	0.001	0.103	0.132	bdl	bdl
Ag ppb	2	19	12	284	286
As ppm	0.1	0.7	0.5	1.5	2.2
Au ppb	0.2	32.6	3.8	755	1032
B ppm	20	bdl	bdl	bdl	bdl
Ba ppm	0.5	40.5	54.3	7.5	7.4
Bi ppm	0.02	0.05	0.03	0.07	0.06
Cd ppm	0.01	0.01	0.01	bdl	0.01
Co ppm	0.1	2.4	3.0	0.3	0.4
Cr ppm	0.5	6.7	8.4	bdl	bdl
Cu ppm	0.01	204	72.7	1940	1852
Ga ppm	0.1	2.5	3.2	0.2	0.2
Hg ppb	5	bdl	bdl	38	45
La ppm	0.5	4.7	5.5	25.3	25.6
Mn ppm	1	53	71	18	10
Mo ppm	0.01	4.8	7.0	1.4	1.4
Ni ppm	0.1	6.0	7.7	0.7	0.3
Pb ppm	0.01	0.77	0.76	0.74	0.67
Sb ppm	0.02	bdl	bdl	0.02	bdl
Sc ppm	0.1	2.6	3.1	0.2	0.1
Se ppm	0.1	0.2	bdl	2.8	2.9
Sr ppm	0.5	21.7	50.3	755	782
Te ppm	0.02	0.02	0.02	0.12	0.13
Th ppm	0.1	0.4	0.4	0.5	0.5
Tl ppm	0.02	0.03	0.04	bdl	bdl
U ppm	0.1	0.1	bdl	bdl	0.1
V ppm	2	94	98	bdl	bdl
Zn ppm	0.1	5.7	8.5	2.1	2.1

Table 7.1: Chemistry of quartz-veined xenoliths and vein anhydrite from Savo. Samples analysed by ICP-MS analysis following aqua regia digestion, as described in Chapter 6.

Fig. 7.2: Typical examples of xenoliths with quartz vein stockworks.

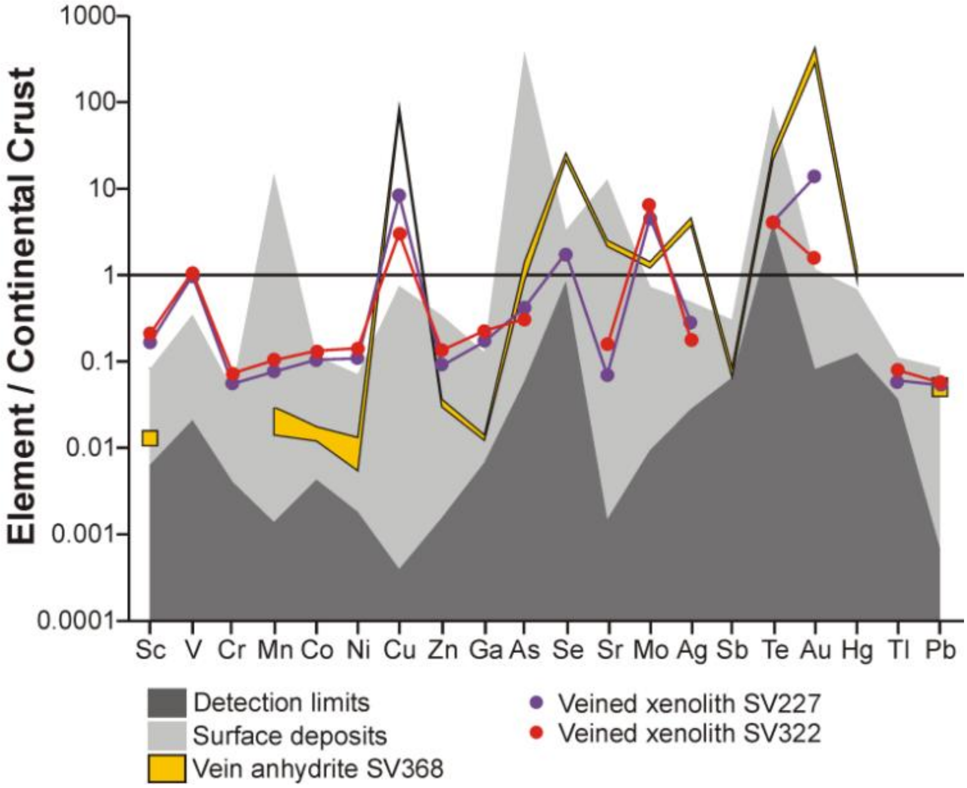

Fig. 7.3: Selected trace elements (analysed by ICP-MS following aqua regia digestion) of veined xenoliths and vein anhydrite (w/ chalcopyrite) vs. continental crust (Wedepohl, 1995). Dark grey field shows detection limits for the technique, normalised to continental crust. Pale grey field shows range of values from sinter, travertine and mixed silica–carbonate deposits discussed in Chapter 6 (Fig. 6.16).

<2 ppm); alkaline suites are the only host for porphyry molybdenum gold deposits (Sillitoe, 2002), and as such molybdenum is an important pathfinder for porphyry style mineralisation. Although the veined samples are not an indicator of economic porphyry mineralisation at Savo, they do at least exhibit characteristics of that deposit class, and are evidence of the movement of Au–Cu–Mo-bearing fluids at depth – sufficiently deep that the altered and veined rocks can be subsequently re-entrained into ductile magma as xenoliths, with no observable chilled margins. Porphyry style mineralisation at depth is a common characteristic of the SW Pacific alkaline epithermal deposits, and although rarely economic, it is key to the transfer of precious metals into the epithermal parts of the systems (Richards, 1995).

7.4 The hydrothermal system and potential for mineralisation at Savo

Direct comparisons between ore deposits and Savo are difficult because the alkaline sulphate fluid types discharging at Savo have not been previously described in modern systems, and as such have not been invoked in the discussion of fossil epithermal equivalents. However, the processes at play in the hydrothermal system are not as unusual as their products might suggest.

There is a paucity of acid alteration in alkaline-hosted epithermal deposits (Jensen and Barton, 2000; Sillitoe, 2002), although not a complete absence (e.g. the Navisi 3 prospect near Emperor, Fiji; Eaton and Setterfield, 1993). Sillitoe (2002) suggested that the dominance of neutral to alkaline fluid conditions in these systems was a result of effective pH buffering by the alkaline host rocks. At Savo such a mechanism is possible, but the input of meteoric water and the bicarbonate it dissolves in the peripheral parts of the system are also important pH controls (Fig. 7.1; Section 4.5.2). Fluid mixing certainly occurs at the south Pacific alkaline epithermal deposits (Richards, 1995), and it may be that it is an important factor in determining the occurrence and distribution of acid-related alteration (or lack thereof) in these systems.

Contributions from magmatic fluids are important, at least in the earliest stages of alkaline epithermal systems (Ahmad et al., 1987; Richards, 1995; Jensen and Barton, 2000; Carman, 2003). The sulphur isotope data from the alkaline sulphate springs indicate magmatic inputs into the hydrothermal system at Savo (Section 5.4.1). The high sulphate and comparatively low chloride contents of the water suggest perhaps that the shallow hydrothermal system is fed by magmatic vapour, separated from an initially more saline fluid (as per Heinrich, 2005; Webster and Mandeville, 2007). A number of studies suggest that low density vapour phase fluids (with salinities of 2–10 wt % NaCl equivalent, and densities similar to 1 g/cm^3) are capable of transporting precious metals in sufficient concentrations to generate mineralisation (Heinrich et al., 2004; Heinrich, 2005; Williams-Jones and Heinrich, 2005). Low salinity vapour is unlikely to be capable of carrying much metal as they will be retained as chloride complexes in the brine (Hedenquist et al., 1994a). However, low salinity hot springs need not indicate that the vapour was necessarily low salinity – in the high rainfall climate of Savo, the chloride may simply have been diluted to low levels (with sulphate concentrations buffered by anhydrite; Section 4.5.2). Hedenquist and Aoki (1991) suggested that the meteoric water-dominated upper zone at Kirishima, Japan, could act as a “condenser” for magmatic vapour, and thus be an environment conducive to ore genesis. Low metal contents in surface discharges would in such a case be a result of dilution and deposition, and not necessarily indicative of a barren system.

The alkaline sulphate springs have $\delta^{34}S_{SO4}$ values ~+6‰, whereas native sulphur from fumaroles and sulphate from low pH springs are within the range −6 to +2‰. Magmatic SO_2 disproportionates into ^{34}S-enriched H_2SO_4 and ^{34}S-depleted H_2S upon reaction with water; H_2S is later oxidised at the surface to low-δ^{34}S native sulphur and sulphate (Section 5.4.1). Although the Savo samples are consistent with this process, the difference between alkaline sulphate and H_2S-derived species is not an equilibrium fractionation value. Sulphide–sulphate equilibrium is slow in high pH conditions (Ohmoto and Lasaga, 1982), and so the samples record only instantaneous kinetic fractionations (Kusakabe et al., 2000), or inherit their isotopic characteristics from fractionation in the magma (Rye, 2005). If the lack of isotopic equilibrium between the species is indeed a result of the high fluid pH, then the neutralisation and dilution processes must occur rapidly; SO_2 disproportionation would generate highly acidic condensates, and equilibrium would be rapidly attained if such conditions persisted. The system may be highly effective as a condenser for magmatic vapour in that case, and the abrupt changes in fluid chemistry and temperature may be ideal conditions for gold precipitation, if indeed metals are transported in a vapour phase.

The role of magmatic vapour phases in gold transport is a source of much debate. Gold can be introduced into the epithermal environment by ascending liquids/ brines (Hedenquist et al., 1994b; Arribas, 1995; Hedenquist et al., 1998); leached out of host rocks (viable in the southwest Pacific deposits, given the close spatial relationships of those deposits to porphyry mineralisation; e.g. Richards et al., 1991), or carried in a foam / aerosol of high salinity brine by an ascending (otherwise barren) low salinity vapour (Fournier, 1999). Potential mechanisms of gold transport at Savo cannot be resolved with the current data. The shallow dilution recorded by stable isotope and water chemistry data means the vapour phase remains cryptic – that is, the data available from the hot springs and fumaroles at Savo provide little indication as to the salinity and density of the magmatic vapour phase that feeds the shallow hydrothermal system.

A float sample of vein anhydrite (SV368; Fig. 7.4) was found in the north of the island, transported to the downstream area of the Tuluka stream (Fig. 2.5). Its initial location is unknown. The anhydrite has δ^{34}S values slightly higher than those of present day alkaline hot springs (7.6‰; analysed by techniques described in Section 5.2.3), but considering this relatively close value, and that anhydrite is predicted by geochemical modelling, it seems highly likely that this sample represents hydrothermal anhydrite formed in the subsurface

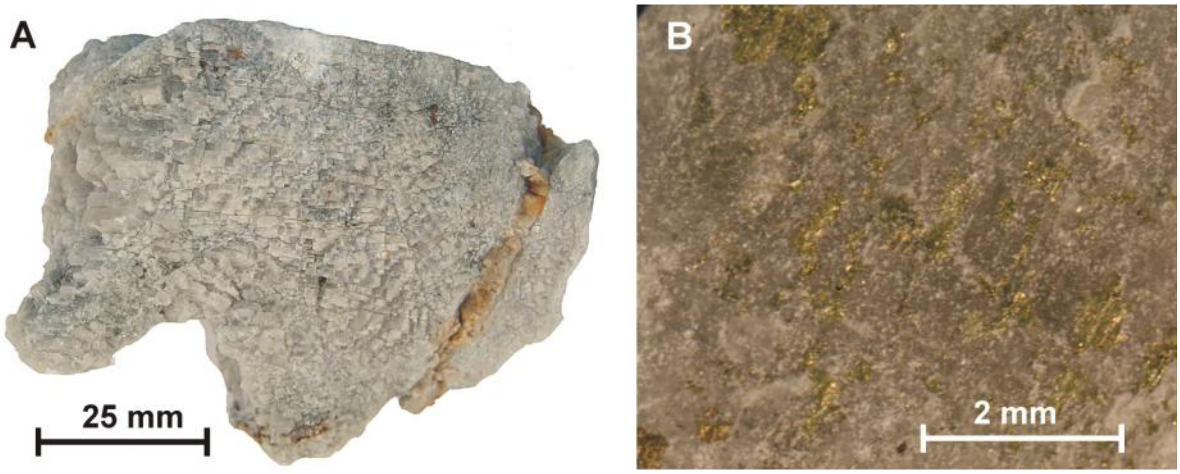

Fig. 7.4: Vein anhydrite sample SV368. B) High magnification view of chalcopyrite on broken surface of SV368 (not visible in view A).

of the present day hydrothermal system. The sample also contains small amounts of chalcopyrite (Fig. 7.4B). SV368 was analysed by ICP-MS following aqua regia digestion (Table 7.1). There is considerable gold grade in this sample (755–1032 ppb), smaller concentrations of silver (285 ppb), and enrichments in pathfinder elements (Se 2.8 ppm; Te 0.12 ppm, Mo 1.4 ppm). Enrichments follow similar patterns to surface deposits (Fig. 7.3). As with the deeper veined samples, this sample indicates the transport of Au and related elements in the hydrothermal fluids at Savo, including in the shallow system, and underlines its potential as a mineralising system.

7.5 Surface deposits

At present on Savo, travertine forms from Ca–Mg–HCO_3^- enriched waters (such as the warm springs of Tanginakulu; Sections 4.5.4 and 6.5.2) sinter precipitates from the alkaline sulphate waters at Rembokola (Section 6.5.3), and silica–carbonate deposits are formed from the mixed waters discharged at the Poghorovorughala alkaline sulphate springs (Sections 4.4.2 and 6.5.4). Older mixed silica–carbonate deposits also occur within the Rembokola valley (SV482; Section 6.5.4), indicating that the springs there are susceptible to fluid mixing, and that the relative contributions of the hydrothermal (Na–K–Si enriched) component versus the lower temperature (Ca–Mg–HCO_3^- enriched) component may vary as a result of a seasonal wet–dry climate in the Solomon Islands. The role of climate on the chemistry and mineralogy of shallow hydrothermal systems may be significant, particularly in high rainfall areas such as the SW Pacific.

The surface deposits show notable enrichments in a number of trace elements – Au is present and in some cases slightly enriched in the sinters (~2 ppb), As is enriched in a number of travertines and the Rembokola mixed silica–carbonate deposit (up to 600 ppm), and Te is enriched in sinter (0.04 ppm) and greatly enriched in carbonate-bearing deposits (up to 0.41 ppm). Te is enriched in the Au-bearing anhydrite + chalcopyrite samples (Section 7.4; Table 7.1), and is associated with gold mineralisation in the southwest Pacific alkaline epithermal deposits, with gold often present as telluride minerals (Ahmad et al., 1987; Richards, 1995; Spry and Scherbarth, 2006). Tellurium may be transported into the shallow hydrothermal system in a magmatic vapour phase (Cooke et al., 1996; Cooke and McPhail, 2001), consistent with the model derived from the fluid chemistry and stable isotope data (Fig. 7.1). Although not *prima facie* evidence of mineralisation at Savo, the Te enrichments in the hydrothermal products are another characteristic shared with regional epithermal deposits, and an indicator of the mineralisation potential at Savo. Sinter and travertine may be useful, particularly in their trace element (Te, As, Se) composition, for the identification of otherwise blind epithermal deposits. This study also highlights the fact that sinter formation is not limited to classic "low sulphidation" type geothermal systems.

7.6 Unresolved problems and suggestions for future work

This body of work represents the first detailed study of Savo volcano from a geochemical perspective. Many of the processes and products described and discussed within the thesis are deserving of further study.

As discussed in Sections 7.2 and 7.3, a number of studies have suggested that mantle conditions and petrogenetic processes can generate fecund magmas. There seems to be little data that indicates gold deposits are related to inherently Au-rich magma (Tilling et al., 1973), but the exceptional gold accumulations within some porphyries are best explained by derivation from such a melt (Connors et al., 1993). Clearly, the best course of action is to analyse the unaltered rocks at Savo for gold concentrations. However, care must be taken as low gold concentrations need not indicate a barren magma – in fact the opposite may be true, and the magma may already have released its metal budget prior to eruption, sampling and analysis.

The role of water in island arc petrogenesis well established, and the igneous rocks of Savo display a number of criteria that suggest high water contents. This study has been limited to a qualitative discussion of the behaviour water; a melt inclusion study on the volatile contents of primitive magmas would allow for more detailed, quantitative discussion of this important aspect of magma evolution. Concentrations of chlorine and sulphur in the primitive melts will also help to constrain the chemistry of any exsolved volatile phase.

Savo has been suggested to be a young extension of the Gallego Volcanic Field of NW Guadalcanal (Petterson and Biliki, 1994; Stanton, 1994). Certainly, the mineralogy and chemistry of unaltered rocks from the two areas show many common features, most obviously the high feldspar phenocryst content and the abundance of ultramafic (cumulate) inclusions. A wider study of volcanism in the central Solomon Islands would provide useful insights into the ambiguous tectonics and melt generation processes – the plate tectonic motions indicate that over time a slab window related to the subducted Woodlark Ridge would move north. As such, the GVF may represent an older, southern surface expression of the slab window now (perhaps) beneath Savo.

Given the range of features displayed at Savo that are consistent with regional epithermal Au deposits, the Gallego Volcanic Field may be a prospective area for mineralisation. The older edifices there will have been more incised and eroded; exposure of deeper levels may allow for the construction of a cross section of Savo-like hydrothermal systems.

Stable isotope data have provided crucial information on the origin of hydrothermal fluids at Savo, and the processes which affect them. Further work on gases and waters can help constrain the models developed during this study. Tritium isotope data can be used to calculate meteoric water residence times in hydrothermal systems (Shevenell and Goff, 1995) as well as constrain relative contributions from magmatic and meteoric sources (Goff and McMurtry, 2000). Noble gas isotopes can be used to identify magmatic contributions to the hydrothermal system, and provide insight into the nature of the magmatic inputs, in particular the origin of anomalously high $\delta^{13}C$ values of fumarole CO_2 (Sumino et al., 2004).

Other key parameters to measure on the hot spring fluids include bisulphide and mercury contents (which require specific chemicals to preserve, are unstable in storage and not routinely analysed in water samples) and Eh. The latter is an important variable in determining the stability of certain minerals (e.g. sulphides) in the hydrothermal system, but it is questionable as to whether the redox potential of the boiling hot springs can be used to directly predict the conditions at depth.

The micro-ecology of the hot springs could well be unique, given the unusual fluid chemistry and geographical isolation of Savo Island. The role that micro-organisms play in the chemistry, mineralogy, distribution and morphology of the surface deposits at Savo was only briefly discussed in Chapter 6, and clearly further attention is needed in this area. Species were tentatively named on the basis of filament casts in the sinters – more thorough microbiological work (dedicated biological sampling, culturing, RNA/ DNA sequencing) would be required to properly establish the ecology of the springs.

Determining rates of precipitation of both carbonate and silica minerals at the surface on Savo may help constrain the role of climate in controlling the hydrothermal chemistry. Although the rhythmic nature of banding in all stream-precipitated sinters and travertines, and particular the mixed silica–carbonate deposits, is strongly suggestive of seasonal wet–dry variations, this hypothesis needs testing. Variations can also be a result of pulses of magmatic activity, and so the timescale of the changes needs to be calculated. Repeat visits to Savo and sampling springs at different times of the year, will help to constrain seasonal variability in the hydrothermal system. Drill core of the mixed silica–carbonate deposits surrounding the Mound Spring will provide a long term record of fluid variation and mineral precipitation at that spring.

The preliminary geochemical analysis of the sinters and travertines provided in this study identified a number of important features, most notably Au and Te enrichments. There is scope for improved analysis, including better digestion techniques, a larger number of samples, and layer-specific sampling and analysis to determine temporal changes in fluid chemistry. In addition, the sinter deposits related to the Emperor gold deposit in Fiji (Eaton and Setterfield, 1993) are not well documented in the literature, but a detailed description and chemical analysis of them may well provide a useful frame of reference for the deposits at Savo.

7.7 Conclusions

The complex tectonic setting of the Solomon Islands involves stalled slabs beneath the arc, subduction polarity reversal and the formation of slab windows. These phenomena have contributed to the generation of sodic magma suites at the volcano. The petrology and chemistry of the igneous suite indicates that water is an important control on magma evolution. Upon ascent and crystallisation, the magmas release water, CO_2, SO_2, and other volatiles into an overlying hydrothermal system. Reactions with the sodic rocks, dilution by meteoric water, and boiling lead to a rapid increase in the pH of the condensed magmatic volatiles. The resulting hydrothermal fluids discharge at the surface as alkaline sulphate hot springs. The sulphur isotope systematics of Savo show atypical features for an active magmatic hydrothermal system as a result of the neutral to alkaline conditions; isotopic equilibrium is prohibitively slow in high pH fluids. The alkaline sulphate waters precipitate sinter and unusual mixed silica–carbonate deposits at the surface; seasonal changes in rainfall affect the chemistry of the hydrothermal waters, and the minerals they precipitate at the surface. Many of the features described at Savo are analogous to major gold deposits of the region, and Savo itself shows promising signs of mineralisation.

Savo shows a range of unusual features and processes, from slab to sinter. The system has a number of features in common with major gold deposits of the region, including tectonic setting, alkaline magmas, magmatic volatile contributions to hydrothermal fluids, and tellurium and gold enrichments. This study makes important contributions to our understanding of island arc petrogenesis with a description of the chemistry, mineralogy and petrogenesis of a suite of sodic magmas, rare in arc settings. It adds to our knowledge of magmatic-hydrothermal systems with a detailed account of previously undescribed alkaline sulphate fluids and their origins, and by providing strong evidence for the role of high rainfall in the chemistry and mineralogy of the shallow hydrothermal system. The thesis documents a new chemical environment of sinter formation, and of globally rare mixed silica–carbonate deposits; anomalous Au and Te contents mean these deposits may be useful in exploration for mineralisation. The combined study of tectonics, igneous petrogenesis, hydrothermal fluids and surface deposits has established Savo as a potential modern analogue for alkaline-related epithermal deposits.

Appendix I: Electron probe microanalysis data

I

Electron probe microanalysis data used in Chapter 3 are collected in the following tables. Minerals are separated onto different tables. Analyses are ordered by increasing sample (SV) number. Additional information (stoichiometry, mineral names, Mg numbers) are included where appropriate. Analyses with low totals (olivine <98%; feldspar <97%; amphibole <96%; clinopyroxene <97%; biotite <93%) have been removed. Samples are listed as MUG (mugearite), BEN (benmoreite), XEN (xenolith /nodule) or blank for main suite (mugearite–trachyte) with no whole data.

I.1 Olivine

Sample	SV1	SV1	SV1	SV1	SV1	SV1	SV1	SV1	SV1	SV1	SV1	SV1	SV158	SV158	SV158	SV158	SV165	SV165
Rock Type	MUG	MUG	MUG	MUG	MUG	MUG	MUG	MUG	MUG	MUG	MUG	MUG	XEN	XEN	XEN	XEN	XEN	XEN
Analysis	05-013	05-019	05-020	05-021	05-022	05-023	05-024	05-027	05-028	05-036	05-037	05-038	12-125	12-126	12-127	12-128	07-056	07-060
SiO_2	38.72	38.31	38.07	38.46	38.52	38.40	38.46	38.13	38.27	38.45	38.51	39.21	39.88	39.76	39.83	40.06	39.21	38.44
TiO_2	0.01	0.01	0.00	0.00	0.00	0.00	0.00	0.00	0.00	0.00	0.01	0.01	0.00	0.00	0.00	0.00	0.04	0.00
Al_2O_3	0.01	0.02	0.05	0.01	0.02	0.01	0.01	0.01	0.02	0.03	0.00	0.00	0.00	0.00	0.00	0.01	0.02	0.03
Cr_2O_3	0.02	0.01	0.00	0.01	0.02	0.00	0.03	0.00	0.02	0.03	0.00	0.00	0.00	0.00	0.00	0.04	0.04	0.00
FeO	20.67	23.22	22.97	23.39	23.33	23.95	23.78	25.08	24.49	23.97	23.37	20.89	18.15	17.89	17.54	17.26	17.77	18.40
MnO	0.50	0.46	0.49	0.57	0.47	0.54	0.61	0.72	0.64	0.48	0.50	0.41	0.29	0.30	0.31	0.29	0.36	0.33
MgO	41.10	39.34	38.74	39.42	38.88	39.01	38.85	37.80	37.82	38.74	39.21	41.47	41.86	42.14	42.45	42.81	43.38	41.57
CaO	0.18	0.20	0.19	0.16	0.15	0.22	0.22	0.17	0.20	0.17	0.19	0.15	0.06	0.03	0.03	0.03	0.08	0.08
Na_2O	0.72	0.02	0.05	0.00	0.04	0.00	0.03	0.01	0.01	0.00	0.00	0.02	0.04	0.02	0.00	0.00	0.02	0.05
K_2O	0.07	0.00	0.02	0.00	0.00	0.00	0.00	0.00	0.00	0.00	0.00	0.00	0.01	0.00	0.00	0.00	0.00	0.01
NiO	0.11	0.07	0.03	0.04	0.07	0.02	0.05	0.01	0.04	0.06	0.01	0.10	0.08	0.03	0.08	0.02	0.15	0.10
Total	102.10	101.65	100.61	102.06	101.50	102.16	102.03	101.92	101.50	101.92	101.80	102.26	100.37	100.17	100.23	100.52	101.08	99.02
Si (4 O)	0.983	0.986	0.990	0.986	0.993	0.986	0.989	0.988	0.992	0.990	0.989	0.991	1.011	1.009	1.009	1.010	0.989	0.993
Ti	0.000	0.000	0.000	0.000	0.000	0.000	0.000	0.000	0.000	0.000	0.000	0.000	0.000	0.000	0.000	0.000	0.001	0.000
Al	0.000	0.000	0.002	0.000	0.001	0.000	0.000	0.000	0.000	0.001	0.000	0.000	0.000	0.000	0.000	0.000	0.001	0.001
Cr	0.000	0.000	0.000	0.000	0.000	0.000	0.001	0.000	0.000	0.001	0.000	0.000	0.000	0.000	0.000	0.001	0.001	0.000
Fe_2	0.439	0.500	0.499	0.502	0.503	0.514	0.511	0.543	0.531	0.516	0.502	0.441	0.385	0.380	0.371	0.364	0.375	0.398
Mn	0.011	0.010	0.011	0.012	0.010	0.012	0.013	0.016	0.014	0.010	0.011	0.009	0.006	0.006	0.007	0.006	0.008	0.007
Mg	1.556	1.509	1.501	1.507	1.494	1.494	1.489	1.460	1.462	1.486	1.502	1.562	1.582	1.594	1.603	1.608	1.631	1.601
Ca	0.005	0.006	0.005	0.005	0.004	0.006	0.006	0.005	0.006	0.005	0.005	0.004	0.001	0.001	0.001	0.001	0.002	0.002
Na	0.035	0.001	0.002	0.000	0.002	0.000	0.001	0.000	0.000	0.000	0.000	0.001	0.002	0.001	0.000	0.000	0.001	0.003
K	0.002	0.000	0.001	0.000	0.000	0.000	0.000	0.000	0.000	0.000	0.000	0.000	0.000	0.000	0.000	0.000	0.000	0.000
Ni	0.002	0.001	0.001	0.001	0.002	0.000	0.001	0.000	0.001	0.001	0.000	0.002	0.002	0.001	0.002	0.000	0.003	0.002
Total	3.035	3.014	3.011	3.013	3.008	3.013	3.011	3.012	3.007	3.010	3.010	3.010	2.990	2.992	2.991	2.990	3.010	3.008
X location	13.542	15.136	14.932	15.006	15.298	14.431	14.534	6.751	6.966	17.462	16.942	16.164	18.087	18.087	20.588	20.589	73.666	75.356
Y location	52.220	49.567	49.567	49.176	48.978	48.611	48.326	51.260	51.174	68.581	68.581	68.623	70.178	67.775	59.936	55.793	58.629	59.063
Crystal #		5	5			6	6	7	7	10	10	10						
Mg %	78	75	75	75	74	74	74	72	73	74	75	78	80	81	81	81	81	80
Fe %	22	25	25	25	25	25	25	27	26	26	25	22	20	19	19	18	19	20
Mn %	1	0	1	1	1	1	1	1	1	1	1	0	0	0	0	0	0	0

Table I.1: Olivine electron microprobe data.

I.2 Feldspar

Sample	SV1	SV1	SV1	SV1	SV1	SV1	SV1	SV1	SV1	SV1	SV1	SV1	SV1	SV1	SV1	SV1	SV1	SV1	SV1	SV1	SV1	SV1	SV1	SV1	SV1
Rock Type	MUG	MUG	MUG	MUG	MUG	MUG	MUG	MUG	MUG	MUG	MUG	MUG	MUG	MUG	MUG	MUG	MUG	MUG	MUG	MUG	MUG	MUG	MUG	MUG	MUG
Analysis	06-002	06-003	06-005	06-006	06-007	06-008	06-009	06-010	06-011	06-012	06-013	06-014	06-015	06-016	06-017	06-018	06-019	06-020	06-021	06-022	06-023	06-024	06-025	06-026	06-027
SiO_2	46.75	48.51	49.53	48.28	49.13	54.56	50.89	51.06	51.00	49.03	50.02	51.03	55.18	52.62	47.03	46.70	47.89	47.04	60.40	48.69	49.24	55.28	54.36	52.40	50.09
TiO_2																									
Al_2O_3	32.86	31.50	30.86	31.74	31.22	27.47	29.98	29.17	29.80	31.21	30.51	29.88	27.06	28.67	32.90	32.73	32.29	32.62	22.39	31.26	30.82	27.09	27.58	28.99	30.38
Cr_2O_3																									
FeO	0.63	0.59	0.60	0.71	0.65	0.81	0.83	0.94	0.80	0.73	0.80	0.74	0.73	0.77	0.55	0.72	0.69	0.67	0.95	0.86	0.78	0.77	0.78	0.72	0.73
MnO																									
MgO																									
CaO	16.84	15.29	14.94	15.89	15.45	10.97	13.92	13.43	13.82	15.32	14.64	13.69	10.63	12.45	17.35	17.35	16.56	17.17	5.57	15.71	15.62	10.34	11.26	12.75	14.59
Na_2O	1.77	2.54	3.13	2.41	2.95	5.19	3.46	3.67	3.61	2.79	3.18	3.64	5.33	4.41	1.89	1.79	2.20	1.93	6.84	2.71	2.84	5.56	5.18	4.19	3.19
K_2O	0.07	0.12	0.16	0.11	0.14	0.38	0.23	0.30	0.33	0.13	0.16	0.18	0.36	0.28	0.07	0.06	0.09	0.09	2.49	0.13	0.16	0.37	0.37	0.25	0.17
NiO																									
BaO	0.03	0.03	0.03	0.05	0.00	0.03	0.00	0.01	0.02	0.00	0.00	0.01	0.02	0.01	0.01	0.04	0.01	0.03	0.08	0.02	0.01	0.04	0.02	0.01	0.00
SrO	0.16	0.15	0.16	0.13	0.18	0.12	0.16	0.15	0.14	0.16	0.19	0.16	0.16	0.16	0.14	0.17	0.15	0.18	0.08	0.18	0.16	0.15	0.14	0.19	0.23
Total	99.11	98.71	99.41	99.33	99.71	99.51	99.47	98.73	99.53	99.37	99.50	99.33	99.47	99.37	99.95	99.56	99.87	99.72	98.80	99.55	99.62	99.60	99.68	99.50	99.38
Si (32 O)	8.696	9.014	9.142	8.941	9.056	9.951	9.360	9.460	9.381	9.061	9.218	9.389	10.049	9.651	8.687	8.671	8.834	8.714	11.017	9.004	9.093	10.056	9.910	9.601	9.240
Ti																									
Al	7.205	6.898	6.714	6.928	6.783	5.905	6.500	6.370	6.461	6.799	6.628	6.481	5.810	6.198	7.163	7.163	7.021	7.122	4.813	6.816	6.707	5.808	5.927	6.260	6.605
Cr																									
Fe_2	0.098	0.092	0.093	0.111	0.100	0.123	0.127	0.146	0.123	0.113	0.123	0.114	0.111	0.118	0.086	0.112	0.106	0.103	0.145	0.132	0.120	0.117	0.119	0.111	0.113
Mn																									
Mg																									
Ca	3.356	3.044	2.956	3.153	3.051	2.143	2.743	2.667	2.724	3.034	2.891	2.699	2.074	2.447	3.434	3.452	3.274	3.407	1.089	3.114	3.089	2.016	2.199	2.504	2.885
Na	0.638	0.914	1.120	0.867	1.053	1.834	1.233	1.319	1.288	0.999	1.137	1.297	1.882	1.570	0.675	0.646	0.786	0.694	2.419	0.972	1.015	1.962	1.830	1.489	1.142
K	0.017	0.028	0.038	0.025	0.033	0.088	0.054	0.070	0.078	0.031	0.037	0.041	0.084	0.065	0.016	0.014	0.021	0.020	0.579	0.030	0.039	0.087	0.086	0.059	0.039
Ni																									
Ba	0.002	0.002	0.002	0.003	0.000	0.002	0.000	0.001	0.001	0.000	0.000	0.001	0.001	0.001	0.001	0.003	0.001	0.002	0.006	0.001	0.001	0.003	0.002	0.001	0.000
Sr	0.017	0.016	0.017	0.014	0.020	0.013	0.017	0.016	0.015	0.018	0.021	0.017	0.017	0.017	0.015	0.018	0.016	0.019	0.009	0.019	0.017	0.016	0.014	0.020	0.024
Total	20.029	20.008	20.080	20.041	20.095	20.058	20.035	20.049	20.072	20.055	20.055	20.039	20.029	20.067	20.077	20.078	20.058	20.082	20.076	20.089	20.081	20.064	20.085	20.043	20.048
X location	4.814	4.850	4.974	5.107	5.144	5.274	8.169	8.232	8.279	8.348	8.412	8.436	8.462	8.456	16.205	16.016	15.904	15.830	15.646	11.765	14.130	14.016	13.200	13.530	12.747
Y location	55.207	55.243	55.400	55.484	55.552	55.597	53.138	53.147	53.142	53.142	53.142	53.142	53.142	53.182	43.963	43.963	43.945	43.945	43.923	43.923	53.441	54.932	57.712	59.710	62.702
Crystal #	1	1	1	1	1	1	2	2	2	2	2	2	2	2	3	3	3	3							
Comments						Rim	Core							Rim	Core			Rim							
An	84	76	72	78	74	53	68	66	67	75	71	67	51	60	83	84	80	83	27	76	75	50	53	62	71
Ab	16	23	27	21	25	45	31	33	31	25	28	32	47	38	16	16	19	17	59	24	25	48	44	37	28
Or	0	1	1	1	1	2	1	2	2	1	1	1	2	2	0	0	1	0	14	1	1	2	2	1	1

Table I.2: Feldspar electron microprobe data. An = mole % anorthite; Ab = albite, Or = orthoclase.

Sample	SV1	SV1	SV1	SV1	SV1	SV1	SV1	SV1	SV1	SV1	SV1	SV1	SV2	SV2	SV2	SV2	SV2	SV2	SV2	SV2	SV2	SV2	SV2	SV2	SV2	SV2
Rock Type	MUG	MUG	MUG	MUG	MUG	MUG	MUG	MUG	MUG	MUG	MUG	MUG	TRAC	TRAC	TRAC	TRAC	TRAC	TRAC	TRAC	TRAC	TRAC	TRAC	TRAC	TRAC	TRAC	TRAC
Analysis	06-028	06-029	06-030	06-031	06-032	06-033	06-034	06-036	06-037	06-038	06-039	06-040	01 -008	01 -009	01 -010	01 -011	01 -012	01 -013	01 -022	01 -023	01 -024	01 -025	01 -026	01 -027	01 -028	01 -029
SiO_2	55.10	47.79	49.39	50.39	50.76	54.94	52.73	50.33	47.31	49.76	49.81	50.10	57.48	49.08	59.15	59.69	58.53	59.96	63.35	64.91	63.16	59.91	59.35	59.47	60.06	65.06
TiO_2													0.00	0.00	0.00	0.00	0.00	0.00	0.00	0.00	0.00	0.00	0.00	0.00	0.00	0.00
Al_2O_3	27.17	32.12	30.79	30.29	29.74	27.06	28.42	30.41	32.43	30.83	30.76	30.43	26.22	31.73	25.03	24.74	25.56	24.79	23.10	22.54	23.31	24.82	25.24	25.10	24.57	22.07
Cr_2O_3													0.03	0.00	0.00	0.00	0.00	0.00	0.00	0.00	0.02	0.00	0.04	0.00	0.00	0.00
FeO	0.58	0.80	0.77	0.75	0.82	0.86	0.89	0.72	0.80	0.71	0.79	0.78	0.35	0.28	0.22	0.21	0.25	0.20	0.20	0.19	0.12	0.11	0.14	0.14	0.17	0.16
MnO													0.00	0.00	0.00	0.00	0.01	0.00	0.00	0.00	0.00	0.00	0.00	0.00	0.00	0.00
MgO													0.01	0.00	0.00	0.00	0.00	0.01	0.00	0.00	0.00	0.00	0.00	0.01	0.00	0.01
CaO	10.64	16.45	14.94	14.31	13.97	10.61	12.39	14.15	17.08	15.09	15.07	14.71	8.19	15.01	6.90	6.67	7.08	6.08	4.16	3.47	4.42	6.13	6.46	6.63	6.48	3.31
Na_2O	5.34	2.13	2.98	3.36	3.83	5.29	4.41	3.44	1.93	3.15	3.22	3.32	6.60	2.77	7.27	7.38	6.70	7.35	8.39	9.14	8.53	7.32	7.10	7.46	7.46	9.44
K_2O	0.40	0.12	0.16	0.17	0.21	0.37	0.26	0.18	0.11	0.13	0.14	0.18	0.24	0.06	0.30	0.33	0.25	0.32	0.47	0.57	0.41	0.30	0.28	0.32	0.37	0.64
NiO													0.00	0.00	0.03	0.00	0.02	0.02	0.00	0.00	0.00	0.00	0.01	0.05	0.00	0.00
BaO	0.04	0.01	0.00	0.00	0.00	0.03	0.04	0.00	0.00	0.02	0.00	0.02														
SrO	0.15	0.12	0.16	0.20	0.17	0.14	0.19	0.18	0.17	0.18	0.18	0.17														
Total	99.41	99.54	99.18	99.47	99.50	99.30	99.32	99.40	99.82	99.86	99.98	99.71	99.12	98.92	98.88	99.02	98.40	98.73	99.66	100.82	99.96	98.58	98.63	99.17	99.11	100.69
Si (32 O)	10.037	8.846	9.139	9.279	9.351	10.030	9.682	9.270	8.753	9.149	9.154	9.221	10.393	9.064	10.671	10.742	10.598	10.792	11.226	11.364	11.172	10.792	10.700	10.691	10.791	11.414
Ti													0.000	0.000	0.000	0.000	0.000	0.000	0.000	0.000	0.000	0.000	0.000	0.000	0.000	0.000
Al	5.835	7.007	6.715	6.575	6.459	5.823	6.150	6.602	7.072	6.683	6.662	6.603	5.588	6.906	5.323	5.249	5.456	5.259	4.824	4.652	4.860	5.269	5.364	5.317	5.203	4.564
Cr													0.004	0.000	0.000	0.000	0.000	0.000	0.000	0.000	0.002	0.000	0.006	0.000	0.000	0.000
Fe_2	0.089	0.124	0.119	0.116	0.126	0.132	0.136	0.111	0.124	0.109	0.122	0.120	0.052	0.043	0.033	0.031	0.037	0.030	0.029	0.027	0.018	0.017	0.021	0.020	0.026	0.024
Mn													0.000	0.000	0.000	0.000	0.001	0.000	0.000	0.000	0.000	0.000	0.000	0.000	0.000	0.000
Mg													0.001	0.000	0.000	0.000	0.000	0.003	0.000	0.000	0.000	0.001	0.000	0.001	0.000	0.002
Ca	2.076	3.263	2.961	2.824	2.758	2.077	2.437	2.792	3.387	2.972	2.968	2.902	1.587	2.969	1.333	1.287	1.373	1.173	0.789	0.652	0.837	1.183	1.248	1.276	1.247	0.622
Na	1.887	0.765	1.071	1.199	1.367	1.874	1.571	1.227	0.692	1.123	1.148	1.184	2.315	0.990	2.541	2.576	2.353	2.566	2.884	3.101	2.924	2.555	2.482	2.601	2.597	3.212
K	0.092	0.027	0.038	0.039	0.048	0.086	0.061	0.042	0.025	0.030	0.034	0.042	0.056	0.014	0.069	0.076	0.059	0.074	0.106	0.128	0.093	0.068	0.065	0.074	0.085	0.142
Ni													0.000	0.000	0.004	0.000	0.003	0.003	0.000	0.000	0.000	0.000	0.001	0.007	0.000	0.000
Ba	0.003	0.001	0.000	0.000	0.000	0.002	0.003	0.000	0.000	0.001	0.000	0.001														
Sr	0.015	0.013	0.017	0.021	0.018	0.015	0.020	0.019	0.018	0.019	0.019	0.018														
Total	20.035	20.047	20.059	20.053	20.128	20.039	20.060	20.063	20.070	20.086	20.106	20.091	19.996	19.986	19.973	19.960	19.880	19.899	19.857	19.924	19.906	19.885	19.888	19.988	19.949	19.981
X location	13.132	13.221	13.095	13.058	13.013	12.991	12.960	17.120	14.159	14.159	12.291	11.919	5.402	6.076	6.147	6.219	6.326	6.468	3.308	3.308	3.308	3.306	3.307	3.307	3.382	3.323
Y location	65.097	68.642	68.642	68.626	68.626	68.626	68.626	71.114	71.721	73.377	73.331	73.226	51.332	52.593	52.593	52.540	52.517	52.526	55.977	56.009	56.036	56.147	56.262	56.423	56.571	56.732
Crystal #		4	4	4	4	4	4							2	2	2	2	2	4	4	4	4	4	4	4	4
Comments		Core												core					Rim			Core	Core			Rim
An	51	80	73	70	66	51	60	69	83	72	72	70	40	75	34	33	36	31	21	17	22	31	33	32	32	16
Ab	47	19	26	30	33	46	39	30	17	27	28	29	58	25	64	65	62	67	76	80	76	67	65	66	66	81
Or	2	1	1	1	1	2	2	1	1	1	1	1	1	0	2	2	2	2	3	3	2	2	2	2	2	4

Sample	SV2	SV2	SV2	SV2	SV2	SV2	SV2	SV2	SV2	SV2	SV2	SV2	SV2	SV2	SV2	SV2	SV2	SV2	SV2	SV2	SV2	SV2	SV2	SV2	SV2	SV2	SV2
Rock Type	TRAC	TRAC	XEN	XEN	XEN	XEN	XEN	XEN	XEN	XEN	XEN	XEN	XEN	XEN	XEN	XEN	XEN	XEN	XEN	XEN	XEN	XEN	XEN	XEN	XEN	XEN	XEN
Analysis	01 -030	01 -032	01 -044	01 -045	01 -046	01 -047	02-007	02-008	02-009	02-027	02-028	02-029	02-030	02-045	02-048	02-049	02-050	02-051	02-052	02-053	02-054	02-056	02-059	02-060	02-063	02-066	02-067
SiO_2	67.62	67.10	63.84	64.28	62.48	58.52	48.33	48.15	48.85	61.10	55.29	57.50	60.37	55.72	54.30	56.84	49.59	49.88	50.69	50.49	49.93	55.11	55.79	53.92	56.16	56.62	55.39
TiO_2	0.00	0.00	0.00	0.01	0.00	0.00	0.00	0.04	0.00	0.00	0.00	0.00	0.00	0.06	0.04	0.00	0.00	0.03	0.03	0.00	0.00	0.00	0.00	0.00	0.00	0.02	0.00
Al_2O_3	20.51	20.73	22.56	22.86	23.29	25.46	31.74	31.91	31.82	23.99	27.11	26.08	24.19	27.01	28.68	26.72	31.59	31.29	30.79	31.04	31.24	27.76	27.12	28.58	27.15	26.53	27.45
Cr_2O_3	0.00	0.00	0.00	0.03	0.03	0.00	0.04	0.00	0.00	0.00	0.00	0.00	0.01	0.00	0.03	0.00	0.00	0.00	0.01	0.03	0.02	0.00	0.00	0.02	0.02	0.03	0.00
FeO	0.18	0.19	0.17	0.15	0.16	0.15	0.46	0.51	0.41	0.31	0.30	0.24	0.30	0.36	0.27	0.74	0.40	0.44	0.48	0.53	0.52	0.33	0.27	0.37	0.51	0.41	0.39
MnO	0.00	0.00	0.00	0.01	0.00	0.03	0.00	0.03	0.00	0.02	0.00	0.00	0.02	0.00	0.00	0.03	0.00	0.00	0.00	0.03	0.01	0.01	0.00	0.03	0.00	0.00	0.00
MgO	0.00	0.00	0.00	0.00	0.00	0.00	0.03	0.05	0.00	0.01	0.00	0.00	0.00	0.00	0.01	0.00	0.00	0.00	0.00	0.01	0.01	0.03	0.00	0.00	0.00	0.01	0.01
CaO	1.52	1.87	3.82	3.81	4.49	7.78	15.71	15.90	15.00	5.46	9.45	8.22	5.72	8.80	10.59	9.01	13.44	13.24	12.71	12.64	13.94	10.10	9.59	11.08	9.17	8.52	9.93
Na_2O	9.75	9.69	9.10	7.45	8.47	7.00	2.69	2.48	2.76	8.18	5.80	6.76	8.03	5.89	5.10	6.41	2.85	2.92	3.30	3.20	3.09	5.74	6.10	5.17	6.12	6.32	5.95
K_2O	0.91	0.90	0.58	0.57	0.42	0.28	0.08	0.10	0.07	0.44	0.18	0.25	0.36	0.19	0.14	0.22	0.03	0.06	0.08	0.06	0.07	0.16	0.19	0.13	0.18	0.23	0.18
NiO	0.02	0.03	0.00	0.01	0.00	0.00	0.00	0.01	0.01	0.00	0.00	0.00	0.00	0.00	0.03	0.01	0.01	0.00	0.02	0.01	0.01	0.00	0.00	0.00	0.03	0.00	0.02
BaO																											
SrO																											
Total	100.50	100.51	100.08	99.18	99.34	99.21	99.06	99.18	98.92	99.50	98.14	99.04	99.00	98.03	99.18	99.98	97.92	97.85	98.10	98.04	98.84	99.24	99.06	99.28	99.34	98.67	99.33
Si (32 O)	11.804	11.732	11.287	11.375	11.133	10.550	8.954	8.916	9.031	10.925	10.131	10.406	10.858	10.198	9.871	10.242	9.195	9.251	9.368	9.336	9.205	10.014	10.140	9.821	10.172	10.297	10.060
Ti	0.000	0.000	0.000	0.001	0.000	0.000	0.000	0.005	0.000	0.000	0.000	0.000	0.000	0.009	0.005	0.000	0.000	0.004	0.004	0.000	0.000	0.000	0.000	0.000	0.000	0.002	0.000
Al	4.220	4.273	4.701	4.767	4.891	5.409	6.930	6.966	6.934	5.056	5.856	5.563	5.129	5.826	6.145	5.676	6.905	6.840	6.706	6.764	6.790	5.946	5.810	6.137	5.797	5.688	5.876
Cr	0.000	0.000	0.000	0.004	0.004	0.000	0.005	0.001	0.000	0.000	0.000	0.000	0.001	0.000	0.004	0.000	0.000	0.000	0.001	0.004	0.004	0.000	0.000	0.003	0.003	0.004	0.000
Fe_2	0.026	0.027	0.025	0.022	0.024	0.023	0.071	0.079	0.064	0.046	0.046	0.036	0.045	0.056	0.041	0.112	0.062	0.068	0.075	0.083	0.081	0.050	0.042	0.056	0.078	0.062	0.060
Mn	0.000	0.000	0.000	0.002	0.001	0.004	0.000	0.004	0.000	0.002	0.000	0.000	0.003	0.000	0.000	0.004	0.000	0.000	0.000	0.004	0.001	0.001	0.000	0.004	0.000	0.000	0.000
Mg	0.000	0.000	0.001	0.000	0.000	0.000	0.007	0.013	0.000	0.002	0.000	0.000	0.000	0.000	0.001	0.000	0.000	0.001	0.000	0.002	0.002	0.007	0.000	0.000	0.000	0.002	0.003
Ca	0.284	0.351	0.724	0.723	0.857	1.503	3.118	3.156	2.971	1.046	1.856	1.593	1.101	1.725	2.063	1.740	2.671	2.630	2.517	2.505	2.754	1.965	1.867	2.162	1.780	1.660	1.933
Na	3.299	3.287	3.119	2.556	2.927	2.448	0.965	0.890	0.989	2.836	2.060	2.372	2.799	2.091	1.797	2.240	1.025	1.050	1.183	1.148	1.106	2.022	2.150	1.824	2.148	2.228	2.095
K	0.202	0.200	0.131	0.129	0.096	0.063	0.019	0.023	0.016	0.101	0.043	0.057	0.082	0.044	0.033	0.050	0.008	0.014	0.018	0.015	0.017	0.038	0.044	0.029	0.042	0.052	0.042
Ni	0.003	0.004	0.000	0.002	0.000	0.000	0.000	0.001	0.001	0.000	0.000	0.001	0.000	0.000	0.004	0.001	0.002	0.000	0.003	0.001	0.001	0.000	0.000	0.000	0.004	0.001	0.002
Ba																											
Sr																											
Total	19.836	19.874	19.988	19.581	19.932	20.001	20.070	20.053	20.005	20.015	19.992	20.027	20.019	19.948	19.965	20.065	19.868	19.858	19.875	19.862	19.959	20.043	20.052	20.036	20.023	19.995	20.070
X location	4.539	4.808	10.943	10.943	12.290	15.764	15.402	15.658	15.281	15.997	16.098	16.103	15.785	11.941	11.793	11.683	11.631	11.585	11.585	11.664	11.683	12.170	12.098	12.089	13.312	14.078	17.561
Y location	62.016	62.016	72.331	72.331	71.295	67.554	48.339	48.339	48.273	49.454	49.291	49.160	49.351	57.075	57.959	58.727	59.431	59.500	59.602	59.667	59.748	59.944	60.211	60.448	60.869	60.930	60.937
Crystal #	5	5	7	7						2	2	2	2				5	5	5	5	5						
Comments										Rim	Rim	Rim	Rim														
An	7	9	18	21	22	37	76	78	75	26	47	40	28	45	53	43	72	71	68	68	71	49	46	54	45	42	47
Ab	87	86	78	75	75	61	24	22	25	71	52	59	70	54	46	56	28	28	32	31	29	50	53	45	54	57	51
Or	5	5	3	4	2	2	0	1	0	3	1	1	2	1	1	1	0	0	0	0	0	1	1	1	1	1	1

Sample	SV2	SV2	SV2	SV2	SV2	SV2	SV2	SV2	SV2	SV2	SV2	SV2	SV2	SV2	SV2	SV2	SV2	SV2	SV2	SV2	SV2	SV2	SV2	SV2	SV2	SV2	SV2	SV2
Rock Type	XEN	XEN	XEN	XEN	XEN	XEN	TRAC	TRAC	TRAC	TRAC	TRAC	TRAC	TRAC	TRAC	TRAC	TRAC	TRAC	TRAC	TRAC	TRAC	TRAC	TRAC	TRAC	TRAC	TRAC	TRAC	TRAC	TRAC
Analysis	02-069	02-071	02-073	02-075	02-076	02-080	02-081	02-082	02-083	02-084	02-085	02-086	02-087	02-088	02-089	02-090	02-091	02-092	02-093	02-094	02-095	02-096	02-098	02-099	02-100	02-101	02-102	02-103
SiO_2	55.43	55.07	54.47	52.95	52.89	54.52	60.30	61.97	62.25	60.25	62.58	61.82	61.57	60.83	65.03	64.81	60.41	64.70	66.45	65.46	66.29	65.42	65.80	64.99	61.98	61.71	60.51	60.31
TiO_2	0.00	0.00	0.00	0.02	0.00	0.00	0.00	0.00	0.00	0.00	0.00	0.00	0.03	0.01	0.00	0.00	0.00	0.00	0.01	0.00	0.04	0.00	0.00	0.00	0.02	0.02	0.00	0.00
Al_2O_3	27.73	27.43	27.98	28.03	28.18	27.74	23.89	22.44	22.58	23.23	22.58	23.16	23.02	23.06	21.03	21.08	23.86	21.13	19.91	20.46	20.17	20.76	20.11	20.87	22.71	22.95	23.68	24.01
Cr_2O_3	0.00	0.02	0.01	0.04	0.00	0.00	0.00	0.00	0.00	0.03	0.01	0.00	0.00	0.00	0.00	0.00	0.00	0.00	0.00	0.01	0.00	0.03	0.01	0.01	0.02	0.00	0.00	0.01
FeO	0.30	0.55	0.43	0.31	0.35	0.45	0.12	0.09	0.14	0.14	0.19	0.13	0.14	0.12	0.15	0.21	0.20	0.18	0.20	0.18	0.18	0.24	0.19	0.14	0.14	0.15	0.18	0.17
MnO	0.00	0.04	0.04	0.02	0.00	0.00	0.01	0.02	0.01	0.01	0.01	0.00	0.01	0.01	0.03	0.00	0.01	0.00	0.00	0.00	0.00	0.01	0.03	0.00	0.00	0.00	0.00	0.02
MgO	0.00	0.08	0.02	0.02	0.01	0.01	0.01	0.00	0.00	0.00	0.00	0.00	0.00	0.00	0.00	0.00	0.00	0.00	0.00	0.00	0.00	0.01	0.00	0.00	0.00	0.00	0.00	0.00
CaO	9.83	10.37	10.88	11.22	10.69	10.19	5.37	3.99	4.11	5.18	4.05	4.82	4.65	5.02	2.36	2.32	5.56	2.58	1.27	1.87	1.49	2.09	1.54	2.31	4.21	4.50	5.31	5.41
Na_2O	5.80	5.71	5.28	4.77	5.11	5.49	8.01	8.78	8.79	8.05	8.85	8.49	8.38	8.22	9.56	9.75	8.01	9.34	9.84	9.68	9.83	9.71	9.64	9.49	8.57	8.35	7.89	8.03
K_2O	0.15	0.19	0.16	0.16	0.18	0.17	0.39	0.53	0.56	0.47	0.54	0.45	0.50	0.50	0.89	0.84	0.36	0.84	1.15	0.95	1.06	0.87	1.10	0.89	0.56	0.44	0.40	0.30
NiO	0.00	0.02	0.00	0.00	0.00	0.01	0.02	0.00	0.03	0.04	0.03	0.00	0.00	0.00	0.05	0.05	0.01	0.00	0.03	0.00	0.00	0.00	0.03	0.00	0.00	0.02	0.00	0.00
BaO																												
SrO																												
Total	99.24	99.46	99.27	97.54	97.43	98.58	98.12	97.82	98.46	97.38	98.84	98.87	98.31	97.77	99.08	99.08	98.41	98.77	98.86	98.62	99.06	99.13	98.44	98.70	98.19	98.13	97.97	98.27
Si (32 O)	10.057	10.011	9.920	9.818	9.814	9.979	10.918	11.214	11.200	10.991	11.216	11.090	11.103	11.046	11.575	11.548	10.913	11.550	11.818	11.685	11.768	11.630	11.759	11.602	11.178	11.135	10.962	10.902
Ti	0.000	0.000	0.000	0.003	0.000	0.000	0.000	0.000	0.000	0.000	0.000	0.000	0.004	0.001	0.000	0.000	0.000	0.000	0.001	0.000	0.005	0.000	0.000	0.000	0.002	0.002	0.000	0.000
Al	5.929	5.877	6.005	6.126	6.164	5.985	5.099	4.788	4.788	4.996	4.770	4.897	4.894	4.935	4.412	4.427	5.081	4.445	4.173	4.306	4.220	4.350	4.236	4.392	4.827	4.880	5.057	5.115
Cr	0.000	0.002	0.001	0.006	0.000	0.000	0.000	0.000	0.000	0.005	0.001	0.000	0.000	0.000	0.000	0.000	0.000	0.000	0.000	0.001	0.000	0.004	0.001	0.002	0.002	0.000	0.000	0.002
Fe_2	0.045	0.083	0.066	0.047	0.055	0.068	0.018	0.013	0.021	0.021	0.028	0.020	0.021	0.018	0.022	0.032	0.030	0.027	0.029	0.027	0.027	0.035	0.028	0.020	0.020	0.022	0.027	0.026
Mn	0.000	0.006	0.007	0.003	0.000	0.000	0.001	0.004	0.002	0.001	0.001	0.000	0.001	0.002	0.004	0.000	0.002	0.000	0.001	0.000	0.000	0.002	0.004	0.000	0.000	0.000	0.000	0.004
Mg	0.000	0.020	0.005	0.005	0.003	0.003	0.002	0.000	0.000	0.000	0.000	0.000	0.000	0.000	0.000	0.001	0.000	0.000	0.000	0.000	0.000	0.001	0.000	0.000	0.000	0.000	0.000	0.000
Ca	1.910	2.019	2.123	2.229	2.126	1.999	1.041	0.773	0.793	1.012	0.778	0.926	0.899	0.977	0.449	0.443	1.076	0.493	0.242	0.358	0.284	0.398	0.294	0.441	0.812	0.871	1.031	1.047
Na	2.041	2.012	1.866	1.715	1.839	1.948	2.811	3.079	3.066	2.847	3.076	2.954	2.932	2.895	3.298	3.368	2.807	3.234	3.393	3.352	3.383	3.347	3.340	3.286	2.996	2.921	2.772	2.816
K	0.034	0.043	0.037	0.037	0.043	0.040	0.091	0.122	0.129	0.109	0.124	0.102	0.116	0.116	0.201	0.192	0.082	0.191	0.261	0.217	0.240	0.198	0.252	0.202	0.129	0.101	0.091	0.068
Ni	0.000	0.003	0.000	0.001	0.000	0.002	0.003	0.000	0.004	0.005	0.005	0.000	0.000	0.000	0.007	0.008	0.001	0.000	0.004	0.000	0.000	0.000	0.004	0.000	0.000	0.003	0.000	0.000
Ba																												
Sr																												
Total	20.016	20.077	20.029	19.990	20.045	20.023	19.984	19.993	20.003	19.987	19.999	19.990	19.970	19.990	19.969	20.019	19.991	19.940	19.922	19.946	19.928	19.965	19.918	19.945	19.968	19.934	19.941	19.981
X location	17.531	17.588	17.647	18.057	18.057	18.091	24.165	24.304	24.327	24.354	24.395	24.395	24.409	24.508	24.508	24.553	24.876	24.876	24.876	24.884	24.851	24.851	23.645	23.645	23.645	23.645	23.645	23.645
Y location	61.244	61.565	61.996	62.374	62.374	62.542	66.612	66.744	66.631	66.535	66.448	66.374	66.291	66.152	66.022	65.953	60.666	60.564	60.496	60.382	60.315	60.256	51.199	51.129	50.976	50.867	50.716	50.641
Crystal #								7	7	7	7	7	7	7	7	7	8	8	8	8	8	8	9	9	9	9	9	9
Comments								Core								Rim	Core					Rim	Rim				Core	
An	48	50	53	56	53	50	26	19	20	26	20	23	23	25	11	11	27	13	6	9	7	10	8	11	21	22	26	27
Ab	51	49	46	43	46	49	71	77	77	72	77	74	74	73	84	84	71	83	87	85	87	85	86	84	76	75	71	72
Or	1	1	1	1	1	1	2	3	3	3	3	3	3	3	5	5	2	5	7	6	6	5	6	5	3	3	2	2

Sample	SV2	SV2	SV2	SV2	SV2	SV2	SV2	SV2	SV2	SV2	SV2	SV2	SV2	SV2
Rock Type	TRAC	TRAC	TRAC	TRAC	TRAC	TRAC	TRAC	TRAC	TRAC	TRAC	TRAC	TRAC	TRAC	TRAC
Analysis	02-104	02-105	02-106	04-091	04-092	04-093	04-094	04-095	04-096	04-097	04-098	04-099	04-100	04-101
SiO_2	61.46	63.16	65.14	61.57	61.43	60.38	63.86	65.69	65.75	59.48	59.94	60.09	60.86	61.31
TiO_2	0.03	0.00	0.02											
Al_2O_3	22.86	21.94	20.47	22.99	22.95	23.84	21.62	20.35	20.12	23.91	24.28	24.02	23.78	22.39
Cr_2O_3	0.02	0.02	0.00											
FeO	0.17	0.15	0.19	0.11	0.14	0.15	0.10	0.16	0.16	0.16	0.16	0.13	0.16	0.15
MnO	0.00	0.02	0.03											
MgO	0.00	0.00	0.00											
CaO	4.34	3.44	1.87	4.59	4.54	5.57	3.13	1.84	1.55	5.85	6.08	5.96	5.54	4.44
Na_2O	8.56	9.15	9.90	8.43	8.43	7.92	9.22	9.65	9.94	7.90	7.84	7.85	8.29	8.38
K_2O	0.41	0.59	0.97	0.43	0.47	0.41	0.70	1.03	1.13	0.24	0.25	0.28	0.33	0.44
NiO	0.02	0.00	0.01											
BaO				0.13	0.11	0.05	0.06	0.14	0.14	0.03	0.06	0.04	0.10	0.10
SrO				0.71	0.66	0.65	0.21	0.04	0.06	0.50	0.59	0.48	0.48	0.32
Total	97.86	98.45	98.61	98.97	98.74	98.96	98.91	98.89	98.84	98.07	99.19	98.83	99.54	97.53
Si (32 O)	11.126	11.342	11.650	11.087	11.086	10.896	11.421	11.708	11.734	10.830	10.802	10.850	10.916	11.165
Ti	0.004	0.000	0.003											
Al	4.877	4.644	4.315	4.880	4.881	5.070	4.558	4.274	4.232	5.132	5.156	5.112	5.029	4.806
Cr	0.002	0.002	0.000											
Fe_2	0.025	0.022	0.028	0.016	0.022	0.023	0.015	0.023	0.024	0.024	0.024	0.020	0.024	0.023
Mn	0.000	0.002	0.005											
Mg	0.001	0.000	0.000											
Ca	0.843	0.661	0.358	0.886	0.878	1.076	0.600	0.352	0.296	1.142	1.174	1.154	1.065	0.867
Na	3.005	3.186	3.434	2.943	2.950	2.770	3.196	3.335	3.440	2.788	2.741	2.747	2.884	2.961
K	0.094	0.135	0.222	0.099	0.108	0.095	0.161	0.234	0.257	0.056	0.057	0.065	0.076	0.101
Ni	0.003	0.000	0.002	0.003	0.005	0.009	0.007	0.003	0.005	0.010	0.010	0.002	0.004	0.003
Ba				0.059	0.033	0.075	0.069	0.068	0.022	0.004	0.006	0.053	0.061	0.050
Sr														
Total	19.980	19.995	20.018	19.994	20.003	20.002	19.978	19.939	19.998	20.026	20.019	20.000	20.050	19.963
X location	23.645	23.645	23.645	23.573	23.573	23.573	23.573	23.573	23.688	24.848	25.048	25.192	25.376	25.418
Y location	50.529	50.436	50.289	50.702	50.766	50.886	51.032	51.123	51.192	60.873	60.873	60.873	60.873	60.831
Crystal #	9	9	9	15	15	15	15	15	15	16	16	16	16	16
Comments			Rim	Core					Rim	Core				
An	21	17	9	23	22	27	15	9	7	29	30	29	26	22
Ab	76	80	86	75	75	70	81	85	86	70	69	69	72	75
Or	2	3	6	3	3	2	4	6	6	1	1	2	2	3

Sample	SV2	SV2	SV2	SV2	SV2	SV2	SV2	SV2	SV2	SV2	SV2	SV2	SV2	SV2
Rock Type	TRAC	TRAC	TRAC	TRAC	TRAC	TRAC	TRAC	TRAC	TRAC	TRAC	TRAC	TRAC	TRAC	TRAC
Analysis	04-102	04-103	04-104	04-105	04-106	04-107	04-108	04-109	04-110	04-111	04-112	04-113	04-114	04-115
SiO_2	66.63	60.80	61.24	58.00	61.13	60.27	64.35	64.52	54.95	54.79	55.27	64.14	64.76	65.11
TiO_2														
Al_2O_3	19.98	23.84	23.54	25.54	23.32	24.21	21.62	21.41	27.75	27.98	27.58	21.79	21.00	21.15
Cr_2O_3														
FeO	0.22	0.08	0.10	0.13	0.16	0.12	0.10	0.24	0.11	0.18	0.17	0.19	0.19	0.17
MnO														
MgO														
CaO	1.34	5.75	5.42	7.77	5.30	6.23	3.15	2.88	10.63	10.69	10.25	3.18	2.15	2.23
Na_2O	10.02	8.15	8.27	6.88	8.31	7.89	9.40	9.33	5.49	5.53	5.81	9.59	9.98	9.99
K_2O	1.06	0.40	0.43	0.30	0.46	0.39	0.75	0.78	0.10	0.12	0.12	0.44	0.53	0.52
NiO														
BaO	0.18	0.04	0.02	0.03	0.07	0.05	0.10	0.16	0.02	0.04	0.02	0.05	0.11	0.09
SrO	0.06	0.28	0.24	0.41	0.30	0.29	0.12	0.23	0.14	0.16	0.13	0.30	0.37	0.39
Total	99.49	99.35	99.26	99.06	99.04	99.45	99.60	99.55	99.19	99.49	99.35	99.67	99.08	99.65
Si (32 O)	11.799	10.911	10.983	10.504	10.999	10.823	11.434	11.475	9.995	9.951	10.037	11.393	11.553	11.548
Ti														
Al	4.171	5.043	4.976	5.451	4.946	5.123	4.529	4.489	5.951	5.989	5.903	4.563	4.416	4.421
Cr														
Fe_2	0.033	0.012	0.015	0.020	0.024	0.018	0.015	0.036	0.017	0.027	0.025	0.028	0.028	0.025
Mn														
Mg														
Ca	0.254	1.106	1.042	1.508	1.021	1.199	0.601	0.549	2.071	2.081	1.995	0.605	0.410	0.425
Na	3.442	2.836	2.876	2.417	2.899	2.746	3.239	3.217	1.936	1.947	2.045	3.302	3.451	3.434
K	0.240	0.092	0.098	0.070	0.106	0.089	0.171	0.178	0.024	0.028	0.029	0.100	0.121	0.117
Ni	0.007	0.007	0.013	0.003	0.001	0.002	0.005	0.004	0.007	0.011	0.001	0.003	0.001	0.003
Ba	0.049	0.034	0.006	0.029	0.025	0.043	0.031	0.031	0.012	0.023	0.014	0.017	0.014	0.031
Sr														
Total	19.956	20.032	20.016	20.014	20.031	20.033	20.007	19.978	20.009	20.042	20.049	20.026	20.025	20.017
X location	25.521	17.729	17.729	17.729	17.729	17.729	17.729	17.729	15.609	15.609	15.609	15.609	15.609	15.609
Y location	60.831	74.794	74.869	74.944	74.991	75.115	75.178	75.232	72.038	72.159	72.232	72.300	72.385	72.460
Crystal #	16	17	17	17	17	17	17	17	18	18	18	18	18	18
Comments	Rim	Core						Rim	Core					
An	6	27	26	38	25	30	15	14	51	51	49	15	10	11
Ab	87	70	72	61	72	68	81	82	48	48	50	82	87	86
Or	6	2	2	2	3	2	4	5	1	1	1	2	3	3

Sample	SV2	SV2	SV10	SV10	SV10	SV10	SV10	SV10	SV10	SV10	SV10	SV10	SV10	SV10	SV10	SV10	SV10	SV10	SV10	SV12	SV12	SV12	SV12	SV12	SV12	SV12	SV12	SV12
Rock Type	TRAC	TRAC	TRAC	TRAC	TRAC	TRAC	TRAC	TRAC	TRAC	TRAC	TRAC	TRAC	TRAC	TRAC	TRAC	TRAC	TRAC	TRAC	TRAC	BEN	BEN	BEN	BEN	BEN	BEN	BEN	BEN	BEN
Analysis	04-116	04-117	09-041	09-042	09-043	09-046	09-050	09-051	09-052	09-053	09-057	09-059	09-061	09-068	09-069	09-070	09-071	09-078	09-079	12-046	12-047	12-048	12-050	12-051	12-053	12-056	12-061	12-062
SiO_2	64.81	64.40	63.14	59.74	56.01	55.98	56.28	58.22	61.24	63.43	59.18	56.78	54.96	59.50	62.53	58.86	59.70	46.59	55.97	48.11	48.40	57.04	51.08	57.89	48.22	56.39	49.23	56.74
TiO_2			0.00	0.03	0.00	0.00	0.00	0.05	0.01	0.00	0.00	0.00	0.00	0.02	0.00	0.02	0.06	0.01	0.00	0.00	0.02	0.00	0.00	0.03	0.01	0.01	0.01	0.00
Al_2O_3	21.29	20.30	21.95	24.51	27.16	26.90	26.65	25.70	23.46	21.97	25.12	26.29	27.89	24.76	22.63	25.21	24.65	33.40	27.12	32.53	31.99	26.51	30.77	25.36	32.13	27.64	31.97	26.69
Cr_2O_3			0.00	0.00	0.00	0.00	0.01	0.03	0.03	0.00	0.00	0.00	0.02	0.00	0.00	0.00	0.00	0.01	0.00	0.00	0.00	0.00	0.01	0.00	0.01	0.02	0.00	0.03
FeO	0.19	0.24	0.28	0.13	0.16	0.12	0.16	0.15	0.16	0.23	0.09	0.33	0.20	0.13	0.08	0.17	0.21	0.13	0.18	0.31	0.37	0.44	0.32	0.53	0.49	0.14	0.52	0.27
MnO			0.02	0.03	0.00	0.02	0.01	0.01	0.00	0.02	0.00	0.01	0.00	0.00	0.02	0.01	0.00	0.00	0.00	0.00	0.00	0.02	0.00	0.02	0.00	0.02	0.00	0.00
MgO			0.00	0.00	0.00	0.00	0.01	0.00	0.00	0.00	0.00	0.00	0.01	0.00	0.01	0.00	0.00	0.00	0.00	0.01	0.00	0.02	0.01	0.18	0.03	0.01	0.01	0.01
CaO	2.41	1.92	3.89	6.59	9.88	9.74	9.64	8.07	5.58	3.89	7.09	8.87	10.69	6.84	4.66	7.57	6.60	17.72	9.92	16.31	15.66	9.23	14.33	8.12	16.13	9.89	15.62	9.80
Na_2O	9.73	9.66	9.05	7.75	5.90	6.07	6.13	7.02	8.23	9.01	7.40	6.27	5.56	7.58	8.90	7.25	7.55	1.67	6.01	2.16	2.40	5.80	3.40	6.46	2.19	5.69	2.61	5.79
K_2O	0.59	0.92	0.73	0.42	0.19	0.23	0.23	0.26	0.49	0.75	0.27	0.32	0.18	0.27	0.45	0.35	0.38	0.02	0.17	0.04	0.07	0.69	0.18	0.45	0.07	0.36	0.06	0.35
NiO			0.00	0.00	0.00	0.00	0.04	0.00	0.00	0.00	0.00	0.05	0.03	0.00	0.02	0.00	0.00	0.04	0.01	0.01	0.00	0.00	0.00	0.04	0.00	0.00	0.00	0.00
BaO	0.11	0.16																										
SrO	0.40	0.14																										
Total	99.52	97.73	99.05	99.20	99.30	99.07	99.16	99.50	99.20	99.30	99.16	98.91	99.53	99.09	99.29	99.43	99.14	99.59	99.39	99.49	98.91	99.74	100.11	99.06	99.27	100.17	100.04	99.68
Si (32 O)	11.516	11.640	11.305	10.749	10.149	10.172	10.215	10.483	10.983	11.321	10.651	10.316	9.969	10.711	11.173	10.592	10.740	8.616	10.141	8.867	8.960	10.294	9.307	10.486	8.911	10.127	9.015	10.241
Ti			0.000	0.004	0.000	0.000	0.001	0.006	0.001	0.000	0.000	0.000	0.000	0.003	0.000	0.003	0.008	0.001	0.000	0.000	0.003	0.000	0.000	0.004	0.001	0.001	0.001	0.000
Al	4.459	4.324	4.631	5.198	5.800	5.760	5.702	5.454	4.960	4.621	5.329	5.629	5.963	5.255	4.766	5.348	5.228	7.282	5.791	7.067	6.981	5.639	6.608	5.415	6.998	5.851	6.899	5.679
Cr			0.000	0.000	0.000	0.000	0.001	0.004	0.004	0.000	0.000	0.000	0.003	0.000	0.000	0.000	0.000	0.001	0.000	0.000	0.000	0.000	0.002	0.000	0.001	0.003	0.000	0.004
Fe_2	0.028	0.037	0.042	0.020	0.025	0.019	0.024	0.023	0.024	0.034	0.014	0.050	0.030	0.019	0.012	0.025	0.031	0.020	0.028	0.048	0.057	0.067	0.048	0.080	0.075	0.021	0.079	0.041
Mn			0.003	0.004	0.000	0.004	0.001	0.001	0.001	0.003	0.000	0.001	0.000	0.000	0.002	0.001	0.000	0.000	0.000	0.000	0.000	0.003	0.000	0.003	0.000	0.003	0.000	0.000
Mg			0.000	0.000	0.000	0.000	0.004	0.000	0.000	0.000	0.001	0.000	0.003	0.000	0.002	0.000	0.000	0.000	0.000	0.004	0.000	0.005	0.003	0.048	0.008	0.003	0.003	0.004
Ca	0.459	0.372	0.745	1.271	1.918	1.896	1.875	1.556	1.073	0.744	1.367	1.726	2.078	1.319	0.892	1.460	1.272	3.511	1.926	3.221	3.107	1.785	2.798	1.575	3.195	1.902	3.065	1.895
Na	3.352	3.385	3.140	2.702	2.073	2.139	2.158	2.449	2.862	3.118	2.582	2.209	1.956	2.645	3.082	2.529	2.634	0.600	2.112	0.772	0.860	2.028	1.203	2.268	0.784	1.980	0.928	2.026
K	0.134	0.212	0.167	0.096	0.044	0.054	0.053	0.060	0.113	0.172	0.063	0.074	0.043	0.062	0.103	0.080	0.086	0.005	0.040	0.009	0.017	0.159	0.042	0.103	0.015	0.083	0.014	0.079
Ni	0.007	0.006	0.000	0.000	0.000	0.000	0.005	0.000	0.000	0.000	0.000	0.007	0.004	0.000	0.003	0.000	0.000	0.006	0.002	0.002	0.000	0.000	0.000	0.005	0.000	0.000	0.000	0.001
Ba	0.038	0.040																										
Sr																												
Total	19.997	19.996	20.034	20.046	20.009	20.044	20.038	20.036	20.021	20.013	20.007	20.011	20.047	20.013	20.036	20.037	19.999	20.044	20.040	19.990	19.985	19.980	20.010	19.988	19.988	19.976	20.005	19.970
X location	15.609	15.609	3.299	4.057	4.001	6.795	11.754	11.754	11.629	11.672	14.905	16.048	15.366	15.097	15.097	15.311	16.062	10.208	10.553	37.926	37.926	37.926	37.839	37.701	37.247	34.738	32.998	32.998
Y location	72.581	72.782	55.000	55.557	54.476	53.853	53.278	53.372	53.418	53.572	52.409	53.880	56.039	62.347	62.495	62.561	62.539	58.054	54.853	46.735	46.830	46.922	47.802	47.904	47.769	48.779	47.400	47.449
Crystal #	18	18	5	5	5		6	6	6	6				9	9	9				6	6	6	7	7			8	8
Comments		Rim	Rim	Core			Core			Rim				Core		Rim				Core		Rim	Core	Rim			Core	
An	12	9	18	31	48	46	46	38	27	18	34	43	51	33	22	36	32	85	47	80	78	45	69	40	80	48	76	47
Ab	85	85	77	66	51	52	53	60	71	77	64	55	48	66	76	62	66	15	52	19	22	51	30	57	20	50	23	51
Or	3	5	4	2	1	1	1	1	3	4	2	2	1	2	3	2	2	0	1	0	0	4	1	3	0	2	0	2

Sample	SV12	SV12	SV12	SV12	SV12	SV12	SV12	SV12	SV12	SV12	SV12	SV12	SV12	SV12
Rock Type	BEN	BEN	BEN	BEN	BEN	BEN	BEN	BEN	BEN	BEN	BEN	BEN	BEN	BEN
Analysis	12-063	12-071	12-076	12-077	12-078	12-079	13-082	13-083	13-084	13-085	13-086	13-087	13-088	13-089
SiO_2	60.16	59.88	57.96	60.63	58.61	59.93	55.32	48.64	49.79	48.31	57.16	50.78	52.36	56.08
TiO_2	0.00	0.01	0.00	0.00	0.00	0.00	0.00	0.03	0.00	0.00	0.04	0.00	0.00	0.00
Al_2O_3	24.44	24.97	26.51	24.73	25.69	25.10	27.63	32.21	31.34	32.16	26.58	28.94	29.22	26.98
Cr_2O_3	0.00	0.00	0.00	0.01	0.01	0.00	0.00	0.01	0.00	0.01	0.00	0.00	0.00	0.00
FeO	0.35	0.27	0.09	0.27	0.28	0.25	0.28	0.30	0.33	0.35	0.33	0.79	0.39	0.28
MnO	0.01	0.00	0.01	0.05	0.00	0.02	0.05	0.00	0.00	0.00	0.00	0.00	0.04	0.00
MgO	0.04	0.00	0.00	0.00	0.02	0.00	0.03	0.02	0.00	0.00	0.00	0.79	0.18	0.03
CaO	6.85	7.32	8.79	6.89	8.10	7.26	10.55	15.92	14.85	16.01	9.08	13.17	12.67	9.58
Na_2O	7.32	7.03	6.33	7.38	6.68	7.17	5.43	2.49	3.15	2.38	6.23	3.48	4.12	5.76
K_2O	0.60	0.71	0.49	0.65	0.52	0.63	0.34	0.12	0.17	0.11	0.41	0.15	0.19	0.34
NiO	0.01	0.00	0.00	0.06	0.00	0.00	0.00	0.01	0.00	0.02	0.00	0.01	0.00	0.01
BaO														
SrO														
Total	99.78	100.19	100.18	100.67	99.90	100.35	99.63	99.76	99.62	99.34	99.83	98.11	99.15	99.06
Si (32 O)	10.772	10.689	10.377	10.762	10.514	10.679	10.024	8.938	9.139	8.918	10.295	9.438	9.592	10.184
Ti	0.000	0.002	0.000	0.000	0.000	0.000	0.000	0.005	0.000	0.000	0.005	0.000	0.000	0.000
Al	5.157	5.254	5.593	5.174	5.431	5.271	5.901	6.978	6.780	6.999	5.643	6.340	6.308	5.775
Cr	0.000	0.000	0.000	0.002	0.001	0.000	0.000	0.002	0.000	0.001	0.000	0.000	0.000	0.000
Fe_2	0.052	0.040	0.014	0.040	0.042	0.038	0.042	0.046	0.050	0.054	0.049	0.122	0.059	0.043
Mn	0.002	0.000	0.001	0.008	0.000	0.003	0.007	0.000	0.000	0.000	0.000	0.000	0.005	0.000
Mg	0.011	0.001	0.000	0.001	0.004	0.000	0.009	0.005	0.001	0.000	0.000	0.220	0.050	0.007
Ca	1.314	1.400	1.686	1.310	1.557	1.386	2.048	3.134	2.921	3.167	1.751	2.624	2.487	1.864
Na	2.542	2.433	2.199	2.539	2.324	2.478	1.908	0.886	1.120	0.852	2.177	1.253	1.462	2.028
K	0.138	0.162	0.112	0.147	0.118	0.142	0.079	0.029	0.040	0.025	0.095	0.036	0.044	0.080
Ni	0.002	0.000	0.000	0.009	0.000	0.000	0.000	0.001	0.000	0.003	0.000	0.002	0.000	0.002
Ba														
Sr														
Total	19.989	19.980	19.982	19.992	19.991	19.996	20.019	20.025	20.051	20.020	20.015	20.036	20.007	19.982
X location	32.998	38.094	39.424	39.424	39.499	36.016	43.900	43.859	43.756	43.736	43.736	44.616	44.566	44.523
Y location	47.470	41.662	40.418	40.360	40.329	40.284	40.130	40.130	40.137	40.166	40.202	40.866	40.866	40.866
Crystal #	8						1	1	1	1	1	2	2	2
Comments	Rim						Core				Rim	Core		
An	33	35	42	33	39	35	51	77	72	78	44	67	62	47
Ab	64	61	55	64	58	62	47	22	27	21	54	32	37	51
Or	3	4	3	4	3	4	2	1	1	1	2	1	1	2

Sample	SV12	SV12	SV12	SV12	SV12	SV12	SV12	SV12	SV12	SV12	SV12	SV12	SV12	SV12
Rock Type	BEN	BEN	BEN	BEN	BEN	BEN	BEN	BEN	BEN	BEN	BEN	BEN	BEN	BEN
Analysis	13-090	13-091	13-092	13-094	13-095	13-096	13-097	13-098	13-099	13-100	13-101	13-102	13-103	13-104
SiO_2	55.12	56.27	59.81	55.82	57.47	53.85	65.20	58.67	58.05	59.13	59.87	59.19	55.38	56.05
TiO_2	0.01	0.00	0.05	0.04	0.00	0.01	0.21	0.00	0.01	0.00	0.00	0.00	0.00	0.01
Al_2O_3	27.68	26.99	24.75	27.20	26.06	27.87	20.24	25.43	25.66	24.75	24.41	24.80	27.45	26.70
Cr_2O_3	0.01	0.00	0.01	0.02	0.01	0.00	0.00	0.00	0.00	0.00	0.00	0.00	0.00	0.00
FeO	0.26	0.25	0.23	0.36	0.37	0.86	1.11	0.25	0.25	0.18	0.22	0.19	0.32	0.32
MnO	0.01	0.00	0.02	0.00	0.02	0.02	0.04	0.01	0.00	0.00	0.00	0.00	0.01	0.00
MgO	0.00	0.00	0.00	0.02	0.18	0.43	0.00	0.00	0.00	0.00	0.02	0.01	0.03	0.03
CaO	10.41	9.72	6.94	9.73	8.83	11.30	4.18	7.73	8.20	7.05	6.65	7.30	10.21	9.64
Na_2O	5.43	5.77	7.13	5.79	6.30	4.73	6.88	6.82	6.44	6.97	7.32	7.04	5.56	5.76
K_2O	0.31	0.40	0.68	0.35	0.39	0.25	1.80	0.49	0.55	0.75	0.81	0.66	0.37	0.39
NiO	0.01	0.00	0.01	0.00	0.00	0.05	0.00	0.00	0.02	0.01	0.01	0.01	0.00	0.00
BaO														
SrO														
Total	99.26	99.41	99.62	99.32	99.61	99.36	99.67	99.40	99.18	98.84	99.31	99.20	99.33	98.90
Si (32 O)	10.018	10.188	10.724	10.126	10.365	9.833	11.607	10.564	10.490	10.692	10.772	10.672	10.059	10.203
Ti	0.001	0.000	0.007	0.005	0.000	0.002	0.028	0.000	0.002	0.000	0.000	0.000	0.000	0.001
Al	5.930	5.760	5.232	5.815	5.541	5.997	4.246	5.396	5.464	5.275	5.177	5.270	5.877	5.730
Cr	0.001	0.000	0.001	0.003	0.002	0.001	0.000	0.000	0.000	0.000	0.000	0.000	0.000	0.000
Fe_2	0.039	0.038	0.034	0.055	0.055	0.132	0.165	0.038	0.038	0.027	0.033	0.029	0.048	0.048
Mn	0.002	0.000	0.003	0.000	0.003	0.003	0.006	0.002	0.000	0.000	0.000	0.001	0.002	0.000
Mg	0.001	0.000	0.000	0.004	0.047	0.117	0.000	0.001	0.000	0.000	0.005	0.001	0.007	0.008
Ca	2.028	1.886	1.334	1.892	1.706	2.210	0.797	1.491	1.587	1.366	1.281	1.411	1.987	1.879
Na	1.915	2.025	2.478	2.035	2.202	1.674	2.375	2.380	2.256	2.445	2.554	2.462	1.958	2.034
K	0.072	0.091	0.156	0.082	0.090	0.058	0.410	0.114	0.127	0.174	0.187	0.152	0.086	0.091
Ni	0.001	0.000	0.001	0.000	0.000	0.007	0.000	0.000	0.004	0.001	0.001	0.002	0.000	0.000
Ba														
Sr														
Total	20.009	19.990	19.969	20.017	20.010	20.032	19.634	19.985	19.967	19.980	20.010	20.000	20.024	19.994
X location	44.498	44.463	44.428	44.411	44.387	44.398	44.421	44.223	44.223	44.223	44.223	44.223	43.418	43.418
Y location	40.866	40.866	40.866	41.211	41.252	41.324	41.434	42.441	42.486	42.526	42.544	42.607	43.679	43.749
Crystal #	2	2	2	3	4	5	6	7	7	7	7	7	8	8
Comments								Core				Rim	Core	
An	51	47	34	47	43	56	22	37	40	34	32	35	49	47
Ab	48	51	62	51	55	42	66	60	57	61	63	61	49	51
Or	2	2	4	2	2	1	11	3	3	4	5	4	2	2

Sample	SV12	SV12	SV12	SV12	SV12	SV12	SV12	SV12	SV12	SV12	SV12	SV12	SV12	SV12	SV12	SV12	SV12	SV12	SV12	SV12	SV12	SV12	SV17	SV17	SV17	SV17	SV17	SV17
Rock Type	BEN	BEN	BEN	BEN	BEN	BEN	BEN	BEN	BEN	BEN	BEN	BEN	BEN	BEN	BEN	BEN	BEN	BEN	BEN	BEN	BEN	BEN	TRAC	TRAC	TRAC	TRAC	TRAC	TRAC
Analysis	13-105	13-106	13-107	13-108	13-109	13-111	13-112	13-113	13-114	13-115	13-116	13-117	13-118	13-119	13-120	13-122	13-123	13-124	13-125	13-126	13-127	13-128	09-004	09-005	09-006	09-007	09-008	09-009
SiO_2	53.15	56.42	57.01	57.28	59.85	51.56	53.98	56.79	50.12	50.39	50.91	96.95	49.09	54.31	56.28	52.17	55.33	55.54	60.60	54.84	54.46	59.55	63.22	61.86	60.66	60.84	60.86	60.84
TiO_2	0.00	0.00	0.07	0.00	0.01	0.00	0.07	0.00	0.02	0.00	0.01	0.03	0.00	0.00	0.00	0.00	0.04	0.00	0.00	0.00	0.02	0.02	0.00	0.00	0.05	0.04	0.00	0.00
Al_2O_3	29.24	27.01	26.64	26.48	24.63	30.06	28.24	26.48	30.63	30.63	30.21	0.89	31.44	27.81	26.64	29.48	27.11	27.19	24.18	27.67	27.90	24.48	22.19	22.95	23.90	23.99	24.03	23.93
Cr_2O_3	0.00	0.00	0.00	0.01	0.04	0.00	0.01	0.00	0.01	0.00	0.01	0.00	0.00	0.01	0.04	0.02	0.00	0.00	0.00	0.00	0.01	0.01	0.00	0.00	0.00	0.00	0.00	0.02
FeO	0.40	0.38	0.24	0.29	0.17	0.25	0.21	0.25	0.44	0.46	0.50	0.02	0.47	0.37	0.43	0.47	0.33	0.42	0.30	0.53	0.47	0.35	0.25	0.09	0.12	0.08	0.11	0.12
MnO	0.00	0.00	0.01	0.00	0.01	0.00	0.00	0.00	0.00	0.03	0.06	0.03	0.03	0.00	0.00	0.04	0.01	0.02	0.02	0.02	0.00	0.03	0.00	0.00	0.04	0.03	0.00	0.00
MgO	0.01	0.02	0.01	0.00	0.00	0.00	0.08	0.06	0.04	0.05	0.04	0.01	0.02	0.02	0.13	0.04	0.10	0.02	0.00	0.01	0.01	0.00	0.00	0.00	0.01	0.00	0.00	0.00
CaO	12.35	9.67	9.10	8.85	7.05	13.47	11.23	9.19	14.33	14.31	13.85	0.13	15.26	11.07	9.85	12.97	10.24	10.29	6.54	10.91	11.01	7.17	4.46	5.00	5.99	5.88	5.89	5.92
Na_2O	4.52	5.79	6.03	6.19	7.16	3.71	4.87	5.90	3.25	3.32	3.47	0.34	2.72	4.99	5.51	4.16	5.47	5.43	7.24	5.10	5.06	6.91	8.52	8.54	8.08	8.15	8.24	8.15
K_2O	0.25	0.35	0.41	0.40	0.57	0.19	0.27	0.43	0.13	0.12	0.18	0.03	0.11	0.34	0.54	0.18	0.37	0.38	0.64	0.38	0.37	0.63	0.85	0.56	0.32	0.32	0.32	0.35
NiO	0.04	0.05	0.02	0.01	0.00	0.01	0.01	0.00	0.01	0.00	0.00	0.00	0.00	0.01	0.04	0.00	0.03	0.00	0.01	0.00	0.00	0.00	0.00	0.00	0.00	0.05	0.00	0.00
BaO																												
SrO																												
Total	99.98	99.68	99.54	99.50	99.47	99.26	98.96	99.10	98.97	99.30	99.22	98.43	99.13	98.91	99.46	99.54	99.03	99.29	99.52	99.45	99.31	99.16	99.50	99.00	99.17	99.37	99.45	99.32
Si (32 O)	9.654	10.191	10.289	10.334	10.741	9.447	9.858	10.294	9.247	9.265	9.358	15.823	9.067	9.929	10.202	9.538	10.082	10.094	10.855	9.974	9.922	10.733	11.272	11.098	10.889	10.896	10.892	10.902
Ti	0.000	0.000	0.009	0.000	0.001	0.000	0.010	0.000	0.003	0.000	0.001	0.004	0.000	0.000	0.000	0.000	0.005	0.000	0.000	0.000	0.002	0.003	0.000	0.000	0.007	0.005	0.000	0.000
Al	6.261	5.750	5.667	5.631	5.210	6.493	6.079	5.657	6.661	6.638	6.545	0.171	6.844	5.993	5.692	6.354	5.823	5.825	5.105	5.932	5.992	5.202	4.664	4.852	5.058	5.064	5.070	5.054
Cr	0.000	0.000	0.000	0.001	0.005	0.000	0.001	0.000	0.001	0.000	0.001	0.000	0.000	0.001	0.005	0.003	0.000	0.000	0.000	0.000	0.002	0.002	0.000	0.000	0.000	0.000	0.000	0.004
Fe_2	0.061	0.057	0.036	0.044	0.026	0.039	0.031	0.037	0.067	0.071	0.077	0.002	0.072	0.056	0.066	0.072	0.051	0.064	0.045	0.081	0.071	0.053	0.037	0.014	0.017	0.012	0.017	0.017
Mn	0.000	0.000	0.002	0.000	0.002	0.000	0.000	0.000	0.000	0.004	0.009	0.004	0.004	0.000	0.000	0.006	0.002	0.003	0.003	0.003	0.000	0.004	0.000	0.000	0.007	0.004	0.000	0.000
Mg	0.004	0.004	0.002	0.000	0.000	0.001	0.020	0.017	0.011	0.014	0.010	0.001	0.005	0.004	0.034	0.012	0.028	0.005	0.000	0.003	0.004	0.000	0.000	0.001	0.002	0.000	0.000	0.000
Ca	2.404	1.871	1.759	1.712	1.355	2.644	2.197	1.784	2.832	2.819	2.728	0.023	3.020	2.168	1.914	2.542	1.998	2.003	1.254	2.127	2.149	1.385	0.852	0.960	1.153	1.128	1.130	1.136
Na	1.591	2.027	2.108	2.164	2.491	1.318	1.725	2.075	1.162	1.185	1.237	0.109	0.975	1.768	1.936	1.475	1.932	1.915	2.514	1.797	1.786	2.414	2.946	2.971	2.811	2.831	2.859	2.833
K	0.059	0.080	0.094	0.091	0.130	0.045	0.062	0.100	0.031	0.027	0.041	0.006	0.025	0.078	0.124	0.043	0.087	0.089	0.146	0.087	0.085	0.146	0.193	0.127	0.073	0.073	0.072	0.080
Ni	0.006	0.007	0.003	0.001	0.000	0.002	0.002	0.000	0.001	0.000	0.000	0.000	0.000	0.001	0.006	0.000	0.004	0.000	0.001	0.000	0.001	0.000	0.000	0.001	0.000	0.007	0.000	0.000
Ba																												
Sr																												
Total	20.040	19.988	19.970	19.977	19.960	19.988	19.986	19.965	20.015	20.023	20.007	16.145	20.012	19.997	19.979	20.043	20.011	19.996	19.923	20.003	20.014	19.942	19.965	20.025	20.017	20.019	20.039	20.026
X location	43.418	43.371	43.335	43.335	38.497	38.516	38.470	38.470	32.563	32.586	32.597	32.620	32.630	32.630	32.630	32.647	32.647	32.665	32.721	32.812	32.837	32.918	37.579	37.469	37.372	37.319	37.319	37.319
Y location	43.830	43.915	43.978	44.082	43.301	43.367	43.410	43.447	48.742	48.670	48.635	48.625	48.592	48.523	48.451	48.347	48.311	48.296	48.286	48.138	48.029	47.879	61.968	61.931	61.818	61.680	61.680	61.680
Crystal #	8	8	8	8	9	9	9	9	10	10	10	10	10	10	10	10	10	10	10	11	12	13	1	1	1	1	1	1
Comments				Rim	Core			Rim	Core										Rim				Rim			Core	Core	Core
An	59	47	44	43	34	66	55	45	70	70	68	17	75	54	48	63	50	50	32	53	53	35	21	24	29	28	28	28
Ab	39	51	53	55	63	33	43	52	29	29	31	79	24	44	49	36	48	48	64	45	44	61	74	73	70	70	70	70
Or	1	2	2	2	3	1	2	3	1	1	1	5	1	2	3	1	2	2	4	2	2	4	5	3	2	2	2	2

Sample	SV17	SV17	SV17	SV17	SV17	SV17	SV17	SV17	SV17	SV17	SV17	SV17	SV17	SV17
Rock Type	TRAC	TRAC	TRAC	TRAC	TRAC	TRAC	TRAC	TRAC	TRAC	TRAC	TRAC	TRAC	TRAC	TRAC
Analysis	09-010	09-014	09-015	09-016	09-017	09-020	09-021	09-022	09-023	09-029	09-030	09-033	09-034	09-036
SiO_2	62.77	60.58	53.57	53.64	55.65	60.68	61.93	64.46	63.17	58.45	57.41	64.13	62.81	60.35
TiO_2	0.00	0.03	0.00	0.00	0.00	0.01	0.00	0.00	0.03	0.00	0.00	0.00	0.00	0.00
Al_2O_3	22.76	24.04	28.80	28.92	27.28	24.20	23.30	21.67	22.11	25.40	26.11	21.66	22.71	24.12
Cr_2O_3	0.00	0.01	0.00	0.00	0.00	0.02	0.00	0.00	0.00	0.00	0.03	0.00	0.00	0.01
FeO	0.23	0.30	0.23	0.45	0.46	0.13	0.19	0.20	0.31	0.22	0.20	0.20	0.10	0.12
MnO	0.02	0.00	0.02	0.01	0.00	0.00	0.00	0.00	0.00	0.00	0.02	0.02	0.01	0.03
MgO	0.02	0.00	0.01	0.03	0.02	0.01	0.00	0.00	0.02	0.00	0.00	0.00	0.00	0.00
CaO	4.55	6.30	11.93	11.98	10.40	6.15	5.34	3.50	4.27	7.91	8.74	3.42	4.63	6.19
Na_2O	8.68	7.97	4.89	4.83	5.72	7.91	8.41	9.24	8.52	7.02	6.65	9.22	8.68	7.88
K_2O	0.75	0.52	0.12	0.16	0.20	0.36	0.42	0.79	1.08	0.39	0.31	0.99	0.58	0.34
NiO	0.00	0.03	0.00	0.00	0.00	0.00	0.00	0.08	0.00	0.02	0.06	0.00	0.00	0.01
BaO														
SrO														
Total	99.78	99.79	99.56	100.01	99.73	99.46	99.58	99.94	99.51	99.41	99.52	99.64	99.52	99.05
Si (32 O)	11.172	10.841	9.746	9.727	10.075	10.861	11.050	11.417	11.275	10.535	10.364	11.403	11.191	10.851
Ti	0.000	0.004	0.000	0.000	0.000	0.001	0.000	0.000	0.004	0.000	0.000	0.000	0.000	0.000
Al	4.774	5.071	6.177	6.183	5.821	5.106	4.900	4.524	4.652	5.396	5.556	4.539	4.769	5.112
Cr	0.001	0.001	0.000	0.000	0.000	0.003	0.000	0.000	0.000	0.000	0.004	0.000	0.000	0.001
Fe_2	0.034	0.044	0.035	0.068	0.069	0.019	0.028	0.029	0.046	0.034	0.030	0.030	0.014	0.018
Mn	0.003	0.000	0.004	0.001	0.001	0.000	0.000	0.000	0.000	0.000	0.003	0.003	0.002	0.004
Mg	0.006	0.001	0.002	0.008	0.006	0.001	0.000	0.000	0.005	0.000	0.000	0.000	0.000	0.000
Ca	0.868	1.208	2.325	2.327	2.016	1.180	1.020	0.665	0.817	1.528	1.690	0.651	0.883	1.192
Na	2.996	2.766	1.725	1.699	2.008	2.746	2.909	3.173	2.948	2.454	2.328	3.178	3.000	2.748
K	0.169	0.119	0.028	0.036	0.046	0.083	0.095	0.179	0.247	0.089	0.071	0.225	0.132	0.079
Ni	0.000	0.005	0.000	0.000	0.000	0.000	0.000	0.011	0.000	0.003	0.008	0.000	0.000	0.002
Ba														
Sr														
Total	20.022	20.061	20.042	20.049	20.042	19.999	20.002	19.997	19.993	20.038	20.055	20.029	19.991	20.006
X location	36.965	37.720	39.828	39.770	39.743	41.157	40.983	40.845	40.621	41.684	44.252	40.670	36.548	36.529
Y location	61.613	58.141	58.231	58.366	55.687	54.758	54.860	55.013	55.001	51.509	49.001	49.778	49.693	54.293
Crystal #	1		2	2		3	3	3	3					
Comments	Rim		Core	Rim		Core			Rim					
An	22	30	57	57	50	29	25	17	20	38	41	16	22	30
Ab	74	68	42	42	49	69	72	79	73	60	57	78	75	68
Or	4	3	1	1	1	2	2	4	6	2	2	6	3	2

Sample	SV17	SV17	SV17	SV19	SV19	SV19	SV19	SV19	SV19	SV19	SV19	SV19	SV19	SV19
Rock Type	TRAC	TRAC	TRAC	MUG	MUG	MUG	MUG	MUG	MUG	MUG	MUG	MUG	MUG	MUG
Analysis	09-037	09-038	09-040	05-063	05-064	06-041	06-042	06-043	06-044	06-045	06-046	06-047	06-048	06-049
SiO_2	60.76	58.91	56.37	48.88	50.21	51.78	51.51	48.16	47.75	47.89	48.29	48.81	47.36	50.67
TiO_2	0.00	0.02	0.00	0.00	0.02									
Al_2O_3	23.84	25.35	26.83	31.43	30.61	29.37	29.66	32.06	32.22	32.22	31.91	31.49	32.46	30.27
Cr_2O_3	0.00	0.00	0.00	0.00	0.02									
FeO	0.11	0.17	0.16	0.81	0.72	0.71	0.69	0.56	0.67	0.70	0.62	0.75	0.65	0.66
MnO	0.00	0.00	0.01	0.03	0.02									
MgO	0.00	0.00	0.01	0.07	0.05									
CaO	5.75	7.41	9.59	15.63	14.24	13.24	13.20	16.38	16.36	16.33	16.21	15.56	16.83	14.28
Na_2O	7.89	7.10	6.12	2.69	3.34	3.93	3.91	2.42	2.25	2.33	2.54	2.71	2.11	3.49
K_2O	0.48	0.23	0.17	0.11	0.18	0.24	0.23	0.12	0.09	0.09	0.12	0.13	0.08	0.21
NiO	0.00	0.00	0.00	0.00	0.04									
BaO						0.02	0.03	0.01	0.02	0.03	0.01	0.00	0.00	0.02
SrO						0.16	0.23	0.21	0.16	0.24	0.18	0.22	0.15	0.15
Total	98.83	99.19	99.26	99.65	99.45	99.45	99.46	99.93	99.51	99.83	99.87	99.65	99.62	99.74
Si (32 O)	10.931	10.604	10.212	9.012	9.237	9.505	9.459	8.879	8.838	8.843	8.905	9.007	8.768	9.301
Ti	0.000	0.003	0.000	0.000	0.003									
Al	5.054	5.379	5.729	6.830	6.638	6.354	6.420	6.967	7.029	7.014	6.936	6.849	7.083	6.550
Cr	0.000	0.000	0.000	0.000	0.003									
Fe_2	0.017	0.025	0.025	0.125	0.111	0.108	0.106	0.087	0.104	0.108	0.096	0.116	0.101	0.101
Mn	0.000	0.000	0.001	0.005	0.002									
Mg	0.000	0.000	0.003	0.019	0.014									
Ca	1.109	1.428	1.860	3.087	2.807	2.604	2.597	3.235	3.244	3.230	3.204	3.076	3.338	2.809
Na	2.752	2.477	2.149	0.962	1.191	1.399	1.394	0.864	0.808	0.835	0.908	0.968	0.756	1.243
K	0.109	0.053	0.040	0.026	0.043	0.056	0.054	0.029	0.022	0.021	0.027	0.029	0.018	0.048
Ni	0.000	0.000	0.000	0.000	0.006									
Ba						0.002	0.002	0.001	0.002	0.003	0.000	0.000	0.000	0.002
Sr						0.018	0.024	0.023	0.017	0.026	0.019	0.023	0.016	0.016
Total	19.972	19.969	20.018	20.067	20.055	20.045	20.056	20.084	20.063	20.078	20.095	20.068	20.078	20.069
X location	35.715	35.715	35.231	48.967	48.999	40.188	38.337	37.379	37.736	37.916	38.026	38.153	38.283	38.434
Y location	56.502	56.778	56.906	72.140	71.228	51.341	51.317	51.300	54.226	54.198	54.203	54.262	54.293	54.307
Crystal #	4	4	4						5	5	5	5	5	5
Comments	Rim		Core						Core					
An	28	36	46	76	69	64	64	78	80	79	77	76	81	69
Ab	69	63	53	24	29	34	34	21	20	20	22	24	18	30
Or	3	1	1	1	1	1	1	1	1	1	1	1	0	1

Sample	SV19	SV19	SV19	SV19	SV19	SV19	SV19
Rock Type	MUG	MUG	MUG	MUG	MUG	MUG	MUG
Analysis	06-050	06-051	06-052	06-053	06-054	06-055	06-056
SiO_2	49.24	52.75	51.29	47.10	53.70	51.48	48.08
TiO_2							
Al_2O_3	31.18	28.91	29.85	32.67	28.08	29.31	31.92
Cr_2O_3							
FeO	0.68	0.67	0.70	0.70	0.74	0.76	0.65
MnO							
MgO							
CaO	15.41	12.51	13.68	17.09	11.63	12.98	15.80
Na_2O	3.03	4.44	3.85	1.91	4.89	4.13	2.53
K_2O	0.14	0.26	0.21	0.09	0.30	0.31	0.10
NiO							
BaO	0.02	0.02	0.04	0.00	0.03	0.03	0.00
SrO	0.21	0.16	0.20	0.18	0.19	0.20	0.18
Total	99.89	99.71	99.80	99.74	99.54	99.20	99.26
Si (32 O)	9.065	9.638	9.401	8.718	9.810	9.487	8.909
Ti							
Al	6.765	6.226	6.449	7.129	6.047	6.365	6.973
Cr							
Fe_2	0.104	0.102	0.108	0.109	0.113	0.118	0.101
Mn							
Mg							
Ca	3.039	2.450	2.687	3.389	2.276	2.563	3.136
Na	1.081	1.572	1.368	0.685	1.732	1.475	0.908
K	0.032	0.059	0.048	0.022	0.069	0.072	0.023
Ni							
Ba	0.001	0.001	0.003	0.000	0.002	0.003	0.000
Sr	0.022	0.017	0.021	0.020	0.020	0.021	0.020
Total	20.109	20.065	20.083	20.071	20.067	20.104	20.070
X location	38.533	38.605	37.664	37.071	36.863	36.881	37.426
Y location	54.307	54.339	54.937	56.209	56.209	61.473	61.514
Crystal #	5	5					
Comments		Rim					
An	73	60	65	83	56	62	77
Ab	26	39	33	17	42	36	22
Or	1	1	1	1	2	2	1

Sample	SV19	SV19	SV19	SV19	SV19	SV19	SV19
Rock Type	MUG	MUG	MUG	MUG	MUG	MUG	MUG
Analysis	06-057	06-058	06-059	06-060	06-061	06-062	06-063
SiO_2	50.64	48.95	50.17	50.40	47.25	47.87	47.53
TiO_2							
Al_2O_3	30.26	31.10	30.87	30.55	32.44	32.22	32.48
Cr_2O_3							
FeO	0.72	0.72	0.66	0.71	0.54	0.66	0.70
MnO							
MgO							
CaO	14.42	14.98	15.04	14.04	16.80	16.76	16.91
Na_2O	3.47	2.80	3.23	3.27	2.18	2.33	2.10
K_2O	0.21	0.13	0.16	0.17	0.09	0.11	0.09
NiO							
BaO	0.00	0.02	0.02	0.03	0.02	0.01	0.01
SrO	0.21	0.20	0.19	0.24	0.18	0.20	0.18
Total	99.93	98.89	100.33	99.39	99.50	100.15	99.98
Si (32 O)	9.289	9.082	9.177	9.276	8.761	8.821	8.772
Ti							
Al	6.542	6.803	6.657	6.628	7.089	6.998	7.065
Cr							
Fe_2	0.111	0.112	0.101	0.109	0.083	0.102	0.108
Mn							
Mg							
Ca	2.835	2.978	2.947	2.768	3.338	3.309	3.343
Na	1.235	1.007	1.144	1.166	0.784	0.831	0.752
K	0.048	0.030	0.037	0.040	0.021	0.027	0.021
Ni							
Ba	0.000	0.001	0.002	0.002	0.001	0.000	0.001
Sr	0.022	0.021	0.020	0.025	0.020	0.021	0.020
Total	20.082	20.035	20.085	20.014	20.097	20.109	20.082
X location	38.054	41.871	42.075	40.777	40.749	40.779	40.943
Y location	61.818	61.818	61.844	64.845	64.690	64.421	68.907
Crystal #				6	6	6	
Comments				Rim		Core	
An	69	74	71	70	81	79	81
Ab	30	25	28	29	19	20	18
Or	1	1	1	1	0	1	0

Sample	SV19	SV19	SV19	SV19	SV19	SV19	SV19
Rock Type	MUG	MUG	MUG	MUG	MUG	MUG	MUG
Analysis	06-064	06-065	06-066	06-067	06-068	06-069	06-070
SiO_2	54.48	53.54	50.23	47.63	49.33	47.80	51.09
TiO_2							
Al_2O_3	27.59	28.20	30.46	32.34	29.70	32.01	30.19
Cr_2O_3							
FeO	0.63	0.72	0.74	0.63	1.40	0.70	0.63
MnO							
MgO							
CaO	11.00	11.91	14.65	16.27	14.63	16.39	13.82
Na_2O	5.15	4.68	3.39	2.09	3.05	2.39	3.63
K_2O	0.37	0.30	0.20	0.08	0.54	0.13	0.20
NiO							
BaO	0.05	0.03	0.01	0.00	0.05	0.02	0.03
SrO	0.20	0.18	0.17	0.19	0.17	0.20	0.23
Total	99.46	99.57	99.85	99.22	98.87	99.62	99.81
Si (32 O)	9.938	9.781	9.230	8.832	9.208	8.849	9.359
Ti							
Al	5.932	6.073	6.597	7.069	6.535	6.985	6.518
Cr							
Fe_2	0.097	0.111	0.113	0.097	0.218	0.108	0.097
Mn							
Mg							
Ca	2.150	2.332	2.885	3.232	2.926	3.252	2.713
Na	1.823	1.658	1.207	0.750	1.104	0.856	1.289
K	0.085	0.071	0.048	0.019	0.129	0.030	0.047
Ni							
Ba	0.003	0.002	0.000	0.000	0.003	0.001	0.002
Sr	0.021	0.019	0.019	0.021	0.019	0.021	0.024
Total	20.050	20.047	20.099	20.019	20.141	20.101	20.050
X location	41.357	45.494	45.672	45.167	42.278	31.944	31.757
Y location	68.870	68.657	68.657	71.046	71.019	78.543	78.543
Crystal #						7	7
Comments						Core	
An	53	57	70	81	70	79	67
Ab	45	41	29	19	27	21	32
Or	2	2	1	0	3	1	1

Sample	SV19	SV19	SV19	SV19	SV19	SV19	SV19
Rock Type	MUG	MUG	MUG	MUG	MUG	MUG	MUG
Analysis	06-071	06-072	06-073	06-074	06-075	06-076	06-077
SiO_2	51.02	54.22	54.17	57.87	48.11	51.12	46.95
TiO_2							
Al_2O_3	29.14	27.82	27.80	24.26	31.97	29.74	32.54
Cr_2O_3							
FeO	1.22	0.64	0.70	0.86	0.58	0.73	0.68
MnO							
MgO							
CaO	13.46	11.24	11.23	7.58	16.22	13.62	17.17
Na_2O	3.88	5.14	5.00	6.54	2.41	3.86	1.90
K_2O	0.46	0.33	0.33	0.92	0.11	0.23	0.09
NiO							
BaO	0.02	0.04	0.02	0.07	0.01	0.02	0.01
SrO	0.20	0.20	0.23	0.14	0.23	0.21	0.22
Total	99.39	99.63	99.49	98.23	99.63	99.53	99.55
Si (32 O)	9.428	9.885	9.887	10.612	8.891	9.399	8.713
Ti							
Al	6.347	5.978	5.982	5.243	6.965	6.445	7.118
Cr							
Fe_2	0.189	0.097	0.107	0.132	0.089	0.113	0.105
Mn							
Mg							
Ca	2.664	2.195	2.196	1.489	3.212	2.683	3.415
Na	1.388	1.816	1.770	2.324	0.865	1.376	0.685
K	0.109	0.077	0.077	0.215	0.025	0.054	0.020
Ni							
Ba	0.002	0.003	0.002	0.005	0.001	0.001	0.001
Sr	0.021	0.021	0.024	0.015	0.024	0.023	0.023
Total	20.148	20.073	20.045	20.036	20.072	20.093	20.080
X location	31.706	31.672	31.653	31.620	33.708	34.463	34.789
Y location	78.543	78.543	78.597	78.621	77.120	74.643	74.663
Crystal #	7	7	7	7		8	8
Comments				Rim			
An	64	54	54	37	78	65	83
Ab	33	44	44	58	21	33	17
Or	3	2	2	5	1	1	0

Sample	SV19	SV19	SV19	SV20	SV20	SV20	SV20	SV20	SV20	SV20	SV20	SV20	SV20	SV20	SV20	SV20	SV20	SV20	SV20	SV20	SV20	SV20	SV20	SV20	SV20	SV20	SV20	SV20
Rock Type	MUG	MUG	MUG	MUG	MUG	MUG	MUG	MUG	MUG	MUG	MUG	MUG	MUG	MUG	MUG	MUG	MUG	MUG	MUG	MUG	MUG	MUG	MUG	MUG	MUG	MUG	MUG	MUG
Analysis	06-078	06-079	06-080	05-083	05-086	06-081	06-082	06-083	06-084	06-085	06-086	06-087	06-088	06-089	06-090	06-091	06-092	06-093	06-094	06-095	06-096	06-097	06-098	06-099	06-100	06-101	06-102	06-103
SiO_2	51.60	54.78	48.64	49.64	53.02	47.71	54.67	47.44	47.24	49.33	52.97	54.34	47.64	55.53	55.32	52.04	50.62	53.88	52.20	53.21	55.23	48.60	51.58	55.73	48.32	49.19	48.72	46.98
TiO_2				0.05	0.01																							
Al_2O_3	29.49	27.28	31.74	31.85	29.26	32.42	27.86	33.06	33.07	31.75	29.25	28.19	32.84	27.52	27.89	29.86	30.90	28.84	29.86	29.11	27.78	32.20	30.15	27.22	31.41	31.49	31.89	33.07
Cr_2O_3				0.05	0.01																							
FeO	0.85	0.71	0.68	0.54	0.71	0.46	0.59	0.61	0.58	0.59	0.53	0.48	0.57	0.46	0.45	0.51	0.58	0.47	0.60	0.45	0.45	0.53	0.49	0.49	0.58	0.64	0.49	0.60
MnO				0.02	0.00																							
MgO				0.02	0.01																							
CaO	13.29	10.60	15.69	14.96	12.33	16.70	11.08	17.10	17.32	15.68	12.58	11.42	17.00	10.59	10.83	13.51	14.59	11.85	13.53	12.24	10.70	16.19	13.75	10.28	16.28	15.49	15.74	17.34
Na_2O	3.89	5.41	2.79	2.87	4.20	2.02	5.15	1.91	1.82	2.82	4.58	5.05	2.10	5.47	5.46	3.98	3.38	4.84	4.00	4.58	5.44	2.47	3.78	5.63	2.44	2.62	2.79	1.86
K_2O	0.22	0.40	0.12	0.19	0.57	0.15	0.49	0.07	0.08	0.12	0.26	0.31	0.12	0.31	0.33	0.23	0.16	0.23	0.22	0.27	0.35	0.09	0.20	0.41	0.10	0.10	0.15	0.07
NiO				0.00	0.02																							
BaO	0.03	0.07	0.00			0.00	0.01	0.01	0.00	0.00	0.05	0.03	0.01	0.00	0.04	0.01	0.00	0.03	0.02	0.01	0.02	0.01	0.02	0.04	0.01	0.00	0.02	0.00
SrO	0.24	0.18	0.20			0.15	0.14	0.16	0.16	0.17	0.15	0.15	0.14	0.14	0.15	0.17	0.17	0.21	0.16	0.19	0.18	0.22	0.17	0.14	0.16	0.18	0.22	0.15
Total	99.59	99.43	99.87	100.17	100.13	99.61	99.98	100.35	100.27	100.45	100.36	99.96	100.43	100.00	100.46	100.31	100.39	100.34	100.58	100.06	100.14	100.32	100.13	99.93	99.29	99.71	100.00	100.07
Si (32 O)	9.471	9.996	8.962	9.070	9.636	8.817	9.920	8.717	8.693	9.021	9.616	9.861	8.749	10.038	9.971	9.467	9.232	9.751	9.474	9.669	9.984	8.912	9.405	10.085	8.957	9.051	8.959	8.668
Ti				0.006	0.001																							
Al	6.381	5.868	6.893	6.859	6.268	7.062	5.959	7.160	7.172	6.843	6.258	6.030	7.110	5.864	5.926	6.404	6.642	6.152	6.389	6.234	5.919	6.960	6.479	5.807	6.863	6.831	6.912	7.191
Cr				0.007	0.002																							
Fe_2	0.130	0.108	0.105	0.082	0.108	0.071	0.089	0.093	0.090	0.090	0.080	0.073	0.088	0.069	0.068	0.077	0.088	0.072	0.091	0.069	0.068	0.081	0.075	0.074	0.090	0.098	0.075	0.092
Mn				0.003	0.000																							
Mg				0.006	0.003																							
Ca	2.614	2.072	3.098	2.928	2.401	3.307	2.154	3.367	3.416	3.072	2.447	2.220	3.346	2.052	2.091	2.634	2.851	2.298	2.632	2.383	2.073	3.181	2.686	1.993	3.233	3.054	3.101	3.427
Na	1.383	1.915	0.997	1.017	1.481	0.723	1.812	0.681	0.648	0.999	1.613	1.775	0.748	1.917	1.908	1.404	1.196	1.698	1.406	1.615	1.906	0.879	1.337	1.976	0.876	0.935	0.994	0.666
K	0.050	0.093	0.028	0.043	0.132	0.036	0.113	0.016	0.018	0.029	0.060	0.071	0.028	0.071	0.075	0.054	0.036	0.054	0.051	0.063	0.082	0.020	0.046	0.094	0.024	0.024	0.035	0.016
Ni				0.000	0.002																							
Ba	0.002	0.005	0.000			0.000	0.001	0.001	0.000	0.000	0.003	0.002	0.001	0.000	0.003	0.001	0.000	0.002	0.001	0.001	0.001	0.001	0.001	0.003	0.001	0.000	0.001	0.000
Sr	0.025	0.019	0.021			0.016	0.015	0.017	0.017	0.018	0.016	0.016	0.015	0.014	0.016	0.018	0.018	0.022	0.017	0.020	0.018	0.024	0.018	0.014	0.018	0.019	0.023	0.016
Total	20.056	20.075	20.104	20.021	20.035	20.032	20.063	20.052	20.054	20.071	20.092	20.047	20.084	20.024	20.057	20.060	20.063	20.049	20.061	20.053	20.051	20.057	20.047	20.047	20.061	20.013	20.100	20.077
X location	34.763	35.422	37.459	67.308	67.472	69.864	69.864	69.864	69.864	69.864	69.864	69.864	73.120	74.635	74.751	74.498	73.239	71.775	70.758	69.363	68.286	68.286	68.286	68.286	63.957	64.742	64.516	64.445
Y location	74.370	73.799	73.766	60.649	63.520	69.836	69.869	69.903	69.941	69.985	70.007	70.027	67.169	69.475	69.320	70.382	71.500	71.769	74.172	74.321	73.477	73.365	73.254	73.129	68.856	65.669	63.277	63.208
Crystal #	8				18	9	9	9	9	9	9	9		10	10						11	11	11	11			12	12
Comments						Core						Rim									Core			Rim				
An	65	51	75	73	60	81	53	83	84	75	59	55	81	51	51	64	70	57	64	59	51	78	66	49	78	76	75	83
Ab	34	47	24	25	37	18	44	17	16	24	39	44	18	47	47	34	29	42	34	40	47	22	33	49	21	23	24	16
Or	1	2	1	1	3	1	3	0	0	1	1	2	1	2	2	1	1	1	1	2	2	1	1	2	1	1	1	0

Sample	SV20	SV20	SV20	SV20	SV20	SV20	SV20	SV20	SV20	SV20	SV20	SV20	SV20	SV20	SV20	SV20	SV20
Rock Type	MUG	MUG	MUG	MUG	MUG	MUG	MUG	MUG	MUG	MUG	MUG	MUG	MUG	MUG	MUG	MUG	MUG
Analysis	06-104	06-105	06-106	06-107	06-108	06-109	06-110	06-111	06-112	06-113	06-114	06-115	06-116	06-117	06-118	06-119	06-120
SiO_2	50.44	50.14	51.66	51.78	50.42	53.74	54.43	47.10	51.09	46.77	46.89	50.37	52.62	57.96	50.82	54.64	55.25
TiO_2																	
Al_2O_3	30.84	31.11	30.00	29.89	30.91	28.92	28.50	33.24	30.45	33.04	33.24	30.68	29.55	25.85	30.76	28.07	27.67
Cr_2O_3																	
FeO	0.54	0.63	0.54	0.52	0.66	0.60	0.54	0.58	0.51	0.51	0.57	0.51	0.49	0.44	0.52	0.48	0.57
MnO																	
MgO																	
CaO	14.70	15.05	13.96	13.50	14.77	11.96	11.34	17.47	14.22	17.65	17.67	14.49	12.88	8.63	14.45	11.21	10.62
Na_2O	3.30	3.17	3.85	4.03	3.34	4.80	4.97	1.76	3.66	1.74	1.75	3.39	4.27	6.62	3.46	5.21	5.41
K_2O	0.16	0.13	0.19	0.19	0.15	0.30	0.30	0.08	0.22	0.06	0.05	0.14	0.22	0.49	0.16	0.30	0.38
NiO																	
BaO	0.00	0.00	0.00	0.01	0.02	0.00	0.02	0.00	0.00	0.00	0.01	0.00	0.02	0.04	0.02	0.02	0.03
SrO	0.11	0.16	0.14	0.19	0.13	0.16	0.10	0.12	0.10	0.14	0.13	0.18	0.12	0.14	0.15	0.17	0.14
Total	100.09	100.38	100.33	100.10	100.40	100.47	100.21	100.34	100.26	99.92	100.31	99.76	100.17	100.18	100.33	100.09	100.06
Si (32 O)	9.225	9.159	9.409	9.445	9.204	9.724	9.844	8.662	9.319	8.645	8.635	9.242	9.564	10.415	9.266	9.897	9.997
Ti																	
Al	6.648	6.698	6.439	6.426	6.651	6.167	6.076	7.207	6.547	7.199	7.215	6.634	6.331	5.475	6.612	5.993	5.902
Cr																	
Fe_2	0.083	0.096	0.083	0.079	0.100	0.090	0.082	0.089	0.078	0.079	0.088	0.078	0.075	0.066	0.079	0.072	0.086
Mn																	
Mg																	
Ca	2.881	2.945	2.725	2.638	2.889	2.318	2.197	3.442	2.780	3.497	3.487	2.848	2.509	1.663	2.823	2.176	2.059
Na	1.170	1.123	1.358	1.424	1.183	1.683	1.744	0.627	1.294	0.623	0.625	1.207	1.506	2.307	1.223	1.829	1.897
K	0.036	0.031	0.043	0.044	0.035	0.069	0.070	0.019	0.051	0.015	0.011	0.033	0.051	0.113	0.037	0.069	0.088
Ni																	
Ba	0.000	0.000	0.000	0.000	0.001	0.000	0.001	0.000	0.000	0.000	0.000	0.000	0.001	0.003	0.001	0.001	0.002
Sr	0.012	0.017	0.015	0.020	0.014	0.017	0.011	0.013	0.010	0.015	0.014	0.019	0.012	0.015	0.016	0.018	0.014
Total	20.054	20.068	20.072	20.076	20.079	20.068	20.025	20.058	20.080	20.074	20.075	20.061	20.049	20.057	20.058	20.055	20.044
X location	64.850	64.878	64.904	64.938	64.968	64.974	64.993	65.883	65.883	65.883	65.883	65.883	65.883	67.022	67.067	67.118	67.073
Y location	60.057	60.092	60.126	60.149	60.172	60.196	60.203	57.922	57.856	57.806	57.761	57.687	57.541	58.208	58.128	58.048	57.821
Crystal #	13	13	13	13	13	13	13	14	14	14	14	14	14	15	15	15	15
Comments	Core						Rim	Core					Rim	Core			Rim
An	70	72	66	64	70	57	55	84	67	85	85	70	62	41	69	53	51
Ab	29	27	33	35	29	41	43	15	31	15	15	30	37	57	30	45	47
Or	1	1	1	1	1	2	2	0	1	0	0	1	1	3	1	2	2

Sample	SV38	SV38	SV38	SV38	SV38	SV38	SV38	SV38	SV38	SV38	SV38
Rock Type	XEN	XEN	XEN	XEN	XEN	XEN	XEN	XEN	TRAC	TRAC	TRAC
Analysis	03-058	03-059	03-060	03-061	03-064	03-068	03-070	03-073	03-075	03-076	03-077
SiO_2	45.90	46.46	45.81	45.90	61.91	46.43	46.17	45.44	61.59	62.30	65.75
TiO_2	0.00	0.00	0.00	0.04	0.01	0.00	0.02	0.00	0.01	0.00	0.02
Al_2O_3	34.60	34.11	34.77	34.29	23.80	34.21	34.34	34.73	24.00	23.18	21.04
Cr_2O_3	0.00	0.04	0.00	0.00	0.01	0.03	0.00	0.00	0.00	0.00	0.02
FeO	0.22	0.27	0.25	0.22	0.17	0.25	0.22	0.26	0.17	0.18	0.17
MnO	0.00	0.00	0.00	0.00	0.04	0.03	0.00	0.01	0.02	0.00	0.01
MgO	0.00	0.00	0.00	0.00	0.00	0.00	0.00	0.00	0.00	0.00	0.00
CaO	18.21	17.81	18.37	18.33	5.25	17.88	18.29	18.34	5.74	4.67	2.25
Na_2O	1.16	1.44	1.20	1.22	8.51	1.49	1.33	1.06	8.09	8.65	9.90
K_2O	0.01	0.01	0.01	0.02	0.41	0.02	0.00	0.01	0.48	0.53	0.92
NiO	0.00	0.00	0.00	0.00	0.04	0.00	0.01	0.00	0.00	0.01	0.01
BaO											
SrO											
Total	100.10	100.14	100.40	100.03	100.15	100.34	100.37	99.85	100.09	99.50	100.08
Si (32 O)	8.451	8.545	8.417	8.465	10.989	8.528	8.484	8.396	10.945	11.108	11.593
Ti	0.000	0.000	0.000	0.006	0.002	0.000	0.003	0.000	0.001	0.000	0.003
Al	7.509	7.395	7.531	7.454	4.980	7.405	7.437	7.563	5.028	4.873	4.372
Cr	0.000	0.006	0.000	0.000	0.002	0.004	0.000	0.000	0.000	0.000	0.002
Fe_2	0.034	0.041	0.038	0.034	0.026	0.039	0.033	0.039	0.025	0.027	0.025
Mn	0.000	0.000	0.000	0.001	0.005	0.004	0.000	0.002	0.002	0.000	0.002
Mg	0.000	0.000	0.000	0.000	0.000	0.000	0.000	0.000	0.001	0.000	0.000
Ca	3.592	3.510	3.617	3.622	0.999	3.518	3.600	3.630	1.092	0.892	0.426
Na	0.416	0.513	0.426	0.436	2.929	0.532	0.473	0.381	2.787	2.989	3.383
K	0.003	0.003	0.001	0.006	0.092	0.005	0.001	0.001	0.108	0.120	0.207
Ni	0.000	0.000	0.000	0.000	0.005	0.000	0.001	0.000	0.000	0.001	0.001
Ba											
Sr											
Total	20.004	20.012	20.031	20.023	20.029	20.036	20.032	20.013	19.988	20.010	20.013
X location	66.369	66.369	66.564	66.728	64.076	65.536	70.715	78.118	75.222	75.072	74.964
Y location	73.706	73.565	73.648	73.648	73.736	76.038	74.004	74.048	69.258	69.258	69.258
Crystal #									3	3	3
Comments									Core		Rim
An	90	87	89	89	25	87	88	90	27	22	11
Ab	10	13	11	11	73	13	12	9	70	75	84
Or	0	0	0	0	2	0	0	0	3	3	5

Sample	SV38	SV38	SV38	SV38	SV38	SV38	SV38	SV38	SV38	SV38	SV38	SV38	SV38	SV38	SV38	SV38	SV38	SV38	SV38	SV38	SV38	SV38	SV38	SV38	SV38	SV38	SV38	SV38
Rock Type	TRAC	TRAC	TRAC	TRAC	TRAC	TRAC	TRAC	TRAC	TRAC	TRAC	TRAC	TRAC	TRAC	TRAC	TRAC	TRAC	TRAC	TRAC	TRAC	TRAC	TRAC	TRAC	TRAC	TRAC	TRAC	TRAC	TRAC	TRAC
Analysis	03-078	03-079	03-080	03-081	03-082	03-083	03-084	03-086	03-087	03-088	03-089	03-090	03-091	03-092	03-093	03-094	03-095	03-096	03-097	03-098	03-099	03-100	03-101	03-102	03-103	04-001	04-002	04-003
SiO_2	56.72	57.46	59.69	63.42	63.51	62.11	63.93	60.30	59.87	60.82	62.20	61.02	60.88	60.39	60.57	63.33	62.88	59.72	60.76	62.92	63.86	66.57	66.64	65.70	64.88	60.66	61.04	62.18
TiO_2	0.00	0.02	0.02	0.01	0.00	0.00	0.00	0.00	0.00	0.00	0.00	0.00	0.00	0.01	0.00	0.00	0.01	0.03	0.01	0.00	0.00	0.00	0.00	0.00	0.00			
Al_2O_3	26.95	26.74	25.31	22.27	22.69	23.47	22.42	24.70	25.37	24.50	23.65	24.49	24.52	24.92	24.78	22.82	23.08	25.07	24.49	23.27	22.58	20.75	20.53	21.11	21.77	24.63	24.28	23.73
Cr_2O_3	0.00	0.00	0.00	0.00	0.01	0.00	0.01	0.00	0.00	0.01	0.00	0.00	0.00	0.00	0.00	0.00	0.00	0.02	0.00	0.02	0.01	0.00	0.02	0.00	0.00			
FeO	0.19	0.16	0.10	0.13	0.17	0.17	0.21	0.13	0.13	0.09	0.08	0.09	0.11	0.09	0.14	0.13	0.14	0.13	0.16	0.09	0.16	0.18	0.23	0.18	0.22	0.12	0.11	0.09
MnO	0.00	0.00	0.02	0.00	0.01	0.00	0.00	0.04	0.01	0.00	0.03	0.00	0.02	0.03	0.00	0.00	0.00	0.03	0.01	0.01	0.00	0.01	0.01	0.00	0.01			
MgO	0.00	0.00	0.00	0.00	0.00	0.00	0.00	0.00	0.00	0.01	0.00	0.00	0.00	0.00	0.00	0.00	0.01	0.01	0.00	0.01	0.00	0.00	0.00	0.01	0.01			
CaO	9.32	9.00	7.09	3.68	4.05	4.97	3.82	6.26	6.97	6.09	5.06	6.09	6.03	6.63	6.33	4.16	4.58	6.98	6.00	4.61	3.87	1.92	1.68	2.32	3.03	6.13	5.94	5.34
Na_2O	6.33	6.46	7.62	9.37	9.07	8.57	9.14	7.98	7.41	7.97	8.38	8.12	8.03	7.65	7.79	8.99	8.89	7.53	7.99	8.98	9.19	10.11	10.01	9.62	9.47	7.94	7.96	8.43
K_2O	0.16	0.15	0.24	0.50	0.50	0.46	0.63	0.34	0.30	0.34	0.41	0.37	0.38	0.34	0.34	0.51	0.49	0.31	0.37	0.49	0.56	1.01	1.12	0.91	0.75	0.33	0.36	0.41
NiO	0.01	0.02	0.01	0.00	0.01	0.00	0.02	0.00	0.02	0.01	0.03	0.04	0.02	0.04	0.01	0.00	0.00	0.00	0.02	0.00	0.02	0.00	0.01	0.00	0.02			
BaO																										0.03	0.03	0.06
SrO																										0.32	0.35	0.26
Total	99.69	100.02	100.11	99.37	100.02	99.73	100.18	99.74	100.09	99.84	99.84	100.20	99.98	100.09	99.96	99.94	100.07	99.82	99.80	100.40	100.26	100.56	100.25	99.85	100.15	100.15	100.06	100.49
Si (32 O)	10.226	10.307	10.646	11.295	11.243	11.056	11.299	10.776	10.669	10.840	11.049	10.844	10.840	10.753	10.790	11.220	11.145	10.679	10.838	11.120	11.276	11.673	11.715	11.597	11.446	10.806	10.875	11.011
Ti	0.000	0.003	0.003	0.001	0.000	0.000	0.000	0.000	0.000	0.000	0.000	0.000	0.000	0.001	0.000	0.000	0.001	0.004	0.001	0.000	0.000	0.000	0.000	0.000	0.000			
Al	5.728	5.654	5.321	4.675	4.735	4.923	4.671	5.203	5.328	5.148	4.952	5.129	5.146	5.230	5.203	4.764	4.822	5.284	5.148	4.847	4.699	4.289	4.254	4.392	4.527	5.172	5.098	4.953
Cr	0.000	0.000	0.000	0.000	0.001	0.000	0.002	0.000	0.000	0.001	0.000	0.000	0.000	0.000	0.001	0.000	0.000	0.003	0.000	0.002	0.002	0.000	0.002	0.000	0.000			
Fe_2	0.029	0.024	0.015	0.020	0.026	0.025	0.031	0.020	0.019	0.013	0.012	0.013	0.017	0.014	0.020	0.019	0.020	0.019	0.024	0.013	0.024	0.027	0.034	0.027	0.033	0.018	0.016	0.013
Mn	0.000	0.000	0.004	0.000	0.002	0.000	0.000	0.006	0.002	0.000	0.005	0.000	0.003	0.004	0.000	0.001	0.000	0.004	0.001	0.002	0.000	0.001	0.002	0.000	0.001			
Mg	0.000	0.000	0.000	0.000	0.000	0.000	0.000	0.000	0.000	0.002	0.000	0.000	0.000	0.000	0.001	0.000	0.002	0.001	0.000	0.003	0.000	0.000	0.000	0.002	0.003			
Ca	1.800	1.731	1.355	0.701	0.768	0.947	0.723	1.198	1.331	1.163	0.964	1.160	1.150	1.265	1.209	0.790	0.869	1.338	1.146	0.873	0.733	0.361	0.316	0.439	0.572	1.170	1.133	1.013
Na	2.213	2.246	2.636	3.237	3.114	2.958	3.132	2.765	2.562	2.756	2.888	2.797	2.771	2.642	2.691	3.089	3.055	2.611	2.765	3.076	3.146	3.438	3.412	3.294	3.241	2.741	2.749	2.893
K	0.036	0.035	0.055	0.113	0.112	0.103	0.142	0.078	0.069	0.078	0.093	0.083	0.085	0.076	0.076	0.116	0.112	0.069	0.085	0.111	0.127	0.226	0.251	0.205	0.168	0.074	0.081	0.093
Ni	0.002	0.004	0.001	0.000	0.002	0.000	0.003	0.000	0.003	0.001	0.004	0.005	0.002	0.006	0.002	0.000	0.000	0.000	0.003	0.000	0.003	0.000	0.002	0.000	0.003			0.002
Ba																												0.033
Sr																												
Total	20.034	20.004	20.036	20.042	20.002	20.013	20.001	20.044	19.982	20.002	19.966	20.032	20.014	19.990	19.992	20.000	20.027	20.013	20.012	20.048	20.009	20.014	19.988	19.956	19.994	20.016	19.991	20.006
X location	73.870	73.834	73.801	73.762	73.729	73.704	73.674	76.249	76.249	76.281	76.250	76.250	76.250	76.250	76.250	76.235	76.235	76.235	76.174	76.174	76.174	76.174	76.174	76.208	76.208	76.243	76.154	76.103
Y location	68.878	68.878	68.878	68.878	68.878	68.878	68.878	67.347	67.274	67.247	67.202	67.161	67.128	67.093	67.077	67.044	66.992	66.946	66.891	66.852	66.815	66.755	66.698	66.669	66.647	67.298	67.229	67.177
Crystal #	4	4	4	4	4	4	4	5	5	5	5	5	5	5	5	5	5	5	5	5	5	5	5	5	5	1	1	1
Comments	Core								Core																Rim	Core		
An	44	43	33	17	19	24	18	30	34	29	24	29	29	32	30	20	22	33	29	22	18	9	8	11	14	29	29	25
Ab	55	56	65	80	78	74	78	68	65	69	73	69	69	66	68	77	76	65	69	76	79	85	86	84	81	69	69	72
Or	1	1	1	3	3	3	4	2	2	2	2	2	2	2	2	3	3	2	2	3	3	6	6	5	4	2	2	2

Sample	SV38	SV38	SV38	SV38	SV38	SV38	SV38	SV38	SV38	SV38	SV38	SV38	SV38	SV38
Rock Type	TRAC	TRAC	TRAC	TRAC	TRAC	TRAC	TRAC	TRAC	TRAC	TRAC	TRAC	TRAC	TRAC	TRAC
Analysis	04-004	04-005	04-006	04-007	04-008	04-009	04-010	04-011	04-012	04-013	04-014	04-015	04-016	04-017
SiO_2	61.73	61.29	62.71	63.37	60.10	60.70	61.05	62.74	65.58	58.34	60.36	59.37	61.45	60.93
TiO_2														
Al_2O_3	24.13	24.22	23.28	22.99	25.07	24.54	24.40	23.24	21.30	25.91	24.95	25.46	24.07	24.45
Cr_2O_3														
FeO	0.10	0.12	0.11	0.17	0.11	0.13	0.11	0.12	0.22	0.07	0.09	0.18	0.13	0.14
MnO														
MgO														
CaO	5.57	5.80	4.85	4.44	6.87	6.40	5.99	4.63	2.74	7.73	6.69	7.27	5.71	6.10
Na_2O	8.15	8.23	8.76	8.85	7.60	7.92	8.07	8.73	9.61	6.80	7.70	7.40	8.30	8.03
K_2O	0.38	0.37	0.46	0.49	0.33	0.38	0.39	0.52	0.97	0.27	0.29	0.26	0.34	0.34
NiO														
BaO	0.04	0.05	0.04	0.05	0.04	0.05	0.07	0.04	0.14	0.03	0.04	0.02	0.03	0.04
SrO	0.31	0.28	0.22	0.19	0.38	0.35	0.33	0.18	0.13	0.71	0.51	0.49	0.30	0.29
Total	100.41	100.36	100.44	100.55	100.49	100.48	100.41	100.19	100.69	99.86	100.63	100.45	100.33	100.32
Si (32 O)	10.943	10.889	11.098	11.184	10.697	10.797	10.852	11.120	11.530	10.487	10.729	10.594	10.917	10.837
Ti														
Al	5.043	5.072	4.857	4.783	5.260	5.145	5.111	4.856	4.415	5.490	5.226	5.356	5.039	5.125
Cr														
Fe_2	0.015	0.018	0.016	0.025	0.016	0.020	0.016	0.018	0.032	0.010	0.013	0.028	0.019	0.021
Mn														
Mg														
Ca	1.057	1.104	0.920	0.840	1.310	1.220	1.140	0.879	0.516	1.490	1.275	1.389	1.087	1.162
Na	2.802	2.836	3.007	3.030	2.623	2.731	2.781	3.000	3.277	2.370	2.655	2.559	2.859	2.771
K	0.085	0.084	0.103	0.110	0.075	0.086	0.089	0.117	0.218	0.062	0.065	0.059	0.078	0.078
Ni	0.002	0.004	0.003	0.004	0.003	0.003	0.003	0.004	0.005	0.003	0.010	0.002	0.003	0.002
Ba	0.036	0.027	0.032	0.028	0.023	0.019	0.039	0.036	0.034	0.018	0.013	0.074	0.053	0.051
Sr														
Total	19.979	20.035	20.028	19.994	20.022	20.039	20.028	20.011	20.010	19.984	20.018	20.037	20.032	20.025
X location	76.059	76.017	75.964	75.948	75.900	75.900	75.900	75.869	75.834	72.265	72.265	72.265	72.265	72.217
Y location	67.127	67.102	67.089	67.070	67.022	66.948	66.906	66.893	66.858	67.858	67.938	67.986	68.023	68.069
Crystal #	1	1	1	1	1	1	1	1	1	2	2	2	2	2
Comments									Rim	Core				Rim
An	27	27	23	21	33	30	28	22	13	38	32	35	27	29
Ab	71	70	75	76	65	68	69	75	82	60	66	64	71	69
Or	2	2	3	3	2	2	2	3	5	2	2	1	2	2

Sample	SV38	SV38	SV38	SV38	SV38	SV38	SV38	SV38	SV38	SV38	SV38	SV38	SV38	SV38
Rock Type	TRAC	TRAC	TRAC	TRAC	TRAC	TRAC	TRAC	TRAC	TRAC	TRAC	TRAC	TRAC	TRAC	TRAC
Analysis	04-018	04-019	04-020	04-021	04-022	04-023	04-024	04-025	04-026	04-027	04-028	04-029	04-030	04-031
SiO_2	59.26	59.29	59.98	66.27	64.97	66.58	65.98	58.41	59.27	60.23	59.20	61.88	62.06	58.84
TiO_2														
Al_2O_3	25.30	25.13	25.01	20.69	21.71	20.66	21.09	26.13	25.47	25.02	25.68	23.82	24.01	25.92
Cr_2O_3														
FeO	0.11	0.11	0.16	0.20	0.18	0.18	0.19	0.07	0.09	0.19	0.16	0.16	0.11	0.18
MnO														
MgO														
CaO	7.12	6.87	6.63	1.86	2.96	1.82	2.30	7.45	6.98	6.57	7.15	5.47	5.36	7.68
Na_2O	7.21	7.32	7.63	9.91	9.42	10.06	9.94	7.06	7.52	7.78	7.48	8.46	8.42	7.08
K_2O	0.35	0.36	0.37	1.02	0.74	1.01	0.91	0.30	0.30	0.29	0.24	0.33	0.33	0.27
NiO														
BaO	0.08	0.03	0.05	0.11	0.09	0.09	0.15	0.03	0.02	0.01	0.05	0.01	0.03	0.03
SrO	0.35	0.65	0.51	0.13	0.10	0.08	0.16	0.66	0.62	0.44	0.52	0.23	0.25	0.51
Total	99.78	99.77	100.33	100.17	100.17	100.48	100.71	100.12	100.28	100.52	100.49	100.34	100.56	100.51
Si (32 O)	10.629	10.648	10.701	11.675	11.465	11.689	11.585	10.472	10.597	10.715	10.564	10.976	10.976	10.505
Ti														
Al	5.348	5.320	5.260	4.296	4.516	4.276	4.366	5.521	5.367	5.246	5.402	4.980	5.005	5.455
Cr														
Fe_2	0.017	0.016	0.024	0.029	0.026	0.026	0.028	0.011	0.014	0.028	0.023	0.023	0.016	0.026
Mn														
Mg														
Ca	1.369	1.323	1.267	0.352	0.560	0.343	0.433	1.432	1.338	1.252	1.367	1.039	1.016	1.469
Na	2.506	2.549	2.641	3.383	3.222	3.426	3.384	2.456	2.608	2.683	2.588	2.910	2.887	2.451
K	0.079	0.082	0.083	0.229	0.168	0.226	0.204	0.069	0.069	0.066	0.056	0.074	0.074	0.062
Ni	0.002	0.003	0.006	0.002	0.004	0.007	0.006	0.006	0.010	0.002	0.002	0.001	0.003	0.001
Ba	0.031	0.030	0.037	0.068	0.053	0.013	0.010	0.008	0.016	0.068	0.064	0.045	0.054	0.023
Sr														
Total	19.990	20.008	20.031	19.983	19.972	20.000	20.026	20.030	20.059	20.036	20.057	20.026	20.002	20.024
X location	71.021	71.057	71.094	71.246	71.246	71.282	71.320	69.929	69.857	69.807	69.742	69.779	69.779	60.048
Y location	67.067	67.030	66.985	66.939	66.888	66.872	66.858	66.573	66.455	66.406	66.364	66.273	66.246	71.800
Crystal #	3	3	3	3	3	3	3	4	4	4	4	4	4	5
Comments	Core						Rim	Core					Rim	Core
An	35	33	32	9	14	9	11	36	33	31	34	26	26	37
Ab	63	64	66	85	82	86	84	62	65	67	65	72	73	62
Or	2	2	2	6	4	6	5	2	2	2	1	2	2	2

Sample	SV38	SV38	SV38	SV38	SV38	SV38	SV38	SV38	SV38	SV38	SV38	SV38	SV38	SV38
Rock Type	TRAC	TRAC	TRAC	TRAC	TRAC	TRAC	TRAC	TRAC	TRAC	TRAC	TRAC	TRAC	TRAC	TRAC
Analysis	04-032	04-033	04-034	04-035	04-036	04-037	04-038	04-039	04-040	04-041	04-042	04-043	04-045	04-046
SiO_2	60.64	60.89	60.59	61.38	63.28	66.22	66.26	58.30	58.75	57.63	62.66	59.77	59.35	60.94
TiO_2														
Al_2O_3	24.71	24.24	24.73	24.05	22.89	21.02	20.73	25.98	25.74	26.54	23.26	25.07	25.50	24.50
Cr_2O_3														
FeO	0.17	0.14	0.14	0.12	0.14	0.19	0.26	0.04	0.10	0.17	0.12	0.18	0.18	0.17
MnO														
MgO														
CaO	6.24	5.80	6.30	5.56	4.44	2.25	2.03	8.03	7.64	8.69	4.83	7.09	7.11	6.06
Na_2O	7.80	8.11	7.68	8.21	8.97	10.00	9.78	6.88	7.11	6.52	8.60	7.45	7.36	8.02
K_2O	0.39	0.41	0.38	0.46	0.55	0.97	1.24	0.38	0.36	0.24	0.49	0.32	0.32	0.40
NiO														
BaO	0.04	0.05	0.08	0.03	0.05	0.11	0.18	0.00	0.04	0.00	0.07	0.04	0.05	0.06
SrO	0.47	0.43	0.44	0.36	0.17	0.09	0.10	0.67	0.64	0.42	0.27	0.33	0.40	0.37
Total	100.45	100.07	100.34	100.16	100.48	100.85	100.58	100.28	100.38	100.21	100.29	100.25	100.28	100.52
Si (32 O)	10.787	10.864	10.786	10.924	11.184	11.606	11.652	10.454	10.516	10.340	11.106	10.671	10.602	10.827
Ti														
Al	5.181	5.097	5.190	5.044	4.769	4.343	4.298	5.491	5.431	5.613	4.858	5.275	5.368	5.132
Cr														
Fe_2	0.026	0.021	0.021	0.018	0.020	0.028	0.039	0.007	0.015	0.026	0.017	0.026	0.026	0.026
Mn														
Mg														
Ca	1.189	1.109	1.203	1.061	0.840	0.423	0.382	1.542	1.465	1.671	0.917	1.357	1.361	1.155
Na	2.692	2.806	2.653	2.833	3.072	3.397	3.335	2.393	2.466	2.268	2.956	2.580	2.549	2.762
K	0.087	0.093	0.086	0.103	0.124	0.217	0.278	0.086	0.083	0.055	0.112	0.073	0.073	0.090
Ni	0.002	0.002	0.002	0.004	0.005	0.002	0.003	0.008	0.012	0.000	0.003	0.000	0.002	0.003
Ba	0.025	0.053	0.048	0.045	0.045	0.037	0.018	0.009	0.010	0.069	0.067	0.044	0.034	0.015
Sr														
Total	20.012	20.037	19.988	20.022	20.030	20.030	20.005	20.040	20.043	20.016	19.999	20.019	20.025	20.033
X location	59.980	59.980	59.980	59.913	59.891	59.822	59.822	59.948	59.879	59.837	59.791	59.791	58.316	58.316
Y location	71.767	71.737	71.706	71.706	71.677	71.691	71.609	73.506	73.506	73.506	73.506	73.464	69.713	69.658
Crystal #	5	5	5	5	5	5	5	6	6	6	6	6	7	7
Comments							Rim	Core					Core	
An	30	28	31	27	21	10	10	38	36	42	23	34	34	29
Ab	68	70	67	71	76	84	83	60	61	57	74	64	64	69
Or	2	2	2	3	3	5	7	2	2	1	3	2	2	2

Sample	SV38	SV38	SV38	SV38	SV38	SV38	SV38	SV38	SV38	SV38	SV38	SV38	SV38	SV38
Rock Type	TRAC	TRAC	TRAC	TRAC	TRAC	TRAC	TRAC	TRAC	TRAC	TRAC	TRAC	TRAC	TRAC	TRAC
Analysis	04-047	04-048	04-049	04-050	04-051	04-053	04-054	04-055	04-056	04-057	04-058	04-059	04-060	04-061
SiO_2	61.52	67.37	66.07	65.88	65.98	62.92	62.69	64.01	65.06	65.62	65.09	64.44	65.68	58.51
TiO_2														
Al_2O_3	24.18	20.35	21.14	21.29	21.43	23.16	23.33	22.56	21.80	21.13	21.84	22.31	20.57	25.95
Cr_2O_3														
FeO	0.17	0.19	0.23	0.18	0.21	0.13	0.11	0.07	0.13	0.22	0.15	0.15	0.24	0.14
MnO														
MgO														
CaO	5.73	1.50	2.34	2.32	2.40	4.70	4.77	3.95	3.09	2.37	2.65	3.18	2.18	7.97
Na_2O	8.16	10.06	9.90	10.08	10.03	8.72	8.55	9.04	9.46	9.58	9.84	9.41	9.67	6.98
K_2O	0.44	1.14	0.98	0.56	0.56	0.51	0.53	0.61	0.71	0.95	0.77	0.69	1.04	0.35
NiO														
BaO	0.09	0.12	0.14	0.15	0.15	0.05	0.07	0.08	0.07	0.10	0.09	0.13	0.12	0.04
SrO	0.29	0.06	0.16	0.19	0.16	0.23	0.24	0.17	0.13	0.12	0.31	0.43	0.15	0.35
Total	100.58	100.80	100.94	100.65	100.92	100.42	100.28	100.49	100.45	100.10	100.73	100.75	99.65	100.28
Si (32 O)	10.909	11.777	11.580	11.562	11.548	11.132	11.107	11.287	11.452	11.580	11.445	11.347	11.648	10.474
Ti														
Al	5.053	4.193	4.367	4.403	4.420	4.830	4.872	4.689	4.522	4.396	4.526	4.631	4.301	5.475
Cr														
Fe_2	0.025	0.028	0.033	0.026	0.031	0.019	0.016	0.010	0.019	0.033	0.022	0.022	0.036	0.021
Mn														
Mg														
Ca	1.088	0.281	0.439	0.436	0.450	0.891	0.905	0.747	0.583	0.449	0.499	0.600	0.414	1.528
Na	2.807	3.411	3.363	3.432	3.406	2.992	2.937	3.090	3.229	3.277	3.353	3.214	3.325	2.422
K	0.100	0.253	0.218	0.125	0.124	0.116	0.119	0.138	0.159	0.215	0.172	0.156	0.235	0.080
Ni	0.004	0.004	0.006	0.008	0.009	0.011	0.009	0.003	0.005	0.006	0.005	0.007	0.006	0.009
Ba	0.042	0.038	0.030	0.006	0.016	0.016	0.015	0.024	0.025	0.017	0.013	0.012	0.032	0.044
Sr														
Total	20.018	19.958	20.027	20.015	20.007	20.007	19.985	19.983	19.982	19.968	20.054	20.023	19.982	20.040
X location	58.316	58.316	58.316	64.663	64.663	64.643	64.643	64.643	64.643	64.643	69.811	69.679	69.448	70.048
Y location	69.618	69.587	69.548	60.812	60.927	59.409	59.334	59.271	59.235	59.201	59.683	59.683	59.683	55.419
Crystal #	7	7	7	8	8	9	9	9	9	9	10	10	10	11
Comments			Rim	Core		Core				Rim	Core		Rim	Core
An	27	7	11	11	11	22	23	19	15	11	12	15	10	38
Ab	70	86	84	86	86	75	74	78	81	83	83	81	84	60
Or	2	6	5	3	3	3	3	3	4	5	4	4	6	2

Sample	SV38	SV38	SV38	SV38	SV38	SV38	SV38	SV38	SV38	SV38	SV38	SV38	SV38	SV38	SV38	SV38	SV38	SV38	SV38	SV38	SV38	SV38	SV38	SV38	SV38	SV38	SV38	SV38
Rock Type	TRAC	TRAC	TRAC	TRAC	TRAC	TRAC	TRAC	TRAC	TRAC	TRAC	TRAC	TRAC	TRAC	TRAC	TRAC	TRAC	TRAC	TRAC	TRAC	TRAC	TRAC	TRAC	TRAC	TRAC	TRAC	TRAC	TRAC	TRAC
Analysis	04-062	04-063	04-064	04-065	04-066	04-067	04-068	04-069	04-070	04-071	04-072	04-073	04-074	04-075	04-076	04-077	04-078	04-079	04-080	04-081	04-082	04-083	04-084	04-085	04-086	04-087	04-088	04-089
SiO_2	59.10	57.96	60.51	62.33	63.62	59.80	57.80	59.50	64.10	66.00	58.85	57.66	57.23	60.30	61.99	66.15	57.83	59.97	59.55	58.31	58.37	59.63	60.89	58.06	61.29	60.83	58.99	57.90
TiO_2																												
Al_2O_3	25.40	26.19	24.41	23.55	22.55	25.12	26.75	25.51	22.59	21.22	25.81	26.62	26.96	25.02	23.75	21.11	25.68	24.98	25.42	26.13	26.05	25.43	24.65	26.58	24.36	24.61	25.73	26.36
Cr_2O_3																												
FeO	0.08	0.12	0.13	0.13	0.13	0.19	0.19	0.13	0.12	0.18	0.14	0.14	0.14	0.14	0.18	0.16	0.04	0.05	0.08	0.06	0.09	0.04	0.05	0.09	0.02	0.03	0.04	0.18
MnO																												
MgO																												
CaO	7.35	8.25	6.39	5.10	4.04	6.97	8.58	7.05	3.76	2.37	7.59	8.73	8.96	6.84	5.35	2.26	7.97	6.70	7.23	8.13	8.08	7.31	6.15	8.29	5.74	6.15	7.57	8.38
Na_2O	7.28	6.71	7.76	8.57	9.13	7.37	6.67	7.32	9.38	9.92	7.11	6.67	6.47	7.60	8.48	9.87	6.91	7.61	7.45	6.81	6.89	7.36	7.95	6.84	8.22	8.05	7.18	6.64
K_2O	0.28	0.23	0.32	0.35	0.48	0.27	0.23	0.32	0.60	0.86	0.30	0.26	0.23	0.34	0.46	0.88	0.29	0.28	0.26	0.23	0.22	0.27	0.30	0.20	0.37	0.35	0.27	0.23
NiO																												
BaO	0.04	0.02	0.03	0.04	0.07	0.04	0.03	0.05	0.05	0.11	0.05	0.00	0.01	0.04	0.06	0.10	0.03	0.01	0.02	0.01	0.03	0.01	0.02	0.02	0.01	0.05	0.02	0.04
SrO	0.61	0.53	0.40	0.34	0.20	0.36	0.39	0.40	0.15	0.11	0.42	0.37	0.36	0.24	0.25	0.11	0.41	0.37	0.39	0.42	0.43	0.39	0.42	0.40	0.37	0.39	0.46	0.56
Total	100.14	100.00	99.93	100.42	100.21	100.10	100.65	100.27	100.76	100.77	100.27	100.45	100.36	100.53	100.52	100.64	99.16	99.96	100.40	100.10	100.16	100.43	100.43	100.47	100.37	100.47	100.27	100.29
Si (32 O)	10.586	10.412	10.812	11.043	11.258	10.680	10.327	10.619	11.279	11.574	10.525	10.325	10.261	10.718	10.988	11.605	10.469	10.715	10.618	10.448	10.457	10.623	10.816	10.376	10.883	10.810	10.543	10.382
Ti																												
Al	5.363	5.546	5.140	4.918	4.703	5.288	5.633	5.365	4.685	4.386	5.440	5.618	5.697	5.243	4.961	4.365	5.480	5.261	5.342	5.520	5.501	5.340	5.161	5.599	5.097	5.156	5.421	5.572
Cr																												
Fe_2	0.011	0.018	0.020	0.019	0.019	0.028	0.029	0.019	0.018	0.026	0.021	0.022	0.021	0.021	0.027	0.024	0.006	0.008	0.012	0.009	0.014	0.006	0.007	0.013	0.003	0.005	0.007	0.027
Mn																												
Mg																												
Ca	1.411	1.588	1.223	0.969	0.766	1.334	1.643	1.349	0.709	0.445	1.454	1.675	1.722	1.303	1.016	0.425	1.545	1.282	1.380	1.561	1.551	1.395	1.171	1.587	1.092	1.171	1.450	1.610
Na	2.527	2.336	2.687	2.945	3.131	2.552	2.310	2.533	3.202	3.372	2.467	2.316	2.250	2.621	2.915	3.358	2.425	2.637	2.576	2.365	2.394	2.542	2.739	2.369	2.829	2.775	2.489	2.310
K	0.065	0.052	0.072	0.079	0.109	0.061	0.053	0.072	0.136	0.193	0.068	0.059	0.053	0.077	0.104	0.196	0.067	0.064	0.059	0.053	0.051	0.062	0.067	0.045	0.083	0.079	0.062	0.053
Ni	0.008	0.003	0.003	0.001	0.002	0.003	0.005	0.003	0.002	0.003	0.003	0.008	0.003	0.000	0.001	0.003	0.004	0.007	0.002	0.001	0.002	0.001	0.002	0.001	0.002	0.001	0.001	0.003
Ba	0.015	0.037	0.064	0.056	0.042	0.035	0.020	0.037	0.040	0.042	0.016	0.012	0.044	0.039	0.037	0.025	0.026	0.011	0.043	0.038	0.040	0.043	0.044	0.041	0.044	0.042	0.038	0.040
Sr																												
Total	20.028	20.009	19.997	20.011	20.011	19.982	20.038	20.001	20.047	20.015	20.023	20.054	20.042	20.010	20.041	19.990	20.038	20.005	20.029	20.000	20.015	20.009	20.007	20.032	20.025	20.039	20.021	20.014
X location	66.433	66.332	66.250	66.250	66.250	66.210	63.699	63.699	63.699	63.704	60.649	60.594	60.594	60.594	60.594	60.567	59.563	59.649	59.681	59.744	59.798	59.840	59.920	59.965	60.028	60.083	60.173	60.265
Y location	56.140	56.140	56.140	56.085	56.002	55.928	56.375	56.453	56.501	56.545	55.245	55.348	55.429	55.522	55.560	55.639	55.388	55.388	55.388	55.350	55.350	55.350	55.350	55.350	55.350	55.350	55.350	55.427
Crystal #	11	11	11	11	11	11	12	12	12	12	13	13	13	13	13	13	14	14	14	14	14	14	14	14	14	14	14	14
Comments						Rim	Core			Rim	Core					Rim	Core											
An	35	40	31	24	19	34	41	34	18	11	36	41	43	33	25	11	38	32	34	39	39	35	29	40	27	29	36	41
Ab	63	59	67	74	78	65	58	64	79	84	62	57	56	65	72	84	60	66	64	59	60	64	69	59	71	69	62	58
Or	2	1	2	2	3	2	1	2	3	5	2	1	1	2	3	5	2	2	1	1	1	2	2	1	2	2	2	1

Sample	SV38	SV39	SV39	SV39	SV39	SV39	SV39	SV39	SV39	SV39	SV39	SV39	SV39	SV39	SV39	SV39	SV39	SV39	SV39	SV40	SV40	SV40	SV40	SV40	SV40	SV40	SV40	SV40
Rock Type	TRAC	XEN	XEN	TRAC	TRAC	TRAC	TRAC	TRAC	TRAC	TRAC	TRAC	TRAC	TRAC	TRAC	TRAC	TRAC	TRAC	TRAC	TRAC	TRAC	TRAC	TRAC	XEN	TRAC	TRAC	TRAC	TRAC	TRAC
Analysis	04-090	12-002	12-003	12-010	12-016	12-017	12-020	12-021	12-022	12-023	12-024	12-025	12-026	12-027	12-029	12-030	12-031	12-032	12-034	11-008	11-009	11-010	11-014	11-021	11-022	11-023	11-024	11-025
SiO_2	61.88	60.79	53.63	61.24	62.34	59.15	67.14	59.05	59.02	59.15	59.41	59.21	58.29	63.82	64.46	57.10	61.04	62.28	60.02	58.85	60.41	65.47	64.29	58.87	62.49	58.45	61.71	63.09
TiO_2		0.00	0.03	0.00	0.00	0.05	0.18	0.00	0.00	0.01	0.00	0.00	0.02	0.00	0.00	0.01	0.00	0.00	0.00	0.00	0.00	0.00	0.00	0.00	0.00	0.00	0.00	0.00
Al_2O_3	23.79	24.78	29.10	24.65	23.92	25.76	18.98	25.97	26.11	25.93	25.54	25.40	25.25	22.64	22.26	25.91	23.83	23.96	24.70	25.16	24.38	21.26	21.90	25.66	22.84	25.63	23.33	22.91
Cr_2O_3		0.00	0.00	0.00	0.02	0.04	0.06	0.04	0.00	0.00	0.00	0.00	0.00	0.00	0.00	0.05	0.00	0.02	0.00	0.00	0.00	0.03	0.02	0.00	0.00	0.00	0.00	0.02
FeO	0.13	0.18	0.19	0.11	0.15	0.24	0.89	0.01	0.04	0.08	0.08	0.09	0.14	0.20	0.11	0.20	0.15	0.14	0.24	0.22	0.19	0.22	0.22	0.15	0.11	0.10	0.08	0.14
MnO		0.00	0.00	0.02	0.02	0.04	0.00	0.00	0.00	0.00	0.00	0.03	0.02	0.01	0.00	0.02	0.00	0.01	0.00	0.01	0.03	0.00	0.01	0.00	0.03	0.00	0.03	0.02
MgO		0.00	0.00	0.00	0.00	0.00	0.65	0.00	0.00	0.01	0.02	0.00	0.00	0.01	0.03	0.00	0.00	0.00	0.01	0.01	0.00	0.01	0.00	0.01	0.00	0.01	0.00	0.00
CaO	5.38	6.67	11.65	6.27	5.42	7.49	2.02	7.85	7.90	7.62	7.35	7.36	7.52	4.03	3.81	8.25	5.80	5.43	6.49	7.24	6.27	2.68	3.51	7.71	4.62	7.79	5.12	4.48
Na_2O	8.48	7.77	4.80	7.88	8.34	6.89	7.54	7.13	6.97	7.12	7.21	7.14	6.90	9.01	9.30	6.60	8.17	8.58	7.62	7.27	7.82	9.38	9.00	6.96	8.64	7.03	8.40	8.76
K_2O	0.35	0.37	0.15	0.41	0.47	0.34	2.48	0.23	0.25	0.26	0.28	0.28	0.28	0.63	0.35	0.18	0.29	0.25	0.36	0.30	0.42	1.15	1.04	0.28	0.52	0.25	0.48	0.54
NiO		0.03	0.00	0.00	0.00	0.00	0.01	0.00	0.00	0.04	0.00	0.01	0.00	0.01	0.00	0.00	0.03	0.02	0.02	0.01	0.00	0.02	0.02	0.03	0.01	0.00	0.00	0.02
BaO	0.07																											
SrO	0.32																											
Total	100.39	100.59	99.56	100.57	100.67	100.00	99.94	100.29	100.29	100.22	99.88	99.53	98.41	100.35	100.32	98.31	99.31	100.69	99.45	99.07	99.51	100.22	100.00	99.67	99.25	99.26	99.15	99.98
Si (32 O)	10.980	10.778	9.743	10.840	11.002	10.567	11.873	10.524	10.515	10.545	10.614	10.619	10.580	11.263	11.350	10.405	10.932	10.988	10.760	10.615	10.820	11.545	11.386	10.556	11.162	10.530	11.050	11.185
Ti		0.000	0.004	0.000	0.000	0.007	0.024	0.000	0.000	0.002	0.000	0.000	0.003	0.000	0.000	0.001	0.000	0.000	0.000	0.000	0.000	0.000	0.000	0.000	0.000	0.000	0.000	0.000
Al	4.975	5.179	6.231	5.142	4.975	5.425	3.957	5.455	5.483	5.447	5.378	5.370	5.402	4.709	4.619	5.565	5.030	4.982	5.219	5.350	5.146	4.419	4.572	5.424	4.810	5.442	4.924	4.787
Cr		0.000	0.000	0.001	0.003	0.005	0.008	0.006	0.000	0.000	0.000	0.000	0.001	0.000	0.001	0.007	0.000	0.002	0.000	0.000	0.000	0.004	0.002	0.000	0.000	0.001	0.001	0.003
Fe_2	0.019	0.026	0.028	0.016	0.022	0.036	0.132	0.002	0.006	0.011	0.012	0.014	0.021	0.030	0.016	0.030	0.022	0.020	0.036	0.033	0.028	0.032	0.033	0.023	0.016	0.015	0.012	0.021
Mn		0.000	0.000	0.002	0.002	0.006	0.000	0.000	0.000	0.000	0.000	0.004	0.003	0.002	0.000	0.003	0.000	0.001	0.000	0.002	0.005	0.000	0.001	0.000	0.004	0.000	0.005	0.003
Mg		0.000	0.000	0.000	0.000	0.001	0.172	0.000	0.000	0.003	0.006	0.000	0.000	0.003	0.008	0.001	0.000	0.001	0.001	0.002	0.000	0.002	0.000	0.001	0.000	0.002	0.000	0.000
Ca	1.022	1.268	2.268	1.189	1.025	1.433	0.382	1.499	1.507	1.456	1.406	1.413	1.462	0.761	0.718	1.610	1.114	1.026	1.246	1.399	1.203	0.506	0.666	1.482	0.885	1.504	0.983	0.851
Na	2.919	2.672	1.692	2.703	2.855	2.386	2.587	2.465	2.407	2.461	2.496	2.483	2.428	3.083	3.174	2.333	2.838	2.935	2.647	2.543	2.715	3.207	3.090	2.420	2.992	2.454	2.918	3.013
K	0.079	0.084	0.035	0.093	0.105	0.078	0.559	0.052	0.056	0.059	0.063	0.065	0.064	0.142	0.079	0.042	0.066	0.057	0.083	0.069	0.096	0.259	0.234	0.064	0.118	0.058	0.110	0.121
Ni	0.001	0.004	0.000	0.000	0.000	0.000	0.001	0.000	0.000	0.005	0.000	0.002	0.000	0.001	0.001	0.000	0.004	0.004	0.003	0.002	0.000	0.003	0.003	0.004	0.001	0.000	0.000	0.004
Ba	0.048																											
Sr																												
Total	20.031	20.011	20.001	19.987	19.989	19.943	19.693	20.004	19.975	19.990	19.976	19.970	19.962	19.995	19.967	19.996	20.005	20.016	19.995	20.016	20.013	19.976	19.988	19.974	19.988	20.005	20.002	19.987
X location	60.298	72.816	72.816	71.304	68.929	68.285	68.151	68.406	68.406	68.406	68.510	68.387	68.477	68.477	67.506	67.506	67.506	67.585	67.459	14.593	14.541	14.509	15.034	13.966	13.860	14.000	13.879	13.748
Y location	55.427	55.316	55.165	53.977	55.650	56.410	57.558	59.152	59.214	59.303	59.500	59.609	59.779	59.884	60.914	61.019	61.178	61.423	61.667	71.532	71.668	71.768	72.829	73.512	73.512	73.512	73.512	73.512
Crystal #	14							2	2	2	2	2	2	2	3	3	3	3	3	2	2	2		5	5	5	5	5
Comments	Rim							Core						Rim	Core				Rim	Core		Rim		Core				
An	25	32	57	30	26	37	11	37	38	37	35	36	37	19	18	40	28	26	31	35	30	13	17	37	22	37	24	21
Ab	73	66	42	68	72	61	73	61	61	62	63	63	61	77	80	59	71	73	67	63	68	81	77	61	75	61	73	76
Or	2	2	1	2	3	2	16	1	1	1	2	2	2	4	2	1	2	1	2	2	2	7	6	2	3	1	3	3

Sample	SV40	SV40	SV40	SV40	SV40	SV40	SV40	SV40	SV40	SV40	SV40	SV40	SV40	SV40	SV40	SV40
Rock Type	TRAC	TRAC	TRAC	TRAC	TRAC	TRAC	TRAC	TRAC	TRAC	TRAC	TRAC	TRAC	TRAC	TRAC	TRAC	TRAC
Analysis	11-026	11-034	11-038	11-046	11-049	11-053	11-054	11-055	11-056	11-058	11-059	11-060	11-061	11-062	11-063	11-064
SiO_2	65.23	64.14	58.63	59.09	59.26	58.48	59.61	59.96	57.76	66.65	64.49	64.52	64.58	66.00	64.40	64.70
TiO_2	0.00	0.00	0.02	0.05	0.01	0.00	0.00	0.00	0.00	0.00	0.00	0.01	0.00	0.00	0.00	0.00
Al_2O_3	21.04	22.52	25.57	25.04	25.09	25.79	25.02	24.93	26.13	20.45	21.60	21.66	21.78	20.66	21.57	21.43
Cr_2O_3	0.01	0.00	0.01	0.00	0.00	0.00	0.01	0.02	0.00	0.01	0.02	0.00	0.02	0.03	0.00	0.01
FeO	0.22	0.15	0.22	0.14	0.10	0.11	0.10	0.10	0.17	0.17	0.09	0.17	0.14	0.16	0.17	0.18
MnO	0.00	0.02	0.00	0.00	0.05	0.03	0.03	0.00	0.02	0.00	0.00	0.00	0.01	0.00	0.02	0.00
MgO	0.01	0.00	0.00	0.00	0.00	0.00	0.00	0.00	0.01	0.00	0.00	0.00	0.00	0.00	0.00	0.00
CaO	2.60	3.83	7.49	6.68	6.96	7.31	6.52	6.41	8.09	1.69	2.87	2.98	3.02	2.07	2.93	2.91
Na_2O	9.27	9.30	6.90	7.21	7.20	6.89	7.38	7.47	6.59	10.46	9.69	9.48	9.49	9.94	9.40	9.22
K_2O	1.30	0.57	0.27	0.40	0.31	0.33	0.34	0.32	0.29	0.60	0.50	0.56	0.60	0.91	0.67	0.94
NiO	0.00	0.00	0.00	0.01	0.01	0.00	0.00	0.04	0.00	0.04	0.00	0.04	0.03	0.00	0.00	0.00
BaO																
SrO																
Total	99.66	100.53	99.11	98.62	98.98	98.94	99.00	99.24	99.06	100.08	99.26	99.41	99.67	99.76	99.15	99.39
Si (32 O)	11.567	11.295	10.564	10.680	10.674	10.549	10.720	10.752	10.435	11.719	11.462	11.454	11.440	11.660	11.464	11.496
Ti	0.000	0.000	0.002	0.006	0.001	0.000	0.000	0.000	0.000	0.000	0.000	0.001	0.000	0.000	0.000	0.000
Al	4.398	4.673	5.431	5.334	5.326	5.482	5.304	5.270	5.564	4.239	4.524	4.533	4.546	4.303	4.525	4.487
Cr	0.002	0.000	0.001	0.001	0.000	0.000	0.001	0.003	0.001	0.001	0.002	0.000	0.002	0.004	0.000	0.001
Fe_2	0.032	0.023	0.033	0.022	0.015	0.017	0.015	0.014	0.026	0.026	0.013	0.025	0.020	0.024	0.025	0.027
Mn	0.000	0.002	0.000	0.000	0.007	0.004	0.004	0.000	0.002	0.000	0.000	0.000	0.002	0.000	0.003	0.000
Mg	0.002	0.000	0.000	0.000	0.001	0.000	0.000	0.000	0.003	0.000	0.000	0.000	0.000	0.000	0.000	0.000
Ca	0.493	0.723	1.447	1.294	1.344	1.413	1.257	1.232	1.565	0.319	0.547	0.567	0.573	0.392	0.559	0.554
Na	3.187	3.175	2.412	2.526	2.515	2.410	2.574	2.596	2.307	3.566	3.340	3.263	3.261	3.404	3.244	3.175
K	0.293	0.128	0.063	0.092	0.070	0.077	0.077	0.073	0.067	0.135	0.113	0.126	0.135	0.205	0.152	0.213
Ni	0.000	0.000	0.000	0.001	0.002	0.000	0.000	0.005	0.000	0.005	0.000	0.006	0.005	0.000	0.000	0.000
Ba																
Sr																
Total	19.973	20.020	19.955	19.955	19.955	19.953	19.953	19.946	19.970	20.011	20.002	19.974	19.984	19.991	19.972	19.953
X location	13.641	6.401	8.984	10.147	9.169	9.685	9.741	9.787	9.846	15.179	15.179	15.179	15.179	15.065	15.226	15.275
Y location	73.512	72.664	72.185	68.672	67.088	66.336	66.336	66.336	66.336	58.545	58.703	58.903	58.982	59.090	59.274	59.590
Crystal #	5					8	8	8	8	9	9	9	9	9	9	9
Comments	Rim					Core			Rim	Core						Rim
An	12	18	37	33	34	36	32	32	40	8	14	14	14	10	14	14
Ab	80	79	62	65	64	62	66	67	59	89	84	82	82	85	82	81
Or	7	3	2	2	2	2	2	2	2	3	3	3	3	5	4	5

Sample	SV43	SV43	SV43	SV43	SV43	SV43	SV43	SV43	SV43	SV43	SV43	SV43
Rock Type	BEN	BEN	BEN	BEN	BEN	BEN	BEN	BEN	BEN	BEN	BEN	BEN
Analysis	13-001	13-002	13-003	13-004	13-005	13-006	13-007	13-008	13-009	13-010	13-011	13-012
SiO_2	56.32	55.99	56.61	59.17	56.43	54.37	55.55	54.80	59.11	53.48	53.77	52.33
TiO_2	0.00	0.06	0.00	0.00	0.02	0.00	0.04	0.00	0.04	0.00	0.04	0.03
Al_2O_3	26.80	26.99	26.70	25.10	26.74	28.21	27.30	28.02	25.22	28.73	28.51	29.68
Cr_2O_3	0.00	0.00	0.00	0.00	0.00	0.00	0.03	0.01	0.00	0.02	0.00	0.04
FeO	0.22	0.23	0.21	0.16	0.37	0.40	0.40	0.36	0.36	0.61	0.58	0.35
MnO	0.03	0.00	0.00	0.02	0.04	0.06	0.04	0.01	0.00	0.02	0.02	0.00
MgO	0.00	0.00	0.02	0.00	0.02	0.01	0.00	0.02	0.00	0.04	0.03	0.01
CaO	9.57	9.93	9.41	7.56	9.73	11.20	10.27	10.71	7.81	11.96	11.79	12.93
Na_2O	6.11	5.87	6.18	7.17	5.94	5.12	5.63	5.39	6.86	4.70	4.86	4.21
K_2O	0.14	0.17	0.18	0.31	0.24	0.19	0.23	0.17	0.44	0.22	0.25	0.10
NiO	0.01	0.01	0.04	0.02	0.00	0.00	0.00	0.02	0.01	0.03	0.03	0.00
BaO												
SrO												
Total	99.21	99.25	99.34	99.50	99.53	99.57	99.49	99.52	99.85	99.80	99.88	99.69
Si (32 O)	10.210	10.155	10.244	10.630	10.209	9.878	10.075	9.945	10.597	9.730	9.772	9.539
Ti	0.000	0.008	0.000	0.000	0.003	0.000	0.005	0.001	0.005	0.000	0.006	0.004
Al	5.727	5.771	5.694	5.315	5.703	6.043	5.836	5.994	5.331	6.160	6.106	6.377
Cr	0.000	0.000	0.000	0.000	0.000	0.000	0.004	0.001	0.000	0.003	0.000	0.006
Fe_2	0.033	0.035	0.032	0.024	0.056	0.060	0.061	0.055	0.053	0.093	0.088	0.054
Mn	0.004	0.000	0.000	0.003	0.005	0.010	0.006	0.001	0.001	0.003	0.004	0.000
Mg	0.000	0.000	0.004	0.000	0.005	0.004	0.000	0.006	0.000	0.011	0.008	0.002
Ca	1.860	1.929	1.824	1.454	1.886	2.180	1.996	2.083	1.500	2.332	2.295	2.526
Na	2.147	2.065	2.170	2.496	2.085	1.804	1.980	1.895	2.385	1.657	1.713	1.489
K	0.033	0.040	0.041	0.072	0.056	0.045	0.054	0.040	0.100	0.052	0.058	0.024
Ni	0.002	0.001	0.005	0.003	0.000	0.000	0.000	0.003	0.001	0.004	0.004	0.000
Ba												
Sr												
Total	20.016	20.004	20.014	19.996	20.008	20.025	20.017	20.024	19.974	20.044	20.054	20.022
X location	8.339	8.477	8.477	8.477	9.432	9.464	9.522	9.560	9.573	9.943	9.954	10.289
Y location	58.967	58.891	58.797	58.766	58.948	58.905	58.863	58.815	58.783	58.692	58.650	58.888
Crystal #	1	1	1	1	2	2	2	2	2	3	3	4
Comments	Core			Rim	Core				Rim	Core	Rim	Core
An	46	48	45	36	47	54	50	52	38	58	56	63
Ab	53	51	54	62	52	45	49	47	60	41	42	37
Or	1	1	1	2	1	1	1	1	3	1	1	1

Sample	SV43	SV43	SV43	SV43	SV43	SV43	SV43	SV43	SV43	SV43	SV43	SV43	SV43	SV43
Rock Type	BEN	BEN	BEN	BEN	BEN	BEN	BEN	BEN	BEN	BEN	BEN	BEN	BEN	BEN
Analysis	13-013	13-014	13-015	13-016	13-018	13-019	13-020	13-021	13-022	13-023	13-024	13-025	13-026	13-027
SiO_2	57.09	57.29	60.46	62.52	59.14	56.20	58.43	59.44	51.63	52.30	53.90	50.61	52.63	52.94
TiO_2	0.03	0.00	0.00	0.00	0.00	0.00	0.06	0.05	0.00	0.01	0.00	0.01	0.00	0.03
Al_2O_3	26.62	26.53	24.42	22.03	24.94	26.82	24.41	24.00	29.13	27.93	27.47	30.24	29.17	28.96
Cr_2O_3	0.00	0.00	0.00	0.00	0.00	0.00	0.00	0.00	0.00	0.03	0.01	0.00	0.00	0.01
FeO	0.22	0.17	0.17	0.30	0.32	0.26	1.03	0.57	0.52	0.35	0.43	0.56	0.40	0.40
MnO	0.01	0.00	0.02	0.05	0.00	0.01	0.01	0.03	0.00	0.01	0.00	0.03	0.00	0.04
MgO	0.02	0.00	0.01	0.01	0.03	0.00	0.30	0.21	0.05	0.04	0.03	0.02	0.03	0.02
CaO	9.32	8.89	6.61	5.52	7.03	9.60	7.15	6.94	12.72	11.91	10.83	13.88	12.72	12.43
Na_2O	6.26	6.43	7.67	6.61	7.39	5.88	6.40	6.55	4.16	4.63	5.16	3.50	4.31	4.52
K_2O	0.18	0.21	0.38	1.52	0.48	0.26	0.41	1.06	0.13	0.17	0.24	0.09	0.11	0.16
NiO	0.01	0.01	0.00	0.00	0.00	0.03	0.00	0.00	0.02	0.01	0.04	0.03	0.05	0.02
BaO														
SrO														
Total	99.75	99.53	99.73	98.57	99.33	99.05	98.20	98.85	98.36	97.37	98.11	98.97	99.42	99.52
Si (32 O)	10.282	10.327	10.807	11.265	10.651	10.206	10.650	10.767	9.548	9.746	9.937	9.331	9.617	9.661
Ti	0.004	0.000	0.000	0.001	0.000	0.000	0.008	0.007	0.000	0.001	0.000	0.002	0.000	0.004
Al	5.651	5.636	5.145	4.678	5.293	5.740	5.245	5.124	6.349	6.133	5.970	6.571	6.283	6.229
Cr	0.000	0.000	0.000	0.000	0.000	0.000	0.000	0.000	0.000	0.004	0.002	0.000	0.000	0.002
Fe_2	0.033	0.025	0.025	0.046	0.049	0.039	0.156	0.086	0.080	0.054	0.067	0.086	0.061	0.060
Mn	0.002	0.001	0.004	0.008	0.001	0.001	0.002	0.004	0.000	0.002	0.000	0.005	0.000	0.006
Mg	0.006	0.000	0.002	0.002	0.008	0.001	0.082	0.056	0.013	0.010	0.008	0.005	0.007	0.006
Ca	1.798	1.718	1.266	1.065	1.356	1.868	1.396	1.347	2.522	2.378	2.140	2.742	2.490	2.431
Na	2.186	2.247	2.657	2.309	2.581	2.071	2.261	2.300	1.492	1.672	1.843	1.250	1.528	1.598
K	0.041	0.048	0.087	0.350	0.110	0.060	0.096	0.246	0.030	0.041	0.056	0.021	0.026	0.036
Ni	0.001	0.001	0.000	0.000	0.000	0.004	0.000	0.000	0.004	0.001	0.006	0.004	0.007	0.002
Ba														
Sr														
Total	20.003	20.003	19.992	19.724	20.048	19.990	19.898	19.936	20.038	20.041	20.027	20.017	20.019	20.036
X location	10.289	10.289	10.289	10.289	11.890	11.814	11.751	11.693	13.217	13.311	13.397	13.429	13.407	13.407
Y location	58.814	58.779	58.742	58.727	57.166	57.158	57.158	57.158	56.770	56.770	56.757	55.510	55.457	55.419
Crystal #	4	4	4	4	5	5	5	5	6	6	6	7	7	7
Comments				Rim				Rim	Core		Rim	Core		
An	45	43	32	29	34	47	37	35	62	58	53	68	62	60
Ab	54	56	66	62	64	52	60	59	37	41	46	31	38	39
Or	1	1	2	9	3	2	3	6	1	1	1	1	1	1

Sample	SV43	SV43	SV43	SV43	SV43	SV43	SV43	SV43	SV43	SV43	SV43	SV43	SV43	SV43
Rock Type	BEN	BEN	BEN	BEN	BEN	BEN	BEN	BEN	BEN	BEN	BEN	BEN	BEN	BEN
Analysis	13-029	13-030	13-031	13-032	13-033	13-034	13-035	13-036	13-037	13-038	13-039	13-041	13-042	13-043
SiO_2	54.62	55.50	56.65	57.25	54.28	56.03	55.09	53.99	58.76	58.59	53.84	54.01	60.16	52.04
TiO_2	0.03	0.00	0.01	0.01	0.01	0.00	0.00	0.01	0.00	0.00	0.00	0.01	0.06	0.00
Al_2O_3	28.18	27.14	26.68	25.96	27.92	26.48	27.79	27.96	25.42	25.50	28.36	28.31	22.72	29.55
Cr_2O_3	0.00	0.00	0.04	0.03	0.02	0.00	0.05	0.01	0.02	0.00	0.03	0.01	0.00	0.00
FeO	0.39	0.38	0.40	0.39	0.52	0.61	0.33	0.33	0.11	0.19	0.30	0.33	0.64	0.45
MnO	0.00	0.05	0.01	0.00	0.00	0.01	0.00	0.00	0.02	0.00	0.00	0.03	0.00	0.00
MgO	0.03	0.02	0.02	0.02	0.04	0.06	0.00	0.01	0.00	0.00	0.03	0.02	0.03	0.03
CaO	11.00	10.12	9.44	8.71	11.19	9.51	10.84	11.48	7.79	7.86	11.71	11.27	6.42	13.18
Na_2O	5.30	5.77	6.01	6.31	5.09	5.81	5.40	4.96	6.95	6.92	4.77	4.85	6.49	4.05
K_2O	0.17	0.19	0.29	0.35	0.24	0.40	0.17	0.15	0.28	0.23	0.13	0.56	1.77	0.11
NiO	0.01	0.00	0.00	0.00	0.00	0.04	0.00	0.00	0.01	0.00	0.00	0.00	0.00	0.01
BaO														
SrO														
Total	99.74	99.17	99.54	99.02	99.30	98.93	99.66	98.89	99.36	99.30	99.16	99.40	98.29	99.41
Si (32 O)	9.901	10.095	10.241	10.382	9.895	10.211	9.981	9.876	10.572	10.550	9.822	9.845	10.972	9.523
Ti	0.004	0.000	0.002	0.001	0.002	0.000	0.000	0.002	0.000	0.000	0.000	0.001	0.008	0.000
Al	6.021	5.818	5.684	5.548	5.999	5.689	5.936	6.029	5.390	5.412	6.099	6.081	4.885	6.374
Cr	0.000	0.000	0.005	0.004	0.002	0.000	0.008	0.001	0.002	0.000	0.004	0.001	0.000	0.000
Fe_2	0.059	0.058	0.060	0.059	0.079	0.092	0.050	0.050	0.017	0.028	0.046	0.050	0.097	0.069
Mn	0.000	0.007	0.001	0.000	0.000	0.002	0.000	0.000	0.004	0.001	0.000	0.005	0.000	0.000
Mg	0.008	0.005	0.006	0.004	0.011	0.015	0.000	0.002	0.000	0.001	0.007	0.005	0.009	0.007
Ca	2.137	1.972	1.828	1.692	2.187	1.857	2.105	2.250	1.502	1.516	2.289	2.201	1.255	2.585
Na	1.864	2.033	2.105	2.220	1.800	2.054	1.897	1.760	2.426	2.416	1.687	1.716	2.296	1.437
K	0.039	0.044	0.066	0.081	0.055	0.092	0.038	0.035	0.063	0.053	0.030	0.129	0.411	0.025
Ni	0.002	0.000	0.000	0.000	0.000	0.005	0.000	0.000	0.002	0.000	0.000	0.000	0.000	0.001
Ba														
Sr														
Total	20.036	20.034	19.998	19.991	20.029	20.017	20.015	20.005	19.977	19.979	19.985	20.035	19.932	20.021
X location	12.733	12.733	12.733	12.733	12.731	12.962	13.124	13.041	13.014	12.940	12.940	11.981	11.820	11.751
Y location	53.985	53.929	53.910	53.902	53.869	53.585	51.593	51.556	51.485	51.435	51.386	51.338	51.338	51.338
Crystal #	8	8	8	9	10	11	12	12	12	12	12	13	13	13
Comments	Core		Rim				Core					Core		
An	53	49	46	42	54	46	52	56	38	38	57	54	32	64
Ab	46	50	53	56	45	51	47	44	61	61	42	42	58	35
Or	1	1	2	2	1	2	1	1	2	1	1	3	10	1

Sample	SV43	SV43	SV43	SV43	SV43	SV43	SV43	SV43	SV43	SV43	SV43	SV43	SV43	SV43	SV43	SV43	SV43	SV43	SV43	SV43	SV43	SV43	SV43	SV43	SV43	SV43	SV43	SV43
Rock Type	BEN	BEN	BEN	BEN	BEN	BEN	BEN	BEN	BEN	BEN	BEN	BEN	BEN	BEN	BEN	BEN	BEN	BEN	BEN	BEN	BEN	BEN	BEN	BEN	BEN	BEN	BEN	BEN
Analysis	13-045	13-046	13-047	13-048	13-049	13-050	13-051	13-052	13-053	13-055	13-057	13-058	13-059	13-060	13-061	13-062	13-063	13-064	13-065	13-066	13-067	13-068	13-069	13-070	13-071	13-072	13-074	13-075
SiO_2	53.41	53.48	55.96	57.15	58.78	57.63	52.90	57.67	50.87	51.91	54.81	52.14	51.96	51.72	51.85	51.60	52.59	50.15	51.64	56.76	51.28	51.61	51.17	53.08	62.39	52.66	50.94	58.77
TiO_2	0.02	0.00	0.00	0.03	0.00	0.07	0.00	0.05	0.02	0.04	0.00	0.01	0.02	0.03	0.00	0.00	0.00	0.01	0.00	0.00	0.00	0.00	0.00	0.00	0.11	0.01	0.00	0.05
Al_2O_3	28.78	28.97	26.39	26.45	25.32	26.25	29.22	25.72	30.43	29.63	27.89	28.97	29.78	29.65	29.68	29.79	29.39	29.93	29.73	25.97	30.15	29.74	29.90	27.68	21.76	27.93	29.71	23.14
Cr_2O_3	0.00	0.00	0.00	0.00	0.01	0.01	0.02	0.02	0.02	0.03	0.00	0.00	0.00	0.01	0.00	0.04	0.00	0.00	0.01	0.00	0.04	0.00	0.00	0.01	0.00	0.02	0.00	0.00
FeO	0.16	0.16	0.13	0.12	0.12	0.17	0.55	0.46	0.39	0.49	0.31	0.62	0.34	0.49	0.32	0.31	0.35	2.24	0.44	0.41	0.48	0.43	0.26	0.54	0.52	0.63	0.52	0.74
MnO	0.02	0.00	0.00	0.00	0.00	0.00	0.02	0.05	0.00	0.00	0.03	0.00	0.02	0.00	0.00	0.00	0.03	0.07	0.03	0.01	0.00	0.00	0.03	0.01	0.04	0.00	0.00	0.00
MgO	0.00	0.00	0.01	0.00	0.00	0.00	0.02	0.00	0.03	0.03	0.00	0.11	0.01	0.08	0.01	0.03	0.02	0.04	0.03	0.03	0.02	0.01	0.02	0.12	0.03	0.06	0.04	0.09
CaO	11.93	11.93	9.21	8.74	7.65	8.59	12.55	10.55	14.00	13.26	11.16	11.71	13.26	12.11	13.09	13.13	12.69	13.72	13.43	8.84	13.77	13.31	13.54	11.11	7.56	11.65	13.81	6.38
Na_2O	4.77	4.79	5.96	6.38	7.10	6.48	4.28	3.64	3.56	3.95	5.16	3.86	4.05	3.88	3.97	4.09	4.39	2.76	3.92	6.19	3.73	4.01	3.95	3.68	4.18	4.07	3.70	6.31
K_2O	0.18	0.18	0.31	0.30	0.38	0.31	0.24	1.26	0.09	0.15	0.16	0.72	0.10	0.10	0.10	0.10	0.12	0.66	0.11	0.36	0.12	0.12	0.12	1.41	2.02	0.53	0.13	1.97
NiO	0.01	0.00	0.00	0.05	0.00	0.04	0.00	0.00	0.03	0.02	0.05	0.01	0.00	0.00	0.01	0.00	0.02	0.00	0.00	0.00	0.00	0.03	0.00	0.00	0.00	0.01	0.03	0.03
BaO																												
SrO																												
Total	99.28	99.50	97.97	99.23	99.36	99.54	99.79	99.42	99.44	99.50	99.56	98.14	99.54	98.07	99.03	99.07	99.60	99.58	99.35	98.57	99.59	99.28	98.98	97.63	98.60	97.58	98.88	97.49
Si (32 O)	9.743	9.732	10.259	10.332	10.581	10.381	9.632	10.428	9.328	9.498	9.948	9.647	9.495	9.553	9.514	9.473	9.593	9.275	9.467	10.347	9.388	9.468	9.417	9.868	11.257	9.789	9.401	10.838
Ti	0.003	0.000	0.000	0.004	0.000	0.010	0.000	0.006	0.002	0.006	0.000	0.001	0.003	0.004	0.000	0.000	0.001	0.002	0.000	0.000	0.000	0.000	0.000	0.000	0.015	0.002	0.000	0.007
Al	6.188	6.213	5.702	5.636	5.373	5.573	6.271	5.482	6.578	6.390	5.967	6.318	6.414	6.456	6.418	6.446	6.318	6.524	6.423	5.580	6.506	6.430	6.485	6.067	4.626	6.120	6.463	5.030
Cr	0.000	0.000	0.000	0.000	0.001	0.001	0.003	0.003	0.003	0.004	0.000	0.000	0.000	0.001	0.000	0.005	0.000	0.000	0.001	0.000	0.005	0.000	0.000	0.001	0.000	0.003	0.000	0.001
Fe_2	0.024	0.025	0.020	0.018	0.018	0.025	0.083	0.070	0.060	0.075	0.047	0.096	0.052	0.076	0.049	0.047	0.053	0.346	0.068	0.063	0.073	0.067	0.040	0.084	0.079	0.098	0.081	0.114
Mn	0.004	0.000	0.000	0.000	0.000	0.000	0.003	0.008	0.000	0.000	0.004	0.000	0.003	0.000	0.000	0.000	0.004	0.011	0.005	0.002	0.000	0.000	0.005	0.001	0.006	0.000	0.000	0.000
Mg	0.000	0.000	0.004	0.001	0.000	0.000	0.006	0.000	0.009	0.007	0.000	0.031	0.004	0.021	0.004	0.007	0.006	0.012	0.008	0.009	0.005	0.003	0.006	0.034	0.008	0.017	0.012	0.023
Ca	2.332	2.326	1.810	1.693	1.475	1.659	2.449	2.045	2.751	2.599	2.171	2.321	2.596	2.397	2.573	2.584	2.481	2.720	2.639	1.726	2.702	2.616	2.669	2.212	1.460	2.320	2.730	1.261
Na	1.687	1.690	2.118	2.238	2.480	2.264	1.509	1.275	1.265	1.400	1.815	1.383	1.435	1.388	1.412	1.454	1.552	0.990	1.395	2.189	1.324	1.428	1.409	1.328	1.462	1.468	1.324	2.258
K	0.041	0.041	0.072	0.070	0.087	0.071	0.056	0.290	0.021	0.034	0.036	0.169	0.024	0.024	0.023	0.023	0.027	0.155	0.027	0.083	0.028	0.029	0.028	0.334	0.465	0.125	0.030	0.463
Ni	0.002	0.000	0.000	0.008	0.000	0.005	0.000	0.000	0.004	0.003	0.007	0.002	0.000	0.000	0.002	0.000	0.004	0.000	0.000	0.000	0.000	0.004	0.000	0.000	0.000	0.002	0.004	0.005
Ba																												
Sr																												
Total	20.024	20.027	19.985	20.000	20.015	19.989	20.013	19.606	20.022	20.016	19.994	19.969	20.024	19.920	19.994	20.040	20.037	20.034	20.032	19.999	20.032	20.045	20.059	19.929	19.379	19.944	20.045	20.000
X location	8.281	8.281	8.281	8.281	8.281	8.281	8.281	6.360	6.282	6.150	5.465	5.080	5.127	5.186	5.239	5.239	5.298	5.424	5.527	5.575	8.144	8.172	8.172	8.172	8.172	8.172	8.219	8.219
Y location	52.582	52.442	52.336	52.253	52.174	52.102	52.033	52.124	52.124	52.124	51.847	45.899	45.928	45.944	45.978	45.978	45.994	46.037	46.037	46.026	44.903	44.846	44.800	44.755	44.723	44.681	44.543	44.516
Crystal #	14	14	14	14	14	14	14	15	15	15	16	17	17	17	17	17	17	17	17	17	18	18	18	18	18	18	18	18
Comments	Core						Rim	Core				Core								Rim	Core							
An	57	57	45	42	36	42	61	57	68	64	54	60	64	63	64	64	61	70	65	43	67	64	65	57	43	59	67	32
Ab	42	42	53	56	61	57	38	35	31	35	45	36	35	36	35	36	38	26	34	55	33	35	34	34	43	38	32	57
Or	1	1	2	2	2	2	1	8	1	1	1	4	1	1	1	1	1	4	1	2	1	1	1	9	14	3	1	12

Sample	SV43	SV43	SV43	SV43	SV44	SV44	SV44	SV44	SV44	SV44	SV44	SV44	SV44	SV44	SV44	SV44	SV44	SV44	SV44	SV44	SV44	SV44	SV44	SV45	SV45	SV45	SV45	SV45
Rock Type	BEN	BEN	BEN	BEN	TRAC	TRAC	TRAC	TRAC	TRAC	TRAC	TRAC	TRAC	TRAC	TRAC	TRAC	TRAC	TRAC	TRAC	TRAC	TRAC	TRAC	TRAC	TRAC	MUG	MUG	MUG	MUG	MUG
Analysis	13-076	13-077	13-078	13-080	09-081	09-082	09-083	09-084	09-090	09-094	09-096	09-100	09-104	09-105	09-106	09-107	09-108	09-109	09-113	09-125	09-126	09-127	09-128	11-067	11-070	11-080	11-082	11-084
SiO_2	52.20	47.50	47.85	60.07	65.35	56.29	52.78	54.74	63.61	63.10	65.72	62.04	60.28	63.17	62.75	63.41	61.34	64.50	59.95	61.16	61.18	61.10	61.12	51.95	49.06	51.41	47.96	49.46
TiO_2	0.00	0.00	0.03	0.00	0.00	0.00	0.03	0.00	0.02	0.03	0.00	0.02	0.04	0.00	0.00	0.01	0.00	0.04	0.00	0.00	0.00	0.00	0.00	0.02	0.03	0.01	0.00	0.00
Al_2O_3	29.43	32.69	31.62	23.68	21.08	26.28	29.51	28.32	22.14	22.37	20.92	23.21	24.22	22.47	22.89	22.49	23.68	21.66	24.67	23.91	23.82	23.91	23.65	29.54	31.48	30.06	32.44	31.20
Cr_2O_3	0.02	0.00	0.00	0.02	0.00	0.02	0.03	0.00	0.00	0.01	0.00	0.00	0.02	0.00	0.01	0.00	0.00	0.01	0.00	0.05	0.00	0.00	0.00	0.04	0.02	0.02	0.00	0.02
FeO	0.50	0.45	0.69	0.40	0.18	0.17	0.24	0.16	0.13	0.12	0.12	0.16	0.09	0.14	0.19	0.15	0.18	0.26	0.13	0.20	0.12	0.15	0.09	0.73	0.67	0.57	0.58	0.99
MnO	0.00	0.06	0.02	0.00	0.03	0.00	0.02	0.04	0.02	0.00	0.02	0.01	0.00	0.00	0.00	0.00	0.00	0.01	0.00	0.01	0.00	0.05	0.00	0.03	0.04	0.00	0.02	0.06
MgO	0.02	0.00	0.12	0.03	0.00	0.00	0.00	0.00	0.00	0.01	0.00	0.00	0.02	0.00	0.01	0.00	0.00	0.02	0.01	0.00	0.01	0.00	0.00	0.13	0.05	0.06	0.02	0.19
CaO	12.98	16.87	16.42	7.59	2.63	8.83	12.48	11.10	3.72	4.21	2.22	5.00	5.91	3.83	4.45	4.01	5.66	3.26	6.42	5.79	6.02	6.03	5.89	12.79	15.10	13.88	16.34	14.82
Na_2O	4.05	2.00	2.15	6.24	9.88	6.35	4.40	5.34	9.15	9.08	9.91	8.66	7.96	9.23	8.82	9.16	8.30	9.55	7.76	8.27	8.30	8.18	8.36	3.75	2.65	3.52	2.11	2.66
K_2O	0.12	0.04	0.17	0.82	0.80	0.23	0.10	0.16	0.66	0.59	0.92	0.48	0.40	0.59	0.52	0.61	0.47	0.82	0.39	0.39	0.41	0.40	0.42	0.23	0.13	0.17	0.09	0.29
NiO	0.00	0.00	0.00	0.00	0.00	0.01	0.01	0.00	0.02	0.00	0.01	0.00	0.00	0.02	0.00	0.05	0.00	0.02	0.00	0.00	0.02	0.00	0.00	0.01	0.02	0.02	0.01	0.00
BaO																												
SrO																												
Total	99.32	99.61	99.06	98.85	99.94	98.18	99.59	99.87	99.47	99.51	99.84	99.57	98.95	99.44	99.63	99.88	99.63	100.15	99.33	99.77	99.88	99.82	99.53	99.20	99.23	99.71	99.58	99.68
Si (32 O)	9.555	8.772	8.892	10.853	11.550	10.294	9.611	9.902	11.321	11.243	11.611	11.069	10.844	11.254	11.167	11.252	10.959	11.408	10.760	10.916	10.916	10.905	10.938	9.526	9.056	9.402	8.849	9.101
Ti	0.000	0.000	0.004	0.001	0.000	0.000	0.004	0.000	0.002	0.004	0.000	0.003	0.006	0.000	0.000	0.001	0.000	0.006	0.000	0.000	0.000	0.000	0.000	0.003	0.004	0.001	0.000	0.000
Al	6.350	7.116	6.925	5.043	4.393	5.664	6.334	6.039	4.644	4.698	4.356	4.881	5.136	4.718	4.802	4.704	4.987	4.516	5.219	5.030	5.009	5.031	4.988	6.384	6.850	6.479	7.055	6.768
Cr	0.003	0.000	0.000	0.002	0.000	0.003	0.004	0.000	0.000	0.001	0.000	0.000	0.003	0.000	0.001	0.000	0.000	0.002	0.000	0.007	0.000	0.001	0.000	0.005	0.002	0.003	0.000	0.003
Fe_2	0.077	0.069	0.107	0.060	0.026	0.027	0.037	0.025	0.020	0.018	0.018	0.024	0.014	0.020	0.028	0.022	0.027	0.039	0.019	0.029	0.018	0.022	0.013	0.112	0.103	0.087	0.089	0.152
Mn	0.000	0.010	0.003	0.000	0.004	0.000	0.004	0.006	0.003	0.000	0.003	0.001	0.000	0.000	0.000	0.000	0.000	0.002	0.000	0.001	0.000	0.007	0.000	0.004	0.006	0.000	0.004	0.009
Mg	0.005	0.001	0.034	0.008	0.000	0.001	0.000	0.000	0.000	0.002	0.000	0.000	0.004	0.001	0.002	0.000	0.000	0.005	0.004	0.000	0.002	0.000	0.001	0.035	0.014	0.017	0.007	0.051
Ca	2.547	3.338	3.269	1.469	0.499	1.729	2.435	2.151	0.709	0.803	0.420	0.956	1.139	0.731	0.849	0.763	1.083	0.617	1.234	1.107	1.150	1.153	1.130	2.513	2.987	2.720	3.231	2.922
Na	1.438	0.716	0.775	2.185	3.386	2.251	1.552	1.874	3.157	3.139	3.396	2.996	2.776	3.189	3.044	3.152	2.876	3.275	2.700	2.860	2.871	2.831	2.902	1.334	0.948	1.247	0.756	0.949
K	0.029	0.009	0.040	0.188	0.179	0.054	0.022	0.037	0.150	0.133	0.206	0.108	0.092	0.134	0.117	0.138	0.106	0.185	0.089	0.089	0.093	0.091	0.097	0.052	0.031	0.039	0.020	0.067
Ni	0.000	0.000	0.000	0.000	0.000	0.002	0.001	0.000	0.003	0.000	0.001	0.000	0.000	0.002	0.000	0.007	0.000	0.003	0.000	0.000	0.004	0.000	0.000	0.002	0.002	0.002	0.002	0.000
Ba																												
Sr																												
Total	20.003	20.032	20.049	19.810	20.036	20.025	20.004	20.034	20.008	20.040	20.012	20.040	20.015	20.049	20.012	20.039	20.038	20.057	20.025	20.040	20.062	20.040	20.068	19.970	20.003	19.999	20.012	20.021
X location	11.552	11.769	11.669	11.570	69.114	68.880	68.631	68.227	63.182	63.047	64.582	64.740	66.533	66.456	66.420	66.399	66.371	66.346	69.715	70.874	70.874	70.896	70.982	69.018	68.907	66.162	65.637	65.248
Y location	44.599	43.920	43.920	43.901	60.357	60.326	60.353	60.589	62.496	64.509	65.089	66.862	67.802	67.802	67.802	67.792	67.792	67.792	67.021	62.509	62.544	62.576	62.523	62.109	62.393	63.888	64.240	64.909
Crystal #	19	20	20	20	10	10	10	10					11	11	11	11	11	11		14	14	14	14					11
Comments	Rim	Core		Rim									Core					Rim										
An	63	82	80	38	12	43	61	53	18	20	10	24	28	18	21	19	27	15	31	27	28	28	27	64	75	68	81	74
Ab	36	18	19	57	83	56	39	46	79	77	84	74	69	79	76	78	71	80	67	71	70	69	70	34	24	31	19	24
Or	1	0	1	5	4	1	1	1	4	3	5	3	2	3	3	3	3	5	2	2	2	2	2	1	1	1	1	2

Sample	SV45	SV45	SV45	SV45	SV45	SV45	SV45	SV45	SV45	SV158	SV158	SV158	SV158	SV158	SV158	SV158	SV158	SV158	SV158	SV165	SV165	SV165	SV165	SV165	SV165	SV165	SV165	SV165
Rock Type	MUG	MUG	MUG	MUG	MUG	MUG	MUG	MUG	MUG																			
Analysis	11-086	11-102	11-103	11-106	11-108	11-116	11-118	11-120	11-121	12-086	12-087	12-088	12-089	12-090	12-098	12-099	12-100	12-101	12-102	07-016	07-017	07-018	07-019	07-020	07-021	07-023	07-024	07-025
SiO_2	47.86	52.83	57.06	48.81	49.25	51.34	50.32	48.64	47.96	61.82	57.51	58.54	63.95	58.42	59.59	60.77	60.55	62.28	64.78	52.41	50.97	48.51	50.61	50.95	55.05	55.57	48.69	47.99
TiO_2	0.05	0.04	0.03	0.20	0.00	0.00	0.00	0.00	0.01	0.02	0.02	0.00	0.00	0.06	0.00	0.00	0.00	0.06	0.04	0.00	0.00	0.00	0.00	0.04	0.01	0.00	0.00	0.00
Al_2O_3	31.19	29.17	25.80	30.90	31.74	30.38	31.25	31.40	32.38	23.41	26.59	25.98	22.49	25.94	25.27	24.58	24.63	23.70	21.58	29.96	30.82	30.57	31.06	30.83	28.39	26.74	32.13	32.47
Cr_2O_3	0.01	0.02	0.02	0.00	0.01	0.00	0.00	0.00	0.00	0.00	0.02	0.03	0.00	0.01	0.03	0.05	0.00	0.00	0.02	0.02	0.00	0.00	0.00	0.00	0.02	0.00	0.00	0.00
FeO	0.81	0.67	0.71	1.18	0.75	0.54	0.65	0.93	0.71	0.29	0.16	0.16	0.13	0.40	0.11	0.12	0.12	0.08	0.14	0.40	0.44	0.47	0.39	0.43	0.39	0.43	0.45	0.50
MnO	0.00	0.00	0.03	0.04	0.00	0.00	0.00	0.03	0.00	0.03	0.00	0.02	0.00	0.03	0.00	0.01	0.00	0.00	0.01	0.00	0.02	0.00	0.00	0.00	0.00	0.02	0.00	0.02
MgO	0.15	0.08	0.08	0.26	0.03	0.04	0.06	0.17	0.10	0.00	0.01	0.00	0.01	0.01	0.00	0.00	0.02	0.00	0.00	0.03	0.03	0.03	0.02	0.01	0.03	0.10	0.03	0.03
CaO	14.83	12.65	9.07	15.41	15.63	13.87	14.64	15.89	16.54	4.86	8.80	8.17	4.22	8.10	7.05	6.29	6.52	5.27	3.19	13.03	14.11	14.43	13.93	13.84	10.79	9.61	16.09	16.46
Na_2O	2.23	4.19	5.37	2.41	2.61	3.51	3.11	2.41	2.16	8.11	6.48	6.70	8.92	6.62	7.18	7.68	7.61	8.37	9.17	4.18	3.56	3.19	3.29	3.40	5.25	5.56	2.60	2.30
K_2O	0.10	0.24	1.59	0.31	0.11	0.14	0.15	0.25	0.12	1.23	0.24	0.30	0.66	0.34	0.36	0.38	0.40	0.57	0.99	0.10	0.09	0.16	0.10	0.09	0.16	0.40	0.11	0.11
NiO	0.03	0.03	0.00	0.00	0.00	0.00	0.00	0.00	0.00	0.00	0.00	0.02	0.02	0.00	0.00	0.00	0.01	0.01	0.00	0.02	0.01	0.03	0.01	0.00	0.00	0.02	0.00	0.01
BaO																												
SrO																												
Total	97.25	99.91	99.75	99.50	100.13	99.81	100.16	99.72	99.98	99.78	99.83	99.92	100.40	99.92	99.58	99.87	99.84	100.34	99.92	100.15	100.05	97.39	99.40	99.59	100.07	98.44	100.11	99.89
Si (32 O)	9.010	9.618	10.347	9.028	9.023	9.374	9.185	8.977	8.830	11.040	10.333	10.486	11.282	10.474	10.669	10.828	10.801	11.026	11.462	9.514	9.294	9.122	9.272	9.314	9.928	10.167	8.932	8.836
Ti	0.007	0.006	0.004	0.028	0.000	0.000	0.000	0.001	0.001	0.003	0.003	0.000	0.000	0.007	0.000	0.000	0.000	0.008	0.005	0.000	0.000	0.000	0.000	0.006	0.002	0.000	0.000	0.000
Al	6.920	6.259	5.515	6.738	6.855	6.539	6.724	6.831	7.026	4.927	5.632	5.485	4.677	5.482	5.333	5.163	5.179	4.945	4.500	6.410	6.623	6.776	6.707	6.644	6.035	5.767	6.948	7.046
Cr	0.001	0.002	0.002	0.000	0.002	0.000	0.000	0.000	0.000	0.000	0.002	0.004	0.000	0.002	0.004	0.008	0.000	0.000	0.003	0.003	0.000	0.000	0.000	0.000	0.003	0.000	0.000	0.000
Fe_2	0.127	0.101	0.107	0.182	0.115	0.082	0.099	0.143	0.110	0.044	0.024	0.023	0.020	0.060	0.016	0.018	0.018	0.012	0.021	0.060	0.066	0.074	0.060	0.066	0.058	0.066	0.070	0.076
Mn	0.000	0.000	0.005	0.006	0.000	0.000	0.000	0.004	0.000	0.005	0.000	0.003	0.000	0.004	0.000	0.001	0.000	0.000	0.001	0.000	0.004	0.000	0.000	0.000	0.000	0.003	0.000	0.004
Mg	0.042	0.022	0.020	0.071	0.008	0.012	0.017	0.048	0.027	0.000	0.003	0.000	0.002	0.001	0.000	0.000	0.004	0.000	0.000	0.008	0.009	0.007	0.004	0.003	0.007	0.027	0.008	0.008
Ca	2.991	2.467	1.762	3.054	3.068	2.714	2.862	3.143	3.263	0.930	1.694	1.567	0.797	1.557	1.353	1.201	1.246	1.000	0.604	2.535	2.757	2.906	2.734	2.712	2.084	1.884	3.163	3.246
Na	0.815	1.479	1.888	0.863	0.927	1.241	1.100	0.862	0.772	2.807	2.259	2.328	3.050	2.300	2.492	2.652	2.632	2.873	3.146	1.469	1.260	1.164	1.167	1.204	1.835	1.972	0.925	0.820
K	0.024	0.056	0.369	0.073	0.026	0.032	0.034	0.058	0.028	0.280	0.056	0.069	0.149	0.078	0.083	0.086	0.090	0.129	0.224	0.024	0.020	0.038	0.023	0.021	0.036	0.093	0.027	0.027
Ni	0.005	0.004	0.000	0.000	0.000	0.000	0.000	0.000	0.000	0.000	0.000	0.003	0.002	0.000	0.000	0.000	0.001	0.001	0.000	0.003	0.001	0.004	0.001	0.000	0.000	0.003	0.000	0.002
Ba																												
Sr																												
Total	19.941	20.013	20.019	20.044	20.024	19.994	20.020	20.066	20.057	20.037	20.005	19.969	19.979	19.965	19.949	19.956	19.970	19.994	19.966	20.027	20.034	20.091	19.969	19.971	19.987	19.982	20.070	20.065
X location	63.917	67.983	68.634	70.277	70.633	70.431	69.659	68.659	68.867	10.174	10.229	10.299	10.335	10.378	13.200	13.199	13.261	13.261	13.279	67.471	67.355	67.154	66.967	66.949	66.722	71.324	71.437	71.439
Y location	65.306	69.192	69.768	69.207	68.895	66.627	65.663	65.153	65.166	42.881	42.881	42.881	42.881	42.858	43.971	43.899	43.867	43.831	43.767	43.730	43.730	43.730	43.730	43.730	43.730	43.853	43.812	43.678
Crystal #	11			12	12					9	9	9	9	9	11	11	11	11	11	3	3	3	3	3	3	4	4	4
Comments										Core				Rim	Core				Rim	RIM		core			RIM	Rim		CORE
An	78	62	44	77	76	68	72	77	80	23	42	40	20	40	34	30	31	25	15	63	68	71	70	69	53	48	77	79
Ab	21	37	47	22	23	31	28	21	19	70	56	59	76	58	63	67	66	72	79	36	31	28	30	31	46	50	22	20
Or	1	1	9	2	1	1	1	1	1	7	1	2	4	2	2	2	2	3	6	1	0	1	1	1	1	2	1	1

Sample	SV165	SV176	SV176	SV181	SV181	SV181	SV181	SV181	SV181	SV181	SV181	SV181	SV181	SV181	SV181	SV181	SV181	SV181	SV181	SV181	SV181	SV181	SV181	SV181	SV181	SV181	SV181	SV181
Rock Type		XEN	XEN	XEN	XEN	XEN	XEN	XEN	XEN	XEN	XEN	XEN	XEN	XEN	XEN	XEN	XEN	XEN	XEN	XEN	XEN	XEN	XEN	XEN	XEN	XEN	XEN	XEN
Analysis	07-027	07-111	07-115	10-006	10-007	10-013	10-014	10-015	10-034	10-035	10-037	10-038	10-039	10-040	10-041	10-042	10-050	10-051	10-052	10-053	10-054	10-055	10-056	10-066	10-069	10-088	10-090	10-094
SiO_2	56.46	55.72	58.58	46.13	46.22	46.50	46.44	46.98	47.04	45.97	46.06	45.93	46.15	45.86	46.29	46.10	46.48	46.64	46.29	46.52	46.49	46.41	46.11	46.81	46.56	46.09	46.67	46.67
TiO_2	0.07	0.03	0.00	0.01	0.00	0.06	0.00	0.02	0.04	0.01	0.00	0.00	0.03	0.00	0.02	0.00	0.00	0.02	0.01	0.04	0.00	0.00	0.02	0.00	0.01	0.00	0.02	0.00
Al_2O_3	27.06	26.90	25.24	33.14	33.92	33.61	33.55	33.41	33.37	33.97	33.77	34.15	33.24	33.30	33.92	34.03	33.51	33.47	33.51	33.62	33.53	33.53	33.62	33.39	33.68	34.11	33.36	34.15
Cr_2O_3	0.01	0.03	0.00	0.00	0.05	0.06	0.00	0.01	0.01	0.00	0.00	0.00	0.01	0.01	0.01	0.00	0.00	0.02	0.02	0.00	0.00	0.00	0.00	0.00	0.02	0.01	0.00	0.00
FeO	0.39	0.20	0.25	0.17	0.21	0.16	0.22	0.26	0.20	0.18	0.23	0.21	0.19	0.16	0.19	0.18	0.24	0.20	0.18	0.18	0.20	0.22	0.21	0.17	0.18	0.20	0.32	0.26
MnO	0.02	0.00	0.00	0.00	0.00	0.03	0.01	0.01	0.00	0.01	0.00	0.04	0.00	0.06	0.00	0.03	0.01	0.00	0.00	0.00	0.00	0.02	0.02	0.00	0.02	0.00	0.01	0.02
MgO	0.02	0.01	0.00	0.02	0.01	0.00	0.01	0.01	0.00	0.00	0.00	0.00	0.03	0.00	0.00	0.00	0.02	0.00	0.00	0.00	0.00	0.00	0.01	0.00	0.00	0.00	0.02	0.00
CaO	9.64	9.89	7.67	17.54	17.62	17.54	17.52	17.07	17.09	17.70	18.00	18.24	17.34	17.34	17.66	17.63	16.98	17.23	17.15	17.20	17.15	17.37	17.78	17.10	17.44	17.86	17.36	17.87
Na_2O	6.09	5.92	7.13	1.51	1.37	1.43	1.51	1.71	1.75	1.24	1.33	1.17	1.72	1.48	1.42	1.31	1.56	1.54	1.51	1.48	1.51	1.47	1.46	1.57	1.57	1.29	1.61	1.40
K_2O	0.24	0.21	0.32	0.02	0.02	0.02	0.03	0.02	0.04	0.00	0.02	0.01	0.03	0.03	0.02	0.02	0.01	0.03	0.02	0.02	0.03	0.03	0.05	0.02	0.04	0.03	0.02	0.02
NiO	0.00	0.01	0.00	0.00	0.04	0.02	0.00	0.01	0.03	0.00	0.00	0.02	0.01	0.03	0.00	0.00	0.01	0.00	0.00	0.01	0.00	0.00	0.00	0.04	0.00	0.03	0.00	0.00
BaO																												
SrO																												
Total	99.98	98.92	99.19	98.55	99.45	99.44	99.29	99.51	99.56	99.08	99.42	99.75	98.75	98.26	99.54	99.30	98.80	99.15	98.69	99.06	98.90	99.06	99.26	99.11	99.51	99.62	99.40	100.39
Si (32 O)	10.172	10.146	10.571	8.617	8.555	8.604	8.607	8.676	8.682	8.536	8.538	8.489	8.605	8.590	8.559	8.541	8.640	8.644	8.619	8.626	8.635	8.616	8.560	8.674	8.607	8.521	8.640	8.560
Ti	0.010	0.004	0.000	0.002	0.000	0.009	0.000	0.003	0.006	0.001	0.000	0.000	0.005	0.000	0.003	0.000	0.000	0.003	0.002	0.006	0.000	0.000	0.002	0.000	0.002	0.000	0.003	0.000
Al	5.746	5.772	5.369	7.296	7.399	7.329	7.329	7.273	7.259	7.434	7.380	7.440	7.306	7.352	7.392	7.432	7.341	7.312	7.354	7.348	7.340	7.338	7.356	7.293	7.339	7.431	7.281	7.383
Cr	0.001	0.004	0.000	0.000	0.007	0.009	0.000	0.001	0.002	0.000	0.000	0.000	0.002	0.002	0.001	0.000	0.000	0.003	0.004	0.000	0.000	0.000	0.000	0.000	0.003	0.002	0.000	0.001
Fe_2	0.059	0.030	0.038	0.027	0.032	0.025	0.035	0.041	0.031	0.028	0.036	0.032	0.029	0.025	0.030	0.028	0.037	0.030	0.027	0.028	0.030	0.034	0.032	0.026	0.027	0.030	0.050	0.040
Mn	0.003	0.000	0.000	0.000	0.000	0.004	0.002	0.001	0.000	0.002	0.000	0.006	0.000	0.010	0.000	0.005	0.001	0.000	0.000	0.000	0.000	0.003	0.002	0.001	0.003	0.000	0.002	0.002
Mg	0.004	0.004	0.000	0.006	0.002	0.001	0.001	0.002	0.000	0.000	0.000	0.000	0.009	0.000	0.000	0.000	0.005	0.000	0.000	0.000	0.000	0.000	0.003	0.000	0.000	0.001	0.006	0.000
Ca	1.860	1.929	1.482	3.510	3.494	3.477	3.479	3.377	3.379	3.521	3.576	3.612	3.464	3.480	3.498	3.500	3.381	3.422	3.421	3.417	3.414	3.455	3.537	3.396	3.455	3.538	3.443	3.512
Na	2.127	2.089	2.495	0.548	0.491	0.511	0.544	0.612	0.625	0.446	0.478	0.420	0.623	0.538	0.510	0.469	0.562	0.552	0.544	0.532	0.542	0.531	0.524	0.564	0.564	0.463	0.578	0.496
K	0.054	0.049	0.074	0.004	0.004	0.006	0.008	0.005	0.009	0.000	0.006	0.001	0.006	0.006	0.005	0.004	0.002	0.008	0.004	0.004	0.007	0.008	0.011	0.005	0.008	0.006	0.005	0.004
Ni	0.000	0.002	0.000	0.000	0.006	0.003	0.000	0.001	0.004	0.000	0.000	0.003	0.002	0.004	0.000	0.000	0.002	0.000	0.000	0.001	0.000	0.000	0.000	0.006	0.000	0.005	0.001	0.000
Ba																												
Sr																												
Total	20.036	20.030	20.029	20.009	19.990	19.978	20.004	19.993	19.998	19.969	20.014	20.002	20.050	20.005	19.999	19.980	19.972	19.975	19.975	19.962	19.970	19.984	20.027	19.964	20.007	19.997	20.008	19.998
X location	77.074	6.300	15.154	20.461	20.724	20.116	20.233	20.591	25.383	25.241	27.980	27.980	28.129	28.103	28.218	28.168	31.713	31.770	31.770	31.788	31.788	31.808	34.273	41.457	52.497	44.500	43.118	54.957
Y location	43.423	70.398	73.465	58.202	58.068	56.853	56.781	56.922	55.441	55.674	55.675	55.926	56.095	56.280	56.383	56.641	55.114	55.114	55.134	55.147	55.162	55.175	54.169	52.316	52.649	60.212	60.104	60.386
Crystal #						2	2	2	4	4	5	5	5	5	5	5	7	7	7	7	7							
Comments																												
An	46	47	37	86	88	87	86	85	84	89	88	90	85	86	87	88	86	86	86	86	86	87	87	86	86	88	86	88
Ab	53	51	62	13	12	13	13	15	16	11	12	10	15	13	13	12	14	14	14	13	14	13	13	14	14	12	14	12
Or	1	1	2	0	0	0	0	0	0	0	0	0	0	0	0	0	0	0	0	0	0	0	0	0	0	0	0	0

Sample	SV181	SV181	SV181	SV181	SV181	SV181	SV181	SV181	SV181	SV181	SV181	SV183	SV183	SV183	SV183	SV183	SV183	SV183	SV183	SV183	SV183	SV183	SV183	SV183	SV183	SV183	SV183	SV183
Rock Type	XEN	XEN	XEN	XEN																	XEN							
Analysis	10-095	10-096	10-097	10-099	10-103	10-104	10-108	10-111	10-118	10-127	10-128	07-066	07-068	07-069	07-070	07-072	07-075	07-076	07-078	07-079	07-090	07-100	07-101	07-106	07-107	07-108	07-109	07-110
SiO_2	46.36	46.60	46.73	47.29	60.22	62.38	62.89	57.09	61.86	63.59	57.35	63.61	63.89	59.09	57.71	56.36	63.06	59.37	60.59	59.57	54.49	57.15	54.40	61.47	56.52	56.48	53.36	62.75
TiO_2	0.00	0.00	0.00	0.00	0.00	0.00	0.07	0.03	0.03	0.00	0.00	0.00	0.00	0.01	0.00	0.02	0.00	0.00	0.02	0.00	0.02	0.00	0.03	0.01	0.00	0.01	0.01	0.04
Al_2O_3	33.09	33.85	33.89	33.66	24.70	23.74	22.52	26.57	23.61	22.51	26.38	22.37	22.17	25.43	26.08	26.88	22.19	25.01	22.70	24.87	27.99	26.20	27.88	23.03	26.59	26.71	28.54	21.28
Cr_2O_3	0.01	0.03	0.02	0.00	0.00	0.00	0.00	0.00	0.01	0.00	0.04	0.02	0.00	0.02	0.00	0.03	0.00	0.01	0.00	0.02	0.00	0.00	0.00	0.00	0.00	0.02	0.00	0.00
FeO	0.35	0.24	0.20	0.24	0.14	0.12	0.16	0.25	0.13	0.18	0.19	0.18	0.17	0.17	0.20	0.23	0.18	0.10	0.20	0.17	0.17	0.12	0.21	0.13	0.17	0.18	0.36	0.42
MnO	0.01	0.01	0.00	0.02	0.00	0.00	0.00	0.02	0.02	0.00	0.00	0.00	0.00	0.00	0.02	0.03	0.00	0.02	0.01	0.00	0.01	0.00	0.01	0.00	0.00	0.02	0.02	0.00
MgO	0.03	0.00	0.00	0.00	0.00	0.00	0.00	0.00	0.00	0.00	0.01	0.00	0.01	0.00	0.01	0.00	0.00	0.00	0.05	0.02	0.01	0.00	0.00	0.00	0.02	0.00	0.03	0.01
CaO	17.09	17.69	17.86	16.86	6.44	5.14	4.40	8.92	5.32	4.16	8.88	4.03	3.61	7.20	8.38	9.31	3.92	7.02	4.95	6.82	11.01	8.89	10.74	4.99	9.11	9.25	11.73	4.02
Na_2O	1.59	1.50	1.35	1.55	7.50	8.44	8.65	6.28	8.25	8.77	6.35	9.03	9.36	7.35	6.73	6.33	9.10	7.51	8.23	7.56	5.45	6.48	5.52	8.38	6.27	6.02	4.84	7.84
K_2O	0.06	0.01	0.03	0.03	0.44	0.42	0.74	0.24	0.44	0.76	0.16	0.59	0.46	0.31	0.20	0.18	0.56	0.29	0.45	0.33	0.15	0.29	0.23	0.58	0.20	0.23	0.17	1.50
NiO	0.00	0.01	0.00	0.01	0.00	0.01	0.00	0.03	0.01	0.01	0.00	0.00	0.00	0.03	0.01	0.00	0.02	0.00	0.00	0.00	0.00	0.01	0.02	0.00	0.00	0.02	0.04	0.00
BaO																												
SrO																												
Total	98.59	99.95	100.08	99.66	99.45	100.24	99.43	99.44	99.69	99.99	99.36	99.83	99.67	99.62	99.34	99.37	99.03	99.33	97.20	99.37	99.31	99.13	99.04	98.59	98.87	98.92	99.11	97.85
Si (32 O)	8.651	8.584	8.592	8.702	10.784	11.041	11.218	10.307	11.020	11.268	10.348	11.284	11.335	10.599	10.412	10.204	11.280	10.670	11.069	10.700	9.916	10.349	9.927	11.074	10.265	10.252	9.760	11.383
Ti	0.000	0.000	0.000	0.000	0.000	0.000	0.009	0.004	0.004	0.000	0.000	0.000	0.000	0.001	0.001	0.003	0.000	0.000	0.003	0.000	0.003	0.000	0.004	0.001	0.000	0.001	0.001	0.005
Al	7.279	7.349	7.344	7.300	5.213	4.953	4.734	5.654	4.957	4.701	5.611	4.678	4.636	5.377	5.545	5.736	4.678	5.297	4.887	5.266	6.004	5.591	5.998	4.891	5.692	5.716	6.152	4.549
Cr	0.002	0.004	0.003	0.000	0.000	0.000	0.000	0.000	0.001	0.000	0.006	0.002	0.000	0.004	0.000	0.004	0.000	0.002	0.000	0.002	0.000	0.000	0.000	0.000	0.000	0.002	0.000	0.000
Fe_2	0.054	0.037	0.031	0.037	0.021	0.017	0.024	0.038	0.020	0.027	0.029	0.027	0.026	0.026	0.030	0.035	0.027	0.015	0.031	0.026	0.026	0.018	0.032	0.019	0.025	0.028	0.055	0.064
Mn	0.002	0.002	0.000	0.002	0.000	0.000	0.000	0.004	0.003	0.000	0.000	0.000	0.000	0.000	0.003	0.004	0.000	0.003	0.001	0.000	0.001	0.000	0.002	0.000	0.000	0.003	0.004	0.000
Mg	0.009	0.000	0.001	0.000	0.000	0.000	0.000	0.000	0.000	0.000	0.003	0.000	0.002	0.000	0.004	0.000	0.000	0.000	0.014	0.005	0.004	0.000	0.000	0.000	0.005	0.000	0.008	0.003
Ca	3.417	3.492	3.519	3.324	1.236	0.974	0.840	1.726	1.016	0.789	1.716	0.766	0.686	1.384	1.620	1.806	0.750	1.351	0.968	1.313	2.146	1.725	2.100	0.963	1.773	1.799	2.299	0.781
Na	0.576	0.534	0.482	0.552	2.606	2.896	2.991	2.197	2.851	3.012	2.223	3.106	3.220	2.558	2.355	2.221	3.157	2.617	2.917	2.633	1.923	2.276	1.955	2.926	2.209	2.117	1.715	2.756
K	0.013	0.003	0.007	0.007	0.100	0.094	0.169	0.055	0.100	0.172	0.038	0.132	0.104	0.070	0.045	0.041	0.127	0.066	0.105	0.076	0.036	0.066	0.052	0.133	0.045	0.053	0.040	0.348
Ni	0.000	0.002	0.000	0.002	0.001	0.001	0.000	0.005	0.001	0.002	0.000	0.000	0.000	0.005	0.002	0.000	0.003	0.000	0.000	0.000	0.000	0.001	0.003	0.000	0.000	0.002	0.006	0.000
Ba																												
Sr																												
Total	20.004	20.008	19.979	19.927	19.962	19.977	19.986	19.989	19.972	19.972	19.974	19.996	20.009	20.023	20.016	20.054	20.023	20.021	19.996	20.021	20.058	20.026	20.073	20.008	20.016	19.973	20.040	19.889
X location	55.064	54.689	54.507	7.136	1.551	2.204	5.641	6.056	8.590	2.338	1.633	38.352	39.416	41.769	41.707	42.242	43.461	43.145	43.327	43.038	33.096	7.824	7.872	11.933	7.938	7.809	7.712	7.712
Y location	60.510	60.299	60.391	60.862	60.615	61.237	62.978	65.491	75.903	70.813	70.505	44.473	44.473	45.359	45.202	50.626	53.858	55.047	57.775	59.325	66.144	50.755	50.654	64.655	66.548	66.548	66.548	66.492
Crystal #		11	11							13	13											7	7		8	8	8	8
Comments										Rim	Core										XEN		Core					
An	85	87	88	86	31	25	21	43	26	20	43	19	17	34	40	44	19	33	24	33	52	42	51	24	44	45	57	20
Ab	14	13	12	14	66	73	75	55	72	76	56	78	80	64	59	55	78	65	73	65	47	56	48	73	55	53	42	71
Or	0	0	0	0	3	2	4	1	3	4	1	3	3	2	1	1	3	2	3	2	1	2	1	3	1	1	1	9

I.3 Amphibole

Sample	SV2	SV2	SV2	SV2	SV2	SV2	SV2	SV2	SV2	SV2	SV2	SV2	SV2	SV2	SV2	SV2	SV2	SV2	SV2	SV2	SV2	SV2	SV2	SV2	SV2
Rock Type	TRAC	TRAC	TRAC	TRAC	TRAC	TRAC	TRAC	TRAC	TRAC	TRAC	TRAC	TRAC	TRAC	TRAC	TRAC	TRAC	XEN	XEN	XEN	XEN	XEN	XEN	XEN	XEN	XEN
Sample	01 -001	01 -002	01 -003	01 -004	01 -005	01 -006	01 -007	01 -016	01 -017	01 -018	01 -019	01 -020	01 -033	01 -034	01 -036	01 -037	01 -038	01 -040	01 -042	01 -043	01 -052	01 -056	02-002	02-004	02-005
SiO_2	44.744	43.217	45.756	44.459	43.537	44.192	45.168	45.034	49.833	46.911	46.178	45.635	49.947	48.185	49.205	49.718	46.508	49.700	48.129	46.440	41.267	41.344	41.572	39.433	41.441
TiO_2	1.419	1.633	1.238	1.398	1.500	1.448	1.208	1.242	1.078	1.115	1.235	1.260	0.999	0.959	0.863	0.771	0.838	0.851	0.134	0.670	1.659	1.828	1.742	1.992	1.797
Al_2O_3	9.667	10.705	8.785	10.065	10.750	10.205	9.481	9.116	5.424	7.489	8.050	8.574	4.943	6.098	5.318	5.158	7.659	5.372	7.450	7.754	12.825	13.376	12.914	14.027	12.896
Cr_2O_3	0.030	0.000	0.000	0.000	0.039	0.051	0.011	0.039	0.000	0.053	0.012	0.057	0.032	0.199	0.109	0.112	0.062	0.075	0.131	0.058	0.014	0.000	0.000	0.003	0.011
MnO	0.330	0.307	0.296	0.290	0.230	0.262	0.272	0.251	0.730	0.586	0.493	0.596	0.713	0.607	0.637	0.687	0.784	0.736	0.396	0.650	0.278	0.233	0.150	0.211	0.142
FeO	13.926	14.813	13.687	13.517	13.981	14.045	13.559	13.473	12.368	12.665	12.714	13.651	11.243	12.685	11.752	11.236	13.221	11.699	12.462	13.173	14.441	11.021	11.650	14.024	11.650
MgO	13.226	12.263	13.495	12.791	12.219	12.564	12.987	13.523	15.556	14.122	14.158	13.636	16.433	15.416	16.022	16.295	14.497	15.783	14.711	14.134	11.829	13.498	13.076	11.072	12.990
CaO	11.833	11.736	11.586	11.106	11.138	11.151	11.371	11.505	10.392	10.911	11.316	11.375	10.717	10.929	11.052	10.855	10.711	10.697	10.788	10.704	11.735	11.759	11.618	11.871	11.896
Na_2O	1.829	2.059	2.314	1.931	2.170	2.160	2.249	2.483	2.155	2.469	2.497	2.580	1.949	1.912	1.859	1.791	2.500	2.037	2.377	2.491	2.814	2.791	2.931	2.863	2.747
K_2O	0.537	0.604	0.467	0.509	0.551	0.533	0.490	0.578	0.497	0.404	0.429	0.446	0.376	0.479	0.398	0.383	0.566	0.344	0.252	0.454	0.749	0.875	0.691	0.943	0.841
NiO	0.000	0.000	0.000	0.000	0.022	0.003	0.019	0.000	0.035	0.018	0.024	0.011	0.016	0.010	0.052	0.000	0.030	0.009	0.045	0.060	0.000	0.027	0.009	0.020	0.000
Total	97.541	97.337	97.624	96.066	96.137	96.614	96.815	97.244	98.068	96.743	97.106	97.821	97.368	97.479	97.267	97.006	97.376	97.303	96.875	96.588	97.611	96.752	96.353	96.459	96.411
Si (23 O)	6.632	6.467	6.760	6.661	6.550	6.611	6.722	6.689	7.227	6.948	6.832	6.745	7.257	7.068	7.189	7.250	6.879	7.241	7.072	6.912	6.186	6.155	6.221	5.999	6.207
Ti	0.158	0.184	0.138	0.158	0.170	0.163	0.135	0.139	0.118	0.124	0.137	0.140	0.109	0.106	0.095	0.085	0.093	0.093	0.015	0.075	0.187	0.205	0.196	0.228	0.202
Al	1.689	1.888	1.530	1.777	1.906	1.799	1.663	1.596	0.927	1.307	1.404	1.493	0.846	1.054	0.916	0.886	1.335	0.922	1.290	1.360	2.266	2.347	2.278	2.515	2.276
Cr	0.004	0.000	0.000	0.000	0.005	0.006	0.001	0.005	0.000	0.006	0.001	0.007	0.004	0.023	0.013	0.013	0.007	0.009	0.015	0.007	0.002	0.000	0.000	0.000	0.001
Mn^{2+}	0.041	0.039	0.037	0.037	0.029	0.033	0.034	0.032	0.090	0.074	0.062	0.075	0.088	0.075	0.079	0.085	0.098	0.091	0.049	0.082	0.035	0.029	0.019	0.027	0.018
Fe^{2+}	1.726	1.854	1.691	1.693	1.759	1.757	1.687	1.673	1.500	1.568	1.573	1.687	1.366	1.556	1.436	1.370	1.635	1.425	1.531	1.640	1.810	1.372	1.458	1.784	1.459
Mg	2.922	2.736	2.972	2.857	2.740	2.802	2.881	2.995	3.363	3.118	3.123	3.005	3.560	3.371	3.490	3.542	3.197	3.428	3.223	3.136	2.643	2.996	2.917	2.511	2.900
Ca	1.879	1.882	1.834	1.782	1.795	1.787	1.813	1.831	1.615	1.731	1.794	1.801	1.668	1.717	1.730	1.696	1.697	1.670	1.698	1.707	1.884	1.875	1.863	1.935	1.909
Na	0.526	0.597	0.663	0.561	0.633	0.626	0.649	0.715	0.606	0.709	0.716	0.739	0.549	0.544	0.527	0.506	0.717	0.575	0.677	0.719	0.818	0.805	0.850	0.844	0.798
K	0.102	0.115	0.088	0.097	0.106	0.102	0.093	0.110	0.092	0.076	0.081	0.084	0.070	0.090	0.074	0.071	0.107	0.064	0.047	0.086	0.143	0.166	0.132	0.183	0.161
Ni	0.000	0.000	0.000	0.000	0.003	0.000	0.002	0.000	0.004	0.002	0.003	0.001	0.002	0.001	0.006	0.000	0.004	0.001	0.005	0.007	0.000	0.003	0.001	0.002	0.000
Total	15.678	15.761	15.713	15.623	15.695	15.687	15.682	15.784	15.541	15.664	15.726	15.777	15.518	15.605	15.553	15.505	15.769	15.520	15.623	15.732	15.974	15.953	15.935	16.029	15.931
Si_T	6.55	6.39	6.69	6.57	6.47	6.52	6.66	6.62	7.10	6.87	6.76	6.67	7.13	6.93	7.07	7.12	6.75	7.13	6.96	6.80	6.13	6.10	6.18	5.97	6.18
$ivAl_T$	1.45	1.61	1.31	1.43	1.53	1.48	1.34	1.38	0.90	1.13	1.24	1.33	0.83	1.03	0.90	0.87	1.25	0.87	1.04	1.20	1.87	1.90	1.82	2.03	1.82
$viAl_C$	0.21	0.25	0.21	0.32	0.35	0.30	0.30	0.20	0.01	0.16	0.15	0.14					0.06	0.03	0.24	0.14	0.37	0.43	0.44	0.47	0.44
Ti_C	0.16	0.18	0.14	0.16	0.17	0.16	0.13	0.14	0.12	0.12	0.14	0.14	0.07	0.07	0.06	0.08	0.09	0.09	0.01	0.07	0.19	0.20	0.19	0.23	0.20
Cr_C						0.01				0.01		0.01		0.02	0.01	0.01	0.01	0.01	0.01	0.01					
Fe^{3+}_C	0.59	0.58	0.44	0.63	0.56	0.59	0.44	0.45	0.78	0.51	0.47	0.53	0.79	0.86	0.76	0.79	0.84	0.72	0.69	0.75	0.45	0.37	0.31	0.23	0.22
Mg_C	2.88	2.70	2.94	2.82	2.71	2.77	2.85	2.97	3.31	3.08	3.09	2.97	3.50	3.31	3.43	3.48	3.14	3.37	3.17	3.08	2.62	2.97	2.90	2.50	2.89
Fe^{2+}_C	1.11	1.25	1.23	1.04	1.18	1.14	1.23	1.21	0.69	1.04	1.09	1.14	0.55	0.66	0.65	0.56	0.76	0.68	0.82	0.86	1.35	0.99	1.13	1.54	1.23
Mn^{2+}_C	0.04	0.04	0.04	0.04	0.03	0.03	0.03	0.03	0.09	0.07	0.06	0.07	0.09	0.07	0.08	0.08	0.10	0.09	0.05	0.08	0.03	0.03	0.02	0.03	0.02
Ni_C															0.01				0.01	0.01					
Ca_B	1.85	1.86	1.82	1.76	1.77	1.76	1.80	1.81	1.59	1.71	1.78	1.78	1.64	1.68	1.70	1.67	1.67	1.64	1.67	1.68	1.87	1.86	1.85	1.92	1.90
Na_B	0.15	0.14	0.18	0.24	0.23	0.24	0.20	0.19	0.41	0.29	0.22	0.22	0.36	0.32	0.30	0.33	0.33	0.36	0.33	0.32	0.13	0.14	0.15	0.08	0.10
Na_A	0.37	0.45	0.47	0.31	0.40	0.38	0.44	0.52	0.18	0.41	0.48	0.51	0.18	0.22	0.22	0.16	0.37	0.21	0.34	0.39	0.68	0.66	0.69	0.76	0.69
K_A	0.10	0.11	0.09	0.10	0.10	0.10	0.09	0.11	0.09	0.08	0.08	0.08	0.07	0.09	0.07	0.07	0.10	0.06	0.05	0.08	0.14	0.16	0.13	0.18	0.16
Na_A+K_A	0.47	0.56	0.56	0.41	0.50	0.48	0.53	0.63	0.27	0.49	0.56	0.59	0.25	0.31	0.29	0.23	0.47	0.27	0.39	0.47	0.82	0.82	0.83	0.95	0.85
Crystal #	1	1	1	1	1	1	1		3	3	3	3	6	6	6	6									
Comments	core		rim		core		rim		Rim		Core		Rim	Core		Rim									
Name	Magnesiohornblende	Magnesiohastingsite	Edenite	Magnesiohornblende	Magnesiohastingsite	Magnesiohornblende	Edenite	Edenite	Ferrian Magnesiohornblende	Magnesiohornblende	Edenite	Edenite	Ferrian Magnesiohornblende	Ferrian Magnesiohornblende	Ferrian Magnesiohornblende	Ferrian Magnesiohornblende	Ferrian Magnesiohornblende	Magnesiohornblende	Magnesiohornblende	Ferrian Magnesiohornblende	Magnesiohastingsite	Pargasite	Pargasite	Pargasite	Pargasite

Table I.3: Amphibole electron microprobe data. Stoichiometry and mineral names by AMPH-CLASS (Esawi, 2004).

Sample	SV2	SV2	SV2	SV2	SV2	SV2	SV2	SV2	SV2	SV2	SV2	SV2	SV2	SV2
Rock Type	XEN	XEN	XEN	XEN	XEN	XEN	XEN	XEN	XEN	XEN	XEN	XEN	XEN	XEN
Sample	02-006	02-011	02-012	02-013	02-014	02-015	02-016	02-017	02-018	02-019	02-020	02-021	02-022	02-023
SiO_2	41.118	41.134	41.161	40.259	40.609	44.307	44.610	40.424	40.250	40.800	40.663	41.087	40.920	40.440
TiO_2	1.839	1.754	1.805	1.858	1.720	1.241	1.273	2.033	1.864	1.950	1.845	1.764	1.887	1.976
Al_2O_3	13.153	13.683	13.599	13.422	13.054	9.520	9.018	13.733	13.979	13.621	14.244	13.616	13.744	12.837
Cr_2O_3	0.000	0.048	0.000	0.023	0.009	0.016	0.000	0.007	0.009	0.000	0.000	0.025	0.000	0.000
MnO	0.159	0.135	0.120	0.055	0.152	0.287	0.205	0.103	0.124	0.111	0.144	0.124	0.125	0.153
FeO	12.719	10.030	10.358	11.025	14.727	14.801	13.916	10.884	11.092	10.877	11.251	12.156	10.713	14.833
MgO	12.693	13.943	14.394	14.551	11.561	13.033	13.516	14.350	13.513	13.732	13.410	13.202	14.090	11.492
CaO	11.942	11.627	12.048	11.930	11.397	11.619	11.498	12.200	12.273	12.458	12.133	11.818	12.354	11.845
Na_2O	2.707	2.744	2.864	2.560	2.879	2.553	2.478	2.621	2.790	2.804	2.759	2.731	2.634	2.787
K_2O	0.977	0.931	0.897	0.943	0.841	0.676	0.615	0.936	0.886	0.908	0.867	0.968	0.964	0.879
NiO	0.000	0.000	0.000	0.023	0.000	0.000	0.000	0.000	0.027	0.016	0.018	0.000	0.000	0.000
Total	97.307	96.029	97.246	96.649	96.949	98.053	97.129	97.291	96.807	97.277	97.334	97.491	97.431	97.242
Si (23 O)	6.141	6.137	6.086	6.016	6.140	6.586	6.656	5.999	6.012	6.057	6.032	6.105	6.055	6.113
Ti	0.207	0.197	0.201	0.209	0.196	0.139	0.143	0.227	0.209	0.218	0.206	0.197	0.210	0.225
Al	2.315	2.406	2.370	2.364	2.326	1.668	1.586	2.402	2.461	2.383	2.490	2.384	2.397	2.287
Cr	0.000	0.006	0.000	0.003	0.001	0.002	0.000	0.001	0.001	0.000	0.000	0.003	0.000	0.000
Mn^{2+}	0.020	0.017	0.015	0.007	0.019	0.036	0.026	0.013	0.016	0.014	0.018	0.016	0.016	0.020
Fe^{2+}	1.589	1.251	1.281	1.378	1.862	1.840	1.736	1.351	1.385	1.350	1.396	1.510	1.325	1.875
Mg	2.826	3.101	3.173	3.242	2.606	2.888	3.006	3.175	3.009	3.039	2.966	2.924	3.108	2.590
Ca	1.911	1.859	1.908	1.910	1.846	1.850	1.838	1.940	1.964	1.981	1.928	1.881	1.958	1.918
Na	0.784	0.794	0.821	0.742	0.844	0.736	0.717	0.754	0.808	0.807	0.793	0.787	0.756	0.817
K	0.186	0.177	0.169	0.180	0.162	0.128	0.117	0.177	0.169	0.172	0.164	0.183	0.182	0.169
Ni	0.000	0.000	0.000	0.003	0.000	0.000	0.000	0.000	0.003	0.002	0.002	0.000	0.000	0.000
Total	15.979	15.945	16.024	16.052	16.003	15.872	15.825	16.038	16.036	16.023	15.996	15.990	16.006	16.012
Si_T	6.10	6.08	6.03	5.92	6.07	6.51	6.58	5.92	5.97	6.03	5.98	6.04	6.00	6.06
$ivAl_T$	1.90	1.92	1.97	2.08	1.93	1.49	1.42	2.08	2.03	1.97	2.02	1.96	2.00	1.94
$viAl_C$	0.39	0.47	0.38	0.24	0.37	0.15	0.15	0.29	0.41	0.40	0.45	0.40	0.38	0.33
Ti_C	0.21	0.20	0.20	0.21	0.19	0.14	0.14	0.22	0.21	0.22	0.20	0.20	0.21	0.22
Cr_C		0.01												
$Fe^{3+}{}_C$	0.34	0.40	0.43	0.76	0.52	0.55	0.53	0.58	0.33	0.22	0.38	0.48	0.38	0.38
Mg_C	2.81	3.07	3.14	3.19	2.58	2.85	2.97	3.13	2.99	3.02	2.94	2.89	3.08	2.57
$Fe^{2+}{}_C$	1.23	0.84	0.83	0.60	1.32	1.27	1.19	0.76	1.04	1.12	1.00	1.01	0.93	1.48
$Mn^{2+}{}_C$	0.02	0.02	0.01	0.01	0.02	0.04	0.03	0.01	0.02	0.01	0.02	0.02	0.02	0.02
Ni_C														
Ca_B	1.90	1.84	1.89	1.88	1.83	1.83	1.82	1.92	1.95	1.97	1.91	1.86	1.94	1.90
Na_B	0.10	0.16	0.11	0.12	0.17	0.17	0.18	0.08	0.05	0.03	0.09	0.14	0.06	0.10
Na_A	0.67	0.63	0.70	0.61	0.66	0.55	0.52	0.66	0.75	0.77	0.70	0.64	0.69	0.71
K_A	0.18	0.18	0.17	0.18	0.16	0.13	0.12	0.17	0.17	0.17	0.16	0.18	0.18	0.17
Na_A+K_A	0.86	0.80	0.87	0.78	0.82	0.68	0.64	0.83	0.92	0.95		0.82	0.87	0.88
Crystal #		1	1	1	1	1	1	1	1	1	1	1	1	1
Comments					Rim						Core			Rim
Name	Pargasite	Pargasite	Magnesiohastingsite	Ferrian Magnesiohastingsite	Magnesiohastingsite	Edenite	Edenite	Magnesiohastingsite	Pargasite	Pargasite	Pargasite	Magnesiohastingsite	Magnesiohastingsite	Magnesiohastingsite

Sample	SV2	SV2	SV2	SV2	SV2	SV2	SV2	SV2	SV2	SV2	SV2	SV2	SV2
Rock Type	XEN	XEN	XEN	XEN	XEN	XEN	XEN	XEN	XEN	XEN	XEN	XEN	XEN
Sample	02-032	02-036	02-038	02-039	02-040	02-041	02-042	02-044	02-055	02-057	02-058	02-062	02-064
SiO_2	46.751	47.135	40.620	43.897	41.603	40.727	40.824	40.169	41.785	46.417	46.480	40.203	43.665
TiO_2	0.936	0.861	1.740	1.452	1.712	1.940	1.905	1.853	1.860	1.020	1.008	1.991	1.379
Al_2O_3	7.849	7.549	12.460	10.071	11.683	14.055	13.386	13.408	11.810	8.055	7.829	13.558	9.674
Cr_2O_3	0.004	0.025	0.000	0.021	0.000	0.021	0.009	0.000	0.000	0.000	0.067	0.000	0.005
MnO	0.271	0.199	0.231	0.261	0.236	0.087	0.243	0.241	0.205	0.209	0.291	0.208	0.220
FeO	13.368	12.322	15.788	13.871	15.233	10.938	12.330	14.697	15.429	12.165	12.568	13.831	13.205
MgO	14.287	14.430	11.099	12.949	11.835	13.704	12.653	11.185	11.473	14.648	14.074	11.943	13.310
CaO	11.480	10.859	11.661	11.541	11.689	12.293	11.951	11.294	11.685	11.634	11.495	11.762	11.590
Na_2O	2.346	2.240	2.818	2.747	2.900	2.760	2.845	2.843	2.842	2.311	2.245	2.824	2.457
K_2O	0.426	0.402	0.888	0.650	0.819	0.952	0.926	0.923	0.558	0.419	0.400	0.871	0.683
NiO	0.014	0.000	0.019	0.015	0.015	0.000	0.008	0.000	0.000	0.000	0.000	0.007	0.000
Total	97.732	96.022	97.324	97.475	97.725	97.477	97.080	96.613	97.647	96.878	96.457	97.198	96.188
Si (23 O)	6.877	6.995	6.161	6.540	6.259	6.030	6.108	6.101	6.279	6.854	6.902	6.051	6.572
Ti	0.104	0.096	0.199	0.163	0.194	0.216	0.214	0.212	0.210	0.113	0.113	0.225	0.156
Al	1.361	1.320	2.227	1.768	2.071	2.452	2.360	2.400	2.092	1.402	1.370	2.405	1.716
Cr	0.000	0.003	0.000	0.002	0.000	0.002	0.001	0.000	0.000	0.000	0.008	0.000	0.001
Mn^{2+}	0.034	0.025	0.030	0.033	0.030	0.011	0.031	0.031	0.026	0.026	0.037	0.027	0.028
Fe^{2+}	1.644	1.529	2.002	1.728	1.916	1.354	1.543	1.866	1.939	1.502	1.561	1.741	1.662
Mg	3.133	3.192	2.510	2.876	2.654	3.025	2.822	2.532	2.570	3.224	3.116	2.680	2.986
Ca	1.809	1.726	1.895	1.842	1.884	1.950	1.916	1.838	1.881	1.840	1.829	1.897	1.869
Na	0.669	0.644	0.829	0.793	0.846	0.792	0.825	0.837	0.828	0.662	0.646	0.824	0.717
K	0.080	0.076	0.172	0.124	0.157	0.180	0.177	0.179	0.107	0.079	0.076	0.167	0.131
Ni	0.002	0.000	0.002	0.002	0.002	0.000	0.001	0.000	0.000	0.000	0.000	0.001	0.000
Total	15.713	15.608	16.027	15.871	16.013	16.013	15.998	15.996	15.932	15.702	15.657	16.017	15.838
Si_T	6.80	6.91	6.10	6.48	6.20	5.99	6.07	6.03	6.22	6.79	6.85	5.99	6.51
$ivAl_T$	1.20	1.09	1.90	1.52	1.80	2.01	1.93	1.97	1.78	1.21	1.15	2.01	1.49
$viAl_C$	0.14	0.21	0.30	0.24	0.25	0.42	0.42	0.41	0.30	0.18	0.21	0.37	0.21
Ti_C	0.10	0.09	0.20	0.16	0.19	0.21	0.21	0.21	0.21	0.11	0.11	0.22	0.15
Cr_C											0.01		
$Fe^{3+}{}_C$	0.54	0.55	0.46	0.39	0.44	0.32	0.28	0.49	0.40	0.42	0.37	0.45	0.42
Mg_C	3.10	3.15	2.48	2.85	2.63	3.00	2.80	2.51	2.55	3.19	3.09	2.65	2.96
$Fe^{2+}{}_C$	1.09	0.96	1.53	1.32	1.46	1.03	1.25	1.35	1.52	1.07	1.18	1.28	1.23
$Mn^{2+}{}_C$	0.03	0.02	0.03	0.03	0.03	0.01	0.03	0.03	0.03	0.03	0.04	0.03	0.03
Ni_C													
Ca_B	1.79	1.71	1.88	1.83	1.87	1.94	1.90	1.82	1.86	1.82	1.81	1.88	1.85
Na_B	0.21	0.29	0.12	0.17	0.13	0.06	0.10	0.18	0.14	0.18	0.19	0.12	0.15
Na_A	0.45	0.34	0.70	0.61	0.70	0.72	0.72	0.65	0.69	0.48	0.46	0.69	0.56
K_A	0.08	0.08	0.17	0.12	0.16	0.18	0.18	0.18	0.11	0.08	0.08	0.17	0.13
Na_A+K_A	0.53	0.42	0.87	0.74	0.86	0.90	0.90	0.82	0.79	0.56	0.53	0.86	0.69
Crystal #	3	3	3	3	3	4	4	4					
Comments	Core	Core			Rim								
Name	Edenite	Magnesiohornblende	Magnesiohastingsite	Magnesiohastingsite	Magnesiohastingsite	Pargasite	Pargasite	Magnesiohastingsite	Magnesiohastingsite	Edenite	Edenite	Magnesiohastingsite	Edenite

Sample	SV2	SV2	SV6A	SV6A	SV6A	SV6A	SV6A	SV6A	SV6A	SV6A	SV6A	SV6A	SV6A	SV6A	SV6A	SV6A	SV6A	SV6A	SV6A	SV6A	SV6A	SV6A	SV6A	SV6A	SV6A	SV6A	SV6A
Rock Type	XEN	XEN	XEN	XEN	XEN	XEN	XEN	XEN	XEN	XEN	XEN	XEN	XEN	XEN	XEN	XEN	XEN	XEN	XEN	XEN	XEN	XEN	XEN	XEN	XEN	XEN	XEN
Sample	02-068	02-072	03-002	03-003	03-007	03-008	03-010	03-012	03-013	03-014	03-015	03-016	03-017	03-019	03-020	03-021	03-023	03-024	03-026	03-027	03-028	03-030	03-031	03-032	03-033	03-035	03-037
SiO_2	43.187	41.284	41.884	42.251	42.946	42.455	42.526	42.512	43.062	43.207	42.080	42.193	42.432	42.823	42.099	42.653	42.372	42.391	42.230	42.449	42.904	41.680	42.161	42.193	42.929	42.639	42.982
TiO_2	1.362	1.637	0.580	0.652	0.520	0.500	0.496	0.545	0.540	0.591	0.584	0.626	0.577	0.559	0.563	0.541	0.548	0.634	0.561	0.558	0.553	0.662	0.642	0.573	0.541	0.598	0.564
Al_2O_3	10.409	11.886	13.223	13.573	12.926	12.791	12.543	13.149	12.829	13.179	12.973	13.482	13.108	13.390	13.230	12.963	13.305	13.361	13.692	12.731	12.932	13.688	12.698	12.911	12.793	12.953	12.564
Cr_2O_3	0.016	0.026	0.171	0.109	0.032	0.064	0.113	0.060	0.118	0.048	0.074	0.106	0.081	0.153	0.164	0.090	0.141	0.076	0.067	0.002	0.132	0.067	0.152	0.125	0.039	0.118	0.051
MnO	0.276	0.308	0.197	0.222	0.190	0.240	0.176	0.209	0.226	0.243	0.204	0.226	0.230	0.226	0.215	0.201	0.192	0.174	0.178	0.225	0.192	0.238	0.227	0.265	0.254	0.261	0.274
FeO	13.354	14.462	11.398	11.510	11.336	11.154	11.078	11.578	11.234	11.155	11.243	11.477	11.413	11.525	11.470	11.250	11.538	11.424	11.748	11.361	11.332	11.564	11.151	11.499	11.505	11.289	11.298
MgO	13.001	12.065	14.281	14.420	14.807	14.517	14.533	14.645	14.906	14.766	14.304	14.364	14.535	14.673	14.198	14.745	14.564	14.583	14.413	14.617	14.830	14.186	14.278	14.335	14.813	14.555	14.759
CaO	11.618	12.094	11.580	11.858	11.831	11.436	11.704	12.005	11.973	11.922	11.817	11.962	11.798	11.792	11.948	11.960	12.059	12.129	11.849	11.602	11.944	11.840	11.787	11.732	11.811	11.961	11.724
Na_2O	2.597	2.668	2.476	2.466	2.429	2.482	2.406	2.438	2.389	2.546	2.380	2.460	2.543	2.520	2.473	2.483	2.530	2.403	2.464	2.447	2.418	2.489	2.441	2.450	2.423	2.391	2.466
K_2O	0.726	0.873	0.499	0.545	0.449	0.488	0.443	0.485	0.428	0.481	0.552	0.548	0.464	0.492	0.522	0.489	0.522	0.529	0.542	0.444	0.481	0.526	0.533	0.484	0.450	0.521	0.465
NiO	0.004	0.000	0.000	0.065	0.051	0.036	0.029	0.000	0.054	0.054	0.035	0.019	0.010	0.000	0.048	0.005	0.000	0.012	0.020	0.028	0.000	0.000	0.047	0.033	0.000	0.025	0.039
Total	96.550	97.303	96.289	97.671	97.517	96.163	96.047	97.626	97.759	98.192	96.246	97.463	97.191	98.153	96.930	97.380	97.771	97.716	97.764	96.464	97.718	96.940	96.117	96.600	97.558	97.311	97.186
Si (23 O)	6.490	6.226	6.242	6.213	6.306	6.319	6.336	6.252	6.308	6.298	6.272	6.219	6.263	6.256	6.241	6.279	6.228	6.228	6.207	6.306	6.291	6.181	6.293	6.273	6.307	6.284	6.335
Ti	0.154	0.186	0.065	0.072	0.057	0.056	0.056	0.060	0.059	0.065	0.065	0.069	0.064	0.061	0.063	0.060	0.061	0.070	0.062	0.062	0.061	0.074	0.072	0.064	0.060	0.066	0.063
Al	1.843	2.112	2.322	2.352	2.237	2.244	2.203	2.279	2.215	2.264	2.279	2.342	2.280	2.305	2.312	2.249	2.305	2.313	2.372	2.229	2.235	2.392	2.234	2.262	2.215	2.250	2.182
Cr	0.002	0.003	0.020	0.013	0.004	0.008	0.013	0.007	0.014	0.006	0.009	0.012	0.009	0.018	0.019	0.010	0.016	0.009	0.008	0.000	0.015	0.008	0.018	0.015	0.005	0.014	0.006
Mn^{2+}	0.035	0.039	0.025	0.028	0.024	0.030	0.022	0.026	0.028	0.030	0.026	0.028	0.029	0.028	0.027	0.025	0.024	0.022	0.022	0.028	0.024	0.030	0.029	0.033	0.032	0.033	0.034
Fe^{2+}	1.678	1.824	1.420	1.415	1.392	1.388	1.380	1.424	1.376	1.360	1.401	1.414	1.409	1.408	1.422	1.385	1.418	1.403	1.444	1.411	1.389	1.434	1.392	1.429	1.413	1.391	1.392
Mg	2.913	2.713	3.173	3.161	3.241	3.221	3.228	3.211	3.255	3.209	3.179	3.156	3.199	3.196	3.138	3.236	3.191	3.194	3.158	3.237	3.242	3.136	3.177	3.177	3.245	3.198	3.243
Ca	1.870	1.954	1.849	1.868	1.861	1.824	1.868	1.892	1.879	1.862	1.887	1.889	1.866	1.846	1.898	1.886	1.899	1.909	1.866	1.846	1.876	1.881	1.885	1.869	1.859	1.889	1.851
Na	0.757	0.780	0.715	0.703	0.691	0.716	0.695	0.695	0.678	0.719	0.688	0.703	0.728	0.714	0.711	0.709	0.721	0.684	0.702	0.705	0.687	0.716	0.706	0.706	0.690	0.683	0.705
K	0.139	0.168	0.095	0.102	0.084	0.093	0.084	0.091	0.080	0.089	0.105	0.103	0.087	0.092	0.099	0.092	0.098	0.099	0.102	0.084	0.090	0.100	0.101	0.092	0.084	0.098	0.087
Ni	0.000	0.000	0.000	0.008	0.006	0.004	0.003	0.000	0.006	0.006	0.004	0.002	0.001	0.000	0.006	0.001	0.000	0.001	0.002	0.003	0.000	0.000	0.006	0.004	0.000	0.003	0.005
Total	15.881	16.005	15.927	15.935	15.904	15.903	15.890	15.937	15.898	15.907	15.915	15.938	15.935	15.924	15.935	15.932	15.960	15.933	15.944	15.912	15.911	15.952	15.913	15.924	15.910	15.908	15.904
Si_T	6.43	6.18	6.12	6.09	6.18	6.19	6.22	6.13	6.18	6.19	6.16	6.10	6.14	6.13	6.13	6.16	6.11	6.11	6.08	6.17	6.17	6.06	6.19	6.15	6.18	6.17	6.21
$ivAl_T$	1.57	1.82	1.88	1.91	1.82	1.81	1.78	1.87	1.82	1.81	1.84	1.90	1.86	1.87	1.87	1.84	1.89	1.89	1.92	1.83	1.83	1.94	1.81	1.85	1.82	1.83	1.79
$viAl_C$	0.26	0.27	0.39	0.40	0.37	0.39	0.38	0.36	0.35	0.41	0.40	0.40	0.38	0.39	0.41	0.37	0.38	0.39	0.40	0.36	0.36	0.41	0.38	0.37	0.34	0.38	0.35
Ti_C	0.15	0.18	0.06	0.07	0.06	0.05	0.05	0.06	0.06	0.06	0.06	0.07	0.06	0.06	0.06	0.06	0.06	0.07	0.06	0.06	0.06	0.07	0.07	0.06	0.06	0.07	0.06
Cr_C			0.02	0.01		0.01	0.01	0.01	0.01	0.01	0.01	0.01	0.01	0.02	0.02	0.01	0.02	0.01	0.01		0.02	0.01	0.02	0.01		0.01	0.01
Fe^{3+}_C	0.40	0.36	0.91	0.89	0.91	0.92	0.83	0.88	0.89	0.81	0.80	0.83	0.87	0.92	0.78	0.83	0.83	0.82	0.93	0.94	0.88	0.87	0.75	0.88	0.94	0.81	0.89
Mg_C	2.89	2.69	3.11	3.10	3.18	3.16	3.17	3.15	3.19	3.15	3.12	3.10	3.14	3.13	3.08	3.18	3.13	3.14	3.09	3.17	3.18	3.08	3.12	3.12	3.18	3.14	3.18
Fe^{2+}_C	1.26	1.45	0.48	0.50	0.46	0.44	0.53	0.51	0.46	0.53	0.57	0.56	0.52	0.45	0.62	0.52	0.56	0.56	0.48	0.44	0.49	0.54	0.62	0.53	0.45	0.55	0.48
Mn^{2+}_C	0.03	0.04	0.02	0.03	0.02	0.03	0.02	0.03	0.03	0.03	0.03	0.03	0.03	0.03	0.03	0.02	0.02	0.02	0.02	0.03	0.02	0.03	0.03	0.03	0.03	0.03	0.03
Ni_C				0.01	0.01				0.01	0.01					0.01								0.01				
Ca_B	1.85	1.94	1.81	1.83	1.82	1.79	1.83	1.85	1.84	1.83	1.85	1.85	1.83	1.81	1.87	1.85	1.86	1.87	1.83	1.81	1.84	1.84	1.85	1.83	1.82	1.85	1.81
Na_B	0.15	0.06	0.19	0.17	0.18	0.21	0.17	0.15	0.16	0.17	0.15	0.15	0.17	0.19	0.13	0.15	0.14	0.13	0.17	0.19	0.16	0.16	0.15	0.17	0.18	0.15	0.19
Na_A	0.60	0.71	0.51	0.52	0.50	0.49	0.52	0.54	0.51	0.54	0.53	0.54	0.54	0.51	0.56	0.55	0.57	0.55	0.51	0.50	0.51	0.55	0.55	0.52	0.50	0.53	0.51
K_A	0.14	0.17	0.09	0.10	0.08	0.09	0.08	0.09	0.08	0.09	0.10	0.10	0.09	0.09	0.10	0.09	0.10	0.10	0.10	0.08	0.09	0.10	0.10	0.09	0.08	0.10	0.09
Na_A+K_A	0.74	0.88	0.61	0.62	0.58	0.58	0.60	0.63	0.59	0.62	0.63	0.65	0.63	0.60	0.66	0.64	0.67	0.64	0.61	0.58	0.60	0.64	0.65	0.61	0.58	0.62	0.59
Crystal #																											
Comments																											
Name	Magnesiohastingsite	Magnesiohastingsite	Ferrian Magnesiohastingsite	Ferrian Magnesiohastingsite	Ferrian Magnesiohastingsite	Ferrian Magnesiohastingsite	Ferrian Magnesiohastingsite	Ferrian Magnesiohastingsite	Ferrian Magnesiohastingsite	Ferrian Magnesiohastingsite	Ferrian Magnesiohastingsite	Ferrian Magnesiohastingsite	Ferrian Magnesiohastingsite	Ferrian Magnesiohastingsite	Ferrian Magnesiohastingsite	Ferrian Magnesiohastingsite	Ferrian Magnesiohastingsite	Ferrian Magnesiohastingsite	Ferrian Magnesiohastingsite	Ferrian Magnesiohastingsite	Ferrian Magnesiohastingsite	Ferrian Magnesiohastingsite	Ferrian Magnesiohastingsite	Ferrian Magnesiohastingsite	Ferrian Magnesiohastingsite	Ferrian Magnesiohastingsite	Ferrian Magnesiohastingsite

Sample	SV6A	SV6A	SV6A	SV6A	SV6A	SV6A	SV6A	SV10	SV10	SV10	SV10	SV10	SV10	SV10	SV10	SV10	SV10	SV10	SV10	SV10	SV12	SV12	SV12	SV12	SV12	SV12	SV12
Rock Type	XEN	XEN	XEN	XEN	XEN	XEN	XEN	TRAC	TRAC	TRAC	TRAC	TRAC	TRAC	TRAC	TRAC	TRAC	TRAC	TRAC	TRAC	TRAC	BEN	BEN	BEN	BEN	BEN	BEN	BEN
Sample	03-038	03-039	03-040	03-046	03-047	03-048	03-050	09-044	09-047	09-049	09-055	09-056	09-060	09-064	09-065	09-066	09-067	09-072	09-074	09-077	12-042	12-043	12-044	12-052	12-054	12-057	12-060
SiO_2	42.690	42.264	41.779	42.555	41.942	41.401	45.427	47.558	39.913	47.130	41.691	46.741	42.044	42.119	42.475	41.977	42.672	39.851	48.861	42.845	42.358	44.024	42.961	41.086	42.863	43.474	41.410
TiO_2	0.566	0.605	0.737	0.592	0.710	0.701	0.453	1.361	1.653	0.994	1.726	1.162	1.119	1.282	1.240	1.427	1.111	1.719	0.360	1.194	1.503	1.473	1.791	1.990	1.512	1.585	2.389
Al_2O_3	13.537	13.376	13.382	13.371	14.131	13.948	9.857	6.784	14.022	7.607	12.237	7.364	12.730	13.075	12.691	13.111	12.524	13.313	6.406	12.384	13.424	10.704	11.908	13.375	12.541	11.746	12.999
Cr_2O_3	0.093	0.159	0.152	0.072	0.051	0.078	0.091	0.000	0.000	0.106	0.053	0.044	0.035	0.050	0.210	0.021	0.264	0.000	0.284	0.270	0.037	0.000	0.015	0.000	0.012	0.021	0.050
MnO	0.222	0.193	0.189	0.171	0.196	0.223	0.286	0.734	0.212	0.326	0.315	0.446	0.431	0.236	0.236	0.233	0.248	0.393	0.495	0.118	0.156	0.190	0.272	0.108	0.112	0.146	0.280
FeO	11.600	11.520	11.430	11.247	11.784	11.652	9.638	12.603	13.904	12.514	14.459	14.393	12.144	12.060	11.201	12.733	11.019	17.106	11.920	8.502	10.103	8.918	11.569	11.258	9.085	10.458	11.956
MgO	14.564	14.433	14.032	14.600	14.270	13.997	14.341	14.592	11.303	14.340	11.636	13.275	13.124	12.745	13.570	12.483	13.783	9.426	15.145	16.188	14.272	15.427	14.037	13.839	15.978	15.554	13.073
CaO	11.705	11.990	11.670	11.311	11.983	11.704	15.964	11.507	11.973	11.648	12.222	12.125	11.903	12.109	12.221	12.117	12.171	11.608	11.567	11.848	12.042	13.052	11.827	12.038	11.749	11.326	11.818
Na_2O	2.492	2.469	2.450	2.616	2.596	2.514	1.665	1.941	2.235	1.728	2.260	1.600	2.697	2.647	2.620	2.703	2.628	2.756	1.748	2.756	2.540	2.293	2.567	2.698	2.466	2.467	2.742
K_2O	0.501	0.491	0.537	0.529	0.540	0.584	0.338	0.560	0.858	0.433	0.699	0.650	0.707	0.539	0.558	0.555	0.510	0.664	0.386	0.808	0.826	0.776	0.609	0.650	1.005	0.714	0.654
NiO	0.076	0.015	0.007	0.009	0.016	0.031	0.018	0.000	0.014	0.000	0.009	0.024	0.047	0.068	0.093	0.026	0.075	0.000	0.000	0.028	0.036	0.007	0.000	0.034	0.000	0.029	0.026
Total	98.046	97.515	96.365	97.073	98.219	96.833	98.078	97.640	96.087	96.826	97.307	97.824	96.981	96.930	97.115	97.386	97.005	96.836	97.172	96.941	97.297	96.864	97.556	97.076	97.323	97.520	97.397
Si (23 O)	6.246	6.225	6.225	6.273	6.144	6.152	6.626	6.983	6.067	6.954	6.263	6.914	6.269	6.268	6.288	6.240	6.315	6.109	7.148	6.279	6.224	6.470	6.331	6.101	6.267	6.361	6.147
Ti	0.062	0.067	0.083	0.066	0.078	0.078	0.050	0.150	0.189	0.110	0.195	0.129	0.125	0.143	0.138	0.160	0.124	0.198	0.040	0.132	0.166	0.163	0.199	0.222	0.166	0.174	0.267
Al	2.334	2.322	2.350	2.323	2.440	2.443	1.694	1.174	2.512	1.323	2.166	1.284	2.237	2.293	2.214	2.297	2.184	2.405	1.104	2.139	2.325	1.854	2.068	2.340	2.161	2.026	2.274
Cr	0.011	0.019	0.018	0.008	0.006	0.009	0.010	0.000	0.000	0.012	0.006	0.005	0.004	0.006	0.025	0.002	0.031	0.000	0.033	0.031	0.004	0.000	0.002	0.000	0.001	0.002	0.006
Mn^{2+}	0.028	0.024	0.024	0.021	0.024	0.028	0.035	0.091	0.027	0.041	0.040	0.056	0.054	0.030	0.030	0.029	0.031	0.051	0.061	0.015	0.019	0.024	0.034	0.014	0.014	0.018	0.035
Fe^{2+}	1.419	1.419	1.424	1.386	1.444	1.448	1.175	1.547	1.767	1.544	1.816	1.780	1.514	1.501	1.387	1.583	1.364	2.193	1.458	1.042	1.241	1.096	1.426	1.398	1.111	1.280	1.484
Mg	3.177	3.169	3.117	3.208	3.117	3.101	3.118	3.194	2.561	3.154	2.606	2.928	2.917	2.827	2.995	2.766	3.041	2.154	3.303	3.537	3.126	3.380	3.084	3.063	3.483	3.393	2.893
Ca	1.835	1.892	1.863	1.786	1.881	1.863	2.494	1.810	1.950	1.841	1.967	1.922	1.901	1.930	1.938	1.930	1.930	1.906	1.813	1.860	1.896	2.055	1.867	1.915	1.840	1.776	1.880
Na	0.707	0.705	0.708	0.748	0.737	0.724	0.471	0.553	0.659	0.494	0.658	0.459	0.780	0.764	0.752	0.779	0.754	0.819	0.496	0.783	0.724	0.653	0.733	0.777	0.699	0.700	0.789
K	0.093	0.092	0.102	0.099	0.101	0.111	0.063	0.105	0.166	0.081	0.134	0.123	0.134	0.102	0.105	0.105	0.096	0.130	0.072	0.151	0.155	0.145	0.114	0.123	0.187	0.133	0.124
Ni	0.009	0.002	0.001	0.001	0.002	0.004	0.002	0.000	0.002	0.000	0.001	0.003	0.006	0.008	0.011	0.003	0.009	0.000	0.000	0.003	0.004	0.001	0.000	0.004	0.000	0.003	0.003
Total	15.920	15.936	15.913	15.920	15.974	15.961	15.739	15.608	15.900	15.556	15.852	15.603	15.942	15.872	15.883	15.893	15.879	15.965	15.528	15.971	15.885	15.840	15.859	15.957	15.929	15.867	15.902
Si_T	6.11	6.11	6.11	6.14	6.03	6.03	6.78	6.91	6.01	6.88	6.22	6.86	6.21	6.23	6.25	6.20	6.27	6.06	7.07	6.19	6.17	6.48	6.26	6.03	6.17	6.24	6.10
$ivAl_T$	1.89	1.89	1.89	1.86	1.97	1.97	1.22	1.09	1.99	1.12	1.78	1.14	1.79	1.77	1.75	1.80	1.73	1.94	0.93	1.81	1.83	1.52	1.74	1.97	1.83	1.76	1.90
$viAl_C$	0.40	0.39	0.42	0.41	0.42	0.42	0.51	0.07	0.50	0.19	0.37	0.14	0.42	0.51	0.45	0.48	0.44	0.44	0.16	0.30	0.48	0.33	0.31	0.35	0.30	0.22	0.35
Ti_C	0.06	0.07	0.08	0.06	0.08	0.08	0.05	0.15	0.19	0.11	0.19	0.13	0.12	0.14	0.14	0.16	0.12	0.20	0.04	0.13	0.16	0.16	0.20	0.22	0.16	0.17	0.26
Cr_C	0.01	0.02	0.02	0.01	0.01	0.01	0.01			0.01	0.01	0.01		0.01	0.02		0.03		0.03	0.03							0.01
$Fe^{3+}{}_C$	0.97	0.84	0.82	0.97	0.87	0.89		0.49	0.44	0.48	0.33	0.35	0.44	0.27	0.30	0.28	0.34	0.38	0.51	0.61	0.38		0.50	0.49	0.69	0.88	0.38
Mg_C	3.11	3.11	3.06	3.14	3.06	3.04	3.19	3.16	2.54	3.12	2.59	2.91	2.89	2.81	2.98	2.75	3.02	2.14	3.27	3.49	3.10	3.38	3.05	3.03	3.43	3.33	2.87
$Fe^{2+}{}_C$	0.42	0.55	0.58	0.39	0.55	0.53	1.20	1.04	1.31	1.05	1.48	1.42	1.06	1.23	1.07	1.29	1.01	1.79	0.93	0.42	0.85	1.10	0.91	0.89	0.40	0.38	1.09
$Mn^{2+}{}_C$	0.03	0.02	0.02	0.02	0.02	0.03	0.04	0.09	0.03	0.04	0.04	0.06	0.05	0.03	0.03	0.03	0.03	0.05	0.06	0.01	0.02	0.02	0.03	0.01	0.01	0.02	0.03
Ni_C	0.01												0.01	0.01	0.01		0.01										
Ca_B	1.80	1.86	1.83	1.75	1.84	1.83	2.55	1.79	1.93	1.82	1.95	1.91	1.88	1.92	1.93	1.92	1.92	1.89	1.79	1.84	1.88	2.06	1.85	1.89	1.81	1.74	1.86
Na_B	0.20	0.14	0.17	0.25	0.16	0.17		0.21	0.07	0.18	0.05	0.09	0.12	0.08	0.07	0.08	0.08	0.11	0.21	0.16	0.12		0.15	0.11	0.19	0.26	0.14
Na_A	0.49	0.55	0.52	0.48	0.57	0.54	0.48	0.34	0.58	0.31	0.61	0.36	0.66	0.68	0.67	0.69	0.66	0.70	0.28	0.61	0.60	0.65	0.57	0.66	0.50	0.43	0.65
K_A	0.09	0.09	0.10	0.10	0.10	0.11	0.06	0.10	0.16	0.08	0.13	0.12	0.13	0.10	0.10	0.10	0.10	0.13	0.07	0.15	0.15	0.15	0.11	0.12	0.18	0.13	0.12
Na_A+K_A	0.58	0.64	0.62	0.58	0.67	0.64	0.55	0.44	0.75	0.39	0.74	0.48	0.79	0.78	0.78	0.80	0.76	0.83	0.35	0.76	0.75	0.80	0.69	0.78	0.68	0.56	0.77
Crystal #											7	7		8	8	8	8				5	5					
Comments												Rim															
Name	Ferrian Magnesiohastingsite	Ferrian Magnesiohastingsite	Ferrian Magnesiohastingsite	Ferrian Magnesiohastingsite	Ferrian Magnesiohastingsite	Ferrian Magnesiohastingsite	Edenite	Magnesiohornblende	Pargasite	Magnesiohornblende	Pargasite	Magnesiohornblende	Magnesiohastingsite	Pargasite	Pargasite	Pargasite	Pargasite	Pargasite	Magnesiohornblende	Magnesiohastingsite	Pargasite	Pargasite	Magnesiohastingsite	Magnesiohastingsite	Magnesiohastingsite	Ferrian Magnesiohastingsite	Titanian Magnesiohastingsite

Sample	SV12	SV12	SV12	SV17	SV17	SV17	SV17	SV17	SV17	SV17	SV17	SV17	SV20	SV20	SV20	SV20	SV20	SV20	SV20	SV20	SV20	SV38	SV38	SV38	SV38	SV38	SV38
Rock Type	BEN	BEN	BEN	TRAC	TRAC	TRAC	TRAC	TRAC	TRAC	TRAC	TRAC	TRAC	MUG	MUG	MUG	MUG	MUG	MUG	MUG	MUG	MUG	XEN	XEN	XEN	XEN	XEN	XEN
Sample	12-070	12-074	12-075	09-001	09-003	09-011	09-013	09-019	09-024	09-032	09-035	09-039	05-085	05-090	05-091	05-093	05-104	05-106	05-114	05-116	05-119	03-051	03-052	03-053	03-054	03-055	03-056
SiO_2	44.363	41.762	44.678	44.296	43.422	41.681	39.697	46.394	51.453	42.108	40.174	40.590	41.903	42.683	41.739	42.376	42.112	41.985	41.984	43.434	41.330	44.445	45.450	43.900	43.552	45.412	44.449
TiO_2	2.248	1.778	2.236	1.034	1.096	1.450	1.721	0.657	0.823	1.473	1.432	1.827	2.635	2.305	2.199	2.188	2.414	1.812	2.067	2.228	2.238	0.492	0.404	0.873	0.798	0.414	0.865
Al_2O_3	10.580	13.419	11.154	10.843	11.916	13.351	14.934	9.824	3.974	13.233	14.146	14.273	11.404	11.663	12.416	13.462	11.620	12.697	11.126	11.383	12.874	11.851	10.677	11.868	11.532	11.239	11.615
Cr_2O_3	0.000	0.025	0.000	0.079	0.082	0.000	0.002	0.246	0.000	0.056	0.000	0.000	0.028	0.011	0.000	0.000	0.000	0.014	0.000	0.000	0.007	0.085	0.035	0.117	0.062	0.131	0.009
MnO	0.293	0.097	0.388	0.204	0.224	0.220	0.223	0.332	0.744	0.091	0.290	0.435	0.207	0.266	0.219	0.204	0.240	0.181	0.238	0.167	0.142	0.211	0.257	0.212	0.185	0.203	0.193
FeO	10.412	9.928	10.482	11.994	12.621	12.267	14.834	12.407	10.434	9.515	13.900	15.798	11.557	11.172	11.484	11.815	10.759	11.655	13.013	10.237	10.265	11.022	10.839	11.482	11.211	10.916	11.077
MgO	14.731	14.854	13.794	13.908	13.450	12.894	10.148	13.985	16.432	15.589	11.252	10.080	14.646	14.750	14.202	14.332	14.996	14.367	14.502	15.440	14.491	15.140	15.357	14.767	14.463	15.518	14.771
CaO	11.581	11.820	10.940	12.401	12.386	12.380	12.202	12.298	11.467	12.022	11.825	11.020	10.761	11.831	11.812	11.234	11.495	11.322	11.046	10.615	11.442	11.953	11.744	11.904	12.003	11.665	11.627
Na_2O	2.493	2.669	2.998	2.539	2.820	2.609	2.462	1.681	1.494	2.468	2.520	3.249	2.592	2.725	2.750	2.957	3.018	2.867	2.961	2.678	2.813	2.704	2.780	2.729	2.691	2.523	2.714
K_2O	0.898	0.796	0.803	0.223	0.126	0.723	1.051	0.430	0.323	1.065	1.235	0.624	0.608	0.637	0.666	0.614	0.580	0.565	0.491	0.598	0.635	0.366	0.329	0.562	0.529	0.359	0.516
NiO	0.012	0.013	0.000	0.006	0.000	0.020	0.000	0.000	0.011	0.021	0.000	0.022	0.000	0.034	0.000	0.000	0.004	0.022	0.000	0.000	0.000	0.000	0.029	0.009	0.030	0.016	0.032
Total	97.611	97.161	97.473	97.527	98.143	97.595	97.274	98.254	97.155	97.641	96.774	97.918	96.341	98.077	97.487	99.182	97.238	97.487	97.428	96.780	96.237	98.269	97.901	98.423	97.056	98.396	97.868
Si (23 O)	6.494	6.148	6.535	6.521	6.380	6.182	5.997	6.753	7.444	6.163	6.077	6.096	6.256	6.262	6.176	6.147	6.226	6.200	6.251	6.387	6.153	6.457	6.612	6.399	6.434	6.565	6.486
Ti	0.247	0.197	0.246	0.114	0.121	0.162	0.196	0.072	0.090	0.162	0.163	0.206	0.296	0.254	0.245	0.239	0.268	0.201	0.231	0.246	0.251	0.054	0.044	0.096	0.089	0.045	0.095
Al	1.825	2.328	1.923	1.881	2.063	2.334	2.659	1.685	0.678	2.283	2.522	2.526	2.006	2.017	2.165	2.301	2.025	2.210	1.952	1.973	2.259	2.029	1.830	2.039	2.008	1.915	1.997
Cr	0.000	0.003	0.000	0.009	0.010	0.000	0.000	0.028	0.000	0.006	0.000	0.000	0.003	0.001	0.000	0.000	0.000	0.002	0.000	0.000	0.001	0.010	0.004	0.013	0.007	0.015	0.001
Mn^{2+}	0.036	0.012	0.048	0.025	0.028	0.028	0.029	0.041	0.091	0.011	0.037	0.055	0.026	0.033	0.027	0.025	0.030	0.023	0.030	0.021	0.018	0.026	0.032	0.026	0.023	0.025	0.024
Fe^{2+}	1.274	1.222	1.282	1.476	1.551	1.521	1.874	1.510	1.262	1.165	1.758	1.984	1.443	1.371	1.421	1.433	1.330	1.439	1.620	1.259	1.278	1.339	1.318	1.399	1.385	1.320	1.351
Mg	3.215	3.260	3.008	3.052	2.946	2.851	2.286	3.035	3.544	3.402	2.537	2.257	3.260	3.226	3.133	3.099	3.305	3.163	3.219	3.385	3.216	3.279	3.330	3.209	3.185	3.345	3.213
Ca	1.816	1.864	1.714	1.956	1.950	1.967	1.975	1.918	1.777	1.885	1.916	1.773	1.721	1.860	1.872	1.746	1.821	1.791	1.762	1.672	1.825	1.860	1.830	1.859	1.900	1.807	1.818
Na	0.707	0.762	0.850	0.725	0.803	0.750	0.721	0.474	0.419	0.700	0.739	0.946	0.750	0.775	0.789	0.832	0.865	0.821	0.855	0.763	0.812	0.762	0.784	0.771	0.771	0.707	0.768
K	0.168	0.149	0.150	0.042	0.024	0.137	0.203	0.080	0.060	0.199	0.238	0.120	0.116	0.119	0.126	0.114	0.109	0.106	0.093	0.112	0.121	0.068	0.061	0.104	0.100	0.066	0.096
Ni	0.001	0.002	0.000	0.001	0.000	0.002	0.000	0.000	0.001	0.002	0.000	0.003	0.000	0.004	0.000	0.000	0.000	0.003	0.000	0.000	0.000	0.000	0.003	0.001	0.004	0.002	0.004
Total	15.784	15.946	15.757	15.803	15.876	15.933	15.939	15.596	15.367	15.979	15.988	15.967	15.877	15.922	15.954	15.936	15.980	15.957	16.015	15.818	15.933	15.884	15.850	15.917	15.905	15.811	15.852
Si_T	6.45	6.07	6.51	6.48	6.33	6.14	5.98	6.69	7.38	6.07	6.03	6.04	6.12	6.18	6.10	6.03	6.14	6.09	6.11	6.26	6.07	6.36	6.52	6.31	6.37	6.45	6.40
$ivAl_T$	1.55	1.93	1.49	1.52	1.67	1.86	2.02	1.31	0.62	1.93	1.97	1.96	1.88	1.82	1.90	1.97	1.86	1.91	1.89	1.74	1.93	1.64	1.48	1.69	1.63	1.55	1.60
$viAl_C$	0.26	0.37	0.43	0.35	0.38	0.46	0.63	0.36	0.05	0.32	0.54	0.54	0.08	0.17	0.24	0.29	0.13	0.26	0.02	0.19	0.30	0.36	0.33	0.32	0.36	0.33	0.37
Ti_C	0.25	0.19	0.25	0.11	0.12	0.16	0.19	0.07	0.09	0.16	0.16	0.20	0.29	0.25	0.24	0.23	0.26	0.20	0.23	0.24	0.25	0.05	0.04	0.09	0.09	0.04	0.09
Cr_C				0.01	0.01			0.03		0.01												0.01		0.01	0.01	0.01	
$Fe^{3+}{}_C$	0.32	0.59	0.15	0.28	0.35	0.28	0.14	0.43	0.38	0.67	0.33	0.44	0.98	0.58	0.58	0.83	0.64	0.82	1.03	0.92	0.60	0.67	0.60	0.63	0.47	0.79	0.59
Mg_C	3.19	3.22	3.00	3.03	2.92	2.83	2.28	3.01	3.51	3.35	2.52	2.23	3.19	3.18	3.09	3.04	3.26	3.11	3.15	3.32	3.17	3.23	3.29	3.16	3.15	3.29	3.17
$Fe^{2+}{}_C$	0.94	0.62	1.13	1.19	1.19	1.24	1.73	1.07	0.87	0.48	1.42	1.52	0.43	0.77	0.83	0.57	0.67	0.60	0.55	0.32	0.66	0.65	0.70	0.75	0.90	0.51	0.74
$Mn^{2+}{}_C$	0.04	0.01	0.05	0.03	0.03	0.03	0.03	0.04	0.09	0.01	0.04	0.05	0.03	0.03	0.03	0.02	0.03	0.02	0.03	0.02	0.02	0.03	0.03	0.03	0.02	0.02	0.02
Ni_C																											
Ca_B	1.80	1.84	1.71	1.94	1.93	1.96	1.97	1.90	1.76	1.86	1.90	1.76	1.68	1.84	1.85	1.71	1.80	1.76	1.72	1.64	1.80	1.83	1.81	1.83	1.88	1.78	1.79
Na_B	0.20	0.16	0.29	0.06	0.07	0.04	0.03	0.10	0.24	0.14	0.10	0.24	0.32	0.16	0.15	0.29	0.20	0.24	0.28	0.36	0.20	0.17	0.19	0.17	0.12	0.22	0.21
Na_A	0.51	0.59	0.56	0.66	0.73	0.70	0.69	0.37	0.18	0.55	0.64	0.69	0.42	0.60	0.63	0.53	0.65	0.56	0.56	0.39	0.60	0.58	0.58	0.59	0.64	0.47	0.55
K_A	0.17	0.15	0.15	0.04	0.02	0.14	0.20	0.08	0.06	0.20	0.24	0.12	0.11	0.12	0.12	0.11	0.11	0.10	0.09	0.11	0.12	0.07	0.06	0.10	0.10	0.07	0.09
Na_A+K_A	0.67	0.74	0.71	0.71	0.76	0.84	0.89	0.45	0.24	0.74	0.87	0.81	0.53	0.72	0.75	0.64	0.76	0.67	0.65	0.50	0.72	0.65	0.64	0.70	0.74	0.54	0.65
Crystal #												4	18	19	19					21	21			1	1	1	
Comments																											
Name	Magnesiohastingsite	Magnesiohastingsite	Edenite	Pargasite	Pargasite	Pargasite	Pargasite	Magnesiohornblende	Magnesiohornblende	Magnesiohastingsite	Pargasite	Pargasite	Ferrian Titanian Magnesiohastingsite	Titanian Magnesiohastingsite	Magnesiohastingsite	Ferrian Magnesiohastingsite	Titanian Magnesiohastingsite	Ferrian Magnesiohastingsite	Ferri-magnesiohastingsite	Ferrian Tschermakite	Magnesiohastingsite	Magnesiohastingsite	Edenite	Magnesiohastingsite	Magnesiohastingsite	Ferrian Magnesiohastingsite	Magnesiohastingsite

Sample	SV38	SV38	SV38	SV38	SV38	SV38	SV38	SV38	SV38	SV38	SV38	SV38	SV38	SV38
Rock Type	XEN	XEN	XEN	XEN	XEN	XEN	XEN	XEN	XEN	XEN	TRAC	TRAC	TRAC	TRAC
Sample	03-057	03-062	03-063	03-065	03-066	03-067	03-069	03-071	03-072	03-074	03-104	03-106	03-110	03-111
SiO_2	44.101	44.608	44.101	45.411	43.892	43.832	45.649	43.808	44.112	44.154	44.971	47.174	42.097	48.842
TiO_2	0.952	0.475	0.452	0.477	0.686	0.524	0.295	0.430	0.565	0.466	0.842	0.905	1.377	1.363
Al_2O_3	11.659	12.269	11.468	10.672	12.294	12.280	10.722	12.151	12.348	12.275	10.695	7.834	13.587	6.170
Cr_2O_3	0.027	0.110	0.064	0.165	0.110	0.049	0.034	0.092	0.097	0.065	0.067	0.023	0.019	0.053
MnO	0.234	0.197	0.229	0.220	0.223	0.212	0.229	0.201	0.193	0.237	0.196	0.789	0.163	0.770
FeO	11.270	11.103	10.819	10.510	10.977	11.165	10.441	11.122	11.174	10.888	12.567	14.660	11.546	11.930
MgO	14.869	14.794	14.675	15.480	14.466	14.525	15.541	14.614	14.720	14.863	14.250	13.743	13.831	16.047
CaO	11.881	11.803	11.962	12.184	12.110	12.181	11.744	12.056	11.933	12.160	11.873	10.772	11.813	11.121
Na_2O	2.647	2.861	2.631	2.565	2.855	2.793	2.591	2.679	2.758	2.838	2.215	2.243	2.937	2.211
K_2O	0.548	0.396	0.347	0.292	0.421	0.430	0.345	0.391	0.371	0.388	0.681	0.409	0.594	0.484
NiO	0.024	0.004	0.055	0.013	0.047	0.000	0.022	0.058	0.005	0.024	0.008	0.049	0.018	0.000
Total	98.212	98.620	96.803	97.989	98.081	97.991	97.613	97.602	98.276	98.358	98.365	98.601	97.982	98.991
Si (23 O)	6.431	6.456	6.503	6.594	6.403	6.404	6.638	6.421	6.415	6.416	6.571	6.910	6.182	7.038
Ti	0.104	0.052	0.050	0.052	0.075	0.058	0.032	0.047	0.062	0.051	0.093	0.100	0.152	0.148
Al	2.004	2.092	1.993	1.826	2.114	2.114	1.838	2.099	2.116	2.102	1.842	1.352	2.352	1.048
Cr	0.003	0.013	0.007	0.019	0.013	0.006	0.004	0.011	0.011	0.007	0.008	0.003	0.002	0.006
Mn^{2+}	0.029	0.024	0.029	0.027	0.028	0.026	0.028	0.025	0.024	0.029	0.024	0.098	0.020	0.094
Fe^{2+}	1.374	1.344	1.334	1.276	1.339	1.364	1.270	1.363	1.359	1.323	1.535	1.796	1.418	1.437
Mg	3.232	3.192	3.226	3.351	3.146	3.164	3.369	3.193	3.191	3.220	3.104	3.001	3.028	3.447
Ca	1.856	1.830	1.890	1.895	1.893	1.907	1.830	1.893	1.859	1.893	1.858	1.690	1.859	1.717
Na	0.748	0.803	0.752	0.722	0.807	0.791	0.730	0.761	0.778	0.799	0.627	0.637	0.836	0.618
K	0.102	0.073	0.065	0.054	0.078	0.080	0.064	0.073	0.069	0.072	0.127	0.076	0.111	0.089
Ni	0.003	0.000	0.007	0.002	0.006	0.000	0.003	0.007	0.001	0.003	0.001	0.006	0.002	0.000
Total	15.887	15.878	15.855	15.819	15.901	15.914	15.806	15.894	15.883	15.914	15.789	15.669	15.963	15.641
Si_T	6.34	6.37	6.43	6.52	6.34	6.34	6.55	6.34	6.33	6.34	6.48	6.77	6.11	6.92
$ivAl_T$	1.66	1.63	1.57	1.48	1.66	1.66	1.45	1.66	1.67	1.66	1.52	1.23	1.89	1.03
$viAl_C$	0.32	0.44	0.40	0.33	0.44	0.43	0.36	0.41	0.42	0.42	0.30	0.10	0.43	
Ti_C	0.10	0.05	0.05	0.05	0.07	0.06	0.03	0.05	0.06	0.05	0.09	0.10	0.15	0.10
Cr_C		0.01	0.01	0.02	0.01	0.01		0.01	0.01	0.01	0.01			0.01
$Fe^{3+}{}_C$	0.62	0.59	0.51	0.51	0.43	0.47	0.63	0.57	0.61	0.52	0.61	0.90	0.54	0.75
Mg_C	3.19	3.15	3.19	3.31	3.12	3.13	3.32	3.15	3.15	3.18	3.06	2.94	2.99	3.39
$Fe^{2+}{}_C$	0.73	0.73	0.81	0.75	0.90	0.88	0.63	0.77	0.73	0.79	0.91	0.86	0.86	0.67
$Mn^{2+}{}_C$	0.03	0.02	0.03	0.03	0.03	0.03	0.03	0.02	0.02	0.03	0.02	0.10	0.02	0.09
Ni_C			0.01		0.01			0.01				0.01		
Ca_B	1.83	1.81	1.87	1.87	1.87	1.89	1.80	1.87	1.83	1.87	1.83	1.66	1.84	1.69
Na_B	0.17	0.19	0.13	0.13	0.13	0.11	0.20	0.13	0.17	0.13	0.17	0.34	0.16	0.31
Na_A	0.57	0.60	0.61	0.59	0.67	0.67	0.52	0.62	0.60	0.66	0.45	0.28	0.66	0.30
K_A	0.10	0.07	0.06	0.05	0.08	0.08	0.06	0.07	0.07	0.07	0.13	0.07	0.11	0.09
Na_A+K_A	0.67	0.67	0.68	0.64	0.75	0.75	0.59	0.69	0.67	0.73	0.58	0.36	0.77	0.38
Crystal #		2	2											
Comments														
Name	Magnesiohastingsite	Magnesiohastingsite	Magnesiohastingsite	Edenite	Pargasite	Magnesiohastingsite	Edenite	Magnesiohastingsite	Magnesiohastingsite	Magnesiohastingsite	Magnesiohastingsite	Ferrian Magnesiohornblende	Magnesiohastingsite	Magnesiohornblende

Sample	SV38	SV38	SV38	SV39	SV39	SV39	SV39	SV39	SV39	SV39	SV40	SV40	SV40
Rock Type	TRAC	TRAC	TRAC	XEN	TRAC	TRAC	TRAC	TRAC	TRAC	TRAC	TRAC	TRAC	TRAC
Sample	03-112	03-113	03-114	12-004	12-008	12-009	12-015	12-035	12-036	12-038	08-071	08-072	08-073
SiO_2	49.713	50.726	49.878	44.773	47.437	48.657	42.220	44.383	43.458	49.902	43.707	45.624	45.740
TiO_2	1.287	0.920	0.984	1.721	1.416	0.712	1.383	1.346	1.441	1.026	1.553	1.144	0.917
Al_2O_3	5.256	4.363	5.083	9.532	7.280	7.155	13.307	10.818	11.317	4.911	11.455	10.572	10.573
Cr_2O_3	0.051	0.000	0.009	0.036	0.027	0.091	0.036	0.145	0.061	0.000	0.047	0.063	0.099
MnO	0.739	0.942	0.681	0.485	0.729	0.708	0.193	0.329	0.412	0.735	0.162	0.081	0.066
FeO	11.929	11.865	12.461	11.516	13.714	13.745	12.812	13.094	13.626	11.285	10.491	8.239	8.273
MgO	16.164	16.135	15.696	14.584	13.902	14.087	12.908	13.448	12.732	15.913	15.458	17.709	17.856
CaO	10.879	11.184	11.434	11.117	11.079	10.964	11.238	11.621	11.411	10.787	11.492	11.508	11.603
Na_2O	2.142	1.903	1.672	3.084	2.238	2.218	2.272	2.710	2.923	2.076	2.734	2.200	2.201
K_2O	0.505	0.401	0.432	0.471	0.594	0.389	1.088	0.480	0.508	0.423	0.960	1.063	1.089
NiO	0.033	0.000	0.019	0.023	0.005	0.000	0.000	0.014	0.027	0.068	0.050	0.047	0.053
Total	98.698	98.439	98.349	97.342	98.421	98.726	97.457	98.388	97.916	97.126	98.192	98.375	98.479
Si (23 O)	7.169	7.319	7.225	6.600	6.943	7.066	6.259	6.512	6.437	7.278	6.368	6.534	6.551
Ti	0.140	0.100	0.107	0.191	0.156	0.078	0.154	0.149	0.161	0.113	0.170	0.123	0.099
Al	0.893	0.742	0.868	1.656	1.256	1.225	2.325	1.871	1.975	0.844	1.967	1.784	1.785
Cr	0.006	0.000	0.001	0.004	0.003	0.010	0.004	0.017	0.007	0.000	0.005	0.007	0.011
Mn^{2+}	0.090	0.115	0.084	0.061	0.090	0.087	0.024	0.041	0.052	0.091	0.020	0.010	0.008
Fe^{2+}	1.438	1.432	1.509	1.419	1.678	1.669	1.588	1.606	1.688	1.376	1.278	0.987	0.991
Mg	3.475	3.471	3.389	3.205	3.034	3.050	2.853	2.942	2.811	3.460	3.358	3.781	3.813
Ca	1.681	1.729	1.774	1.756	1.737	1.706	1.785	1.827	1.811	1.685	1.794	1.766	1.780
Na	0.599	0.532	0.470	0.881	0.635	0.624	0.653	0.771	0.839	0.587	0.772	0.611	0.611
K	0.093	0.074	0.080	0.089	0.111	0.072	0.206	0.090	0.096	0.079	0.178	0.194	0.199
Ni	0.004	0.000	0.002	0.003	0.001	0.000	0.000	0.002	0.003	0.008	0.006	0.005	0.006
Total	15.588	15.513	15.509	15.864	15.644	15.587	15.851	15.826	15.879	15.520	15.983	15.897	15.859
Si_T	7.05	7.22	7.12	6.53	6.86	6.97	6.16	6.44	6.37	7.18	6.28	6.42	6.42
$ivAl_T$	0.88	0.73	0.86	1.47	1.14	1.03	1.84	1.56	1.63	0.82	1.72	1.58	1.58
$viAl_C$				0.17	0.10	0.17	0.45	0.29	0.33	0.02	0.23	0.17	0.17
Ti_C	0.07	0.05	0.08	0.19	0.15	0.08	0.15	0.15	0.16	0.11	0.17	0.12	0.10
Cr_C	0.01					0.01		0.02	0.01		0.01	0.01	0.01
$Fe^{3+}{}_C$	0.74	0.61	0.64	0.48	0.56	0.64	0.71	0.48	0.46	0.58	0.66	0.88	0.90
Mg_C	3.42	3.42	3.34	3.17	3.00	3.01	2.81	2.91	2.78	3.42	3.31	3.71	3.74
$Fe^{2+}{}_C$	0.68	0.80	0.85	0.92	1.10	1.01	0.85	1.11	1.21	0.77	0.60	0.09	0.07
$Mn^{2+}{}_C$	0.09	0.11	0.08	0.06	0.09	0.09	0.02	0.04	0.05	0.09	0.02	0.01	0.01
Ni_C										0.01	0.01	0.01	0.01
Ca_B	1.65	1.71	1.75	1.74	1.72	1.68	1.76	1.81	1.79	1.66	1.77	1.73	1.75
Na_B	0.35	0.29	0.25	0.26	0.28	0.32	0.24	0.19	0.21	0.34	0.23	0.27	0.25
Na_A	0.24	0.23	0.21	0.61	0.34	0.30	0.40	0.57	0.62	0.24	0.53	0.33	0.34
K_A	0.09	0.07	0.08	0.09	0.11	0.07	0.20	0.09	0.10	0.08	0.18	0.19	0.20
Na_A+K_A	0.33	0.30	0.29	0.70	0.45	0.37	0.60	0.66	0.72	0.32	0.71	0.53	0.54
Crystal #					1	1		4	4	4	11	11	11
Comments								Core		Rim	Rim		
Name	Magnesiohornblende	Magnesiohornblende	Magnesiohornblende	Edenite	Magnesiohornblende	Magnesiohornblende	Magnesiohastingsite	Magnesiohastingsite	Magnesiohastingsite	Magnesiohornblende	Magnesiohastingsite	Ferrian Magnesiohastingsite	Ferrian Magnesiohastingsite

Sample	SV40	SV40	SV40	SV40	SV40	SV40	SV40	SV40	SV40	SV40	SV40	SV40	SV40	SV40
Rock Type	TRAC	TRAC	TRAC	TRAC	TRAC	TRAC	TRAC	TRAC	TRAC	TRAC	TRAC	TRAC	TRAC	TRAC
Sample	08-074	08-075	08-076	08-077	08-078	08-079	08-080	08-081	08-082	08-083	08-084	08-085	08-086	08-087
SiO_2	44.749	45.359	44.567	45.389	42.139	45.276	45.782	45.390	45.396	45.426	43.172	46.550	40.330	40.284
TiO_2	0.921	0.968	0.991	1.031	1.451	1.037	0.903	0.996	1.057	1.255	1.568	1.763	1.636	1.364
Al_2O_3	10.687	10.809	10.234	10.432	12.631	10.520	10.630	10.632	10.725	10.554	12.285	14.169	14.403	15.475
Cr_2O_3	0.212	0.191	0.174	0.158	0.013	0.229	0.245	0.008	0.101	0.084	0.013	0.000	0.021	0.000
MnO	0.147	0.106	0.053	0.085	0.147	0.106	0.059	0.116	0.132	0.085	0.130	0.168	0.254	0.369
FeO	8.185	8.305	7.914	8.525	15.702	8.055	7.694	8.323	8.212	8.384	11.039	11.282	16.384	16.098
MgO	17.515	17.773	17.304	17.294	11.526	17.688	17.990	17.598	17.740	17.413	14.822	12.165	9.935	10.076
CaO	11.220	11.385	11.528	11.243	11.140	11.379	11.402	11.516	11.329	11.746	11.597	7.684	11.296	11.071
Na_2O	2.222	2.291	2.069	2.215	2.636	2.427	2.285	2.262	2.169	2.184	2.404	2.610	3.157	2.805
K_2O	1.070	1.051	1.175	1.026	0.827	1.145	1.102	1.025	1.119	1.044	1.065	3.486	1.078	1.061
NiO	0.119	0.049	0.015	0.030	0.051	0.069	0.090	0.036	0.018	0.070	0.024	0.006	0.013	0.035
Total	97.140	98.398	96.075	97.540	98.280	97.974	98.317	97.990	98.149	98.290	98.231	99.998	98.516	98.681
Si (23 O)	6.503	6.501	6.545	6.562	6.280	6.525	6.547	6.533	6.515	6.528	6.300	6.621	6.055	6.014
Ti	0.101	0.104	0.109	0.112	0.163	0.112	0.097	0.108	0.114	0.136	0.172	0.189	0.185	0.153
Al	1.830	1.826	1.771	1.777	2.219	1.787	1.792	1.803	1.814	1.787	2.113	2.375	2.548	2.722
Cr	0.024	0.022	0.020	0.018	0.002	0.026	0.028	0.001	0.011	0.010	0.001	0.000	0.002	0.000
Mn^{2+}	0.018	0.013	0.007	0.010	0.019	0.013	0.007	0.014	0.016	0.010	0.016	0.020	0.032	0.047
Fe^{2+}	0.995	0.995	0.972	1.031	1.957	0.971	0.920	1.002	0.986	1.007	1.347	1.342	2.057	2.009
Mg	3.795	3.798	3.789	3.727	2.561	3.800	3.835	3.776	3.796	3.730	3.224	2.580	2.224	2.242
Ca	1.747	1.748	1.814	1.741	1.779	1.757	1.747	1.776	1.742	1.808	1.813	1.171	1.817	1.771
Na	0.626	0.637	0.589	0.621	0.762	0.678	0.634	0.631	0.604	0.608	0.680	0.720	0.919	0.812
K	0.198	0.192	0.220	0.189	0.157	0.210	0.201	0.188	0.205	0.191	0.198	0.632	0.206	0.202
Ni	0.014	0.006	0.002	0.003	0.006	0.008	0.010	0.004	0.002	0.008	0.003	0.001	0.002	0.004
Total	15.910	15.929	15.869	15.873	15.909	15.915	15.908	15.899	15.919	15.852	15.954	15.708	16.048	15.982
Si_T	6.37	6.37	6.44	6.44	6.18	6.41	6.43	6.41	6.39	6.42	6.22	6.56	6.01	5.93
$ivAl_T$	1.63	1.63	1.56	1.56	1.82	1.59	1.57	1.59	1.61	1.58	1.78	1.44	1.99	2.07
$viAl_C$	0.16	0.16	0.18	0.19	0.37	0.16	0.19	0.18	0.17	0.18	0.30	0.91	0.53	0.61
Ti_C	0.10	0.10	0.11	0.11	0.16	0.11	0.10	0.11	0.11	0.13	0.17	0.19	0.18	0.15
Cr_C	0.02	0.02	0.02	0.02		0.03	0.03		0.01	0.01				
$Fe^{3+}{}_C$	0.97	0.98	0.77	0.90	0.71	0.85	0.89	0.88	0.97	0.77	0.69	0.50	0.37	0.66
Mg_C	3.71	3.72	3.73	3.66	2.52	3.73	3.77	3.71	3.72	3.67	3.18	2.55	2.21	2.21
$Fe^{2+}{}_C$			0.19	0.11	1.22	0.10	0.01	0.10		0.22	0.64	0.83	1.67	1.32
$Mn^{2+}{}_C$	0.02	0.01	0.01	0.01	0.02	0.01	0.01	0.01	0.02	0.01	0.02	0.02	0.03	0.05
Ni_C	0.01	0.01			0.01	0.01	0.01			0.01				
Ca_B	1.71	1.71	1.78	1.71	1.75	1.72	1.72	1.74	1.71	1.78	1.79	1.16	1.80	1.74
Na_B	0.29	0.29	0.22	0.29	0.25	0.28	0.28	0.26	0.29	0.22	0.21	0.71	0.20	0.26
Na_A	0.32	0.34	0.36	0.32	0.50	0.39	0.34	0.36	0.30	0.38	0.46		0.71	0.54
K_A	0.19	0.19	0.22	0.19	0.15	0.21	0.20	0.18	0.20	0.19	0.20	0.63	0.20	0.20
Na_A+K_A	0.52	0.53	0.58	0.50	0.66	0.60	0.54	0.55	0.50	0.57	0.66	0.63	0.92	0.74
Crystal #	11	11	11	11	11	11	11	11	11	11	11	12	12	12
Comments					Core						Rim	Core		
Name	Ferrian Magnesiohastingsite	Ferrian Magnesiohastingsite	Ferrian Magnesiohastingsite	Ferrian Magnesiohastingsite	Magnesiohastingsite	Ferrian Magnesiohastingsite	Ferrian Magnesiohastingsite	Ferrian Magnesiohastingsite	Ferrian Magnesiohastingsite	Ferrian Magnesiohastingsite	Magnesiohastingsite	Potassic Magnesiokatophorite	Pargasite	Magnesiohastingsite

Sample	SV40	SV40	SV40	SV40	SV40	SV40	SV40	SV40	SV40	SV40	SV40	SV40	SV40
Rock Type	TRAC	TRAC	TRAC	TRAC	TRAC	TRAC	TRAC	TRAC	TRAC	TRAC	TRAC	TRAC	TRAC
Sample	08-088	08-089	08-091	08-092	08-094	08-095	08-096	08-097	08-098	08-099	08-100	08-101	08-103
SiO_2	42.551	42.391	39.747	41.778	41.224	43.510	43.780	44.265	44.407	42.745	43.464	43.247	42.728
TiO_2	1.278	1.251	1.658	1.342	1.463	1.432	1.164	1.192	1.182	1.275	1.247	1.677	1.272
Al_2O_3	13.179	13.067	14.658	13.488	13.325	11.796	11.649	11.060	10.500	12.986	11.927	11.708	12.475
Cr_2O_3	0.023	0.000	0.009	0.004	0.000	0.045	0.000	0.036	0.053	0.047	0.063	0.021	0.017
MnO	0.186	0.220	0.368	0.420	0.284	0.155	0.178	0.135	0.176	0.128	0.180	0.225	0.155
FeO	13.487	12.647	15.151	14.904	15.963	11.765	10.857	9.023	8.791	10.581	9.257	13.848	10.287
MgO	12.874	14.075	10.610	10.893	11.340	14.590	15.521	16.855	16.780	14.841	15.718	12.915	14.975
CaO	11.115	11.238	11.374	11.016	11.044	11.436	11.398	11.089	11.543	11.691	11.541	10.912	11.238
Na_2O	2.360	2.467	2.749	3.128	2.691	2.261	2.477	2.322	2.144	2.286	2.566	2.170	2.106
K_2O	1.080	1.064	1.187	1.340	1.188	1.273	1.109	1.114	1.280	1.316	1.245	1.040	1.203
NiO	0.000	0.025	0.000	0.022	0.000	0.012	0.030	0.083	0.045	0.027	0.000	0.000	0.002
Total	98.226	98.465	97.562	98.523	98.534	98.423	98.254	97.224	96.906	97.942	97.275	97.792	96.574
Si (23 O)	6.272	6.224	5.999	6.215	6.161	6.357	6.380	6.457	6.504	6.257	6.366	6.407	6.319
Ti	0.142	0.138	0.188	0.150	0.164	0.157	0.128	0.131	0.130	0.140	0.137	0.187	0.141
Al	2.289	2.261	2.607	2.365	2.347	2.031	2.001	1.901	1.812	2.240	2.059	2.044	2.174
Cr	0.003	0.000	0.001	0.000	0.000	0.005	0.000	0.004	0.006	0.005	0.007	0.002	0.002
Mn^{2+}	0.023	0.027	0.047	0.053	0.036	0.019	0.022	0.017	0.022	0.016	0.022	0.028	0.019
Fe^{2+}	1.662	1.553	1.912	1.854	1.995	1.437	1.323	1.101	1.077	1.295	1.134	1.715	1.272
Mg	2.829	3.081	2.387	2.416	2.527	3.178	3.372	3.665	3.664	3.239	3.432	2.852	3.302
Ca	1.755	1.768	1.839	1.756	1.768	1.790	1.779	1.733	1.811	1.833	1.811	1.732	1.781
Na	0.674	0.702	0.804	0.902	0.780	0.640	0.700	0.657	0.609	0.649	0.729	0.623	0.604
K	0.203	0.199	0.229	0.254	0.226	0.237	0.206	0.207	0.239	0.246	0.233	0.197	0.227
Ni	0.000	0.003	0.000	0.003	0.000	0.001	0.004	0.010	0.005	0.003	0.000	0.000	0.000
Total	15.905	15.962	16.035	16.091	16.004	15.960	15.976	15.902	15.881	15.930	15.958	15.798	15.892
Si_T	6.17	6.09	5.93	6.19	6.05	6.27	6.27	6.32	6.40	6.16	6.29	6.29	6.21
$ivAl_T$	1.83	1.91	2.07	1.81	1.95	1.73	1.73	1.68	1.60	1.84	1.71	1.71	1.79
$viAl_C$	0.42	0.30	0.51	0.54	0.36	0.27	0.24	0.18	0.18	0.37	0.32	0.30	0.35
Ti_C	0.14	0.14	0.19	0.15	0.16	0.16	0.13	0.13	0.13	0.14	0.14	0.18	0.14
Cr_C						0.01			0.01	0.01	0.01		
$Fe^{3+}{}_C$	0.80	0.98	0.51	0.32	0.79	0.74	0.84	0.98	0.76	0.68	0.57	0.82	0.84
Mg_C	2.78	3.01	2.36	2.41	2.48	3.13	3.31	3.59	3.60	3.19	3.39	2.80	3.24
$Fe^{2+}{}_C$	0.83	0.54	1.38	1.53	1.18	0.67	0.46	0.09	0.30	0.60	0.55	0.87	0.41
$Mn^{2+}{}_C$	0.02	0.03	0.05	0.05	0.04	0.02	0.02	0.02	0.02	0.02	0.02	0.03	0.02
Ni_C								0.01	0.01				
Ca_B	1.73	1.73	1.82	1.75	1.74	1.76	1.75	1.70	1.78	1.81	1.79	1.70	1.75
Na_B	0.27	0.27	0.18	0.25	0.26	0.24	0.25	0.30	0.22	0.19	0.21	0.30	0.25
Na_A	0.39	0.42	0.61	0.65	0.50	0.40	0.44	0.34	0.38	0.45	0.51	0.31	0.34
K_A	0.20	0.19	0.23	0.25	0.22	0.23	0.20	0.20	0.24	0.24	0.23	0.19	0.22
Na_A+K_A	0.59	0.61	0.84	0.90	0.73	0.63	0.64	0.54	0.61	0.69	0.74	0.51	0.57
Crystal #	12	12	13	13	13	13	13	13	13	13	13	13	13
Comments			Rim										
Name	Ferrian Magnesiohastingsite	Ferrian Magnesiohastingsite	Magnesiohastingsite	Potassian Pargasite	Ferrian Magnesiohastingsite	Magnesiohastingsite	Ferrian Magnesiohastingsite	Ferrian Magnesiohastingsite	Ferrian Magnesiohastingsite	Magnesiohastingsite	Magnesiohastingsite	Ferrian Magnesiohastingsite	Ferrian Magnesiohastingsite

Sample	SV40	SV40	SV40	SV40	SV40	SV40	SV40	SV40	SV40	SV40	SV40	SV40	SV40	SV40	SV40	SV40	SV40	SV40	SV40	SV40	SV40	SV40	SV40	SV40	SV40	SV40	SV40
Rock Type	TRAC	TRAC	TRAC	TRAC	TRAC	TRAC	TRAC	TRAC	TRAC	TRAC	TRAC	TRAC	TRAC	TRAC	TRAC	TRAC	TRAC	TRAC	TRAC	TRAC	TRAC	TRAC	TRAC	TRAC	TRAC	TRAC	TRAC
Sample	08-104	08-105	08-106	08-107	08-108	08-111	08-112	08-113	08-114	08-115	08-116	08-117	08-118	08-119	08-120	08-121	08-122	08-123	08-124	08-125	08-126	08-127	08-128	11-001	11-002	11-005	11-006
SiO_2	41.041	41.275	38.971	40.434	42.482	43.403	42.800	43.645	43.541	42.590	41.652	39.347	44.845	45.082	45.397	44.551	42.393	45.538	42.306	43.352	44.091	43.998	42.588	43.911	43.622	42.545	45.547
TiO_2	1.620	1.615	1.799	1.887	1.295	1.286	1.186	1.278	1.270	1.345	1.593	1.723	1.255	1.255	1.156	1.275	1.728	1.289	1.463	1.772	1.698	1.385	1.564	1.210	1.158	1.412	1.266
Al_2O_3	14.799	13.213	15.397	14.103	12.812	12.148	12.637	12.045	12.054	12.474	13.354	16.062	10.848	10.475	10.617	11.394	12.666	10.127	12.987	11.668	10.524	10.929	12.111	11.065	10.960	11.702	9.173
Cr_2O_3	0.000	0.015	0.017	0.000	0.049	0.057	0.000	0.038	0.027	0.021	0.000	0.006	0.000	0.000	0.000	0.011	0.044	0.000	0.045	0.070	0.027	0.009	0.019	0.178	0.082	0.111	0.057
MnO	0.277	0.404	0.356	0.313	0.219	0.146	0.165	0.141	0.108	0.234	0.230	0.325	0.157	0.088	0.167	0.138	0.189	0.195	0.193	0.165	0.085	0.149	0.259	0.322	0.218	0.231	0.517
FeO	14.173	13.982	16.333	14.240	12.163	11.539	12.100	10.488	11.000	12.326	13.121	15.343	8.953	8.954	9.671	10.544	11.658	10.682	13.708	11.569	9.751	10.710	12.219	13.038	13.040	13.446	12.771
MgO	11.527	11.351	9.335	11.386	13.907	14.771	13.998	15.221	14.862	13.645	13.107	9.957	16.701	16.975	16.547	15.618	14.109	15.915	12.565	14.680	16.188	15.972	14.262	13.376	13.391	12.560	13.963
CaO	11.228	10.749	11.462	11.470	11.199	11.190	11.164	11.371	11.342	11.366	11.524	11.539	11.500	11.408	11.515	11.291	11.482	11.061	11.451	11.465	11.684	11.729	11.691	11.394	11.477	11.402	11.246
Na_2O	2.861	3.273	2.674	2.762	3.125	2.220	2.237	2.439	2.090	2.243	2.647	2.713	2.251	2.176	2.151	2.157	2.917	2.216	2.461	2.281	2.286	2.377	2.845	2.577	2.615	2.837	2.838
K_2O	1.273	1.073	1.107	1.045	1.047	1.172	1.035	1.127	1.151	1.083	1.081	1.162	1.068	0.976	0.996	1.018	1.108	1.075	1.318	1.140	1.015	1.134	1.039	0.530	0.538	0.590	0.585
NiO	0.012	0.000	0.032	0.000	0.032	0.000	0.031	0.046	0.004	0.000	0.006	0.009	0.000	0.000	0.009	0.026	0.020	0.000	0.025	0.031	0.005	0.040	0.014	0.036	0.039	0.038	0.000
Total	98.873	97.107	97.576	97.698	98.442	97.982	97.487	97.893	97.572	97.392	98.429	98.385	97.634	97.427	98.305	98.023	98.355	98.195	98.669	98.292	97.521	98.463	98.749	97.637	97.140	96.874	97.963
Si (23 O)	6.062	6.204	5.914	6.056	6.236	6.355	6.314	6.371	6.380	6.306	6.148	5.882	6.503	6.542	6.547	6.475	6.222	6.602	6.236	6.341	6.438	6.404	6.242	6.491	6.485	6.372	6.699
Ti	0.180	0.183	0.205	0.213	0.143	0.142	0.132	0.140	0.140	0.150	0.177	0.194	0.137	0.137	0.125	0.139	0.191	0.141	0.162	0.195	0.186	0.152	0.172	0.135	0.129	0.159	0.140
Al	2.576	2.341	2.754	2.489	2.216	2.096	2.197	2.072	2.081	2.177	2.323	2.830	1.854	1.791	1.805	1.952	2.191	1.730	2.256	2.011	1.811	1.875	2.092	1.928	1.920	2.065	1.590
Cr	0.000	0.002	0.002	0.000	0.006	0.007	0.000	0.004	0.003	0.002	0.000	0.001	0.000	0.000	0.000	0.001	0.005	0.000	0.005	0.008	0.003	0.001	0.002	0.021	0.010	0.013	0.007
Mn^{2+}	0.035	0.051	0.046	0.040	0.027	0.018	0.021	0.017	0.013	0.029	0.029	0.041	0.019	0.011	0.020	0.017	0.023	0.024	0.024	0.020	0.011	0.018	0.032	0.040	0.027	0.029	0.064
Fe^{2+}	1.751	1.757	2.072	1.783	1.493	1.413	1.493	1.280	1.348	1.526	1.619	1.918	1.086	1.087	1.166	1.281	1.431	1.295	1.690	1.415	1.191	1.304	1.498	1.611	1.621	1.684	1.571
Mg	2.538	2.544	2.112	2.542	3.043	3.224	3.079	3.312	3.246	3.012	2.884	2.219	3.611	3.672	3.558	3.384	3.087	3.440	2.761	3.201	3.524	3.466	3.117	2.948	2.968	2.804	3.061
Ca	1.777	1.731	1.863	1.840	1.761	1.755	1.764	1.778	1.780	1.803	1.822	1.848	1.787	1.774	1.779	1.758	1.805	1.718	1.808	1.797	1.828	1.829	1.836	1.804	1.828	1.829	1.772
Na	0.819	0.954	0.787	0.802	0.889	0.630	0.640	0.690	0.594	0.644	0.757	0.786	0.633	0.612	0.601	0.608	0.830	0.623	0.703	0.647	0.647	0.671	0.808	0.738	0.754	0.824	0.809
K	0.240	0.206	0.214	0.200	0.196	0.219	0.195	0.210	0.215	0.205	0.204	0.222	0.198	0.181	0.183	0.189	0.207	0.199	0.248	0.213	0.189	0.211	0.194	0.100	0.102	0.113	0.110
Ni	0.001	0.000	0.004	0.000	0.004	0.000	0.004	0.005	0.000	0.000	0.001	0.001	0.000	0.000	0.001	0.003	0.002	0.000	0.003	0.004	0.001	0.005	0.002	0.004	0.005	0.005	0.000
Total	16.019	16.071	16.034	16.012	16.090	15.892	15.910	15.922	15.883	15.906	16.026	16.087	15.869	15.837	15.848	15.807	16.022	15.834	15.995	15.917	15.946	15.959	16.083	15.820	15.849	15.898	15.823
Si_T	6.00	6.17	5.86	6.00	6.16	6.23	6.20	6.27	6.28	6.21	6.06	5.84	6.40	6.42	6.44	6.35	6.15	6.49	6.17	6.25	6.36	6.30	6.17	6.40	6.40	6.31	6.63
$ivAl_T$	2.00	1.83	2.14	2.00	1.84	1.77	1.80	1.73	1.72	1.79	1.94	2.16	1.60	1.58	1.56	1.65	1.85	1.51	1.83	1.75	1.64	1.70	1.83	1.60	1.60	1.69	1.37
$viAl_C$	0.54	0.49	0.60	0.46	0.34	0.29	0.36	0.31	0.33	0.35	0.35	0.65	0.22	0.18	0.21	0.27	0.32	0.19	0.40	0.23	0.15	0.14	0.23	0.30	0.30	0.35	0.21
Ti_C	0.18	0.18	0.20	0.21	0.14	0.14	0.13	0.14	0.14	0.15	0.17	0.19	0.13	0.13	0.12	0.14	0.19	0.14	0.16	0.19	0.18	0.15	0.17	0.13	0.13	0.16	0.14
Cr_C					0.01	0.01											0.01		0.01	0.01				0.02	0.01	0.01	0.01
Fe^{3+}_C	0.54	0.38	0.44	0.47	0.65	0.90	0.88	0.73	0.81	0.74	0.68	0.44	0.76	0.85	0.82	0.86	0.55	0.85	0.57	0.73	0.68	0.79	0.63	0.61	0.57	0.46	0.46
Mg_C	2.51	2.53	2.09	2.52	3.00	3.16	3.02	3.26	3.19	2.97	2.84	2.20	3.55	3.61	3.50	3.32	3.05	3.38	2.73	3.15	3.48	3.41	3.08	2.91	2.93	2.78	3.03
Fe^{2+}_C	1.20	1.36	1.62	1.29	0.82	0.49	0.58	0.53	0.52	0.76	0.92	1.47	0.31	0.22	0.33	0.40	0.86	0.42	1.10	0.66	0.50	0.49	0.85	0.98	1.03	1.21	1.10
Mn^{2+}_C	0.03	0.05	0.05	0.04	0.03	0.02	0.02	0.02	0.01	0.03	0.03	0.04	0.02	0.01	0.02	0.02	0.02	0.02	0.02	0.02	0.01	0.02	0.03	0.04	0.03	0.03	0.06
Ni_C								0.01																			
Ca_B	1.76	1.72	1.85	1.82	1.74	1.72	1.73	1.75	1.75	1.78	1.80	1.84	1.76	1.74	1.75	1.72	1.78	1.69	1.79	1.77	1.80	1.80	1.81	1.78	1.80	1.81	1.75
Na_B	0.24	0.28	0.15	0.18	0.26	0.28	0.27	0.25	0.25	0.22	0.20	0.16	0.24	0.26	0.25	0.28	0.22	0.31	0.21	0.23	0.20	0.20	0.19	0.22	0.20	0.19	0.25
Na_A	0.57	0.67	0.63	0.62	0.62	0.34	0.36	0.43	0.34	0.41	0.54	0.62	0.38	0.34	0.34	0.32	0.60	0.30	0.49	0.41	0.44	0.46	0.61	0.51	0.55	0.63	0.56
K_A	0.24	0.20	0.21	0.20	0.19	0.21	0.19	0.21	0.21	0.20	0.20	0.22	0.19	0.18	0.18	0.19	0.21	0.20	0.25	0.21	0.19	0.21	0.19	0.10	0.10	0.11	0.11
Na_A+K_A	0.81	0.87	0.84	0.82	0.81	0.55	0.55	0.64	0.55	0.61	0.75	0.84	0.58	0.52	0.52	0.51	0.81	0.50	0.73	0.62	0.63	0.66	0.80	0.61	0.65	0.74	0.66
Crystal #	13	13	13	13	14	14	14	14	14	14	14	15	15	15	15	15	15	16	16	16	16	16	16	1	1	1	1
Comments				Rim	Rim		Core				Rim	Core					Rim	Core					Rim	Core			Rim
Name	Pargasite	Pargasite	Pargasite	Magnesiohastingsite	Magnesiohastingsite	Ferrian Magnesiohastingsite	Ferrian Magnesiohastingsite	Magnesiohastingsite	Ferrian Magnesiohastingsite	Magnesiohastingsite	Magnesiohastingsite	Pargasite	Ferrian Magnesiohastingsite	Ferrian Magnesiohastingsite	Ferrian Magnesiohastingsite	Ferrian Magnesiohastingsite	Magnesiohastingsite	Ferrian Tschermakite	Magnesiohastingsite	Magnesiohastingsite	Magnesiohastingsite	Ferrian Magnesiohastingsite	Magnesiohastingsite	Magnesiohastingsite	Magnesiohastingsite	Magnesiohastingsite	Edenite

Sample	SV40	SV40	SV40	SV40	SV41	SV41	SV41	SV41	SV41	SV41	SV41	SV41	SV41	SV41
Rock Type	XEN	TRAC	TRAC	TRAC	MUG	MUG	MUG	MUG	MUG	MUG	MUG	MUG	MUG	MUG
Sample	11-016	11-042	11-043	11-047	08-001	08-002	08-004	08-006	08-007	08-008	08-009	08-010	08-012	08-013
SiO_2	51.037	45.141	44.642	41.087	45.597	40.860	44.188	41.560	41.346	41.468	41.729	41.818	43.786	43.674
TiO_2	0.948	1.327	1.203	1.644	1.632	2.160	1.958	1.688	1.736	1.766	1.754	1.712	1.681	1.655
Al_2O_3	4.672	10.619	11.216	13.627	9.178	12.607	10.711	12.757	13.036	13.079	12.898	13.017	10.424	10.431
Cr_2O_3	0.000	0.041	0.037	0.021	0.019	0.030	0.000	0.000	0.000	0.019	0.028	0.000	0.024	0.000
MnO	0.873	0.149	0.114	0.222	0.417	0.267	0.302	0.165	0.180	0.077	0.092	0.129	0.258	0.310
FeO	11.100	9.143	9.571	13.983	12.875	14.927	13.590	12.689	12.534	11.970	11.240	11.082	13.241	12.894
MgO	15.915	16.750	16.292	11.332	14.416	11.793	13.630	13.418	13.517	13.594	14.061	14.246	13.908	13.838
CaO	10.769	11.252	11.235	11.282	11.705	11.832	11.526	12.114	12.406	12.234	11.974	12.267	11.820	11.962
Na_2O	2.239	2.153	2.201	2.512	2.355	2.611	2.590	2.462	2.597	2.686	2.584	2.635	2.468	2.374
K_2O	0.452	1.166	1.144	0.960	0.443	0.665	0.477	0.633	0.654	0.635	0.660	0.577	0.590	0.611
NiO	0.028	0.032	0.004	0.034	0.000	0.000	0.000	0.000	0.041	0.000	0.008	0.030	0.025	0.027
Total	98.033	97.773	97.659	96.704	98.774	97.808	99.051	97.588	98.123	97.602	97.093	97.558	98.322	97.865
Si (23 O)	7.358	6.540	6.488	6.189	6.642	6.133	6.453	6.170	6.113	6.138	6.182	6.165	6.448	6.457
Ti	0.103	0.145	0.132	0.186	0.179	0.244	0.215	0.188	0.193	0.197	0.195	0.190	0.186	0.184
Al	0.794	1.813	1.921	2.419	1.576	2.230	1.844	2.232	2.271	2.281	2.252	2.262	1.809	1.817
Cr	0.000	0.005	0.004	0.003	0.002	0.004	0.000	0.000	0.000	0.002	0.003	0.000	0.003	0.000
Mn^{2+}	0.107	0.018	0.014	0.028	0.051	0.034	0.037	0.021	0.023	0.010	0.012	0.016	0.032	0.039
Fe^{2+}	1.338	1.108	1.163	1.761	1.568	1.874	1.660	1.575	1.549	1.481	1.392	1.366	1.631	1.594
Mg	3.421	3.618	3.530	2.545	3.131	2.639	2.968	2.970	2.979	3.000	3.105	3.131	3.053	3.050
Ca	1.663	1.746	1.749	1.821	1.827	1.903	1.803	1.927	1.965	1.940	1.900	1.937	1.865	1.895
Na	0.626	0.605	0.620	0.734	0.665	0.760	0.733	0.709	0.744	0.771	0.742	0.753	0.705	0.680
K	0.083	0.215	0.212	0.184	0.082	0.127	0.089	0.120	0.123	0.120	0.125	0.109	0.111	0.115
Ni	0.003	0.004	0.000	0.004	0.000	0.000	0.000	0.000	0.005	0.000	0.001	0.004	0.003	0.003
Total	15.496	15.817	15.834	15.873	15.803	15.952	15.839	15.969	16.020	15.999	15.947	15.959	15.889	15.863
Si_T	7.29	6.42	6.36	6.13	6.57	6.06	6.37	6.10	6.05	6.09	6.11	6.10	6.37	6.39
$ivAl_T$	0.71	1.58	1.64	1.87	1.43	1.94	1.63	1.90	1.95	1.91	1.89	1.90	1.63	1.61
$viAl_C$	0.08	0.20	0.25	0.52	0.12	0.26	0.19	0.30	0.30	0.35	0.34	0.34	0.15	0.18
Ti_C	0.10	0.14	0.13	0.18	0.18	0.24	0.21	0.19	0.19	0.19	0.19	0.19	0.18	0.18
Cr_C														
Fe^{3+}_C	0.43	0.85	0.86	0.47	0.60	0.55	0.64	0.60	0.51	0.44	0.53	0.49	0.61	0.53
Mg_C	3.39	3.55	3.46	2.52	3.10	2.61	2.93	2.93	2.95	2.97	3.07	3.10	3.02	3.02
Fe^{2+}_C	0.90	0.24	0.28	1.28	0.96	1.30	0.99	0.96	1.02	1.03	0.85	0.87	1.00	1.05
Mn^{2+}_C	0.11	0.02	0.01	0.03	0.05	0.03	0.04	0.02	0.02	0.01	0.01	0.02	0.03	0.04
Ni_C														
Ca_B	1.65	1.71	1.72	1.80	1.81	1.88	1.78	1.90	1.95	1.92	1.88	1.92	1.84	1.87
Na_B	0.35	0.29	0.28	0.20	0.19	0.12	0.22	0.10	0.05	0.08	0.12	0.08	0.16	0.13
Na_A	0.27	0.31	0.32	0.53	0.46	0.63	0.50	0.60	0.68	0.69	0.61	0.66	0.54	0.55
K_A	0.08	0.21	0.21	0.18	0.08	0.13	0.09	0.12	0.12	0.12	0.12	0.11	0.11	0.11
Na_A+K_A	0.35	0.52	0.53	0.71	0.54	0.76	0.59	0.72	0.80	0.81	0.74	0.77	0.65	0.66
Crystal #	3	6	6		1	1	1	2	2	2	2	2	3	3
Comments		Core	Rim		Core		Rim	Core				Rim	Rim	
Name	Magnesiohornblende	Ferrian Magnesiohastingsite	Ferrian Magnesiohastingsite	Pargasite	Edenite	Magnesiohastingsite	Magnesiohastingsite	Magnesiohastingsite	Magnesiohastingsite	Magnesiohastingsite	Magnesiohastingsite	Magnesiohastingsite	Magnesiohastingsite	Magnesiohastingsite

Sample	SV41	SV41	SV41	SV41	SV41	SV41	SV41	SV41	SV41	SV41	SV41	SV41	SV41
Rock Type	MUG	MUG	MUG	MUG	MUG	MUG	MUG	MUG	MUG	MUG	MUG	MUG	MUG
Sample	08-014	08-015	08-016	08-017	08-018	08-019	08-020	08-021	08-022	08-023	08-024	08-025	08-026
SiO_2	43.466	42.462	42.852	41.845	41.412	43.293	43.961	41.078	41.033	41.771	41.569	41.446	43.220
TiO_2	1.717	1.640	1.498	1.537	1.850	1.777	1.791	1.598	1.678	1.585	1.653	1.761	2.407
Al_2O_3	10.644	12.674	12.013	12.962	12.394	10.058	10.144	13.092	13.558	13.478	13.467	13.268	10.761
Cr_2O_3	0.000	0.051	0.064	0.000	0.004	0.000	0.013	0.006	0.000	0.023	0.000	0.004	0.007
MnO	0.291	0.266	0.300	0.315	0.323	0.268	0.251	0.103	0.091	0.109	0.093	0.147	0.318
FeO	12.534	12.043	10.968	12.017	13.556	12.782	12.738	10.168	10.938	10.689	10.452	11.065	13.662
MgO	13.088	13.783	14.374	13.767	12.452	13.497	13.644	14.267	14.084	14.708	14.846	14.261	12.984
CaO	11.454	12.090	12.089	12.078	12.031	11.731	11.811	12.254	12.340	12.337	12.472	12.279	11.837
Na_2O	2.128	2.435	2.370	2.467	2.478	2.325	2.504	2.557	2.585	2.679	2.622	2.691	2.577
K_2O	0.690	0.697	0.693	0.752	0.755	0.716	0.697	0.800	0.763	0.696	0.704	0.690	0.359
NiO	0.015	0.006	0.000	0.000	0.000	0.000	0.033	0.017	0.000	0.023	0.030	0.067	0.005
Total	96.155	98.173	97.228	97.760	97.283	96.574	97.811	96.185	97.155	98.225	97.972	97.721	98.195
Si (23 O)	6.510	6.242	6.325	6.186	6.206	6.486	6.491	6.140	6.081	6.107	6.093	6.114	6.390
Ti	0.193	0.181	0.166	0.171	0.209	0.200	0.199	0.180	0.187	0.174	0.182	0.195	0.268
Al	1.879	2.196	2.090	2.258	2.189	1.776	1.765	2.306	2.368	2.322	2.326	2.307	1.875
Cr	0.000	0.006	0.007	0.000	0.000	0.000	0.002	0.001	0.000	0.003	0.000	0.000	0.001
Mn^{2+}	0.037	0.033	0.038	0.039	0.041	0.034	0.031	0.013	0.011	0.013	0.012	0.018	0.040
Fe^{2+}	1.570	1.480	1.354	1.486	1.699	1.601	1.573	1.271	1.355	1.307	1.281	1.365	1.689
Mg	2.922	3.020	3.163	3.034	2.782	3.014	3.004	3.179	3.111	3.206	3.244	3.136	2.862
Ca	1.838	1.904	1.912	1.913	1.932	1.883	1.868	1.962	1.959	1.932	1.958	1.941	1.875
Na	0.618	0.694	0.678	0.707	0.720	0.675	0.717	0.741	0.743	0.759	0.745	0.770	0.739
K	0.132	0.131	0.130	0.142	0.144	0.137	0.131	0.153	0.144	0.130	0.132	0.130	0.068
Ni	0.002	0.001	0.000	0.000	0.000	0.000	0.004	0.002	0.000	0.003	0.004	0.008	0.001
Total	15.764	15.889	15.864	15.940	15.925	15.858	15.915	16.001	16.024	16.046	16.025	15.988	15.807
Si_T	6.45	6.17	6.26	6.10	6.15	6.43	6.46	6.10	6.03	6.04	6.03	6.05	6.33
$ivAl_T$	1.55	1.83	1.74	1.90	1.85	1.57	1.54	1.90	1.97	1.96	1.97	1.95	1.67
$viAl_C$	0.32	0.34	0.32	0.33	0.31	0.19	0.21	0.39	0.38	0.34	0.33	0.33	0.19
Ti_C	0.19	0.18	0.16	0.17	0.21	0.20	0.20	0.18	0.19	0.17	0.18	0.19	0.27
Cr_C		0.01	0.01										
Fe^{3+}_C	0.45	0.55	0.50	0.60	0.44	0.44	0.37	0.37	0.46	0.55	0.54	0.50	0.44
Mg_C	2.90	2.98	3.13	2.99	2.76	2.99	2.99	3.16	3.08	3.17	3.21	3.10	2.83
Fe^{2+}_C	1.10	0.91	0.84	0.86	1.24	1.15	1.20	0.89	0.88	0.74	0.73	0.85	1.24
Mn^{2+}_C	0.04	0.03	0.04	0.04	0.04	0.03	0.03	0.01	0.01	0.01	0.01	0.02	0.04
Ni_C												0.01	
Ca_B	1.82	1.88	1.89	1.89	1.91	1.87	1.86	1.95	1.94	1.91	1.94	1.92	1.86
Na_B	0.18	0.12	0.11	0.11	0.09	0.13	0.14	0.05	0.06	0.09	0.06	0.08	0.14
Na_A	0.43	0.57	0.56	0.59	0.63	0.54	0.57	0.68	0.68	0.66	0.67	0.68	0.59
K_A	0.13	0.13	0.13	0.14	0.14	0.14	0.13	0.15	0.14	0.13	0.13	0.13	0.07
Na_A+K_A	0.57	0.70	0.69	0.73	0.77	0.67	0.70	0.84	0.82	0.79	0.80	0.81	0.66
Crystal #	3	3	3	3	3	3	3	4	4	4	4	4	5
Comments			Core				Rim	Core				Rim	Rim
Name	Magnesiohastingsite	Magnesiohastingsite	Magnesiohastingsite	Magnesiohastingsite	Magnesiohastingsite	Magnesiohastingsite	Magnesiohastingsite	Pargasite	Magnesiohastingsite	Magnesiohastingsite	Magnesiohastingsite	Magnesiohastingsite	Titanian Magnesiohastingsite

Sample	SV41	SV41	SV41	SV41	SV41	SV41	SV41	SV41	SV41	SV41	SV41	SV41	SV41	SV41	SV41	SV41	SV41	SV41	SV41	SV41	SV41	SV41	SV41	SV41	SV41	SV41	SV41
Rock Type	MUG	MUG	MUG	MUG	MUG	MUG	MUG	MUG	MUG	MUG	MUG	MUG	MUG	MUG	MUG	MUG	MUG	MUG	MUG	MUG	MUG	MUG	MUG	MUG	MUG	MUG	MUG
Sample	08-027	08-028	08-029	08-030	08-032	08-033	08-034	08-035	08-036	08-037	08-038	08-041	08-043	08-044	08-046	08-047	08-048	08-049	08-050	08-051	08-052	08-053	08-054	08-055	08-056	08-057	08-058
SiO_2	45.852	43.204	42.567	44.839	44.701	50.103	45.182	43.547	42.230	44.002	44.210	41.515	43.688	45.823	46.581	44.645	43.527	43.945	44.322	45.673	43.205	42.691	42.622	42.370	41.333	42.037	41.590
TiO_2	1.517	1.837	1.872	1.554	1.623	1.206	1.449	2.357	1.906	1.627	1.497	1.727	1.516	1.098	1.027	1.218	2.035	1.093	0.972	0.914	1.012	1.690	1.709	1.740	1.798	2.070	2.350
Al_2O_3	8.945	10.824	10.948	9.691	8.929	10.842	9.140	10.411	10.656	9.962	9.868	11.780	11.453	9.093	9.037	10.194	10.458	10.888	10.833	9.313	10.841	11.194	11.314	11.146	11.228	11.690	11.895
Cr_2O_3	0.000	0.000	0.000	0.000	0.006	0.000	0.000	0.015	0.007	0.006	0.000	0.000	0.135	0.147	0.111	0.156	0.034	0.017	0.028	0.068	0.062	0.006	0.000	0.000	0.009	0.006	0.000
MnO	0.422	0.384	0.337	0.393	0.389	0.291	0.349	0.342	0.346	0.282	0.262	0.301	0.370	0.285	0.307	0.257	0.334	0.264	0.251	0.222	0.274	0.254	0.257	0.305	0.245	0.296	0.274
FeO	13.284	14.826	15.102	14.410	13.801	13.278	14.455	13.577	14.936	14.241	13.761	13.545	12.847	11.878	11.813	12.411	12.590	13.681	13.220	12.202	12.767	14.105	14.357	14.805	15.098	15.673	15.656
MgO	14.274	12.606	12.205	13.218	13.485	10.742	13.414	13.087	12.038	13.062	13.216	12.747	13.692	14.674	15.290	14.215	14.015	13.571	13.623	14.656	13.750	12.661	12.546	12.458	11.777	11.945	11.641
CaO	11.613	11.726	11.659	11.603	11.627	9.772	11.372	11.689	11.545	11.650	11.774	12.060	11.736	11.780	11.616	11.720	11.734	11.788	11.890	12.013	11.875	11.801	11.584	11.869	11.759	11.765	11.888
Na_2O	2.100	2.383	2.381	2.299	2.148	2.699	2.122	2.673	2.347	2.249	2.286	2.591	2.644	2.149	2.087	2.272	2.462	2.408	2.334	2.049	2.406	2.376	2.534	2.427	2.306	2.404	2.462
K_2O	0.308	0.578	0.663	0.476	0.303	0.734	0.337	0.339	0.630	0.659	0.660	0.606	0.582	0.495	0.543	0.620	0.549	0.522	0.529	0.429	0.454	0.754	0.733	0.692	0.729	0.690	0.669
NiO	0.045	0.039	0.000	0.018	0.003	0.000	0.020	0.000	0.019	0.006	0.000	0.000	0.000	0.029	0.013	0.026	0.017	0.000	0.006	0.000	0.026	0.000	0.005	0.025	0.000	0.001	0.013
Total	98.441	98.521	97.871	98.528	97.096	99.755	97.855	98.182	96.754	97.842	97.596	97.002	98.745	97.523	98.546	97.761	97.875	98.299	98.074	97.562	96.721	97.561	97.782	97.885	96.309	98.587	98.453
Si (23 O)	6.701	6.397	6.359	6.601	6.660	7.102	6.680	6.425	6.383	6.528	6.565	6.235	6.399	6.721	6.744	6.570	6.418	6.469	6.521	6.706	6.452	6.374	6.361	6.335	6.299	6.261	6.212
Ti	0.167	0.205	0.210	0.172	0.182	0.129	0.161	0.262	0.217	0.182	0.167	0.195	0.167	0.121	0.112	0.135	0.226	0.121	0.108	0.101	0.114	0.190	0.192	0.196	0.206	0.232	0.264
Al	1.541	1.889	1.927	1.681	1.568	1.811	1.593	1.810	1.898	1.742	1.727	2.085	1.977	1.572	1.542	1.768	1.817	1.889	1.878	1.611	1.908	1.970	1.990	1.964	2.016	2.052	2.094
Cr	0.000	0.000	0.000	0.000	0.001	0.000	0.000	0.002	0.001	0.001	0.000	0.000	0.016	0.017	0.013	0.018	0.004	0.002	0.003	0.008	0.007	0.001	0.000	0.000	0.001	0.001	0.000
Mn^{2+}	0.052	0.048	0.043	0.049	0.049	0.035	0.044	0.043	0.044	0.035	0.033	0.038	0.046	0.035	0.038	0.032	0.042	0.033	0.031	0.028	0.035	0.032	0.032	0.039	0.032	0.037	0.035
Fe^{2+}	1.623	1.836	1.886	1.774	1.719	1.574	1.787	1.675	1.888	1.767	1.709	1.701	1.573	1.457	1.430	1.527	1.552	1.684	1.626	1.498	1.594	1.761	1.792	1.851	1.924	1.952	1.955
Mg	3.110	2.783	2.718	2.901	2.995	2.270	2.957	2.879	2.713	2.889	2.926	2.854	2.990	3.209	3.300	3.119	3.081	2.978	2.988	3.208	3.061	2.818	2.792	2.777	2.676	2.652	2.592
Ca	1.818	1.860	1.866	1.830	1.856	1.484	1.801	1.848	1.870	1.852	1.873	1.941	1.841	1.851	1.802	1.848	1.854	1.859	1.874	1.890	1.900	1.888	1.852	1.901	1.920	1.877	1.902
Na	0.595	0.684	0.690	0.656	0.620	0.742	0.608	0.765	0.688	0.647	0.658	0.754	0.751	0.611	0.586	0.648	0.704	0.687	0.666	0.583	0.697	0.688	0.733	0.704	0.681	0.694	0.713
K	0.057	0.109	0.126	0.089	0.058	0.133	0.064	0.064	0.121	0.125	0.125	0.116	0.109	0.093	0.100	0.116	0.103	0.098	0.099	0.080	0.086	0.144	0.140	0.132	0.142	0.131	0.127
Ni	0.005	0.005	0.000	0.002	0.000	0.000	0.002	0.000	0.002	0.001	0.000	0.000	0.000	0.003	0.002	0.003	0.002	0.000	0.001	0.000	0.003	0.000	0.001	0.003	0.000	0.000	0.002
Total	15.707	15.884	15.925	15.761	15.717	15.322	15.699	15.871	15.886	15.844	15.810	16.004	15.868	15.739	15.750	15.784	15.894	15.893	15.829	15.719	15.881	15.869	15.892	15.909	15.899	15.896	15.900
Si_T	6.60	6.32	6.29	6.51	6.57	7.15	6.57	6.38	6.31	6.46	6.50	6.18	6.32	6.65	6.65	6.48	6.35	6.38	6.44	6.62	6.37	6.30	6.28	6.26	6.23	6.17	6.14
$ivAl_T$	1.40	1.68	1.71	1.49	1.43	0.85	1.43	1.62	1.69	1.54	1.50	1.82	1.68	1.35	1.35	1.52	1.65	1.62	1.56	1.38	1.63	1.70	1.72	1.74	1.77	1.83	1.86
$viAl_C$	0.12	0.18	0.20	0.17	0.12	0.97	0.13	0.18	0.19	0.18	0.21	0.25	0.27	0.21	0.17	0.23	0.15	0.25	0.30	0.22	0.25	0.25	0.25	0.20	0.22	0.19	0.21
Ti_C	0.16	0.20	0.21	0.17	0.18	0.13	0.16	0.26	0.21	0.18	0.17	0.19	0.16	0.12	0.11	0.13	0.22	0.12	0.11	0.10	0.11	0.19	0.19	0.19	0.20	0.23	0.26
Cr_C													0.02	0.02	0.01	0.02				0.01	0.01						
$Fe^{3+}{}_C$	0.72	0.63	0.59	0.63	0.61		0.77	0.43	0.56	0.57	0.46	0.46	0.58	0.52	0.70	0.59	0.58	0.68	0.58	0.56	0.62	0.51	0.56	0.57	0.53	0.65	0.53
Mg_C	3.06	2.75	2.69	2.86	2.96	2.28	2.91	2.86	2.68	2.86	2.90	2.83	2.95	3.18	3.26	3.08	3.05	2.94	2.95	3.17	3.02	2.79	2.76	2.74	2.64	2.61	2.56
$Fe^{2+}{}_C$	0.88	1.19	1.27	1.12	1.09	1.58	0.99	1.23	1.30	1.18	1.23	1.22	0.98	0.92	0.71	0.91	0.95	0.98	1.03	0.92	0.95	1.23	1.21	1.25	1.37	1.27	1.40
$Mn^{2+}{}_C$	0.05	0.05	0.04	0.05	0.05	0.04	0.04	0.04	0.04	0.04	0.03	0.04	0.05	0.04	0.04	0.03	0.04	0.03	0.03	0.03	0.03	0.03	0.03	0.04	0.03	0.04	0.03
Ni_C	0.01																										
Ca_B	1.79	1.84	1.85	1.80	1.83	1.49	1.77	1.83	1.85	1.83	1.86	1.92	1.82	1.83	1.78	1.82	1.83	1.83	1.85	1.87	1.87	1.87	1.83	1.88	1.90	1.85	1.88
Na_B	0.21	0.16	0.15	0.20	0.17	0.51	0.23	0.17	0.15	0.17	0.14	0.08	0.18	0.17	0.22	0.18	0.17	0.17	0.15	0.13	0.13	0.13	0.17	0.12	0.10	0.15	0.12
Na_A	0.38	0.51	0.53	0.45	0.44	0.24	0.37	0.59	0.53	0.47	0.51	0.67	0.56	0.44	0.35	0.46	0.53	0.51	0.51	0.44	0.56	0.55	0.55	0.57	0.57	0.53	0.58
K_A	0.06	0.11	0.12	0.09	0.06	0.13	0.06	0.06	0.12	0.12	0.12	0.12	0.11	0.09	0.10	0.11	0.10	0.10	0.10	0.08	0.09	0.14	0.14	0.13	0.14	0.13	0.13
Na_A+K_A	0.43	0.62	0.65	0.54	0.50	0.37	0.43	0.66	0.65	0.59	0.63	0.79	0.67	0.53	0.45	0.58	0.63	0.61	0.61	0.52	0.65	0.69	0.69	0.70	0.71	0.66	0.71
Crystal #	5	5	5	5	5	5	5	5	6	6	6	6	7	7	7	7	7	8	8	8	9	9	9	9	9	9	9
Comments								Rim	Core			Rim					Rim	Core		Rim	Rim						Core
Name	Magnesiohornblende	Magnesiohastingsite	Magnesiohastingsite	Edenite	Edenite	Barroisite	Ferrian Magnesiohornblende	Titanian Magnesiohastingsite	Magnesiohastingsite	Magnesiohastingsite	Edenite	Magnesiohastingsite	Magnesiohastingsite	Edenite	Magnesiohornblende	Magnesiohastingsite	Magnesiohastingsite	Magnesiohastingsite	Magnesiohastingsite	Edenite	Magnesiohastingsite	Magnesiohastingsite	Magnesiohastingsite	Magnesiohastingsite	Magnesiohastingsite	Magnesiohastingsite	Titanian Magnesiohastingsite

Sample	SV41	SV41	SV41	SV44	SV44	SV44	SV44	SV44	SV158	SV158	SV158	SV158
Rock Type	MUG	MUG	MUG	TRAC	TRAC	TRAC	TRAC	TRAC				
Sample	08-059	08-060	08-062	09-091	09-093	09-099	09-112	09-121	12-081	12-082	12-091	12-092
SiO_2	41.747	41.825	46.502	38.672	43.489	41.517	42.170	47.326	43.387	48.723	47.509	39.408
TiO_2	2.307	2.311	1.728	1.389	1.724	1.708	1.355	1.305	1.395	1.366	1.588	1.955
Al_2O_3	11.781	11.836	12.640	15.682	11.236	13.696	12.712	6.037	11.941	6.319	7.535	15.341
Cr_2O_3	0.000	0.004	0.021	0.000	0.033	0.000	0.019	0.113	0.149	0.006	0.000	0.025
MnO	0.225	0.230	0.230	0.378	0.190	0.215	0.249	0.844	0.139	0.723	0.717	0.361
FeO	15.190	15.263	14.029	16.916	11.726	13.476	11.891	11.762	8.417	11.128	12.625	16.680
MgO	11.662	11.764	14.743	8.159	14.200	12.632	13.630	15.103	15.150	15.190	14.224	8.916
CaO	11.847	11.761	11.574	11.244	10.940	11.191	11.523	10.449	12.287	11.578	11.346	11.555
Na_2O	2.447	2.436	2.894	2.400	2.237	2.363	2.598	2.277	2.472	1.941	2.103	2.660
K_2O	0.699	0.712	0.659	1.353	0.971	1.144	1.158	0.806	0.789	0.537	0.684	0.810
NiO	0.019	0.000	0.031	0.000	0.039	0.000	0.000	0.000	0.000	0.009	0.005	0.032
Total	97.948	98.208	105.152	96.193	96.785	97.942	97.305	96.022	96.126	97.520	98.336	97.743
Si (23 O)	6.250	6.247	6.379	5.969	6.447	6.156	6.260	7.050	6.398	7.098	6.928	5.965
Ti	0.260	0.260	0.178	0.161	0.192	0.190	0.151	0.146	0.155	0.150	0.174	0.223
Al	2.079	2.084	2.044	2.852	1.963	2.393	2.224	1.060	2.075	1.085	1.295	2.737
Cr	0.000	0.000	0.002	0.000	0.004	0.000	0.002	0.013	0.017	0.001	0.000	0.003
Mn^{2+}	0.029	0.029	0.027	0.049	0.024	0.027	0.031	0.106	0.017	0.089	0.089	0.046
Fe^{2+}	1.902	1.906	1.609	2.183	1.454	1.671	1.476	1.465	1.038	1.356	1.539	2.111
Mg	2.603	2.620	3.015	1.877	3.138	2.793	3.016	3.354	3.331	3.299	3.092	2.012
Ca	1.900	1.882	1.701	1.859	1.737	1.778	1.832	1.668	1.941	1.807	1.772	1.874
Na	0.710	0.705	0.770	0.718	0.643	0.679	0.748	0.658	0.707	0.548	0.595	0.781
K	0.133	0.136	0.115	0.266	0.184	0.216	0.219	0.153	0.148	0.100	0.127	0.156
Ni	0.002	0.000	0.003	0.000	0.005	0.000	0.000	0.000	0.000	0.001	0.001	0.004
Total	15.876	15.874	15.880	15.936	15.791	15.904	15.960	15.673	15.828	15.533	15.612	15.911
Si_T	6.19	6.18	6.26	5.93	6.34	6.05	6.18	6.95	6.38	7.06	6.87	5.92
$ivAl_T$	1.81	1.82	1.74	2.07	1.66	1.95	1.82	1.04	1.62	0.94	1.13	2.08
$viAl_C$	0.25	0.24	0.26	0.76	0.27	0.40	0.38		0.45	0.13	0.15	0.63
Ti_C	0.26	0.26	0.17	0.16	0.19	0.19	0.15	0.13	0.15	0.15	0.17	0.22
Cr_C								0.01	0.02			
$Fe^{3+}{}_C$	0.44	0.51	0.91	0.32	0.77	0.79	0.55	0.67	0.11	0.27	0.41	0.35
Mg_C	2.58	2.59	2.96	1.86	3.08	2.74	2.98	3.30	3.32	3.28	3.06	2.00
$Fe^{2+}{}_C$	1.44	1.38	0.67	1.85	0.65	0.85	0.90	0.78	0.92	1.07	1.12	1.75
$Mn^{2+}{}_C$	0.03	0.03	0.03	0.05	0.02	0.03	0.03	0.10	0.02	0.09	0.09	0.05
Ni_C												
Ca_B	1.88	1.86	1.67	1.85	1.71	1.75	1.81	1.64	1.94	1.80	1.76	1.86
Na_B	0.12	0.14	0.33	0.15	0.29	0.25	0.19	0.36	0.06	0.20	0.24	0.14
Na_A	0.59	0.56	0.42	0.56	0.34	0.41	0.55	0.29	0.64	0.34	0.35	0.63
K_A	0.13	0.13	0.11	0.26	0.18	0.21	0.22	0.15	0.15	0.10	0.13	0.16
Na_A+K_A	0.72	0.69	0.54	0.82	0.52	0.63	0.77	0.44	0.79	0.44	0.47	0.79
Crystal #	9	9	9					12				
Comments			Rim									
Name	Titanian Magnesiohastingsite	Titanian Magnesiohastingsite	Ferrian Magnesiohastingsite	Potassian Pargasite	Ferrian Magnesiohastingsite	Ferrian Magnesiohastingsite	Magnesiohastingsite	Magnesiohornblende	Pargasite	Magnesiohornblende	Magnesiohornblende	Pargasite

Sample	SV158	SV158	SV158	SV158	SV158	SV158	SV158	SV165	SV165	SV165	SV165	SV165	SV165	SV165	SV165
Rock Type	XEN	XEN	XEN	XEN	XEN	XEN	XEN								
Sample	12-111	12-114	12-115	12-117	12-118	12-122	12-124	07-001	07-002	07-003	07-004	07-006	07-007	07-009	07-010
SiO_2	43.349	43.086	43.818	43.049	43.157	43.082	43.918	43.345	42.114	42.335	42.711	43.994	40.839	41.416	41.779
TiO_2	1.185	1.338	1.265	1.485	1.402	1.442	1.079	1.919	1.972	2.197	2.247	2.057	2.362	2.777	2.800
Al_2O_3	10.320	12.322	12.417	12.734	12.366	12.451	11.874	10.967	11.973	11.808	11.850	11.792	11.594	12.179	12.243
Cr_2O_3	0.120	0.383	0.424	0.227	0.282	0.238	0.012	0.000	0.030	0.016	0.032	0.000	0.000	0.000	0.005
MnO	0.500	0.085	0.075	0.087	0.068	0.073	0.081	0.407	0.318	0.286	0.293	0.227	0.268	0.316	0.268
FeO	12.931	8.795	8.871	8.513	9.032	9.110	9.021	13.415	14.525	14.579	14.071	13.381	13.637	13.213	13.383
MgO	13.031	15.192	15.552	15.540	15.327	15.240	16.135	13.703	12.459	12.418	12.234	11.939	12.133	12.366	12.310
CaO	11.338	12.195	12.414	12.107	12.216	12.217	11.770	11.871	11.786	11.964	11.716	11.640	11.877	11.880	12.132
Na_2O	2.775	1.986	1.974	2.290	2.259	2.101	2.255	2.742	2.602	2.605	3.034	2.614	2.645	2.533	2.536
K_2O	0.713	0.812	0.792	0.741	0.739	0.809	0.681	0.574	0.712	0.723	0.755	0.709	0.649	0.649	0.638
NiO	0.000	0.012	0.027	0.019	0.000	0.044	0.027	0.012	0.000	0.004	0.026	0.010	0.000	0.004	0.073
Total	96.262	96.206	97.629	96.792	96.848	96.807	96.853	98.955	98.491	98.935	98.969	98.363	96.004	97.333	98.167
Si (23 O)	6.524	6.352	6.363	6.301	6.329	6.323	6.418	6.362	6.250	6.257	6.296	6.463	6.214	6.190	6.195
Ti	0.134	0.148	0.138	0.163	0.155	0.159	0.119	0.212	0.220	0.244	0.249	0.227	0.270	0.312	0.312
Al	1.830	2.141	2.125	2.196	2.137	2.154	2.045	1.897	2.094	2.057	2.059	2.041	2.079	2.145	2.139
Cr	0.014	0.045	0.049	0.026	0.033	0.028	0.001	0.000	0.004	0.002	0.004	0.000	0.000	0.000	0.001
Mn^{2+}	0.064	0.011	0.009	0.011	0.008	0.009	0.010	0.051	0.040	0.036	0.037	0.028	0.035	0.040	0.034
Fe^{2+}	1.627	1.084	1.077	1.042	1.108	1.118	1.102	1.646	1.802	1.802	1.734	1.644	1.735	1.651	1.659
Mg	2.924	3.339	3.367	3.391	3.351	3.335	3.515	2.998	2.756	2.736	2.688	2.615	2.752	2.755	2.721
Ca	1.828	1.926	1.931	1.898	1.919	1.921	1.843	1.867	1.874	1.894	1.850	1.832	1.936	1.902	1.927
Na	0.810	0.568	0.556	0.650	0.642	0.598	0.639	0.780	0.749	0.746	0.867	0.744	0.780	0.734	0.729
K	0.137	0.153	0.147	0.138	0.138	0.151	0.127	0.107	0.135	0.136	0.142	0.133	0.126	0.124	0.121
Ni	0.000	0.001	0.003	0.002	0.000	0.005	0.003	0.001	0.000	0.000	0.003	0.001	0.000	0.000	0.009
Total	15.893	15.767	15.764	15.819	15.821	15.801	15.823	15.922	15.923	15.911	15.929	15.728	15.929	15.854	15.847
Si_T	6.47	6.29	6.30	6.24	6.27	6.26	6.31	6.28	6.17	6.19	6.26	6.45	6.17	6.15	6.16
$ivAl_T$	1.53	1.71	1.70	1.76	1.73	1.74	1.69	1.72	1.83	1.81	1.74	1.55	1.83	1.85	1.84
$viAl_C$	0.28	0.41	0.40	0.41	0.39	0.39	0.33	0.15	0.24	0.23	0.31	0.49	0.24	0.28	0.29
Ti_C	0.13	0.15	0.14	0.16	0.15	0.16	0.12	0.21	0.22	0.24	0.25	0.23	0.27	0.31	0.31
Cr_C	0.01	0.04	0.05	0.03	0.03	0.03									
$Fe^{3+}{}_C$	0.41	0.42	0.45	0.46	0.42	0.45	0.73	0.58	0.57	0.46	0.24	0.07	0.30	0.33	0.25
Mg_C	2.90	3.31	3.33	3.36	3.32	3.30	3.46	2.96	2.72	2.71	2.67	2.61	2.73	2.74	2.71
$Fe^{2+}{}_C$	1.20	0.65	0.61	0.57	0.68	0.65	0.35	1.05	1.21	1.32	1.48	1.57	1.42	1.31	1.40
$Mn^{2+}{}_C$	0.06	0.01	0.01	0.01	0.01	0.01	0.01	0.05	0.04	0.04	0.04	0.03	0.03	0.04	0.03
Ni_C						0.01									0.01
Ca_B	1.81	1.91	1.91	1.88	1.90	1.90	1.81	1.84	1.85	1.88	1.84	1.83	1.92	1.89	1.92
Na_B	0.19	0.09	0.09	0.12	0.10	0.10	0.19	0.16	0.15	0.12	0.16	0.17	0.08	0.11	0.08
Na_A	0.61	0.47	0.46	0.52	0.54	0.49	0.44	0.61	0.59	0.61	0.70	0.57	0.70	0.62	0.64
K_A	0.14	0.15	0.15	0.14	0.14	0.15	0.12	0.11	0.13	0.13	0.14	0.13	0.13	0.12	0.12
Na_A+K_A	0.75	0.62	0.61	0.66	0.67	0.64	0.57	0.72	0.72	0.75	0.84	0.71	0.82	0.74	0.76
Crystal #								1	1	1	1	2	2	2	2
Comments															
Name	Magnesiohastingsite	Magnesiohastingsite	Magnesiohastingsite	Magnesiohastingsite	Magnesiohastingsite	Magnesiohastingsite	Magnesiohastingsite	Magnesiohastingsite	Magnesiohastingsite	Magnesiohastingsite	Pargasite	Pargasite	Titanian Magnesiohastingsite	Titanian Magnesiohastingsite	Titanian Pargasite

Sample	SV165	SV165	SV165	SV165	SV165	SV165	SV165	SV165	SV165	SV165	SV165	SV165	SV165	SV176
Rock Type			XEN				XEN	XEN	XEN	XEN	XEN	XEN	XEN	XEN
Sample	07-011	07-012	07-013	07-015	07-022	07-026	07-032	07-033	07-034	07-036	07-041	07-043	07-053	07-113
SiO_2	42.931	42.412	43.561	41.577	42.236	48.308	44.446	43.501	44.748	42.799	42.830	43.342	44.222	42.766
TiO_2	1.769	1.895	1.766	1.405	1.704	0.504	1.477	1.612	1.050	1.117	1.065	1.246	0.251	1.097
Al_2O_3	11.477	11.575	10.801	13.660	12.603	7.756	10.480	10.793	10.731	13.060	12.442	12.062	11.308	12.609
Cr_2O_3	0.000	0.000	0.005	0.000	0.005	0.081	0.129	0.098	0.133	0.059	0.248	1.032	0.266	0.131
MnO	0.288	0.313	0.287	0.161	0.245	0.264	0.305	0.348	0.251	0.178	0.150	0.132	0.146	0.264
FeO	14.076	13.640	13.409	11.817	12.173	11.371	12.659	11.846	11.692	10.621	9.983	7.634	8.178	11.895
MgO	12.955	12.956	13.499	14.157	14.182	16.233	14.295	14.163	15.142	15.128	15.071	16.564	16.855	14.129
CaO	12.069	11.766	11.764	12.206	12.111	12.047	11.703	11.919	11.949	11.969	11.615	12.031	11.827	12.019
Na_2O	2.409	2.984	2.506	2.582	2.621	2.250	2.775	2.442	2.502	2.606	2.542	2.378	2.927	2.687
K_2O	0.642	0.606	0.506	0.770	0.678	0.302	0.280	0.334	0.377	0.557	0.512	0.578	0.423	0.622
NiO	0.029	0.000	0.004	0.023	0.000	0.000	0.027	0.017	0.034	0.014	0.000	0.039	0.054	0.071
Total	98.645	98.147	98.108	98.358	98.558	99.116	98.576	97.073	98.609	98.108	96.458	97.038	96.457	98.290
Si (23 O)	6.336	6.293	6.430	6.105	6.195	6.927	6.496	6.443	6.503	6.241	6.326	6.314	6.477	6.273
Ti	0.196	0.211	0.196	0.155	0.188	0.054	0.162	0.180	0.115	0.123	0.118	0.137	0.028	0.121
Al	1.996	2.024	1.879	2.364	2.179	1.311	1.805	1.884	1.838	2.244	2.166	2.071	1.952	2.180
Cr	0.000	0.000	0.001	0.000	0.001	0.009	0.015	0.011	0.015	0.007	0.029	0.119	0.031	0.015
Mn^{2+}	0.036	0.039	0.036	0.020	0.030	0.032	0.038	0.044	0.031	0.022	0.019	0.016	0.018	0.033
Fe^{2+}	1.737	1.692	1.655	1.451	1.493	1.363	1.547	1.467	1.421	1.295	1.233	0.930	1.002	1.459
Mg	2.850	2.866	2.971	3.099	3.101	3.470	3.115	3.127	3.281	3.289	3.318	3.597	3.680	3.090
Ca	1.908	1.870	1.860	1.920	1.903	1.851	1.832	1.891	1.860	1.870	1.838	1.878	1.856	1.889
Na	0.689	0.858	0.717	0.735	0.745	0.626	0.786	0.701	0.705	0.737	0.728	0.672	0.831	0.764
K	0.121	0.115	0.095	0.144	0.127	0.055	0.052	0.063	0.070	0.104	0.096	0.107	0.079	0.116
Ni	0.003	0.000	0.000	0.003	0.000	0.000	0.003	0.002	0.004	0.002	0.000	0.005	0.006	0.008
Total	15.874	15.970	15.840	15.997	15.963	15.699	15.851	15.812	15.843	15.931	15.871	15.844	15.959	15.949
Si_T	6.26	6.23	6.35	6.01	6.11	6.84	6.41	6.37	6.40	6.14	6.23	6.22	6.38	6.19
$ivAl_T$	1.74	1.77	1.65	1.99	1.89	1.16	1.59	1.63	1.60	1.86	1.77	1.78	1.62	1.81
$viAl_C$	0.23	0.24	0.20	0.34	0.25	0.13	0.19	0.23	0.21	0.34	0.36	0.27	0.31	0.34
Ti_C	0.19	0.21	0.19	0.15	0.19	0.05	0.16	0.18	0.11	0.12	0.12	0.13	0.03	0.12
Cr_C						0.01	0.01	0.01	0.02	0.01	0.03	0.12	0.03	0.01
$Fe^{3+}{}_C$	0.54	0.44	0.58	0.68	0.65	0.58	0.62	0.54	0.71	0.76	0.72	0.65	0.66	0.62
Mg_C	2.82	2.84	2.93	3.05	3.06	3.43	3.07	3.09	3.23	3.23	3.27	3.55	3.63	3.05
$Fe^{2+}{}_C$	1.18	1.24	1.06	0.75	0.83	0.77	0.90	0.91	0.69	0.52	0.50	0.27	0.32	0.82
$Mn^{2+}{}_C$	0.04	0.04	0.04	0.02	0.03	0.03	0.04	0.04	0.03	0.02	0.02	0.02	0.02	0.03
Ni_C													0.01	0.01
Ca_B	1.89	1.85	1.84	1.89	1.88	1.83	1.81	1.87	1.83	1.84	1.81	1.85	1.83	1.86
Na_B	0.11	0.15	0.16	0.11	0.12	0.17	0.19	0.13	0.17	0.16	0.19	0.15	0.17	0.14
Na_A	0.57	0.70	0.54	0.62	0.61	0.44	0.58	0.56	0.53	0.56	0.53	0.51	0.65	0.62
K_A	0.12	0.11	0.09	0.14	0.13	0.05	0.05	0.06	0.07	0.10	0.09	0.11	0.08	0.11
Na_A+K_A	0.69	0.82	0.64	0.76	0.74	0.50	0.63	0.62	0.59	0.66	0.62	0.62	0.73	0.73
Crystal #	2	2	2											
Comments														
Name	Magnesiohastingsite	Magnesiohastingsite	Magnesiohastingsite	Magnesiohastingsite	Magnesiohastingsite	Magnesiohornblende	Magnesiohastingsite	Magnesiohastingsite	Magnesiohastingsite	Ferrian Magnesiohastingsite	Magnesiohastingsite	Magnesiohastingsite	Magnesiohastingsite	Magnesiohastingsite

Sample	SV181	SV181	SV181	SV181	SV181	SV181	SV181	SV181	SV181	SV183	SV183	SV183	SV183
Rock Type	XEN	XEN	XEN	XEN	XEN	XEN							
Sample	10-001	10-005	10-008	10-011	10-019	10-020	10-121	10-122	10-126	07-061	07-073	07-074	07-077
SiO_2	40.269	40.158	40.498	40.444	40.268	40.478	43.002	47.463	42.361	48.601	45.968	44.901	41.686
TiO_2	1.559	1.708	1.513	1.625	1.501	1.448	1.265	1.345	1.469	0.955	1.104	1.426	1.451
Al_2O_3	14.896	14.881	14.849	14.842	15.108	14.992	12.138	7.155	12.613	6.128	8.486	9.933	12.366
Cr_2O_3	0.069	0.000	0.006	0.000	0.030	0.000	0.166	0.017	0.012	0.016	0.005	0.029	0.009
MnO	0.179	0.220	0.204	0.223	0.236	0.277	0.336	0.640	0.280	0.817	0.470	0.357	0.129
FeO	14.465	13.711	14.151	14.581	13.980	13.641	12.724	11.850	12.288	12.339	12.676	13.250	12.114
MgO	11.054	10.878	11.013	10.891	11.084	11.305	12.999	14.263	12.766	15.468	14.056	13.616	13.962
CaO	11.564	11.780	11.584	11.511	11.488	11.720	11.435	11.271	11.610	11.333	11.428	11.587	11.911
Na_2O	2.586	2.606	2.602	2.605	2.577	2.559	2.732	2.097	2.526	1.723	2.136	2.230	2.303
K_2O	0.804	0.753	0.776	0.711	0.760	0.772	0.467	0.620	0.698	0.340	0.380	0.489	1.257
NiO	0.003	0.003	0.000	0.000	0.000	0.012	0.053	0.000	0.000	0.051	0.005	0.000	0.000
Total	97.448	96.698	97.196	97.433	97.032	97.204	97.317	96.721	96.623	97.771	96.714	97.818	97.188
Si (23 O)	6.036	6.049	6.073	6.060	6.044	6.058	6.377	7.005	6.322	7.091	6.816	6.615	6.215
Ti	0.176	0.194	0.171	0.183	0.169	0.163	0.141	0.149	0.165	0.105	0.123	0.158	0.163
Al	2.632	2.642	2.624	2.621	2.672	2.644	2.121	1.245	2.218	1.054	1.483	1.725	2.173
Cr	0.008	0.000	0.001	0.000	0.004	0.000	0.019	0.002	0.001	0.002	0.001	0.003	0.001
Mn^{2+}	0.023	0.028	0.026	0.028	0.030	0.035	0.042	0.080	0.035	0.101	0.059	0.045	0.016
Fe^{2+}	1.813	1.727	1.774	1.827	1.755	1.707	1.578	1.462	1.533	1.505	1.572	1.632	1.510
Mg	2.470	2.443	2.462	2.433	2.480	2.523	2.874	3.138	2.840	3.365	3.107	2.991	3.103
Ca	1.857	1.901	1.861	1.848	1.847	1.879	1.817	1.782	1.856	1.772	1.815	1.829	1.902
Na	0.752	0.761	0.756	0.757	0.750	0.743	0.785	0.600	0.731	0.487	0.614	0.637	0.666
K	0.154	0.145	0.148	0.136	0.146	0.147	0.088	0.117	0.133	0.063	0.072	0.092	0.239
Ni	0.000	0.000	0.000	0.000	0.000	0.001	0.006	0.000	0.000	0.006	0.001	0.000	0.000
Total	15.921	15.889	15.897	15.893	15.896	15.901	15.849	15.581	15.835	15.551	15.662	15.727	15.988
Si_T	5.96	6.01	6.01	5.99	5.97	6.00	6.30	6.96	6.27	6.97	6.73	6.53	6.13
$ivAl_T$	2.04	1.99	1.99	2.01	2.03	2.00	1.70	1.04	1.73	1.03	1.27	1.47	1.87
$viAl_C$	0.56	0.64	0.61	0.58	0.61	0.62	0.40	0.20	0.46		0.20	0.23	0.27
Ti_C	0.17	0.19	0.17	0.18	0.17	0.16	0.14	0.15	0.16	0.10	0.12	0.16	0.16
Cr_C	0.01						0.02						
$Fe^{3+}{}_C$	0.55	0.29	0.45	0.53	0.53	0.46	0.55	0.29	0.40	0.78	0.56	0.58	0.62
Mg_C	2.44	2.43	2.44	2.40	2.45	2.50	2.84	3.12	2.82	3.31	3.07	2.95	3.06
$Fe^{2+}{}_C$	1.24	1.43	1.30	1.28	1.20	1.23	1.01	1.17	1.12	0.70	1.00	1.03	0.87
$Mn^{2+}{}_C$	0.02	0.03	0.03	0.03	0.03	0.03	0.04	0.08	0.04	0.10	0.06	0.04	0.02
Ni_C							0.01			0.01			
Ca_B	1.83	1.89	1.84	1.83	1.83	1.86	1.79	1.77	1.84	1.74	1.79	1.81	1.88
Na_B	0.17	0.11	0.16	0.17	0.17	0.14	0.21	0.23	0.16	0.26	0.21	0.19	0.12
Na_A	0.58	0.65	0.59	0.57	0.57	0.60	0.57	0.37	0.56	0.22	0.40	0.43	0.53
K_A	0.15	0.14	0.15	0.13	0.14	0.15	0.09	0.12	0.13	0.06	0.07	0.09	0.24
Na_A+K_A	0.73	0.79	0.74	0.71	0.71	0.74	0.66	0.48	0.70	0.28	0.47	0.52	0.77
Crystal #					3	3	12				5	5	
Comments													
Name	Pargasite	Pargasite	Pargasite	Pargasite	Pargasite	Pargasite	Magnesiohastingsite	Magnesiohornblende	Pargasite	Ferrian Magnesiohornblende	Magnesiohornblende	Edenite	Magnesiohastingsite

Sample	SV183	SV183	SV183	SV183	SV183	SV183	SV183	SV183	SV183	SV183
Rock Type	XEN	XEN	XEN	XEN	XEN	XEN	XEN	XEN	XEN	
Sample	07-081	07-082	07-083	07-084	07-085	07-088	07-093	07-096	07-102	07-104
SiO_2	48.651	47.928	44.118	43.346	45.618	45.445	42.931	41.223	44.959	48.908
TiO_2	1.182	1.082	1.277	1.346	0.704	0.586	0.105	1.440	1.441	1.035
Al_2O_3	6.030	6.224	9.675	10.066	8.763	8.942	13.375	13.646	11.457	5.614
Cr_2O_3	0.000	0.014	0.021	0.078	0.007	0.102	0.044	0.043	0.000	0.000
MnO	0.769	0.731	0.416	0.356	0.323	0.417	0.126	0.165	0.438	0.745
FeO	11.480	11.870	14.152	14.022	12.739	13.828	7.475	10.528	13.487	11.040
MgO	15.784	15.190	13.051	12.838	14.411	13.829	16.350	14.348	11.008	15.680
CaO	11.273	11.124	11.844	11.820	12.041	11.884	13.082	12.279	10.715	12.080
Na_2O	1.736	1.720	2.016	2.163	1.940	2.083	2.351	2.652	3.395	2.120
K_2O	0.347	0.337	0.773	0.713	0.566	0.590	0.658	0.747	1.520	0.289
NiO	0.033	0.030	0.000	0.005	0.000	0.039	0.000	0.005	0.007	0.029
Total	97.285	96.250	97.343	96.753	97.112	97.745	96.497	97.076	98.427	97.540
Si (23 O)	7.103	7.088	6.586	6.517	6.754	6.726	6.283	6.104	6.622	7.131
Ti	0.130	0.120	0.143	0.152	0.078	0.065	0.012	0.160	0.160	0.114
Al	1.038	1.085	1.702	1.783	1.529	1.560	2.307	2.381	1.989	0.965
Cr	0.000	0.002	0.002	0.009	0.001	0.012	0.005	0.005	0.000	0.000
Mn^{2+}	0.095	0.092	0.053	0.045	0.041	0.052	0.016	0.021	0.055	0.092
Fe^{2+}	1.402	1.468	1.767	1.763	1.577	1.711	0.915	1.304	1.661	1.346
Mg	3.436	3.349	2.905	2.877	3.181	3.052	3.567	3.167	2.417	3.408
Ca	1.763	1.763	1.894	1.904	1.910	1.884	2.051	1.948	1.691	1.887
Na	0.491	0.493	0.583	0.630	0.557	0.598	0.667	0.761	0.970	0.599
K	0.065	0.064	0.147	0.137	0.107	0.111	0.123	0.141	0.286	0.054
Ni	0.004	0.004	0.000	0.001	0.000	0.005	0.000	0.001	0.001	0.003
Total	15.526	15.527	15.783	15.818	15.734	15.777	15.945	15.993	15.851	15.599
Si_T	6.99	6.98	6.51	6.44	6.67	6.63	6.23	6.04	6.67	7.10
$ivAl_T$	1.01	1.02	1.49	1.56	1.33	1.37	1.77	1.96	1.33	0.90
$viAl_C$	0.01	0.04	0.19	0.21	0.18	0.17	0.52	0.39	0.67	0.06
Ti_C	0.13	0.12	0.14	0.15	0.08	0.06	0.01	0.16	0.16	0.11
Cr_C				0.01		0.01	0.01			
$Fe^{3+}{}_C$	0.71	0.71	0.55	0.51	0.56	0.63	0.36	0.50		0.21
Mg_C	3.38	3.30	2.87	2.85	3.14	3.01	3.54	3.13	2.44	3.39
$Fe^{2+}{}_C$	0.67	0.73	1.20	1.23	1.00	1.06	0.55	0.79	1.67	1.13
$Mn^{2+}{}_C$	0.09	0.09	0.05	0.04	0.04	0.05	0.02	0.02	0.06	0.09
Ni_C										
Ca_B	1.74	1.73	1.87	1.88	1.89	1.86	2.03	1.93	1.70	1.88
Na_B	0.26	0.27	0.13	0.12	0.11	0.14		0.07	0.30	0.12
Na_A	0.22	0.22	0.45	0.51	0.44	0.45	0.66	0.68	0.68	0.47
K_A	0.06	0.06	0.15	0.14	0.11	0.11	0.12	0.14	0.29	0.05
Na_A+K_A	0.28	0.28	0.59	0.64	0.54	0.56	0.78	0.82	0.97	0.53
Crystal #		6	6	6	6	6				
Comments										
Name	Magnesiohornblende	Magnesiohornblende	Edenite	Magnesiohastingsite	Edenite	Edenite	Pargasite	Magnesiohastingsite	Potassian Edenite	Edenite

I.4 Clinopyroxene

Sample	SV1	SV1	SV1	SV1	SV1	SV1	SV1	SV1	SV1	SV1	SV1	SV1	SV1	SV1	SV1
Rock Type	MUG	MUG	MUG	MUG	MUG	MUG	MUG	MUG	MUG	MUG	MUG	MUG	MUG	MUG	MUG
Analysis	05-001	05-002	05-004	05-005	05-006	05-007	05-008	05-009	05-010	05-011	05-012	05-014	05-015	05-016	05-017
SiO_2	52.54	51.58	48.92	51.73	51.48	51.20	51.08	51.16	50.84	51.56	53.20	51.34	50.90	52.27	51.91
TiO_2	0.49	0.44	0.65	0.41	0.54	0.37	0.56	0.46	0.57	0.38	0.16	0.49	0.47	0.22	0.44
Al_2O_3	2.97	2.47	4.59	2.49	2.53	3.38	2.99	3.31	3.47	2.69	1.66	2.89	3.40	2.10	1.95
FeO	7.37	7.50	8.46	7.01	8.26	6.22	7.92	7.76	7.94	7.08	3.65	7.41	7.60	4.84	8.13
MnO	0.23	0.26	0.26	0.25	0.30	0.17	0.26	0.25	0.23	0.16	0.11	0.18	0.24	0.13	0.32
MgO	15.17	15.71	14.07	15.77	15.39	15.71	15.64	15.57	15.64	15.83	17.37	15.49	15.52	16.56	16.28
CaO	20.42	21.58	21.66	22.15	20.80	22.44	21.14	21.29	21.45	21.68	23.25	21.92	21.92	22.99	20.72
K_2O	0.03	0.00	0.00	0.00	0.00	0.01	0.00	0.01	0.00	0.00	0.01	0.01	0.01	0.00	0.00
Na_2O	0.48	0.38	0.42	0.38	0.43	0.29	0.41	0.50	0.41	0.41	0.27	0.46	0.31	0.28	0.37
NiO	0.03	0.00	0.02	0.00	0.01	0.00	0.00	0.02	0.01	0.00	0.00	0.04	0.01	0.00	0.02
Cr2O3	0.01	0.00	0.06	0.03	0.03	0.21	0.04	0.03	0.01	0.19	0.70	0.05	0.00	0.60	0.03
Total	99.75	99.91	99.11	100.22	99.76	99.99	100.03	100.35	100.57	99.98	100.39	100.28	100.39	99.98	100.19
Si (6 O)	1.941	1.900	1.826	1.898	1.905	1.879	1.881	1.875	1.861	1.895	1.929	1.884	1.867	1.911	1.907
Ti	0.014	0.012	0.018	0.011	0.015	0.010	0.015	0.013	0.016	0.010	0.004	0.014	0.013	0.006	0.012
Al (T)	0.059	0.100	0.174	0.102	0.095	0.121	0.119	0.125	0.139	0.105	0.071	0.116	0.133	0.089	0.084
Al (M1)	0.071	0.007	0.028	0.005	0.015	0.025	0.010	0.018	0.010	0.011	0.000	0.009	0.013	0.002	0.000
Fe^{3+} (T)	0.000	0.000	0.000	0.000	0.000	0.000	0.000	0.000	0.000	0.000	0.000	0.000	0.000	0.000	0.008
Fe^{3+} (M1)	0.000	0.096	0.139	0.101	0.080	0.091	0.106	0.117	0.127	0.097	0.061	0.112	0.117	0.078	0.094
Fe^{2+}	0.228	0.135	0.125	0.114	0.176	0.100	0.137	0.121	0.116	0.120	0.049	0.115	0.116	0.070	0.148
Mn	0.007	0.008	0.008	0.008	0.009	0.005	0.008	0.008	0.007	0.005	0.003	0.006	0.008	0.004	0.010
Mg	0.836	0.863	0.783	0.862	0.849	0.859	0.858	0.850	0.853	0.867	0.939	0.847	0.849	0.903	0.892
Ca	0.808	0.852	0.866	0.871	0.824	0.882	0.834	0.836	0.841	0.853	0.903	0.862	0.861	0.901	0.816
K	0.002	0.000	0.000	0.000	0.000	0.001	0.000	0.001	0.000	0.000	0.000	0.000	0.000	0.000	0.000
Na	0.034	0.027	0.031	0.027	0.031	0.021	0.029	0.035	0.029	0.029	0.019	0.033	0.022	0.020	0.027
Ni	0.001	0.000	0.000	0.000	0.000	0.000	0.000	0.001	0.000	0.000	0.000	0.001	0.000	0.000	0.001
Cr	0.000	0.000	0.002	0.001	0.001	0.006	0.001	0.001	0.000	0.006	0.020	0.001	0.000	0.017	0.001
Total	4.000	4.000	4.000	4.000	4.000	4.000	4.000	4.000	4.000	4.000	4.000	4.000	4.000	4.000	4.000
Crystal #	1	1	2	2	3	3	3	3	3	3	4	4	4	4	4
Comments															
Enstatite %	44	44	41	44	44	44	44	44	44	45	48	44	44	46	45
Ferrosillite %	13	12	14	11	14	10	13	13	13	11	6	12	12	8	13
Wollastonite %	43	44	45	45	43	46	43	43	43	44	46	44	44	46	41
Adjective	aluminian	aluminian	aluminian ferrian	aluminian ferrian	aluminian	aluminian	aluminian ferrian	aluminian ferrian	aluminian ferrian	aluminian	chromian	aluminian ferrian	aluminian ferrian	chromian	ferrian
Pyroxene	augite	augite	diopside	augite	augite	diopside	augite	augite	augite	augite	diopside	augite	augite	diopside	augite

Table I.4: Clinopyroxene electron microprobe data. Mineral names and stoichiometry from PX-NOM (Sturm, 2002)

Sample	SV1	SV1	SV1	SV1	SV1	SV1	SV1	SV1	SV1	SV1	SV1	SV6A	SV6A	SV6A	SV6A	SV6A	SV6A	SV6A	SV6A	SV6A	SV6A	SV12	SV12	SV19
Rock Type	MUG	MUG	MUG	MUG	MUG	MUG	MUG	MUG	MUG	MUG	MUG	XEN	XEN	XEN	XEN	XEN	XEN	XEN	XEN	XEN	XEN	BEN	BEN	MUG
Analysis	05-018	05-030	05-031	05-032	05-033	05-034	05-035	05-003	05-025	05-026	05-040	03-004	03-005	03-006	03-009	03-022	03-029	03-034	03-041	03-042	03-043	12-059	12-069	05-041
SiO_2	52.01	53.57	51.05	51.27	51.01	51.34	51.27	50.74	51.94	52.95	51.75	50.99	50.81	50.32	50.56	50.39	50.89	50.94	50.91	49.36	50.38	53.03	50.73	49.51
TiO_2	0.43	0.07	0.49	0.38	0.43	0.39	0.49	0.36	0.43	0.22	0.26	0.13	0.13	0.14	0.14	0.16	0.15	0.10	0.13	0.25	0.23	0.32	0.58	0.70
Al_2O_3	1.98	1.14	3.32	3.38	3.77	2.92	2.60	3.55	2.30	1.48	3.02	3.60	3.96	4.31	4.32	4.18	3.94	3.88	3.92	4.73	4.35	1.71	3.71	4.91
FeO	8.61	3.53	7.44	6.42	6.78	6.94	7.77	6.66	8.08	4.36	4.92	7.45	7.51	7.65	7.53	7.66	7.44	7.43	7.43	7.42	7.32	7.77	8.05	7.84
MnO	0.37	0.09	0.27	0.16	0.16	0.18	0.25	0.12	0.34	0.08	0.06	0.31	0.28	0.32	0.34	0.30	0.31	0.36	0.24	0.22	0.28	0.54	0.48	0.17
MgO	16.00	17.40	15.82	15.59	15.46	15.57	16.02	15.55	16.34	17.06	16.22	14.38	14.19	13.83	13.92	13.92	14.24	14.22	14.15	13.37	14.09	13.81	12.98	14.41
CaO	20.23	23.31	20.70	22.48	21.89	22.21	20.78	22.20	20.44	23.78	23.81	23.00	22.87	23.30	22.39	22.98	22.63	21.72	23.13	22.94	23.04	22.79	22.42	22.14
K_2O	0.01	0.02	0.00	0.01	0.01	0.01	0.01	0.01	0.02	0.01	0.01	0.00	0.00	0.01	0.00	0.00	0.00	0.00	0.00	0.00	0.00	0.00	0.01	0.00
Na_2O	0.45	0.22	0.54	0.32	0.36	0.37	0.41	0.35	0.36	0.30	0.22	0.43	0.42	0.39	0.42	0.39	0.39	0.41	0.44	0.44	0.41	0.44	0.53	0.39
NiO	0.04	0.00	0.00	0.06	0.00	0.02	0.00	0.06	0.03	0.01	0.00	0.02	0.01	0.00	0.00	0.04	0.01	0.00	0.02	0.00	0.00	0.04	0.00	0.00
Cr2O3	0.00	0.56	0.12	0.09	0.11	0.05	0.00	0.07	0.00	0.34	0.21	0.04	0.08	0.07	0.08	0.04	0.08	0.06	0.11	0.03	0.01	0.04	0.00	0.07
Total	100.11	99.91	99.76	100.16	99.98	99.99	99.59	99.67	100.27	100.59	100.49	100.35	100.25	100.33	99.70	100.07	100.07	99.11	100.47	98.76	100.10	100.50	99.48	100.15
Si (6 O)	1.916	1.952	1.878	1.879	1.874	1.887	1.893	1.868	1.906	1.919	1.882	1.875	1.871	1.854	1.873	1.861	1.877	1.897	1.870	1.847	1.857	1.961	1.895	1.824
Ti	0.012	0.002	0.014	0.010	0.012	0.011	0.014	0.010	0.012	0.006	0.007	0.003	0.004	0.004	0.004	0.004	0.004	0.003	0.004	0.007	0.006	0.009	0.016	0.020
Al (T)	0.084	0.048	0.122	0.121	0.126	0.113	0.107	0.132	0.094	0.063	0.118	0.125	0.129	0.146	0.127	0.139	0.123	0.103	0.130	0.153	0.143	0.039	0.105	0.176
Al (M1)	0.001	0.001	0.023	0.026	0.037	0.014	0.006	0.022	0.005	0.000	0.012	0.031	0.043	0.041	0.062	0.043	0.049	0.067	0.040	0.055	0.046	0.036	0.058	0.038
Fe^{3+} (T)	0.000	0.000	0.000	0.000	0.000	0.000	0.000	0.000	0.000	0.017	0.000	0.000	0.000	0.000	0.000	0.000	0.000	0.000	0.000	0.000	0.000	0.000	0.000	0.000
Fe^{3+} (M1)	0.092	0.044	0.107	0.095	0.087	0.102	0.104	0.113	0.092	0.080	0.101	0.117	0.107	0.124	0.085	0.114	0.091	0.058	0.111	0.114	0.113	0.016	0.052	0.125
Fe^{2+}	0.174	0.063	0.122	0.102	0.121	0.111	0.136	0.092	0.156	0.035	0.048	0.112	0.125	0.111	0.149	0.123	0.138	0.173	0.117	0.118	0.113	0.224	0.199	0.117
Mn	0.011	0.003	0.008	0.005	0.005	0.006	0.008	0.004	0.011	0.002	0.002	0.010	0.009	0.010	0.011	0.009	0.010	0.011	0.007	0.007	0.009	0.017	0.015	0.005
Mg	0.878	0.945	0.868	0.852	0.847	0.853	0.882	0.853	0.894	0.922	0.880	0.788	0.779	0.760	0.769	0.767	0.783	0.790	0.775	0.746	0.774	0.761	0.723	0.792
Ca	0.798	0.910	0.816	0.883	0.862	0.875	0.822	0.876	0.804	0.923	0.928	0.906	0.902	0.920	0.889	0.909	0.895	0.867	0.910	0.920	0.910	0.903	0.897	0.874
K	0.000	0.001	0.000	0.000	0.000	0.000	0.000	0.001	0.001	0.000	0.000	0.000	0.000	0.001	0.000	0.000	0.000	0.000	0.000	0.000	0.000	0.000	0.000	0.000
Na	0.032	0.016	0.039	0.023	0.026	0.026	0.029	0.025	0.026	0.021	0.016	0.031	0.030	0.028	0.030	0.028	0.028	0.029	0.032	0.032	0.029	0.032	0.038	0.028
Ni	0.001	0.000	0.000	0.002	0.000	0.000	0.000	0.002	0.001	0.000	0.000	0.000	0.000	0.000	0.000	0.001	0.000	0.000	0.001	0.000	0.000	0.001	0.000	0.000
Cr	0.000	0.016	0.004	0.003	0.003	0.002	0.000	0.002	0.000	0.010	0.006	0.001	0.002	0.002	0.002	0.001	0.002	0.002	0.003	0.001	0.000	0.001	0.000	0.002
Total	4.000	4.000	4.000	4.000	4.000	4.000	4.000	4.000	4.000	4.000	4.000	4.000	4.000	4.000	4.000	4.000	4.000	4.000	4.000	4.000	4.000	4.000	4.000	4.000
Crystal #	4	8	8	9	9	9	9																	11
Comments																								
Enstatite %	45	48	45	44	44	44	45	44	46	47	45	41	41	39	40	40	41	42	40	39	40	40	38	41
Ferrosillite %	14	6	12	10	11	11	13	11	13	7	8	12	12	13	13	13	12	13	12	13	12	13	14	13
Wollastonite %	41	46	42	46	45	45	42	45	41	47	47	47	47	48	47	47	47	46	47	48	47	47	48	46
Adjective		chromian	aluminian ferrian	aluminian	aluminian	aluminian ferrian	aluminian ferrian	aluminian ferrian			aluminian ferrian	aluminian ferrian	aluminian ferrian	aluminian ferrian	aluminian	aluminian ferrian	aluminian	aluminian	aluminian ferrian	aluminian ferrian	aluminian ferrian		aluminian	aluminian ferrian
Pyroxene	augite	diopside	augite	diopside	augite	augite	augite	diopside	augite	diopside	diopside	diopside	diopside	diopside	diopside	diopside	diopside	diopside	diopside	diopside	diopside	diopside	diopside	diopside

Sample	SV19	SV19	SV19	SV19	SV19	SV19	SV19	SV19	SV19	SV19	SV19	SV19	SV19
Rock Type	MUG	MUG	MUG	MUG	MUG	MUG	MUG	MUG	MUG	MUG	MUG	MUG	MUG
Analysis	05-042	05-045	05-046	05-054	05-055	05-056	05-057	05-058	05-059	05-060	05-065	05-066	05-067
SiO_2	51.08	50.65	51.84	50.15	52.68	51.85	52.30	51.69	51.35	51.56	49.98	50.44	50.97
TiO_2	0.59	0.63	0.52	0.67	0.15	0.43	0.31	0.53	0.52	0.32	0.73	0.62	0.49
Al_2O_3	3.04	3.64	2.33	3.64	1.39	2.69	2.21	2.54	2.93	3.16	4.37	3.85	3.23
FeO	7.82	7.88	8.07	8.15	7.05	6.15	5.69	7.41	7.95	6.18	7.13	7.44	7.84
MnO	0.24	0.26	0.32	0.22	0.40	0.17	0.15	0.21	0.24	0.18	0.12	0.21	0.21
MgO	15.64	15.36	16.11	14.97	15.14	16.09	16.57	15.84	15.32	15.99	14.50	15.03	15.07
CaO	21.46	21.55	20.11	21.27	22.90	22.41	22.83	21.32	21.31	22.44	23.13	22.02	21.71
K_2O	0.00	0.00	0.00	0.01	0.00	0.00	0.00	0.00	0.01	0.00	0.01	0.00	0.00
Na_2O	0.42	0.43	0.54	0.46	0.45	0.22	0.17	0.38	0.48	0.25	0.31	0.39	0.47
NiO	0.03	0.00	0.00	0.01	0.00	0.01	0.01	0.00	0.06	0.04	0.03	0.00	0.00
Cr2O3	0.00	0.11	0.00	0.00	0.02	0.03	0.12	0.00	0.03	0.11	0.02	0.00	0.03
Total	100.32	100.50	99.84	99.56	100.17	100.06	100.35	99.92	100.17	100.21	100.31	100.00	100.03
Si (6 O)	1.874	1.857	1.909	1.858	1.939	1.901	1.909	1.903	1.890	1.887	1.838	1.858	1.878
Ti	0.016	0.017	0.014	0.019	0.004	0.012	0.009	0.015	0.014	0.009	0.020	0.017	0.014
Al (T)	0.126	0.143	0.091	0.142	0.060	0.099	0.091	0.097	0.110	0.113	0.162	0.142	0.122
Al (M1)	0.006	0.014	0.011	0.017	0.000	0.017	0.004	0.013	0.017	0.023	0.027	0.025	0.019
Fe^{3+} (T)	0.000	0.000	0.000	0.000	0.000	0.000	0.000	0.000	0.000	0.000	0.000	0.000	0.000
Fe^{3+} (M1)	0.117	0.121	0.090	0.121	0.084	0.072	0.079	0.081	0.099	0.087	0.117	0.111	0.109
Fe^{2+}	0.122	0.120	0.159	0.132	0.133	0.116	0.094	0.147	0.146	0.102	0.102	0.118	0.133
Mn	0.008	0.008	0.010	0.007	0.013	0.005	0.004	0.007	0.007	0.006	0.004	0.007	0.006
Mg	0.856	0.839	0.885	0.827	0.831	0.879	0.902	0.869	0.840	0.872	0.795	0.825	0.828
Ca	0.844	0.847	0.793	0.844	0.903	0.880	0.893	0.841	0.840	0.880	0.911	0.869	0.857
K	0.000	0.000	0.000	0.000	0.000	0.000	0.000	0.000	0.000	0.000	0.000	0.000	0.000
Na	0.030	0.030	0.038	0.033	0.032	0.016	0.012	0.027	0.034	0.017	0.022	0.028	0.034
Ni	0.001	0.000	0.000	0.000	0.000	0.000	0.000	0.000	0.002	0.001	0.001	0.000	0.000
Cr	0.000	0.003	0.000	0.000	0.000	0.001	0.003	0.000	0.001	0.003	0.001	0.000	0.001
Total	4.000	4.000	4.000	4.000	4.000	4.000	4.000	4.000	4.000	4.000	4.000	4.000	4.000
Crystal #	11	12	12	13	13	13	13	13	13	13	14	14	15
Comments													
Enstatite %	44	43	46	43	42	45	46	45	43	45	41	43	43
Ferrosillite %	13	13	13	13	12	10	9	12	13	10	12	12	13
Wollastonite %	43	44	41	44	46	45	45	43	43	45	47	45	44
Adjective	aluminian ferrian	aluminian ferrian	aluminian	aluminian ferrian		aluminian		aluminian	aluminian	aluminian	aluminian ferrian	aluminian ferrian	aluminian ferrian
Pyroxene	augite	augite	augite	augite	diopside	diopside	diopside	augite	augite	diopside	diopside	diopside	augite

Sample	SV19	SV19	SV19	SV19	SV19	SV19	SV19	SV19	SV19	SV19	SV19	SV19	SV19
Rock Type	MUG	MUG	MUG	MUG	MUG	MUG	MUG	MUG	MUG	MUG	MUG	MUG	MUG
Analysis	05-068	05-069	05-070	05-071	05-072	05-073	05-076	05-077	05-043	05-044	05-049	05-050	05-052
SiO_2	50.54	51.18	50.16	49.73	52.60	49.64	52.23	51.13	50.22	50.82	52.68	50.50	51.77
TiO_2	0.39	0.34	0.72	0.72	0.19	0.81	0.32	0.55	0.77	0.62	0.39	0.51	0.43
Al_2O_3	3.91	3.30	3.82	4.12	1.87	3.95	2.23	3.31	3.93	3.06	1.73	4.10	2.33
FeO	7.81	5.65	8.14	7.68	5.03	8.40	6.68	7.63	7.70	7.98	7.06	7.64	7.89
MnO	0.28	0.15	0.23	0.21	0.19	0.27	0.35	0.25	0.34	0.26	0.38	0.24	0.32
MgO	14.18	15.80	14.93	14.40	16.33	14.68	16.22	15.43	14.96	15.26	16.77	15.05	15.97
CaO	22.54	23.33	21.38	21.68	22.93	21.27	21.51	20.92	21.50	21.45	20.66	21.94	20.98
K_2O	0.00	0.01	0.00	0.00	0.00	0.00	0.00	0.01	0.00	0.00	0.00	0.01	0.01
Na_2O	0.46	0.25	0.45	0.46	0.35	0.52	0.35	0.39	0.46	0.47	0.39	0.40	0.39
NiO	0.00	0.08	0.01	0.02	0.01	0.02	0.02	0.02	0.00	0.01	0.04	0.00	0.01
Cr2O3	0.01	0.24	0.02	0.01	0.80	0.02	0.00	0.05	0.00	0.05	0.02	0.01	0.00
Total	100.11	100.33	99.86	99.03	100.29	99.57	99.90	99.68	99.88	99.97	100.11	100.40	100.10
Si (6 O)	1.865	1.870	1.853	1.853	1.921	1.841	1.918	1.889	1.853	1.874	1.930	1.852	1.904
Ti	0.011	0.009	0.020	0.020	0.005	0.022	0.009	0.015	0.021	0.017	0.011	0.014	0.012
Al (T)	0.135	0.130	0.147	0.147	0.079	0.159	0.082	0.111	0.147	0.126	0.070	0.148	0.096
Al (M1)	0.035	0.012	0.020	0.034	0.001	0.014	0.015	0.033	0.024	0.007	0.005	0.030	0.005
Fe^{3+} (T)	0.000	0.000	0.000	0.000	0.000	0.000	0.000	0.000	0.000	0.000	0.000	0.000	0.000
Fe^{3+} (M1)	0.111	0.111	0.118	0.106	0.069	0.138	0.074	0.075	0.113	0.117	0.071	0.118	0.096
Fe^{2+}	0.130	0.061	0.133	0.133	0.085	0.123	0.131	0.161	0.124	0.129	0.145	0.116	0.147
Mn	0.009	0.005	0.007	0.007	0.006	0.008	0.011	0.008	0.011	0.008	0.012	0.007	0.010
Mg	0.780	0.861	0.822	0.800	0.889	0.811	0.888	0.850	0.823	0.839	0.916	0.823	0.876
Ca	0.891	0.913	0.846	0.866	0.897	0.845	0.847	0.828	0.850	0.847	0.811	0.862	0.827
K	0.000	0.001	0.000	0.000	0.000	0.000	0.000	0.000	0.000	0.000	0.000	0.001	0.000
Na	0.033	0.018	0.032	0.033	0.024	0.038	0.025	0.028	0.033	0.034	0.028	0.028	0.028
Ni	0.000	0.002	0.000	0.001	0.000	0.000	0.001	0.000	0.000	0.000	0.001	0.000	0.000
Cr	0.000	0.007	0.001	0.000	0.023	0.001	0.000	0.001	0.000	0.002	0.001	0.000	0.000
Total	4.000	4.000	4.000	4.000	4.000	4.000	4.000	4.000	4.000	4.000	4.000	4.000	4.000
Crystal #	15	15	15	15	16	16	17	17					
Comments													
Enstatite %	41	44	43	42	46	42	46	44	43	43	47	43	45
Ferrosillite %	13	9	13	13	8	14	11	13	13	13	12	13	13
Wollastonite %	46	47	44	45	46	44	43	43	44	44	41	45	42
Adjective	aluminian ferrian	aluminian ferrian	aluminian ferrian	aluminian ferrian	chromian	aluminian ferrian		aluminian	aluminian ferrian	aluminian ferrian		aluminian ferrian	aluminian
Pyroxene	diopside	diopside	augite	diopside	diopside	augite	augite	augite	augite	augite	augite	augite	augite

Sample	SV19	SV19	SV19	SV19	SV19	SV19	SV19	SV19	SV20	SV20	SV20	SV20	SV20	SV20	SV20	SV20	SV20	SV20	SV20	SV20	SV20	SV20	SV45	SV45	SV45
Rock Type	MUG	MUG	MUG	MUG	MUG	MUG	MUG	MUG	MUG	MUG	MUG	MUG	MUG	MUG	MUG	MUG	MUG	MUG	MUG	MUG	MUG	MUG		MUG	MUG
Analysis	05-053	05-061	05-062	05-074	05-075	05-078	05-079	05-080	05-087	05-094	05-095	05-089	05-097	05-098	05-099	05-100	05-102	05-103	05-109	05-110	05-111	05-112	11-065	11-074	11-075
SiO_2	50.64	52.02	50.80	51.11	50.36	49.72	51.43	51.25	49.00	52.34	51.66	52.19	51.92	52.08	52.23	51.55	51.86	51.54	51.58	50.91	51.85	50.64	50.74	51.01	50.63
TiO_2	0.51	0.48	0.65	0.33	0.36	0.96	0.35	0.51	0.30	0.33	0.34	0.21	0.31	0.37	0.28	0.47	0.37	0.55	0.40	0.55	0.33	0.52	0.61	0.66	0.76
Al_2O_3	3.42	2.41	3.12	2.94	3.55	3.78	3.14	2.82	2.27	2.52	2.80	2.43	2.17	2.46	2.30	2.75	2.56	3.04	2.92	3.69	2.66	3.84	3.08	3.87	4.11
FeO	7.43	7.32	7.69	7.26	6.92	8.74	5.32	7.42	7.00	6.97	7.95	7.47	7.21	6.97	7.19	7.14	6.75	7.29	6.96	7.28	7.56	7.49	8.52	7.61	7.99
MnO	0.23	0.40	0.23	0.26	0.15	0.26	0.11	0.23	0.39	0.35	0.36	0.32	0.39	0.37	0.44	0.37	0.33	0.32	0.27	0.30	0.31	0.31	0.26	0.23	0.23
MgO	15.45	16.07	15.10	14.89	15.02	14.77	16.03	15.79	14.44	15.34	14.18	14.91	13.67	15.39	15.25	15.75	15.52	15.43	15.40	14.73	14.88	14.30	15.38	14.71	14.37
CaO	21.76	21.11	21.71	22.01	22.22	20.94	23.17	21.45	21.98	22.53	22.98	22.59	22.91	22.46	22.29	21.92	22.14	21.99	22.54	22.72	22.61	22.58	20.62	21.25	20.75
K_2O	0.01	0.01	0.01	0.02	0.00	0.00	0.03	0.00	0.00	0.02	0.00	0.00	0.00	0.01	0.01	0.00	0.02	0.00	0.00	0.02	0.00	0.01	0.03	0.00	0.02
Na_2O	0.47	0.51	0.45	0.49	0.29	0.54	0.22	0.38	0.40	0.47	0.53	0.45	0.51	0.46	0.51	0.44	0.41	0.44	0.32	0.43	0.45	0.47	0.38	0.45	0.49
NiO	0.00	0.00	0.00	0.03	0.04	0.00	0.00	0.00	0.05	0.01	0.00	0.00	0.01	0.02	0.03	0.00	0.00	0.00	0.03	0.00	0.00	0.02	0.00	0.00	0.01
Cr2O3	0.00	0.00	0.00	0.03	0.02	0.00	0.25	0.00	0.00	0.00	0.02	0.02	0.02	0.00	0.02	0.00	0.04	0.00	0.00	0.01	0.03	0.01	0.00	0.00	0.03
Total	99.91	100.34	99.75	99.38	98.93	99.72	100.04	99.85	95.81	100.88	100.81	100.57	99.12	100.57	100.54	100.38	100.00	100.60	100.42	100.63	100.68	100.18	99.63	99.79	99.38
Si (6 O)	1.863	1.904	1.877	1.894	1.873	1.842	1.882	1.888	1.885	1.910	1.896	1.915	1.941	1.906	1.914	1.888	1.907	1.886	1.891	1.865	1.901	1.866	1.880	1.886	1.883
Ti	0.014	0.013	0.018	0.009	0.010	0.027	0.010	0.014	0.009	0.009	0.009	0.006	0.009	0.010	0.008	0.013	0.010	0.015	0.011	0.015	0.009	0.014	0.017	0.018	0.021
Al (T)	0.137	0.096	0.123	0.106	0.127	0.158	0.118	0.112	0.103	0.090	0.104	0.085	0.059	0.094	0.086	0.112	0.093	0.114	0.109	0.135	0.099	0.134	0.120	0.114	0.117
Al (M1)	0.011	0.008	0.013	0.023	0.029	0.008	0.017	0.010	0.000	0.018	0.017	0.020	0.036	0.012	0.013	0.006	0.018	0.017	0.017	0.025	0.016	0.033	0.014	0.054	0.063
Fe^{3+} (T)	0.000	0.000	0.000	0.000	0.000	0.000	0.000	0.000	0.012	0.000	0.000	0.000	0.000	0.000	0.000	0.000	0.000	0.000	0.000	0.000	0.000	0.000	0.000	0.000	0.000
Fe^{3+} (M1)	0.132	0.098	0.106	0.100	0.098	0.135	0.091	0.101	0.127	0.089	0.105	0.086	0.041	0.095	0.094	0.112	0.084	0.099	0.093	0.112	0.096	0.106	0.101	0.056	0.048
Fe^{2+}	0.097	0.126	0.132	0.125	0.117	0.136	0.072	0.127	0.086	0.124	0.139	0.143	0.184	0.118	0.126	0.107	0.124	0.124	0.120	0.111	0.136	0.125	0.163	0.179	0.201
Mn	0.007	0.012	0.007	0.008	0.005	0.008	0.003	0.007	0.013	0.011	0.011	0.010	0.012	0.011	0.014	0.011	0.010	0.010	0.008	0.009	0.010	0.010	0.008	0.007	0.007
Mg	0.847	0.877	0.832	0.823	0.833	0.816	0.875	0.867	0.828	0.834	0.776	0.815	0.762	0.839	0.833	0.860	0.851	0.842	0.841	0.805	0.813	0.786	0.849	0.811	0.797
Ca	0.858	0.828	0.860	0.874	0.886	0.832	0.909	0.846	0.906	0.881	0.904	0.888	0.917	0.881	0.875	0.860	0.872	0.862	0.885	0.892	0.888	0.892	0.818	0.842	0.827
K	0.000	0.001	0.000	0.001	0.000	0.000	0.001	0.000	0.000	0.001	0.000	0.000	0.000	0.001	0.000	0.000	0.001	0.000	0.000	0.001	0.000	0.000	0.001	0.000	0.001
Na	0.034	0.036	0.032	0.035	0.021	0.039	0.015	0.027	0.029	0.033	0.038	0.032	0.037	0.032	0.036	0.031	0.029	0.031	0.023	0.030	0.032	0.034	0.028	0.032	0.035
Ni	0.000	0.000	0.000	0.001	0.001	0.000	0.000	0.000	0.001	0.000	0.000	0.000	0.000	0.001	0.001	0.000	0.000	0.000	0.001	0.000	0.000	0.000	0.000	0.000	0.000
Cr	0.000	0.000	0.000	0.001	0.000	0.000	0.007	0.000	0.000	0.000	0.000	0.000	0.001	0.000	0.000	0.000	0.001	0.000	0.000	0.000	0.001	0.000	0.000	0.000	0.001
Total	4.000	4.000	4.000	4.000	4.000	4.000	4.000	4.000	4.000	4.000	4.000	4.000	4.000	4.000	4.000	4.000	4.000	4.000	4.000	4.000	4.000	4.000	4.000	4.000	4.000
Crystal #									18	20	20													10	10
Comments																								Rim	
Enstatite %	44	45	43	43	43	42	45	44	42	43	40	42	40	43	43	44	44	43	43	42	42	41	44	43	42
Ferrosillite %	12	12	13	12	11	14	9	12	12	12	13	12	12	12	12	12	11	12	11	12	12	13	14	13	14
Wollastonite %	44	43	44	45	46	43	47	43	46	45	47	46	48	45	45	44	45	45	45	46	46	46	42	44	44
Adjective	aluminian ferrian	aluminian	aluminian ferrian	aluminian ferrian	aluminian	aluminian ferrian	aluminian	aluminian ferrian	aluminian ferrian	aluminian	aluminian ferrian	aluminian		aluminian		aluminian ferrian	aluminian	aluminian	aluminian	aluminian ferrian	aluminian	aluminian ferrian	aluminian ferrian	aluminian	aluminian
Pyroxene	augite	augite	augite	diopside	diopside	augite	diopside	augite	diopside	diopside	diopside	diopside	diopside	diopside	diopside	augite	augite	augite	diopside	diopside	diopside	diopside	augite	augite	augite

Sample	SV45	SV45	SV45	SV45	SV45	SV45	SV45	SV45	SV45	SV45	SV45	SV45	SV45	SV45	SV45	SV158	SV158	SV158	SV158	SV158	SV158	SV158	SV165	SV165	SV165
Rock Type	MUG	MUG	MUG	MUG	MUG	MUG	MUG	MUG	MUG	MUG	MUG	MUG	MUG	MUG	MUG		XEN	XEN	XEN	XEN	XEN	XEN			
Analysis	11-076	11-077	11-078	11-079	11-087	11-088	11-096	11-097	11-098	11-099	11-104	11-111	11-112	11-113	11-117	12-083	12-104	12-106	12-107	12-108	12-110	12-113	07-005	07-014	07-029
SiO_2	51.30	42.14	50.27	54.13	52.95	45.80	43.01	51.64	53.37	51.46	51.37	50.29	51.13	52.74	51.59	53.30	52.13	52.00	51.57	51.59	52.12	52.37	51.44	51.88	51.53
TiO_2	0.73	0.66	0.75	0.46	0.43	0.57	0.90	0.48	0.23	0.74	0.71	0.61	0.67	0.33	0.52	0.26	0.34	0.39	0.43	0.43	0.34	0.36	0.36	0.26	0.27
Al_2O_3	3.51	4.00	4.23	8.76	2.50	2.79	8.08	3.44	1.20	3.16	3.16	3.46	3.70	2.45	3.38	1.96	3.00	3.01	3.20	3.10	2.87	2.66	2.71	1.93	1.59
FeO	7.78	7.63	7.73	4.84	6.42	7.05	6.19	7.26	7.47	7.48	7.84	6.75	7.43	5.74	6.34	4.68	5.31	5.23	5.22	5.33	5.33	5.10	8.24	9.55	7.11
MnO	0.27	0.18	0.21	0.11	0.25	0.24	0.15	0.28	0.39	0.26	0.25	0.17	0.25	0.26	0.19	0.10	0.10	0.12	0.11	0.14	0.13	0.07	0.31	0.81	0.38
MgO	15.02	10.96	14.36	10.07	15.96	13.14	7.15	14.81	15.74	15.00	15.10	14.62	14.83	15.97	14.83	15.32	15.49	15.42	15.18	15.20	15.40	15.29	13.49	12.90	14.26
CaO	21.02	18.21	21.54	15.51	21.39	20.29	13.98	21.81	21.38	21.30	21.19	21.30	21.09	21.99	22.59	24.28	22.86	23.07	23.19	23.35	23.03	23.38	23.53	23.15	22.65
K_2O	0.01	0.06	0.00	1.36	0.01	0.05	0.89	0.03	0.01	0.00	0.01	0.01	0.02	0.00	0.00	0.00	0.00	0.01	0.00	0.00	0.00	0.00	0.02	0.00	0.01
Na_2O	0.44	0.56	0.49	2.21	0.44	0.51	1.10	0.44	0.46	0.46	0.46	0.45	0.44	0.37	0.41	0.23	0.25	0.28	0.26	0.26	0.23	0.25	0.45	0.42	0.41
NiO	0.00	0.00	0.00	0.00	0.04	0.00	0.00	0.00	0.01	0.00	0.02	0.02	0.03	0.02	0.00	0.00	0.03	0.00	0.01	0.00	0.01	0.00	0.00	0.02	0.01
Cr2O3	0.01	0.05	0.00	0.11	0.15	0.00	0.01	0.04	0.06	0.04	0.00	0.22	0.02	0.23	0.04	0.05	0.09	0.19	0.24	0.13	0.23	0.15	0.05	0.01	0.03
Total	100.08	84.44	99.58	97.55	100.54	90.44	81.47	100.21	100.32	99.90	100.11	97.89	99.59	100.09	99.88	100.17	99.59	99.71	99.40	99.52	99.70	99.62	100.59	100.90	98.24
Si (6 O)	1.891	1.854	1.864	2.030	1.934	1.869	1.968	1.900	1.961	1.900	1.893	1.892	1.893	1.933	1.901	1.954	1.920	1.913	1.905	1.903	1.920	1.930	1.900	1.924	1.940
Ti	0.020	0.022	0.021	0.013	0.012	0.017	0.031	0.013	0.006	0.020	0.020	0.017	0.019	0.009	0.014	0.007	0.009	0.011	0.012	0.012	0.009	0.010	0.010	0.007	0.008
Al (T)	0.109	0.146	0.136	0.000	0.066	0.131	0.032	0.100	0.039	0.100	0.107	0.108	0.107	0.067	0.099	0.046	0.080	0.087	0.095	0.097	0.080	0.070	0.100	0.076	0.060
Al (M1)	0.044	0.061	0.048	0.387	0.041	0.004	0.403	0.049	0.013	0.038	0.031	0.046	0.055	0.038	0.048	0.038	0.050	0.044	0.044	0.038	0.044	0.046	0.017	0.008	0.011
Fe^{3+} (T)	0.000	0.000	0.000	0.000	0.000	0.000	0.000	0.000	0.000	0.000	0.000	0.000	0.000	0.000	0.000	0.000	0.000	0.000	0.000	0.000	0.000	0.000	0.000	0.000	0.000
Fe^{3+} (M1)	0.056	0.091	0.082	0.000	0.028	0.135	0.000	0.057	0.044	0.053	0.070	0.054	0.047	0.030	0.051	0.009	0.027	0.035	0.039	0.050	0.027	0.018	0.095	0.084	0.063
Fe^{2+}	0.183	0.190	0.158	0.152	0.168	0.106	0.237	0.167	0.185	0.178	0.172	0.158	0.184	0.145	0.145	0.135	0.136	0.126	0.122	0.115	0.137	0.139	0.159	0.212	0.160
Mn	0.008	0.007	0.007	0.003	0.008	0.008	0.006	0.009	0.012	0.008	0.008	0.005	0.008	0.008	0.006	0.003	0.003	0.004	0.004	0.004	0.004	0.002	0.010	0.025	0.012
Mg	0.826	0.719	0.794	0.563	0.869	0.800	0.487	0.812	0.862	0.826	0.829	0.820	0.818	0.872	0.814	0.837	0.851	0.846	0.836	0.836	0.846	0.840	0.743	0.713	0.800
Ca	0.830	0.858	0.856	0.623	0.837	0.887	0.685	0.860	0.842	0.843	0.837	0.859	0.837	0.863	0.892	0.954	0.902	0.910	0.918	0.923	0.909	0.923	0.931	0.920	0.914
K	0.000	0.003	0.000	0.065	0.000	0.002	0.052	0.001	0.000	0.000	0.000	0.001	0.001	0.000	0.000	0.000	0.000	0.000	0.000	0.000	0.000	0.000	0.001	0.000	0.001
Na	0.032	0.048	0.035	0.161	0.031	0.041	0.097	0.032	0.033	0.033	0.033	0.033	0.032	0.026	0.029	0.016	0.018	0.020	0.019	0.018	0.017	0.018	0.033	0.030	0.030
Ni	0.000	0.000	0.000	0.000	0.001	0.000	0.000	0.000	0.000	0.000	0.001	0.001	0.001	0.001	0.000	0.000	0.001	0.000	0.000	0.000	0.000	0.000	0.000	0.000	0.000
Cr	0.000	0.002	0.000	0.003	0.004	0.000	0.001	0.001	0.002	0.001	0.000	0.006	0.001	0.007	0.001	0.001	0.003	0.005	0.007	0.004	0.007	0.004	0.001	0.000	0.001
Total	4.000	4.000	4.000	4.000	4.000	4.000	4.000	4.000	4.000	4.000	4.000	4.000	4.000	4.000	4.000	4.000	4.000	4.000	4.000	4.000	4.000	4.000	4.000	4.000	4.000
Crystal #	10	10																12	12	12					
Comments		Core																							
Enstatite %	43	39	42	42	46	41	34	43	44	43	43	43	43	45	43	43	44	44	44	43	44	44	38	36	41
Ferrosillite %	13	15	13	12	11	13	17	12	12	13	13	11	13	10	11	8	9	9	9	9	9	8	14	16	12
Wollastonite %	44	46	45	46	44	46	48	45	43	44	44	45	44	45	47	49	47	47	48	48	47	48	48	47	47
Adjective	aluminian	aluminian	aluminian	aluminian sodian	aluminian	aluminian ferrian	aluminian	aluminian		aluminian	aluminian	aluminian	aluminian	aluminian	aluminian		aluminian	aluminian	aluminian	aluminian	aluminian	aluminian	aluminian		
Pyroxene	augite	diopside	diopside	diopside	augite	diopside	diopside	diopside	augite	augite	augite	diopside	augite	augite	diopside	diopside	diopside	diopside	diopside	diopside	diopside	diopside	diopside	diopside	diopside

Sample	SV165	SV165	SV165	SV165	SV165	SV165	SV165	SV165	SV165	SV165	SV165	SV165	SV165	SV165	SV165	SV165	SV165	SV176	SV176	SV176	SV176	SV183	SV183	SV183	SV183
Rock Type		XEN	XEN	XEN	XEN	XEN	XEN	XEN	XEN	XEN	XEN	XEN	XEN	XEN	XEN	XEN	XEN					XEN	XEN	XEN	XEN
Analysis	07-031	07-037	07-038	07-039	07-040	07-042	07-044	07-045	07-046	07-047	07-048	07-049	07-052	07-054	07-055	07-057	07-059	07-117	07-118	07-119	07-120	07-087	07-091	07-092	07-094
SiO_2	52.75	52.16	53.45	51.59	52.94	53.62	53.80	53.28	52.33	53.79	54.19	53.31	54.09	54.33	54.16	53.93	53.67	53.22	53.35	51.44	53.08	53.37	52.36	51.63	51.01
TiO_2	0.24	0.17	0.09	0.14	0.10	0.04	0.06	0.00	0.15	0.03	0.04	0.04	0.00	0.05	0.07	0.00	0.04	0.06	0.10	0.08	0.00	0.04	0.13	0.18	0.13
Al_2O_3	1.53	2.93	1.51	2.47	1.99	2.37	1.71	1.66	2.87	1.15	1.38	1.67	0.74	1.28	1.01	1.55	1.53	1.49	1.52	3.64	1.08	1.16	2.43	3.61	2.63
FeO	7.28	5.87	5.01	5.41	3.87	2.67	2.55	3.86	3.29	4.25	3.59	4.80	3.85	5.73	3.96	3.97	4.79	3.12	3.75	5.69	5.58	6.45	3.88	5.23	4.22
MnO	0.42	0.17	0.22	0.19	0.14	0.11	0.13	0.12	0.09	0.20	0.13	0.18	0.09	0.19	0.11	0.21	0.16	0.08	0.11	0.25	0.22	0.44	0.08	0.18	0.21
MgO	15.02	16.84	16.52	16.33	16.40	17.65	17.63	17.15	17.66	17.30	17.99	17.64	18.11	20.77	17.65	17.55	17.33	17.27	16.39	13.44	15.51	15.27	16.02	16.85	15.79
CaO	23.23	21.25	23.79	21.89	24.19	23.97	24.98	22.92	21.30	23.01	23.30	22.60	22.72	18.17	22.84	22.61	22.57	23.92	23.82	21.47	24.05	23.15	25.18	21.52	23.72
K_2O	0.01	0.02	0.00	0.01	0.01	0.00	0.00	0.04	0.05	0.01	0.01	0.00	0.00	0.02	0.01	0.01	0.00	0.00	0.00	0.04	0.00	0.02	0.01	0.01	0.01
Na_2O	0.46	0.76	0.29	0.48	0.27	0.11	0.12	0.52	0.57	0.31	0.27	0.26	0.20	0.30	0.26	0.29	0.35	0.24	0.35	0.39	0.40	0.46	0.13	0.62	0.32
NiO	0.01	0.08	0.04	0.06	0.00	0.03	0.02	0.03	0.01	0.02	0.07	0.01	0.00	0.02	0.00	0.01	0.03	0.00	0.01	0.03	0.08	0.03	0.02	0.00	0.00
Cr2O3	0.00	0.58	0.31	0.46	0.48	0.66	0.28	0.47	0.75	0.89	0.42	0.41	0.27	0.13	0.36	0.49	0.17	0.83	0.93	0.02	0.00	0.05	0.05	0.11	0.13
Total	100.95	100.83	101.22	99.01	100.40	101.23	101.27	100.05	99.07	100.95	101.38	100.92	100.07	100.98	100.44	100.60	100.63	100.23	100.33	96.48	100.01	100.43	100.28	99.93	98.17
Si (6 O)	1.929	1.885	1.933	1.903	1.925	1.923	1.928	1.935	1.910	1.944	1.941	1.924	1.963	1.941	1.962	1.951	1.943	1.932	1.943	1.966	1.949	1.957	1.907	1.877	1.896
Ti	0.007	0.005	0.002	0.004	0.003	0.001	0.002	0.000	0.004	0.001	0.001	0.001	0.000	0.001	0.002	0.000	0.001	0.002	0.003	0.002	0.000	0.001	0.003	0.005	0.004
Al (T)	0.066	0.115	0.064	0.097	0.075	0.077	0.072	0.065	0.090	0.049	0.058	0.071	0.032	0.054	0.038	0.049	0.057	0.064	0.057	0.034	0.047	0.043	0.093	0.123	0.104
Al (M1)	0.000	0.010	0.000	0.010	0.011	0.023	0.000	0.006	0.034	0.000	0.000	0.000	0.000	0.000	0.006	0.017	0.008	0.000	0.008	0.130	0.000	0.007	0.012	0.032	0.012
Fe^{3+} (T)	0.005	0.000	0.003	0.000	0.000	0.000	0.000	0.000	0.000	0.007	0.000	0.005	0.005	0.005	0.000	0.000	0.000	0.004	0.000	0.000	0.004	0.000	0.000	0.000	0.000
Fe^{3+} (M1)	0.091	0.135	0.074	0.100	0.064	0.040	0.068	0.084	0.069	0.051	0.064	0.081	0.044	0.075	0.036	0.039	0.066	0.058	0.041	0.000	0.080	0.066	0.082	0.122	0.104
Fe^{2+}	0.127	0.043	0.075	0.067	0.054	0.041	0.008	0.033	0.032	0.070	0.044	0.060	0.068	0.091	0.084	0.080	0.080	0.032	0.073	0.182	0.087	0.132	0.036	0.037	0.027
Mn	0.013	0.005	0.007	0.006	0.004	0.003	0.004	0.004	0.003	0.006	0.004	0.005	0.003	0.006	0.003	0.006	0.005	0.002	0.003	0.008	0.007	0.014	0.003	0.006	0.006
Mg	0.819	0.907	0.890	0.898	0.889	0.944	0.942	0.929	0.961	0.932	0.961	0.949	0.980	1.106	0.953	0.946	0.935	0.935	0.890	0.766	0.849	0.835	0.870	0.913	0.875
Ca	0.910	0.823	0.922	0.865	0.942	0.921	0.959	0.892	0.833	0.891	0.894	0.874	0.884	0.695	0.887	0.876	0.876	0.930	0.930	0.879	0.946	0.909	0.983	0.838	0.945
K	0.000	0.001	0.000	0.000	0.001	0.000	0.000	0.002	0.002	0.001	0.000	0.000	0.000	0.001	0.001	0.000	0.000	0.000	0.000	0.002	0.000	0.001	0.001	0.000	0.000
Na	0.033	0.053	0.020	0.034	0.019	0.007	0.008	0.036	0.040	0.022	0.018	0.018	0.014	0.021	0.018	0.020	0.024	0.017	0.025	0.029	0.029	0.033	0.009	0.044	0.023
Ni	0.000	0.002	0.001	0.002	0.000	0.001	0.001	0.001	0.000	0.000	0.002	0.000	0.000	0.000	0.000	0.000	0.001	0.000	0.000	0.001	0.002	0.001	0.000	0.000	0.000
Cr	0.000	0.016	0.009	0.014	0.014	0.019	0.008	0.013	0.022	0.025	0.012	0.012	0.008	0.004	0.010	0.014	0.005	0.024	0.027	0.001	0.000	0.001	0.001	0.003	0.004
Total	4.000	4.000	4.000	4.000	4.000	4.000	4.000	4.000	4.000	4.000	4.000	4.000	4.000	4.000	4.000	4.000	4.000	4.000	4.000	4.000	4.000	4.000	4.000	4.000	4.000
Crystal #																						6			
Comments																									
Enstatite %	42	47	45	46	46	48	48	48	51	48	49	48	49	56	49	49	48	48	46	42	43	43	44	48	45
Ferrosillite %	12	10	8	9	6	4	4	6	5	7	6	8	6	9	6	6	8	5	6	10	9	11	6	9	7
Wollastonite %	46	43	47	45	48	47	48	46	44	46	45	44	45	35	45	45	45	47	48	48	48	47	50	44	48
Adjective		aluminian chromian ferrian		aluminian chromian	chromian	aluminian chromian		chromian	aluminian chromian	chromian	chromian	chromian			chromian	chromian		chromian	chromian	aluminian			aluminian	aluminian ferrian	aluminian ferrian
Pyroxene	diopside	augite	diopside	augite	diopside	diopside	diopside	diopside	augite	diopside	diopside	augite	augite	augite	diopside	augite	augite	diopside	diopside	diopside	diopside	diopside	diopside	augite	diopside

I.5 Biotite

Sample	SV2	SV2	SV2	SV2	SV2	SV2	SV38	SV38	SV38	SV39	SV39	SV39	SV39	SV40	SV40	SV40
Rock Type	XEN	XEN	XEN	XEN	XEN	XEN	TRAC	TRAC	TRAC	TRAC	TRAC	TRAC	TRAC	TRAC	TRAC	TRAC
Analysis	01 -048	01 -049	01 -050	01 -051	02-024	02-077	03-107	03-108	03-109	12-007	12-013	12-018	12-040	11-007	11-027	11-030
SiO_2	37.12	37.58	38.19	37.38	36.87	37.22	36.66	36.64	36.73	37.66	36.80	38.85	45.89	36.42	37.28	48.83
TiO_2	2.40	1.76	2.54	1.87	3.23	2.14	2.67	2.61	2.49	4.08	2.59	4.03	2.04	2.74	2.47	2.67
Al_2O_3	14.10	14.49	13.27	14.87	13.54	15.59	14.77	15.30	15.08	13.12	15.39	12.94	18.86	15.97	14.20	14.41
Cr_2O_3	0.00	0.02	0.07	0.01	0.02	0.00	0.00	0.00	0.02	0.04	0.00	0.00	0.00	0.03	0.00	0.00
FeO	13.99	13.06	13.80	13.07	14.17	12.68	14.98	14.22	14.73	14.02	13.76	14.04	10.27	15.54	14.16	10.35
MnO	0.33	0.35	0.27	0.27	0.16	0.25	0.39	0.37	0.37	0.30	0.38	0.40	0.25	0.36	0.39	0.34
MgO	16.51	17.00	17.06	16.77	16.00	16.20	15.69	15.97	16.11	15.46	15.12	16.12	8.66	14.08	15.83	10.88
CaO	0.00	0.02	0.00	0.00	0.10	0.01	0.01	0.04	0.05	0.03	0.02	0.03	2.64	0.02	0.04	0.08
Na_2O	0.82	0.80	0.77	0.80	0.81	0.84	0.85	0.84	0.90	0.92	0.81	0.89	2.51	0.78	0.86	2.27
K_2O	8.90	8.63	8.87	8.59	8.67	8.73	8.44	7.87	8.01	8.76	8.78	8.94	6.25	9.04	9.12	8.22
NiO	0.02	0.06	0.03	0.04	0.05	0.00	0.01	0.04	0.00	0.01	0.00	0.00	0.03	0.01	0.01	0.00
F																
Cl																
Total	94.20	93.75	94.86	93.66	93.62	93.65	94.45	93.90	94.50	94.39	93.67	96.24	97.39	94.97	94.36	98.05
Si (24 O)	5.515	5.556	5.594	5.531	5.520	5.502	5.454	5.442	5.439	5.569	5.488	5.602	6.065	5.419	5.536	6.363
Ti	0.268	0.196	0.280	0.208	0.363	0.238	0.298	0.291	0.277	0.454	0.290	0.437	0.203	0.306	0.276	0.262
Al iv	2.470	2.444	2.291	2.469	2.390	2.498	2.546	2.558	2.561	2.287	2.512	2.200	1.935	2.581	2.464	1.637
Al vi	0.000	0.080	0.000	0.125	0.000	0.218	0.045	0.122	0.071	0.000	0.193	0.000	1.004	0.219	0.021	0.576
Cr	0.000	0.002	0.008	0.001	0.003	0.000	0.000	0.000	0.003	0.004	0.000	0.000	0.000	0.004	0.000	0.000
Fe_2	1.738	1.614	1.690	1.618	1.775	1.567	1.864	1.766	1.824	1.734	1.717	1.693	1.135	1.933	1.758	1.128
Mn	0.042	0.044	0.033	0.034	0.020	0.031	0.049	0.047	0.046	0.038	0.048	0.049	0.028	0.045	0.049	0.037
Mg	3.655	3.745	3.726	3.699	3.571	3.568	3.481	3.535	3.557	3.409	3.361	3.465	1.706	3.123	3.503	2.114
Ca	0.000	0.003	0.000	0.000	0.016	0.001	0.001	0.007	0.007	0.005	0.004	0.004	0.374	0.003	0.006	0.011
Na	0.236	0.230	0.218	0.230	0.234	0.242	0.246	0.243	0.260	0.263	0.233	0.249	0.644	0.224	0.246	0.574
K	1.687	1.626	1.658	1.620	1.657	1.646	1.602	1.491	1.514	1.652	1.670	1.645	1.053	1.716	1.728	1.367
Ni	0.002	0.007	0.003	0.004	0.006	0.000	0.001	0.004	0.000	0.001	0.000	0.000	0.003	0.001	0.002	0.000
F	0.000	0.000	0.000	0.000	0.000	0.000	0.000	0.000	0.000	0.000	0.000	0.000	0.000	0.000	0.000	0.000
Cl	0.000	0.000	0.000	0.000	0.000	0.000	0.000	0.000	0.000	0.000	0.000	0.000	0.000	0.000	0.000	0.000
Li	0.658	0.734	0.830	0.699	0.620	0.673	0.579	0.576	0.590	0.747	0.606	0.926	1.923	0.539	0.686	2.338
OH	4.000	4.000	4.000	4.000	4.000	4.000	4.000	4.000	4.000	4.000	4.000	4.000	4.000	4.000	4.000	4.000
Total	20.273	20.281	20.330	20.238	20.175	20.182	20.166	20.082	20.148	26.549	20.124	20.271	20.073	20.112	20.275	20.408
X location	9.237	10.302	15.871	15.761	15.884	18.175	61.250	61.416	61.416	72.398	69.698	67.742	67.159	15.078	13.475	13.496
Y location	71.869	71.894	66.879	65.911	49.292	62.344	54.439	54.439	54.584	54.345	54.606	57.177	63.322	71.353	74.140	74.835
Crystal #					2	6	6	6	6							
mgli	2.997	3.011	2.896	2.999	2.951	2.896	2.901	2.960	2.967	2.662	2.755	2.539	-0.218	2.584	2.818	-0.224
feal	2.048	1.773	2.004	1.734	2.158	1.618	2.166	1.982	2.076	2.226	1.862	2.179	0.362	2.065	2.063	0.851

Sample	SV40	SV40	SV40	SV40	SV40	SV40	SV40	SV44	SV44	SV44	SV44	SV44	SV183	SV183	SV183	SV183
Rock Type	TRAC	TRAC	TRAC	TRAC	TRAC	TRAC	TRAC	TRAC	TRAC	TRAC	TRAC	TRAC				
Analysis	11-052	08-065	08-066	08-067	08-068	08-069	08-070	09-085	09-087	09-097	09-101	09-117	07-062	07-063	07-064	07-067
SiO_2	42.41	38.29	38.25	38.30	38.68	39.19	38.71	37.93	37.36	39.05	37.49	36.54	37.58	36.39	36.12	37.55
TiO_2	1.43	3.90	3.91	3.89	3.80	3.92	3.84	3.00	4.08	4.02	4.00	2.45	3.49	3.34	3.88	3.67
Al_2O_3	12.85	13.37	13.37	13.38	12.87	12.78	12.85	14.67	13.12	12.77	13.20	15.47	13.42	13.57	12.57	13.38
Cr_2O_3	0.00	0.05	0.00	0.01	0.00	0.00	0.00	0.02	0.04	0.00	0.01	0.05	0.07	0.05	0.01	0.08
FeO	12.95	14.39	14.65	14.48	13.45	14.07	13.95	14.34	14.27	13.04	14.59	16.68	15.54	16.30	15.17	15.57
MnO	0.17	0.34	0.42	0.41	0.36	0.38	0.44	0.36	0.33	0.32	0.40	0.38	0.45	0.64	0.40	0.45
MgO	13.24	16.15	16.08	16.25	16.29	16.56	16.39	12.22	15.63	15.79	15.47	13.19	15.05	15.81	14.49	14.95
CaO	10.79	0.00	0.00	0.00	0.04	0.00	0.00	0.15	0.02	0.06	0.02	0.00	0.03	0.00	0.03	0.07
Na_2O	2.37	0.91	0.88	0.87	0.80	0.92	0.88	1.28	1.03	1.06	0.97	0.91	0.65	0.62	0.53	0.77
K_2O	1.03	9.05	9.07	9.07	8.78	9.10	9.07	8.42	8.86	8.84	9.00	9.08	8.28	7.55	8.73	8.38
NiO	0.00	0.03	0.04	0.05	0.00	0.03	0.06	0.00	0.07	0.00	0.04	0.02	0.02	0.03	0.00	0.03
F		0.21	0.04	0.38	0.48	0.27	0.58									
Cl		0.03	0.01	0.00	0.02	0.01	0.01									
Total	97.22	96.65	96.69	96.92	95.47	97.14	96.57	92.38	94.81	94.97	95.20	94.76	94.57	94.29	91.92	94.89
Si (24 O)	5.826	5.538	5.531	5.531	5.628	5.606	5.595	5.703	5.527	5.670	5.531	5.481	5.569	5.453	5.569	5.555
Ti	0.147	0.424	0.425	0.423	0.416	0.422	0.417	0.340	0.454	0.438	0.444	0.276	0.389	0.376	0.449	0.408
Al iv	2.080	2.280	2.279	2.277	2.207	2.155	2.189	2.297	2.287	2.186	2.296	2.519	2.344	2.396	2.285	2.333
Al vi	0.000	0.000	0.000	0.000	0.000	0.000	0.000	0.304	0.000	0.000	0.000	0.216	0.000	0.000	0.000	0.000
Cr	0.000	0.005	0.000	0.001	0.000	0.000	0.000	0.002	0.005	0.000	0.002	0.006	0.008	0.006	0.001	0.009
Fe_2	1.487	1.741	1.772	1.749	1.637	1.683	1.686	1.803	1.766	1.584	1.801	2.092	1.926	2.042	1.957	1.926
Mn	0.020	0.041	0.052	0.050	0.044	0.046	0.054	0.046	0.041	0.039	0.050	0.048	0.057	0.081	0.052	0.056
Mg	2.711	3.481	3.466	3.498	3.533	3.532	3.532	2.740	3.448	3.418	3.401	2.949	3.324	3.532	3.330	3.298
Ca	1.588	0.000	0.000	0.000	0.006	0.000	0.000	0.024	0.004	0.010	0.004	0.000	0.005	0.000	0.005	0.011
Na	0.630	0.255	0.246	0.242	0.225	0.255	0.246	0.373	0.294	0.299	0.277	0.264	0.186	0.179	0.158	0.220
K	0.181	1.670	1.674	1.670	1.630	1.661	1.673	1.615	1.673	1.638	1.693	1.737	1.566	1.444	1.718	1.582
Ni	0.000	0.004	0.004	0.005	0.000	0.004	0.007	0.000	0.008	0.000	0.004	0.002	0.002	0.004	0.000	0.003
F	0.000	0.097	0.016	0.173	0.220	0.120	0.263	0.000	0.000	0.000	0.000	0.000	0.000	0.000	0.000	0.000
Cl	0.000	0.008	0.002	0.000	0.004	0.003	0.003	0.000	0.000	0.000	0.000	0.000	0.000	0.000	0.000	0.000
Li	1.448	0.836	0.829	0.836	0.907	0.975	0.906	0.806	0.696	0.967	0.717	0.564	0.735	0.537	0.504	0.729
OH	4.000	3.895	3.981	3.827	3.776	3.877	3.734	4.000	4.000	4.000	4.000	4.000	4.000	4.000	4.000	4.000
Total	20.116	20.276	20.278	20.282	20.233	20.340	20.306	20.053	20.204	20.250	20.219	20.155	20.109	20.050	20.029	20.131
X location	8.483							66.942	64.793	63.999	65.136	69.800	37.905	38.062	38.200	38.583
Y location	66.785							60.501	61.551	65.774	66.540	64.648	44.470	44.470	44.481	44.473
Crystal #	7	10	10	10	10	10	10									
mgli	1.263	2.646	2.637	2.662	2.627	2.557	2.626	1.934	2.752	2.451	2.685	2.385	2.589	2.995	2.826	2.570
feal	1.654	2.207	2.249	2.222	2.097	2.151	2.158	1.885	2.262	2.062	2.295	2.200	2.372	2.500	2.458	2.391

Table I.5: Biotite electron microprobe data. Named according to the scheme of (Tischendorf et al., 2004). Stoichiometry calculated with spreadsheet designed by Jeremy Preston, University of Aberdeen.

I.6 Iron oxides

Sample	SV2	SV2	SV2	SV2	SV2	SV10	SV10	SV12	SV12	SV12	SV17	SV17	SV17	SV17	SV17	SV39
Rock Type	XEN	XEN	XEN	XEN	TRAC	TRAC	TRAC	BEN	BEN	BEN	TRAC	TRAC	TRAC	TRAC	TRAC	TRAC
Analysis	01 -054	01 -053	01 -039	01 -041	02-097	09-080	09-045	12-073	12-072	12-049	09-026	09-027	09-012	09-002	09-028	12-014
SiO_2	0.00	0.00	0.01	0.01	0.04	0.03	0.05	0.00	0.00	0.05	0.00	0.01	0.03	0.03	0.04	0.00
TiO_2	2.29	2.90	3.71	3.82	3.98	4.77	4.57	1.84	9.27	4.65	4.99	0.39	6.14	5.84	4.07	2.51
Al_2O_3	2.25	1.49	0.73	0.65	0.78	1.02	0.91	1.10	0.61	0.65	0.88	1.31	0.76	1.27	1.06	0.89
Cr_2O_3	0.00	0.03	0.15	0.49	0.05	0.10	0.02	0.51	0.06	0.12	0.05	0.02	0.06	0.76	0.00	0.10
FeO	84.21	86.70	84.22	86.09	86.12	84.98	83.73	82.27	82.23	76.85	80.98	80.58	82.35	76.67	78.90	82.83
MnO	1.01	0.82	1.26	1.25	1.16	1.36	1.71	1.13	0.75	0.64	1.68	2.58	1.48	0.95	1.27	1.50
MgO	0.72	0.91	0.85	0.88	0.85	0.73	0.89	2.32	1.75	1.27	1.42	2.29	1.09	2.61	1.19	1.03
CaO	0.07	0.00	0.08	0.00	0.00	0.00	0.00	0.03	0.00	0.05	0.02	0.04	0.04	0.00	0.05	0.01	0.00
Na_2O	0.06	0.00	0.00	0.00	0.05	0.00	0.07	0.00	0.00	0.00	0.00	0.09	0.01	0.00	0.05	0.00
K_2O	0.00	0.00	0.02	0.01	0.00	0.00	0.00	0.00	0.02	0.00	0.00	0.00	0.00	0.01	0.02	0.02
NiO	0.00	0.07	0.00	0.00	0.04	0.06	0.00	0.01	0.00	0.00	0.02	0.00	0.01	0.00	0.00	0.00
Total	90.60	92.91	91.03	93.20	93.07	93.04	91.98	89.17	94.73	84.24	90.05	87.32	91.92	88.18	86.61	88.89
Fe_2O_3	59.9	61.4	59.1	60.3	60.0	58.0	57.9	61.7	51.2	52.4	56.0	63.5	54.9	52.2	54.9	60.0
FeO	30.3	31.4	31.0	31.9	32.1	32.8	31.7	26.8	36.2	29.7	30.6	23.5	32.9	29.7	29.5	28.8
Total	96.6	99.1	97.0	99.2	99.1	98.8	97.8	95.3	99.9	89.5	95.7	93.7	97.4	93.4	92.1	94.9
X location	17.898	15.316	15.963	15.556	22.390	9.974	6.409	40.057	38.920	38.310	40.004	40.080	37.264	38.114	40.347	69.485
Y location	62.193	65.074	67.850	68.722	52.197	55.341	53.853	41.024	41.867	47.820	51.824	51.687	60.015	63.035	51.597	54.529
Crystal #																

Sample	SV39	SV39	SV39	SV39	SV40	SV40	SV40	SV40	SV40	SV40	SV44	SV44	SV44	SV44	SV45	SV45
Rock Type	TRAC	TRAC	TRAC	TRAC	XEN	XEN	XEN	TRAC	TRAC	TRAC	TRAC	TRAC	TRAC	TRAC	MUG	MUG
Analysis	12-028	12-006	12-019	12-039	11-019	11-020	11-018	11-028	11-012	11-029	09-124	09-123	09-122	09-111	11-114	11-094
SiO_2	0.00	0.00	0.02	0.04	0.00	0.04	0.09	0.01	0.06	0.47	0.03	0.09	0.22	0.00	0.00	0.03
TiO_2	3.66	4.19	4.75	3.04	0.78	0.75	0.83	0.76	0.57	0.63	4.03	4.04	4.00	3.95	6.82	7.16
Al_2O_3	0.90	0.92	0.89	0.94	1.04	0.95	0.99	0.61	0.39	0.38	0.76	0.71	0.71	0.67	4.27	4.28
Cr_2O_3	0.11	0.05	0.06	0.01	0.45	0.48	0.64	0.07	0.09	0.03	0.07	0.10	0.03	0.03	0.15	0.07
FeO	82.62	84.16	81.61	84.21	84.72	84.36	83.21	83.90	85.50	82.29	81.66	80.09	79.62	82.19	76.78	75.95
MnO	1.48	1.14	1.45	1.48	1.74	1.83	1.83	1.82	1.53	1.75	1.47	1.42	1.56	1.60	0.49	0.52
MgO	0.91	0.72	1.01	0.91	2.28	2.18	2.01	1.23	1.25	1.21	0.93	0.97	0.93	1.04	4.02	4.08
CaO	0.00	0.11	0.00	0.00	0.00	0.00	0.02	0.00	0.04	0.10	0.00	0.12	0.26	0.00	0.02	0.02
Na_2O	0.00	0.00	0.00	0.00	0.00	0.04	0.00	0.13	0.10	0.05	0.06	0.32	0.33	0.07	0.01	0.00
K_2O	0.00	0.02	0.03	0.00	0.00	0.01	0.02	0.01	0.04	0.06	0.00	0.00	0.02	0.04	0.00	0.01
NiO	0.03	0.00	0.02	0.02	0.02	0.03	0.00	0.03	0.00	0.03	0.00	0.01	0.00	0.00	0.02	0.03
Total	89.70	91.30	89.83	90.66	91.04	90.67	89.63	88.57	89.58	87.02	89.00	87.86	87.67	89.59	92.57	92.15
Fe_2O_3	58.1	58.2	56.0	60.1	65.3	65.0	63.7	63.8	65.1	62.1	57.0	55.9	55.5	57.9	51.2	50.2
FeO	30.3	31.8	31.2	30.1	25.9	25.9	25.9	26.5	26.9	26.4	30.4	29.8	29.6	30.1	30.7	30.8
Total	95.5	97.1	95.4	96.7	97.6	97.2	96.0	95.0	96.1	93.2	94.7	93.5	93.2	95.4	97.7	97.2
X location	66.993	72.208	67.192	67.265	15.850	15.722	15.686	13.464	14.608	13.322	71.787	71.758	71.758	69.579	73.243	63.028
Y location	60.484	54.507	57.165	62.539	73.240	73.404	73.240	74.945	71.960	74.836	64.794	64.794	64.794	68.688	67.503	67.285
Crystal #					4	4	4				13	13	13			

Sample	SV45	SV45	SV45	SV45	SV45	SV158	SV158	SV158	SV158	SV158	SV158	SV158	SV181	SV181	SV181	SV181
Rock Type	MUG	MUG	MUG	MUG	MUG						XEN	XEN	XEN	XEN	XEN	XEN
Analysis	11-089	11-066	11-110	11-073	11-119	12-097	12-095	12-093	12-096	12-094	12-112	12-120	10-047	10-046	10-048	10-045
SiO_2	0.09	0.11	0.15	0.27	0.38	0.00	0.04	0.04	0.04	0.05	0.00	0.00	0.05	0.06	0.06	0.11
TiO_2	6.00	4.96	6.97	6.37	6.82	4.11	4.17	3.49	3.98	3.99	4.09	3.87	4.07	3.94	3.98	4.04
Al_2O_3	5.88	3.49	4.43	5.12	4.66	0.61	0.59	0.69	0.64	0.67	3.48	5.29	2.53	2.58	2.60	2.64
Cr_2O_3	0.13	0.38	0.15	0.14	0.19	0.03	0.04	0.03	0.05	0.06	4.99	5.13	0.04	0.06	0.05	0.05
FeO	71.16	73.10	74.37	73.24	74.78	80.37	79.67	80.35	79.44	80.20	70.93	72.95	81.98	82.03	81.85	82.40
MnO	0.39	0.65	0.41	0.50	0.56	1.43	1.39	1.56	1.48	1.54	0.28	0.28	0.51	0.57	0.47	0.50
MgO	4.50	4.00	4.09	4.15	4.18	1.26	1.22	1.24	1.24	1.25	2.17	2.73	1.44	1.37	1.42	1.39
CaO	0.04	0.09	0.00	0.03	0.03	0.00	0.02	0.00	0.02	0.00	0.00	0.03	0.00	0.00	0.03	0.02
Na_2O	0.02	0.00	0.03	0.05	0.00	0.00	0.01	0.00	0.01	0.01	0.01	0.03	0.04	0.00	0.00	0.01
K_2O	0.00	0.04	0.00	0.00	0.02	0.02	0.00	0.00	0.00	0.00	0.01	0.00	0.03	0.02	0.02	0.00
NiO	0.06	0.03	0.00	0.06	0.05	0.00	0.01	0.00	0.00	0.06	0.05	0.07	0.01	0.00	0.06	0.00
Total	88.27	86.85	90.60	89.91	91.65	87.83	87.15	87.41	86.91	87.82	86.01	90.37	90.69	90.62	90.53	91.16
Fe_2O_3	47.7	51.3	48.9	48.5	49.1	56.5	55.8	57.3	55.9	56.5	46.6	48.2	56.2	56.3	56.1	56.3
FeO	28.2	27.0	30.4	29.6	30.6	29.6	29.5	28.8	29.1	29.4	29.0	29.6	31.4	31.4	31.4	31.7
Total	93.0	92.0	95.5	94.8	96.6	93.5	92.7	93.1	92.5	93.5	90.7	95.2	96.3	96.3	96.2	96.8
X location	62.111	69.874	70.773	69.396	69.020	12.593	12.593	12.593	12.593	12.593	5.975	3.497	30.865	30.865	30.865	30.865
Y location	66.516	61.729	68.398	63.388	65.631	44.167	44.167	44.167	44.167	44.167	50.854	70.713	55.134	55.134	55.134	55.134
Crystal #						10	10	10	10	10			6	6	6	6

Table I.6: Iron oxide electron microprobe data. Total for all analyses are low, as iron is displayed as FeO. Recalculation to Fe_2O_3 + FeO on a magnetite–ulvöspinel basis (Carmichael, 1967; shown on tables) does not consistently yield 100% totals. Possible explanations for this are:

1) The oxides are not pure magnetite, but maghemite;
2) Analyses were not tailored specifically towards oxide analyses, and the use of 10 μm beam may lead to the analysis of inhomogeneous surfaces (exsolution fabrics);
3) Important trace elements such as vanadium or zinc may be present, but were not included in the list of measured minerals.

Sample	SV181	SV181	SV181	SV181	SV181	SV181	SV181	SV181	SV181	SV181	SV181	SV181	SV181	SV181
Rock Type	XEN	XEN	XEN	XEN	XEN	XEN	XEN	XEN		XEN		XEN	XEN	
Analysis	10-049	10-009	10-010	10-036	10-087	10-018	10-032	10-017	10-113	10-068	10-102	10-089	10-093	10-125
SiO_2	0.14	0.00	0.09	0.00	0.00	0.00	0.00	0.04	0.06	0.11	0.16	0.19	0.22	0.31
TiO_2	3.93	4.04	4.15	4.14	1.88	4.26	4.01	4.17	5.87	4.01	3.32	3.82	1.82	4.71
Al_2O_3	2.59	2.68	2.78	2.69	2.92	2.43	2.35	2.70	1.07	2.22	0.99	2.68	2.74	0.84
Cr_2O_3	0.07	0.02	0.04	0.02	0.36	0.04	0.03	0.02	0.01	0.10	0.03	0.04	0.04	0.07
FeO	82.19	82.90	84.37	75.87	81.15	81.51	85.26	79.85	79.85	79.77	80.76	80.37	82.08	78.63
MnO	0.54	0.59	0.47	0.51	0.61	0.56	0.46	0.39	1.33	0.51	1.56	0.62	0.58	1.73
MgO	1.33	1.94	1.17	1.23	2.05	1.47	1.29	1.28	1.09	1.19	1.10	1.82	1.69	1.26
CaO	0.01	0.04	0.01	0.00	0.00	0.00	0.00	0.00	0.02	0.00	0.00	0.05	0.00	0.03
Na_2O	0.00	0.00	0.00	0.00	0.04	0.00	0.00	0.00	0.07	0.00	0.04	0.00	0.01	0.08
K_2O	0.00	0.02	0.01	0.00	0.01	0.00	0.02	0.00	0.00	0.01	0.02	0.01	0.00	0.00
NiO	0.00	0.00	0.02	0.00	0.00	0.05	0.01	0.09	0.00	0.06	0.00	0.00	0.00	0.01
Total	90.80	92.21	93.10	84.47	89.00	90.33	93.42	88.55	89.36	87.98	87.97	89.58	89.17	87.69
Fe_2O_3	56.2	57.7	57.3	51.3	59.1	55.8	58.6	54.1	53.1	54.3	57.2	55.6	59.2	53.9
FeO	31.6	31.0	32.8	29.7	27.9	31.3	32.5	31.2	32.0	30.9	29.3	30.3	28.8	30.1
Total	96.4	98.0	98.8	89.6	94.9	95.9	99.3	94.0	94.7	93.4	93.7	95.2	95.1	93.1
X location	30.865	18.618	18.879	28.121	46.233	17.547	26.212	20.982	9.266	43.770	2.638	42.853	55.149	2.879
Y location	55.134	57.807	57.943	55.178	52.610	53.852	54.724	56.718	68.845	51.500	60.527	60.254	60.301	71.221
Crystal #	6	1	1											

Appendix II: Sulphur chemistry and isotopes

II

II.1 Introduction

The isotopic composition and speciation of sulphur are important variables in hydrothermal systems, and for Savo provides a crucial tool for the determination of fluid sources. However, sulphur species can be metastable with respect to oxidation, resulting in the presence of sulphide (reduced) species alongside sulphates (oxidised), and care is required to ensure that samples for isotopic analysis represent the appropriate species only, rather than a mixture. In addition, samples can deteriorate over time due to bacterial action or exposure to the atmosphere, and unwanted fractionations can occur. The sampling methods and analytical techniques used can have significant influence on the final dataset. Techniques used and the results obtained are compared below.

II.2 Sampling and analytical techniques

Samples were collected and analysed as in Chapters 4 and 5.

II.3 Results

II.3.1 Sulphate content

Data from ICP-AES, IC and gravimetric calculation from recovered $BaSO_4$ are shown in Table II.1. Blanks for the procedures show that minimal contamination from preceding samples occurred.

Long term data for ICP-AES and IC analysed at the British geological Survey, Keyworth, are reviewed annually. Percentage uncertainty was better than 2.1% (ICP-AES; Table 4.2) and 4% (IC) for sulphate in the relevant analytical periods.

Comparison of the ICP-AES and IC data (Fig. II.1) show some deviation between the two (standard error of estimate on y = 101, excluding SV205 due to its disproportionate influence), particularly for alkaline hot springs and stream samples downstream of those springs collected in 2006, which show lower sulphate contents by IC than ICP-AES.

Comparison of IC and gravimetric data (Fig. II.2) shows scatter (standard error of estimate on y = 135), particularly amongst the 2006 samples from the Rembokola area.

Sample	Area	Type	AES	IC	GRAV
SV197	Lemboni	Well	58	61.6	27
SV198	Lemboni	Rain Tank	2	2.29	
SV199	Lemboni	Well	113	123	76
SV200	Lemboni	Well	103	113	73
SV201	Vutu.	Acid	332	362	307
SV202	Vutu.	Stream	97	106	40
SV203	Vutu.	Stream	98	108	63
SV204	Vutu.	Well	24	23.2	
SV205	Lemboni	Seawater	2576	2899	1649
SV206	Pogho.	Alk.	602	689	552
SV207	Pogho.	Alk.	623	684	657
SV208	Pogho.	Alk.	619	670	665
SV209	Pogho.	Acid	481	529	430
SV210	Pogho.	Stream	635	626	652
SV211	Pogho.	Cold	213	240	212
SV212	Reoka	Acid	342	373	267
SV213	Reoka	Acid	516	549	514
SV214	Reoka	Stream	258	287	239
SV215	Reoka	Stream	257	290	243
SV229	Remb.	Alk.	639	696	645
SV230	Remb.	Alk.	633	692	640
SV231	Remb.	Alk.	642	705	687
SV232	Remb.	Alk.	635	546	681
SV233	Remb.	Alk.	653	714	661
SV234	Remb.	Stream	698	763	
SV235	Remb.	Cold	107	118	112
SV250	Lemboni	Rain Tank	1	0.632	
SV377		Blank	0	<0.050	
SV378		Blank	0	<0.050	
SV379	Lemboni	Well	162	165	151
SV380	Remb.	Stream	739	824	756
SV410	Lemboni	Well	94	98.8	
SV411		Blank	0	0.146	
SV422	Tang.	Warm	294	333	292
SV428	Tang.	Stream	286	309	288
SV433	Tang.	Stream	268	304	
SV435	Vutu.	Acid	508	578	480
SV436	Vutu.	Acid	151	162	96
SV438	Tang.	Stream	266	298	241

Sample	Area	Type	AES	IC	GRAV
SV440	Tang.	Stream	190	199	195
SV443	Reoka	Stream	309	335	307
SV444	Reoka	Stream	308	341	327
SV446	Reoka	Stream	307	334	273
SV447	Reoka	Stream	309	339	306
SV449	Reoka	Acid	419	495	451
SV452	Reoka	Stream	284	318	269
SV453	Reoka	Acid	561	645	558
SV454	Reoka	Acid	247	278	243
SV457	Reoka	Stream	316	358	
SV458	Reoka	Acid	865	961	905
SV460	Reoka	Stream	311	344	273
SV462	Reoka	Stream	248	280	245
SV467	Remb.	Stream	713	799	718
SV469	Remb.	Stream	713	813	716
SV471	Remb.	Stream	717	822	757
SV473	Remb.	Stream	716	815	723
SV474	Remb.	Stream	715	415	735
SV476	Remb.	Stream	719	423	756
SV478	Remb.	Stream	711	439	739
SV480	Remb.	Stream	710	446	738
SV483	Remb.	Stream	696	443	
SV485	Remb.	Alk.	627	419	646
SV487	Remb.	Alk.	614	442	
SV488	Remb.	Alk.	643	464	674
SV489	Remb.	Stream	668	502	719
SV490	Remb.	Alk.	620	471	655
SV491	Remb.	Alk.	624	473	668
SV493	Remb.	Stream	684	539	775
SV496		Blank	0	0.196	
SV498	Pogho.	Alk.	681	522	689
SV499	Pogho.	Alk.	679	529	698
SV500	Pogho.	Alk.	669	530	702
SV503	Pogho.	Acid	817	650	871
SV515	Pogho.	Acid	774	628	845
SV516	Pogho.	Alk.	661	539	742
SV520	Pogho.	Cold	329	272	339
GR1	Gold Ridge	Warm	1119	888	1254

Table II.1: Sulphate content data, obtained by ICP-AES, IC, and calculated from gravimetric data for precipitated barium sulphate. All values in mg/l. Alk. = alkaline sulphate hot spring; Vutu. = Vutusuala; Pogho. = Poghorovorughala; Remb. = Rembokola. Gold Ridge spring is within the mining lease area on Guadalcanal.

ICP-AES and gravimetric data (Fig. II.3) compare very well (standard error of estimate on y = 26) excluding seawater.

The seawater sample (SV205) has lower gravimetric values compared to ICP-AES and IC.

II.3.2 Sulphur isotopes

Sulphur isotope data for samples and standards are shown on Tables II.2 and II.3. Data presented in Chapter 5 are averaged values of multiple analyses where appropriate. Detailed examination of the two seawater sulphate samples, NBS 127 (standard) and SV205 (sampled this study) shows an important relationship between SO_2 yield (measured after the combustion of the sample) and $\delta^{34}S$ value, with yields below 70% of the maximum possible SO_2 generally leading to lower than expected $\delta^{34}S$ values (Fig. II.4).

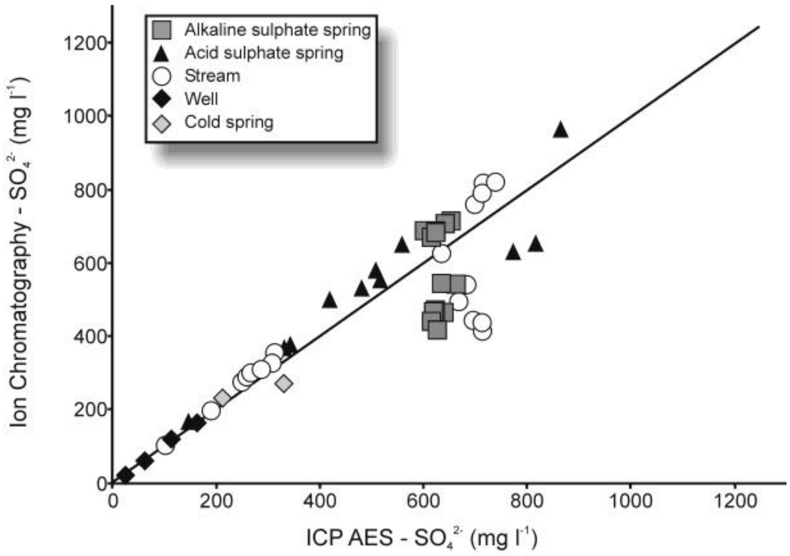

Fig. II.1: Sulphate content as determined by ICP-AES vs. IC. Seawater sample SV205 not shown.

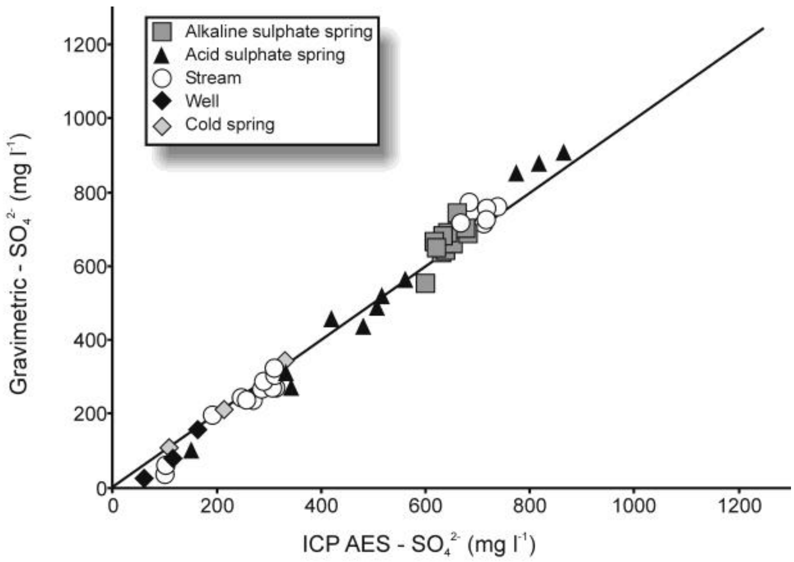

Fig. II 2: Sulphate content as determined by ICP-AES vs. calculated SO_4^{2-} from gravimetric analysis of precipitated $BaSO_4$. Seawater sample SV205 not shown.

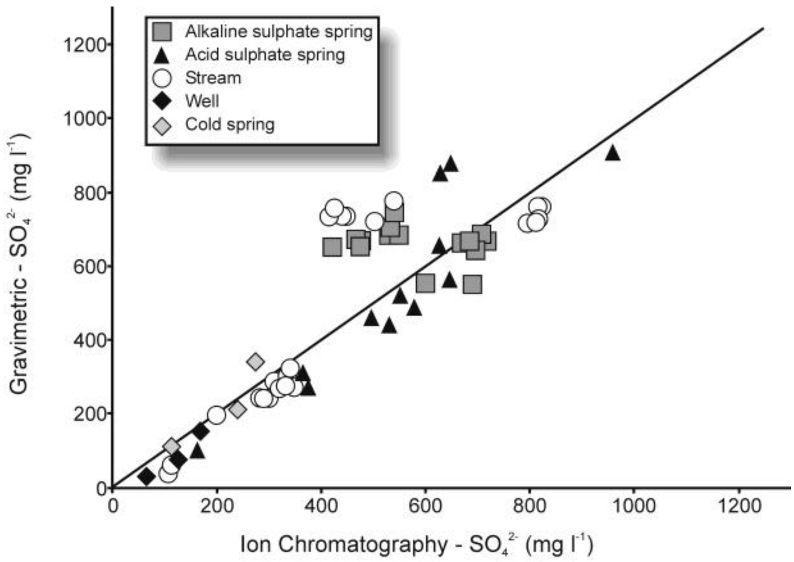

Fig. II 3: Sulphate content as determined by IC vs. calculated SO_4^{2-} from gravimetric analysis of precipitated $BaSO_4$. Seawater sample SV205 not shown.

Sample	Date	Mineral	Yield	δ^{34}S	Line #
CP1	08/09/05	$CuFeS_2$	89	−4.2	SA11127
CP1	23/11/05	$CuFeS_2$	93	−4.2	SA11195
CP1	28/11/05	$CuFeS_2$	99	−4.5	SA11209
CP1	03/02/06	$CuFeS_2$	101	−5.0	SA11304
CP1	06/02/06	$CuFeS_2$	98	−4.7	SA11307
CP1	07/02/06	$CuFeS_2$		−4.4	SA11317
CP1	23/01/07	$CuFeS_2$	84	−5.1	SA11662
CP1	25/01/07	$CuFeS_2$	112	−4.1	SA11673
CP1	26/01/07	$CuFeS_2$	111	−4.6	SA11681
CP1	30/01/07	$CuFeS_2$	112	−4.5	SA11694
CP1	30/01/07	$CuFeS_2$	95	−4.5	SA11696
CP1	19/03/07	$CuFeS_2$	103	−4.3	SA11748
CP1	19/03/07	$CuFeS_2$	88	−4.7	SA11749
CP1	21/03/07	$CuFeS_2$	84	−4.5	SA11761
CP1	22/03/07	$CuFeS_2$	99	−4.8	SA11773
CP1	22/03/07	$CuFeS_2$	91	−4.8	SA11774
CP1	28/03/07	$CuFeS_2$	94	−4.0	SA11794
CP1	21/05/07	$CuFeS_2$	92	−4.7	SA11828
CP1	21/05/07	$CuFeS_2$	95	−4.5	SA11829
CP1	24/05/07	$CuFeS_2$	100	−4.7	SA11844
CP1	17/09/07	$CuFeS_2$	87	−4.0	SA12042
CP1	17/09/07	$CuFeS_2$	74	−4.5	SA12045
CP1	18/09/07	$CuFeS_2$	77	−3.5	SA12053
CP1	02/02/07	$CuFeS_2$	88	−4.7	
GR	25/05/07	$BaSO_4$	64	18.9	SA11850
GR	25/09/07	$BaSO_4$	44	17.5	SA12061
IAEA S3	03/02/06	Ag_2S	101	−31.3	SA11303
IAEA S3	06/02/06	Ag_2S		−31.5	SA11309
IAEA S3	23/01/07	Ag_2S	96	−31.2	SA11661
IAEA S3	25/01/07	Ag_2S	97	−31.7	SA11670
IAEA S3	29/01/07	Ag_2S	100	−31.3	SA11684
IAEA S3	29/01/07	Ag_2S	105	−31.8	SA11685
IAEA S3	19/03/07	Ag_2S	99	−31.4	SA11750
IAEA S3	19/03/07	Ag_2S	87	−32.4	SA11751
IAEA S3	21/03/07	Ag_2S	90	−31.4	SA11762
IAEA S3	22/03/07	Ag_2S	100	−31.4	SA11771
IAEA S3	22/03/07	Ag_2S	92	−32.1	SA11772
IAEA S3	21/05/07	Ag_2S	94	−31.6	SA11830
IAEA S3	21/05/07	Ag_2S	97	−31.4	SA11831
IAEA S3	17/09/07	Ag_2S	93	−31.9	SA12043
IAEA S3	17/09/07	Ag_2S	98	−31.4	SA12046
IAEA S3	18/09/07	Ag_2S	102	−31.7	SA12055
NBS123	09/09/05	(Zn,Fe)S	101	16.9	SA11131
NBS123	06/02/06	(Zn,Fe)S	100	17.3	SA11308
NBS123	23/01/07	(Zn,Fe)S	102	17.2	SA11663
NBS123	30/01/07	(Zn,Fe)S	82	16.8	SA11695
NBS123	30/01/07	(Zn,Fe)S	99	17.3	SA11697
NBS123	19/03/07	(Zn,Fe)S	104	16.8	SA11752
NBS123	19/03/07	(Zn,Fe)S	100	17.8	SA11753
NBS123	20/03/07	(Zn,Fe)S	103	17.5	SA11760
NBS123	22/03/07	(Zn,Fe)S	97	17.2	SA11769
NBS123	22/03/07	(Zn,Fe)S	97	17.3	SA11770
NBS123	21/05/07	(Zn,Fe)S	101	17.1	SA11833
NBS123	21/05/07	(Zn,Fe)S	97	17.1	SA11834
NBS123	25/05/07	(Zn,Fe)S	104	17.1	SA11848
NBS123	17/09/07	(Zn,Fe)S	87	16.7	SA12044
NBS123	18/09/07	(Zn,Fe)S	94	17.0	SA12052
NBS123	18/09/07	(Zn,Fe)S	95	17.2	SA12054
NBS127	23/11/05	BaSO4	57	20.3	SA11198
NBS127	24/11/05	BaSO4	61	19.3	SA11203
NBS127	25/11/05	BaSO4	72	21.0	SA11207
NBS127	29/11/05	BaSO4	78	21.4	SA11217
NBS127	01/12/05	BaSO4	47	19.3	SA11223
NBS127	01/12/05	BaSO4	77	21.5	SA11225
NBS127	31/01/06	BaSO4	59	18.1	SA11285
NBS127	02/02/06	BaSO4	64	18.3	SA11297
NBS127	24/01/07	BaSO4	83	20.9	SA11664
NBS127	30/01/07	BaSO4	69	18.9	SA11691
NBS127	19/03/07	BaSO4	76	21.5	SA11754
NBS127	20/03/07	BaSO4	86	22.2	SA11755
NBS127	21/03/07	BaSO4	82	21.5	SA11767
NBS127	26/03/07	BaSO4	92	21.0	SA11778
NBS127	29/03/07	BaSO4	81	20.6	SA11803
NBS127	30/03/07	BaSO4	87	21.2	SA11807
NBS127	22/05/07	BaSO4	95	20.9	SA11839
NBS127	25/05/07	BaSO4	94	21.4	SA11851
NBS127	17/09/07	BaSO4	59	20.6	SA12047
NBS127	18/09/07	$BaSO_4$	61	20.6	SA12051
NBS127	19/09/07	$BaSO_4$	81	22.5	SA12056
NBS127	19/09/07	$BaSO_4$	89	21.1	SA12057
NBS127	19/09/07	$BaSO_4$	87	21.4	SA12058A
NBS127	25/09/07	$BaSO_4$	79	21.3	SA12064
SV131	21/11/05	S	86	−1.9	SA11182
SV133	21/11/05	S	96	−5.4	SA11184
SV201	06/09/05	$BaSO_4$	67	-4.6	SA11116
SV201	22/11/05	$BaSO_4$	59	-2.9	SA11191
SV201	23/11/05	$BaSO_4$	54	-3.0	SA11197
SV202	06/09/05	$BaSO_4$	53	1.2	SA11117
SV203	07/09/05	$BaSO_4$	65	2.5	SA11121
SV205	07/09/05	$BaSO_4$	63	19.8	SA11123
SV205	02/12/05	$BaSO_4$	51	20.8	SA111230
SV205	22/11/05	$BaSO_4$	79	21.1	SA11192
SV205	23/11/05	$BaSO_4$	66	21.2	SA11200
SV205	25/11/05	$BaSO_4$	100	22.1	SA11205
SV206	07/09/05	$BaSO_4$	74	5.0	SA11125
SV206	29/11/05	$BaSO_4$	63	5.2	SA11219
SV207	05/09/05	$BaSO_4$	30	3.6	SA11111
SV207	29/11/05	$BaSO_4$	73	6.3	SA11216
SV207	01/12/05	$BaSO_4$	60	5.1	SA11222
SV207	21/03/07	$BaSO_4$	65	5.6	SA11764
SV207	26/03/07	$BaSO_4$	80	6.0	SA11782
SV208	07/09/05	$BaSO_4$	65	3.7	SA11119
SV208	22/11/05	$BaSO_4$	68	4.6	SA11190
SV208	23/11/05	$BaSO_4$	55	4.6	SA11196
SV208	21/03/07	$BaSO_4$	102	5.0	SA11765
SV208	27/03/07	$BaSO_4$	80	3.8	SA11785
SV209	06/09/05	$BaSO_4$	74	0.3	SA11113
SV209	28/11/05	$BaSO_4$	61	0.8	SA11212
SV209	21/03/07	$BaSO_4$	45	-1.5	SA11766
SV209	22/03/07	$BaSO_4$	64	1.1	SA11768
SV210	07/09/05	$BaSO_4$	56	3.6	SA11124
SV210	28/11/05	$BaSO_4$	62	3.5	SA11213
SV211	07/09/05	$BaSO_4$	78	4.5	SA11120
SV211	01/12/05	$BaSO_4$	74	5.4	SA11224
SV212	09/09/05	$BaSO_4$	69	-3.1	SA11135
SV212	28/11/05	$BaSO_4$	56	-2.1	SA11211
SV212	29/11/05	$BaSO_4$	65	-2.3	SA11218
SV213	06/09/05	$BaSO_4$	83	-3.0	SA11112
SV213	25/11/05	$BaSO_4$	68	-2.8	SA11208
SV214	29/11/05	$BaSO_4$	63	2.6	SA111220
SV214	09/09/05	$BaSO_4$	59	2.5	SA11133
SV215	08/09/05	$BaSO_4$	68	2.5	SA11129
SV215	22/11/05	$BaSO_4$	67	2.8	SA11194
SV215	23/11/05	$BaSO_4$	82	3.0	SA11199
SV216	09/09/05	S	95	−3.9	SA11138
SV216	21/11/05	S	81	−4.3	SA11183
SV216	21/11/05	S	45	−5.1	SA11185
SV216	22/11/05	S	98	−4.5	SA11188
SV217	09/09/05	S	99	−5.6	SA11134
SV229	08/09/05	$BaSO_4$	69	4.8	SA11130
SV229	28/11/05	$BaSO_4$	73	6.1	SA11210
SV229	29/11/05	$BaSO_4$	59	5.3	SA11215
SV229	02/12/05	$BaSO_4$	85	5.6	SA11227
SV230	08/09/05	$BaSO_4$	87	5.0	SA11128
SV230	02/12/05	$BaSO_4$	54	5.5	SA11228
SV230	23/03/07	$BaSO_4$	75	5.1	SA11775
SV231	09/09/05	$BaSO_4$	80	5.7	SA11139
SV231	28/11/05	$BaSO_4$	63	4.9	SA11214
SV231	02/12/05	$BaSO_4$	53	3.9	SA11229
SV231	23/03/07	$BaSO_4$	64	4.6	SA11776
SV231	27/03/07	$BaSO_4$	79	5.7	SA11789
SV232	08/09/05	$BaSO_4$	73	5.1	SA11126
SV232	22/11/05	$BaSO_4$	75	5.6	SA11189
SV232	22/11/05	$BaSO_4$	42	5.7	SA11193
SV233	09/09/05	$BaSO_4$	83	5.4	SA11132
SV233	25/11/05	$BaSO_4$	77	5.9	SA11206
SV237	21/11/05	S	74	−6.1	SA11181
SV237	21/11/05	S	94	−5.5	SA11186

Table II.2: Sulphur isotope data. All δ^{34}S values presented in standard notation, compared to V-CDT. Yield is percentage of maximum possible SO_2 generated by combustion of sample.

Sample	Date	Mineral	Yield	$\delta^{34}S$	Line #
SV237	21/11/05	S	96	−6.2	SA11187
SV368	29/01/07	$CaSO_4$	77	7.6	SA11689
SV380	30/01/07	$BaSO_4$	46	5.7	SA11693
SV380	31/01/07	$BaSO_4$	50	4.8	SA11699
SV380	20/02/07	$BaSO_4$	70	3.6	
SV40	27/09/07	$BaSO_4$	29	6.5	SA12068
SV40	27/09/07	$BaSO_4$	72	8.6	SA12069
SV40	27/09/07	$BaSO_4$	83	7.8	SA12070
SV40	27/09/07	$BaSO_4$	76	8.0	SA12071
SV422	31/01/07	$BaSO_4$	53	5.0	SA11698
SV422	20/03/07	$BaSO_4$	89	6.1	SA11757
SV422	17/09/07	$BaSO_4$	67	6.0	SA12048
SV428	22/05/07	$BaSO_4$	65	4.8	SA11835
SV433	22/05/07	$BaSO_4$	73	14.8	SA11836
SV433	18/09/07	$BaSO_4$	37	4.5	SA12049
SV435	26/03/07	$BaSO_4$	79	−2.4	SA11783
SV435	27/03/07	$BaSO_4$	59	−4.5	SA11792
SV435		$BaSO_4$	77	−4.1	SA11808
SV436	24/05/07	$BaSO_4$	86	-4.2	SA11846
SV435	22/05/07	$BaSO_4$	41	-2.4	SA11837
SV435	24/05/07	$BaSO_4$	86	-4.2	SA11846
SV436	22/05/07	$BaSO_4$	41	-2.4	SA11837
SV438	22/05/07	$BaSO_4$	48	1.1	SA11838
SV440	22/05/07	$BaSO_4$	75	5.3	SA11840
SV443	22/05/07	$BaSO_4$	61	1.8	SA11841
SV443	24/05/07	$BaSO_4$	63	2.0	SA11845
SV444	23/05/07	$BaSO_4$	60	2.4	SA11842
SV444	25/09/07	$BaSO_4$	56	-0.5	SA12063
SV446	24/05/07	$BaSO_4$	78	2.9	SA11843
SV447	27/03/07	$BaSO_4$	73	2.8	SA11786
SV449	29/01/07	$BaSO_4$	56	1.9	SA11687
SV449	20/03/07	$BaSO_4$	66	2.8	SA11759
SV449	01/02/07	$BaSO_4$	76	2.8	
SV452	24/05/07	$BaSO_4$	75	3.1	SA11847
SV453	26/03/07	$BaSO_4$	76	1.3	SA11784
SV454	29/01/07	$BaSO_4$	56	3.7	SA11690
SV454	18/09/07	$BaSO_4$		-4.6	SA12050
SV457	27/03/07	$BaSO_4$	84	2.8	SA11787
SV458	29/01/07	$BaSO_4$	62	-2.3	SA11686
SV458	25/05/07	$BaSO_4$	75	-0.8	SA11849
SV458	02/02/07	$BaSO_4$	88	-1.3	
SV460	25/05/07	$BaSO_4$	77	0.6	SA11852
SV462	02/02/07	$BaSO_4$	73	3.7	
SV467	28/03/07	$BaSO_4$	70	4.9	SA11796
SV467	29/03/07	$BaSO_4$	81	6.1	SA11804
SV469	28/03/07	$BaSO_4$	87	5.7	SA11797
SV471	28/03/07	$BaSO_4$	75	5.7	SA11798
SV473	28/03/07	$BaSO_4$	86	6.2	SA11799
SV474	29/03/07	$BaSO_4$	79	5.7	SA11802
SV476	25/09/07	$BaSO_4$	61	5.6	SA12062
SV478	24/01/07	$BaSO_4$	76	5.9	SA11665
SV480	24/01/07	$BaSO_4$	82	5.6	SA11666
SV483	24/01/07	$BaSO_4$	72	5.8	SA11669
SV485	24/01/07	$BaSO_4$	86	5.8	SA11668
SV487	25/01/07	$BaSO_4$	73	5.2	SA11671
SV488	25/01/07	$BaSO_4$	72	5.8	SA11672
SV489	26/01/07	$BaSO_4$	60	5.4	SA11677
SV489	21/03/07	$BaSO_4$	78	5.9	SA11763
SV490	26/03/07	$BaSO_4$	64	5.7	SA11779
SV490	27/03/07	$BaSO_4$	76	6.2	SA11788
SV490	20/09/07	$BaSO_4$	47	4.9	SA12058B
SV490	26/09/07	$BaSO_4$	79	5.5	SA12067
SV491	26/01/07	$BaSO_4$	48	5.5	SA11678
SV491	20/09/07	$BaSO_4$	63	4.9	SA12059
SV491	20/02/07	$BaSO_4$	73	5.2	
SV493	26/03/07	$BaSO_4$	72	6.3	SA11780
SV493	28/03/07	$BaSO_4$	68	5.0	SA11793
SV498	26/01/07	$BaSO_4$	49	6.1	SA11679
SV498	20/03/07	$BaSO_4$	57	6.5	SA11756
SV498	20/03/07	$BaSO_4$	89	6.8	SA11758
SV498	20/09/07	$BaSO_4$	75	8.3	SA12060
SV499	26/01/07	$BaSO_4$	60	5.9	SA11680
SV499	30/03/07	$BaSO_4$	60	6.2	SA11806
SV499	02/02/07	$BaSO_4$	68	5.8	
SV500	25/01/07	$BaSO_4$	70	6.2	SA11676
SV500	30/01/07	$BaSO_4$	49	7.2	SA11692
SV500	01/02/07	$BaSO_4$	69	5.9	SA11701
SV500	20/02/07	$BaSO_4$	75	5.4	
SV503	25/01/07	$BaSO_4$	80	2.0	SA11674
SV503	25/01/07	$BaSO_4$	71	1.9	SA11675
SV503	01/02/07	$BaSO_4$	71	2.0	
SV515	26/03/07	$BaSO_4$	81	1.3	SA11781
SV515	27/03/07	$BaSO_4$	70	0.3	SA11790
SV515		$BaSO_4$	75	−0.2	SA11809
SV515	26/05/07	$BaSO_4$	83	−2.2	SA11853
SV516	23/03/07	$BaSO_4$	69	−1.5	SA11777
SV516	27/03/07	$BaSO_4$	72	5.2	SA11791
SV516	26/09/07	$BaSO_4$	84	3.4	SA12065
SV520	29/03/07	$BaSO_4$	47	1.6	SA11801
SV520	30/03/07	$BaSO_4$	77	5.0	SA11805
SV520	26/09/07	$BaSO_4$	75	4.9	SA12066

Table II.2: contd.

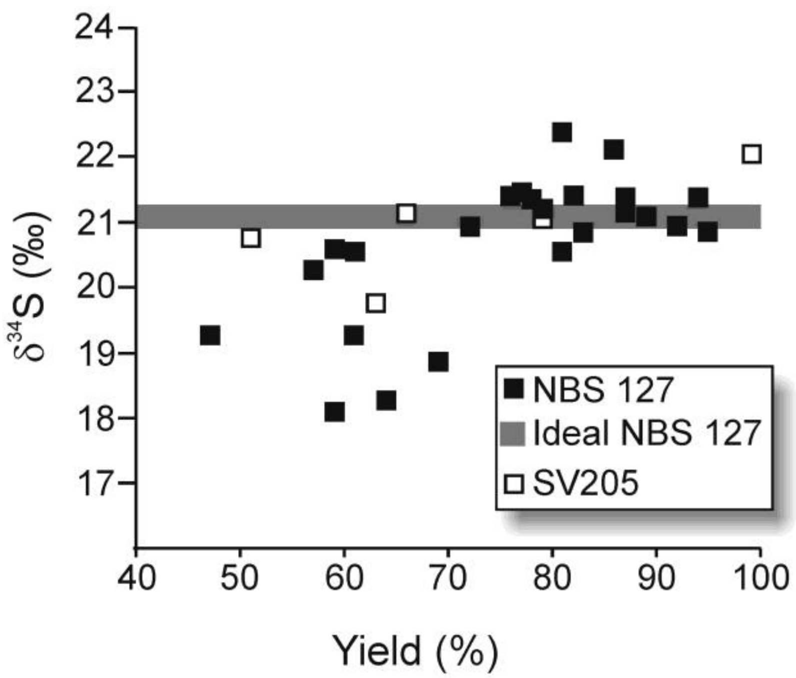

Fig. II.4: $\delta^{34}S$ of seawater sulphate samples NBS 127 and SV205 vs. SO_2 yield, as determined after combustion of sulphate sample. Ideal values shown for reference. Yields below 70% typically produce lower than expected $\delta^{34}S$ values.

Standard	This study	1σ	N	Accepted Value	Reference
CP-1	−4.6	0.7	24	−4.6	Lipfert et al. 2007
IAEA S3	−31.6	0.3	16	−31.5	Lipfert et al. 2007
NBS 123	17.7	0.3	16	17.4	Coplen et al. 2002
NBS 127	21.2	0.8	17	21.1	Coplen et al. 2002

Table II.3: Sulphur isotope standard data, excluding single calibration samples and those with low or anomalous yields. All numbers in standard notation, $\delta^{34}S_{V\text{-}CDT}$. 1σ is one standard deviation. N is number of analyses.

II.4 Discussion

II.4.1 Sulphate content

ICP-AES is the most reliable method of analysing sulphate (at total sulphur) content of the fluids. Blanks show evidence of little cross contamination between samples; multiple samples from the same springs reproduce well (i.e. less than 10% variation between three samples from Rembokola F1 spring over both years of study); and the data correlate very well with those calculated from the mass of recovered $BaSO_4$ (Fig. II.2). Post-sampling bacterial action and precipitation of solid sulphate minerals such as $CaSO_4$ should be inhibited by the low pH of the acidified samples. In addition, any sulphur present as HS^- should be driven off at low pH, so later exposure to the atmosphere and oxidation would not appreciably affect (i.e.. increase) the sulphate contents.

Samples for IC analysis were not acidified, and these samples may be subject to bacterial action (sulphate reduction), mineral precipitation (sulphate removal) and sulphide oxidation (sulphate addition). This is the most likely explanation for the scatter present in the IC data when compared to the other two methods. Where unacidified samples had significantly different sulphate contents to acidified equivalents, they had lower SO_4^{2-} contents, suggesting that mineral precipitation and/or sulphate reduction where the dominant processes.

In light of the differences in the data, the ICP-AES data have been used throughout the thesis in preference to the IC values, as the acidified samples appear to have been more robust and less subject to post-sampling processes.

Gravimetric data should and do reproduce the ICP-AES data, as both are based on acidified samples. The gravimetric data shows lower than expected yields for the highest sulphate content sample (SV205) most likely as a result of insufficient $BaCl_2$ addition to the fluid when sampled. Although there are differences in the two datasets, they are relatively minor, and no attempt has been made to correct for interference from solids that may co-precipitate in trace amounts with $BaSO_4$, such as $Ba(NO_3)_2$ and SiO_2.

II.4.2 Sulphur isotopes

The comparison between ICP-AES and gravimetric data suggests that the samples used for isotopic analysis were representative of the fluid sulphate content, and that any fractionation induced by precipitation will therefore be minimal. Excluding samples with total $BaSO_4$ yields too small to use for isotope analysis, the mean recovery of sulphate (determined by comparison with ICP-AES data) was 99%, with $1\sigma = 11$.

Low SO_2 yields during the combustion of sulphates led to lower than expected $\delta^{34}S$ values (Fig. II.4). Consequently, samples where yields were consistently below 70% are excluded from further discussion. Sulphide and native sulphur samples showed no consistent yield-related problems. A number of factors may contribute to the low yields and resulting fractionations:

- The temperature of combustion for sulphate samples (1125°C) is higher than for sulphide and sulphur samples (1075°C). The temperature required for sulphate combustion is at the upper limit of the furnace used; it is possible that for a number of samples, the furnace temperature was insufficient for complete combustion.
- A secondary copper furnace is used for sulphate samples to reduce any SO_3 to SO_2. The copper within becomes oxidised with use. A number of the samples may have generated low SO_2 yields due to the copper in the furnace being too oxidised to completely convert all SO_3 present.
- Samples may have contained co-precipitates, which would lead to an apparently low yield (although this should not have affected sulphur isotope results).

II.5 Summary

Data reported for aqueous sulphate samples analysed in this study report values obtained by ICP-AES in preference to IC, due to sample degradation of IC (unacidified) samples over time, and poor correlation between IC and gravimetric data.

The recovery of sulphate for isotopic analysis, as determined by comparison of ICP-AES and gravimetric data, was high (mean = 99%), and any isotopic fractionation induced by incomplete precipitation of $BaSO_4$ is assumed to be small to negligible.

Repeat analysis of sulphate samples showed that expected values of $\delta^{34}S$ are only reliably achieved with SO_2 yields >70% during the sulphate combustion process. As a result, low yield data have been omitted.

Appendix III: Well water chemistry

III

Sample	SV197	SV410	SV199	SV379	SV200	SV204
Location	Main Well	Main Well	Crab Well	Crab Well	Sea Well	Well
Area	Lemboni	Lemboni	Lemboni	Lemboni	Lemboni	Volivolila
Date	24/05/05	03/10/06	24/05/05	28/09/06	24/05/05	24/05/05
T (°C)	33	34	34	36	39	29
pH	7.2	7.2	6.9	7.3	6.3	7.0
HCO_3^- eqv.		212		352		
Ag (µg/l)		bdl		0.2		
Al (µg/l)	bdl	7	bdl	6	bdl	bdl
As (µg/l)	bdl	27	bdl	66	bdl	bdl
B	0.77	1.20	1.43	2.07	1.46	bdl
Ba (µg/l)	bdl	38.4	bdl	22.5	bdl	0.069
Be (µg/l)	bdl	0.3	bdl	0.5	bdl	bdl
Ca	50.19	72.6	81.93	101.6	72.69	41.78
Co (µg/l)	bdl	0.3	bdl	0.5	bdl	bdl
Cs (µg/l)		0.94		3.54		
Cu (µg/l)	bdl	4	bdl	2	bdl	bdl
Fe	bdl	bdl	bdl	0.03	bdl	bdl
K	6.7	8.7	9.6	12.3	10.6	2.9
Li (µg/l)	63	67	110	170	118	bdl
Mg	23.87	36.06	38.02	58.73	39.51	9.05
Mn	bdl	0.034	bdl	0.152	0.089	bdl
Mo (µg/l)	bdl	6.2	bdl	5.7	bdl	bdl
Na	69.83	96.7	134.10	186.1	156.00	33.39
Ni (µg/l)	bdl	3	bdl	4	bdl	bdl
P	bdl	0.38	bdl	0.34	bdl	bdl
Pb (µg/l)	bdl	1.9	bdl	1.7	bdl	bdl
Rb (µg/l)		12.6		28.8		
Si	46.43	47.13	53.86	65.90	57.27	30.20
SO_4^{2-}	58.39	93.8	112.58	161.8	102.88	23.95
Sr	0.636	0.903	0.984	1.313	0.974	0.527
Tl (µg/l)		bdl		0.04		
U (µg/l)		0.10		0.12		
V (µg/l)	bdl	13	bdl	4	bdl	bdl
Y (µg/l)	bdl	0.03	bdl	0.07	bdl	bdl
Zn (µg/l)	bdl	13	bdl	10	bdl	bdl
Zr (µg/l)	bdl	0.04	bdl	0.07	bdl	bdl
Cl^-	71.1	94.5	128	180	171	25.2
NO_3^-	bdl	0.026	0.044	bdl	0.578	0.508
Br	0.187	0.319	0.377	0.573	0.508	0.052
HPO_4^{2-}	bdl	0.500	bdl	bdl	bdl	bdl
F^-	0.199	0.133	0.230	bdl	0.281	0.187
CBE (%)	41	19	38	15	33	57

Table III.1: Water chemistry data for coastal wells at Savo. Wells contain traces of hydrothermal fluids and seawater. Analysed as per Section 4.3). All values in mg/l unless noted otherwise. bdl = below detection limits. Blank cells denote no analysis. The following elements were below detection limits for all analyses, and are omitted from the table: Bi, Cd, Ce, Cr, La, Nd, Sb, Se, Sn, Te, Th, Ti, NO_2^-.

Appendix IV: Whole rock oxygen isotopes

IV

IV.1 Analysis

Unaltered rocks were powdered as in section 3.2.1. Oxygen isotope analyses were carried out at the Scottish Universities Environmental Research Centre (SUERC) by laser fluorination of approximately 2 mg powder with excess ClF_3 using a CO_2 laser as a heat source (temperature in excess of 1500°C; following Sharp, 1990). Liberated O_2 was converted to CO_2 by reaction with hot graphite, then analysed on-line by a VG SIRA 10 mass spectrometer. Reproducibility is better than ±0.6‰ (1σ) based on repeated analyses of internal laboratory standard SES-1 (+10.1‰). Data are presented in standard permil notation relative to V-SMOW.

Sample	Analysis	Date	$\delta^{18}O_{SMOW}$
SES	10006	07/08/06	10.3
SES	10015	07/08/06	9.0
SES	10019	08/08/06	11.0
SES	10020	08/08/06	10.1
SES	10029	08/08/06	10.0
SES	10042	11/08/06	10.0
SES	10043	11/08/06	10.0
SES	10050	11/08/06	10.1
SES	Average		10.1
SES	1σ		0.6
SV1	10007	07/08/06	6.6
SV2	10008	07/08/06	8.2
SV6A	10016	07/08/06	6.1
SV6A	10048	11/08/06	6.7
SV10	10010	07/08/06	7.7
SV10	10044	11/08/06	7.3
SV12	10011	07/08/06	10.2
SV12	10021	08/08/06	9.4
SV12	10045	11/08/06	7.0
SV12	10046	11/08/06	6.9
SV12	Average		8.4
SV12	1σ		1.6

Sample	Analysis	Date	$\delta^{18}O_{SMOW}$
SV17	10013	07/08/06	7.9
SV19	10014	07/08/06	6.3
SV19	10047	11/08/06	6.6
SV20	10022	08/08/06	6.9
SV33	10023	08/08/06	7.4
SV38	10024	08/08/06	8.0
SV38	10025	08/08/06	9.1
SV38	10049	11/08/06	8.1
SV38	Average		8.4
SV38	1σ		0.6
SV39	10026	08/08/06	8.2
SV44	10027	08/08/06	7.4
SV45	10028	08/08/06	6.8

Table IV.1: Whole rock oxygen isotope data for unaltered igneous samples.

Appendix V: Analytical details

V

This appendix summarises selected analytical details (precision, accuracy, detection limits) in table format. Values are contained in the relevant chapters as text. Analytical details already summarised within the relevant chapters in table format are not repeated here.

V.1 XRF errors and detection limits

	Precision	Detection Limits (wt %)
SiO_2	<3%	0.0065
TiO_2	<7%	0.0015
Al_2O_3	<3%	0.0064
Fe_2O_3	<3%	0.0024
MnO	<7%	0.0018
MgO	<3%	0.018
CaO	<3%	0.0024
Na_2O	<3%	0.022
K_2O	<10%	0.0024
P_2O_5	<10%	

	Precision (contents >10 ppm)	Precision (contents <10 ppm)	Detection Limits (ppm)
Ba	<15%	<4 ppm	8.11
Ce	<10%		2.00
Co	<10%	<2 ppm	5.72
Cr	<10%	<4 ppm	5.09
Cu	<10%	<2 ppm	3.46
Ga	<5%	<1 ppm	2.37
La		<2 ppm	1.00
Nb		<1 ppm	1.51
Nd		<2 ppm	2.00
Ni	<10%	<2 ppm	6.41
Pb	<10%	<4 ppm	6.95
Rb	<5%	<1 ppm	1.08
Sc	<10%		12.30
Sr	<5%		1.00
Th		<4 ppm	4.16
U		<2 ppm	5.39
V	<5%		4.01
Y		<2 ppm	1.59
Zn	<5%		5.05
Zr	<5%	<4 ppm	4.57

Table V.1: Typical precision and detection limits for XRF technique (Chapter 3). Precision determined as 1σ on repeat analysis of reference materials, and expressed as percentage or ppm. Comparison of reference materials analysed in this study with accepted values indicated no systematic bias to higher or lower values for any element. Therefore precision is the largest contributor to analytical uncertainty.

V.2 REE ICP-MS Errors

	Precision (ppm)	Recovery (%)
La	0.45	90
Ce	0.98	94
Pr	0.06	100
Nd	0.62	95
Sm	0.18	92
Eu	0.06	95
Gd	0.62	101
Tb	0.03	90
Dy	0.15	99
Ho	0.02	96
Er	0.11	101
Tm	0.04	92
Yb	0.19	97
Lu	0.01	92

Table V.2: Typical precision and recovery (accuracy) for REE ICP-MS technique (Chapter 3). Precision determined as 1σ on repeat analysis of reference materials, and expressed as ppm. Recovery is measured vs. accepted concentration of element in a reference material, expressed as a percentage.

V.3 Ion chromatography Errors

	Precision (%)	Accuracy (%)
Cl^-	5	6
NO_2^-	3	1
NO_3^-	4	2
Br^-	2	1
F^-	3	1
HPO_4^-	3	1

Table V.3: Typical precision and accuracy for IC technique (Chapter 4). Precision determined as 1σ on repeat analysis of quality control solutions, and expressed as a percentage. Accuracy is typical difference between measured and accepted values for quality control solutions, expressed as a percentage

V.4 ICP-MS Errors

Analyte	Unit	Detection Limit	DS7 Expected	DS7 Measured Value	DS7 Measured Value	2σ	Precision (%)	Accuracy (%)
Ag	ppb	2	890	907	828	55.86	12.88	-2.5
Al	%	0.01	0.959	1.04	1.00	0.03	5.55	6.4
As	ppm	0.1	48.2	53.3	52.1	0.85	3.22	9.3
Au	ppb	0.2	70	58.1	91.7	23.76	63.44	7.0
B	ppm	20	38.6	42	40	1.41	6.90	6.2
Ba	ppm	0.5	370.3	406.7	392.4	10.11	5.06	7.9
Bi	ppm	0.02	4.51	5.05	5.04	0.01	0.28	11.9
Ca	%	0.01	0.93	0.98	0.94	0.03	5.89	3.2
Cd	ppm	0.01	6.38	7.05	6.96	0.06	1.82	9.8
Co	ppm	0.1	9.7	9.3	9.4	0.07	1.51	-3.6
Cr	ppm	0.5	163	178.7	187.0	5.87	6.42	12.2
Cu	ppm	0.01	109	142.03	104.38	26.62	43.22	13.0
Fe	%	0.01	2.39	2.41	2.36	0.04	2.96	-0.2
Ga	ppm	0.1	4.6	4.7	4.7	0.00	0.00	2.2
Hg	ppb	5	200	217	200	12.02	11.53	4.3
K	%	0.01	0.44	0.51	0.50	0.01	2.80	14.8
La	ppm	0.5	12.7	13.5	12.7	0.57	8.64	3.1
Mg	%	0.01	1.05	1.09	1.05	0.03	5.29	1.9
Mn	ppm	1	627	648	639	6.36	1.98	2.6
Mo	ppm	0.01	20.92	21.71	21.44	0.19	1.77	3.1
Na	%	0.001	0.073	0.095	0.089	0.00	9.22	26.0
Ni	ppm	0.1	56	54.4	55.6	0.85	3.09	-1.8
P	%	0.001	0.08	0.081	0.081	0.00	0.00	1.3
Pb	ppm	0.01	70.6	71.27	68.70	1.82	5.19	-0.9
S	%	0.02	0.21	0.19	0.19	0.00	0.00	-9.5
Sb	ppm	0.02	5.86	5.14	5.21	0.05	1.91	-11.7
Sc	ppm	0.1	2.5	2.8	2.6	0.14	10.48	8.0
Se	ppm	0.1	3.5	3.5	3.2	0.21	12.66	-4.3
Sr	ppm	0.5	68.7	78.9	78.0	0.64	1.62	14.2
Te	ppm	0.02	1.08	1.28	1.30	0.01	2.19	19.4
Th	ppm	0.1	4.4	4.6	4.6	0.00	0.00	4.5
Ti	%	0.001	0.124	0.117	0.115	0.00	2.44	-6.5
Tl	ppm	0.02	4.19	4.33	4.30	0.02	0.98	3.0
U	ppm	0.1	4.9	5.1	5.0	0.07	2.80	3.1
V	ppm	2	86	82	81	0.71	1.74	-5.2
W	ppm	0.1	3.8	3.6	3.6	0.00	0.00	-5.3
Zn	ppm	0.1	411	425.6	392.6	23.33	11.41	-0.5

Table V.4: Typical detection limits, precision and accuracy for ICP-MS technique used in the analysis of sinter and travertine samples (Chapters 6 & 7). Precision determined as 2σ on repeat analysis of standard DS7, and expressed as a percentage. Accuracy is typical difference between measured and accepted values for standard DS7, expressed as a percentage

Bibliography

Ahmad, M., Solomon, M. and Walshe, J.L., 1987. Mineralogical and geochemical studies of the Emperor gold telluride deposit, Fiji. Economic Geology, 82(2): 345-370.

Alderton, D.H.M. and Fallick, A.E., 2000. The nature and genesis of gold-silver-tellurium mineralization in the Metaliferi Mountains of western Romania. Economic Geology, 95(3): 495-515.

Amherst, W.A.T.A., Thompson, B., Gallegos, H., Sarmiento, P., Mendaña, A. and Hernandez, G., 1901. The a in 1568. Hakluyt Society, London.

Amundson, R. and Kelly, E., 1987. The chemistry and mineralogy of a CO_2-rich travertine depositing spring in the California Coast Range. Geochimica et Cosmochimica Acta, 51(11): 2883-2890.

Annen, C., Blundy, J.D. and Sparks, R.S.J., 2006. The genesis of intermediate and silicic magmas in deep crustal hot zones. Journal of Petrology, 47(3): 505-539.

Arculus, R.J., Johnson, R.W., Chappell, B.W., McKee, C.O. and Sakai, H., 1983. Ophiolite-contaminated andesites, trachybasalts, and cognate inclusions of Mount Lamington, Papua New Guinea: anhydrite -amphibole-bearing lavas and the 1951 cumulodome. Journal of Volcanology and Geothermal Research, 18: 215-247.

Arnórsson, S. (Editor), 2000. Isotopic and Chemical Techniques in Geothermal Exploration, Development and Use: Sampling Methods, Data Handling, Interpretation International Atomic Energy Agency, Vienna, 351 pp.

Arnórsson, S., Bjarnason, J.O., Giroud, N., Gunnarsson, I. and Stefansson, A., 2006. Sampling and analysis of geothermal fluids. Geofluids, 6(3): 203-216.

Arribas, A., 1995. Characteristics of high sulfidation epithermal deposits, and their relation to magmatic fluid. In: J.F.H. Thompson (Editor), Magmas, Fluids, Ore Deposits. Mineralogical Association of Canada Short Course Series, pp. 419-454.

Arribas, A., Hedenquist, J.W., Itaya, T., Okada, T., Concepcion, R.A. and Garcia, J.S., 1995. Contemporaneous formation of adjacent porphyry and epithermal Cu-Au deposits over 300 ka in northern Luzon, Philippines. Geology, 23(4): 337-340.

Atherton, M.P. and Petford, N., 1993. Generation of sodium-rich magmas from newly underplated basaltic crust. Nature, 362(6416): 144-146.

Ault, L., Green, K.A. and Perkins, K.M., 1999. Validation of the procedure for the determination of major and trace cations in aqueous samples by inductively coupled plasma-atomic emission spectrometry (Fisons/ARL 3580). British Geological Survey Technical Report WI/00/6.

Auzende, J.-M., Kroenke, L.W., Collot, J.Y., Lafoy, Y., Pelletier, B. and Collot, J.-Y., 1996. Compressive tectonism along the eastern margin of Malaita Island (Solomon Islands). Marine Geophysical Researches, 18: 289-304.

Ayers, J.C. and Eggler, D.H., 1995. Partitioning of elements between silicate melt and H_2O - NaCl fluids at 1.5 and 2.0 GPa pressure: Implications for mantle metasomatism. Geochimica et Cosmochimica Acta, 59(20): 4237-4246.

Baker, P.E., 1982. Evolution and classification of orogenic volcanic rocks. In: R.S. Thorpe (Editor), Andesites: orogenic andesites and related rocks. John Wiley and Sons, Chichester, pp. 11-23.

Barclay, J. and Carmichael, I.S.E., 2004. A hornblende basalt from western Mexico: Water-saturated phase relations constrain a pressure-temperature window of eruptibility. Journal of Petrology, 45(3): 485-506.

Berly, T.J., Hermann, J., Arculus, R.J. and Lapierre, H., 2006. Supra-subduction zone pyroxenites from San Jorge and Santa Isabel (Solomon Islands). Journal of Petrology, 47(8): 1531-1555.

Bernard, A., Demaiffe, D., Mattielli, N. and Punongbayan, R.S., 1991. Anhydrite-bearing pumices from Mount Pinatubo: further evidence for the existence of sulphur-rich silicic magmas. Nature, 354: 139 -140

Birkhold, A.L., Neal, C.R., Jain, J.C., Mahoney, J.J., Duncan, R.A. and Petterson, M.G., 1998. The evolution of the Ontong Java Plateau (OJP); is San Cristobal, Solomon Islands, the missing link? Geological Society of America, 1998 Annual Meeting Abstracts with Programs, 30(7): 377.

Birnbaum, S.J. and Wireman, J.W., 1984. Bacterial sulfate reduction and pH: Implications for early diagenesis. Chemical Geology, 43(1-2): 143-149.

Bolognesi, L., 2000. Earthquake-induced variations in the composition of the water in the geothermal reservoir at Vulcano Island, Italy. Journal of Volcanology and Geothermal Research, 99(1-4): 139-150.

Boyce, A.J., Fulignati, P., Sbrana, A. and Fallick, A.E., 2007. Fluids in early stage hydrothermal alteration of high-sulfidation epithermal systems: A view from the Vulcano active hydrothermal system (Aeolian Island, Italy). Journal of Volcanology and Geothermal Research, 166: 76-90.

Boynton, W.V., 1984. Geochemistry of the rare earth elements: meteorite studies. In: P. Henderson (Editor), Rare Earth Element Geochemistry. Elsevier, pp. 63-114.

Breitsprecher, K., Thorkelson, D.J., Groome, W.G. and Dostal, J., 2003. Geochemical confirmation of the Kula-Farallon slab window beneath the Pacific Northwest in Eocene time. Geology, 31(4): 351-354.

Brombach, T., Caliro, S., Chiodini, G., Fiebig, J., Hunziker, J.C. and Raco, B., 2003. Geochemical evidence for mixing of magmatic fluids with seawater, Nisyros hydrothermal system, Greece. Bulletin of Volcanology, 65(7): 505-516.

Brown, K.L., 1986. Gold deposition from geothermal discharges in New Zealand. Economic Geology, 81(4): 979-983.

Bureau, H. and Keppler, H., 1999. Complete miscibility between silicate melts and hydrous fluids in the upper mantle: experimental evidence and geochemical implications. Earth and Planetary Science Letters, 165(2): 187-196.

Burnham, C.W., 1979. Magmas and hydrothermal fluids. In: H.L. Barnes (Editor), Geochemistry of Hydrothermal Ore Deposits, 2nd Edition. John Wiley and Sons.

Burnham, C.W., 1994. Development of the Burnham Model for prediction of H_2O solubility in magmas. In: M.R. Carroll and J.R. Holloway (Editors), Volatiles in Magmas. Reviews in Mineralogy, pp. 123-130.

Cabon, J.Y. and Cabon, N., 2000. Determination of arsenic species in seawater by flow injection hydride generation in situ collection followed by graphite furnace atomic absorption spectrometry: Stability of As(III). Analytica Chimica Acta, 418(1): 19-31.

Campbell, A., Rye, D. and Petersen, U., 1984. A hydrogen and isotope study of the San Cristobal mine, Peru: implications of the role of water to rock ratio for the genesis of wolframite deposits. Economic Geology, 79(8): 1818-1832.

Campbell, K.A., Rodgers, K.A., Brotheridge, J.M.A. and Browne, P.R.L., 2002. An unusual modern silica-carbonate sinter from Pavlova spring, Ngatamariki, New Zealand. Sedimentology, 49(4): 835-854.

Canet, C., Prol-Ledesma, R.M., Torres-Alvarado, I., Gilg, H.A., Villanueva, R.E. and Cruz, R.L.-S., 2005. Silica-carbonate stromatolites related to coastal hydrothermal venting in Bahía Concepción, Baja California Sur, Mexico. Sedimentary Geology, 174(1-2): 97-113.

Carman, G.D., 2003. Geology, mineralization and hydrothermal evolution of the Ladolam gold deposit, Lihir Island, Papua New Guinea. In: S.F. Simmons and I. Graham (Editors), Volcanic, Geothermal and Ore-Forming Fluids: Rulers and Witnesses of Processes within the Earth. Special Publication No. 10. Society of Economic Geologists, Littleton, Colorado, pp. 247-284.

Carmichael, I.S.E., 1967. The iron-titanium oxides of sialic volcanic rocks and their associated ferromagnesian silicates. Contributions to Mineralogy and Petrology, 14(1): 36-64.

Carroll, M.R. and Rutherford, M.J., 1987. The stability of igneous anhydrite: experimental results and implications for sulfur behavior in the 1982 El Chichon trachyandesite and other evolved magmas. Journal of Petrology, 28(5): 781-801.

Carroll, M.R. and Webster, J.D., 1994. Solubilities of sulfur, noble gases, nitrogen, chlorine, and fluorine in magmas. In: M.R. Carroll and J.R. Holloway (Editors), Volatiles in Magmas. Reviews in Mineralogy, pp. 231-279.

Castillo, P.R., 2006. An overview of adakite petrogenesis. Chinese Science Bulletin, 51(3): 258-268.

Castillo, P.R., Janney, P.E. and Solidum, R.U., 1999. Petrology and geochemistry of Camiguin Island, southern Philippines: insights into the source of adakites and other lavas in a complex arc setting. Contributions to Mineralogy and Petrology, 134: 33-51.

Chacko, T., Cole, D.R. and Horita, J., 2001. Equilibrium oxygen, hydrogen and carbon isotope fractionation factors applicable to geologic systems. In: J.W. Valley and D.R. Cole (Editors), Stable Isotope Geochemistry. Reviews in Mineralogy and Geochemistry, pp. 1-81.

Chafetz, H.S. and Folk, R.L., 1984. Travertines; depositional morphology and the bacterially constructed constituents Journal of Sedimentary Research, 54(1): 289-316.

Chafetz, H.S. and Guidry, S.A., 1999. Bacterial shrubs, crystal shrubs, and ray-crystal shrubs: bacterial vs. abiotic precipitation. Sedimentary Geology, 126(1-4): 57-74.

Chafetz, H.S., Rush, P.F. and Utech, N.M., 1991. Microenvironmental controls on mineralogy and habit of $CaCO_3$ precipitates: an example from an active travertine system. Sedimentology, 38(1): 107-126.

Charlton, B.D., Reeder, S. and Watts, M.J., 2003. Method validation for the determination of major and trace anions by Ion Chromatography (DX-600). British Geological Survey Internal Report IR/03/79.

Chiodini, G., Cioni, R., Marini, L. and Panichi, C., 1995. Origin of the fumarolic fluids of Vulcano Island, Italy and implications for volcanic surveillance. Bulletin of Volcanology, 57(2): 99-110.

Chivas, A.R., 1978. Porphyry copper mineralization at the Koloula igneous complex, Guadalcanal, Solomon Islands. Economic Geology, 73(5): 645-677.

Chivas, A.R., 1981. Geochemical evidence for magmatic fluids in porphyry copper mineralization.1. Mafic silicates from the Koloula Igneous Complex. Contributions to Mineralogy and Petrology, 78(4): 389 -403.

Christenson, B.W., Mroczek, E., Kennedy, B.M., van Soest, M.C., Stewart, M.K. and Lyon, G., 2002. Ohaaki reservoir chemistry: characteristics of an arc-type hydrothermal system in the Taupo Volcanic Zone, New Zealand. Journal of Volcanology and Geothermal Research, 115(1-2): 53-82.

Chung, S.L., Liu, D.Y., Ji, J.Q., Chu, M.F., Lee, H.Y., Wen, D.J., Lo, C.H., Lee, T.Y., Qian, Q. and Zhang, Q., 2003. Adakites from continental collision zones: Melting of thickened lower crust beneath southern Tibet. Geology, 31(11): 1021-1024.

Coleman, M.L. and Moore, M.P., 1978. Direct reduction of sulfates to sulfur dioxide for isotopic analysis. Analytical Chemistry, 50(11): 1594-1595.

Coleman, P.J., 1966. The Solomon Islands as an island arc. Nature, 211(5055): 1249-1251.

Coleman, P.J., 1991. Dynamic strike-slip fault systems with respect to the Solomon Islands, and their effect on mineral potential. Marine Geology, 98(2-4): 167-176.

Coleman, P.J. and Kroenke, L.W., 1981. Subduction without volcanism in the Solomon Islands arc. Geo-Marine Letters, 1(2): 129-134.

Connors, K.A., Noble, D.C., Bussey, S.D. and Weiss, S.I., 1993. Initial gold contents of silicic volcanic rocks: Bearing on the behavior of gold in magmatic systems. Geology, 21(10): 937-940.

Conrey, R.M., Hooper, P.R., Larson, P.B., Chesley, J. and Ruiz, J., 2001. Trace element and isotopic evidence for two types of crustal melting beneath a High Cascade volcanic center, Mt. Jefferson, Oregon. Contributions to Mineralogy and Petrology, 141(6): 710-732.

Cook, J.M., Robinson, J.J., Chenery, S.R.N. and Perkins, K.M., 2002. Validation report for the analysis of aqueous solutions by ICP-MS, AGN 2.3.3. British Geological Survey Internal Report IR/02/091R.

Cooke, D.R. and Hollings, P., 2005. Giant porphyry deposits: characteristics, distribution and tectonic controls. Economic Geology, 100(5): 801-818.

Cooke, D.R. and McPhail, D.C., 2001. Epithermal Au-Ag-Te mineralization, Acupan, Baguio district, Philippines: Numerical simulations of mineral deposition. Economic Geology, 96(1): 109-131.

Cooke, D.R., McPhail, D.C. and Bloom, M.S., 1996. Epithermal gold mineralization, Acupan, Baguio district, Philippines: Geology, mineralization, alteration and the thermochemical environment of ore deposition. Economic Geology, 91(2): 243-272.

Cooke, D.R. and Simmons, S.F., 2000. Characteristics and genesis of epithermal gold deposits. In: S.G. Hagemann and P.E. Brown (Editors), Gold in 2000. Reviews in Economic Geology. Society of Economic Geologists, Littleton, Colorado, pp. 221-244.

Cooper, P. and Taylor, B., 1987. The spatial distribution of earthquakes, focal mechanisms and subducted lithosphere in the Solomon Islands. In: B. Taylor and N.F. Exon (Editors), Marine Geology, Geophysics and Geochemistry of the Woodlark Basin-Solomon Islands. Circum-Pacific Council for Energy and Mineral Resources, Earth Science Series, pp. 67-80.

Coplen, T.B., Hopple, J.A., Böhlke, J.K., Peiser, H.S., Rieder, S.E., Krouse, H.R., Rosman, K.J.R., Ding, T., Vocke Jr, R.D., Révész, K.M., Lamberty, A., Taylor, P. and De Bièvre, P., 2002. Compliation of minimum and maximum isotope ratios of selected elements in naturally occurring terrestrial materials and reagents. USGS Water Resources Investigation Report 01-4222.

Cowley, S., Mann, P., Coffin, M.F. and Shipley, T.H., 2004. Oligocene to Recent tectonic history of the Central Solomon intra-arc basin as determined from marine seismic reflection data and compilation of onland geology. Tectonophysics, 389(3-4): 267-307.

Craig, H., 1961. Isotopic variations in meteoric waters. Science, 133(3465): 1702-1703.

Craig, H., 1963. The isotopic geochemistry of water and carbon in geothermal areas. In: E. Tongiorgi (Editor), Nuclear Geology on Geothermal Areas, pp. 17-53.

Crook, K.A.W. and Taylor, B., 1994. Structure and Quaternary tectonic history of the Woodlark Triple Junction region, Solomon Islands. Marine Geophysical Researches, 16(1): 65-89.

Dandurand, J.L., Gout, R., Hoefs, J., Menschel, G., Schott, J. and Usdowski, E., 1982. Kinetically Controlled Variations of Major Components and Carbon and Oxygen Isotopes in a Calcite-Precipitating Spring. Chemical Geology, 36(3-4): 299-315.

Darling, W.G., Armannsson, H. and Groenvold, K., 1989. Stable isotopic aspects of fluid flow in the Krafla, Namafjall and Theistareykir geothermal systems of Northeast Iceland. Chemical Geology, 76: 197-213.

Darling, W.G. and Talbot, J.C., 1991. Evaluation and development of gas geothermometry for geothermal exploration in the East African Rift System. WD/91/72, British Geological Survey.

de Jongh, W.K., 1973. X-ray fluorescence analysis applying theoretical matrix corrections. Stainless steel. X-ray Spectrometry, 2: 151-158.

Deer, W.A., Howie, R.A. and Zussman, J., 1992. An Introduction to the Rock-Forming Minerals - 2nd ed. Longman Scientific and Technical, 696 pp.

Defant, M. and Drummond, M.S., 1990. Derivation of some modern arc magmas by melting of young subducted lithosphere. Nature, 347(6294): 662-665.

Deines, P., Langmuir, D. and Harmon, R.S., 1974. Stable carbon isotope ratios and the existence of a gas phase in the evolution of carbonate ground waters. Geochimica et Cosmochimica Acta, 38(7): 1147-1164.

Delmelle, P., Bernard, A., Kusakabe, M., Fischer, T.P. and Takano, B., 2000. Geochemistry of the magmatic-hydrothermal system of Kawah Ijen Volcano, East Java, Indonesia. Journal of Volcanology and Geothermal Research, 97: 31-53.

Delmelle, P., Kusakabe, M., Bernard, A., Fischer, T., de Brouwer, S. and del Mundo, E., 1998. Geochemical and isotopic evidence for seawater contamination of the hydrothermal system of Taal Volcano, Luzon, the Philippines. Bulletin of Volcanology, 59(8): 562-576.

DeLong, S.E., Hodges, F.N. and Arculus, R., 1975. Ultramafic and mafic inclusions, Kanaga Island, Alaska, and the occurrence of alkaline rocks in island arcs. Journal of Geology, 83: 721-736.

DeLong, S.E., Schwarz, W.M. and Anderson, R.N., 1979. Thermal effects of ridge subduction. Earth and Planetary Science Letters, 44(2): 239-246.

Dilles, J.H. and Einaudi, M.T., 1992. Wall rock alteration and hydrothermal flow paths about the Ann-Mason porphyry copper deposit, Nevada - a 6 km vertical reconstruction. Economic Geology, 87: 1963-2001.

Donnelly, T., Waldron, S., Tait, A., Dougans, J. and Bearhop, S., 2001. Hydrogen isotope analysis of natural abundance and deuterium-enriched waters by reduction over chromium on-line to a dynamic dual inlet isotope-ratio mass spectrometer. Rapid Communications in Mass Spectrometry, 15(15): 1297-1303.

Dreher, S.T., Macpherson, C.G., Pearson, D.G. and Davidson, J.P., 2005. Re-Os isotope studies of Mindanao adakites: Implications for sources of metals and melts. Geology, 33(12): 957-960.

Driesner, T. and Heinrich, C.A., 2007. The system H_2O-NaCl. Part I: Correlation formulae for phase relations in temperature-pressure-composition space from 0 to 1000°C, 0 to 5000 bar, and 0 to 1 X_{NaCl}. Geochimica et Cosmochimica Acta, 71(20): 4880-4901.

Eaton, P.C. and Setterfield, T.N., 1993. The relationship between epithermal and porphyry hydrothermal systems within the Tavua Caldera, Fiji. Economic Geology, 88: 1053-1083.

Elderfield, H., 1986. Strontium isotope stratigraphy. Palaeogeography, Palaeoclimatology, Palaeoecology, 57 (1): 71-90.

Ellis, A.J. and Mahon, W.A.J., 1977. Chemistry and Geothermal Systems. Academic Press, New York, 392 pp.

Epstein, S. and Mayeda, T., 1953. Variation of O^{18} content of waters from natural sources. Geochimica et Cosmochimica Acta, 4(5): 213-224.

Esawi, E.K., 2004. AMPH-CLASS: An Excel spreadsheet for the classification and nomenclature of amphiboles based on the 1997 recommendations of the International Mineralogical Association. Computers & Geosciences, 30(7): 753-760.

Feeley, T.C. and Hacker, M.D., 1995. Intracrustal derivation of Na-rich andesitic and dacitic magmas - an example from Volcan Ollague, Andean Central Volcanic Zone. Journal of Geology, 103(2): 213-225.

Fernandez-Turiel, J.L., Garcia-Valles, M., Gimeno-Torrente, D., Saavedra-Alonso, J. and Martinez-Manent, S., 2005. The hot spring and geyser sinters of El Tatio, Northern Chile. Sedimentary Geology, 180(3-4): 125-147.

Field, C.W. and Fifarek, R.H., 1985. Light stable isotope systematics in the epithermal environment. In: B.R. Berger and P.M. Bethke (Editors), Geology and Geochemistry of Epithermal Systems. Reviews in Economic Geology Volume 2. Society of Economic Geologists, Littleton, Colorado, pp. 99-128.

Fifarek, R.H. and Rye, R.O., 2005. Stable-isotope geochemistry of the Pierina high-sulfidation Au-Ag deposit, Peru: influence of hydrodynamics on SO_4^{2-}-H_2S sulfur isotopic exchange in magmatic-steam and steam-heated environments. Chemical Geology, 215(1-4): 253-279.

Fisher, R.V. and Heiken, G., 1982. Mt. Pelée, Martinique: May 8 and 20, pyroclastic flows and surges. Journal of Volcanology and Geothermal Research, 13(3-4): 339-371.

Folk, R.L., Chafetz, H.S. and Tiezzi, P.A., 1985. Bizarre forms of depositional and diagenetic calcite in hot spring travertine, central Italy. In: N. Schneidermann and P.M. Harris (Editors), Carbonate Cements. Society of Economic Palaeontologists and Mineralogists, pp. 349-369.

Fouke, B.W., Farmer, J.D., Des Marais, D.J., Pratt, L., Sturchio, N.C., Burns, P.C. and Discipulo, M.K., 2000. Depositional Facies and Aqueous-Solid Geochemistry of Travertine-Depositing Hot Springs (Angel Terrace, Mammoth Hot Springs, Yellowstone National Park, U.S.A.). Journal of Sedimentary Research, 70(3): 565-585.

Fournier, R.O., 1979. A revised equation for the Na/K geothermometer. Geothermal Resources Council Transactions, 3: 221-224.

Fournier, R.O., 1985. The behaviour of silica in hydrothermal solutions. In: B.R. Berger and P.M. Bethke (Editors), Geology and Geochemistry of Epithermal Systems. Reviews in Economic Geology. Society of Economic Geologists, Littleton, Colorado, pp. 45-62.

Fournier, R.O., 1999. Hydrothermal processes related to movement of fluid from plastic into brittle rock in the magmatic-epithermal environment. Economic Geology, 94(8): 1193-1211.

Friedman, I., 1970. Some investigations of the deposition of travertine from Hot Springs—I. The isotopic chemistry of a travertine-depositing spring. Geochimica et Cosmochimica Acta, 34(12): 1303-1315.

Fulignati, P., Gioncada, A. and Sbrana, A., 1998. Geologic model of the magmatic-hydrothermal system of Vulcano (Aeolian Islands, Italy). Mineralogy and Petrology, 62(3-4): 195-222.

Gaetani, G.A., Grove, T.L. and Bryan, W.B., 1993. The influence of water on the petrogenesis of subduction related igneous rocks. Nature, 365(6444): 332-334.

Garrison, J.M. and Davidson, J.P., 2003. Dubious case for slab melting in the Northern volcanic zone of the Andes. Geology, 31(6): 565-568.

Giggenbach, W.F., 1988. Geothermal solute equilibria. Derivation of Na-K-Mg-Ca geoindicators. Geochimica et Cosmochimica Acta, 52(12): 2749-2765.

Giggenbach, W.F., 1992. Isotopic shifts in waters from geothermal and volcanic systems along convergent plate boundaries and their origin. Earth and Planetary Science Letters, 113(4): 495-510.

Giggenbach, W.F., 1997. The origin and evolution of fluids in magmatic-hydrothermal systems. In: H.L. Barnes (Editor), Geochemistry of Hydrothermal Ore Deposits, 3rd Edition. John Wiley and Sons, pp. 737-796.

Giggenbach, W.F., Garcia P., N., Londono C., A., Rodriguez V., L., Rojas G., N. and Calvache V., M.L., 1990. The chemistry of fumarolic vapor and thermal-spring discharges from the Nevado del Ruiz volcanic-magmatic-hydrothermal system, Colombia. Journal of Volcanology and Geothermal Research, 42(1-2): 13-39.

Giggenbach, W.F., Shinohara, H., Kusakabe, M. and Ohba, T., 2003. Formation of acid volcanic brines through interaction of magmatic gases, seawater, and rock within the White Island volcanic-hydrothermal system, New Zealand. In: S.F. Simmons and I. Graham (Editors), Volcanic, Geothermal and Ore-Forming Fluids: Rulers and Witnesses of Processes within the Earth. Special Publication No. 10. Society of Economic Geologists, Littleton, Colorado, pp. 19-40.

Giggenbach, W.F. and Stewart, M.K., 1982. Processes controlling the isotopic composition of steam and water discharges from steam vents and steam-heated pools in geothermal areas. Geothermics, 11(2): 71-80.

Gill, J.B., 1981. Orogenic Andesites and Plate Tectonics. Springer-Verlag, New York, 390 pp.

GNIP, 2004. Global Network of Isotopes in Precipitation Database. IAEA / WMO, accessible at http://isohis.iaea.org.

Goff, F. and McMurtry, G.M., 2000. Tritium and stable isotopes of magmatic waters. Journal of Volcanology and Geothermal Research, 97(1-4): 347-396.

Govindaraju, K., 1994. 1994 Compilation of working values and sample description for 383 geostandards. Geostandards Newsletter 18 (Special Issue): 1-158.

Gow, P.A. and Walshe, J.L., 2005. The role of preexisting geologic architecture in the formation of giant porphyry-related Cu +/- Au deposits: Examples from New Guinea and Chile. Economic Geology, 100(5): 819-833.

Graham, C.M., Viglino, J.A. and Harmon, R.S., 1987. Experimental study of hydrogen isotope exchange between aluminous chlorite and water and of hydrogen diffusion in chlorite. American Mineralogist, 72(5-6): 566-579.

Gregoire, M., McInnes, B.I.A. and O'Reilly, S.Y., 2001. Hydrous metasomatism of oceanic sub-arc mantle, Lihir, Papua New Guinea - Part 2. Trace element characteristics of slab-derived fluids. Lithos, 59 (3): 91-108.

Grover, J.C., 1958. Savo volcano - a potential danger to its inhabitants, The Solomon Islands - geological exploration and research, 1953 - 56. Geological Survey of the British Solomon Islands Memoir, pp. 108-111.

Guidry, S.A. and Chafetz, H.S., 2003a. Anatomy of siliceous hot springs: examples from Yellowstone National Park, Wyoming, USA. Sedimentary Geology, 157(1-2): 71-106.

Guidry, S.A. and Chafetz, H.S., 2003b. Siliceous shrubs in hot springs from Yellowstone National Park, Wyoming, USA. Canadian Journal of Earth Sciences, 40(11): 1571-1583.

Gutscher, M.-A., Maury, R., Eissen, J.-P. and Bourdon, E., 2000. Can slab melting be caused by flat subduction? Geology, 28: 535-538.

Hackman, B.D., 1980. The geology of Guadalcanal, Solomon Islands. Institute of Geological Sciences Overseas Memoir 6. Her Majesty's Stationery Office, London, 115 pp.

Haggerty, S.E., 1976. Oxidation of opaque mineral oxides in basalts. In: D. Rumble III (Editor), Oxide Minerals. Reviews in Mineralogy.

Hall, A.J., Boyce, A.J., Fallick, A.E. and Hamilton, P.J., 1991. Isotopic evidence of the depositional environment of Late Proterozoic stratiform barite mineralization, Aberfeldy, Scotland. Chemical Geology, 87(2): 99-114.

Hammarstrom, J.M. and Zen, E.A., 1986. Aluminum in hornblende; an empirical igneous geobarometer. American Mineralogist, 71(11-12): 1297-1313.

Hammer, Ø., Dysthe, D.K. and Jamtveit, B., 2007. The dynamics of travertine dams. Earth and Planetary Science Letters, 256(1-2): 258-263.

Hattori, K. and Sakai, H., 1979. D-H ratios, origins, and evolution of the ore-forming fluids for the Neogene veins and Kuroko deposits of Japan. Economic Geology, 74(3): 535-555.

Heald, P., Foley, N.K. and Hayba, D.O., 1987. Comparative anatomy of volcanic-hosted epithermal deposits - acid-sulfate and adularia-sericite types. Economic Geology, 82(1): 1-26.

Hedenquist, J.W. and Aoki, M., 1991. Meteoric interaction with magmatic discharges in Japan and the significance for mineralization. Geology, 19(10): 1041-1044.

Hedenquist, J.W., Aoki, M. and Shinohara, H., 1994a. Flux of volatiles and ore-forming metals from the magmatic-hydrothermal system of Satsuma Iwojima volcano. Geology, 22(7): 585-588.

Hedenquist, J.W., Arribas, A. and Reynolds, T.J., 1998. Evolution of an intrusion-centered hydrothermal system: Far Southeast-Lepanto porphyry and epithermal Cu-Au deposits, Philippines. Economic Geology, 93(4): 373-404.

Hedenquist, J.W., Arribas, A.R. and Gonzalez-Urien, E., 2000. Exploration for epithermal gold deposits. In: S.G. Hagemann and P.E. Brown (Editors), Gold in 2000. Reviews in Economic Geology. Society of Economic Geologists, Littleton, Colorado, pp. 245-277.

Hedenquist, J.W. and Henley, R.W., 1985. Hydrothermal eruptions in the Waiotapu geothermal system, New Zealand; their origin, associated breccias, and relation to precious metal mineralization. Economic Geology, 80: 1640-1668.

Hedenquist, J.W. and Lowenstern, J.B., 1994. The role of magmas in the formation of hydrothermal ore deposits. Nature, 370(6490): 519-527.

Hedenquist, J.W., Matsuhisa, Y., Izawa, E., White, N.C., Giggenbach, W.F. and Aoki, M., 1994b. Geology, geochemistry, and origin of high sulfidation Cu-Au mineralization in the Nansatsu District, Japan. Economic Geology, 89(1): 1-30.

Hedenquist, J.W., Simmons, S.F., Giggenbach, W.F. and Eldridge, C.S., 1993. White Island, New Zealand, volcanic-hydrothermal system represents the geochemical environment of high-sulfidation Cu and Au ore deposition. Geology, 21: 731-734.

Heinrich, C., 2005. The physical and chemical evolution of low-salinity magmatic fluids at the porphyry to epithermal transition: a thermodynamic study. Mineralium Deposita, 39(8): 864-889.

Heinrich, C.A., Driesner, T., Stefansson, A. and Seward, T.M., 2004. Magmatic vapor contraction and the transport of gold from the porphyry environment to epithermal ore deposits. Geology, 32(9): 761-764.

Henley, R.W., 1984. Chemical structure of geothermal systems. In: R.W. Henley, A.H. Truesdell and P.B. Barton Jr. (Editors), Fluid-Mineral Equilibria in Hydrothermal Systems. Society of Economic Geologists, pp. 9-28.

Henley, R.W. and Ellis, A.J., 1983. Geothermal systems ancient and modern: a geochemical review. Earth-Science Reviews, 19(1): 1-50.

Henley, R.W. and McNabb, A., 1978. Magmatic vapour plumes and groundwater interaction in porphyry copper emplacement Economic Geology, 73: 1-20.

Hill, K.C., Kendrick, R.D., Crowhurst, P.V. and Gow, P.A., 2002. Copper-gold mineralisation in New Guinea: tectonics, lineaments, thermochronology and structure. Australian Journal of Earth Sciences, 49(4): 737-752.

Hinman, N.W. and Lindstrom, R.F., 1996. Seasonal changes in silica deposition in hot spring systems. Chemical Geology, 132(1-4): 237-246.

Hoefs, J., 1997. Stable Isotope Geochemistry. Springer, 201 pp.

Hofmann, A.W., 1997. Mantle geochemistry: the message from oceanic volcanism. Nature, 385(6613): 219-229.

Hole, M.J. and Saunders, A.D., 1996. The generation of small melt-fractions in truncated melt columns: constraints from magmas erupted above slab windows and implications for MORB genesis. Mineralogical Magazine, 60: 173-189.

Holland, H.D., 1965. Some applications of thermochemical data to problems of ore deposits; Part 2, Mineral assemblages and the composition of ore forming fluids. Economic Geology, 60(6): 1101-1166.

Hou, Z.Q., Gao, Y.F., Qu, X.M., Rui, Z.Y. and Mo, X.X., 2004. Origin of adakitic intrusives generated during mid-Miocene east-west extension in southern Tibet. Earth and Planetary Science Letters, 220 (1-2): 139-155.

Hughes, G.W., 2004. Accretion of the Ontong Java Plateau to the Solomon arc: a historical perspective. Tectonophysics, 389(3-4): 127-136.

Ishikawa, A., Maruyama, S. and Komiya, T., 2004. Layered lithospheric mantle beneath the Ontong Java Plateau: Implications from xenoliths in alnöite, Malaita, Solomon Islands. Journal of Petrology, 45 (10): 2011-2044.

Jensen, E.P. and Barton, M.D., 2000. Gold deposits related to alkaline magmatism. In: S.G. Hagemann and P.E. Brown (Editors), Gold in 2000. Reviews in Economic Geology. Society of Economic Geologists, Littleton, Colorado, pp. 279-314.

Jochum, K.P., Seufert, H.M. and Thirlwall, M.F., 1990. High-sensitivity Nb analysis by spark source mass spectrometry (SSMS) and calibration of XRF Nb and Zr. Chemical Geology, 81: 1-16.

Jochum, K.P., Nohl, U., Herwig, K., Lammel, E., Stoll, B. and Hofmann, A.W., 2005. GeoReM: A new geochemical database for reference materials and isotopic standards. Geostandards and Geoanalytical Research, 29(3): 333-338.

Johnson, R.W., Jaques, A.L., Langmuir, C.H., Perfit, M.R., Staudigel, H., Dunkley, P.N., Chappell, B.W., Taylor, S.R. and Baekisapa, M., 1987. Ridge subduction and forearc volcanism; petrology and geochemistry of rocks dredged from the western Solomon Arc and Woodlark Basin. In: B. Taylor and N.F. Exon (Editors), Marine Geology, Geophysics and Geochemistry of the Woodlark Basin-Solomon Islands. Circum-Pacific Council for Energy and Mineral Resources, Earth Science Series, pp. 155-226.

Johnson, R.W. and Tuni, D., 1987. Kavachi, an active forearc volcano in the western Solomon Islands: reported eruptions between 1950 and 1982. In: B. Taylor and N.F. Exon (Editors), Marine Geology, Geophysics and Geochemistry of the Woodlark Basin-Solomon Islands. Circum-Pacific Council for Energy and Mineral Resources, Earth Science Series, pp. 89-112.

Johnston, S.T. and Thorkelson, D.J., 1997. Cocos-Nazca slab window beneath Central America. Earth and Planetary Science Letters, 146(3-4): 465-474.

Jones, B. and Renaut, R.W., 2003a. Hot spring and geyser sinters: the integrated product of precipitation, replacement, and deposition. Canadian Journal of Earth Sciences, 40(11): 1549-1569.

Jones, B. and Renaut, R.W., 2003b. Petrography and genesis of spicular and columnar geyserite from the Whakarewarewa and Orakeikorako geothermal areas, North Island, New Zealand. Canadian Journal of Earth Sciences, 40(11): 1585-1610.

Jones, B., Renaut, R.W. and Konhauser, K.O., 2005. Genesis of large siliceous stromatolites at Frying Pan Lake, Waimangu geothermal field, North Island, New Zealand. Sedimentology, 52: 1229-1252.

Jones, B., Renaut, R.W. and Rosen, M.R., 1996. High-temperature (>90°C) calcite precipitation at Waikite Hot Springs, North Island, New Zealand. Journal of the Geological Society, 153: 481-496.

Jones, B., Renaut, R.W. and Rosen, M.R., 1997. Biogenicity of silica precipitation around geysers and hot-spring vents, North Island, New Zealand. Journal of Sedimentary Research, 67(1): 88-104.

Jones, B., Renaut, R.W. and Rosen, M.R., 2000. Stromatolites Forming in Acidic Hot-Spring Waters, North Island, New Zealand. Palaios, 15(5): 450-475.

Jones, B., Renaut, R.W. and Rosen, M.R., 2003. Taxonomic fidelity of silicified filamentous microbes from hot-spring systems in the Taupo Volcanic Zone, North Island, New Zealand. Transactions of the Royal Society of Edinburgh: Earth Sciences, 94: 475-483.

Jouzel, J., Russell, G.L., Suozzo, R.J., Koster, D., White, J.W.C. and Broecker, W.S., 1987. Simulations of the HDO and $H_2^{18}O$ atmospheric cycles using the NASA GISS general circulation model: The seasonal cycle for present-day conditions. Journal of Geophysical Research - Atmospheres, 92: 14739-14760.

Kamenov, G.D., Perfit, M.R., Mueller, P.A. and Jonasson, I.R., 2008. Controls on magmatism in an island arc environment: study of lavas and sub-arc xenoliths from the Tabar-Lihir-Tanga-Feni island chain, Papua New Guinea. Contributions to Mineralogy and Petrology, 155(5): 635-656.

Keenan, J.H., Keyes, F.G., Hill, P.G. and Moore, J.G., 1969. Steam tables - thermodynamic properties of water including vapor, liquid and solid phases (International Edition - metric units). Wiley, New York, 162 pp.

Kempton, P.D. and McGill, R., 2002. Procedures for the analysis of common lead at the NERC Isotope Geosciences Laboratory and an assessment of data quality. NIGL Report Series 178, NERC Isotope Geosciences Laboratory.

Kepezhinskas, P.K., Defant, M.J. and Drummond, M.S., 1995. Na metasomatism in the island-arc mantle by slab melt- peridotite interaction: Evidence from mantle xenoliths in the north Kamchatka arc. Journal of Petrology, 36(6): 1505-1527.

Kim, S.-T. and O'Neil, J.R., 1997. Equilibrium and nonequilibrium oxygen isotope effects in synthetic carbonates. Geochimica et Cosmochimica Acta, 61(16): 3461-3475.

Konhauser, K.O. and Ferris, F.G., 1996. Diversity of iron and silica precipitation by microbial mats in hydrothermal waters, Iceland: Implications for Precambrian iron formations. Geology, 24(4): 323-326.

Konhauser, K.O., Jones, B., Phoenix, V.R., Ferris, G. and Renaut, R.W., 2004. A model for hot spring silicification. Ambio, 33: 552-558.

König, S., Schuth, S., Münker, C. and Qopoto, C., 2007. The role of slab melting in the petrogenesis of high-Mg andesites: evidence from Simbo Volcano, Solomon Islands. Contributions to Mineralogy and Petrology, 153(1): 85-103.

Kornexl, B.E., Werner, R.A. and Gehre, M., 1999. Standardization for oxygen isotope ratio measurement - still an unsolved problem. Rapid Communications in Mass Spectrometry, 13(13): 1248-1251.

Kroenke, L.W., 1995. A morphotectonic interpretation of SOPACMAPS 1:500 000 charts, Central Solomon Islands - Southern Tuvalu. Technical Report 220, SOPAC, Fiji.

Kusakabe, M., Komoda, Y., Takano, B. and Abiko, T., 2000. Sulfur isotopic effects in the disproportionation reaction of sulfur dioxide in hydrothermal fluids: implications for the $\delta^{34}S$ variations of dissolved bisulfate and elemental sulfur from active crater lakes. Journal of Volcanology and Geothermal Research, 97: 287-307.

Lange, R.A., 1994. The effect of H_2O, CO_2 and F on the density and viscosity of silicate melts. In: M.R. Carroll and J.R. Holloway (Editors), Reviews in Mineralogy, pp. 331-369.

Le Maitre, R.W., Bateman, P., Dudek, A., Keller, J., Lameyre, J., Le Bas, M.J., Sabine, P.A., Schmid, R., Sorensen, H., Streckeisen, A., Woolley, A.R. and Zanettin, B., 1989. A Classification of Igneous Rocks and Glossary of Terms: Recommendations of the International Union of Geological Sciences Subcommission on the Systematics of Igneous Rocks. Blackwell Scientific, Oxford.

Leake, B.E., Woolley, A.R., Arps, C.E.S., Birch, W.D., Gilbert, M.C., Grice, J.D., Hawthorne, F.C., Kato, A., Kisch, H.J., Krivovichev, V.G., Linthout, K., Laird, J., Mandarino, J.A., Maresch, W.V., Nickel, E.H., Rock, N.M.S., Schumacher, J.C., Smith, D.C., Stephenson, N.C.N., Ungaretti, L., Whittaker, E.J.W. and Guo, Y.Z., 1997. Nomenclature of amphiboles: Report of the subcommittee on amphiboles of the International Mineralogical Association, commission on new minerals and mineral names. American Mineralogist, 82(9-10): 1019-1037.

Lebron, M.C. and Perfit, M.R., 1993. Stratigraphic and petrochemical data support subduction polarity reversal of the Cretaceous Caribbean Island Arc. Journal of Geology, 101(3): 389-396.

Leeman, W.P., Tonarini, S., Pennisi, M. and Ferrara, G., 2005. Boron isotopic variations in fumarolic condensates and thermal waters from Vulcano Island, Italy: Implications for evolution of volcanic fluids. Geochimica et Cosmochimica Acta, 69(1): 143-163.

Lipfert, G., Sidle, W.C., Reeve, A.S., Ayuso, R.A. and Boyce, A.J., 2007. High arsenic concentrations and enriched sulfur and oxygen isotopes in a fractured-bedrock ground-water system. Chemical Geology, 242: 385-399.

Luhr, J.F., Carmichael, I.S.E. and Varekamp, J.C., 1984. The 1982 eruptions of El Chichon volcano, Chiapas, Mexico - mineralogy and petrology of the anhydrite bearing pumices. Journal of Volcanology and Geothermal Research, 23(1-2): 69-108.

Luhr, J.F. and Logan, M.A.V., 2002. Sulfur isotope systematics of the 1982 El Chichon trachyandesite: An ion microprobe study. Geochimica et Cosmochimica Acta, 66(18): 3303-3316.

Lynne, B.Y. and Campbell, K.A., 2003. Diagenetic transformations (opal-A to quartz) of low- and mid-temperature microbial textures in siliceous hot-spring deposits, Taupo Volcanic Zone, New Zealand. Canadian Journal of Earth Sciences, 40(11): 1679-1696.

Macpherson, C.G., Dreher, S.T. and Thirlwall, M.F., 2006. Adakites without slab melting: High pressure differentiation of island arc magma, Mindanao, the Philippines. Earth and Planetary Science Letters, 243(3-4): 581-593.

Mann, P., Taylor, F.W., Lagoe, M.B., Quarles, A. and Burr, G., 1998. Accelerating late Quaternary uplift of the New Georgia Island Group (Solomon island arc) in response to subduction of the recently active Woodlark spreading center and Coleman seamount. Tectonophysics, 295(3-4): 259-306.

Marshak, R.S. and Karig, D.E., 1977. Triple junctions as a cause for anomalously near-trench igneous activity between the trench and volcanic arc. Geology, 5: 233-236.

McCrea, J.M., 1950. On the isotopic chemistry of carbonates and a paleotemperature scale. Journal of Chemical Physics, 18(6): 849-857.

McInnes, B.I.A. and Cameron, E.M., 1994. Carbonated, alkaline hybridizing melts from a sub-arc environment: Mantle wedge samples from the Tabar-Lihir-Tanga-Feni arc, Papua New Guinea. Earth and Planetary Science Letters, 122(1-2): 125-141.

McInnes, B.I.A., Gregoire, M., Binns, R.A., Herzig, P.M. and Hannington, M.D., 2001. Hydrous metasomatism of oceanic sub-arc mantle, Lihir, Papua New Guinea: petrology and geochemistry of fluid-metasomatised mantle wedge xenoliths. Earth and Planetary Science Letters, 188(1-2): 169-183.

McKenzie, W.F. and Truesdell, A.H., 1977. Geothermal reservoir temperatures estimated from the oxygen isotope compositions of dissolved sulfate and water from hot springs and shallow drillholes. Geothermics, 5(1-4): 51-61.

Meffre, S. and Crawford, A.J., 2001. Collision tectonics in the New Hebrides arc (Vanuatu). Island Arc, 10 (1): 33-50.

Michaelis, J., Usdowski, E. and Menschel, G., 1985. Partitioning of ^{13}C and ^{12}C on the Degassing of CO_2 and the Precipitation of Calcite - Rayleigh-Type Fractionation and a Kinetic-Model. American Journal of Science, 285(4): 318-327.

Miyabuchi, Y., 1999. Deposits associated with the 1990-1995 eruption of Unzen volcano, Japan. Journal of Volcanology and Geothermal Research, 89(1-4): 139-158.

Moore, G. and Carmichael, I.S.E., 1998. The hydrous phase equilibria (to 3 kbar) of an andesite and basaltic andesite from western Mexico: constraints on water content and conditions of phenocryst growth. Contributions to Mineralogy and Petrology, 130(3-4): 304-319.

Müller, D., 2002. Gold-copper mineralization in alkaline rocks. Mineralium Deposita, 37(1): 1-3.

Müller, D., Franz, L., Herzig, P.M. and Hunt, S., 2001. Potassic igneous rocks from the vicinity of epithermal gold mineralization, Lihir Island, Papua New Guinea. Lithos, 57(2-3): 163-186.

Mungall, J.E., 2002. Roasting the mantle: Slab melting and the genesis of major Au and Au-rich Cu deposits. Geology, 30(10): 915-918.

Muntean, J.L. and Einaudi, M.T., 2001. Porphyry-epithermal transition: Maricunga belt, northern Chile. Economic Geology, 96(4): 743-772.

Naden, J., Kilias, S.P. and Darbyshire, D.P.F., 2005. Active geothermal systems with entrained seawater as modern analogues for transitional volcanic-hosted massive sulfide and continental magmato-hydrothermal mineralization: the example of Milos Island, Greece. Geology, 33(7): 541-544.

Nesbitt, R.W., Mastins, H., Stolz, G.W. and Bruce, D.R., 1976. Matrix corrections in trace-element analysis by X-ray fluorescence: An extension of the Compton scattering technique to long wavelengths. Chemical Geology, 18(3): 203-213.

Notsu, K., Sugiyama, K., Hosoe, M., Uemura, A., Shimoike, Y., Tsunomori, F., Sumino, H., Yamamoto, J., Mori, T. and Hernandez, P.A., 2005. Diffuse CO_2 efflux from Iwojima volcano, Izu-Ogasawara arc, Japan. Journal of Volcanology and Geothermal Research, 139(3-4): 147-161.

Ohmoto, H., 1986. Stable isotope geochemistry of ore deposits. In: J.W. Valley, H.P. Taylor Jr. and J.R. O'Neil (Editors), Stable Isotopes in High Temperature Geological Processes. Reviews in Mineralogy, pp. 491-559.

Ohmoto, H. and Lasaga, A.C., 1982. Kinetics of reactions between aqueous sulfates and sulfides in hydrothermal systems. Geochimica et Cosmochimica Acta, 46(10): 1727-1745.

Ohmoto, H. and Rye, R.O., 1979. Isotopes of sulfur and carbon. In: H.L. Barnes (Editor), Geochemistry of Hydrothermal Ore Deposits, 2nd Edition. John Wiley and Sons, pp. 509-567.

Ohsawa, S. and Yusa, Y., 2001. High $\delta^{13}C$ fumarolic CO_2 discharged from Ogasawara-Iwojima, an active volcanic island in the Izu–Bonin arc. Journal of the Geothermal Research Society of Japan, 23(3): 197-204.

Oki, Y. and Hirano, T., 1978. Geochemistry of Hakone, Yugawara and Atami hydrothermal systems. Transactions-American Geophysical Union, 59(12): 1220-1220.

Oyarzun, R., Márquez, A., Lillo, J., López, I. and Rivera, S., 2001. Giant versus small porphyry copper deposits of Cenozoic age in northern Chile: adakitic versus normal calc-alkaline magmatism. Mineralium Deposita, 36(8): 794-798.

Pals, D.W. and Spry, P.G., 2003. Telluride mineralogy of the low-sulfidation epithermal Emperor gold deposit, Vatukoula, Fiji. Mineralogy and Petrology, 79(3): 285-307.

Peacock, S.M., Rushmer, T. and Thompson, A.B., 1994. Partial melting of subducting oceanic crust. Earth and Planetary Science Letters, 121: 227-244.

Pearce, J.A., 1982. Trace element characteristics of lavas from destructive plate boundaries. In: R.S. Thorpe (Editor), Andesites: Orogenic Andesites and Related Rocks. John Wiley and Sons, Chichester, pp. 525-548.

Pearce, J.A. and Peate, D.W., 1995. Tectonic implications of the composition of volcanic arc magmas. Annual Review of Earth and Planetary Sciences, 23: 251-285.

Peate, D.W., Pearce, J.A., Hawkesworth, C.J., Colley, H., Edwards, C.M.H. and Hirose, K., 1997. Geochemical variations in Vanuatu arc lavas: the role of subducted material and a variable mantle wedge composition. Journal of Petrology, 38(10): 1331-1358.

Pentecost, A., 2003. Cyanobacteria associated with hot spring travertines. Canadian Journal of Earth Sciences, 40(11): 1447-1457.

Perfit, M.R., Langmuir, C.H., Baekisapa, M., Chappell, B.W., Johnson, R.W., Staudigel, H. and Taylor, S.R., 1987. Geochemistry and petrology of volcanic rocks from the Woodlark Basin; addressing questions of ridge subduction. In: B. Taylor and N.F. Exon (Editors), Marine Geology, Geophysics and Geochemistry of the Woodlark Basin-Solomon Islands. Circum-Pacific Council for Energy and Mineral Resources, Earth Science Series, pp. 113-154.

Petterson, M.G., Babbs, T., Neal, C.R., Mahoney, J.J., Saunders, A.D., Duncan, R.A., Tolia, D., Magu, R., Qopoto, C., Mahoa, H. and Natogga, D., 1999. Geological-tectonic framework of Solomon Islands, SW Pacific; crustal accretion and growth within an intra-oceanic setting. Tectonophysics, 301(1-2): 35-60.

Petterson, M.G. and Biliki, N., 1994. A volcano-morphological map of the Gallego volcanic field, Western Guadalcanal. Technical Report TR4/94, Water & Mineral Resources Division, Ministry of Energy, Water & Mineral Resources, Honiara, Solomon Islands.

Petterson, M.G., Coleman, P.J., Tolia, D.H., Mahoa, H. and Magu, R., 2004. Application of terrain modelling of Solomon Islands, SW Pacific, to the metallogenesis and mineral exploration in composite arc-ocean floor terrain collages. In: M.G. Petterson (Editor), Pacific Minerals in the New Millenium: Science, Exploration, Mining and Community: The Jackson Lum Volume. Technical Bulletin 11. SOPAC, pp. 93-113.

Petterson, M.G., Cronin, S.J., Taylor, P.W., Tolia, D., Papabatu, A., Toba, T. and Qopoto, C., 2003. The eruptive history and volcanic hazards of Savo, Solomon Islands. Bulletin of Volcanology, 65(2-3): 165-181.

Petterson, M.G., Neal, C.R., Mahoney, J.J., Kroenke, L.W., Saunders, A.D., Babbs, T.L., Duncan, R.A., Tolia, D. and McGrail, B., 1997. Structure and deformation of north and central Malaita, Solomon Islands; tectonic implications for the Ontong Java Plateau-Solomon arc collision, and for the fate of oceanic plateaus. Tectonophysics, 283(1-4): 1-33.

Phinney, E.J., Mann, P., Coffin, M.F. and Shipley, T.H., 2004. Sequence stratigraphy, structural style, and age of deformation of the Malaita accretionary prism (Solomon arc–Ontong Java Plateau convergent zone). Tectonophysics, 389(3-4): 221-246.

Plank, T. and Langmuir, C.H., 1988. An evaluation of the global variations in the major element chemistry of arc basalts. Earth and Planetary Science Letters, 90(4): 349-370.

Poli, S. and Schmidt, M.W., 2002. Petrology of subducted slabs. Annual Review of Earth and Planetary Sciences, 30: 207-235.

Pound, K.S., 1986. Correlation of rock units in the central and western Solomon Islands. In: J.G. Vedder, K.S. Pound and S.Q. Boundy (Editors), Geology and offshore resources of Pacific island arcs - central and western Solomon Islands. Circum-Pacific Council for Energy and Mineral Resources, Houston, TX, pp. 89-97.

Rabbia, O., Hernández, L., King, R. and López-Escobar, L., 2002. Discussion on "Giant versus small porphyry copper deposits of Cenozoic age in northern Chile: adakitic versus normal calc-alkaline magmatism" by Oyarzun et al. (Mineralium Deposita 36:794-798, 2001). Mineralium Deposita, 37 (8): 791-794.

Rapp, R.P., Shimizu, N., Norman, M.D. and Applegate, G.S., 1999. Reaction between slab-derived melts and peridotite in the mantle wedge: experimental constraints at 3.8 GPa. Chemical Geology, 160: 335-356.

Reed, M.H., 1982. Calculation of multicomponent chemical equilibria and reaction processes in systems involving minerals, gases and an aqueous phase. Geochimica et Cosmochimica Acta, 46(4): 513-528.

Reed, M.H., 1997. Hydrothermal alteration and its relationship to ore fluid composition. In: H.L. Barnes (Editor), Geochemistry of Hydrothermal Ore Deposits, 3rd Edition. John Wiley and Sons, pp. 303-366.

Reed, M.H., 1998. Calculation of simultaneous chemical equilibria in aqueous-mineral-gas systems and its application to modeling hydrothermal processes. In: J. Richards and P. Larson (Editors), Techniques in Hydrothermal Ore Deposits Geology. Reviews in Economic Geology. Society of Economic Geologists, pp. 109-124.

Reed, M.H. and Spycher, N., 1984. Calculation of pH and mineral equilibria in hydrothermal waters with application to geothermometry and studies of boiling and dilution. Geochimica et Cosmochimica Acta, 48(7): 1479-1492.

Reyes, A.G., Grapes, R. and Clemente, V.C., 2003. Fluid-rock interaction at the magmatic-hydrothermal interface of the Mount Cagua geothermal system, Philippines. In: S.F. Simmons and I. Graham (Editors), Special Publication 10. Society of Economic Geologists, pp. 197-222.

Reynolds, R.C., 1967. Estimation of mass absorption coefficient by Compton scattering: Improvements and extensions of the method. American Mineralogist, 52: 1493-1502.

Richards, J., 2002. Discussion on "Giant versus small porphyry copper deposits of Cenozoic age in northern Chile: adakitic versus normal calc-alkaline magmatism" by Oyarzun et al. (Mineralium Deposita 36: 794-798, 2001). Mineralium Deposita, 37(8): 788-790.

Richards, J.P., 1995. Alkalic-type epithermal gold deposits - a review. In: J.F.H. Thompson (Editor), Magmas, Fluids, Ore Deposits. Mineralogical Association of Canada Short Course Series, pp. 367-400.

Richards, J.P., Bray, C.J., Channer, D.M.D. and Spooner, E.T.C., 1997. Fluid chemistry and processes at the Porgera gold deposit, Papua New Guinea. Mineralium Deposita, 32(2): 119-132.

Richards, J.P., Chappell, B.W. and McCulloch, M.T., 1990. Intraplate-type magmatism in a continent island-arc collision zone: Porgera intrusive complex, Papua New Guinea. Geology, 18: 958-961.

Richards, J.P. and Kerrich, R., 1993. The Porgera gold mine, Papua New Guinea - magmatic hydrothermal to epithermal evolution of an alkalic-type precious-metal deposit. Economic Geology, 88(5): 1017-1052.

Richards, J.P. and Kerrich, R., 2007. Special Paper: Adakite-like rocks: their diverse origins and questionable role in metallogenesis. Economic Geology, 102(4): 537-576.

Richards, J.P., McCulloch, M.T., Chappell, B.W. and Kerrich, R., 1991. Sources of metals in the Porgera gold deposit, Papua New Guinea: Evidence from alteration, isotope, and noble metal geochemistry. Geochimica et Cosmochimica Acta, 55(2): 565-580.

Rimstidt, J.D., 1997. Gangue mineral transport and deposition. In: H.L. Barnes (Editor), Geochemistry of Hydrothermal Ore Deposits, 3rd Edition. John Wiley and Sons, pp. 487-515.

Rimstidt, J.D. and Cole, D.R., 1983. Geothermal mineralization; I, The mechanism of formation of the Beowawe, Nevada, siliceous sinter deposit. American Journal of Science, 283(8): 861-875.

Robinson, B.W. and Kusakabe, M., 1975. Quantitative Preparation of Sulfur-Dioxide, for ^{34}S-^{32}S Analyses, from Sulfides by Combustion with Cuprous-Oxide. Analytical Chemistry, 47(7): 1179-1181.

Rodgers, K.A., Browne, P.R.L., Buddle, T.F., Cook, K.L., Greatrex, R.A., Hampton, W.A., Herdianita, N.R., Holland, G.R., Lynne, B.Y., Martin, R., Newton, Z., Pastars, D., Sannazarro, K.L. and Teece, C.I.A., 2004. Silica phases in sinters and residues from geothermal fields of New Zealand. Earth-Science Reviews, 66(1-2): 1-61.

Rodriguez, C., Selles, D., Dungan, M., Langmuir, C. and Leeman, W., 2007. Adakitic dacites formed by intracrustal crystal fractionation of water-rich parent magmas at Nevado de Longavi Volcano (36.2° S; Andean Southern Volcanic Zone, Central Chile). Journal of Petrology, 48(11): 2033-2061.

Rogers, G., Saunders, A.D., Terrell, D.J., Verma, S.P. and Marriner, G.F., 1985. Geochemistry of Holocene volcanic rocks associated with ridge subduction in Baja California, Mexico. Nature, 315: 389-392.

Roggensack, K., Hervig, R.L., McKnight, S.B. and Williams, S.N., 1997. Explosive basaltic volcanism from Cerro Negro volcano: Influence of volatiles on eruptive style. Science, 277(5332): 1639-1642.

Rohrbach, A., Schuth, S., Ballhaus, C., Munker, C., Matveev, S. and Qopoto, C., 2005. Petrological constraints on the origin of arc picrites, New Georgia Group, Solomon Islands. Contributions to Mineralogy and Petrology, 149(6): 685-698.

Rohrbach, A., Schuth, S., Münker, C. and Ballhaus, C., 2003. Island arc picrites from the solomon islands-origin by mantle matrix collapse. Geophysical Research Abstracts, 5: 11716.

Rollinson, H.R., 1993. Using geochemical data: evaluation, presentation, interpretation. Longman Scientific & Technical, Harlow, England, 352 pp.

Rose, W.I., Pearson, T. and Bonis, S., 1976. Nuée ardente eruption from the foot of a dacite lava flow, Santiaguito volcano, Guatemala. Bulletin of Volcanology, 40(1): 23-38.

Rosenbaum, J.M. and Sheppard, S.M.F., 1986. An isotopic study of siderites, dolomites and ankerites at high temperatures. Geochimica et Cosmochimica Acta, 50: 1147-1159.

Royse, K.R., Kempton, P.D. and Darbyshire, D.P.F., 1998. Procedure for the analysis of rubidium-strontium and samarium-neodymium isotopes at the NERC Isotope Geosciences Laboratory. NIGL Report Series No. 121.

Rye, R.O., 1993. The evolution of magmatic fluids in the epithermal environment; the stable isotope perspective. Economic Geology, 88(3): 733-752.

Rye, R.O., 2005. A review of the stable-isotope geochemistry of sulfate minerals in selected igneous environments and related hydrothermal systems. Chemical Geology, 215(1-4): 5-36.

Rye, R.O., Bethke, P.M. and Wasserman, M.D., 1992. The stable isotope geochemistry of acid sulfate alteration. Economic Geology, 87(2): 225-262.

Rye, R.O., Luhr, J.F. and Wasserman, M.D., 1984. Sulfur and oxygen isotopic systematics of the 1982 eruptions of El Chichon volcano, Chiapas, Mexico. Journal of Volcanology and Geothermal Research, 23(1-2): 109-123.

Sajona, F.G. and Maury, R.C., 1998. Association of adakites with gold and copper mineralization in the Philippines. Comptes Rendus de l'Academie des Sciences - Series IIA - Earth and Planetary Science, 326(1): 27-34.

Sakai, H., 1968. Isotopic properties of sulfur compounds in hydrothermal processes. Geochemical Journal, 2: 29-49.

Saleeby, J., Ducea, M. and Clemens-Knott, D., 2003. Production and loss of high-density batholithic root, southern Sierra Nevada, California. Tectonics, 22(6).

Sano, Y. and Marty, B., 1995. Origin of carbon in fumarolic gas from island arcs. Chemical Geology, 119(1-4): 265-274.

Saunders, A.D., Rogers, G., Marriner, G.F., Terrell, D.J. and Verma, S.P., 1987. Geochemistry of Cenezoic volcanic rocks, Baja California, Mexico: Implications for the petrogenesis of post-subduction magmas. Journal of Volcanology and Geothermal Research, 32(1-3): 223-245.

Schuth, S., Munker, C., Konig, S., Basi, S., Qopoto, C. and Ballhaus, C., 2006. High precision Pb and Sr-Nd-Hf isotope constraints on mantle source variations along the Solomon arc. Geochimica et Cosmochimica Acta, 70(18): A566-A566.

Schuth, S., Munker, C., Scherer, E.E. and Konig, S., 2007. High-precision Pb isotope measurements discriminate different subduction components along the Solomon island arc. Geochimica et Cosmochimica Acta, 71(15): A909-A909.

Schuth, S., Rohrbach, A., Münker, C., Ballhaus, C., Garbe-Schönberg, D. and Qopoto, C., 2004. Geochemical constraints on the petrogenesis of arc picrites and basalts, New Georgia Group, Solomon Islands. Contributions to Mineralogy and Petrology, 148(3): 288-304.

Seward, T.M., 1991. The hydrothermal geochemistry of gold. In: R.P. Forster (Editor), Gold Metallogeny and Exploration. Blackie and Son, London, pp. 37-62.

Seward, T.M. and Barnes, H.L., 1997. Metal tranpsort by hydrothermal ore fluids. In: H.L. Barnes (Editor), Geochemistry of Hydrothermal ore Deposits, 3rd edition. John Wiley and Sons, pp. 435-486.

Sharp, Z.D., 1990. A laser-based microanalytical method for the in situ determination of oxygen isotope ratios of silicates and oxides. Geochimica et Cosmochimica Acta, 54(5): 1353-1357.

Shelton, K.L. and Rye, D.M., 1982. Sulfur isotopic compositions of ores from Mines Gaspe, Quebec - an example of sulfate-sulfide isotopic disequilibria in ore-forming fluids with applications to other porphyry-type deposits. Economic Geology, 77(7): 1688-1709.

Shevenell, L. and Goff, F., 1993. Addition of magmatic volatiles into the hot spring waters of Loowit Canyon, Mount St. Helens, Washington, USA. Bulletin of Volcanology, 55: 489-503.

Shevenell, L. and Goff, F., 1995a. Evolution of hydrothermal waters at Mount St. Helens, Washington, USA. Journal of Volcanology and Geothermal Research, 69(1-2): 73-94.

Shevenell, L. and Goff, F., 1995b. The use of tritium in groundwater to determine fluid mean residence times of Valles caldera hydrothermal fluids, New Mexico, USA. Journal of Volcanology and Geothermal Research, 67(1-3): 187-205.

Sillitoe, R.H., 1994. Erosion and collapse of volcanoes; causes of telescoping in intrusion-centered ore deposits. Geology, 22(10): 945-948.

Sillitoe, R.H., 1997. Characteristics and controls of the largest porphyry copper-gold and epithermal gold deposits in the circum-Pacific region. Australian Journal of Earth Sciences, 44: 373-388.

Sillitoe, R.H., 2002. Some metallogenic features of gold and copper deposits related to alkaline rocks and consequences for exploration. Mineralium Deposita, 37(1): 4-13.

Sillitoe, R.H. and Hedenquist, J.W., 2003. Linkages between volcanotectonic settings, ore-fluid compositions, and epithermal precious metal deposits. In: S.F. Simmons and I. Graham (Editors), Volcanic, Geothermal and Ore-Forming Fluids: Rulers and Witnesses of Processes within the Earth. Special Publication No. 10. Society of Economic Geologists, Littleton, Colorado, pp. 315-343.

Simmons, S.F. and Brown, K.L., 2006. Gold in magmatic hydrothermal solutions and the rapid formation of a giant ore deposit. Science, 314(5797): 288-291.

Simmons, S.F. and Browne, P.R.L., 2000. Hydrothermal minerals and precious metals in the Broadlands-Ohaaki geothermal system: Implications for understanding low- sulfidation epithermal environments. Economic Geology, 95(5): 971-999.

Simmons, S.F. and Christenson, B.W., 1994. Origins of calcite in a boiling geothermal system. American Journal of Science, 294: 361-400.

Simmons, S.F., White, N.C. and John, D.A., 2005. Geological characteristics of epithermal precious and base metal deposits, Economic Geology 100th Anniversary Volume. Society of Economic Geologists, pp. 485-522.

Sisson, T.W. and Grove, T.L., 1993. Experimental investigations of the role of H_2O in calc-alkaline differentiation and subduction zone magmatism. Contributions to Mineralogy and Petrology, 113(2): 143-166.

Sisson, T.W. and Layne, G.D., 1993. H_2O in basalt and basaltic andesite glass inclusions from 4 subduction-related volcanoes. Earth and Planetary Science Letters, 117(3-4): 619-635.

Solomon, M., 1990. Subduction, arc reversal, and the origin of porphyry copper-gold deposits in island arcs. Geology, 18(7): 630-633.

Sourirajan, S. and Kennedy, G.C., 1962. The system H_2O-NaCl at elevated temperatures and pressures. American Journal of Science, 260(2): 115-141.

Sparks, R.S.J., 1997. Causes and consequences of pressurisation in lava dome eruptions. Earth and Planetary Science Letters, 150(3-4): 177-189.

Spry, P.G. and Scherbarth, N.L., 2006. The gold–vanadium–tellurium association at the Tuvatu gold–silver prospect, Fiji: conditions of ore deposition. Mineralogy and Petrology, 87(3-4): 171-186.

Stanton, R.L., 1994. Ore Elements in Arc Lavas. Oxford monographs on geology and geophysics; no.24. Oxford University Press.

Staudigel, H., McCulloch, M.T., Zindler, A. and Perfit, M.R., 1987. Complex ridge subduction and island arc magmatism; an isotopic study of the New Georgia Forearc and the Woodlark Basin. In: B. Taylor and N.F. Exon (Editors), Marine geology, geophysics and geochemistry of the Woodlark Basin-Solomon Islands. Circum-Pacific Council for Energy and Mineral Resources, Earth Science Series, pp. 227-240.

Stimac, J.A., Goff, F., Counce, D., Larocque, A.C.L., Hilton, D.R. and Morgenstern, U., 2004. The crater lake and hydrothermal system of Mount Pinatubo, Philippines: evolution in the decade after eruption. Bulletin of Volcanology, 66(2): 149-167.

Stoffregen, R.E., 1987. Genesis of acid-sulfate alteration and Au-Cu-Ag mineralization at Summitville, Colorado. Economic Geology, 82(6): 1575-1591.

Streck, M.J., Leeman, W.P. and Chesley, J., 2007. High-magnesian andesite from Mount Shasta: A product of magma mixing and contamination, not a primitive mantle melt. Geology, 35(4): 351-354.

Sturm, R., 2002. PX-NOM - an interactive spreadsheet program for the computation of pyroxene analyses derived from the electron microprobe. Computers & Geosciences, 28(4): 473-483.

Sumino, H., Notsu, K., Nakai, S., Sato, M., Nagao, K., Hosoe, M. and Wakita, H., 2004. Noble gas and carbon isotopes of fumarolic gas from Iwojima volcano, Izu-Ogasawara arc, Japan: implications for the origin of unusual arc magmatism. Chemical Geology, 209(1-2): 153-173.

Symonds, R.B., Gerlach, T.M. and Reed, M.H., 2001. Magmatic gas scrubbing: implications for volcano monitoring. Journal of Volcanology and Geothermal Research, 108(1-4): 303-341.

Taran, Y., Fischer, T.P., Pokrovsky, B., Sano, Y., Armienta, M.A. and Macias, J.L., 1998. Geochemistry of the volcano-hydrothermal system of El Chichón Volcano, Chiapas, Mexico. Bulletin of Volcanology, 59(6): 436-449.

Taran, Y.A., Hedenquist, J.W., Korzhinsky, M.A., Tkachenko, S.I. and Shmulovich, K.I., 1995. Geochemistry of magmatic gases from Kudryavy volcano, Iturup, Kuril Islands. Geochimica et Cosmochimica Acta, 59(9): 1749-1761.

Taylor, B., 1987. A geophysical survey of the Woodlark-Solomons region. In: B. Taylor and N.F. Exon (Editors), Marine Geology, Geophysics and Geochemistry of the Woodlark Basin-Solomon Islands. Circum-Pacific Council for Energy and Mineral Resources, Earth Science Series, pp. 25-48.

Taylor, B. and Exon, N.F., 1987. An investigation of ridge subduction in the Woodlark-Solomons region: introduction and overview. In: B. Taylor and N.F. Exon (Editors), Marine Geology, Geophysics and Geochemistry of the Woodlark Basin-Solomon Islands. Circum-Pacific Council for Energy and Mineral Resources, Earth Science Series, pp. 1-24.

Taylor, B.E., 1986. Magmatic volatiles: isotopic variation of C, H, and S. In: J.W. Valley, H.P. Taylor Jr. and J.R. O'Neil (Editors), Stable Isotopes in High temperature Geological Processes. Mineralogical Society of America, pp. 185-225.

Tejada, M.L.G., Mahoney, J.J., Duncan, R.A. and Hawkins, M.P., 1996. Age and geochemistry of basement and alkalic rocks of Malaita and Santa Isabel, Solomon Islands, southern margin of Ontong Java plateau. Journal of Petrology, 37(2): 361-394.

Tejada, M.L.G., Mahoney, J.J., Neal, C.R., Duncan, R.A. and Petterson, M.G., 2002. Basement geochemistry and geochronology of central Malaita, Solomon Islands, with implications for the origin and evolution of the Ontong Java Plateau. Journal of Petrology, 43(3): 449-484.

Thieblemont, D., Stein, G. and Lescuyer, J., 1997. Gisements epithermaux et porphyriques: la connexion adakite. Comptes Rendus de l'Academie des Sciences - Series IIA - Earth and Planetary Science, 325(2): 103-109.

Thinh, T. and Leroux, J., 1979. New basic empirical expression for computing tables of X-ray mass attenuation coefficients. X-ray Spectrometry, 8(2): 85-91.

Thirlwall, M.F., 2002. Multicollector ICP-MS analysis of Pb isotopes using a ^{207}Pb-^{204}Pb double spike demonstrates up to 400 ppm/amu systematic errors in Tl-normalization. Chemical Geology, 184(3-4): 255-279.

Thorkelson, D.J., 1996. Subduction of diverging plates and the principles of slab window formation. Tectonophysics, 255(1-2): 47-63.

Thorkelson, D.J. and Breitsprecher, K., 2005. Partial melting of slab window margins: genesis of adakitic and non-adakitic magmas. Lithos, 79(1-2): 25-41.

Tilling, R.I., Gottfried, D. and Rowe, J.J., 1973. Gold Abundance in Igneous Rocks; bearing on Gold Mineralization. Economic Geology, 68(2): 168-186.

Tischendorf, G., Forster, H.J., Gottesmann, B. and Rieder, M., 2007. True and brittle micas: composition and solid-solution series. Mineralogical Magazine, 71: 285-320.

Tischendorf, G., Rieder, M., Forster, H.J., Gottesmann, B. and Guidotti, C.V., 2004. A new graphical presentation and subdivision of potassium micas. Mineralogical Magazine, 68(4): 649-667.

Toba, T., 1995. Geothermal activity of Savo Volcanic Island, Solomon Islands. A review and interpretation of temperature data obtained from geothermal vents during the period 1956 - 1993. TR6/95, Seismology Unit, Water and Mineral Resources Division, Ministry of Water and Mineral Resources, Honiara, Solomon Islands.

Todt, W., Cliff, R.A., Hanser, A. and Hofmann, A.W., 1996. Evaluation of a ^{202}Pb-^{205}Pb double spike for high-precision lead isotope analysis, Geophysical Monograph 95, Earth Processes: Reading the Isotopic Code, pp. 429-437.

Tolia, D.H. and Petterson, M.G., 2005. The Gold Ridge Mine, Guadalcanal, Solomon Islands' first gold mine: a case study in stakeholder consultation. In: B.R. Marker, M.G. Petterson and M.H. Stephenson (Editors), Sustainable Minerals Operations in the Developing World. Geological Society, London, pp. 149-160.

Truesdell, A.H., 1984a. Chemical geothermometers for geothermal exploration. In: R.W. Henley, A.H. Truesdell and P.B. Barton Jr. (Editors), Fluid-Mineral Equilibria in Hydrothermal Systems. Society of Economic Geologists, pp. 31-44.

Truesdell, A.H., 1984b. Stable isotopes in hydrothermal systems. In: R.W. Henley, A.H. Truesdell and P.B. Barton Jr. (Editors), Fluid-Mineral Equilibria in Hydrothermal Systems. Review in Economic Geology. Society of Economic Geologists, pp. 129-142.

Truesdell, A.H., Nathenson, M. and Rye, R.O., 1977. The effects of subsurface boiling and dilution on the isotopic compositions of Yellowstone thermal waters. Journal of Geophysical Research, B, Solid Earth and Planets, 82(26): 3694-3704.

Ui, T., Matsuwo, N., Sumita, M. and Fujinawa, A., 1999. Generation of block and ash flows during the 1990-1995 eruption of Unzen Volcano, Japan. Journal of Volcanology and Geothermal Research, 89(1-4): 123-137.

Usdowski, E., Hoefs, J. and Menschel, G., 1979. Relationship between ^{13}C and ^{18}O fractionation and changes in major element composition in a recent calcite-depositing spring -- A model of chemical variations with inorganic $CaCO_3$ precipitation. Earth and Planetary Science Letters, 42(2): 267-276.

Varekamp, J.C. and Kreulen, R., 2000. The stable isotope geochemistry of volcanic lakes, with examples from Indonesia. Journal of Volcanology and Geothermal Research, 97(1-4): 309-327.

Vikre, P.G., 2007. Sinter-Vein Correlations at Buckskin Mountain, National District, Humboldt County, Nevada. Economic Geology, 102(2): 193-224.

Wagner, T., Williams-Jones, A.E. and Boyce, A.J., 2005. Stable isotope-based modeling of the origin and genesis of an unusual Au–Ag–Sn–W epithermal system at Cirotan, Indonesia. Chemical Geology, 219: 237-260.

Wang, Q., McDermott, F., Xu, J.-f., Bellon, H. and Zhu, Y.-t., 2005. Cenozoic K-rich adakitic volcanic rocks in the Hohxil area, northern Tibet: Lower-crustal melting in an intracontinental setting. Geology, 33 (6): 465-468.

Webster, J.D., 2004. The exsolution of magmatic hydrosaline chloride liquids. Chemical Geology, 210(1-4): 33-48.

Webster, J.D. and De Vivo, B., 2002. Experimental and modeled solubilities of chlorine in aluminosilicate melts, consequences of magma evolution, and implications for exsolution of hydrous chloride melt at Mt. Somma-Vesuvius. American Mineralogist, 87(8-9): 1046-1061.

Webster, J.D. and Mandeville, C.W., 2007. Fluid immiscibility in volcanic environments. Reviews in Mineralogy and Geochemistry, 65: 313-362.

Wedepohl, K.H., 1995. The composition of the continental crust. Geochimica et Cosmochimica Acta, 59(7): 1217-1232.

White, N.C. and Hedenquist, J.W., 1995. Epithermal gold deposits: styles, characteristics and exploration. SEG Newsletter(23): 1-13.

White, N.C., Leake, M.J., McCaughey, S.N. and Parris, B.W., 1995. Epithermal gold deposits of the southwest Pacific. Journal of Geochemical Exploration, 54(2): 87-136.

Williams-Jones, A.E. and Heinrich, C.A., 2005. Vapor transport of metals and the formation of magmatic-hydrothermal ore deposits. Economic Geology, 100(7): 1287-1312.

Wilson, A.J., Cooke, D.R., Stein, H.J., Fanning, C.M., Holliday, J.R. and Tedder, I.J., 2007. U-Pb and Re-Os geochronologic evidence for two alkalic porphyry ore-forming events in the Cadia District, New South Wales, Australia. Economic Geology, 102(1): 3-26.

Woodhead, J.D., Eggins, S.M. and Johnson, R.W., 1998. Magma Genesis in the New Britain island arc: further insights into melting and mass transfer processes. Journal of Petrology, 39(8): 1641-1668.

Wright, J.V., Smith, A.L. and Self, S., 1980. A working terminology of pyroclastic deposits. Journal of Volcanology and Geothermal Research, 8(2-4): 315-336.

Wyborn, D., 1992. The tectonic significance of Ordovician magmatism in the eastern Lachlan Fold Belt. Tectonophysics, 214: 177-192.

Yi, W., Halliday, A., Alt, J., Lee, D., Rehkamper, M., Garcia, M., Langmuir, C.H. and Su, Y., 2000. Cadmium, indium, tin, tellurium, and sulfur in oceanic basalts: Implications for chalcophile element fractionation in the Earth. Journal of Geophysical Research, 105(B8): 18927-18948.

Yogodzinski, G.M., Lees, J.M., Churikova, T.G., Dorendorf, F., Woerner, G. and Volynets, O.N., 2001. Geochemical evidence for the melting of subducting oceanic lithosphere at plate edges. Nature, 409 (6819): 500-504.

Yumul, G.P., Dimalanta, C.B., Bellon, H., Faustino, D.V., De Jesus, J.V., Tamayo, R.A. and Jumawan, F.T., 2000. Adakitic lavas in the Central Luzon back-arc region, Philippines: lower crust partial melting products? Island Arc, 9(4): 499-512.

Zhang, R., 1986. Sulfur isotopes and pyrite-anhydrite equilibria in a volcanic-basin hydrothermal system of the Middle to Lower Yangtze River Valley. Economic Geology, 81(1): 32-45.

Zhao, Z.-F. and Zheng, Y.-F., 2003. Calculation of oxygen isotope fractionation in magmatic rocks. Chemical Geology, 193(1-2): 59-80.